University of Alberta

Fluorogenic and fluorescent bioorthogonal labelling strategies for examining glycoproteins and phospholipids

by

Jessie Adam Key

A thesis submitted to the Faculty of Graduate Studies and Research
in partial fulfillment of the requirements for the degree of

Doctor of Philosophy

Department of Chemistry

Fall 2011
Edmonton, Alberta

Abstract

Traditional genetically-encoded imaging strategies are problematic for use in analysing cell surface interactions due to the heterogeneous nature of the cell surface, and the high level of post-translational modifications. Small molecule fluorophores can provide dynamic information on cell surface interactions due to their small size, low detection limits and environmental sensitivity. Recent advances in bioconjugate strategies such as the Staudinger ligation, Sharpless-Meldal reaction and periodate oxidation with aniline-catalyzed ligation (PAL) and hydrazone/oxime forming reactions have imparted improved specificity. However, there remains a need for chromophores with improved specificity. This thesis describes the synthesis and application of novel chromophores for cell surface imaging. We employed selective labelling strategies to combat background signal, and enable detection of specific post-translational modifications.

We generated a small library of alkynyl coumarin profluorophores and characterized the corresponding alkyne and triazole derivatives. We observed increased fluorescence emission quantum yields of up to 9-fold and bathochromic shift of up to 23 nm due to the formation of the triazole linkage. Although these dyes are useful for fluorogenic labelling strategies, their relatively low brightness and short excitation wavelength inspired us to examine a new series of alkynyl and azido benzoxadiazole fluorophores for labelling cell surface glycoconjugates. We were able to identify reactive chromophores which act as fluorogenic,

quenched, and static fluorescent labels. The fluorogenic dye showed an almost 50-fold increase of intensity, and the quenched dyes showed up to 500-fold loss of intensity.

To quantify sialic acid content, using PAL methodology, we developed a novel 4-aminooxy-7-nitro- benzoxadiazole (NBDAO) fluorophore, and compared its performance with commercially available dyes. NBDAO was excited by a 488 nm laser line and found to be suitable for *in vitro* and *in vivo* labelling studies using SDS-PAGE, microplate assays, fluorescence spectroscopy, and flow cytometry. As well, a series of bioorthogonal cyanine-5 fluorophores and choline derivatives were synthesized and examined for suitability in phospholipid metabolic labelling experiments. Propargyl- and azido- choline readily incorporated as metabolic labels of phospholipids. However, a carbonyl-choline analog did not show any incorporation. The Cy 5 dyes were found to have exceptionally high absorption coefficients and long-wavelength absorption and emission.

Acknowledgements

I would like to take this chance to thank and acknowledge those that have helped me along my path. There have been so many influences that have contributed to the experiences that have shaped my knowledge and personality. Firstly I would like to thank my family and friends, who contributed to my basic foundations and well being. As well, I thank all of my teachers and educators who provided such an exceptional learning environment; in particular, the truly remarkable instructors at Kamloops Secondary School and Thompson Rivers University.

Graduate school has been a challenging experience in so many ways, and those who have supported me during this time deserve special acknowledgement:

- My advisor Chris Cairo, a great mentor and friend.
- My supervisory committee, always willing to lend advice, and write last minute reference letters.
- My colleagues and friends, especially my lab mates and fiancée, without your support and friendship, I can honestly say that I would not have gotten to the point of writing this document.

Table of Contents

List of Tables

List of Figures

List of Schemes

List of Abbreviations

ABDH	4-4-aminosulphonyl-7-hydrazino-2,1,3-benzoxadiazole
AD_E2	Electrophilic addition, bimolecular
APT	Attached proton test
Boc	Butyloxy carbonyl
Bodipy	4,4-Difluoro-4-bora-3a,4a-diaza-*s*-indacene
Bodipy FL	4,4-difluoro-5,7-dimethyl-4-bora-3a,4a-diaza-*s*-indacene-3-propionic acid
Cbz/Z	Carboxybenzyl
CDP	Cytidine diphosphate
CFP	Cyan fluorescent protein
CuAAC	Copper catalyzed alkyne-azide cycloaddition
Cy	Cyanine
DAABD-MHz	4-[2-(*N*,*N*-dimethylamino)ethylaminosulfonyl]-7-*N*-methylhydrazino-benz-2,1,3-oxadiazole
DBDH	4-(*N*,*N*-dimethylaminosulphonyl)-7-hydrazino-benz-2,1,3-oxadiazole
DCC	*N,N′*-Dicyclohexylcarbodiimide
DCM	Dichloromethane
DPH	diphenylhexatriene
DIC	Differential interference contrast
DIFO	difluorinated cyclooctynes
DIPEA	*N*,*N*-Diisopropylethylamine
DMF	Dimethylformamide

DNA	Deoxyribonucleic acid
DPBS	Dulbecco's phosphate buffered saline
EI	Electron impact
ES	Electrospray
EtOAc	Ethyl acetate
EtOH	Ethanol
Fmoc	Fluorenylmethyloxycarbonyl
FRET	Fluorescence Resonance Energy Transfer
GFP	Green fluorescent protein
h	Hour
HOMO	Highest occupied molecular orbital
HPLC	High-performance liquid chromatography
HRMS	High-resolution mass spectrometry
IR	Infrared spectroscopy
LUMO	Lowest unoccupied molecular orbital
MAE	Mean absolute error
MDBDH	4-(*N*,*N*-dimethylaminosulfonyl)-7-*N*-methylhydrazino-benz-2,1,3-oxadiazole
mDHFR	murine dihydrofolate reductase
MNBDH	*N*-methyl-4-hydrazino-7-nitrobenzofurazan
MeOH	Methanol
MEK	Methyl ethyl ketone
min	Minute

MFI	Mean fluorescence intensity
MW	Molecular weight
NBD	7-Nitrobenz[2,1,3-d]oxadiazole
NBDAO	*O*-(7-Nitrobenzo-[2,1,3-d]-oxadiazol-4-yl)hydroxylamine
NBDH	4-Hydrazinyl-7-nitrobenz-[2,1,3-d]-oxadiazole
NBD-Cl	7-nitro-4-chlorobenz-2,1,3-oxadiazole
NEU	Neuraminidase
NMR	Nuclear magnetic resonance
PAL	Periodate oxidation and aniline-catalyzed ligation
Pd/C	Palladium on Carbon
R*f*	Retention factor
RP	Reverse phase
RPMI	Roswell Park Memorial Institute
rt	Room temperature
SBD-F	ammonium 7-fluoro-2,1,3-benzoxadiazole-4-sulphonate
SDS-PAGE	Sodium dodecyl sulfate polyacrylamide gel electrophoresis
SMFS	Single-molecule fluorescence spectroscopy
S_NAR	Nucleophilic aromatic substitution
TBAF	Tetrabutylammonium fluoride
TD DFT	Time-dependent density functional theory
TEA	Triethyl amine
TES	Triethyl silane
TFA	Trifluoroacetic acid

THF	Tetrahydrofuran
TLC	Thin layer chromatography
TMSOTf	Trimethylsilyl trifluoromethanesulfonate
QY	Quantum yield
Quant	Quantitative
UV	Ultraviolet
UV-vis	Ultraviolet–visible

Chapter 1

Fluorogenic and static fluorophore probes for examining post-translational modifications[1]

[1] Portions of the work described in this chapter have been published in Key, J.A., Koh, S., Timerghazin, Q.K., Brown, A. and Cairo, C.W. (2009) Photophysical characterization of triazole-substituted coumarin fluorophores. *Dyes and Pigments*, 82, 196-203. Key, J.A. and Cairo, C.W. (2011) Identification of fluorogenic and quenched benzoxadiazole reactive chromophores. *Dyes and Pigments*, 88, 95-102. Sandbhor, M.S., Key, J.A., Strelkov, I.S. and Cairo, C.W. (2009) A Modular Synthesis of Alkynyl-Phosphocholine Headgroups for Labeling Sphingomyelin and Phosphatidylcholine. *The Journal of Organic Chemistry*, 74, 8669-8674. and Key, J.A., Li, C. and Cairo, C.W. (Submitted) Detection of cellular sialic acid content using nitrobenzoxadiazole carbonyl-reactive chromophores. *Bioconjugate Chemistry*.

1.1 The heterogeneous nature of the cell surface

The cell surface is a dynamic and heterogeneous environment which plays vital roles - both structural and functional - in processes like cell-cell communication, and homeostasis (**Figure 1.1**).(Cairo, C.W., Key, J.A., et al. 2010) Therefore, studying the interactions that occur on the cell surface remains an important research target. The lipid bilayer is composed primarily of three classes of macromolecules: lipids, proteins, and sterols. However, areas of high diversity arise from the proportion of, and structural diversity within, these broad classes of macromolecules. Post-translational modifications further contribute to this heterogeneity.

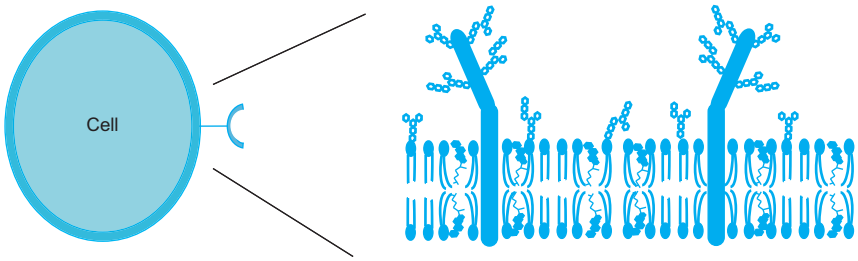

Figure 1.1. Schematic representation of the cell surface. The lipid bilayer is represented as a heterogeneous composite of lipids, proteins, and sterols in glycosylated and unglycosylated forms.

Glycosylation, one of the most prevalent post-translational modifications, accounts for approximately half of all protein modifications.(Kiessling, L.L. and Splain, R.A. 2010) Glycolipids are less prevalent than glycoproteins, typically making up about 5% of outer membrane lipids, but their functions and interactions are still relatively poorly understood. Traditional genetically-encoded

probing strategies are often impractical due to the heterogeneous nature of the cell surface, and because glycosylation is not directly template controlled like protein and nucleotide synthesis. In addition, there are several genetic and epigenetic (non-sequence determined) factors which contribute to glycolipid expression levels.(Maccioni, H.J.F., Quiroga, R., et al. 2011)

1.2 Small molecule fluorophores

Small molecule fluorophores possess several favourable characteristics which make them viable alternatives for examination of the cell surface. Small molecule fluorophores can provide dynamic information on cell surface interactions due to their small size, low detection limits and environmental sensitivity.(Cairo, C.W., Key, J.A., et al. 2010, Demchenko, A.P., Mély, Y., et al. 2009) Green Fluorescent Protein (GFP) is over 235 amino acids in length (~28 kDa), and can mask or alter the localization, quaternary structure and activities of the native proteins.(Ayoob, J.C., Sanger, J.M., et al. 2000, Lisenbee, C.S., Karnik, S.K., et al. 2003, Tsien, R.Y. 1998) Antibody and lectin probes are even larger, ranging in size from 150-900 kDa, with plant lectins ranging between 36-120 kDa.(Cohen, S. 1975, Etzler, M.E. 1985) As well, antibodies and lectins are known to perturb endogenous functions by crosslinking receptor molecules – limiting live cell applications.(Hernandez, J.D. and Baum, L.G. 2002) Thus small molecule fluorophores are advantageous for many *in vivo* cell labelling applications.

Judicious choice of an appropriate small molecule fluorophore can afford very low detection limits, down to the single molecule level. Single-molecule

fluorescence spectroscopy (SMFS) is a highly demanding method of monitoring the structure, dynamics and interactions of biomolecules. This methodology requires fluorophores with high absorption coefficients, high quantum yields, long wavelength absorption/emission, large Stokes shifts and good photostability. SMFS can give critical information on sub-populations which may be hidden or obscured by analysis using averaged-population methods.(Kapanidis, A.N. and Weiss, S. 2002)

Several small molecule fluorophores are sensitive to changes in the pH, hydrophobicity, polarity and microviscosity of their local environments. For example, 7-hydroxycoumarin shows decreased fluorescence emission under acidic conditions, while dansyl derivatives undergo bathochromic shifts under polar conditions.(Maier, O., Oberle, V., et al. 2002) The rod shaped probe diphenylhexatriene (DPH) is commonly used to examine microviscosity by fluorescence anisotropy.(Demchenko, A.P., Mély, Y., et al. 2009) In less viscous environments, DPH will rotate more freely, thereby depolarizing its fluorescence emission compared to its polarized excitation source. However, in highly ordered environments rotation will be hindered, and less depolarization will be observed.

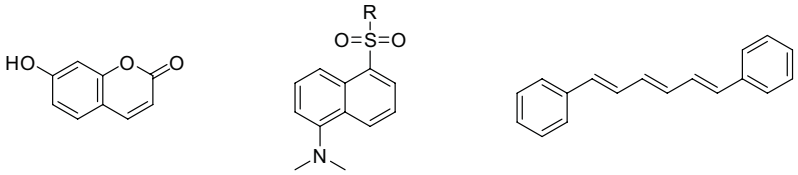

7-hydroxycoumarin dansyl diphenylhexatriene

Figure 1.2. Selected environmentally sensitive fluorophores. The fluorophores 7-hydroxycoumarin, dansyl and diphenylhexatriene (left to right) represent pH, solvatochromic and microviscosity sensitive probes.

Although there are numerous advantages to using small molecule fluorophores, to examine biomolecular interactions, high cost and background signal from non-specific binding have posed challenges for this methodology. Traditional fluorophore bioconjugation techniques, which rely on reactive endogenous functional groups such as the amine and thiol side chains of some amino acid residues, lack specificity and have limited applications *in vivo*. Thus, much research effort has focused on bioorthogonal labelling strategies, to improve specificity.(Best, M.D. 2009, Hackenberger, C.P.R. and Schwarzer, D. 2008, Lim, R.K.V. and Lin, Q. , Sletten, E.M. and Bertozzi, C.R. 2009)

1.3 Bioorthogonal labelling strategies

Bioorthogonal labelling strategies are defined as reactions which can be performed under aqueous conditions in the presence of endogenous functional groups, while retaining specificity for the intended target. The first step in a bioorthogonal labelling strategy is the introduction or generation of a bioorthogonal reactive handle. This may be accomplished by metabolic labelling, where an analogue of a natural substrate functionalized with a reactive moiety is introduced and biosynthetically incorporated into the cell. Alternatively, *in situ* generation may be performed by a treatment that unmasks a bioorthogonal reactive handle. The second step of a bioorthogonal labelling strategy is the ligation of a probe molecule that bears the complementary reactivity to the installed handle. The most desirable strategies are those which minimally perturb endogenous function, have fast reaction rates and are not cytotoxic. (Best, M.D. 2009, Lim, R.K.V. and Lin, Q. , Sletten, E.M. and Bertozzi, C.R. 2009)

Existing bioorthogonal labelling strategies each have strengths and weaknesses. The most popular of these strategies use the azide moiety, which is an excellent bioorthogonal handle due to its small size, narrow reaction profile, and ease of synthetic incorporation (**Figure 1.3**). The Staudinger ligation employs the selective conjugation of an azide with a phosphine, and has been successfully used for numerous labelling experiments *in vitro* and *in vivo*. The main limitation of the Staudinger ligation is that it suffers from relatively slow reaction rates (2 x 10^{-3} $M^{-1}s^{-1}$).(Agard, N.J., Baskin, J.M., et al. 2006, Kiick, K.L., Saxon, E., et al. 2002, Köhn, M. and Breinbauer, R. 2004, Saxon, E., Luchansky, S.J., et al. 2002)

Another popular methodology is the Sharpless-Meldal reaction, a Cu(I)-catalyzed Huisgen azide alkyne 1,3-dipolar cycloaddition (CuAAC).(Molteni, G. 2006, Prescher, J.A. and Bertozzi, C.R. 2005, Rostovtsev, V.V., Green, L.G., et al. 2002, Tornoe, C.W., Christensen, C., et al. 2002, Tornoe, C.W. and Meldal, M. 2001) The high selectivity and reactivity of the azide and alkyne groups, mild aqueous reaction conditions, and small size of the functional groups make this reaction ideal for many biological applications.(Molteni, G. 2006, Sen Gupta, S., Kuzelka, J., et al. 2005) However, use of these conditions *in vivo* has been limited by the toxicity of Cu(I), which can kill mammalian cells at concentrations of 1 mM or greater.(Sletten, E.M. and Bertozzi, C.R. 2009)

The Huisgen 1,3-dipolar cycloaddition between azides and alkynes is performed at high temperatures and long durations. Electron deficient alkynes exhibit good regioselectivity, while other alkynes give mixtures of 1,4- and 1,5-triazole regioisomers.(Bock, V.D., Hiemstra, H., et al. 2005, Molteni, G. 2006)

The Cu(I)-catalyzed form of the reaction uses much milder conditions and is known as the Sharpless-Meldal reaction, as both research groups independently reported the finding.(Rostovtsev, V.V., Green, L.G., et al. 2002, Tornoe, C.W., Christensen, C., et al. 2002) The group of Meldal demonstrated the initial copper catalysis, while the Sharpless group later showed this could be performed under aqueous conditions. The reaction has been employed in numerous biochemical studies to detect binding partners, enzymes and substrates, or engineered proteins.(Manetsch, R., Krasinski, A., et al. 2004, Speers, A.E. and Cravatt, B.F. 2004, Stubbs, K.A., Scaffidi, A., et al. 2008, Xie, J. and Seto, C.T. 2007)

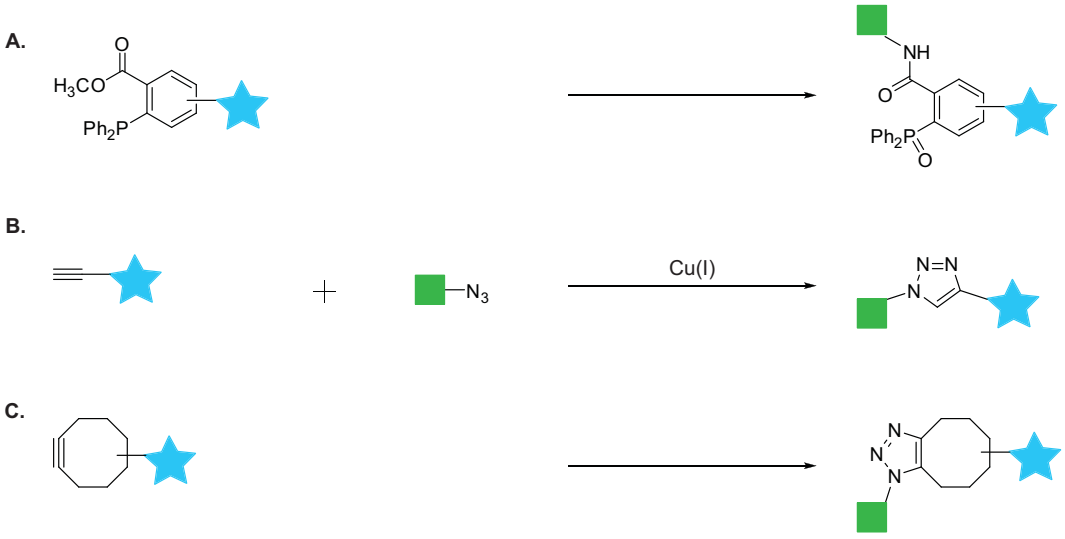

Figure 1.3. Bioorthogonal ligations using an azide reactive handle. A) The Staudinger ligation between azides and phosphines. **B)** The Sharpless-Meldal reaction between azides and alkynes. **C)** The strain-promoted Huisgen 1,3-dipolar cycloaddition between azides and cyclooctynes.

Recently, copper-free, strain-promoted variants have emerged from the Boons and Bertozzi groups which avoid Cu(I) toxicity issues. Cyclooctynes are

highly strained molecules, having a perturbed alkyne bond angle of 163^{o} and ring strain of 18 kcal mol^{-1}. This strain imparts significant rate acceleration, compared to unstrained alternatives, enabling the use copper-free conditions.(Agard, N.J., Prescher, J.A., et al. 2004) However, the first strain-promoted cyclooctynes suffered from relatively slow reaction rates; on the same order as the Staudinger ligation (10^{-3} $M^{-1}s^{-1}$). Second generation compounds were based on difluorinated cyclooctynes (DIFO), and were later developed to incorporate two propargylic fluorines to lower the LUMO thereby increasing interaction with the azide HOMO. This modification improved reaction rates by 60-fold (10^{-1} $M^{-1}s^{-1}$) similar to the rate observed with CuAAC. The synthesis of DIFO compounds proved very challenging, and required twelve synthetic steps with a total yield of 1%.(Codelli, J.A., Baskin, J.M., et al. 2008) Alternatively, the Boons group developed a series of dibenzocyclooctynols which were found to have similar reaction kinetics to the DIFO compounds, but only required five synthetic steps and gave the desired products in superior yield (15%).

Aldehydes and ketones are another class of reactive handle commonly used in bioorthogonal reactions. The small size, easy synthetic incorporation, and inertness of carbonyls are advantageous properties. However, their use is limited primarily to cell surface applications where these functional groups are normally absent. As well, native electrophiles within the cell, such as pyruvate, may impede the desired reactivity. Aldehydes and ketones selectively react with nucleophiles enhanced by the alpha effect, such as hydrazines and amino-oxy compounds, to form imines (**Figure 1.4**).(Fina, N.J. and Edwards, J.O. 1973) Sayer and

colleagues have shown this reaction performs optimally at pH 5-6, showing less sensitivity to the nucleophile pK_a, however it still suffers from relatively slow reaction rates (3.3 x 10^{-2} $M^{-1}s^{-1}$).(Sayer, J.M., Peskin, M., et al. 1973) Recently, Dawson and colleagues have revived aniline catalysis, which they observed to increase reaction rates 30-400%, via formation of an aniline Schiff base intermediate, for hydrazone and oxime forming reactions. The observed variability in rate is attributed to substrate ability, pH and concentrations explored.(Cordes, E.H. and Jencks, W.P. 1962, Dirksen, A., Dirksen, S., et al. 2006, Kohler, J.J. 2009)

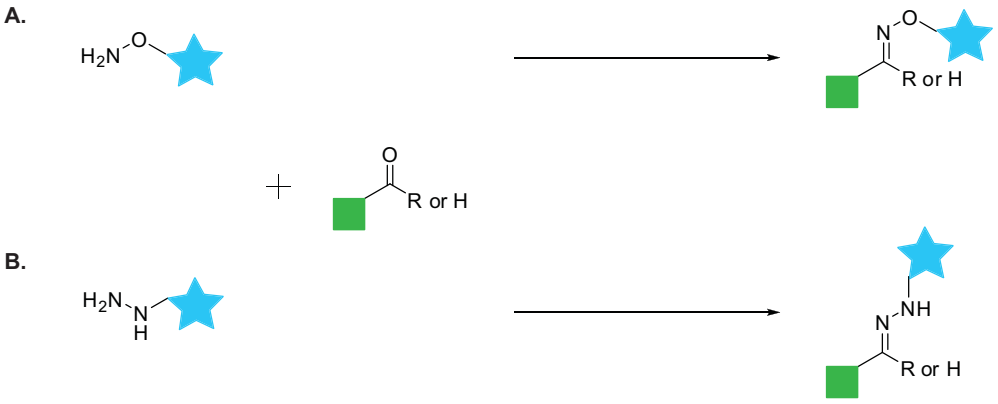

Figure 1.4. Bioorthogonal reactions using a carbonyl reactive handle. A) Reaction of a carbonyl with an amino-oxy label resulting in an oxime conjugate. **B)** Reaction of a carbonyl with a hydrazine label resulting in a hydrazone conjugate.

Alkenes are another bioorthogonal handle which have been increasingly explored for reaction with tetrazoles by a nitrile-imine mediated 1,3-dipolar cycloaddition under mild UV photoirradiation (**Figure 1.5**).(Song, W., Wang, Y., et al. 2008) The formation of a nitrile-imine intermediate is quite rapid. However, a wide range of reaction rates are observed for the subsequent 1,3-dipolar

cycloaddition depending on the alkene substrate. Lower energy HOMO alkenes, like acrylamide, can react up to 75 times faster (0.15 $M^{-1}s^{-1}$) than those with higher energy LUMO levels such as allyl phenyl ether (2 x 10^{-3} $M^{-1}s^{-1}$).(Song, W., Yu, Z., et al. 2010, Wang, Y., Rivera Vera, C.I., et al. 2007) If an alkene is sufficiently strained, such as trans-cyclooctene, it can selectively react with tetrazines through an inverse-electron demand hetero-Diels-Alder reaction to form dihydropyridazine products with surprisingly fast reaction kinetics (2-4 x 10^3 $M^{-1}s^{-1}$).(Blackman, M.L., Royzen, M., et al. 2008, Devaraj, N.K., Weissleder, R., et al. 2008) The two orders of magnitude increase in reaction kinetics over alternative bioorthogonal strategies makes the tetrazine-cyclooctene reaction promising for use in examining otherwise unobservable fast-timescale biological events.(Lim, R.K.V. and Lin, Q. 2010)

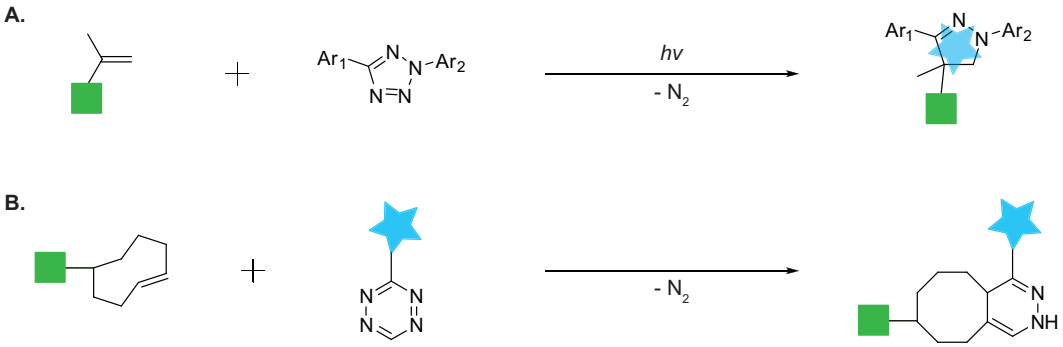

Figure 1.5. Bioorthogonal reactions using an alkene reactive handle. A) Reaction of an alkene with a tetrazole under mild UV photoirradiation, forming a fluorescent pyrazoline ligation product. **B)** Reaction of a strained alkene with a tetrazine reporter forming a dihydropyridazine product.

1.4 Fluorogenic bioorthogonal probes

The specificity afforded to probes using bioorthogonal ligation strategies is tremendously powerful and has enabled the interrogation of many biological phenomena. (Best, M.D., Rowland, M.M. and Bostic, H.E. 2011, Song, W., Yu, Z., et al. 2010, Li, K., Lee, L.A., et al. 2010) However, there is a need to develop better probes which can match these high levels of selectivity with enhanced sensitivity. Many traditional non-fluorogenic probes feature multi-step labelling techniques or require multiple wash/purification steps to obtain the signal to noise required. Therefore, developing fluorogenic bioorthogonal probes, which simultaneously undergo fluorescence enhancement upon selective bond formation, is a promising area of fluorophore research (**Figure 1.6**).

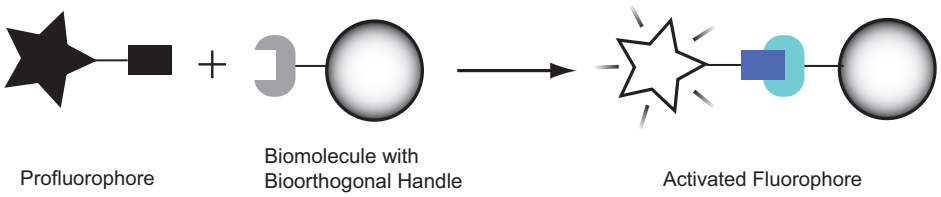

Figure 1.6. Schematic example of a fluorogenic bioorthogonal biolabelling reaction. Fluorogenic bioorthogonal labelling strategies combine selective reactivity in biological environments with an enhancement in fluorescence.

Traditional bioconjugate strategies focus on ligation to reactive endogenous functional groups, such as the amine and thiol side chains of amino acid residues, and can therefore lack desired specificity, limiting applications *in vivo*. Numerous colourimetric, fluorescent and fluorogenic probes have been developed for these applications and are reviewed elsewhere.(Chen, X., Zhou, Y., et al. 2010, Elbashir, A.A., Suliman, F.E.O., et al. 2011, Imai, K., Uzu, S., et al. 1989) While the fluorogenic probes from these strategies are not discussed here,

many of the principles of their design have been carried forward to the synthesis of fluorogenic bioorthogonal probes.

The rational design of fluorogenic bioorthogonal probes remains a challenging endeavour despite advancements in fluorophore synthesis and computational modelling. Although time-dependent density functional theory (TD-DFT) analysis is fairly reliable for determining absorption maxima, accurate prediction of emission properties has proven to be much more difficult.(Brown, A., Ngai, T., et al. Submitted, Key, J.A., Koh, S., et al. 2009) Most examples of fluorogenic bioorthogonal probes in the literature use the following general strategies: loss of a quencher, induced electronic changes, or extension of conjugation. The loss of a known quenching motif upon product formation is one of the surest ways to produce a fluorogenic probe; however, the chemical transformation of the bioorthogonal strategy must lend itself appropriately. Induced electronic change strategies place a bioorthogonal handle on known 'sensitive positions' of a fluorophore core. This strategy is most effective for 'push-pull' fluorophores, which have electron donating and electron accepting groups across a rigid conjugated backbone. Small changes in the electronic balance of such fluorophores can have dramatic effects on excited state energy levels and correspondingly, the fluorescence properties observed. Extension of conjugation strategies generate new conjugated systems (fluorochromes) from non-fluorescent components upon ligation. Ultimately, the discovery of new fluorogenic bioorthogonal probes is truly an interdisciplinary exercise, integrating

biological, synthetic organic, analytical, physical, and computational chemistry methodologies.

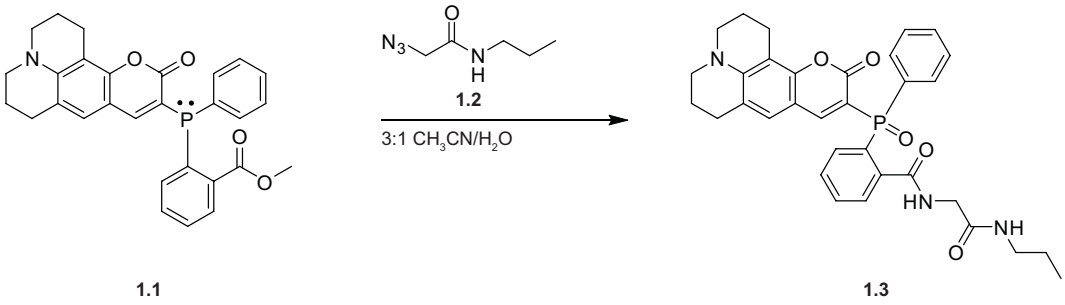

Scheme 1.1. Coumarin-phosphine fluorogenic Staudinger ligation. Oxidation of the phosphine restores fluorescence for this probe.(Lemieux, G.A., de Graffenried, C.L., et al. 2003)

The Staudinger ligation is a popular bioorthogonal ligation strategy, and several fluorogenic reagents have been developed based on this platform. The first example, by Lemieux and colleagues, utilized a 7-aminocoumarin profluorophore **1.1**, substituted with a phosphine at the sensitive 3-position (**Scheme 1.1**). The lone pair of electrons present on the phosphorous is an efficient quencher, reducing the quantum yield (QY) of **1.1** to 0.01. However, upon reaction with an azide (**1.2**) to generate **1.3**, the phosphorous becomes oxidized, restoring fluorescence with a 65-fold increase in QY.(Lemieux, G.A., de Graffenried, C.L., et al. 2003) Cai and colleagues later developed a Staudinger ligation probe consisting of a fluorescein ester of 2-carboxytriphenylphosphine **1.4** (**Scheme 1.2**). Di-*O*-substituted fluoresceins, such as **1.4**, are known to exist in the non-fluorescent lactone form. Upon Staudinger ligation with a model azide (**1.5**) the

ester linkage is broken, giving the mono-substituted product **1.7** and restoring fluorescence. Unfortunately, the photophysical properties of this probe were not discussed by the authors, but **1.4** was shown to successfully discriminate between DNA template mismatches using fluorescence-monitored kinetics studies.(Cai, J., Li, X., et al. 2004)

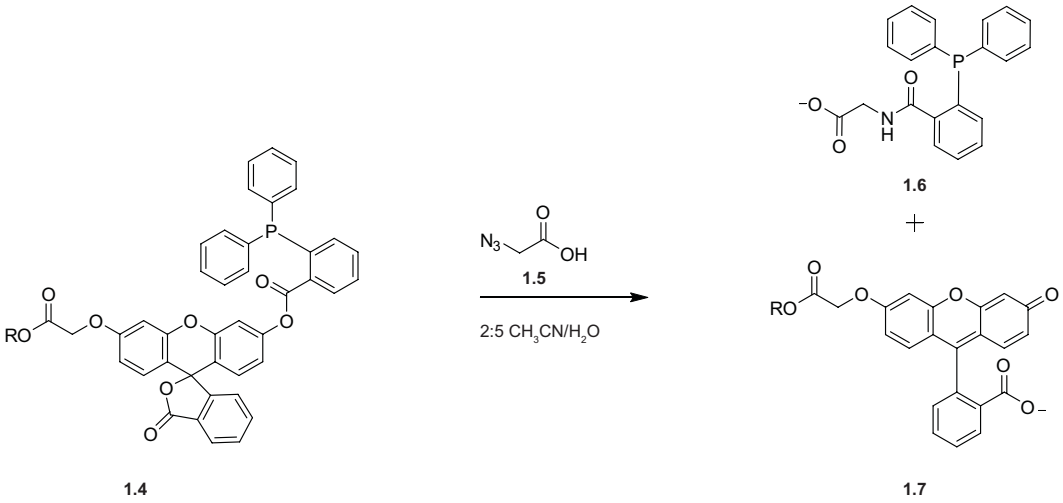

Scheme 1.2. Fluorogenic Staudinger ligation probe based on di-*O*-substituted fluorescein 1.4. Conversion of the fluorescein to its mono-*O*-substituted form restores fluorescence by lactone ring opening. R = tBu or H.(Cai, J., Li, X., et al. 2004)

A known disadvantage of the Staudinger ligation is the susceptibility of phosphine reagents to oxidation. This limitation may hinder the application of reagent **1.1** in live cell experiments due to increased background signal. To address this problem, Hangauer and colleagues developed a fluorogenic probe, **1.8**, which featured a fluorescein-phosphine that is quenched by Fluorescence Resonance Energy Transfer (FRET) to the ester-linked quencher: Disperse Red 1.(Clegg, R.M. 1995, Hangauer, M.J. and Bertozzi, C.R. 2008) Upon Staudinger

ligation to a model azide (**1.9**), the ester linkage is cleaved releasing the quencher group (**1.11**) and the activated fluorophore (**1.10**); the fluorescence quantum yield is improved from 0.00 to 0.64. An azide-modified protein, murine dihydrofolate reductase (mDHFR), containing azidohomoalanine was treated with fluorophore **1.8** and visualized with SDS-PAGE fluorescence imaging. The authors demonstrated the applicability of this compound for use in live cell imaging by performing metabolic labelling of HeLa cells with the azido mannose derivative Ac_4ManNAz. Labelled cell glycoconjugates were visualized with fluorescence microscopy and fluorescence intensity was quantified by flow cytometry.

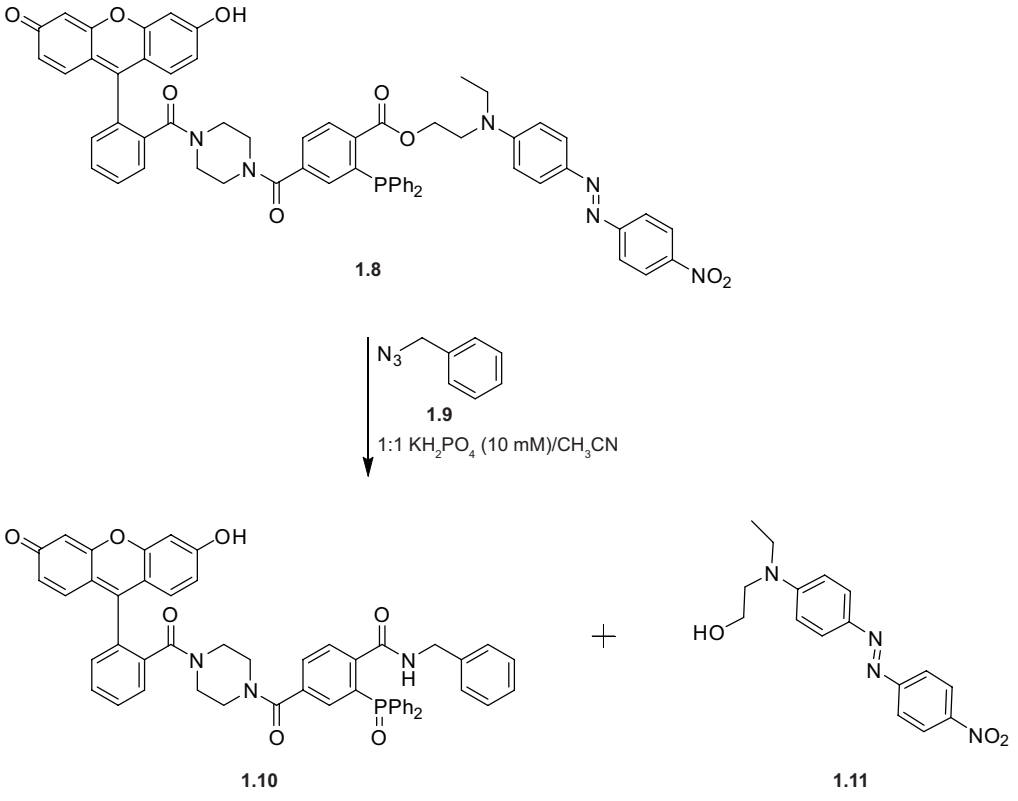

Scheme 1.3. Fluorescein-disperse red 1 fluorogenic Staudinger ligation probe. Fluorescence is restored upon loss of the quencher disperse red 1 (**1.11**). (Hangauer, M.J. and Bertozzi, C.R. 2008)

The Cu(I)-catalyzed Huisgen 1,3-dipolar cycloaddition between azides and alkynes, often referred to as a "click reaction," or more specifically as the Sharpless-Meldal reaction or copper catalyzed azide-alkyne cycloaddition (CuAAC), is one of the most popular bioorthogonal labelling strategies found in the literature.(Rostovtsev, V.V., Green, L.G., et al. 2002, Tornoe, C.W., Christensen, C., et al. 2002) The formation of a triazole product from the Sharpless-Meldal reaction has been shown to alter the spectral properties from an initial azide or alkyne.(Key, J.A., Koh, S., et al. 2009, Sivakumar, K., Xie, F., et al. 2004, Xie, F., Sivakumar, K., et al. 2008, Zhou, Z. and Fahrni, C.J. 2004) Both azido and alkynyl substituted fluorophore cores have been developed for fluorogenic labelling strategies, showing dramatic changes in photophysical properties following triazole formation (**Scheme 1.4**). The first examples were performed on coumarins, but soon expanded to several other fluorophore backbones.(Key, J.A., Koh, S., et al. 2009, LeDroumaguet, C., Wang, C., et al. 2010, Sawa, M., Hsu, T.L., et al. 2006, Sivakumar, K., Xie, F., et al. 2004, Xie, F., Sivakumar, K., et al. 2008, Zhou, Z. and Fahrni, C.J. 2004)

Zhou and Fahrni examined an alkynyl coumarin substituted at the sensitive 7-position, synthesized by Sonogashira alkynylation **1.12**. Upon triazole formation (**1.15**), an 18–fold increase in quantum yield (from 0.01 to 0.25, and a bathochromic shift of emission by 27 nm) was observed.(Zhou, Z. and Fahrni, C.J. 2004) Similarly, Sivakumar and colleagues took a combinatorial approach to synthesize numerous click-ligation products from a library of 3-azido coumarin profluorophores and terminal alkynes. The resulting triazole compounds were

examined by a plate reader assay and found that generally emission intensities significantly increased upon triazole formation. Among these examples, the largest differences were QY increases from 0.0 (**1.16**) to 0.3 (**1.18**).(Sivakumar, K., Xie, F., et al. 2004) Our group has addressed the generality of this strategy for other coumarins, using a small library of alkynyl-coumarin derivatives (such as **2.6.1**) and their triazole products (such as **2.6.3**) (see Chapter 2). Similar photophysical trends were found including increases in emission quantum yield ranging from 1.2 - 9 fold, and bathochromic shifts of up to 23 nm. The extent of these effects were found to be highly dependent on the substitution pattern of the fluorophore core.(Key, J.A., Koh, S., et al. 2009)

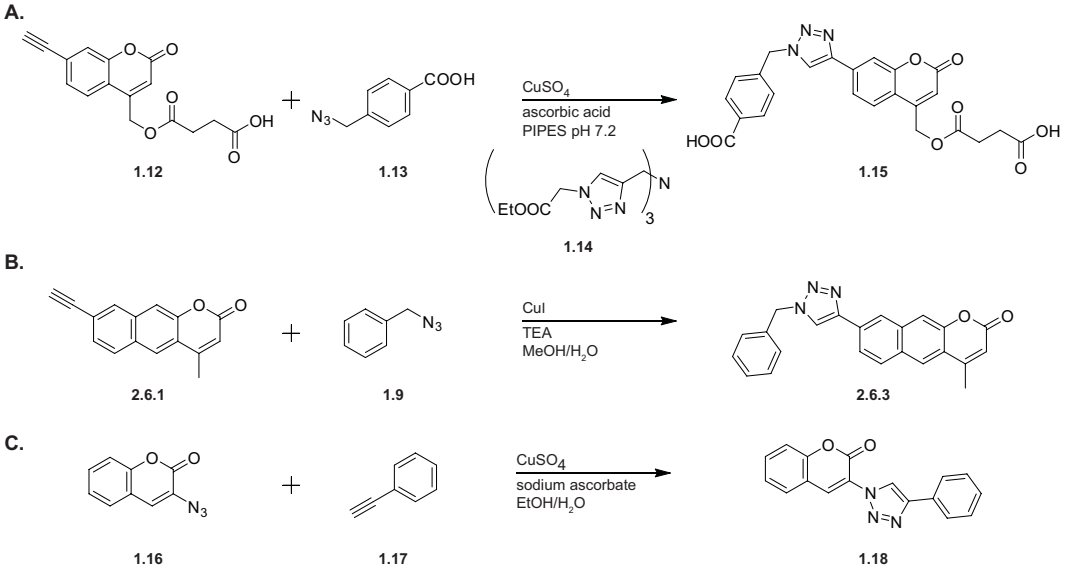

Scheme 1.4 Fluorogenic alkynyl and azido coumarin Sharpless-Meldal ligations. A) Alkynyl coumarin profluorophore strategy of Zhou and Farni. **B)** An alkynyl benzocoumarin profluorophore strategy examined by Key et al. **C)** An azido-coumarin profluorophore strategy examined by Sivakumar et al.(Key, J.A.,

Koh, S., et al. 2009, Sivakumar, K., Xie, F., et al. 2004, Zhou, Z. and Fahrni, C.J. 2004)

Fluorogenic azido-coumarins have found many labelling applications with several classes of biomolecules since their introduction. Beatty and colleagues have examined expression of proteins bearing unnatural alkynyl amino acids, while Gierlich et al, Seela et al, and Li et al, have used fluorogenic coumarins for applications with alkynyl nucleotides.(Beatty, K.E., Liu, J.C., et al. 2006, Gierlich, J., Burley, G.A., et al. 2006, Li, K., Lee, L.A., et al. 2010, Seela, F. and Pujari, S.S. 2010) Recently, Jolck and colleagues have used azido coumarins and strained alkynes to quantify liposome-ligand densities. (Jølck, R.I., Sun, H., et al. 2011) As well, Hsu and colleagues have used fluorogenic coumarins to examine glycoconjugates following metabolic labelling with alkynyl fucose or alkynyl ManNAc derivatives. (Hsu, T.L., Hanson, S.R., et al. 2007)

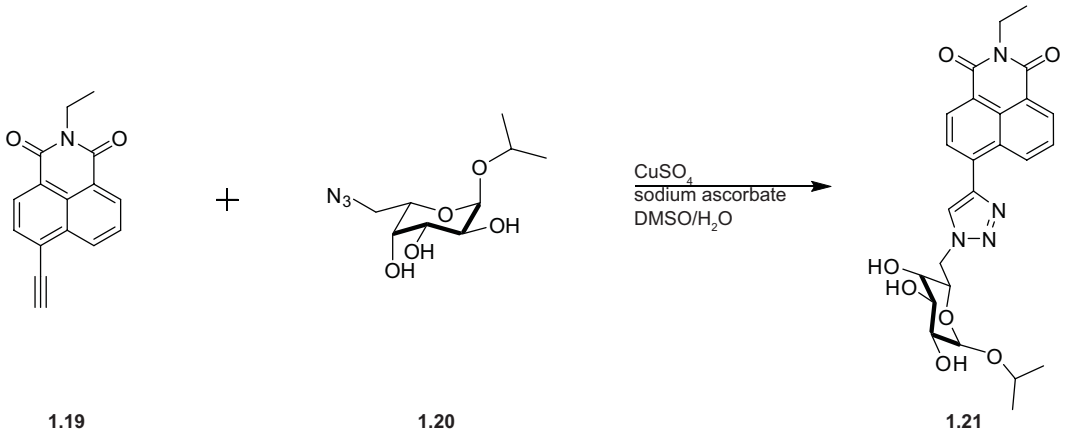

1.19 1.20 1.21

Scheme 1.5. Fluorogenic reaction of 4-Alkynyl 1,8-napthalimide (1.19) Sharpless-Meldal ligation probe with 6-azidomethyl fucose analogue (1.20). Significant fluorescence enhancement is noticed upon triazole formation, however

this probe suffers from slow reaction kinetics compared to an azide analogue. (Sawa, M., Hsu, T.L., et al. 2006)

Previous efforts from the same research group towards visualizing fucosylated glycoconjugates utilized novel fluorogenic 4-alkynyl and 4-azido dyes based on the 1,8-napthalimide backbone (**Scheme 1.5**).(Sawa, M., Hsu, T.L., et al. 2006) Both alkynyl-(**1.19**) and azido-profluorophores are reported to have essentially no fluorescence; however, the azido probe was observed to slowly decompose into a strongly fluorescent amine derivative. Upon triazole formation, their emission quantum yields are enhanced to 0.36 (from alkyne **1.19**) and 0.29 (from azide). The authors noted dramatically slower reaction kinetics (ca. 48 fold) for the alkynyl fluorophore **1.19** compared to the azide. Despite its slower reaction kinetics, the alkynyl napthalimide **1.19** has since been used to demonstrate a DNA-template driven click reaction.(Jentzsch, E. and Mokhir, A. 2009)

Xie and colleagues expanded upon previous work with azido-coumarins by developing a series of fluorogenic azidoanthracenes (**Scheme 1.6**).(Xie, F., Sivakumar, K., et al. 2008) Azidoanthracenes were readily synthesized from commercially available halogen, hydroxyl, carboxyl, and amine-bearing starting materials. Examination of the photophysical properties of these compounds demonstrated that the best reported profluorophores showed 49-fold QY enhancements upon triazole formation (**1.22** to **1.23**). The authors then examined the applicability of these compounds for conjugation to alkynyl-substituted cow

pea mosaic and tobacco mosaic virus particles, visualized using SDS-PAGE with fluorescence imaging. Derivatives of these triazolyl-anthracenes have since been examined for applications in Cu(II) ion sensing.(Varazo, K., Xie, F., et al. 2008)

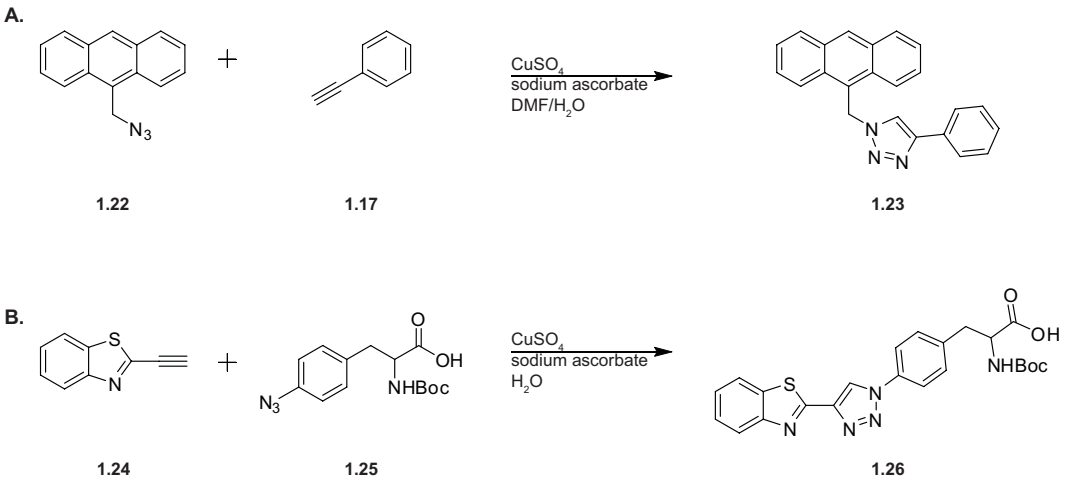

Scheme 1.6. Fluorogenic azidoanthracene and alkynyl-benzothiazole Sharpless-Meldal ligation probes. A) The azidoanthracene probe shows a 49-fold QY enhancement (0.02 to 0.97) upon triazole formation. **B)** The akynyl-benzothiazole shows a 158-fold enhancement in fluorescence emission. (Qi, J. and Tung, C.-H. 2011, Xie, F., Sivakumar, K., et al. 2008)

Qi and colleagues have recently introduced another example of a fluorogenic alkynyl profluorophore, with 2-alkynyl-benzothiazole (**1.24**). This compound was readily synthesized from 2-iodo-benzothiazole by Sonogashira cross-coupling. The authors perform ligation with a model azido-substituted amino acid (**1.26**) and nucleic acids. Following triazole formation (**1.26**), they observe a 158-fold increase in fluorescence emission, but unfortunately do not report the QY of their triazole conjugates. The authors attempted to synthesize the

2-azido-benzothiazole for comparison, but noted it was unstable and spontaneously formed an undesired cyclization product.

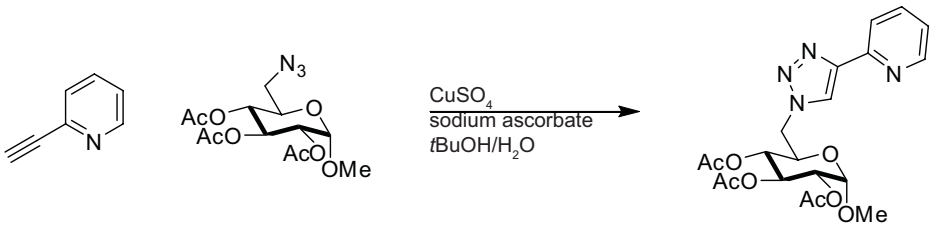

1.27 **1.28** **1.29**

Scheme 1.7. Fluorogenic Sharpless-Meldal ligation between 2-ethynylpyridine and an azido-glucopyranoside. Ethynylpyridine triazole-conjugates have been shown to be fluorogenic, solvatochomic and capable of zinc ion-sensing. (David, O., Maisonneuve, S., et al. 2007)

David and colleagues have reported an interesting discovery of an ethynylpyridine fluorogenic probe (**1.27**).(David, O., Maisonneuve, S., et al. 2007) Upon ligation to per-(6-azido)-β-cyclodextrin they noticed the generation of a fluorescent product. Photophysical characterization of these pyridyl-triazole conjugates demonstrated strong solvatochromism, with dramatic increases in QY and bathochromic shifts in high-polarity protic solvent systems. In THF, the QY was found to be 0.04, with an emission maximum of 302 nm; while in acetonitrile/H_2O the QY increased to 0.36, with an emission maximum of 362 nm. Model monosaccharide compounds were then synthesized from methyl 2,3,4-tri-*O*-acetyl-6-azido-6-deoxy-α-D-glucopyranoside, **1.28**, with 2-ethynylpyridine **1.27**, 2-ethynylbenzene or propargyl alcohol to confirm the fluorogenic nature of pyridyl-triazole (**Scheme 1.7**). Only the ethynylpyridine conjugate **1.29** possessed

similar fluorescence properties. The cyclodextrin compounds and model pyridyl-triazole monosaccharide were also found to have fluorogenic chelating properties in the presence of Zn^{2+}.

To further expand the fluorophore cores amenable to activation by triazole formation; our group examined a series of benzoxadiazole and nitrobenzoxadiazole (NBD) alkynyl and azido derivatives (**Scheme 1.8**) (see Chapter 3). The high solvatochromic sensitivity of this fluorophore core has facilitated its widespread use in environment sensing in lipid-bilayer experiments. (Loura, L.M., Fernandes, F., et al. 2008)

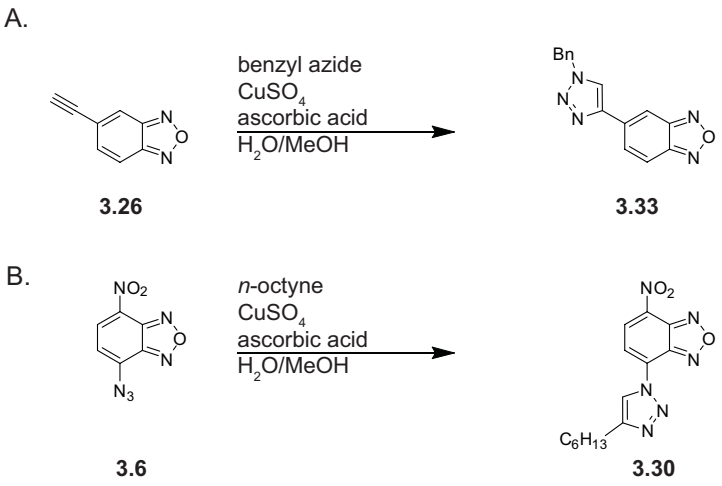

Scheme 1.8. Fluorogenic and quenching Sharpless-Meldal ligation of benzoxadiazoles with model azide and alkyne compounds. A) The alkynyl benzoxadiazole **3.26** shows a 48-fold enhancement in QY, 0.001 to 0.048, upon triazole formation **3.33**. **B)** The nitrobenzoxadiazole azide **3.6** shows a dramatic 470-fold decrease in emission quantum yield, 0.47 to <0.001, upon triazole formation **3.30**. (Key, J.A. and Cairo, C.W. 2011)

However, there were no previous reports of CuAAC-based fluorogenic strategies with the benzoxadiazole core. The alkynyl and azido compounds could be readily synthesized from commercially available halogenated starting materials by nucleophilic substitution and Sonogashira alkynylation, respectively, in good yields. Within this series of compounds we found an alkynyl benzoxadiazole (**3.26**) which exhibited a 48-fold enhancement in QY, from 0.001 to 0.048, upon triazole formation (**3.33**), and a nitrobenzoxadiazole azide (**3.6**) which had a dramatic 470-fold decrease in emission quantum yield, 0.47 to <0.001, upon triazole formation (**3.30**). However, it should be noted that the extent of the fluorogenic and quenching phenomena are highly dependent on solvent environment.(Key, J.A. and Cairo, C.W. 2011) (see Chapter 3)

Aldehydes and ketones are another class of reactive handle commonly employed in bioorthogonal ligation strategies. Fluorogenic compounds targeted to the labelling of aldehydes and ketones are well known in the literature, particularly those based on the nitrobenzoxadiazole backbone (**Figure 1.7**). These compounds feature nucleophiles enhanced by the alpha effect, such as hydrazines and amino-oxy compounds. The resulting hydrazones or oximes often have increased fluorescence emission. Reported fluorogenic NBD-hydrazines include 7-hydrazino-4-nitrobenzo-2-oxa-1,3,-diazole (NBDH) (Gubitz, G., Wintersteiger, R., et al. 1984), 4-(*N*,*N*-dimethylaminosulphonyl)-7-hydrazino-benz-2,1,3-oxadiazole (DBDH) (Uzu, S., Kanda, S., et al. 1990), 4-4-aminosulphonyl-7-hydrazino-2,1,3-benzoxadiazole (ABDH) (Uzu, S., Kanda, S., et al. 1990). Several of these derivatives are commercially available and have found

application in biological assays like the recent work by Raindlova and colleagues who examined polymerase synthesis of aldehyde-functionalized DNA. (Raindlová, V., Pohl, R., et al. 2010) Fluorogenic hydrazines have also been commonly used for detection of trace carbonyls in environmental samples such as automobile exhaust (Jachmann, N. and Karst, U. 2001, Vogel, M., Büldt, A., et al. 2000).

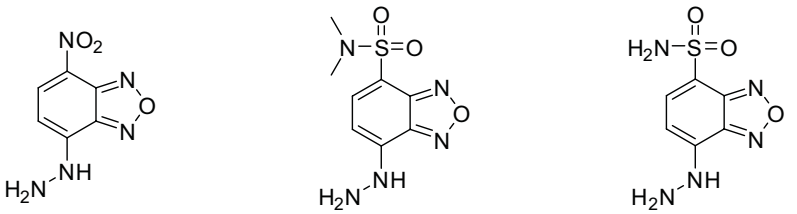

Figure 1.7. A series of known fluorogenic NBD hydrazine derivatives. These compounds show enhanced fluorescence upon hydrazone formation.(Gubitz, G., Wintersteiger, R., et al. 1984, Uzu, S., Kanda, S., et al. 1990)

We have recently developed a novel fluorogenic amino-oxy derivative, NBDAO **4.5**, which has a remarkable Stokes shift and can be used to detect sialic acid in combination with periodate oxidation of cellular glycans. (**Scheme 1.9**) (see Chapter 4). The conversion of NBDAO (**4.5**) to the oxime (**4.6**) was fluorogenic in certain solvent environments, such as ethanol, with a 3-fold QY increase from 0.05 to 0.16, but is relatively static in non-polar solvents. We examined the applicability of this dye for live cell sialic acid labelling following periodate oxidation (Kohler, J.J. 2009, Zeng, Y., Ramya, T.N.C., et al. 2009). Fluorescence labelling was examined by plate reader, fluorescence microscopy and flow cytometry. The NBDAO dye showed significant staining of sialic acids

over background (6.7-fold); which was superior to the commercially available fluorogenic NBDH (2.9-fold) and static dye Bodipy FL hydrazide (2.5-fold).

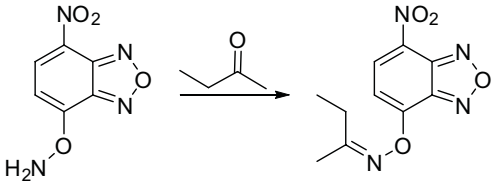

4.5
NBDAO

4.6

Scheme 1.9. Fluorogenic oxime formation of NBDAO (4.5). NBDAO has been utilized for the detection of sialic acid content in live cells following PAL treatment.

Dilek and colleagues have reported several fluorogenic 4,4-Difluoro-4-bora-3a,4a-diaza-*s*-indacene (Bodipy) hydrazine compounds, which increase in QY and have a bathochromic shift in both absorption and emission upon hydrazone formation (**Scheme 1.10**). Hydrazine **1.30** undergoes a 25-30 fold increase in QY upon hydrazone formation (**1.32**) with aliphatic carbonyls, and shifts in emission maximum of up to 21 nm. Reaction with aromatic carbonyls resulted in hydrazones with QY increases of approximately 49-54 fold and bathochromic emission shifts of 37 nm.(Dilek, Ö. and Bane, S.L. 2008) The authors also show the applicability of fluorophore **1.30** by labelling the protein α-tubulin after incorporation of the unnatural amino acid 3-formyltyrosine.(Dilek, O. and Bane, S. 2011)

The use of alkenes as bioorthogonal handles has become popular with the tetrazine and tetrazole reporters. Tetrazines can selectively react with strained dienophile like trans-cyclooctenes (**Scheme 1.11**). (Devaraj, N.K., Weissleder, R.,

et al. 2008) Deveraj and colleagues found that the tetrazine moiety itself can successfully act as a quencher for several classes of fluorophore probes (**1.33**).

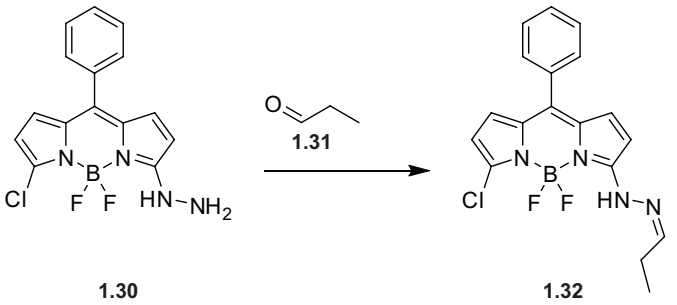

Scheme 1.10. Fluorogenic Bodipy hydrazone formation. Fluorogenic Bodipy hydrazines show large bathochromic shifts and enhanced emission quantum yield upon hydrazone formation (Dilek, Ö. and Bane, S.L. 2008)

Upon reaction with the strained dienophile (**1.34**), fluorescence is restored, enhancing emission quantum yields 3-21 fold.(Devaraj, N.K., Hilderbrand, S., et al. 2010) However, the authors postulate this quenching effect is wavelength-dependant. Green and red emitting fluorophores like Oregon Green 488 and Bodipy (**1.35**) show the strongest effect (15-21 fold QY increases), while a shorter wavelength coumarin and a longer wavelength near-infrared fluorophore (vivo-tag 680) show minimal (3 fold) and no enhancement, respectively. The authors demonstrate the applicability of these probes by visualizing alpha tubulin in PtK2 cells and compare it to the binding of taxol, a compound with high affinity for tubulin. (Devaraj, N.K., Hilderbrand, S., et al. 2010) After treatment with a trans-cyclooctene taxol derivative and Bodipy FL tetrazine, fluorescence microscopy reveals strong staining similar to anti-α-tubulin immunostaining.

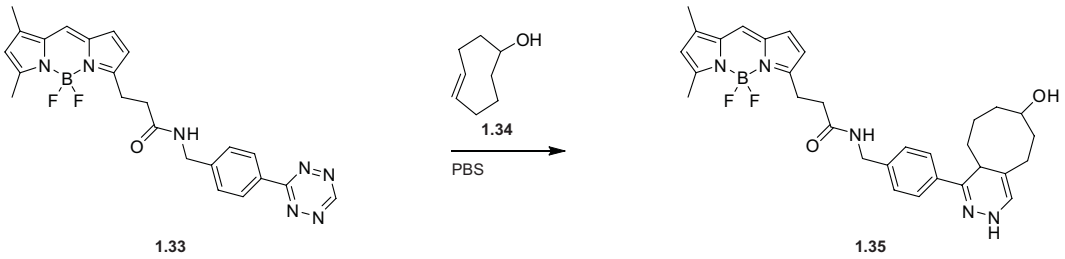

Scheme 1.11. Fluorogenic ligation of Bodipy FL tetrazine reagent with a strained alkene. The tetrazine moiety is itself a potent quencher of green and red fluorophores. (Devaraj, N.K., Hilderbrand, S., et al. 2010)

Tetrazoles such as **1.37** can react selectively with alkenes using a mild UV-photoirradiation catalyzed, nitrile imine mediated 1,3-dipolar cycloaddition.(Song, W., Wang, Y., et al. 2008) The resulting pyrazoline products are fluorescent with good QY's of 0.29, and similar in excitation/emission profile to cyan fluorescent protein (CFP). Song and colleagues took advantage of these fluorogenic ligation products to examine *E. coli* protein synthesis of a mutant Z-domain protein (**1.36**) which was genetically encoded to have an O-allyl-tyrosine at residue 7 (**Scheme 1.12**). Analysis of conjugate **1.38** was performed by in-gel SDS-PAGE fluorescence imaging of the protein from cell lysate, and in cells by fluorescence microscopy using the CFP excitation and filter set.(Song, W., Wang, Y., et al. 2008)

The fluorogenic bioorthogonal probes examined here are valuable new tools for the examination of biological phenomena. These fluorophores offer a one step method to selectively probe a biomolecule of interest, while simultaneously enhancing fluorescence. Therefore these probes are capable of improving signal to noise, by reducing background signal. However, there remains great opportunity in this field to develop new fluorogenic probes. In

particular, there is a need for longer wavelength fluorogenic bioorthogonal probes. The majority of examples here do not exceed green emission wavelengths, and therefore must contend with autofluorescence present in many biological systems.(Weissleder, R. 2001) Properties such as quantum yield, absorption coefficient, Stokes-shift, photostability and reaction rate may be optimized by design of next generation probes. The development of additional fluorogenic backbones will facilitate use of multicolour, pulse-chase and FRET experiments, enabling better interrogation of biomolecular interactions.

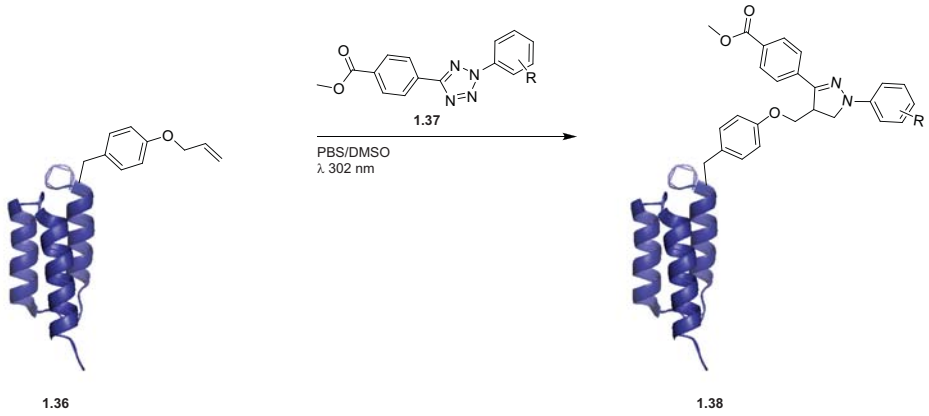

Scheme 1.12. Fluorogenic labelling of O-allyl-tyrosine mutant Z-domain protein with tetrazole reagent 1.37.(Song, W., Wang, Y., et al. 2008) Z-domain protein structure obtained from PDB: 1Q2N (Zheng, D., Aramini, J.M., et al. 2004)

1.5 References

Agard, N.J., Baskin, J.M., Prescher, J.A., Lo, A. and Bertozzi, C.R. (2006) A comparative study of bioorthogonal reactions with azides. *ACS Chemical Biology*, 1, 644-648.

Agard, N.J., Prescher, J.A. and Bertozzi, C.R. (2004) A Strain-Promoted [3 + 2] Azide-Alkyne Cycloaddition for Covalent Modification of Biomolecules in Living Systems. *Journal of the American Chemical Society*, 126, 15046-15047.

Ayoob, J.C., Sanger, J.M. and Sanger, J.W. (2000) Visualization of the Expression of Green Fluorescent Protein (GFP)-Linked Proteins. pp. 153-157.

Beatty, K.E., Liu, J.C., Xie, F., Dieterich, D.C., Schuman, E.M., Wang, Q. and Tirrell, D.A. (2006) Fluorescence Visualization of Newly Synthesized Proteins in Mammalian Cells. *Angewandte Chemie International Edition*, 45, 7364-7367.

Best, M.D. (2009) Click Chemistry and Bioorthogonal Reactions: Unprecedented Selectivity in the Labeling of Biological Molecules. *Biochemistry*, 48, 6571-6584.

Best, M.D., Rowland, M.M. and Bostic, H.E. (ASAP) Exploiting Bioorthogonal Chemistry to Elucidate Protein-Lipid Binding Interactions and Other Biological Roles of Phospholipids. *Accounts of Chemical Research*.

Blackman, M.L., Royzen, M. and Fox, J.M. (2008) Tetrazine Ligation: Fast Bioconjugation Based on Inverse-Electron-Demand Diels-Alder Reactivity. *Journal of the American Chemical Society*, 130, 13518-13519.

Bock, V.D., Hiemstra, H. and van Maarseveen, J.H. (2005) Cu-I-catalyzed alkyne-azide "click" cycloadditions from a mechanistic and synthetic perspective. *European Journal of Organic Chemistry*, 51-68.

Brown, A., Ngai, T., Key, J. and Cairo, C. (Submitted) Substituted benzoxadiazoles as fluorogenic probes: A computational study of absorption and fluorescence. *Journal of Chemical Theory and Computation*.

Cai, J., Li, X., Yue, X. and Taylor, J.S. (2004) Nucleic Acid-Triggered Fluorescent Probe Activation by the Staudinger Reaction. *Journal of the American Chemical Society*, 126, 16324-16325.

Cairo, C.W., Key, J.A. and Sadek, C.M. (2010) Fluorescent small-molecule probes of biochemistry at the plasma membrane. *Current Opinion in Chemical Biology*, 14, 57-63.

Chen, X., Zhou, Y., Peng, X. and Yoon, J. (2010) Fluorescent and colorimetric probes for detection of thiols. *Chemical Society Reviews*, 39, 2120-2135.

Clegg, R.M. (1995) Fluorescence resonance energy transfer. *Current Opinion in Biotechnology*, 6, 103-110.

Codelli, J.A., Baskin, J.M., Agard, N.J. and Bertozzi, C.R. (2008) Second-Generation Difluorinated Cyclooctynes for Copper-Free Click Chemistry. *Journal of the American Chemical Society*, 130, 11486-11493.

Cohen, S. (1975) Antibody Structure. *Journal of Clinical Pathology Supplement* 6, 1-7.

Cordes, E.H. and Jencks, W.P. (1962) Nucleophilic catalysis of semicarbazone formation by anilines. *Journal of the American Chemical Society*, 84, 826-831.

David, O., Maisonneuve, S. and Xie, J. (2007) Generation of new fluorophore by Click chemistry: synthesis and properties of [beta]-cyclodextrin substituted by 2-pyridyl triazole. *Tetrahedron Letters*, 48, 6527-6530.

Demchenko, A.P., Mély, Y., Duportail, G. and Klymchenko, A.S. (2009) Monitoring Biophysical Properties of Lipid Membranes by Environment-Sensitive Fluorescent Probes. *Biophysical Journal*, 96, 3461-3470.

Devaraj, N.K., Hilderbrand, S., Upadhyay, R., Mazitschek, R. and Weissleder, R. (2010) Bioorthogonal Turn-On Probes for Imaging Small Molecules inside Living Cells. *Angewandte Chemie International Edition*, 49, 2869-2872.

Devaraj, N.K., Weissleder, R. and Hilderbrand, S.A. (2008) Tetrazine-Based Cycloadditions: Application to Pretargeted Live Cell Imaging. *Bioconjugate Chemistry*, 19, 2297-2299.

Dilek, O. and Bane, S. (2011) Synthesis and Spectroscopic Characterization of Fluorescent Boron Dipyrromethene-Derived Hydrazones. *Journal of Fluorescence*, 21, 347-354.

Dilek, Ö. and Bane, S.L. (2008) Synthesis of boron dipyrromethene fluorescent probes for bioorthogonal labeling. *Tetrahedron Letters*, 49, 1413-1416.

Dirksen, A., Dirksen, S., Hackeng, T.M. and Dawson, P.E. (2006) Nucleophilic Catalysis of Hydrazone Formation and Transimination: Implications for Dynamic Covalent Chemistry. *Journal of the American Chemical Society*, 128, 15602-15603.

Elbashir, A.A., Suliman, F.E.O. and Aboul-Enein, H.Y. (2011) The Application of 7-Chloro-4-nitrobenzoxadiazole (NBD-Cl) for the Analysis of Pharmaceutical-Bearing Amine Group Using Spectrophotometry and Spectrofluorimetry Techniques. *Applied Spectroscopy Reviews*, 46, 222 - 241.

Etzler, M.E. (1985) Plant Lectins: Molecular and Biological Aspects. *Annual Review of Plant Physiology*, 36, 209-234.

Fina, N.J. and Edwards, J.O. (1973) The alpha effect. A review. *International Journal of Chemical Kinetics*, 5, 1-26.

Gierlich, J., Burley, G.A., Gramlich, P.M.E., Hammond, D.M. and Carell, T. (2006) Click Chemistry as a Reliable Method for the High-Density Postsynthetic Functionalization of Alkyne-Modified DNA. *Organic Letters*, 8, 3639-3642.

Gubitz, G., Wintersteiger, R. and Frei, R.W. (1984) Fluorogenic labeling of carbonyl compounds with 7-hydrazino-4-nitrobenzo-2-oxa-1,3,-diazole (NBD-H). *Journal of Liquid Chromatography*, 7, 839-854.

Hackenberger, C.P.R. and Schwarzer, D. (2008) Chemoselective Ligation and Modification Strategies for Peptides and Proteins. *Angewandte Chemie International Edition*, 47, 10030-10074.

Hangauer, M.J. and Bertozzi, C.R. (2008) A FRET-Based Fluorogenic Phosphine for Live-Cell Imaging with the Staudinger Ligation. *Angewandte Chemie International Edition*, 47, 2394-2397.

Hernandez, J.D. and Baum, L.G. (2002) Ah, sweet mystery of death! Galectins and control of cell fate. *Glycobiology*, 12, 127R-136R.

Hsu, T.L., Hanson, S.R., Kishikawa, K., Wang, S.K., Sawa, M. and Wong, C.H. (2007) Alkynyl sugar analogs for the labeling and visualization of glycoconjugates in cells. *Proceedings of the National Academy of Sciences of the United States of America*, 104, 2614-2619.

Imai, K., Uzu, S. and Toyo'oka, T. (1989) Fluorogenic reagents, having benzofurazan structure, in liquid chromatography. *Journal of Pharmaceutical and Biomedical Analysis*, 7, 1395-1403.

Jachmann, N. and Karst, U. (2001) Synthesis and application of 4-(N,N-dimethylaminosulfonyl)-7-N-methylhydrazino-2,1,3-benzoxadiazole (MDBDH) as a new derivatizing agent for aldehydes. *Fresenius' Journal of Analytical Chemistry*, 369, 47-53.

Jentzsch, E. and Mokhir, A. (2009) A Fluorogenic, Nucleic Acid Directed Click Reaction. *Inorganic Chemistry*, 48, 9593-9595.

Jølck, R.I., Sun, H., Berg, R.H. and Andresen, T.L. (2011) Catalyst-Free Conjugation and In Situ Quantification of Nanoparticle Ligand Surface Density Using Fluorogenic Cu-Free Click Chemistry. *Chemistry – A European Journal*, 17, 3326-3331.

Kapanidis, A.N. and Weiss, S. (2002) Fluorescent probes and bioconjugation chemistries for single-molecule fluorescence analysis of biomolecules. *The Journal of Chemical Physics*, 117, 10953-10964.

Key, J.A. and Cairo, C.W. (2011) Identification of fluorogenic and quenched benzoxadiazole reactive chromophores. *Dyes and Pigments*, 88, 95-102.

Key, J.A., Koh, S., Timerghazin, Q.K., Brown, A. and Cairo, C.W. (2009) Photophysical characterization of triazole-substituted coumarin fluorophores. *Dyes and Pigments*, 82, 196-203.

Kiessling, L.L. and Splain, R.A. (2010) Chemical Approaches to Glycobiology. *Annual Review of Biochemistry*, 79, 619-653.

Kiick, K.L., Saxon, E., Tirrell, D.A. and Bertozzi, C.R. (2002) Incorporation of azides into recombinant proteins for chemoselective modification by the Staudinger ligation. *Proceedings of the National Academy of Sciences of the United States of America*, 99, 19-24.

Kohler, J.J. (2009) Aniline: A Catalyst for Sialic Acid Detection. *ChemBioChem*, 10, 2147-2150.

Köhn, M. and Breinbauer, R. (2004) The Staudinger Ligation - A Gift to Chemical Biology. *Angewandte Chemie International Edition*, 43, 3106-3116.

LeDroumaguet, C., Wang, C. and Wang, Q. (2010) Fluorogenic click reaction. *Chemical Society Reviews*, 1233 - 1239.

Lemieux, G.A., de Graffenried, C.L. and Bertozzi, C.R. (2003) A Fluorogenic Dye Activated by the Staudinger Ligation. *Journal of the American Chemical Society*, 125, 4708-4709.

Li, K., Lee, L.A., Lu, X.B. and Wang, Q.A. (2010) Fluorogenic "click" reaction for labeling and detection of DNA in proliferating cells. *BioTechniques*, 49, 525-527.

Lim, R.K.V. and Lin, Q. Bioorthogonal chemistry: recent progress and future directions. *Chemical Communications (Cambridge, United Kingdom)*, 46, 1589-1600.

Lisenbee, C.S., Karnik, S.K. and Trelease, R.N. (2003) Overexpression and Mislocalization of a Tail-Anchored GFP Redefines the Identity of Peroxisomal ER. *Traffic*, 4, 491-501.

Loura, L.M., Fernandes, F., Fernandes, A.C. and Ramalho, J.P. (2008) Effects of fluorescent probe NBD-PC on the structure, dynamics and phase transition of DPPC. A molecular dynamics and differential scanning calorimetry study. *Biochimica et Biophysica Acta*, 1778, 491-501.

Maccioni, H.J.F., Quiroga, R. and Ferrari, M.L. (2011) Cellular and molecular biology of glycosphingolipid glycosylation. *Journal of Neurochemistry*, 117, 589-602.

Maier, O., Oberle, V. and Hoekstra, D. (2002) Fluorescent lipid probes: some properties and applications (a review). *Chemistry and Physics of Lipids*, 116, 3-18.

Manetsch, R., Krasinski, A., Radic, Z., Raushel, J., Taylor, P., Sharpless, K.B. and Kolb, H.C. (2004) In situ click chemistry: enzyme inhibitors made to their own specifications. *Journal of the American Chemical Society*, 126, 12809-12818.

Molteni, G. (2006) 1,3-dipolar cycloadditions in aqueous media. *Heterocycles*, 68, 2177-2202.

Prescher, J.A. and Bertozzi, C.R. (2005) Chemistry in living systems. *Nature Chemical Biology*, 1, 13-21.

Qi, J. and Tung, C.-H. (2011) Development of benzothiazole `click-on' fluorogenic dyes. *Bioorganic & Medicinal Chemistry Letters*, 21, 320-323.

Raindlová, V., Pohl, R., Scaronanda, M. and Hocek, M. (2010) Direct Polymerase Synthesis of Reactive Aldehyde-Functionalized DNA and Its Conjugation and Staining with Hydrazines. *Angewandte Chemie International Edition*, 49, 1064-1066.

Rostovtsev, V.V., Green, L.G., Fokin, V.V. and Sharpless, K.B. (2002) A stepwise huisgen cycloaddition process: copper(I)-catalyzed regioselective "ligation" of azides and terminal alkynes. *Angewandte Chemie, International Edition*, 41, 2596-2599.

Sawa, M., Hsu, T.L., Itoh, T., Sugiyama, M., Hanson, S.R., Vogt, P.K. and Wong, C.H. (2006) Glycoproteomic probes for fluorescent imaging of fucosylated glycans in vivo. *Proceedings of the National Academy of Sciences of the United States of America*, 103, 12371-12376.

Saxon, E., Luchansky, S.J., Hang, H.C., Yu, C., Lee, S.C. and Bertozzi, C.R. (2002) Investigating cellular metabolism of synthetic azidosugars with the Staudinger ligation. *Journal of the American Chemical Society*, 124, 14893-14902.

Sayer, J.M., Peskin, M. and Jencks, W.P. (1973) Imine-Forming Elimination Reactions. I. General Base Acid Catalysis and Influence of the Nitrogen Substituent on Rates and Equilibria for Carbinolamine Dehydration. *Journal of the American Chemical Society*, 95, 4277-4287.

Seela, F. and Pujari, S.S. (2010) Azide-Alkyne "Click" Conjugation of 8-Aza-7-deazaadenine-DNA: Synthesis, Duplex Stability, and Fluorogenic Dye Labeling. *Bioconjugate Chemistry*, 21, 1629-1641.

Sen Gupta, S., Kuzelka, J., Singh, P., Lewis, W.G., Manchester, M. and Finn, M.G. (2005) Accelerated bioorthogonal conjugation: a practical method for the ligation of diverse functional molecules to a polyvalent virus scaffold. *Bioconjugate Chemistry*, 16, 1572-1579.

Sivakumar, K., Xie, F., Cash, B.M., Long, S., Barnhill, H.N. and Wang, Q. (2004) A fluorogenic 1,3-dipolar cycloaddition reaction of 3-azidocoumarins and acetylenes. *Organic Letters*, 6, 4603-4606.

Sletten, E.M. and Bertozzi, C.R. (2009) Bioorthogonal chemistry: fishing for selectivity in a sea of functionality. *Angew Chem Int Ed Engl*, 48, 6974-6998.

Song, W., Wang, Y., Qu, J. and Lin, Q. (2008) Selective Functionalization of a Genetically Encoded Alkene-Containing Protein via "Photoclick Chemistry" in Bacterial Cells. *Journal of the American Chemical Society*, 130, 9654-9655.

Song, W., Wang, Y., Qu, J., Madden, M.M. and Lin, Q. (2008) A Photoinducible 1,3-Dipolar Cycloaddition Reaction for Rapid, Selective Modification of Tetrazole-Containing Proteins. *Angewandte Chemie International Edition*, 47, 2832-2835.

Song, W., Yu, Z., Madden, M.M. and Lin, Q. (2010) A bioorthogonal chemistry strategy for probing protein lipidation in live cells. *Molecular BioSystems*, 6, 1576-1578.

Speers, A.E. and Cravatt, B.F. (2004) Profiling enzyme activities in vivo using click chemistry methods. *Chemistry & Biology*, 11, 535-546.

Stubbs, K.A., Scaffidi, A., Debowski, A.W., Mark, B.L., Stick, R.V. and Vocadlo, D.J. (2008) Synthesis and use of mechanism-based protein-profiling probes for retaining beta-D-glucosaminidases facilitate identification of Pseudomonas aeruginosa NagZ. *Journal of the American Chemical Society*, 130, 327-335.

Tornoe, C.W., Christensen, C. and Meldal, M. (2002) Peptidotriazoles on solid phase: [1,2,3]-triazoles by regiospecific copper(i)-catalyzed 1,3-dipolar cycloadditions of terminal alkynes to azides. *Journal of Organic Chemistry*, 67, 3057-3064.

Tornoe, C.W. and Meldal, M. (2001) Peptidotriazoles: Copper(I)-catalyzed 1,3-dipolar cycloadditions on solid-phase. In Lebl, M. and Houghten, R.A. (eds), Peptides 2001, Proc. Am. Pept. Symp. American Peptide Society and Kluwer Academic Publishers, San Diego, pp. 263-264.

Tsien, R.Y. (1998) The green fluorescent protein. *Annual Review of Biochemistry*, 67, 509-544.

Uzu, S., Kanda, S., Imai, K., Nakashima, K. and Akiyama, S. (1990) Fluorogenic Reagents - 4-Aminosulphonyl-7-Hydrazino-2,1,3-Benzoxadiazole, 4-(*N*,*N*-Dimethylaminosulphonyl)-7-Hydrazino-2,1,3-Benzoxadiazole and 4-Hydrazino-7-Nitro-2,1,3-Benzoxadiazole Hydrazine for Aldehydes and Ketones. *Analyst*, 115, 1477-1482.

Varazo, K., Xie, F., Gulledge, D. and Wang, Q. (2008) Synthesis of triazolyl anthracene as a selective fluorescent chemosensor for the Cu(II) ion. *Tetrahedron Letters*, 49, 5293-5296.

Vogel, M., Büldt, A. and Karst, U. (2000) Hydrazine reagents as derivatizing agents in environmental analysis – a critical review. *Fresenius' Journal of Analytical Chemistry*, 366, 781-791.

Wang, Y., Rivera Vera, C.I. and Lin, Q. (2007) Convenient Synthesis of Highly Functionalized Pyrazolines via Mild, Photoactivated 1,3-Dipolar Cycloaddition. *Organic Letters*, 9, 4155-4158.

Weissleder, R. (2001) A clearer vision for in vivo imaging. *Nature Biotechnology*, 19, 316-317.

Xie, F., Sivakumar, K., Zeng, Q., Bruckman, M.A., Hodges, B. and Wang, Q. (2008) A fluorogenic `click' reaction of azidoanthracene derivatives. *Tetrahedron*, 64, 2906-2914.

Xie, J. and Seto, C.T. (2007) A two stage click-based library of protein tyrosine phosphatase inhibitors. *Bioorganic & Medicinal Chemistry*, 15, 458-473.

Zeng, Y., Ramya, T.N.C., Dirksen, A., Dawson, P.E. and Paulson, J.C. (2009) High-efficiency labeling of sialylated glycoproteins on living cells. *Nature Methods*, 6, 207-209.

Zheng, D., Aramini, J.M. and Montelione, G.T. (2004) Validation of helical tilt angles in the solution NMR structure of the Z domain of Staphylococcal protein A by combined analysis of residual dipolar coupling and NOE data. *Protein Science*, 13, 549-554.

Zhou, Z. and Fahrni, C.J. (2004) A fluorogenic probe for the copper(I)-catalyzed azide-alkyne ligation reaction: modulation of the fluorescence emission via 3(n,pi)-1(pi,pi) inversion. *Journal of the American Chemical Society*, 126, 8862-8863.

Chapter 2

Synthesis and photophysical characterization of triazole-substituted coumarin fluorophores[2]

[2] Portions of the work described in this chapter have been published in Key, J.A., Cairo, C.W. and Ferguson, M.J. (2008) 7,7 '-(3,3 '-dibenzyl-3H,3 ' H-4,4 '-bi-1,2,3-triazole-5,5 '-diyl)bis(4-methyl-2H-chromen-2-one). *Acta Crystallographica Section E-Structure Reports Online*, 64, O1910-U3631. and Key, J.A., Koh, S., Timerghazin, Q.K., Brown, A. and Cairo, C.W. (2009) Photophysical characterization of triazole-substituted coumarin fluorophores. *Dyes and Pigments*, 82, 196-203.

2.1 Introduction

The characterization of biomolecular systems has been revolutionized by concurrent developments in fluorescence spectroscopy and biomolecular labeling strategies. The advent of sensitive fluorescence detectors has enabled advances in biological imaging and the emergence of the field of single molecule spectroscopy. Bioconjugate strategies for the ligation of fluorescent labels to biomolecules have become important for biochemical characterization, as they allow detection of these species in complex mixtures, and their diversity provides access to previously intractable systems.(Meares, C. 1990) The specificity of any labelling strategy is critical to success in biological assays, whether used for research, commercial, or therapeutic purposes. Successful applications of bioconjugate methods have been applied to proteins, nucleic acids, carbohydrates, lipids and cells.(Hermanson, G. 1996, Kapanidis, A.N. and Weiss, S. 2002, Means, G.E. and Feeney, R.E. 1990, Medintz, I.L., Uyeda, H.T., et al. 2005, Niemeyer, C. 2004, Weiss, S. 1999) However, there remains a need for bioconjugate strategies with improved sensitivity and selectivity.

Traditionally, the Huisgen 1,3-dipolar cycloaddition between azides and alkynes is performed at high temperatures and long durations.(Bock, V.D., Hiemstra, H., et al. 2005) Generally, electron deficient alkynes exhibit good regioselectivity, while other alkynes give mixtures of 1,4- and 1,5-triazole regioisomers.(Bock, V.D., Hiemstra, H., et al. 2005, Molteni, G. 2006) The Cu(I)-catalyzed form of the reaction uses much milder conditions and has many names in the literature including: the Sharpless-Meldal reaction, CuAAC, or the click

reaction.(Rostovtsev, V.V., Green, L.G., et al. 2002, Tornoe, C.W., Christensen, C., et al. 2002) The reaction has been employed in numerous biochemical studies to detect binding partners, enzymes and substrates, or engineered proteins.(Manetsch, R., Krasinski, A., et al. 2004, Speers, A.E. and Cravatt, B.F. 2004, Stubbs, K.A., Scaffidi, A., et al. 2008, Xie, J. and Seto, C.T. 2007)

The product of the Sharpless-Meldal reaction is a triazole moiety, which has been proposed to provide a means to alter the spectral properties of the initial azide or alkyne. Known examples include attachment of the azide or the alkyne to the fluorophore core.(Hsu, T.L., Hanson, S.R., et al. 2007, Sawa, M., Hsu, T.L., et al. 2006, Sivakumar, K., Xie, F., et al. 2004, Xie, F., Sivakumar, K., et al. 2008, Zhou, Z. and Fahrni, C.J. 2004) Subsequent formation of the triazole leads to varying increases in emission intensity and changes in emission wavelength, properties desirable in fluorogenic probes. Combinatorial approaches to identifying new fluorophores have been employed to identify suitable substrates.(Sivakumar, K., Xie, F., et al. 2004) It is notable that even small changes to these structures can have a significant impact on the resulting emission properties. For example, switching the attachment point on the fluorochrome from the *N*1 to the *C*4 position of the triazole can result in significant differences in emission properties.(Sawa, M., Hsu, T.L., et al. 2006)

Substitution of coumarin fluorophores with azide or alkyne groups is known to induce changes in fluorescence properties.(LeDroumaguet, C., Wang, C., et al. 2010, Sivakumar, K., Xie, F., et al. 2004, Zhou, Z. and Fahrni, C.J. 2004) The 3- and 7-positions of the coumarin backbone have been shown to strongly

modulate fluorescence by affecting the energy of the molecule's two lowest excited states.(Sivakumar, K., Xie, F., et al. 2004, Zhou, Z. and Fahrni, C.J. 2004) This property has been used extensively for detection of enzymatic activity by substitution at the 7-position, exploiting the increase in emission upon unmasking of a hydroxycoumarin.(Blum, M.M., Timperley, C.M., et al. 2008, Kage, K.L., Richardson, P.L., et al. 2007, Sun, W.C., Gee, K.R., et al. 1998, Zhu, Q., Uttamchandani, M., et al. 2003) Conjugation of an electron-donating triazole ring to the coumarin backbone at one of these positions causes an increase in quantum yield and a bathochromic shift in emission relative to the starting alkyne.(Hsu, T.L., Hanson, S.R., et al. 2007, Sawa, M., Hsu, T.L., et al. 2006, Sivakumar, K., Xie, F., et al. 2004, Zhou, Z. and Fahrni, C.J. 2004) This observation was first reported by Sivakumar and colleagues with a series of eight 3-azido substituted coumarins.(Sivakumar, K., Xie, F., et al. 2004)

Zhou and Fahrni examined the influence of triazole formation on a single 7-ethynyl substituted succinic acid coumarin ester.(Zhou, Z. and Fahrni, C.J. 2004) Applications of triazole structures to fluorogenic probe strategies have capitalized on an increase in fluorescence emission to enhance signal to noise in labeling and imaging experiments. Recent examples have favoured the use of 3-azido-7-hydroxy coumarin in the labeling of proteins, DNA, and glycoconjugates.(Beatty, K.E., Liu, J.C., et al. 2006, Hsu, T.L., Hanson, S.R., et al. 2007, O'Reilly, R.K., Joralemon, M.J., et al. 2006, Seela, F., Sirivolu, V.R., et al. 2008, Sivakumar, K., Xie, F., et al. 2004, Zhou, Z. and Fahrni, C.J. 2004) Although this fluorophore shows a large increase in emission quantum yield (QY,

Φ) upon triazole formation, hydroxycoumarins are environmentally sensitive due to the acidic hydroxyl group.(Adamczyk, M., Cornwell, M., et al. 1997, Sun, W.C., Gee, K.R., et al. 1998) Therefore, quantitative use of these dyes can be complicated by pH sensitivity to the biological microenvironment.(Sun, W.C., Gee, K.R., et al. 1998, Valeur, B. 2002, Weiss, S. 1999) Ethynyl substitutions of these structures can, therefore, provide an alternative strategy that avoids pH sensitivity.(Zhou, Z. and Fahrni, C.J. 2004)

In this study, we undertook a systematic examination of changes to fluorescent properties among a group of related fluorophore backbones. We chose to examine coumarin fluorophores since similar structures have been used successfully in fluorogenic strategies.(Sivakumar, K., Xie, F., et al. 2004, Zhou, Z. and Fahrni, C.J. 2004) These derivatives are synthetically accessible by established precedents for introduction of alkyne or azide groups onto the coumarin structure at the 3-,(O'Reilly, R.K., Joralemon, M.J., et al. 2006, Seela, F., Sirivolu, V.R., et al. 2008, Sivakumar, K., Xie, F., et al. 2004) 4-(Wu, J., Liao, Y., et al. 2001) and 7-positions.(Zhou, Z. and Fahrni, C.J. 2004) We sought to examine the modulating effects of conjugated triazole formation on this series of ethynyl coumarin and benzocoumarin structures for changes in UV-Vis absorbance, emission quantum yield, molar absorption coefficient, and fluorescence emission. Comparison of the experimental data with theoretical calculations of the absorbance properties of the fluorophores allowed us to test the accuracy of electronic models.

2.2 Fluorophore synthesis

Synthesis of the pre- and post-click compounds used in this study was performed using established methods, as depicted in **Scheme 2.1**. Coumarin fluorophores were generated by Pechmann and Knoevenagel condensations of the corresponding diols, generating four different hydroxycoumarins. To generate the 7-hydroxy-4-methylcoumarin backbone (**2.4.1**, 4-methylumbelliferone), resorcinol (**2.1**) was reacted with ethyl acetoacetate in a $TiCl_4$-catalyzed Pechmann condensation.(Valizadeh, H. and Shockravi, A. 2005) Two isomers of benzocoumarin were generated from 2,7-dihydroxynapthalene (**2.2**) in a sulfuric acid-catalyzed Pechmann condensation with ethyl acetoacetate, providing the angular- (**2.5.1**) and linear-benzocoumarins (**2.6.1**) after purification.(Kolancilar, H. 2002, Kolancilar, H. and Oyman, U. 2003, Tao, Z.F., Qian, X.H., et al. 1997)

A second umbelliferone derivative was generated by a piperidine catalyzed Knoevenagel condensation of diethyl glutaconate with 2,4-dihydroxybenzaldehyde to form compound **2.7.1**.(Padmanabhan, S., Peri, R., et al. 1996) The hydroxyl derivatives (**2.4.1, 2.5.1, 2.6.1,** and **2.7.1**) were then converted to the corresponding triflic ethers. The intermediate triflates were used without purification to generate trimethylsilyl-protected alkyne intermediates (**2.4.1a, 2.5.1a, 2.6.1a,** and **2.7.1a**) via Pd(0)-catalyzed Sonogashira cross-coupling with trimethylsilyl acetylene.(Chinchilla, R. and Najera, C. 2007, Zhou, Z. and Fahrni, C.J. 2004) Deprotection with tetrabutylammonium fluoride (TBAF) resulted in the ethynyl compounds (**2.4.2, 2.5.2, 2.6.2,** and **2.7.2**).(Zhou, Z. and Fahrni, C.J. 2004)

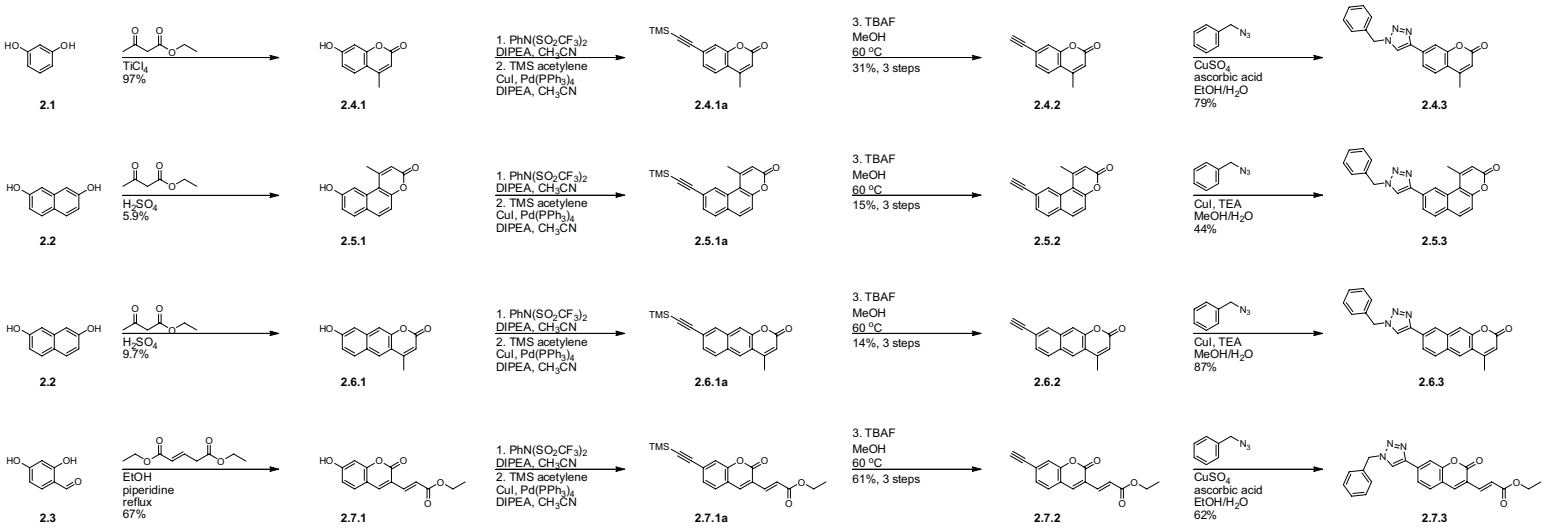

Scheme 2.1. Synthetic scheme for the generation of click substrates and fluorophores. Hydroxyl compounds were obtained by Pechmann and Knoevenagel condensations. Alkynyl compounds were generated by Pd(0)-catalyzed Sonogashira cross-coupling.

With the conjugated alkyne derivatives in hand, we proceeded to generate the click products to characterize their properties. Although an azide coupling partner that is conjugated to an aromatic moiety could enhance the fluorogenic properties of the products,(Sivakumar, K., Xie, F., et al. 2004) we chose to use benzylazide to more closely mimic a triazole product that might be formed in a bioconjugate addition. A variety of conditions have been used for similar reactions, with variables including the choice of base/ligand, solvent, reducing agent, and source of copper.(Bock, V.D., Hiemstra, H., et al. 2005) The triazolyl-click products (**2.4.3, 2.5.3, 2.6.3,** and **2.7.3**) were generated using two sets of conditions, in the first, Cu(I) catalyzed Sharpless-Meldal reaction with benzylazide was performed using CuI in 1:1 methanol/water with triethylamine as base.(Bock, V.D., Hiemstra, H., et al. 2005) These reactions proceeded in good to moderate yields (44% – 87%). However, we observed minor amounts of the 5,5'-bistriazole products under these conditions, as evidenced by the appearance of a new ^{1}H-NMR signal between 4 – 5 ppm and the observation of a peak in the mass spectrum for [$2M^{+}$-$2H$] (**Figure 2.1**).(Angell, Y. and Burgess, K. 2007)

In one case, we were successful in obtaining crystals of the side product suitable for X-ray diffraction.(Key, J.A., Cairo, C.W., et al. 2008) This contaminant was only observed in detectable amounts in the synthesis of **2.4.3** (23% of bistriazole) and **2.7.3** (7% of bistriazole) (**Figure 2.2**). We obtained exclusive formation of the desired products **2.4.3** and **2.7.3** with good yields (ca. 62 – 79%) by altering the conditions used for these substrates to 0.2 equivalents $CuSO_4$ and 0.3 equivalents ascorbic acid in 1:1ethanol/water. In reactions with

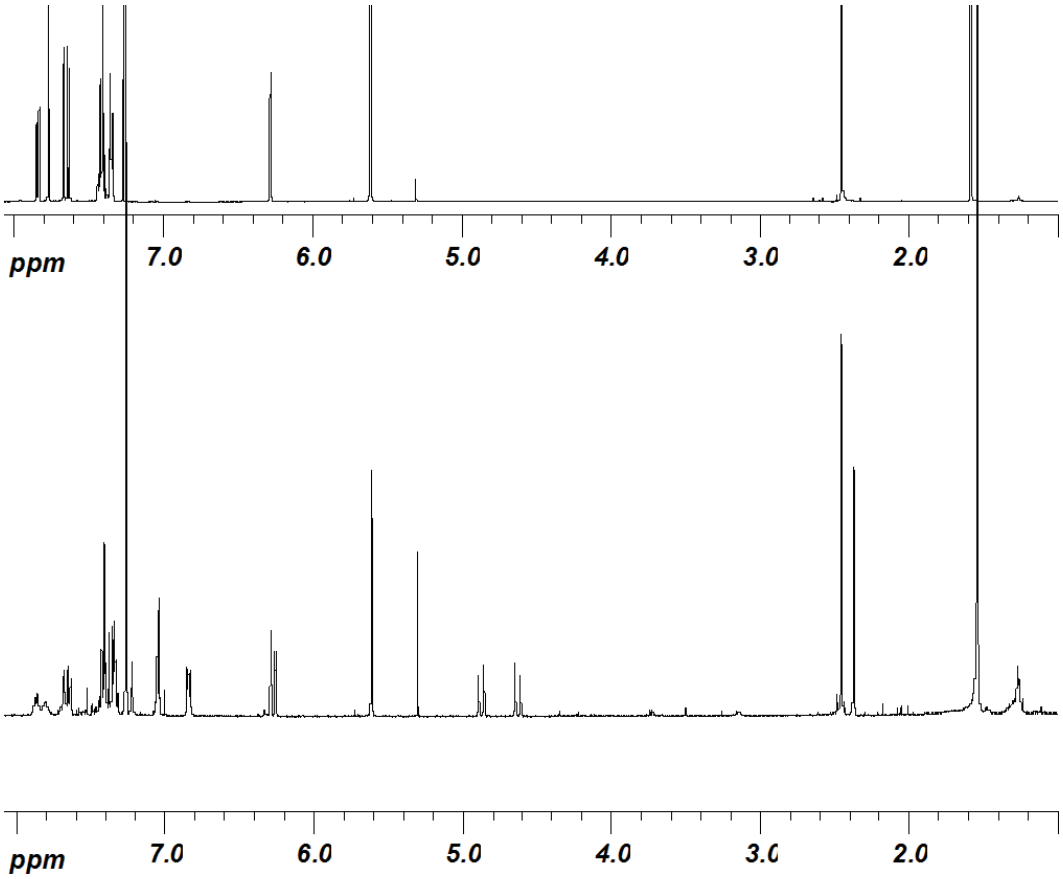

Figure 2.1. Comparison of 1H NMR signals of desired triazole product 2.4.3 (above), and its crude bistriazole byproduct (Below). Doubled signals are observed in the bistriazole spectrum for the methyl group (2.2-2.6 ppm) and also for shielded benzylic protons (4.4-5.0 ppm). NMR were performed at room temperature in $CDCl_3$ (7.26 ppm) at 500 MHz (above) and 400 MHz (below).

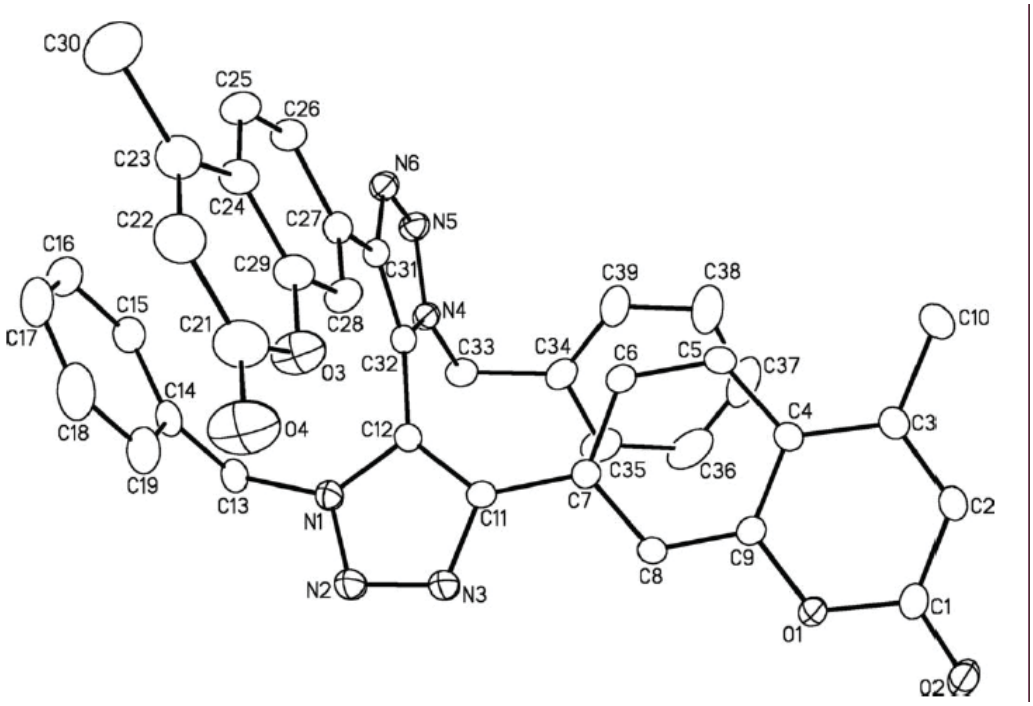

Figure 2.2. Perspective view of 5,5'-bis-triazole dimer showing the atom labelling scheme. Non-hydrogen atoms are represented by Gaussian ellipsoids at the 20% probability level. Hydrogen atoms are not shown.(Key, J.A., Cairo, C.W., et al. 2008)

equimolar $CuSO_4$ and ascorbic acid at pH 4, we observed the formation of a fluorescent contaminant. The contaminant could be generated in the absence of the alkyne derivative and showed fluorescent emission at 450 nm (see Figure 2.5, Section 2.6.11). The triazole compounds were, therefore, purified by flash chromatography before characterization.

The use of fluorination to improve the fluorescence properties of coumarins is well known, and is demonstrated by the popular fluorophores

Marina Blue and Pacific Blue. (Sun, W.-C., Gee, K.R., et al. 1998, Sun, W.-C., Gee, K.R., et al. 1997) The main benefits of fluorination include increased quantum yields, reduced pKa's, and improved photostability compared to the parent compound. A precedented and commercially available fluorinated starting material amenable to our alkynylation methodology, 2,4-difluororesorcinol, was also synthesized (**Scheme 2.2**) but alkynylation was not pursued further.[11,12]

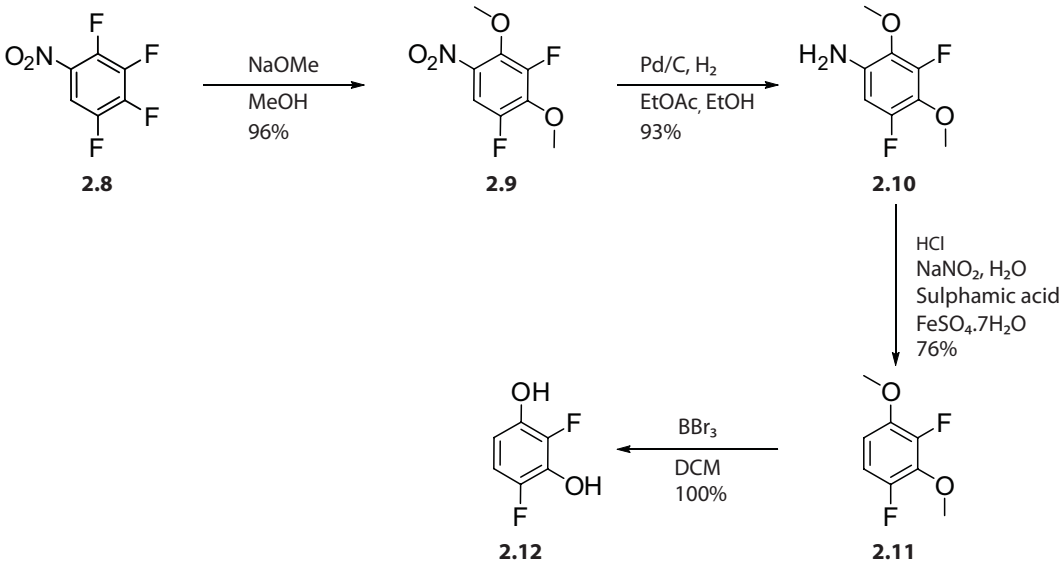

Scheme 2.2. Synthesis of 2,4-difluororesorcinol 2.12. Synthesis was performed following the protocol of Sun et al, employing nucleophilic substitution, reduction, hydrodediazoniation and demethylation.(Sun, W.-C., Gee, K.R., et al. 1997)

The starting material, 2,4-difluororesorcinol (**2.12**) was synthesized in 4 steps in an overall yield of 68%, based on the protocol of Sun and colleagues who reported a yield of 80%.(Sun, W.-C., Gee, K.R., et al. 1998, Sun, W.-C., Gee, K.R., et al. 1997) 1,2,3,4-tetrafluoro-5-nitrobenzene (**2.8**) was first subjected to a bis-methoxy addition, where the nitro group served to direct the nucleophilic

aromatic substitutions at the ortho and para positions giving **2.9** in excellent yield (96%). The nitro group was then hydrogenated using Pd/C catalysis in excellent yield (93%), and subsequently removed by hydrodediazoniation to give **2.11** in good yield (76%). The final step was the demethylation of **2.11** with BBr_3 providing 2,4-difluororesorcinol (**2.12**) in quantitative yields. Caution must be taken when working with fluorobenzenes, as they are volatile and are readily lost under high vacuum.

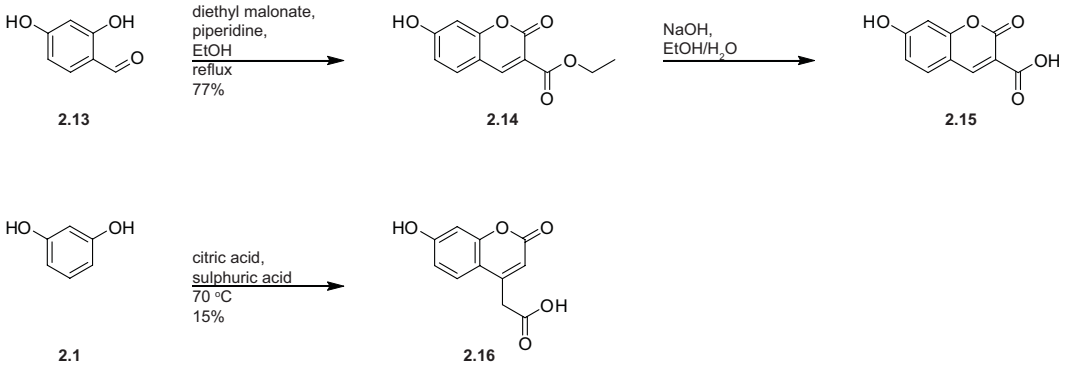

Scheme 2.3. Synthesis of carboxylic acid substituted coumarins 2.15 and 2.16. Compounds were formed by Knoevenagel and sulphuric acid-catalyzed Pechmann condensations, respectively.

Two additional coumarin backbones (**2.15, 2.16**) were synthesized but were not further elaborated to their alkynyl derivatives (**Scheme 2.3**). These compounds were synthesized to have a carboxylic acid reactive handle, which could be further derivatized by amide bond formation with amine-bearing substrates. The coumarin ester, **2.14**, was synthesized by condensation of 2,4-dihydroxybenzaldehyde and diethyl malonate in the presence of catalytic piperidine in good yield (77%). Subsequent saponification with NaOH afforded acid **2.15** with high salt contamination, obscuring yield calculations. The acid,

2.16, was generated by sulphuric acid catalyzed condensation of resorcinol (**2.1**) with citric acid with heating in modest yields (15%). These compounds are useful bifunctional coumarin fluorophores, that can be used for generating static bioorthogonal probes upon amide bond formation to amine-bearing bioorthogonal linkers.

2.3 Fluorophore characterization

To quantitate changes in photophysical properties after triazole formation, we characterized the properties of the hydroxyl-(**2.4.1, 2.5.1, 2.6.1,** and **2.7.1**), ethynyl- (**2.4.2, 2.5.2, 2.6.2,** and **2.7.2**), and triazolyl- (**2.4.3, 2.5.3, 2.6.3,** and **2.7.3**) compounds. These compounds were characterized to determine their UV-vis absorbance spectra, fluorescence emission, molar absorption coefficients, and emission quantum yields (**Table 2.1**). Spectral characterization was performed in ethanol at pH 7 using a quinine sulfate standard in 0.5 M sulfuric acid.(Valeur, B. 2002, Williams, A.T.R., Winfield, S.A., et al. 1983) Our results confirmed that triazole formation generally enhances the fluorescence of alkyne derivatives and can induce shifts in emission wavelength (**Table 2.1**). In all four alkynes, we observed a large decrease in QY relative to the starting hydroxyl derivatives (ca. 20 - 90%) with **2.4.2** (from 0.33 to 0.02) and **2.6.2** (from 0.35 to 0.01) showing the most significant changes. Three of the alkyne structures (**2.4.2**, **2.6.2**, and **2.7.2**) showed a significant increase in extinction coefficient relative to the hydroxyl derivatives.

	Experimental							*Theoretical*		
Cmpd	*Abs λ_{Max} (nm)*	*Emission λ_{Max} (nm)*	*ε Absorption Coefficient (cm^{-1} M^{-1})*	*Φ Quantum Yield*[b]	*$\Delta\ \Phi$ b → c*	*$\varepsilon \times \Phi$ Brightness (cm^{-1} M^{-1})*	*Δ Brightness b → c*	*Abs λ_{Max} (nm)*	*Corrected Abs λ_{Max} (nm)*[a]	*f*[e]
2.4.1	323	380	11,600	0.33[c]		3800		302	324	0.44
2.4.2	325	380	22,000	0.02		440		309	328	0.54
2.4.3	329	381	17,500	0.17	850%	3000	680%	318 [d]	333	0.69
2.5.1	350	450	13,800	0.30		4100		351	354	0.33
2.5.2	362	403	3,100	0.23		710		346	350	0.41
2.5.3	352	420	18,000	0.35	120%	6300	890%	349 [d]	352	0.48
2.6.1	357	466	7,400	0.35		2600		365	362	0.19
2.6.2	334	437	16,300	0.01		160		329	340	0.53
2.6.3	339	445	11,600	0.02	200%	230	140%	335 [d]	344	0.49
2.7.1	367	430	11,400	0.52		5900		353	355	1.11
2.7.2	360	412	18,000	0.36		6500		360	359	1.24
2.7.3	358	435	7,700	0.44	120%	3400	50%	370 [d]	365	1.38

Table 2.1. Photophysical characterization of coumarin compounds.

a. The corrected values were obtained based on the linear correlation (eq. 1).See section 2.6.3 for additional data used.

b. Spectra were obtained in ethanol (pH 7), emission quantum yields were determined using quinine sulfate as a standard in 0.5 M H_2SO_4.(Valeur, B. 2002, Williams, A.T.R., Winfield, S.A., et al. 1983)

c. The emission quantum yield of **2.4.1** was found to agree to within 11% of literature values in ethanol at pH 10.(Adamczyk, M., Cornwell, M., et al. 1997, Sun, W.C., Gee, K.R., et al. 1998)

d. For triazole-substituted coumarins, lower-energy 1,4-isomers were used for calculations.

e. Oscillator strength.

Conversion of the alkyne structures to the corresponding triazole increased the QY of all structures, with **2.4.3** and **2.6.3** showing the largest relative changes. With the exception of compound **2.5.2**, triazole formation caused a slight decrease in the extinction coefficients as compared to the corresponding alkyne. The increased brightness ($\varepsilon \times \Phi$, $cm^{-1}M^{-1}$) of compounds **2.4.3** and **2.5.3** suggest that these may be the most suitable as fluorogenic probes, while compounds **2.6.3** and **2.7.3** show only minor changes by this analysis. Although relatively large bathochromic shifts have been reported for related compounds, we only observed modest changes in emission wavelength upon triazole formation, with the largest of these seen in compounds **2.5.3** (17 nm) and **2.7.3** (23 nm) (**Figure 2.3**).(Zhou, Z. and Fahrni, C.J. 2004)

Previous studies have suggested that triazole formation on conjugated alkyne fluorophores can induce large increases in fluorescence. We found that the extent of the increase is highly dependent on the fluorophore backbone. Several of the coumarin-based fluorophores examined here showed substantial increases in brightness upon triazole formation, and could prove useful as biological probes. The results obtained demonstrate that the impact of substitutions on the fluorophore backbone must be carefully considered. It is worth noting that hydroxycoumarin structures are often assessed at higher pH where their anionic forms are more prevalent.

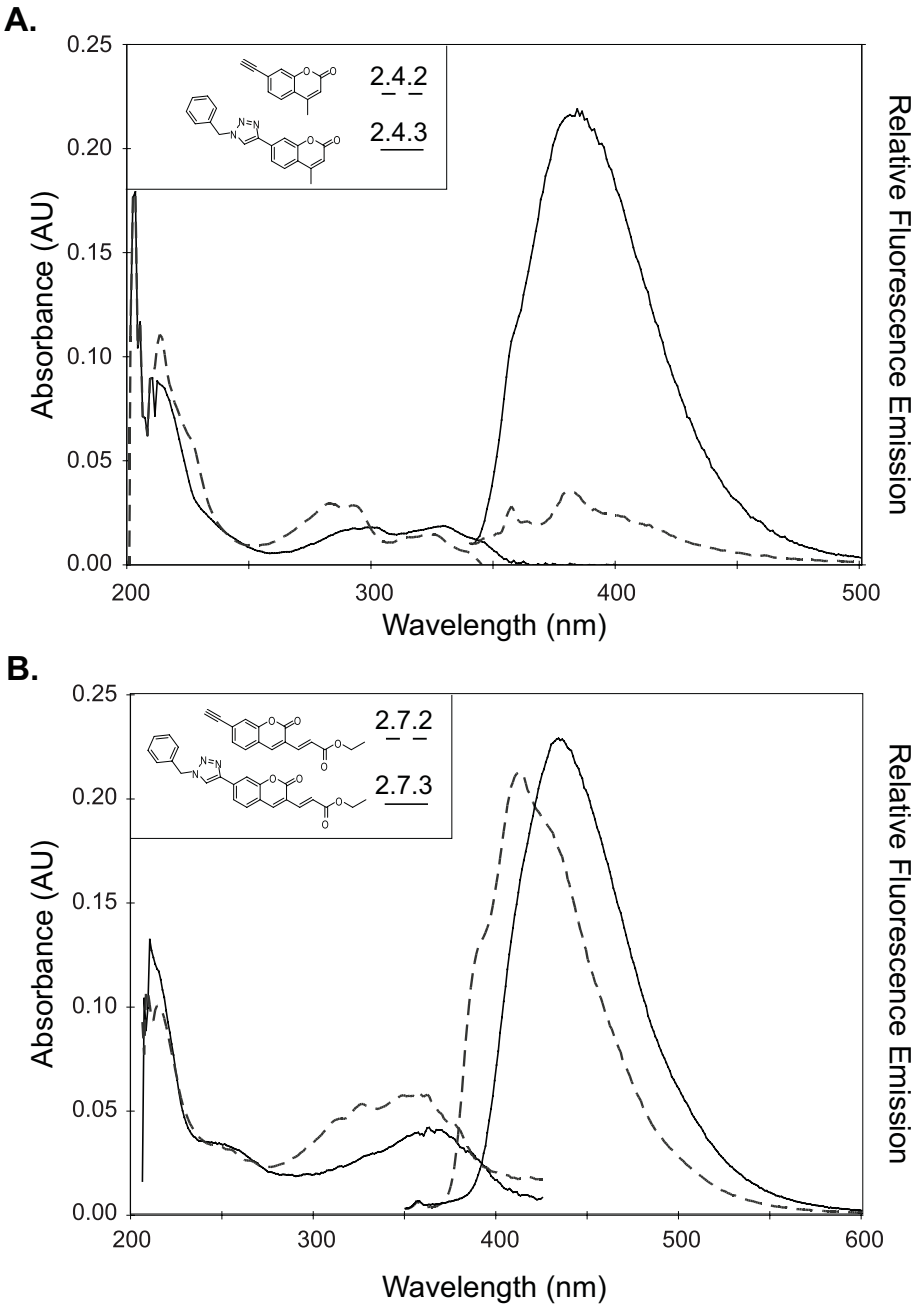

Figure 2.3. Absorbance and relative fluorescence emission of alkyne and triazole structures. A) 2.4.2, 2.4.3 and **B) 2.7.2, 2.7.3.** Spectra were obtained at equimolar concentrations in EtOH (pH 7) with an excitation wavelength of 325 nm.

Replacement of the hydroxyl group with an alkyne, triazole, or methoxy group reduces the emission of the fluorophore as a result.(Seixas de Melo, J.B., RS. and Macanita, AL. 1994, Zhou, Z. and Fahrni, C.J. 2004, Zhu, Q., Uttamchandani, M., et al. 2003) We examined the properties of our fluorophores at high pH and confirmed they were similar to neutral conditions. Therefore, while dyes that take advantage of this design suffer from reduced brightness, they are conversely less environmentally sensitive.

We found that the alkyne-triazole fluorogenic strategy manifests a variety of effects in each of the backbones studied. The largest increases in total fluorescence emission were seen in series **2.4** and **2.6**, with increases in QY between 1.2- to 9-fold. When the brightness of the fluorophore is considered, series **2.4** and **2.5** show large increases of 7- and 9-fold, respectively. The intensity of emission is not the only consideration for fluorogenic strategies, shifts in emission wavelength can be used to enhance the selectivity of detection. We found that the 3-substituted coumarin backbone in series **2.7** showed the largest shift in emission wavelength (**Figure 2.3**), similar to previous reports.(Zhou, Z. and Fahrni, C.J. 2004) Although the shift in λ_{Max} is small in the other derivatives, even these compounds could be used as suitable probes through judicious choice of excitation and emission filters. For example, the tail region of the emission spectra for these compounds (~450 – 600 nm) can show substantial differences between the alkyne and triazole (**Figure 2.3**).

2.4 Theoretical prediction of fluorophore absorption

To guide the design of future fluorogenic probes, we explored theoretical methods to predict the properties of alkyne- and triazole-conjugated coumarin fluorophores. Computational quantum chemistry methods are readily available; however, careful testing of the performance of any method is necessary before it can be applied to a particular class of fluorophores. Here, we used the experimental data presented in **Table 2.2** to benchmark the performance of time-dependent density functional theory(Casida, M.E., Jamorski, C., et al. 1998) (TD DFT) in the determination of absorption wavelengths for coumarins. TD DFT is one of the most widely used single-reference approaches to model excited states of organic molecules.(Dreuw, A. and Head-Gordon, M. 2005) Prediction of the fluorescence wavelengths is a significantly more challenging task compared to the absorption properties; thus, we postpone the presentation of computational modeling of the emission of the substituted coumarins to future work.

The calculated absorption wavelengths listed in **Table 2.2** correspond to the transitions with the largest oscillator strengths (*f*) for coumarins in ethanol solution. These were also considered to be bright excited states and correspond to $\pi \rightarrow \pi^*$ type transitions (normally HOMO to LUMO).

Cmpd	*Calculated*			*Experimental Abs* λ_{Max} *(nm)*
	Abs λ_{Max} *(nm)*	*Corrected Abs* λ_{Max} *(nm)*[a]	*f*	
2.4.1, anion	361	360	0.46	374
2.5.1, anion	456	417	0.28	418
2.6.1, anion	452	415	0.41	410
2.7.1, anion[b]	402	384	1.28	434

Table 2.2. Absorption wavelengths of substituted coumarins (Figure 2.3), calculated with PCM-TD-PBE0/6-31+G(d) method.

a. The corrected values were obtained based on the linear correlation (eq. 1).

b. Excluded from correlation (**Figure 2.4**) due to the unusually large differences between the calculated and experimental λ_{Max} values (32 nm and 50 nm for uncorrected and corrected theoretical values, respectively). Preliminary Complete Active Space Self-Consistent Field (CASSCF)(Knowles, P.J. and Werner, H.J. 1985, Werner, H.-J., Knowles, P.J., et al. 2006, Werner, H.J. and Knowles, P.J. 1985) calculations suggest that the failure of TD DFT in the case of **2.7.1** anion may be related to a high contribution of the doubly-excited configurations in its bright excited state, which can not be properly treated by the standard TD DFT implementation.

In most cases, these transitions are to the lowest-energy bright excited states ($S_0 \rightarrow S_1$); in the case of **2.6.2** and **2.6.3**, S_1 had a much smaller oscillator strength when compared with S_2 (0.12 and 0.21 *vs.* 0.53 and 0.49, respectively). Therefore, for these two structures we chose the next higher excited state (S_2) to correlate with the experimentally observed absorption bands giving rise to fluorescence, omitting the lowest-energy excited state, S_1. The calculated

absorption wavelengths significantly deviate from the experimental data, with mean absolute error (MAE) of 13.6 nm. Thus, it is not advisable to use the TD DFT calculated values directly in order to predict the absorption wavelengths. However, we found that there is a good linear correlation between the calculated and experimental absorption λ_{Max} values ($R^2 = 0.936$, **Figure 2.4**):

$$\lambda_{Max}^{exptl} = 140.0 + 0.6082\ \lambda_{Max}^{calc} \qquad \text{(eq. 1)}$$

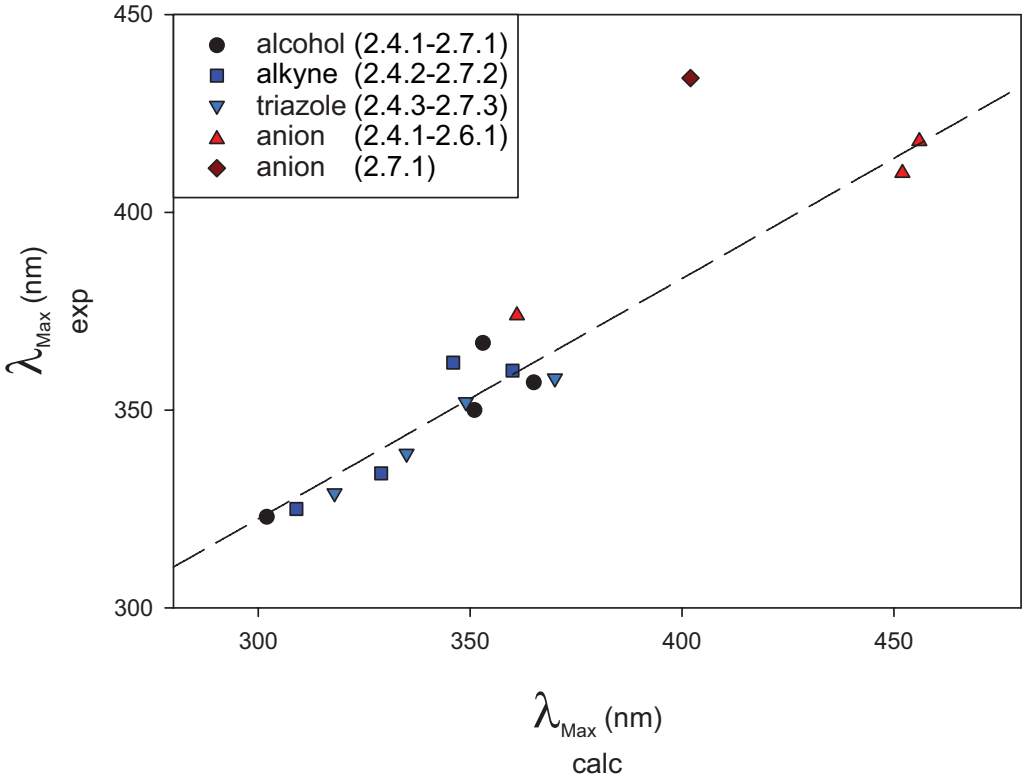

Figure 2.4. Correlation of experimental and theoretical absorbance values calculated with PCM-TD-PBE0/6-31+G(d) method, R2 = 0.936. Note that anion values for compounds **2.4.1**, **2.5.1**, and **2.6.1** are included, whereas the anion of **2.7.1** was excluded. Exclusion of all anionic forms gives $R^2 = 0.827$.

This correlation can be used to correct the computed values.(Timerghazin, Q.K., Carlson, H.J., et al. 2008) Indeed, when the corrected values are used

(**Table 2.2**), the MAE decreases to 5.3 nm. Similar correlations have been reported;(Jacquemin, D., Preat, J., et al. 2006) however, this is the first study to include experimental data for alkyne- and triazole-substituted species and anionic forms of the hydroxycoumarins. It has been proposed that the lower fluorescence emission quantum yields of the alkyne- vs. triazole-substituted coumarins can be explained by the predominance of the intersystem crossing from the lowest lying singlet state (S_1) to a low lying $(n\pi^*)^3$ triplet state.(Zhou, Z. and Fahrni, C.J. 2004) Indeed, semi-empirical calculations(Zhou, Z. and Fahrni, C.J. 2004) suggest that for alkyne-substituted coumarins the triplet state is lower in energy than the singlet, and this difference is responsible for the higher fluorescence emission quantum yields of the triazole. However, higher-level TD DFT calculations performed in this work suggest that for the majority of the alkyne-substituted coumarins the $(n\pi^*)^3$ triplet state is also significantly (*ca.* 0.5 eV) higher in energy than the S_1 state at the ground state equilibrium geometry. Thus, alternative mechanisms of the fluorescence emission quantum yield enhancement for triazole- vs. alkyne-substituted coumarins may be involved.

2.5 Conclusion

The fluorophores used here may be useful for fluorogenic labeling strategies in bioconjugate chemistry. The excitation wavelengths for the triazole structures range from 330 – 370 nm, similar to that of commonly employed dyes such as DAPI and Hoescht.(Lavis, L.D. and Raines, R.T. 2008) The triazole dyes generated for this study leave room for improvement to become optimal fluorogenic probes. The brightness of all fluorophores studied is low compared to

many common dyes, primarily due to their reduced extinction coefficients. We demonstrate here that absorbance wavelength can be accurately predicted for a range of coumarin based structures, including triazole- and alkyne-containing compounds. Employing rational design and computational prediction, future generations of fluorophores can be tuned to specific applications. In particular, fluorophores with superior water solubility, enhanced brightness and longer absorption/emission wavelengths are desirable for bioorthogonal fluorogenic labelling applications. Therefore, examination of additional fluorophore cores better endowed with these properties, as fluorogenic bioorthogonal labels, merits further investigation.

2.6 Experimental

2.6.1 General information

Reagents were purchased reagent grade from Sigma-Aldrich (Oakville, Ont) and used without additional purification. Proton and carbon NMR were performed on Varian 300, 400, or 500 MHz instruments at room temperature as noted. Deuterated solvents were obtained from Cambridge Isotope Laboratories (Andover, MA). CD_3OD, $(CD_3)_2SO$, and $CDCl_3$ solvent peaks (3.31, 2.50, and 7.26 for ^1H; 49.0, 39.5, and 77.2 for ^{13}C, respectively) were used as an internal chemical shift references. Some spectra contain small amounts of contaminating solvents.(Gottlieb, H.E., Kotlyar, V., et al. 1997) Mass spectrometry was performed using an MS50G positive electron impact instrument from Kratos Analytical (Manchester, UK) and a Mariner Biospectrometry positive ion electrospray instrument from Applied Biosystems (Foster City, CA).

2.6.2 Spectroscopy

Absorbance spectra for all compounds were collected at room temperature with a Hewlett-Packard (Palo Alto, CA) model 8453 diode array UV-visible spectro-photometer. Absorbance measurements were taken using Eppendorf (Hamburg, Germany) UVette cuvettes (220 – 1600 nm). Fluorescence spectra for all compounds were collected at room temperature with a Photon Technology International model (Birmingham, NJ) MP1 steady-state fluorimeter. Fluorescence measurements were taken using NSG Precision Cells (Farmingdale, NY) ES quartz cuvettes (190 – 2000 nm).

2.6.3 Quantum chemistry calculations

TD DFT calculations were performed using parameter-free Perdew, Burke and Ernzerhof (PBE0) hybrid functional(Perdew, J.P., Burke, K., et al. 1996) and the standard 6-31+G(d) basis set,(Hehre, W.J., Radom, L., et al. 1985) as implemented in the Gaussian03 program package.(Frisch, M.J., Trucks, G.W., et al.) Ground state geometry optimizations for the coumarins were performed at the PBE0/6-31+G(d) level, and the solvent (EtOH) effects were included using an IEF-PCM polarizable continuum model.(Cances, E., Mennucci, B., et al. 1997, Cossi, M., Scalmani, G., et al. 2002)

2.6.4 General synthesis of trifluoromethanesulfonic acid ester intermediates

Hydroxy compound (**2.4.1, 2.5.1, 2.6.1,** and **2.7.1**) (1 equiv) and *N*-phenyl bis-trifluoromethane sulfonimide ($PhN(SO_2CF_3)_2$, 1.3 equiv) were added to an oven dried round bottom flask and dissolved in acetonitrile (approximately 0.3 M).

N,N-Diisopropylethylamine (DIPEA, 1.3 equiv) was then added by syringe, briefly turning the solution a dark orange. The reaction was allowed to stir for approximately 1 to 2 h. The reaction mixture was then diluted with EtOAc, washed with water and dried over $MgSO_4$. The compound was concentrated in vacuo and carried forward without further purification.

2.6.5 General synthesis of trimethylsilanylethynyl intermediates

Trifluoro-methanesulfonic acid ester intermediates (1 equiv) were dissolved in acetonitrile (approximately 0.4 M). $Pd(PPh_3)_4$ (0.1 equiv) was then added, giving the reaction mixture a light brown colour. CuI (0.2 equiv) was added, turning the reaction mixture dark brown/black. Trimethylsilyl acetylene (5 equiv) and DIPEA (3.77 equiv) were then added to the reaction mixture. The solution was degassed by three freeze/thaw cycles and allowed to stir for 48 h. The reaction mixture was then diluted with EtOAc, washed with NH_4Cl and dried over $MgSO_4$. The crude product was concentrated in vacuo, and purified by gradient flash column chromatography (EtOAc/hexanes).

2.6.6 General synthesis of ethynyl profluorophores (2.4.2, 2.5.2, 2.6.2, and 2.7.2)

Trimethylsilanylethynyl intermediates (1 equiv) were dissolved in MeOH (approximately 0.03 M) and heated to 60 ^{o}C. Tributylammonium fluoride (TBAF, 3 equiv) was then added dropwise, and the reaction was allowed to stir for 15 min, turning a dark brown. The reaction was quenched with distilled water and filtered; the filtrate then formed a white precipitate under reduced pressure. The precipitate

was filtered to give crude product, and was purified by gradient flash column chromatography (EtOAc/hexanes).

2.6.7 General synthesis of click reaction products (2.4.3, 2.5.3, 2.6.3, and 2.7.3)

The alkynyl compounds (**2.4.2, 2.5.2, 2.6.2,** and **2.7.2**, 1 equiv) and benzyl azide (4 – 5 equiv) were dissolved in a 1:1 solution of methanol:water (0.02 M). CuI (0.2 equiv) was then added, followed by triethylamine (TEA, 2 equiv). The reaction proceeded at room temperature and was monitored by thin layer chromatography. Reactions were usually complete within 2 – 48 h. The crude product was concentrated in vacuo, extracted with chloroform and purified by flash column chromatography (CH_2Cl_2/MeOH). In some cases these conditions showed formation of the 5,5'-bistriazole side product (< 25%) as evidenced by an additional resonance in the ^{1}H-NMR spectrum between 4 – 5 ppm.(Angell, Y. and Burgess, K. 2007) To avoid this side product, alternative conditions were used as follows: The alkynyl compounds (**2.4.2** and **2.7.2)** (1 equiv) and benzyl azide (4 – 5 equiv) were dissolved in a 1:1 solution of methanol:water (0.03 M alkyne). $CuSO_4$ (0.2 equiv) and ascorbic acid (0.3 equiv) were then added, and the reaction was allowed to proceed at room temperature. Reactions were sluggish, and required 2 – 7 d. The crude product was concentrated in vacuo, extracted with chloroform and purified by flash column chromatography (CH_2Cl_2/MeOH).

2.6.8 Synthesis and characterization

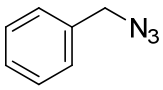

Azidomethylbenzene (**benzylazide**).

Bromomethylbenzene (0.7 mL, 5.85 mmol, 1 equiv) was dissolved in 15 mL of DMSO, followed by addition of sodium azide (0.57 g, 8.8 mmol, 1.5 equiv). The reaction mixture was heated to 40 ^{o}C, then quenched after 1 h with distilled water. Extraction was performed with diethyl ether, followed by water and brine washes. The organic layer was dried over $MgSO_4$ and concentrated in vacuo. Proton NMR data matched that previously reported.(Alvarez, S.G. and Alvarez, M.T. 1997)

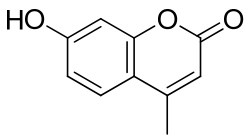

7-Hydroxy-4-methyl-chromen-2-one (**7-hydroxy-4-methyl coumarin, 2.4.1**). Resorcinol (4 g, 36.32 mmol, 1 equiv) was added to an oven dried round bottom flask, and dissolved in ethyl acetoacetate (7 mL, 54.48 mmol, 1.5 equiv). $TiCl_4$ (2 mL, 18.16 mmol, 0.5 equiv) was then added by pipet, driving the reaction to immediate completion. The reaction was quenched with water, forming a yellow precipitate. The water was then decanted off, and the precipitate recrystallized in EtOH obtained in 97% yield. (Valizadeh, H. and Shockravi, A. 2005) ^{1}H NMR (300 MHz, DMSO): δ 10.50 (s, 1H), 7.57 (d, 1H, ^{3}J = 8.7 Hz), 6.78 (dd, 1H, ^{3}J = 8.7 Hz, ^{4}J = 2.4 Hz), 6.68 (d, 1H, ^{4}J = 2.3 Hz), 6.10 (s, 1H), 2.35 (s, 3H). R_f = 0.5 (9:1 CH_2Cl_2/MeOH).

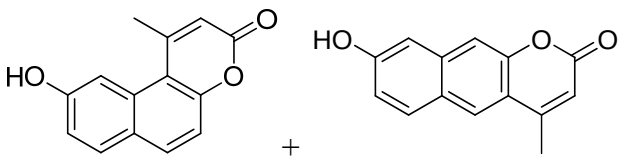

9-Hydroxy-1-methyl-benzo[f]chromen-3-one (**2.5.1**) and **8-Hydroxy-4-methyl-benzo[g]chromen-2-one** (**2.6.1**).

2,7-dihydroxynapthalene (4.8 g, 29.44 mmol, 1 equiv) was dissolved in ethyl acetoacetate (9.4 mL, 73.6 mmol, 2.5 equiv) and approximately 30 mL of 80% sulfuric acid was added dropwise. The reaction was allowed to stir for 24 h under argon. The reaction was then quenched with water, and the resulting precipitate was filtered. The precipitate was then dissolved in EtOH, filtering off the insoluble material, and concentrated in vacuo. The concentrated solid was then dissolved in 10% NaOH (aq) and the insoluble material was filtered, acidified and recrystallized with EtOH to obtain the white crystalline linear benzocoumarin (**2.6.1**). The filtrate was then acidified with concentrated HCl to pH 1 and allowed to crystallize at 4 °C, yielding the yellow angular benzocoumarin solid (**2.5.1**). (Kolancilar, H. 2002, Kolancilar, H. and Oyman, U. 2003)

(**2.5.1**) Obtained in 5.9% yield. ^{1}H NMR (400 MHz, DMSO): δ 10.13 (s, 1H), 8.03 (d, 1H, ^{3}J = 8.8 Hz), 7.99 (s, 1H), 7.89 (d, 1H, ^{3}J =8.8 Hz), 7.27 (d, 1H, ^{3}J = 8.8 Hz), 7.12 (d, 1H, ^{3}J = 8.8 Hz), 2.85 (s, 3H). R_f = 0.67 (10:1 CH_2Cl_2/MeOH).

(**2.6.1**) Obtained in 9.7% yield. ^{1}H NMR (300 MHz, DMSO): δ 10.17 (s, 1H), 8.27 (s, 1H), 7.94 (d, 1H, ^{3}J = 9.0 Hz), 7.60 (s, 1H), 7.16 (d, 1H, ^{4}J = 2.4 Hz), 7.10 (d, 1H, ^{3}J = 9.0 Hz) 6.33 (d, 1H, 1.2 Hz), methyl overlapping DMSO ~2.5 (3H). R_f = 0.73 (9:1 CH_2Cl_2/MeOH).

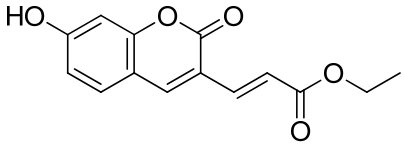

(E)-ethyl 3-(7-Hydroxy-2-oxo-chromen-3-yl)-acrylate (**2.7.1**).

2,4-dihydroxy benzaldehyde (300 mg, 2.18 mmol, 1 equiv) was dissolved in approximately 6 mL of ethanol. Diethyl glutaconate was then added (0.40 mL, 2.29 mmol, 1.05 equiv), followed by 3 drops of piperidine. The reaction mixture was refluxed at 89 ^{o}C for 24 h, then cooled to room temperature providing a yellow precipitate, that was then filtered. (Padmanabhan, S., Peri, R., et al. 1996) Obtained in 67% yield (**2.7.1**). ^{1}H NMR (300 MHz, CD_3OD): δ 8.14 (s, 1H), 7.56 (dd, 1H, ^{3}J = 16.5 Hz, ^{4}J = 0.6 Hz), 7.52 (d, 1H, ^{3}J = 8.6 Hz), 6.92 (d, 1H, ^{3}J = 16.5 Hz), 6.80 (dd, 1H, ^{3}J = 8.6 Hz, ^{4}J = 2.4 Hz), 6.71 (d, 1H, ^{4}J = 2.4 Hz, ^{4}J = 0.6 Hz), 4.23 (q, 2H, ^{3}J = 6.9 Hz), 1.31 (t, 3H, ^{3}J = 6.9 Hz). R_f = 0.49 (1:1 EtOAc/hexanes).

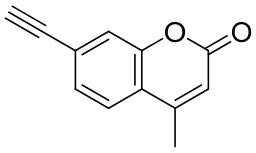

7-ethynyl-4-methyl-chromen-2-one (**2.4.2**).

See protocol for general synthesis of trimethylsilanylethynyl intermediates and ethynyl profluorophores (sections 2.6.5 and 2.6.6). Obtained in 31% yield over three steps from **2.4.1.**

^{1}H NMR (400 MHz, DMSO): δ 7.75 (d, 1H, ^{3}J = 8.1 Hz), 7.49 (d, 1H, ^{4}J = 1.5 Hz), 7.44 (dd, 1H, ^{3}J = 8.1 Hz, ^{4}J = 1.6 Hz), 6.42 (d, 1H, ^{4}J = 1.2 Hz), 4.48 (s, 1H), 2.41 (d, 3H, ^{4}J = 1.3 Hz). APT ^{13}C NMR (100 MHz, DMSO): δ 159.1, 152.5, 152.4, 127.3, 125.6, 124.7, 119.9, 119.1, 114.8, 83.7, 82.0, 17.7. EI-MS

calculated for $C_{12}H_8O_2$: 184.0524; observed: 184.0524. R_f = 0.37 (1:3 EtOAc/hexanes).

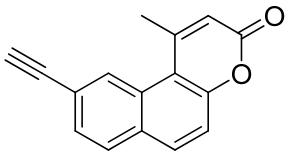

9-ethynyl-1-methyl-benzo[f]chromen-3-one (**2.5.2**).

See protocol for general synthesis of trimethylsilanylethynyl intermediates and ethynyl profluorophores (sections 2.6.5 and 2.6.6). Obtained in 15% yield over three steps from **2.5.1.**

^{1}H NMR (600 MHz, $CDCl_3$): δ 8.77 (s, 1H), 7.95 (d, 1H, ^3J = 8.9 Hz), 7.86 (d, 1H, ^3J = 8.4 Hz), 7.61 (dd, 1H, ^3J = 8.3 Hz, ^4J = 1.4 Hz), 7.49 (d, 1H, ^3J = 8.9 Hz), 6.40 (d, 1H, ^4J = 1.1 Hz), 3.23 (s, 1H), 2.95 (s, 3H). APT ^{13}C NMR (100 MHz, $CDCl_3$): δ 159.9, 154.9, 153.5, 133.1, 130.9, 129.8, 129.6, 129.1, 128.1, 121.5, 118.7, 116.9, 114.2, 83.7, 78.7, 26.2. EI-MS calculated for $C_{16}H_{10}O_2$: 234.0681; observed: 234.0682. R_f = 0.39 (1:3 EtOAc/hexanes).

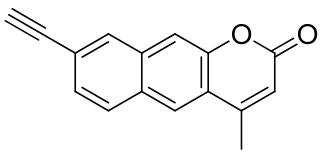

8-ethynyl-4-methyl-benzo[g]chromen-2-one (**2.6.2**).

See protocol for general synthesis of trimethylsilanylethynyl intermediates and ethynyl profluorophores (sections and 2.6.5 2.6.6). Obtained in 14% yield over three steps from **2.6.1.**

^{1}H NMR (600 MHz, $CDCl_3$): δ 8.07 (s, 1H), 8.04 (s, 1H), 7.89 (d, 1H, ^3J = 8.6 Hz), 7.67 (s, 1H), 7.53 (dd, 1H, ^3J = 8.5 Hz, ^4J = 1.5 Hz), 6.37 (d, 1H, ^4J = 1.3

Hz), 3.24 (s, 1H), 2.56 (s, 3H). APT ^{13}C NMR (100 MHz, $CDCl_3$): δ 160.2, 151.4, 150.6, 133.9, 131.4, 129.2, 128.5, 128.3, 124.7, 121.8, 120.7, 116.2, 112.7, 83.3, 79.1, 18.6. EI-MS calculated for $C_{16}H_{10}O_2$: 234.0681; observed: 234.0676. R_f = 0.30 (1:3 EtOAc/hexanes).

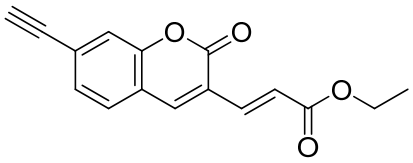

(E)-ethyl 3-(7-ethynyl-2-oxo-chromen-3-yl)-acrylate (**2.7.2**).

See protocol for general synthesis of trimethylsilanylethynyl intermediates and ethynyl profluorophores (sections 2.6.5 and 2.6.6). Obtained in 61% yield over three steps from **2.7.1.**

^{1}H NMR (400 MHz, $CDCl_3$): δ 7.84 (s, 1H), 7.55 (dd, 1H, ^3J = 16.0 Hz, ^4J = 0.7 Hz), 7.49 (d, 1H, ^3J = 8.0 Hz) 7.44 (m, 1H), 7.40 (d, 1H, ^3J = 8.0 Hz, ^4J = 1.5 Hz), 7.10 (d, 1H, ^3J = 16.0 Hz), 4.27 (q, 2H, ^3J = 7.8 Hz), 3.33 (s, 1H), 1.34 (t, 3H, ^3J = 7.8 Hz). APT ^{13}C NMR (100 MHz, $CDCl_3$): δ 166.7, 158.5, 152.9, 142.3, 137.3, 128.3, 128.2, 126.5, 124.3, 122.8, 119.9, 119.1, 81.4, 60.7, 60.7, 14.2. EI-MS calculated for $C_{16}H_{12}O_4$: 268.0736; observed: 268.0740. R_f = 0.34 (1:3 EtOAc/hexanes).

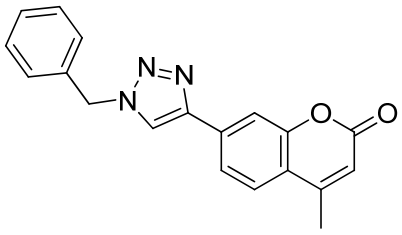

7-(1-Benzyl-[1,2,3]triazol-4-yl)-4-methyl-chromen-2-one (**2.4.3**).

See protocol for general synthesis of click reaction products (section 2.6.7). Obtained in 79% yield from **2.4.2**.

^{1}H NMR (500 MHz, $CDCl_3$): δ 7.84 (dd, 1H, ^{3}J = 8.2 Hz, ^{4}J = 1.7 Hz), 7.77 (s, 1H), 7.67 (d, 1H, ^{4}J = 1.6 Hz), 7.64 (d, 1H, ^{3}J = 8.2 Hz), 7.43 – 7.34 (m, 5H), 6.29 (s, 1H), 5.61 (s, 2H), 2.45 (s, 3H). APT ^{13}C NMR (125 MHz, $CDCl_3$): δ 160.7, 153.9, 152.0, 146.5, 134.3, 134.1, 129.3, 129.0, 128.2, 125.1, 121.5, 120.5, 119.6, 115.0, 113.6, 54.4, 18.6. Pos-ES-MS calculated for $C_{19}H_{15}N_3O_2Na$: 340.1057; observed: 340.1057 ($[M+Na]^+$). R_f = 0.68 (10:1 CH_2Cl_2/MeOH).

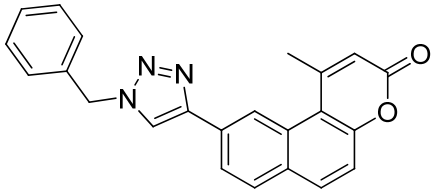

9-(1-Benzyl-[1,2,3]triazol-4-yl)-1-methyl-benzo[f]chromen-3-one (**2.5.3**).

See protocol for general synthesis of click reaction products (section 2.6.7). Obtained in 44% yield from **2.5.2**.

^{1}H NMR (500 MHz, $CDCl_3$): δ 9.32 (broad s, 1H), 7.95 (d, 1H, ^{3}J = 9.0 Hz), 7.92 (d, 1H, ^{3}J = 8.0 Hz), 7.80 (d, 1H, ^{3}J = 8.0 Hz), 7.46 (d, 1H, ^{3}J = 9.0 Hz), 7.40 – 7.35 (m, 6H), 6.41 (s, 1H), 3.06 (s, 3H). APT ^{13}C NMR (125 MHz, $CDCl_3$): δ 160.3, 155.1, 154.3, 134.5, 134.5, 133.3, 131.0, 130.6, 130.2, 129.8, 129.2, 128.9, 128.1, 123.1, 121.9, 118.0, 116.6, 114.8, 54.5, 50.9, 26.5. EI-MS calculated for $C_{23}H_{17}N_3O_2$: 367.1321; observed: 367.1319. R_f = 0.38 (30:1 CH_2Cl_2/MeOH).

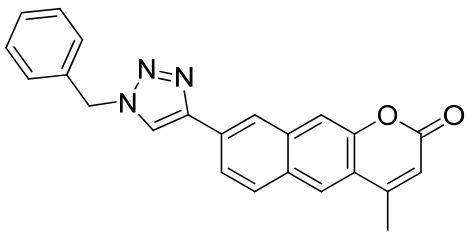

8-(1-Benzyl-[1,2,3]triazol-4-yl)-4-methyl-benzo[g]chromen-2-one (**2.6.3**).

See protocol for general synthesis of click reaction products (section 2.6.7). Obtained in 87% yield from **2.6.2**.

^{1}H NMR (500 MHz, $CDCl_3$): δ 8.29 (s, 1H), 8.09 (s, 1H), 7.99 (s, 2H), 7.84 (s, 1H), 7.73 (s, 1H), 7.45 – 7.40 (m, 3H), 7.35 – 7.30 (m, 2H), 6.36 (d, 1H, ^{3}J = 1.0 Hz), 5.64 (s, 2H), 2.55 (d, 3H, ^{3}J = 1.5 Hz). APT ^{13}C NMR (125 MHz, $CDCl_3$): δ 160.6, 151.7, 150.6, 134.8, 134.4, 130.3, 129.6, 129.3, 129.0, 128.2, 124.9, 123.9, 123.5, 120.3, 120.2, 116.4, 115.8, 113.1, 54.4, 18.7. EI-MS calculated for $C_{23}H_{17}N_3O_2$: 367.1321; observed: 367.1321. R_f = 0.39 (30:1 CH_2Cl_2/MeOH).

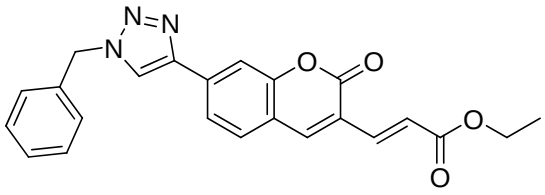

(E)-ethyl 3-[7-(1-Benzyl-[1,2,3]triazol-4-yl)-2-oxo-chromen-3-yl]-acrylate (**2.7.3**).

See protocol for general synthesis of click reaction products (section 2.6.7). Obtained in 62% yield from **2.7.2.**

^{1}H NMR (500 MHz, $CDCl_3$): δ 7.86 (s, 1H), 7.84 (dd, 1H, ^{3}J = 8.1 Hz, ^{4}J = 1.6 Hz), 7.78 (s, 1H), 7.73 (d, 1H, ^{4}J = 1.6 Hz), 7.58 (d, 1H, ^{3}J = 7.8 Hz), 7.57 (d, 1H, ^{3}J = 16.0 Hz), 7.46-40 (m, 3H), 7.36-7.33 (m, 2H), 7.10 (d, 1H ,^{3}J = 16.0 Hz), 5.61 (s, 2H), 4.28 (q, 2H, ^{3}J = 7.2 Hz), 1.35 (t, 3H, ^{3}J = 7.2 Hz). ^{13}C NMR (125 MHz, $CDCl_3$): δ 166.9, 159.0, 154.1, 154.0, 146.4, 142.9, 137.8, 135.2, 134.2, 129.3, 129.05, 128.98, 128.2, 123.7, 122.1, 120.7, 118.6, 113.1, 60.7, 54.4, 14.3. EI-MS calculated for $C_{23}H_{19}N_3O_4$: 401.1375; observed: 401.1375. R_f = 0.52 (30:1 CH_2Cl_2/MeOH).

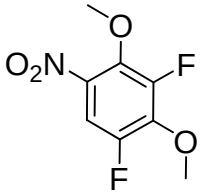

3,5-difluoro-2,4-dimethoxynitrobenzene (**2.9**).

Commercially available 2,3,4,5-Tetrafluoronitrobenzene (**2.8**) (0.5 mL, 4.3 mmol, 1 equiv) was dissolved in approximately 8 mL of methanol. In a separate round bottom flask, sodium metal (0.3 g, 12.9 mmol, 3 equiv) was dissolved in 3 mL of methanol, generating sodium methoxide upon stirring. The solution of sodium methoxide was added to the reaction mixture, on ice, resulting in a bright yellow solution. The reaction was quenched with 4 mL of 1 M citric acid after approximately 30 min. The crude product was concentrated *in vacuo*, and taken up in ether. The crude product was then washed twice with citric acid, once with brine, dried with magnesium sulphate and concentrated *in vacuo* giving a yellow oil (0.9 g, 96%). ^{1}H NMR (300 MHz, CD_3OD): δ 7.66 (dd, 1H, ^{3}J = 11.1 Hz, ^{4}J = 1.8 Hz), 4.11 (s, 3H), 3.99 (s, 3H). R_f = 0.55 (5:1 hexanes/MeOH).

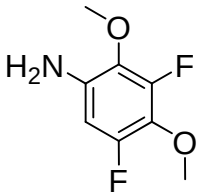

1-amino-3,5-difluoro-2,4-dimethoxybenzene (**2.10**).

3,5-difluoro-2,4-dimethoxynitrobenzene (**2.9**) (0.9 g, 4.1 mmol, 1 equiv) was dissolved in 8 mL of 1:1 ethyl acetate/ethanol and placed in a Parr shaker vessel. Palladium on charcoal (25 mg, 0.235 mmol, 0.05 equiv) was then added and the reaction mixture was subjected to hydrogenation at 45 psi for approximately 6 h.

The heterogeneous catalyst was removed by filtration, and the crude product was concentrated *in vacuo* giving a brown oil (0.717 g, 93%). ^{1}H NMR (300 MHz, $CDCl_3$): δ 6.27 (dd, 1H, ^{3}J = 12.0 Hz, ^{4}J = 2.4 Hz), 3.87 (s, 6H), 3.620 Broad, not always present (s, 2H). R_f = 0.19 (1:5 EtOAc/hexanes).

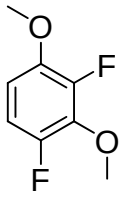

1,3-dimethoxy-2,4-difluoro benzene (**2.11**).

1-amino-3,5-difluoro-2,4-dimethoxybenzene (**2.10**) (260 mg, 1.2 mmol, 1 equiv) was dissolved in a mixture of concentrated HCl (0.6 mL)/ice (3 g). Sodium nitrite (91 mg, 1.3 mmol, 1.1 equiv) dissolved in a minimal amount of water was then added after cooling in an ice bath. The reaction was allowed to stir for approximately 20 minutes at room temperature. Sulphamic acid (60 mg, 0.6 mmol, 0.5 equiv) was then added to destroy any remaining HNO_2. The reaction mixture was then added dropwise to a solution of $FeSO_4 \cdot 7H_2O$ (0.33 g, 1.2 mmol, 1eq) dissolved in approximately 5 mL of DMF. The reaction was allowed to stir for 2 h at room temperature, then diluted with water. NaOH (10%) was then added until pH 7 was achieved. Three ether extractions were performed, followed by a water and brine wash. The crude product was dried with sodium sulphate and concentrated *in vacuo* (160 mg, 76%). ^{1}H NMR (400 MHz, $CDCl_3$): δ 6.78 (ddd, 1H, ^{3}J = 10.5 Hz, ^{4}J = 2.4 Hz), 6.56 (td, 1H, ^{3}J = 8.8 Hz, ^{4}J = 4.6 Hz), 3.98 (s, 3H), 3.85 (s, 3H). R_f = 0.49 (1:5 EtOAc/hexanes).

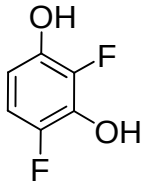

2,4-difluororesorcinol (**2.12**).

1,3-dimethoxy-2,4-difluoro benzene (**2.11**) (0.9 g, 5.1 mmol, 1equiv) was dissolved in approximately 15 mL of dry dichloromethane. BBr_3 (5.3 mL, 31.01 mmol, 6 equiv) was then added slowly and the reaction mixture was allowed to stir under argon for approximately 30 h. The reaction mixture was then quenched with water, and extracted three times with ether. A brine wash was performed, and the crude reaction mixture was dried using sodium sulphate before concentrating *in vacuo* resulting in a red-brown oil (0.757 g, 100%). ^{1}H NMR (300, $CDCl_3$): δ 6.79 (ddd, 1H, ^3J = 9.6 Hz, ^4J = 2.6 Hz, ^{5}J = 0.3), 6.49 (td, 1H, ^3J = 9.0 Hz, ^4J = 4.7 Hz), 5.23 (broad s, 1H), 4.99 (broad s, 1H). R_f = 0.14 (1:4 EtOAc/hexanes).

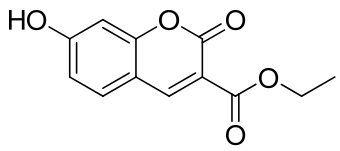

Ethyl 7-hydroxy-2-oxo-2H-chromene-3-carboxylate (**2.14**).

Commercially available 2,4-dihydroxybenzaldehyde (**2.13**) (1 g, 7.24 mmol, 1 equiv) and diethyl malonate (1.15 mL, 7.6 mmol, 1.05 equiv) were dissolved in EtOH (15 mL). A catalytic amount of piperidine (5 drops) was then added and the reaction was heated at reflux for 48 h. The reaction mixture was then cooled to -20 ^{o}C, the product formed a bright yellow precipate which was then filtered and dried (1.3 g, 77%). ^{1}H NMR (400 MHz, DMSO-D_6): δ 8.64 (s, 1H), 7.72 (d, 1H,

^{3}J = 8.6 Hz), 6.81 (dd, 1H, ^{3}J = 8.6 Hz, ^{4}J = 2.3 Hz), 6.70 (d, 1H, ^{4}J = 2.3 Hz), 4.24 (q, 2H, ^{3}J = 7.1 Hz), 1.27 (t, 3H, ^{3}J = 7.1 Hz); APT ^{13}C NMR (100 MHz, DMSO-D_6): δ 165.0, 163.6, 157.8, 157.1, 150.1, 132.8, 114.8, 112.7, 111.0, 102.5, 61.5, 14.8. EI-MS calculated for $C_{12}H_{10}O_5$: 234.0528; observed: 234.0528. R_f = 0.08 (1:3 EtOAc/hexanes).

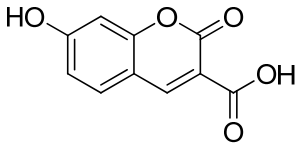

7-hydroxy-2-oxo-chromene-3-carboxylic acid (**2.15**).

Ethyl 7-hydroxy-2-oxo-2H-chromene-3-carboxylate (**2.14**) (50 mg, 0.21 mmol, 1 equiv) was dissolved in water and ethanol (0.65 mL each). To this reaction mixture was added NaOH (100 mg, 1.25 mmol, 6 equiv) and the reaction was allowed to stir for 5 min. The reaction mixture was then acidified with concentrated HCl until an off-white precipitate formed and was filtered (127 mg of sodium salt adduct). ^{1}H NMR (400 MHz, DMSO-D_6): δ 11.43 (broad s, 1H), 8.66 (s, 1H), 7.72 (d, 1H, ^{3}J = 8.6 Hz), 6.90 (dd, 1H, ^{3}J = 8.6 Hz, ^{4}J = 2.3 Hz), 6.80 (d, 1H, ^{4}J = 2.3 Hz); APT ^{13}C NMR (100 MHz, DMSO-D_6): δ 165.0, 14.92, 158.4, 157.6, 150.1, 132.6, 114.9, 113.0, 111.2, 102.5. ESI-HRMS calculated for $C_{10}H_5O_5$: 205.0143; observed: 205.0140. R_f = 0.0 (1:3 EtOAc/hexanes).

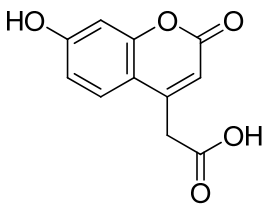

(7-hydroxy-2-oxo-chromen-4-yl)acetic acid (**2.16**).

Commercially available citric acid (2.5 g, 13 mmol, 1 equiv) was dissolved in concentrated sulphuric acid (7.5 mL). This solution was then gently heated to 70 ^{o}C and allowed to stir for approximately 20 min until no more bubbling was observed. The solution of citric acid was then allowed to cool in ice and resorcinol (**2.1**) (1.15g, 10.4 mmol, 0.8 equiv) dissolved in an additional 7.5 mL of concentrated sulphuric acid was added slowly. The reaction was allowed to proceed for approximately 4 h and quenched with ice. The pH was then adjusted between 1-2 with NaOH until awhite precipitate (**2.16**) was observed, and then filtered. The solid was dried *in vacuo* and characterized to match that previously reported (435 mg, 15%). (Laskowski, S.C. and Clinton, R.O. 1950) ^{1}H NMR (500 MHz, CH_3OD): δ 7.56 (d, 1H, ^{3}J = 8.5 Hz), 6.81(d, 1H, ^{3}J = 8.5 Hz), 6.72 (s, 1H), 6.20 (s, 1H), 3.83 (s, 2H), 2.42 (s, 0.6H). IR (microscope): ν = 3176 (broad), 1706, 1617, 1568, 1210 cm^{-1}; ES-MS calculated for $C_{12}H_{10}O_5$ Na: 243.02640; observed: 243.02639. R_f = 0.51 (10:1 DCM/MeOH with acetic acid spike)

2.6.9 Normalized absorbance and emission data. All spectra were obtained in ethanol (pH 7) with an excitation wavelength of 325 nm.

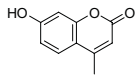

2.4.1

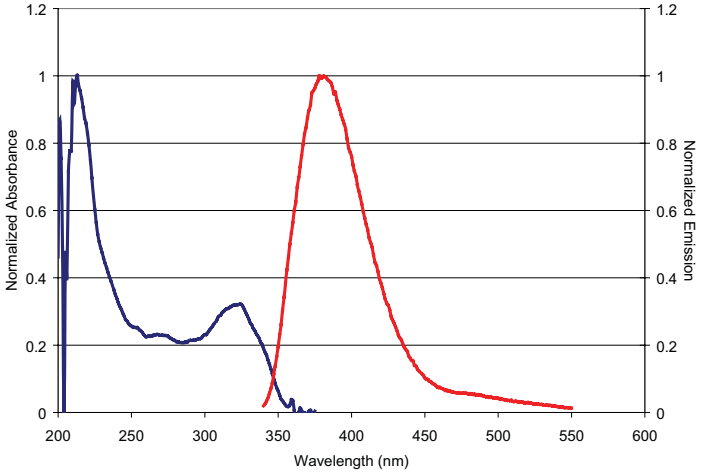

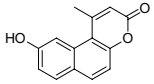

2.5.1

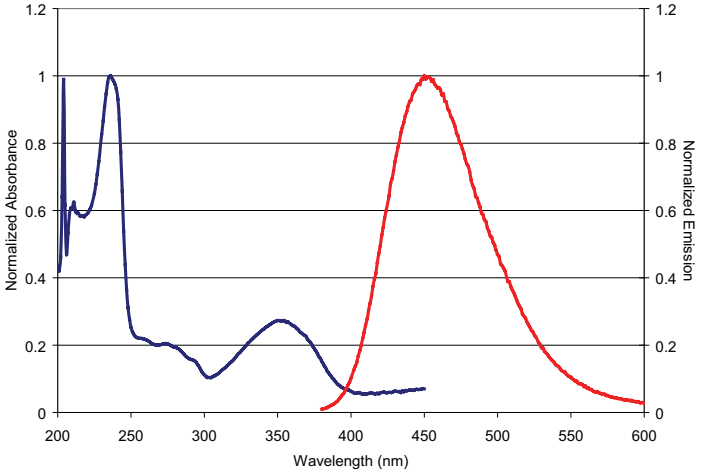

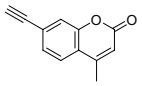

2.4.2

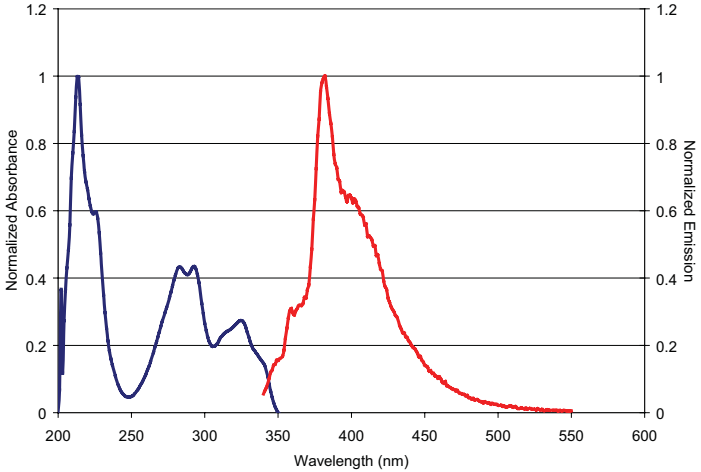
Normalized Absorbance
Normalized Emission
Wavelength (nm)
0
0.2
0.4
0.6
0.8
1
1.2
200
250
300
350
400
450
500
550
600

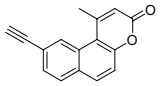

2.5.2

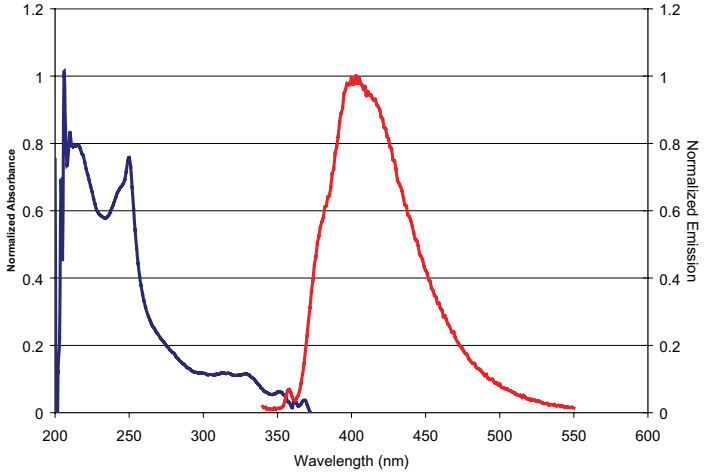
Normalized Absorbance
Normalized Emission
Wavelength (nm)
0
0.2
0.4
0.6
0.8
1
1.2
200
250
300
350
400
450
500
550
600

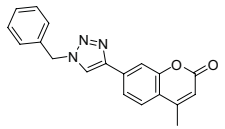

2.4.3

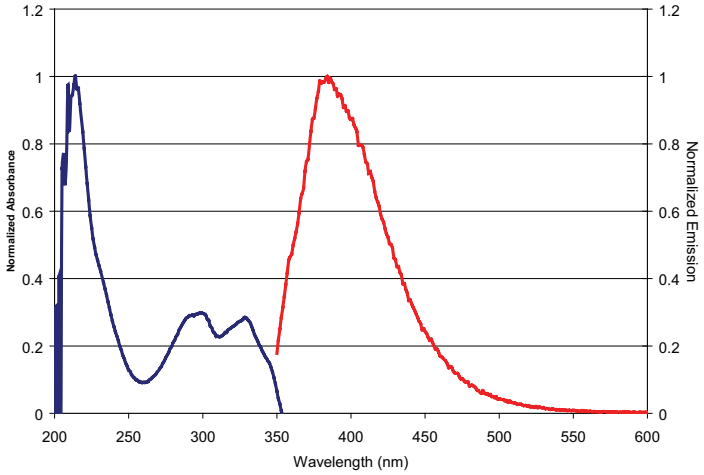
Normalized Absorbance
Normalized Emission
Wavelength (nm)
0
0.2
0.4
0.6
0.8
1
1.2
200
250
300
350
400
450
500
550
600

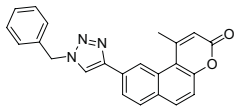

2.5.3

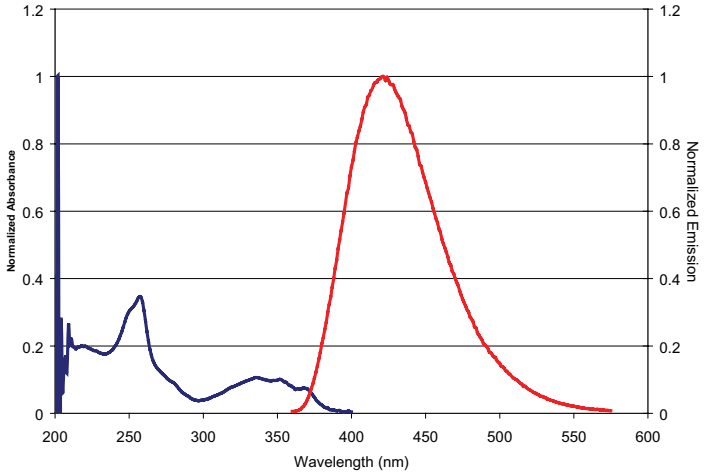
Normalized Absorbance
Normalized Emission
Wavelength (nm)
0
0.2
0.4
0.6
0.8
1
1.2
200
250
300
350
400
450
500
550
600

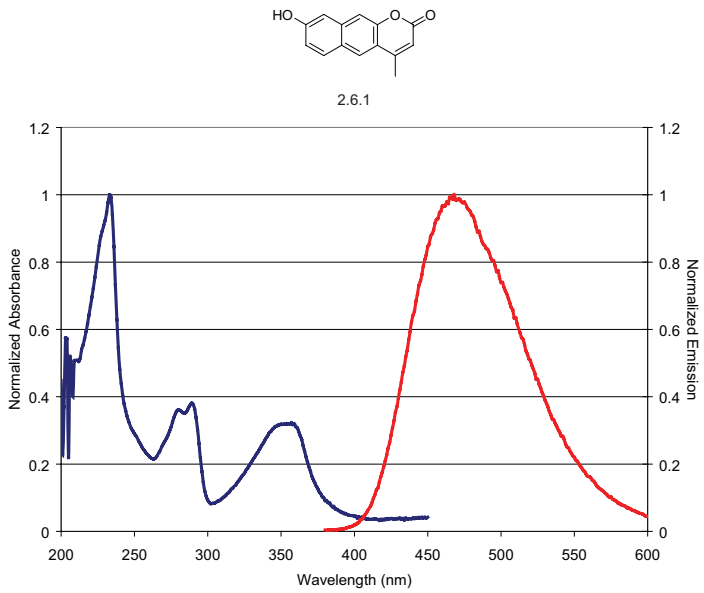
HO
O
O
2.6.1
1.2
1
0.8
0.6
0.4
0.2
0
200
250
300
350
400
450
500
550
600
Wavelength (nm)
Normalized Absorbance
Normalized Emission

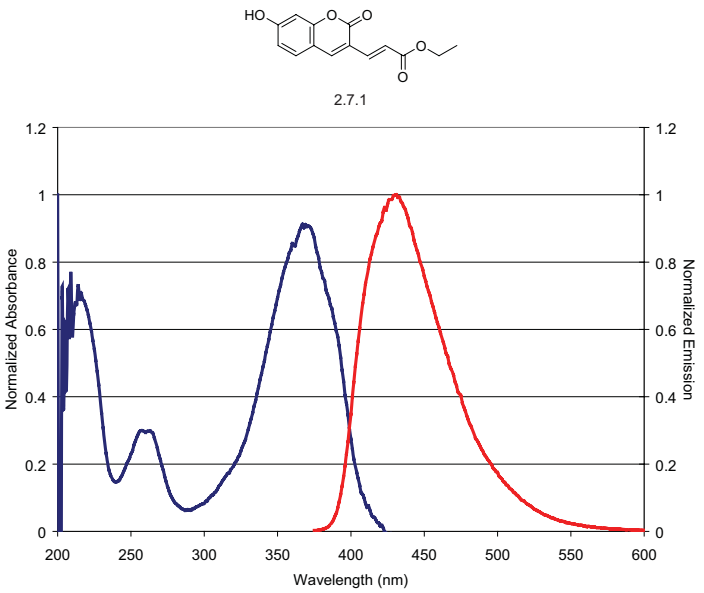
HO
O
O
O
O
2.7.1
1.2
1
0.8
0.6
0.4
0.2
0
200
250
300
350
400
450
500
550
600
Wavelength (nm)
Normalized Absorbance
Normalized Emission

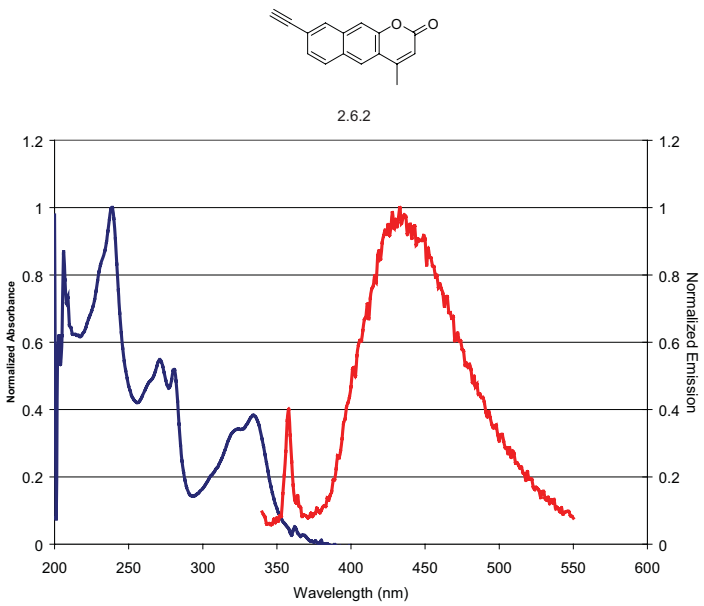
2.6.2
Normalized Absorbance
Normalized Emission
Wavelength (nm)
0
0.2
0.4
0.6
0.8
1
1.2
200
250
300
350
400
450
500
550
600

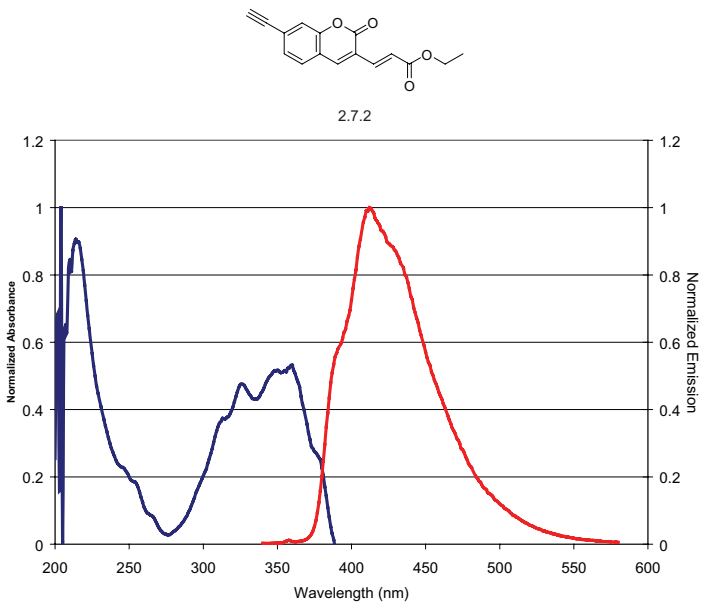
2.7.2
Normalized Absorbance
Normalized Emission
Wavelength (nm)
0
0.2
0.4
0.6
0.8
1
1.2
200
250
300
350
400
450
500
550
600

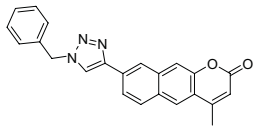

2.6.3

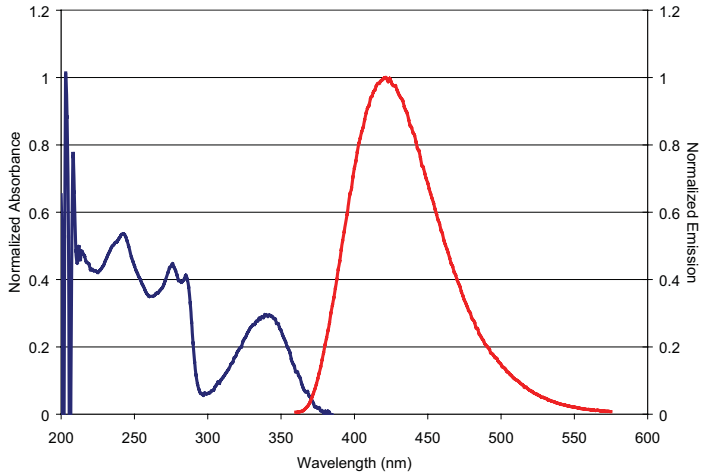
Normalized Absorbance
Normalized Emission
Wavelength (nm)
0
0.2
0.4
0.6
0.8
1
1.2
200
250
300
350
400
450
500
550
600

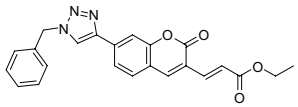

2.7.3

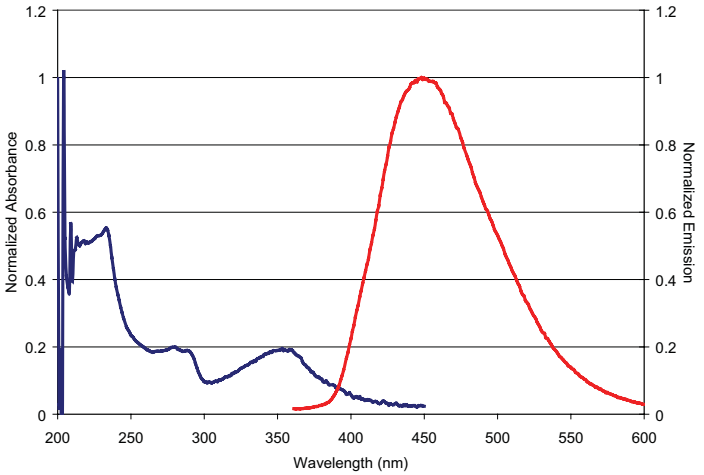
Normalized Absorbance
Normalized Emission
Wavelength (nm)
0
0.2
0.4
0.6
0.8
1
1.2
200
250
300
350
400
450
500
550
600

2.6.10 Quantum yield determination

2.6.10.1 Selecting a Fluorescence Standard

A QY standard is required as a comparison when performing a quantum yield calculation, as every fluorometer varies in lamp and detector intensities. As well, changing parameters such as the slit widths greatly affect the results obtained. The standard's absorption and excitation ranges should overlap with the experimental compound. It is often necessary to do a quick characterization of your compound to ensure proper selection of the fluorescence standard. Quinine sulphate is a popular standard due to its broad absorption and emission spectra and is highly recommended in the emission range of 400-600 nm. Fluorescein is a popular choice for emission ranges of 500-600 nm, and Cresyl violet is commonly used for longer wavelength samples in the emission range of 600-650 nm. Other quantum yield standards may be found in the literature or in a textbook such as Principles of Fluorescence Spectroscopy.(Lakowicz, J.R. 2006)

2.6.10.2 Sample Preparation and UV-Vis absorbance

Very little compound is required for quantum yield measurements. Typically, enough to cover the very tip of a small spatula can be dissolved in approximately 2-3 mL of solvent. From this stock solution, a series of serial dilutions were performed, ensuring a final volume sufficient for the cuvette size. UV-Vis absorbance measurements were performed in triplicate, measuring samples from lowest to highest concentrations to minimize carry-over. Both experimental compound and standard must share an excitation wavelength. Only

samples with absorbances below 0.05 at the desired excitation wavelength were used for quantum yield determination as self quenching, exciplex formation and inner-filter effects may occur at higher concentrations.

2.6.10.3 Fluorescence Measurements

Fluoresence emission was measured, using quarts cuvettes (190 – 2000 nm), by emission scan using the Felix32 software on a Photon Technology International model MP1 steady-state fluorimeter. The 'HW configuration' was set to 'digital' with an integration of 0.1 sec. Using the same excitation wavelength, each sample was scanned for emission, from lowest to highest concentration. All measurements were performed in the same sitting for accurate comparison. Emission spectra were integrated over the same wavelength ranges (encompassing the entirety of the emission peaks) between experimental compound and the standard.

2.6.10.3 Calculations

The fluorescence emission integration values were plotted against averaged absorbance values for each sample. The slope was calculated for each graph, ensuring an R^2 value above 0.8. The quantum yield was then determined using equation 2:

$$\Phi_{unknown} = \Phi_{standard} \text{ (slope unknown/slope standard)}(n_{unknown}/n_{standard}) \qquad \text{(eq. 2)}$$

Where n is the refractive index of the solvent used.

2.6.11 Fluorescent impurity observed using copper sulphate ascorbic acid conditions

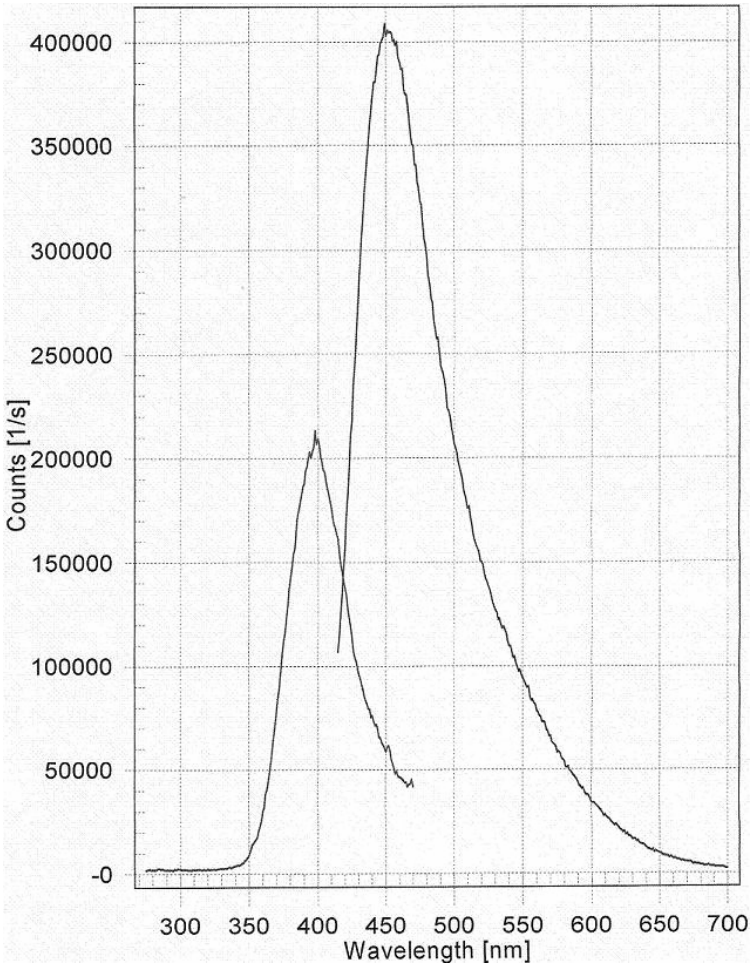

Figure 2.5. Excitation (left) and emission spectrum (right) of aqueous copper sulphate (4 M) and ascorbic acid byproduct (4 M). Excitation scan was monitored at 500 nm, and the emission scan was performed with excitation at 400 nm. Control experiments of copper sulfate or ascorbic acid alone did not show any significant fluorescence.

2.7 References

Adamczyk, M., Cornwell, M., Huff, J., Rege, S. and Rao, T.V.S. (1997) Novel 7-hydroxycoumarin based fluorescent labels. *Bioorganic & Medicinal Chemistry Letters*, 7, 1985-1988.

Alvarez, S.G. and Alvarez, M.T. (1997) A practical procedure for the synthesis of alkyl azides at ambient temperature in dimethyl sulfoxide in high purity and yield. *Synthesis-Stuttgart*, 413-414.

Angell, Y. and Burgess, K. (2007) Base dependence in copper-catalyzed Huisgen reactions: Efficient formation of bistriazoles. *Angewandte Chemie, International Edition*, 46, 3649-3651.

Beatty, K.E., Liu, J.C., Xie, F., Dieterich, D.C., Schuman, E.M., Wang, Q. and Tirrell, D.A. (2006) Fluorescence visualization of newly synthesized proteins in mammalian cells. *Angewandte Chemie, International Edition*, 45, 7364-7367.

Blum, M.M., Timperley, C.M., Williams, G.R., Thiermann, H. and Worek, F. (2008) Inhibitory potency against human acetylcholinesterase and enzymatic hydrolysis of fluorogenic nerve agent mimics by human paraoxonase 1 and squid diisopropyl fluorophosphatase. *Biochemistry*, 47, 5216-5224.

Bock, V.D., Hiemstra, H. and van Maarseveen, J.H. (2005) Cu-I-catalyzed alkyne-azide "click" cycloadditions from a mechanistic and synthetic perspective. *European Journal of Organic Chemistry*, 51-68.

Cances, E., Mennucci, B. and Tomasi, J. (1997) A new integral equation formalism for the polarizable continuum model: Theoretical background and applications to isotropic and anisotropic dielectrics. *Journal of Chemical Physics*, 107, 3032-3041.

Casida, M.E., Jamorski, C., Casida, K.C. and Salahub, D.R. (1998). *Journal of Chemical Physics*, 108, 4439.

Chinchilla, R. and Najera, C. (2007) The Sonogashira Reaction: A Booming Methodology in Synthetic Organic Chemistry *Chemical Reviews*, 107, 874-922.

Cossi, M., Scalmani, G., Rega, N. and Barone, V. (2002) New developments in the polarizable continuum model for quantum mechanical and classical calculations on molecules in solution. *Journal of Chemical Physics*, 117, 43-54.

Dreuw, A. and Head-Gordon, M. (2005) Single-Reference ab Initio Methods for the Calculation of Excited States of Large Molecules. *Chemical Reviews*, 105, 4009-4037.

Frisch, M.J., Trucks, G.W., Schlegel, H.B., Scuseria, G.E., Robb, M.A., Cheeseman, J.R., Montgomery, J.A., Jr., T.V., Kudin, K.N., Burant, J.C., Millam, J.M., Iyengar, S.S., Tomasi, J., Barone, V., Mennucci, B., Cossi, M., Scalmani, G., Rega, N., Petersson, G.A., Nakatsuji, H., Hada, M., Ehara, M., Toyota, K., Fukuda, R., Hasegawa, J., Ishida, M., Nakajima, T., Honda, Y., Kitao, O., Nakai, H., Klene, M., Li, X., Knox, J.E., Hratchian, H.P., Cross, J.B., Bakken, V., Adamo, C., Jaramillo, J., Gomperts, R., Stratmann, R.E., Yazyev, O., Austin, A.J., Cammi, R., Pomelli, C., Ochterski, J.W., Ayala, P.Y., Morokuma, K., Voth, G.A., Salvador, P., Dannenberg, J.J., Zakrzewski, V.G., Dapprich, S., Daniels, A.D., Strain, M.C., Farkas, O., Malick, D.K., Rabuck, A.D., Raghavachari, K., Foresman, J.B., Ortiz, J.V., Cui, Q., Baboul, A.G., Clifford, S., Cioslowski, J., Stefanov, B.B., Liu, G., Liashenko, A., Piskorz, P., Komaromi, I., Martin, R.L., Fox, D.J., Keith, T., Al-Laham, M.A., Peng, C.Y., Nanayakkara, A., Challacombe, M., Gill, P.M.W., Johnson, B., Chen, W., Wong, M.W., Gonzalez, C. and Pople, J.A. *Gaussian 03*, Revision B.05; Gaussian Inc., Pittsburgh, PA, 2003.

Gottlieb, H.E., Kotlyar, V. and Nudelman, A. (1997) NMR Chemical Shifts of Common Laboratory Solvents as Trace Impurities. *Journal of Organic Chemistry*, 62, 7512-7515.

Hehre, W.J., Radom, L., Schleyer, P.v.R. and Pople, J.A. (1985) *Ab Initio* Molecular Orbital Theory. John Wiley and Sons, New York et al.

Hermanson, G. (1996) Bioconjugate Techniques. Academic Press, New York.

Hsu, T.L., Hanson, S.R., Kishikawa, K., Wang, S.K., Sawa, M. and Wong, C.H. (2007) Alkynyl sugar analogs for the labeling and visualization of glycoconjugates in cells. *Proceedings of the National Academy of Sciences of the United States of America*, 104, 2614-2619.

Jacquemin, D., Preat, J., Wathelet, V., Fontaine, M. and Perpete, E.A. (2006) Thioindigo dyes: Highly accurate visible spectra with TD-DFT. *Journal of the American Chemical Society*, 128, 2072-2083.

Kage, K.L., Richardson, P.L., Traphagen, L., Severin, J., Pereda-Lopez, A., Lubben, T., Davis-Taber, R., Vos, M.H., Bartley, D., Walter, K., Harlan, J., Solomon, L., Warrior, U., Holzman, T.F., Faltynek, C., Surowy, C.S. and Scott, V.E. (2007) A high throughput fluorescent assay for measuring the activity of fatty acid amide hydrolase. *Journal of Neuroscience Methods*, 161, 47-54.

Kapanidis, A.N. and Weiss, S. (2002) Fluorescent probes and bioconjugation chemistries for single-molecule fluorescence analysis of biomolecules. *Journal of Chemical Physics*, 117, 10953-10964.

Key, J.A., Cairo, C.W. and Ferguson, M.J. (2008) 7,7 '-(3,3 '-dibenzyl-3H,3 ' H-4,4 '-bi-1,2,3-triazole-5,5 '-diyl)bis(4-methyl-2H-chromen-2-one). *Acta Crystallographica Section E-Structure Reports Online*, 64, O1910-U3631.

Knowles, P.J. and Werner, H.J. (1985) An efficient second-order MC SCF method for long configuration expansions. *Chemical Physics Letters*, 115, 259-267.

Kolancilar, H. (2002) Investigation of pechmann condensation products of ethyl acetoacetate with 2,7-dihydroxynapthalene. *Trakya Universitesi bilimsel Arasturmalar Dergisi*, 7-10.

Kolancilar, H. and Oyman, U. (2003) Investigation of the Pechmann reaction between 2,7-dihydroxynaphthalene and ethyl a cetoacetate with different condensing agents. Synthesis of benzocoumarin and benzochromone systems and their bi- and bis-derivatives. *Journal of the Indian Chemical Society*, 80, 853-857.

Lakowicz, J.R. (2006) Principles of Fluorescence Spectroscopy. Springer, New York, NY.

Laskowski, S.C. and Clinton, R.O. (1950) Coumarins .2. Derivatives of Coumarin-3-Acetic and Coumarin-4-Acetic Acids. *Journal of the American Chemical Society*, 72, 3987-3991.

Lavis, L.D. and Raines, R.T. (2008) Bright Ideas for Chemical Biology. *ACS Chemical Biology*, 3, 142-155.

LeDroumaguet, C., Wang, C. and Wang, Q. (2010) Fluorogenic click reaction. *Chemical Society Reviews*, 1233 - 1239.

Manetsch, R., Krasinski, A., Radic, Z., Raushel, J., Taylor, P., Sharpless, K.B. and Kolb, H.C. (2004) In situ click chemistry: enzyme inhibitors made to their own specifications. *Journal of the American Chemical Society*, 126, 12809-12818.

Means, G.E. and Feeney, R.E. (1990) Chemical modifications of proteins: history and applications. *Bioconjugate Chemistry*, 1, 2-12.

Meares, C. (1990) Editorial: Introduction to Bioconjugate Chemistry. *Bioconjugate Chemistry*, 1, 1-2.

Medintz, I.L., Uyeda, H.T., Goldman, E.R. and Mattoussi, H. (2005) Quantum dot bioconjugates for imaging, labelling and sensing. *Nature Materials*, 4, 435-446.

Molteni, G. (2006) 1,3-dipolar cycloadditions in aqueous media. *Heterocycles*, 68, 2177-2202.

Niemeyer, C. (2004) Bioconjugation Protocols: Strategies and Methods. Humana Press, New Jersey.

O'Reilly, R.K., Joralemon, M.J., Hawker, C.J. and Wooley, K.L. (2006) Fluorogenic 1,3-dipolar cycloaddition within the hydrophobic core of a shell cross-linked nanoparticle. *Chemistry*, 12, 6776-6786.

Padmanabhan, S., Peri, R. and Triggle, D.J. (1996) Formation of chromenes and coumarin derivatives from salicyladehydes and 2-pentenedioate: Facile route to 3-formylcoumarins. *Synthetic Communications*, 26, 827-831.

Perdew, J.P., Burke, K. and Ernzerhof, M. (1996) Generalized gradient approximation made simple. *Physical Review Letters*, 77, 3865-3868.

Rostovtsev, V.V., Green, L.G., Fokin, V.V. and Sharpless, K.B. (2002) A stepwise huisgen cycloaddition process: copper(I)-catalyzed regioselective "ligation" of azides and terminal alkynes. *Angewandte Chemie, International Edition*, 41, 2596-2599.

Sawa, M., Hsu, T.L., Itoh, T., Sugiyama, M., Hanson, S.R., Vogt, P.K. and Wong, C.H. (2006) Glycoproteomic probes for fluorescent imaging of fucosylated glycans in vivo. *Proceedings of the National Academy of Sciences of the United States of America*, 103, 12371-12376.

Seela, F., Sirivolu, V.R. and Chittepu, P. (2008) Modification of DNA with octadiynyl side chains: synthesis, base pairing, and formation of fluorescent coumarin dye conjugates of four nucleobases by the alkyne--azide "click" reaction. *Bioconjugate Chemistry*, 19, 211-224.

Seixas de Melo, J.B., RS. and Macanita, AL. (1994) Photophysical Behavior of Coumarins as a Function of Substitution and Solvent: Experimental
Evidence for the Existence of a Lowest Lying (n,π*) State. *Journal of Physical Chemistry*, 98, 6054-6058.

Sivakumar, K., Xie, F., Cash, B.M., Long, S., Barnhill, H.N. and Wang, Q. (2004) A fluorogenic 1,3-dipolar cycloaddition reaction of 3-azidocoumarins and acetylenes. *Organic Letters*, 6, 4603-4606.

Speers, A.E. and Cravatt, B.F. (2004) Profiling enzyme activities in vivo using click chemistry methods. *Chemistry & Biology*, 11, 535-546.

Stubbs, K.A., Scaffidi, A., Debowski, A.W., Mark, B.L., Stick, R.V. and Vocadlo, D.J. (2008) Synthesis and use of mechanism-based protein-profiling probes for retaining beta-D-glucosaminidases facilitate identification of Pseudomonas aeruginosa NagZ. *Journal of the American Chemical Society*, 130, 327-335.

Sun, W.-C., Gee, K.R. and Haugland, R.P. (1998) Synthesis of novel fluorinated coumarins: Excellent UV-light excitable fluorescent dyes. *Bioorganic & Medicinal Chemistry Letters*, 8, 3107-3110.

Sun, W.-C., Gee, K.R., Klaubert, D.H. and Haugland, R.P. (1997) Synthesis of Fluorinated Fluoresceins. *The Journal of Organic Chemistry*, 62, 6469-6475.

Sun, W.C., Gee, K.R. and Haugland, R.P. (1998) Synthesis of novel fluorinated coumarins: excellent UV-light excitable fluorescent dyes. *Bioorganic & Medicinal Chemistry Letters*, 8, 3107-3110.

Tao, Z.F., Qian, X.H. and Fan, M.C. (1997) Regioselective synthesis and photooxygenations of furonaphthopyrones starting from 2,7-naphthalenediol. *Tetrahedron*, 53, 13329-13338.

Timerghazin, Q.K., Carlson, H.J., Liang, C., Campbell, R.E. and Brown, A. (2008) Computational Prediction of Absorbance Maxima for a Structurally Diverse Series of Engineered Green Fluorescent Protein Chromophores. *The Journal of Physical Chemistry B*, 112, 2533-2541.

Tornoe, C.W., Christensen, C. and Meldal, M. (2002) Peptidotriazoles on solid phase: [1,2,3]-triazoles by regiospecific copper(i)-catalyzed 1,3-dipolar cycloadditions of terminal alkynes to azides. *Journal of Organic Chemistry*, 67, 3057-3064.

Valeur, B. (2002) Molecular fluorescence : principles and applications. Wiley-VCH, Weinheim.

Valizadeh, H. and Shockravi, A. (2005) An efficient procedure for the synthesis of coumarin derivatives using TiCl4 as catalyst under solvent-free conditions. *Tetrahedron Letters*, 46, 3501-3503.

Weiss, S. (1999) Fluorescence spectroscopy of single biomolecules. *Science*, 283, 1676-1683.

Werner, H.-J., Knowles, P.J. and Manby, F.R.M.S., P. Celani, G. Knizia, T. Korona, R. Lindh, A. Mitrushenkov, G. Rauhut, T. B. Adler, R. D. Amos, A. Bernhardsson, A. Berning, D. L. Cooper, M. J. O. Deegan, A. J. Dobbyn, F. Eckert, E. Goll, C. Hampel, A. Hesselmann, G. Hetzer, T. Hrenar, G. Jansen, C. Köppl, Y. Liu, A. W. Lloyd, R. A. Mata, A. J. May, S. J. McNicholas, W. Meyer, M. E. Mura, A. Nicklaß, P. Palmieri, K. Pflüger, R. Pitzer, M. Reiher, T. Shiozaki, H. Stoll, A. J. Stone, R. Tarroni, T. Thorsteinsson, M. Wang, A. Wolf . (2006) Molpro version 2006.1, A package of ab initio programs.

Werner, H.J. and Knowles, P.J. (1985) A second order multiconfiguration SCF procedure with optimum convergence. *Journal of Chemical Physics*, 82, 5053-5063.

Williams, A.T.R., Winfield, S.A. and Miller, J.N. (1983) Relative Fluorescence Quantum Yields Using a Computer-Controlled Luminescence Spectrometer. *Analyst*, 108, 1067-1071.

Wu, J., Liao, Y. and Yang, Z. (2001) Synthesis of 4-Substituted Coumarins via the Palladium-Catalyzed Cross-Couplings of 4-Tosylcoumarins with Terminal Acetylenes and Organozinc Reagents. *Journal of Organic Chemistry*, 66, 3642-3645.

Xie, F., Sivakumar, K., Zeng, Q.B., Bruckman, M.A., Hodges, B. and Wang, Q. (2008) A fluorogenic 'click' reaction of azidoanthracene derivatives. *Tetrahedron*, 64, 2906-2914.

Xie, J. and Seto, C.T. (2007) A two stage click-based library of protein tyrosine phosphatase inhibitors. *Bioorganic & Medicinal Chemistry*, 15, 458-473.

Zhou, Z. and Fahrni, C.J. (2004) A fluorogenic probe for the copper(I)-catalyzed azide-alkyne ligation reaction: modulation of the fluorescence emission via 3(n,pi)-1(pi,pi) inversion. *Journal of the American Chemical Society*, 126, 8862-8863.

Zhu, Q., Uttamchandani, M., Li, D., Lesaicherre, M.L. and Yao, S.Q. (2003) Enzymatic profiling system in a small-molecule microarray. *Organic Letters*, 5, 1257-1260.

Chapter 3

Synthesis and characterization of fluorogenic, quenched and static benzoxadiazole reactive chromophores[3]

[3] Portions of the work described in this chapter have been published in Key, J.A., Li, M.D. and Cairo, C.W. (2011) A Fluorogenic Aromatic Nucleophilic Substitution Reaction for Demonstrating Normal-Phase Chromatography and Isolation of Nitrobenzoxadiazole Chromophores. *Journal of Chemical Education*, 88, 98-100. Key, J.A. and Cairo, C.W. (2011) Identification of fluorogenic and quenched benzoxadiazole reactive chromophores. *Dyes and Pigments*, 88, 95-102. and Sandbhor, M.S., Key, J.A., Strelkov, I.S. and Cairo, C.W. (2009) A Modular Synthesis of Alkynyl-Phosphocholine Headgroups for Labeling Sphingomyelin and Phosphatidylcholine. *The Journal of Organic Chemistry*, 74, 8669-8674.

3.1 Introduction

We have previously generated a series of structurally similar fluorophores which incorporated a conjugated alkyne on a coumarin backbone (**Chapter 2**).(Key, J.A., Koh, S., et al. 2009) Upon conversion of these fluorophores to the corresponding triazole, we found that subtle differences in substitution were able to modulate changes in fluorescence arising from triazole formation. Comparison of the photophysical properties of these compounds after triazole formation identified increases in emission quantum yields of up to 9–fold, and bathochromic shifts of as much as 23 nm. Although these dyes are useful for fluorogenic labelling strategies, their relatively low brightness and short excitation wavelength inspired us to examine a new series of alkynyl- and azido-benzoxadiazole fluorophores which we expected to have longer wavelength emission.

Design of this new series took into account many considerations. We sought a fluorophore backbone that was synthetically amenable to functionalization and had readily available, inexpensive starting materials. As well, its photophysical properties should display an excitation profile that is compatible with a commonly used laser line to facilitate use in biochemical assays. Finally, we wanted to use a fluorophore backbone known to demonstrate significant changes in its photophysical properties upon chemical reaction. These 'reactive chromophores' offer the potential to greatly simplify biochemical assays and improve sensitivity.(LeDroumaguet, C., Wang, C., et al. 2010, Lemieux, G.A., de Graffenried, C.L., et al. 2003) The increased excitation or emission maxima or altered emission quantum yield of reactive chromophores have clear

advantages; however, it remains difficult to predict desired spectral changes in specific chromophores.

Nitrobenzoxadiazole (NBD) fluorophores are an important class of small molecule labels used in chemical biology and bioanalytical studies.(Lakowicz, J.R. 2006, Lavis, L.D. and Raines, R.T. 2008, Loura, L.M.S., Fernandes, F., et al. 2008) NBDs are a class of environmentally sensitive dyes which exhibit dramatic changes in excitation and emission spectra due to the polarity and hydration of their environment.(Demchenko, A.P., Mély, Y., et al. 2009) Their small size, strong fluorescence, and sensitivity to environmental changes make them ideal for biological applications. As well, NBDs are known to have excitation maxima close to the commonly used 488 nm laser line.

We chose to examine the photophysical properties of a series of alkynyl-, azido-, and triazolyl-benzoxadiazole and nitro-benzoxadiazole fluorophores. Nitro substitution at the 4-position and alkyne or azide substitution at the 5- and 7-positions were selected as they have previously been shown to strongly influence fluorescent properties.(Uchiyama, S., Santa, T., et al. 1998, Uchiyama, S., Takehira, K., et al. 2002) The modulating effects of solvent polarity, conjugation, and attachment point of the fluorochrome to the triazole were examined. Characterization of these compounds revealed that ligation to model alkynes or azides by Sharpless-Meldal reaction imparts dramatic photophysical changes to these dyes. We were able to identify reactive chromophores which act as fluorogenic, quenched, and invariant fluorescent labels. Fluorogenic dyes with increases of intensity of almost 50-fold, and quenched dyes which show an almost

500-fold loss of intensity were identified. This is the largest quantified increase in emission quantum yield for a reactive alkynyl dye, and the largest quenching effect known upon triazole formation. These reaction-sensitive dyes should be of interest for use in bioconjugate chemistry.

3.2 Fluorophore Synthesis

We identified the most direct route to substituted benzoxadiazoles as nucleophilic substitution of the appropriate halo starting materials (**Scheme 3.1**). The 5-azidomethyl-benzoxadiazole **3.2** was synthesized from commercially available 5-bromomethyl-benzoxadiazole **3.1** using sodium azide in DMSO at 45 °C in good yield. Direct substitution of the aromatic ring was accomplished by nucleophilic aromatic substitution (S_NAr) of a commercially available 5-bromo-benzoxadiazole **3.3**, to provide the 5-azido-benzoxadiazole **3.4** in quantitative yield. We employed the 4-chloro-7-nitro-benzoxadiazole (NBD-Cl) **3.5** as a common substrate for S_NAr reactions. The para-nitro substitution of the ring in addition to the oxadiazole ring allowed for excellent yields of the 4-azido-7-nitro-benzoxadiazole **3.6** upon reaction with sodium azide at room temperature. A chromophore with an unconjugated azido-group was generated by first introducing an alkylbromide via S_NAr of NBD-Cl **3.5** with bromopropylamine, providing the 7-nitro-N-(prop-2-ynyl)benzoxadiazole-4-amine **3.7**. The bromide was then converted by nucleophilic displacement with sodium azide to provide *N*-(3-azidopropyl)-7-nitro-benzoxadiazole-4-amine, **3.8**, in good yield. An alternate route was also examined, but proved to be lower yielding and more synthetically challenging. This alternate route featured the nucleophilic aromatic substitution of

NBD-Cl **3.5** with ethanolamine to generate the alcohol (**3.9**). Iodination of the alcohol to **3.10** was performed with I_2, imidazole and triphenylphosphine in modest yields. Subsequent nucleophilic displacement with sodium azide afforded the azide **3.11** in low total yield. We generated a propargyl-amine derivative using a similar route, by reaction of NBD-Cl **3.5** with propargyl-amine which provided *N*-(propynyl)-7-nitro-benzoxadiazole-4-amine, **3.12**, in moderate yield.

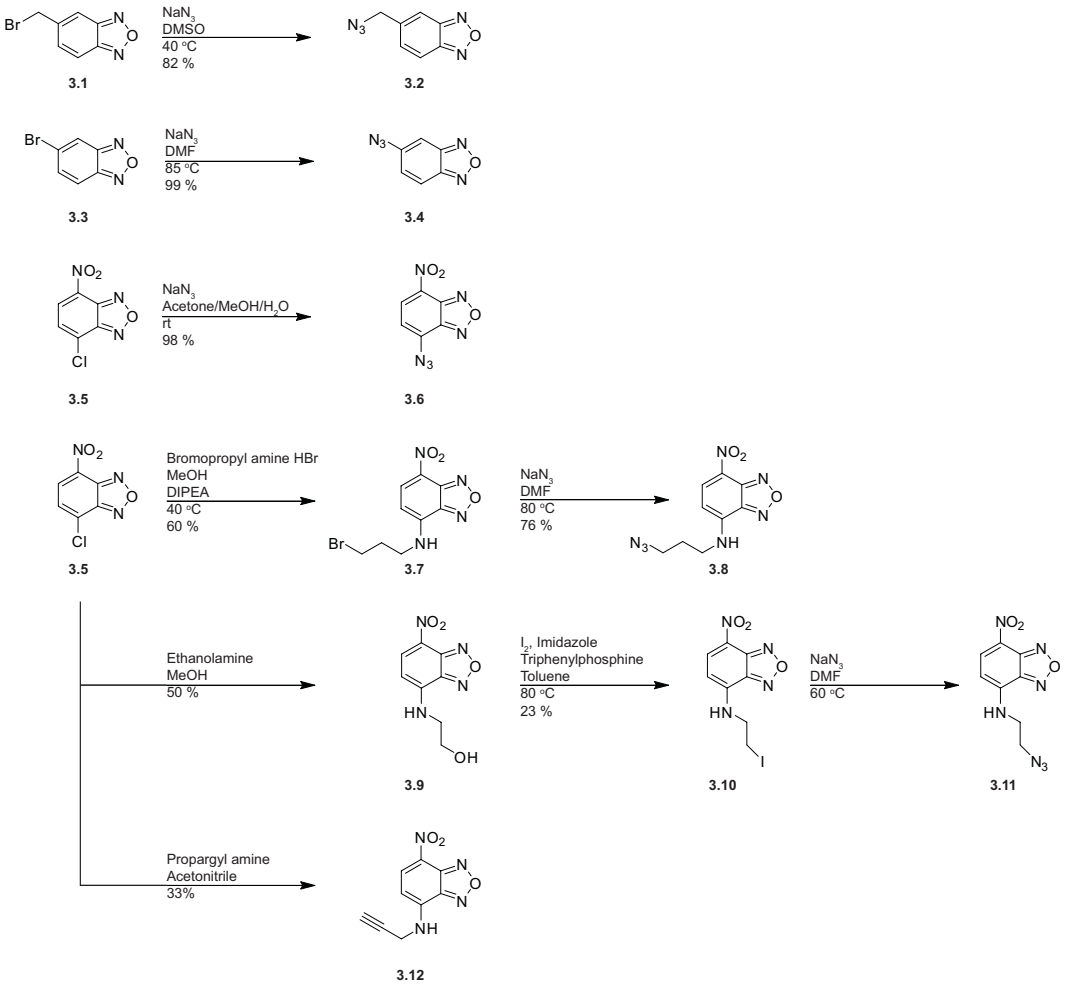

Scheme 3.1. Synthetic scheme for the generation of azido and alkynyl benzoxadiazoles. Azides and alkyne were generated by bimolecular nucleophilic substitution, S_NAr or a combination of both.

Additional nucleophilic aromatic substitutions of NBD-Cl (**3.5**) were examined using a variety of substrates, giving insight into the scope of this reaction (**Scheme 3.2**). Generally, it was found that more basic amine nucleophiles such as piperidine (pKa 11, formation of **3.17**) had faster reaction times and higher yields than less basic amines such as glycine (pKa 9.6, formation of **3.14**) and hydroxyl nucleophiles which required higher reaction temperatures or addition of a base, such as sodium carbonate, to force the reaction. This conforms to expectations, as typically the rate determining step is nucleophilic attack at the ipso carbon (**Figure 3.1**). Base catalysis is believed to aid during the second step of the reaction, by accelerating the removal of Hydrogen from a less stable zwitterionic intermediate (**Figure 3.1B**).(Smith, M.B. and March, J. 2007) Polar solvents were found to be beneficial, however they must be chosen carefully as solvolysis by-products may be observed. In the attempted synthesis of phenol **3.16** if methanol is used as a co-solvent, with water and sodium carbonate, a methoxy byproduct (**3.15**) is observed in a 1:5 ratio with phenol **3.16**.

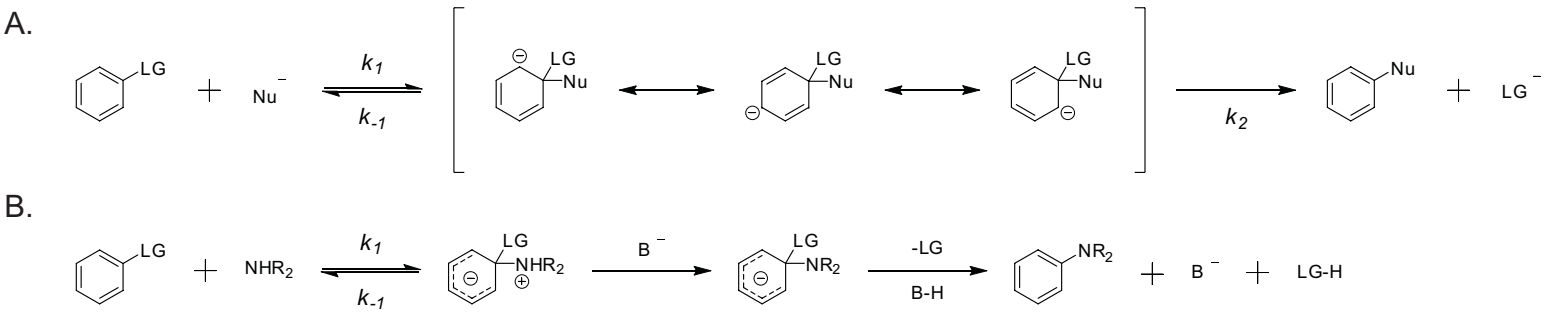

Figure 3.1. Nucleophilic aromatic substitution (S_NAr) mechanism. A) Generic mechanism. **B)** Base-catalyzed mechanism. LG = leaving group, B = base, Nu = nucleophile.(Smith, M.B. and March, J. 2007)

The benzoxadiazole backbone is also amenable to further functionalization by Electrophilic Aromatic Substitution (EAS) (**Scheme 3.3**). Nitration and sulphonation of commercially available 5-halo benzoxadiazoles is possible at the 4- position in moderate yield (33-48%). Sulphonation can be performed by heating in neat chlorosulphonic acid giving the sulphonyl chlorides (**3.19**, **3.22**) followed by substitution to the sulphonate by heating in the presence of mild aqueous bases.(Dorogov, M.V., Filimonov, S.I., et al. 2004) Extreme caution should be observed when working with chlorosulphonic acid, it is extremely hazardous and highly reactive with moisture. Attempts to substitute the sulphonyl chlorides and sulphonates with sodium azide in DMF proved problematic. Sulphonyl chloride **3.19** rapidly formed an undesired, potentially highly explosive diazide **3.21** at room temperature. However, sulphonate **3.20** reacted much more slowly, giving mixtures of starting material, amine and sulphonamide decomposition by-products and trace amounts of the 5-azido product (observed by mass spectrometry) at a range of temperatures (45-80 ^{o}C).

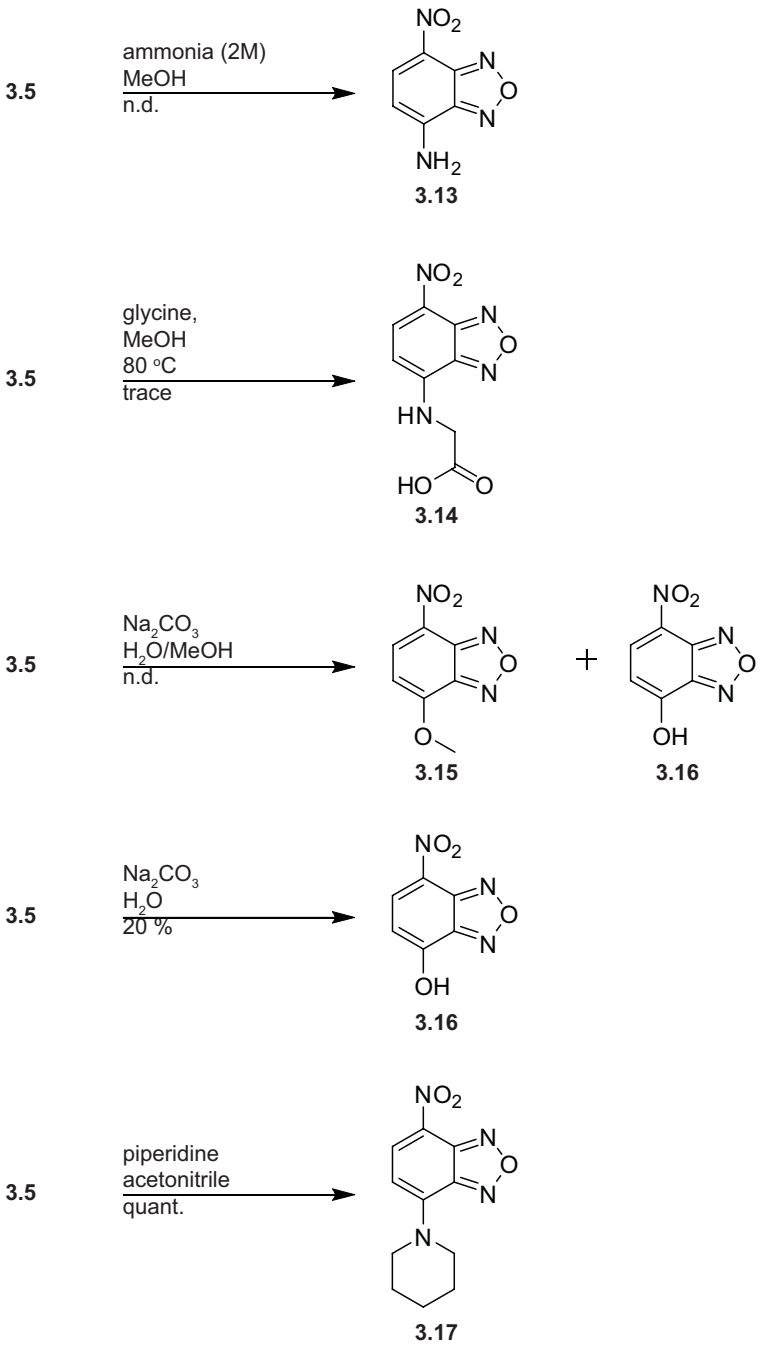

Scheme 3.2. Synthetic scheme of the generation of S_NAr products from NBD-Cl (3.5). Reactivity roughly follows trends in nucleophile basicity. Reactions denoted with n.d. or trace had very low yields, however, enough material was purified to characterize by at least ^1H NMR.

The 5-halo-4-nitro-benzoxadiazoles (**3.23**, **3.24**) were generated in moderate yields by standard nitration methodology using nitric acid and sulphuric acid. Attempts at azide substitution of compound **3.23** to 5-azido-4-nitrobenzoxadiazole proved unsuccessful. At 45 ^{o}C, using sodium azide in DMF, many decomposition products could be observed by TLC, however, at room temperature little reactivity was observed. The unusual reactivity of these compounds hindered this line of investigation. We chose to refocus our efforts on the 5-halo benzoxadiazole and 4-nitro-7-chloro-benzoxadiazole backbones.

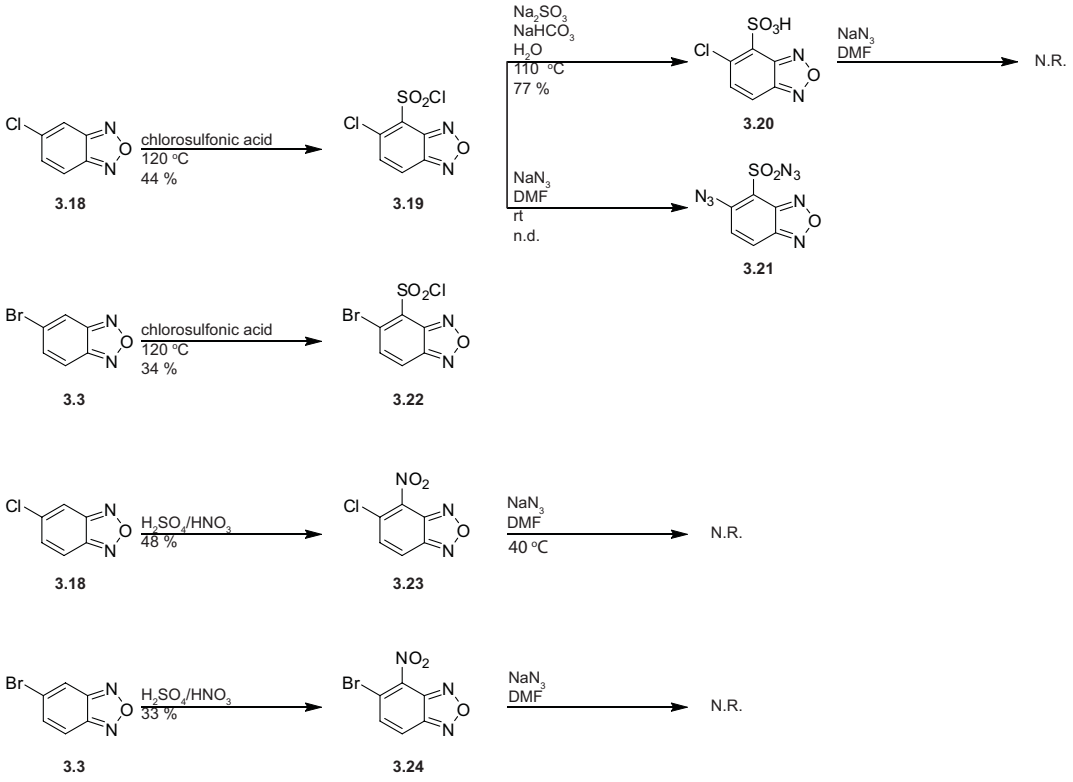

Scheme 3.3. Synthetic scheme examining EAS products of 5-halo benzoxadiazoles 3.3 and 3.18. EAS occurred primarily at the 4- position in moderate yield (33-48%). Further elaboration of EAS products proved difficult, requiring additional studies.

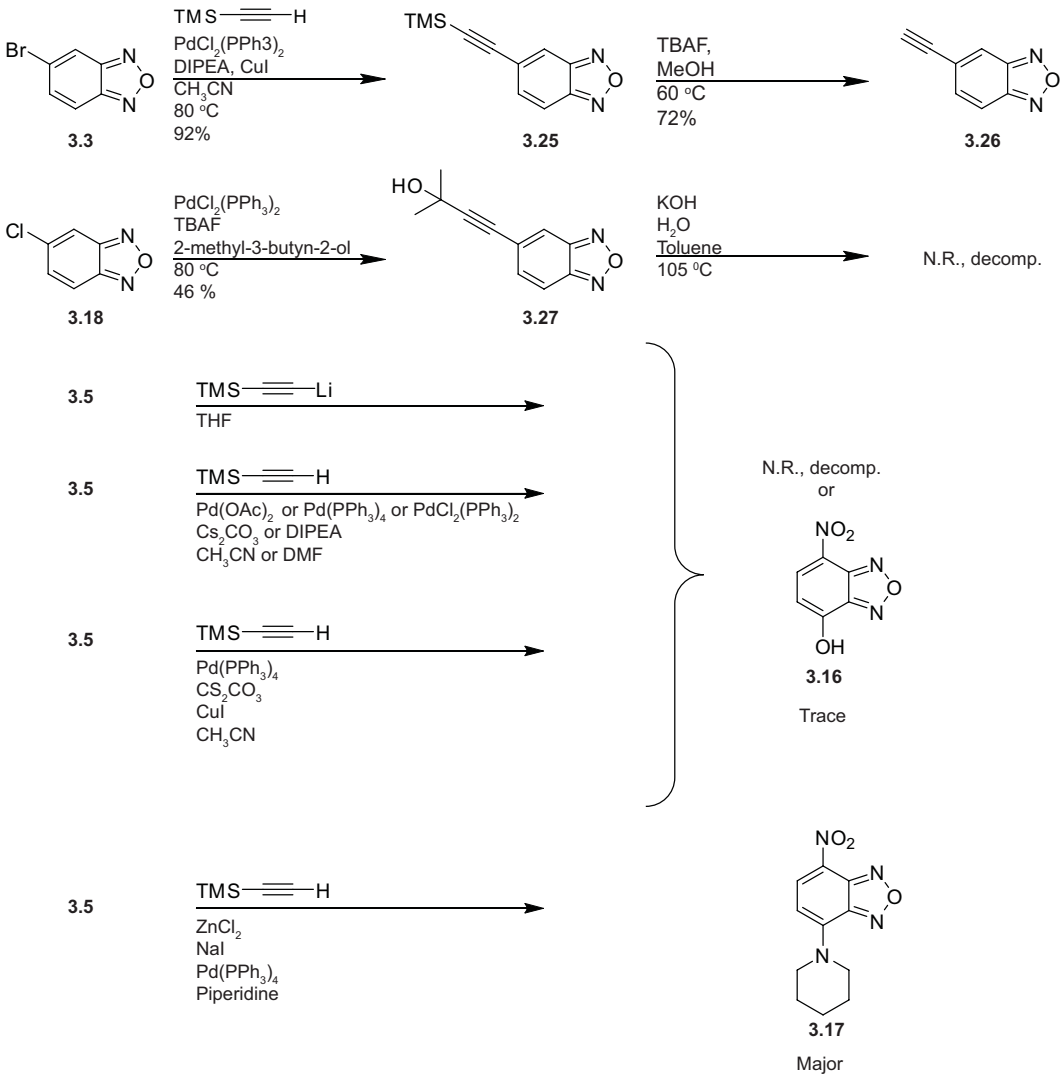

Scheme 3.4. Synthetic scheme of alkynyl benzoxadiazoles generated by Sonogashira alkynylation of benzoxadiazoles 3.3, 3.18 and 3.5. Reactions of the 5-halo benzoxadiazoles (**3.3** and **3.18**) can be successfully alkynylated by Sonogashira cross-coupling. However, NBD-Cl (**3.5**) formed undesired side products (**3.16** and **3.17**) or did not react.

To install an alkyne group directly onto the benzoxadiazole, we investigated application of Pd-catalyzed Sonogashira cross-coupling (**Scheme**

3.4).(Key, J.A., Koh, S., et al. 2009) The 5-trimethylsilylethynyl-benzoxadiazole, **3.25**, was generated from bromide **3.3** by reaction with trimethylsilyl acetylene under standard conditions in excellent yield. Compound **3.25** was then deprotected using tetrabutylammonium fluoride (TBAF) to afford the 5-ethynyl-benzoxadiazole, **3.26**, in good yield. An alternative methodology, using a copper, base, and solvent-free variant of Sonogashira cross-coupling is known.(Liang, Y., Xie, Y.-X., et al. 2005) Using this protocol we obtained the protected alkynyl derivative **3.27** in moderate yield, however, the strongly basic conditions required for deprotection resulted in decomposition. Direct alkynylation was attempted on NBD-Cl, **3.5**, using a variety of conditions; however, the extreme reactivity of this substrate towards S_NAr substitution interfered. Several palladium catalysts and alternative bases were examined in acetonitrile and DMF, however all conditions failed to produce the desired alkynyl product. Trimethylsilyl ethynyl lithium was generated *in situ* and reacted with NBD-Cl, however, again the desired alkynyl product was not observed. We proceeded to study the properties of the alkyne derivatives we were able to obtain.

With azide and alkyne benzoxadiazole derivatives (**3.2, 3.4, 3.6, 3.8, 3.12,** and **3.26**) in hand, we examined the properties of the dyes and their click-reaction products. Azide and alkyne dyes were reacted with either *n*-octyne or benzylazide, respectively (**Scheme 3.5**).

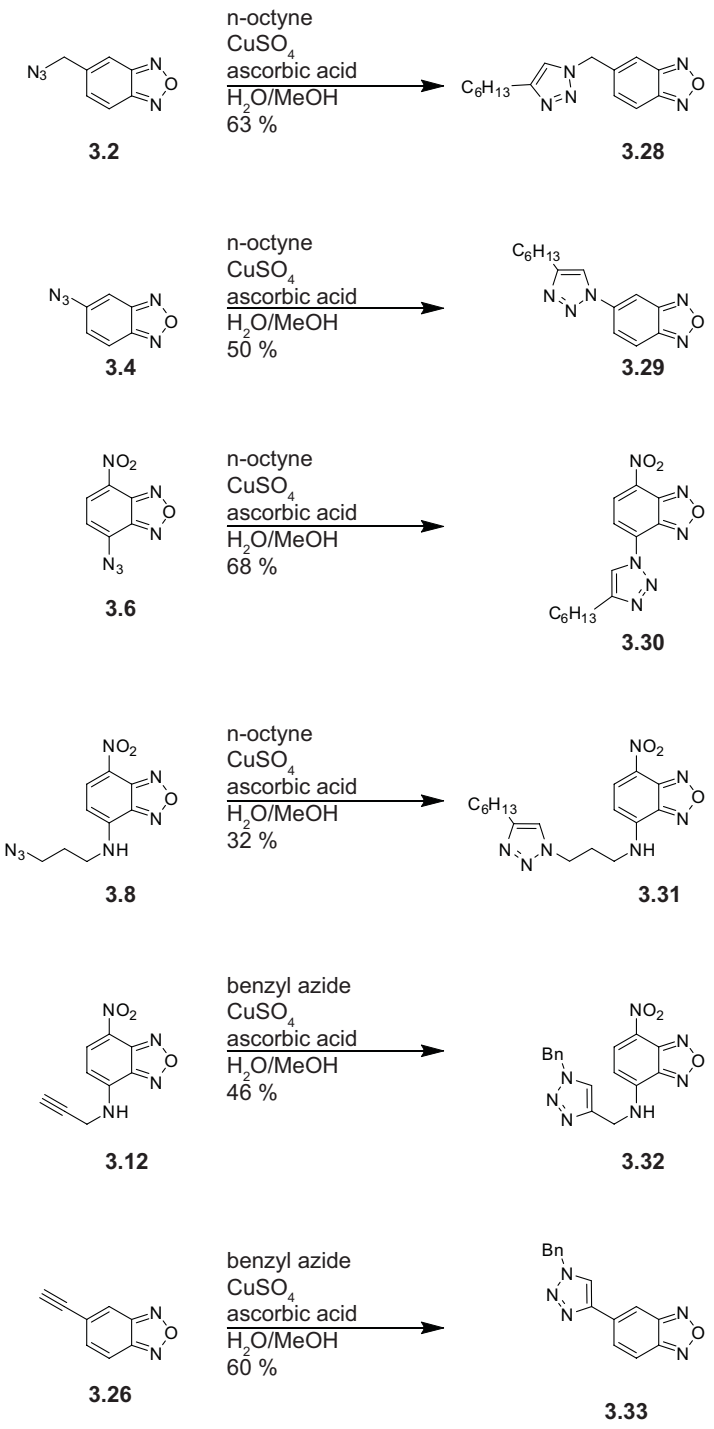

Scheme 3.5. Synthetic scheme for the generation of triazole click products by Sharpless-Meldal reaction of azido and alkynyl benzoxadiazoles. Azido compounds were reacted with n-octyne to mimic an alkynyl lipid side chain, while alkynes were reacted with benzyl azide under aqueous conditions.

A variety of conditions are known for the Sharpless-Meldal reaction; however, care must be taken when choosing appropriate reaction conditions to avoid undesired 5,5-bistriazole side products when using alkynyl fluorophores.(Angell, Y. and Burgess, K. 2007, Key, J.A., Cairo, C.W., et al. 2008, Meldal, M. and Tornoe, C.W. 2008) Variables can include the choice of copper source, reducing agent, ligand/base, and solvent conditions. Copper sulphate with ascorbic acid in a 1:1 methanol/water mixture gave consistent yields in our hands.(Key, J.A., Koh, S., et al. 2009) The alkynes (**3.12**, **3.26**) were reacted with benzyl azide, a substrate that lacks conjugation to the alkyne in order to mimic the triazole product of a bioconjugate addition. The azide benzoxadiazoles (**3.2**, **3.4**, **3.6**, and **3.8**) were subjected to click reaction conditions with n-octyne, an alkynyl mimic of a lipid acyl chain. Yields and reaction times varied between 32 - 68% and 0.75 - 6 h for the fluorophore substrates. Compounds **3.4**, **3.8** and **3.12** gave the lowest yields and required the longest reaction times.

3.3 Fluorophore characterization

To quantitate the utility of these dyes as reactive chromophores, changes in photophysical properties were determined after triazole formation. We isolated and characterized the alkynyl (**3.12**, **3.26**), azido (**3.2**, **3.4**, **3.6**, **3.8**), and triazolyl compounds (**3.28**-**3.33**) in both polar and non-polar solvents. Absorbance, fluorescence emission, molar absorption coefficient, emission quantum yield, and brightness were determined (**Table 3.1**). Spectral characterization was performed in ethanol and *n*-hexane, using quinine sulphate in 0.5 M sulphuric acid,

Cmpd	*Abs (nm)*[a]	*Em (nm)*	*ε*	*Φ*[b]	*ΔΦ*[c]	*Brightness*	*Δ Brightness*[d]
3.2	**278**, 290	nd	7100	nd	na	na	na
3.28	**278**, 289	nd	8400	nd	na	na	na
3.4	**286**, 298, 329	481	30400	0.003	na	91.2	na
3.29	**301**	406	7800	0.003	1.0	0.2	0.02
3.6	**388**, 454	530	14100	0.47	na	6630	na
3.30	267, **371**	539	26000	<0.001	<0.002	<52	<0.008
3.8	331, **461**	524	22100	0.51	na	11300	na
3.31	329, **461**	524	38600	0.52	1.0	20100	1.83
3.12	324, **453**	517	34300	0.57	na	19600	na
3.32	326, **453**	522	16300	0.58	1.0	9450	0.48
3.26	**300**	428	45600	0.001	na	31.9	na
3.33	293, **305**, 325	421	18300	0.048	48	878	28

Table 3.1. Spectral properties of benzoxadiazoles in ethanol

a. Absorbance maxima are listed with the most intense peak shown in bold face

b. Quantum yield standards were quinine sulphate in 0.5 M sulphuric acid, fluorescein in 0.1 M sodium hydroxide or rhodamine 6G in ethanol

c. $\Delta\Phi$ calculated as $\Phi_{\text{click product}}/\Phi_{\text{azide or alkyne}}$

d. Δ Brightness calculated as $\text{brightness}_{\text{click product}}/\text{brightness}_{\text{azide or alkyne}}$

Cmpd	*Abs (nm)*[a]	*Em (nm)*[b]	ε^c	Φ	$\Delta\Phi^d$	*Brightness*	Δ *Brightness*
3.2	**278**, 289	nd	24300	nd	na	na	na
3.28	**278**, 289	nd	11200	nd	na	na	na
3.4	**275**, 285, 297, 325	424	9000	0.01	na	304	na
3.29	290, **300**, 318	370	18900	0.002	0.2	15.6	0.05
3.6	260, **375**	522	30500	0.03	na	915	na
3.30	260, **380**	501	21900	<0.001	<0.03	<21.9	0.02
3.8	305, **420**	523	12200	<0.001	na	<12.2	na
3.31	nd	nd	nd	nd	na	na	na
3.12	296, **410**	520	17100	0.28	na	4790	na
3.32	347, 467, **504**	525	28300	0.02	0.07	566	0.12
3.26	**283**, 298	406	4800	0.008	na	38	na
3.33	293, **305**, 324	375	9000	0.008	1.0	72	1.9

Table 3.2. Spectral properties of benzoxadiazoles in *n*-hexane

a. Absorbance maxima are listed with the most intense peak shown in boldface

b. Quantum yield standards were quinine sulphate in 0.5 M sulphuric acid, fluorescein in 0.1 M sodium hydroxide or rhodamine 6G in ethanol

c. $\Delta\Phi$ calculated as $\Phi_{\text{click product}}/\Phi_{\text{azide or alkyne}}$

d. Δ Brightness calculated as $\text{brightness}_{\text{click product}}/\text{brightness}_{\text{azide or alkyne}}$

fluorescein in 0.1 M sodium hydroxide or rhodamine 6G in ethanol as fluorescence standards (See section 2.10).

In general, the NBD fluorophores showed greater absorbance, emission, emission quantum yield and brightness, and had greater solubility in ethanol (**Tables 3.1** and **3.2**). Substitution of the nitro group on the benzoxadiazole ring system resulted in longer wavelength excitation/emission and increased in the emission intensity and emission quantum yield. These observations correspond well with previous reports linking enhanced fluorescence to an electron rich and polarized benzoxadiazole ring, presumably via an intramolecular charge transfer fluorescent excited state.(Uchiyama, S., Santa, T., et al. 1998, Uchiyama, S., Santa, T., et al. 1999) Strong electron donating or withdrawing groups, such as the nitro group in compounds **3.6**, **3.8**, and **3.12**, increase the dipole moment contributing to greater charge transfer character. The observed fluorescence enhancement in the more polar ethanol may be attributed to relaxation of this charge transfer excited state by the solvent dipole.(Lakowicz, J.R. 2006) The benzoxadiazole core can still have a remarkably strong absorbance even in the absence of the nitro group, as seen in compound **3.4**, however the low emission quantum yield of this dye reduces its overall brightness.

Our results show several interesting trends upon fluorophore conversion from alkyne or azide to triazole when measured in ethanol. Azide **3.6** has been recently examined for its use as a photoactivatable probe, and was observed to undergo photochemical conversion to a more fluorescent amine upon UV irradiation.(Lord, S.J., Lee, H.-l.D., et al. 2009) In our experiments we examined

the properties of this dye before and after conversion to a triazole derivative. Conjugated azido-benzoxadiazoles (**3.4**, **3.6**) exhibited a significant quenching effect upon triazole formation (**3.29**, **3.30**) (**Figure 3.2**). The emission quantum yield of compound **3.6** decreases from 0.47 to <0.001 upon forming the click-reaction product **3.30** (470-fold). To the best of our knowledge, this is the first example of such a significant quenching effect upon triazole formation. This trend was also observed in *n*-hexane, but to a lesser extent (30-fold).

In contrast, the conjugated 5-ethynyl-benzoxadiazole **3.26** shows a 48-fold increase in emission quantum yield upon formation of triazole **3.33** (**Figure 3.3**). These results demonstrate the extreme sensitivity of the NBD fluorophore, as triazole products **3.29** and **3.30**, differ only in the triazole attachment point to the fluorochrome. From these observations we conclude that linkage of the triazole through *N*1 results in quenching and attachment through *C*4 results in fluorogenicity. This trend differs from that previously seen with 1,8-napthalimides, where linkage of the triazole through the *N*1 and *C*4 both elicit an increase in fluorescence.(Sawa, M., Hsu, T.L., et al. 2006) However, it should be noted that a larger emission quantum yield (0.36) was observed for the *C*4 linked 1,8-napthalimide than the *N*1-linked (0.29).(Sawa, M., Hsu, T.L., et al. 2006)

Fluorophores which feature alkyne and azide moieties that are not conjugated to the benzoxadiazole core (**3.2**, **3.8**, **3.12**) exhibited only minor changes in molar absorption coefficient (ε) upon triazole formation, resulting in small changes to their brightness, while their emission quantum yields remained fairly constant (**Figure 3.4**).

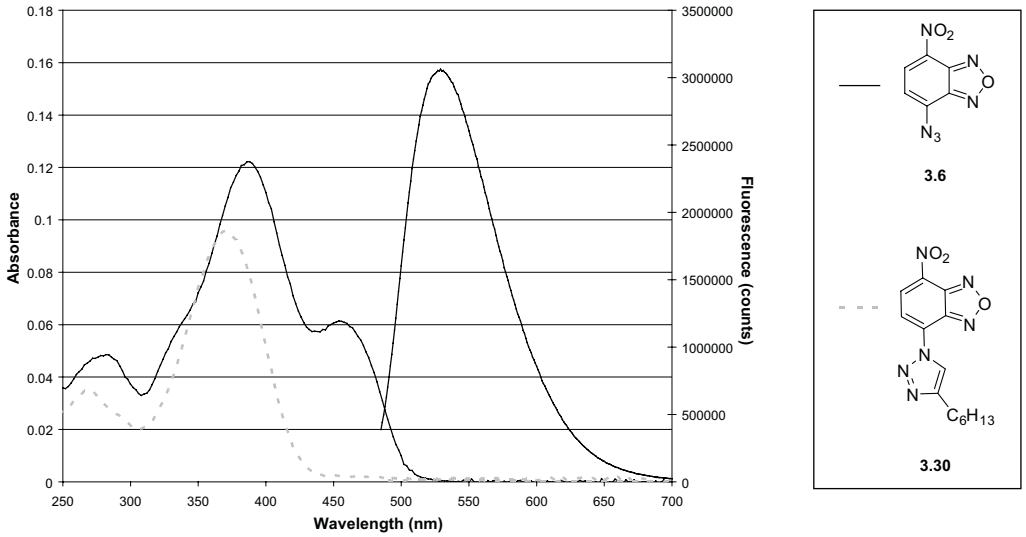

Figure 3.2. Equimolar Absorbance and fluorescence emission of azide 3.6 and triazole 3.30. Spectra were obtained at equimolar concentrations in EtOH, excitation 470 nm.

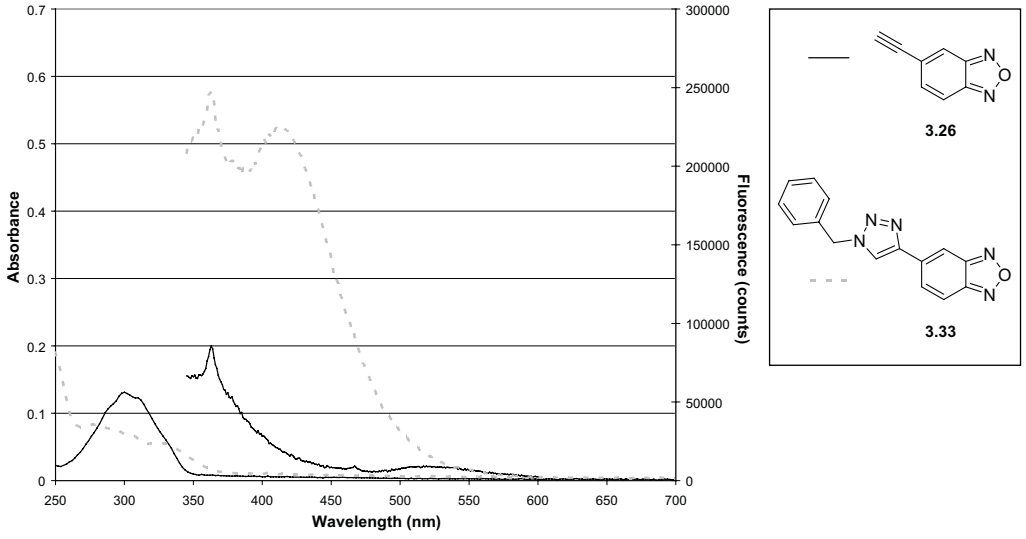

Figure 3.3. Equimolar Absorbance and fluorescence emission of alkyne 3.26 and triazole 3.33. Spectra were obtained at equimolar concentrations in EtOH, excitation 330 nm.

Although azide **3.2** and triazole **3.28** have very low fluorescence in both *n*-hexane and ethanol, an alkynyl sphingomyelin analogue **3.35** was labelled with azide **3.2** to give triazole **3.36** which exhibited stronger fluorescence in other solvent environments (**Scheme 3.6**).(Sandbhor, M.S., Key, J.A., et al. 2009) The absorption coefficient and brightness decreased approximately 52% upon conversion of azide **3.8** to triazole **3.31**. However, the opposite effect was observed for alkyne **3.12**, nearly doubling upon conversion to triazole **3.32**.

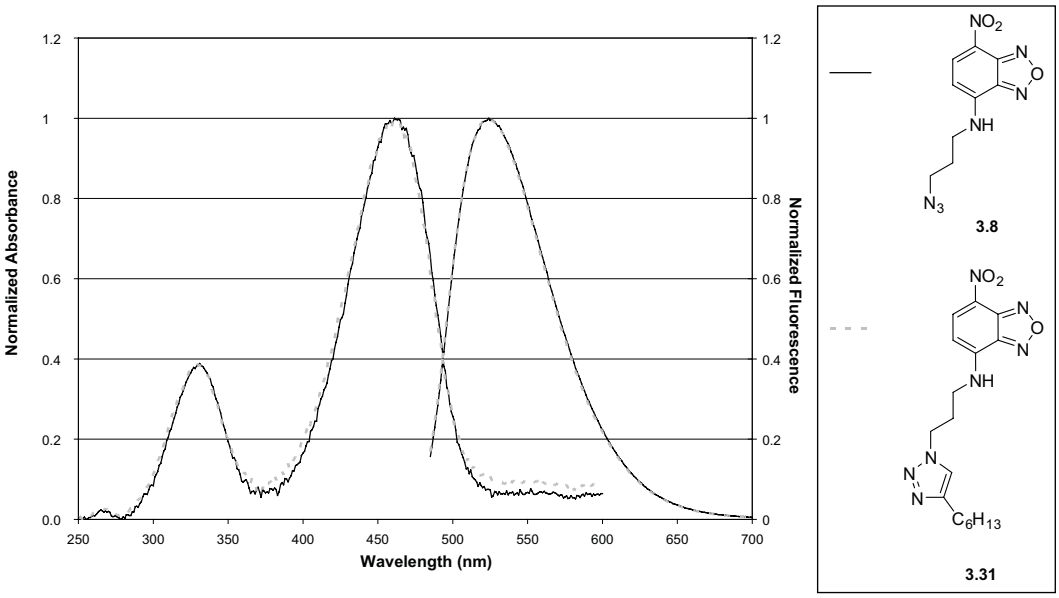

Figure 3.4. Normalized Absorbance and fluorescence emission of azide 3.8 and triazole 3.31. Spectra were obtained in EtOH, excitation 470 nm.

Our results add important new examples of reactive chromophores based upon triazole formation as a result of the Sharpless-Meldal reaction. We have identified a series of reactive chromophores based on the NBD core, exhibiting a range of activities including dramatic quenching and fluorogenic effects. Notably, the quenching observed upon conversion of compound **3.6** to **3.30** exceeds the

fluorogenic increase observed in previous reports.(Sawa, M., Hsu, T.L., et al. 2006, Sivakumar, K., Xie, F., et al. 2004, Zhou, Z. and Fahrni, C.J. 2004) As well, the 48-fold increase in emission quantum yield and 28-fold increase in brightness upon conversion of alkyne **3.26** to triazole **3.33** significantly exceeds the results observed in our previous studies with a series of alkynyl coumarin derivatives and other alkynyl fluorophores in previous reports.(Key, J.A., Koh, S., et al. 2009, Zhou, Z. and Fahrni, C.J. 2004)

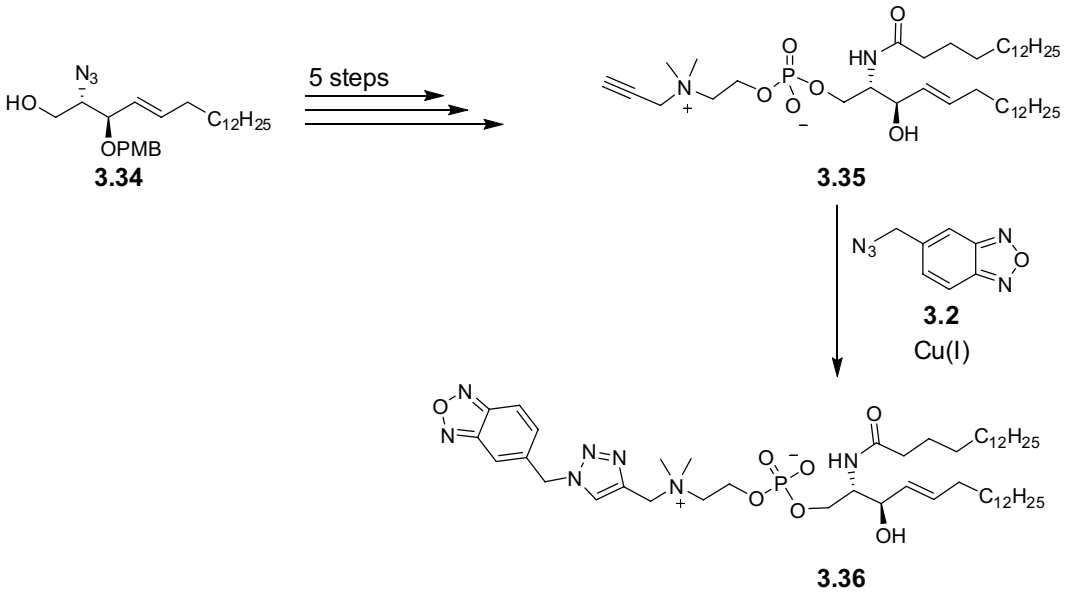

Scheme 3.6. Synthesis of sphingomyelin probe 3.36. Alkynyl phospholipid analogue **3.35** was synthesized in 5 steps in 53% yield from **3.34**, then substituted with azido-substituted benzoxadiazole probe (**3.2**) to generate the triazole product **3.36**.(Sandbhor, M.S., Key, J.A., et al. 2009)

3.4 Conclusion

The reactive chromophores studied here will be useful for a variety of labelling strategies in bioconjugate chemistry. The benzoxadiazole derivatives

reported were generated in good yield using nucleophilic substitution of commercially available starting materials. The 5-ethynyl-benzoxadiazole, **3.26**, shows a dramatic fluorogenic increase in emission quantum yield (48–fold) and brightness upon conversion to the triazole, **3.33**. While the NBD-azide, **3.6**, undergoes a dramatic quenching (470–fold) after conversion to triazole **3.30**. The alkynyl- and azido-NBD amines (**3.8** and **3.12**) and their triazole products (**3.31** and **3.32**) exhibit high quantum yields and brightness, and should be suitable for use with 488 nm laser line. The NBD backbone is amenable to functionalization using S_NAr and EAS strategies, generally following trends in reactivity as previously described in the literature. Taking advantage of this reactivity, novel probes may be developed by substitution of the NBD core, including potentially fluorogenic bioorthogonal labels.

3.5 Experimental

3.5.1 General

Reagents were purchased reagent grade from commercial sources such as Sigma-Aldrich (Oakville, Ont) and used without additional purification. ^{1}H and ^{13}C NMR were performed on Varian 300, 400, or 500 MHz instruments at room temperature as noted. Deuterated solvents were obtained from Cambridge Isotope Laboratories (Andover, MA). CD_3OD, $(CD_3)_2SO$, and $CDCl_3$ solvent peaks (3.31, 2.50, and 7.26 ppm for ^{1}H; 49.0, 39.5, and 77.2 ppm for ^{13}C, respectively) were used as internal chemical shift references. Some spectra contain small amounts of contaminating solvents.(Gottlieb, H.E., Kotlyar, V., et al. 1997) Mass spectrometry was performed using an MS-50G positive electron impact

instrument from Kratos Analytical (Manchester, UK) and a Mariner Biospectrometry positive ion electrospray instrument from Applied Biosystems (Foster City, CA).

3.5.2 Spectroscopy

Absorbance spectra for all compounds were collected at room temperature with a Hewlett-Packard (Palo Alto, CA) model 8453 diode array UV-visible spectrophotometer or Varian (Walnut Creek, CA) Cary 50 spectrophotometer. Absorbance measurements were taken using Eppendorf (Hamburg, Germany) UVette cuvettes (220 – 1600 nm) or NSG Precision Cells (Farmingdale, NY) ES quartz cuvettes (190 – 2000 nm). Fluorescence spectra for all compounds were collected at room temperature with a Photon Technology International (Birmingham, NJ) model MP1 steady-state fluorimeter. Fluorescence measurements were taken using NSG Precision Cells (Farmingdale, NY) ES quartz cuvettes (190 – 2000 nm).

3.5.3 Synthesis

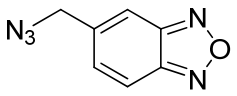

5-(Azidomethyl)benz-[2,1,3-*d*]-oxadiazole (**3.2**).

5-(Bromomethyl)benzoxadiazole (**3.1**) (200 mg, 0.93 mmol, 1 equiv) was dissolved in DMSO (15 mL), followed by the addition of sodium azide (0.57 g, 8.8 mmol, 1.5 equiv). The reaction mixture was heated to 40 °C, then quenched after 45 m with distilled water. Extraction was performed with diethyl ether, followed by water and brine washes. The organic layer was dried over $MgSO_4$

and concentrated in vacuo giving a yellow oil (133 mg, 82%). ^{1}H NMR (400 MHz, $CDCl_3$): δ 7.90 (d, 1H, ^{3}J = 10.4 Hz), 7.80 (s, 1H), 7.36 (d, 1H, ^{3}J = 10.4 Hz), 4.51 (s, 2H); ^{13}C NMR (100 MHz, $CDCl_3$) δ 149.0, 148.7, 139.5, 131.7, 117.3, 114.2, 54.2. IR (neat film): ν = 3064, 2107, 1635 cm^{-1}; EI-HRMS calculated for $C_7H_5N_5O$: 175.0494; observed: 175.0495. R_f = 0.50 (1:3 EtOAc/hexanes).

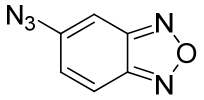

5-Azidobenz-[2,1,3-*d*]-oxadiazole (**3.4**).

5-bromobenzoxadiazole (**3.3**) (200 mg, 1 mmol, 1 equiv) was dissolved in dimethylformamide (20 mL). Sodium azide (195 mg, 3 mmol, 3 equiv) was then added and the reaction mixture was heated at 85 ^{o}C for approximately 24 h. The reaction was then quenched with distilled water, and extracted with ethyl ether. The organic layer was then dried over $MgSO_4$, concentrated in vacuo giving a yellow solid which was purified by gradient flash column chromatography (EtOAc/hexanes). The product was obtained in 99% yield as a brown-yellow powder (160 mg, 99%). 98.9-100.0 ^{o}C; ^{1}H NMR (400 MHz, $CDCl_3$): δ 7.85 (dd, 1H, ^{4}J = 0.96 Hz, ^{3}J = 9.6 Hz), 7.39 (dd, 1H, ^{4}J = 0.96 Hz, ^{4}J = 1.96 Hz), 7.07 (dd, 1H, ^{4}J = 1.96 Hz, ^{3}J = 9.6 Hz); APT ^{13}C NMR (100 MHz, $CDCl_3$): δ 149.5, 147.9, 144.0, 127.8, 118.6, 101.9; IR (microscope): ν = 3119, 3058, 3050, 2177, 2136, 1626, 1536 cm^{-1}; EI-HRMS calculated for $C_{12}H_{14}O$: 161.0338; observed: 161.0337. R_f = 0.71 (1:3 EtOAc/hexanes).

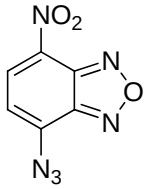

4-Azido-7-nitrobenz-[2,1,3-*d*]-oxadiazole (**3.6**).

4-Chloro-7-nitrobenzoxadiazole (**3.5**) (250 mg, 1.25 mmol, 1 equiv) was dissolved in 10 mL of 1:1 acetone/methanol. Sodium azide (90 mg, 1.38 mmol, 1.1 equiv) was then dissolved in 1:2:1 acetone/methanol/water and added slowly. The reaction was allowed to proceed at room temperature for approximately 1 h until the starting material was not visible by TLC. Solvent was removed in vacuo, and the resulting residue was recrystallized with 100% ethanol and allowed to cool at -20 °C giving brown-yellow crystals (252 mg, 98%). m.p. 95.3-97.0 ^{o}C; ^{1}H NMR (400 MHz, $CDCl_3$): δ 8.53 (dd, 1H, ^{4}J = 0.64 Hz,^{3}J = 8.0 Hz), 7.08 (dd, 1H, ^{4}J = 0.64 Hz,^{3}J = 8.0 Hz); APT ^{13}C NMR (100 MHz, $CDCl_3$): δ 145.9, 143.5, 138.1, 132.5, 132.1, 114.9; IR (cast film): ν = 3092, 2139, 2118, 1536, 1338 1321 cm^{-1}; EI-HRMS calculated for $C_6H_2N_6O_3$: 206.0188; observed: 206.0187. R_f = 0.33 (1:3 EtOAc/hexanes).

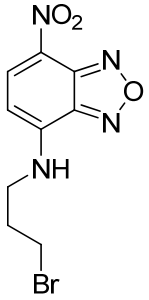

***N*-(3-Bromopropyl)-7-nitrobenzo-[2,1,3-*d*]-oxadiazol-4-amine** (**3.7**).

4-Chloro-7-nitrobenzoxadiazole (**3.5**) (200 mg, 1 mmol, 1 equiv) and bromopropyl amine·HBr (658 mg, 3 mmol, 3 equiv) were dissolved in methanol

(8 mL) and heated to 40 °C. DIPEA (0.2 mL, 1.14 mmol, 1.1 equiv) was then added, turning the reaction mixture a dark red colour. Upon consumption of starting materials by TLC (approximately 6 h), the solvent was removed in vacuo. The resulting red oily residue was purified by column chromatography (EtOAc/hexanes), obtained as an orange-brown powder (180 mg, 60%). m.p. 72.1-73.8 °C; ^{1}H NMR (400 MHz, CD_3OD): δ 8.46 (d, 1H, ^{3}J = 8.8 Hz), 6.33 (d, 1H, ^{3}J = 9.2 Hz), 3.71 (broad s, 2H), 3.59 (t, 2H, ^{3}J = 6.8 Hz), 3.31 (q, 2H, ^{4}J = 1.64 Hz), 2.30 (q, 2H, ^{4}J = 6.8 Hz); ^{13}C NMR (100 MHz, CD_3OD): δ 146.6, 145.9, 145.5, 138.3, 123.5, 99.8, 43.2, 32.4, 31.1; IR (microscope): ν = 3382, 3096, 2967, 2922, 1621, 1586 , 1502, 1357 and 1334, cm^{-1}; ES-HRMS calculated for $C_9H_9N_4O_3Na$: 322.9750; observed: 322.9755. R_f = 0.67 (3:2 EtOAc/hexanes);

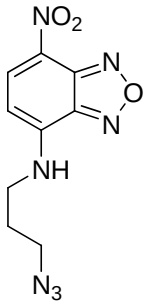

***N*-(3-Azidopropyl)-7-nitrobenz-[2,1,3-*d*]-oxadiazol-4-amine** (**3.8**).

N-(3-Bromopropyl)-7-nitrobenzoxadiazol-4-amine (**3.7**) (76 mg, 0.254 mmol, 1 equiv) and sodium azide (50 mg, 0.762 mmol, 3 equiv) were dissolved in dimethylformamide and heated at 80 °C for approximately 3 h. The reaction was quenched with distilled water and extracted with ethyl ether. Water and brine washes were performed, the organic layer was then dried over $MgSO_4$ and concentrated in vacuo. Purification was performed by column chromatography (EtOAc/hexanes). The product was obtained as an orange powder (50 mg, 76%).

m.p. 68.7-70.4 °C; ^{1}H NMR (400 MHz, $CDCl_3$): δ 8.49 (d, 1H, ^{3}J = 8.4 Hz), 6.60 (broad s, 1H), 6.24 (d, 1H, ^{3}J = 8.8 Hz), 3.68 (q, 2H, ^{3}J = 6.8 Hz), 3.62 (t, 2H, ^{3}J = 6.8 Hz), 2.11 (q, 2H, ^{3}J = 6.8 Hz); ^{13}C NMR (100 MHz, $CDCl_3$): δ 144.5, 144.1, 144.0, 136.7, 124.4, 99.0, 49.4, 41.9, 28.0; IR (microscope): ν = 3325, 3101, 2973, 2933, 2856, 2137, 2108, 1620, 1586, 1362 cm^{-1}; ES-HRMS calculated for $C_9H_{10}N_7O_3$: 263.0840; observed: 264.0843. R_f = 0.35 (1:1 EtOAc/hexanes).

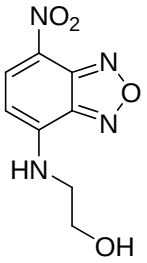

2-(7-nitrobenz-[2,1,3-*d*]-oxadiazol-4-ylamino)ethanol (**3.9**).

4-chloro-7-nitrobenzoxadiazole (**3.5**) (25 mg, 0.125 mmol, 1 equiv) was dissolved in 3 mL of methanol. Five drops of ethanolamine was then added by pipette. The reaction occured rapidly at room temperature, turning the reaction mixture a red-brown color. 2-(7-nitrobenzo[c][1,2,5]oxadiazol-4-ylamino)ethanol (**3.9**) is produced as a yellow fluorescent spot. The product was purified using normal phase flash column chromatography and obtained in 50% yield. ^{1}H NMR (400 MHz, CD_3OD): δ 8.51 (d, 1H, ^{3}J = 8.8 Hz), 6.41 (d, 1H, ^{3}J = 8.8 Hz), 3.85 (t, 2H, ^{3}J = 5.6 Hz), 3.67 (br s, 2H) may be obscured by solvent peak. IR microscope: ν = 3432.1, 3248.3, 3160.4, 3077.0, 2957.5, 2924.6, 2542.9, 2385.2 cm^{-1}. ESI-MS calculated for $C_8H_8N_4O_4Na$ (M+Na) 247.0438; observed: 247.0439. R_f = 0.11 (3:2 EtOAc/hexanes), 0.33 (EtOAc). λ_{max} (methanol): absorbance 464 nm; emission 535 nm. ε_{450} = 1.6 x 10^{6} M^{-1}cm^{-1}. R_f = 0.11 (3:2 EtOAc/hexanes)

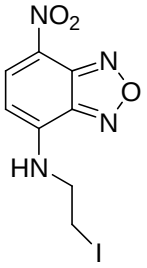

***N*-(2-iodoethyl)-7-nitrobenz-[2,1,3-*d*]-oxadiazol-4-amine** (**3.10**).

The starting material 2-(7-nitrobenzoxadiazol-4-ylamino)ethanol (**3.9**) (25 mg, 0.11 mmol, 1 equiv) was dissolved in toluene with I_2 (31 mg, 0.12 mmol, 1.1 equiv), imidazole (17 mg, 0.25 mmol, 2.2 equiv), triphenylphosphine (32 mg, 0.12 mmol, 1.1 equiv) and the reaction was heated to 80 ^{o}C. The reaction was allowed to proceed for 30 min, then diluted with EtOAc and washed with Na_2SO_3, $NaHCO_3$ and brine. The organic layer was concentrated in vacuo then further purified by normal phase flash column chromatography (6 mg, 23%). ^{1}H NMR (400 MHz, $CDCl_3$): δ 8.53 (d, 1H, ^{3}J = 8.5 Hz), 6.41 (broad s, 1H), 6.27 (d, 1H, ^{3}J = 8.5 Hz), 3.95 (q, 2H, ^{3}J = 6.6 Hz), 3.49 (t, 2H, ^{3}J = 6.6 Hz); ^{13}C NMR (100 MHz, $CDCl_3$): δ 144.3, 143.8, 142.6, 135.8, 125.3, 99.0, 45.6; ESI-HRMS calculated for $C_8H_7N_4O_3$ NaI: 356.9455; observed 356.9446. R_f = 0.65 (3:2 EtOAc/hexanes).

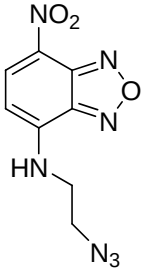

***N*-(2-azidoethyl)-7-nitrobenzo-[2,1,3-*d*]-oxadiazol-4-amine** (**3.11**).

N-(2-iodoethyl)-7-nitrobenzoxadiazol-4-amine (**3.10**) (6 mg, 0.026 mmol, 1 equiv) and NaN_3 (5mg, 0.077 mmol, 3 equiv) were dissolved in DMF (5 mL) and heated at 60 ^oC for 20 min. The reaction mixture was quenched with water, and the crude product extracted out with ethyl ether (4 x 10 mL), dried over magnesium sulphate and the solvent removed in vacuo. The product was purified by normal phase flash column chromatography and obtained in trace amounts (EtOAc/hexanes). ^1H NMR (400 MHz, $CDCl_3$): δ 8.53 (d, 1H, ^3J = 8.5 Hz), 6.32 (broad s, 1H), 6.28 (d, 1H, ^3J = 8.5 Hz), 3.79 (m, 2H), 3.73 (m, 2H); IR (microscope): ν = 3248, 3072, 2934, 2868, 2118, 1620, 1584, 1484, 1279, 1247 cm^{-1}; ESI-HRMS calculated for $C_8H_7N_7O_3$: 250.0683; observed 250.0684. R_f = 0.59 (3:2 EtOAc/hexanes).

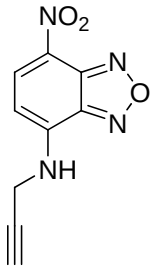

7-Nitro-*N*-(prop-2-ynyl)benz-[2,1,3-*d*]-oxadiazol-4-amine (**3.12**).

4-Chloro-7-nitrobenzoxadiazole (**3.5**) (500 mg, 2.5 mmol, 1 equiv) was dissolved in acetonitrile (20 mL). Propargyl amine (0.32 mL, 5 mmol, 2 equiv) was then added, turning the reaction mixture a dark green colour, and was allowed to stir at room temperature for 1.5 h. The solvent was removed in vacuo and the crude product was purified by column chromatography (EtOAc/hexanes). Product was obtained as an orange-brown powder (600 mg, 33%). m.p. 134.0-137.6 ^oC; ^1H NMR (400 MHz, $CDCl_3$): δ 8.56 (d, 1H, ^3J = 8.4 Hz), 6.4 (broad s, 1H), 6.38 (br

s, 1H, ^{3}J = 8.4 Hz), 4.35-4.33 (dd, 2H, ^{4}J = 2.4 Hz, ^{3}J = 5.6 Hz), 2.54 (t, 1H, ^{4}J = 2.4 Hz,); ^{13}C NMR (100 MHz, $CDCl_3$): δ 144.6, 144.0, 142.5, 136.1, 100.2, 74.4, 33.7; IR (microscope): ν = 3392, 3366, 3310 and 3291, 3077, 3038, 2124, 1621, 1585 cm^{-1}; ES-HRMS calculated for $C_9H_6N_4O_3$: 241.0332; observed: 241.0334. R_f = 0.10 (1:3 EtOAc/hexanes).

7-nitrobenzo-[2,1,3-*d*]-oxadiazol-4-amine (**3.13**).

The starting material 4-chloro-7-nitrobenzoxadiazole (**3.5**) (25 mg, 0.125 mmol, 1 equiv) was dissolved in 3 mL of methanol. Ammonia in methanol (2 M) (0.082 mL, 0.325 mmol, 1.3 equiv) was added by syringe or pipette. The reaction proceeded at room temperature, and the product can be visualized by longwave-UV lamp on TLC after 0.5 - 1 h. 7-nitrobenzo[c][1,2,5]oxadiazol-4-amine (**3.13**) was produced as a yellow fluorescent spot. The product was purified by normal phase flash column chromatography and obtained in trace amounts (EtOAc/hexanes). ^{1}H NMR (400 MHz, CD_3OD): δ 8.49 (d, 1H, ^{3}J = 8.8 Hz), 6.39 (d, 1H, ^{3}J = 8.8 Hz). IR cast film: ν = 3344.8, 2901.1, 1636.4, 1427.7, 1315.1, 1160.7, 1106.9, 1030.9 cm^{-1}. EI-MS calculated for $C_6H_4O_3N_4$ (M^+) 180.0283; observed: 180.0280. R_f = 0.42 (3:2 EtOAc/hexanes). λ_{max} (methanol): absorbance 458 nm; emission 534 nm. ε_{450} = 6.9 x 10^{5} M^{-1}cm^{-1}. R_f = 0.42 (3:2 v:v EtOAc/hexanes).

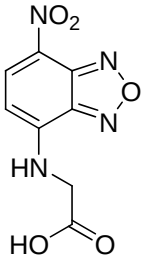

2-(7-nitrobenz-[2,1,3-*d*]-oxadiazol-4-ylamino)acetic acid (**3.14**).

The starting material 4-chloro-7-nitrobenzoxadiazole (**3.5**) (25 mg, 0.125 mmol, 1 equiv) was dissolved in 3 mL of methanol. Glycine (24 mg, 0.325 mmol, 1.3 equiv) was then added, and heated at 80 – 85 ^{o}C. The product can be visualized by longwave-UV lamp TLC after 0.5 - 1 h. 2-(7-nitrobenzo[c][1,2,5]oxadiazol-4-ylamino)acetic acid (**3.14**) is produced as a fluorescent spot. The reaction may need to be covered with a vented rubber septum to reduce evaporation of solvent, or else methanol should be added to the mixture to maintain the volume. The product was purified by normal phase flash column chromatography and obtained in trace amounts (DCM/MeOH). ^{1}H NMR (300 MHz, D_2O): δ 8.60 (δ, 1H, ^{3}J = 9.0 Hz), 6.29 (br s, 1H), 4.78 (br s, 2H), 4.20 (br s, 1H). IR cast film: ν = 3427.5, 3338.0, 3233.5, 2918.0, 2849.8, 1642.7, 1554.9, 1491.4, 1446.4, 1422.5, 1308.1, 1285.0 cm^{-1}; ESI-MS calculated for $C_6H_5N_4O_5$ $(M-H)^-$ 237.0265; observed: 237.0266. λ_{max} (methanol): absorbance 462 nm; emission 534 nm. ε_{450} = 6.3 x 10^{5} M^{-1}cm^{-1}. R_f = 0.0 (3:2 EtOAc/hexanes).

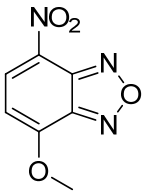

4-methoxy-7-nitrobenzo-[2,1,3-*d*]-]oxadiazole (**3.15**).

4-chloro-7-nitrobenzoxadiazole (**3.5**) (50 mg, 0.25 mmol, 1 equiv) was dissolved in a 3:1 water/methanol mixture (4 mL). Na_2CO_3 (100 mg) was added to bring the solution to pH 9. The reaction was allowed to stir at room temperature for 48 h and the product was purified by normal phase flash column chromatography and obtained in approximately 4% yield (DCM/MeOH). In the presence of base and trace amounts of water or methanol, products are formed in a 1:5 mixture of methoxy (**3.15**) and phenol (**3.16**). ^{1}H NMR (400 MHz, MeOD): δ 8.63 (d, 1H, ^3J = 8.4 Hz), 6.93 (d, 1H, ^3J = 8.4 Hz), 3.34 (s, 3H).

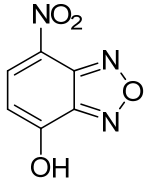

7-nitrobenz-[2,1,3-*d*]-oxadiazol-4-ol (**3.16**).

4-chloro-7-nitrobenzoxadiazole (**3.5**) (250 mg, 1.25 mmol, 1 equiv), and Na_2CO_3 (1 g, 9.4 mmol, 7.5 equiv) were dissolved in water (15 mL), and allowed to stir for 2 h at room temperature. The crude reaction mixture was neutralized with HCl and further diluted with water. The solvent removed in vacuo then purified by normal phase flash column chromatography (DCM/Methanol) (45 mg, 20%). ^{1}H NMR (400 MHz, MeOD): δ 8.43 (d, 1H, ^3J = 9.6 Hz), 6.02 (d, 1H, ^3J = 9.6 Hz); ^{13}C NMR (100 MHz, MeOD): δ 173.6, 148.5, 146.4, 139.0, 115.1, 111.0; IR (microscope): ν = 3458, 2919, 1618, 1569, 1410 cm^{-1}; ESI-HRMS calculated for

$C_6H_2N_3O_4$: 180.0051; observed 180.0055. R_f = 0.31 (3:2 EtOAc/hexanes).

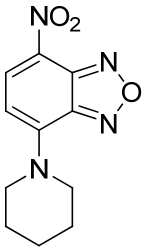

4-nitro-7-(piperidin-1-yl)benz-[2,1,3-*d*]-oxadiazole (**3.17**).

4-chloro-7-nitrobenzoxadiazole (**3.5**) (200 mg, 1 mmol, 1 equiv) was dissolved in acetonitrile (3 mL) and piperidine (0.13 mL, 1.3 mmol, 1.3 equiv) was added. The reaction occurs very rapidly producing a bright red colour, and was allowed to stir at room temperature for approximately 15 min. The solvent and excess piperidine were then removed in vacuo (270 mg, quant). ^{1}H NMR (400 MHz, $CDCl_3$): δ 8.38 (d, 1H, ^3J = 9.1 Hz), 6.27 (d, 1H, ^3J = 9.1 Hz), 4.12 (broad s, 4 H), 1.86 (broad s, 6H); ^{13}C NMR (100 MHz, $CDCl_3$): δ 145.4, 145.2, 145.0, 135.7, 122.5, 102.2, 51.5, 26.3, 24.2; IR (microscope): ν = 3118, 2954, 2874, 1604, 1552, 1483, 1276, 1199 cm^{-1}; ESI-HRMS calculated for $C_{11}H_{11}N_4O_3$: 249.0982; observed 249.0983. R_f = 0.11 (1:3 EtOAc/hexanes).

5-chlorobenz-[2,1,3-*d*]-oxadiazole-4-sulfonyl chloride (**3.19**).

5-chlorobenzoxadiazole (**3.18**) (0.5 g, 3.25 mmol, 1 equiv) was dissolved in chlorosulfonic acid (0.65 mL, 9.7 mmol, 3 equiv) and heated at 120 ^{o}C for 3 h. The reaction was allowed to cool to rt then quenched on ice, where the product precipitates out as a white powder (0.36 g, 44%). ^{1}H NMR (400 MHz, $CDCl_3$): δ

8.22 (d, 1H, ^{3}J = 9.3 Hz), 7.63 (d, 1H, ^{3}J = 9.3 Hz); ^{13}C NMR (100 MHz, $CDCl_3$): δ 147.9, 145.1, 142.1, 135.3, 129.6, 124.1; EI-MS calculated for $C_6H_2N_2O_3SCl2$: 251.9163; observed: 251.9166. R_f = 0.45 (1:3 EtOAc/hexanes).

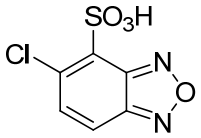

5-chlorobenz-[2,1,3-*d*]-oxadiazole-4-sulfonic acid (**3.20**).

5-chlorobenzoxadiazole-4-sulfonyl chloride (**3.19**) (100 mg, 0.395 mmol, 1 equiv), Na_2SO_3 (50 mg, 0.395 mmol, 1 equiv) and $NaHCO_3$ (3.3 mg, 0.0395 mmol, 0.1 equiv) were dissolved in water (150 mL) and heated at 110 ^{o}C for 1 h. The solvent was then removed in vacuo, and the crude product was crystallized upon cooling to -20 ^{o}C from 5:1 DCM/Methanol as a yellow powder (70 mg, 77%). ^{1}H NMR (400 MHz, CD_3OD): δ 7.98 (d, 1H, ^{3}J = 9.4 Hz), 7.56 (d, 1H, ^{3}J = 9.4 Hz), 1.90 (s, 1H); ^{13}C NMR (100 MHz, CD_3OD): δ 148.6, 147.4, 136.5, 135.9, 131.0, 118.5; IR (microscope): ν = 3499, 3091, 3049, 1643, 1565, 1438, 1236, 1069 cm^{-1}. ESI-HRMS calculated for $(M-H)^-$ $C_6H_2N_2O_4S$: 239.9833; observed 239.9837. R_f = 0.20 (5:1 DCM/MeOH).

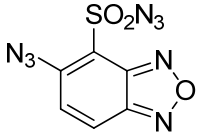

5-azidobenz-[2,1,3-*d*]-oxadiazole-4-sulfonyl azide (**3.21**).

5-chlorobenzoxadiazole-4-sulfonyl chloride (**3.19**) (40 mg, 0.15, 1 equiv) and sodium azide (30 mg, 0.47 mmol, 3 equiv) was dissolved in DMF (5 mL) and allowed to react at rt for 1 h. The reaction was quenched with distilled water, and the product was extracted wtih ethyl ether (3 x 10 mL), dried with magnesium

sulphate and the solvent was removed in vacuo. This compound was quickly disposed of after characterization, as it is suspected to be unstable. Yield was not determined. ^{1}H NMR (400 MHz, $CDCl_3$): δ 8.28 (d, 1H, ^{3}J = 9.4 Hz), 7.52 (d, 1H, ^{3}J = 9.5 Hz); ^{13}C NMR (100 MHz, $CDCl_3$): δ 147.3, 145.9, 145.3, 125.0, 124.8; IR (microscope): ν = 3282, 3105, 2925, 2148, 2127, 1617, 1464, 1377, 1172 cm^{-1}. ESI-HRMS calculated for $(M+Na)^+$ $C_6H_2N_8O_3S$: 288.9863; observed 288.9862. R_f = 0.25 (1:3 EtOAc/hexanes).

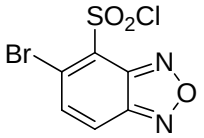

5-**bromobenz-[2,1,3-*d*]-oxadiazole-4-sulfonyl chloride** (**3.22**).

5-bromobenzoxadiazole (**3.3**) (100 mg, 0.5 mmol, 1 equiv) was dissolved in chlorosulphonic acid (0.1 mL, 1.5 mmol, 3 equiv) and heated at 130 ^{o}C for 2 h. The reaction mixture was quenched onto ice (10 mL) and the resulting brown-gray precipitate was filtered (51 mg, 34%). ^{1}H NMR (400 MHz, $CDCl_3$): δ 8.12 (d, 1H, ^{3}J = 9.3 Hz), 7.84 (d, 1H, ^{3}J = 9.3 Hz); APT ^{13}C NMR (100 MHz, $CDCl_3$): δ 148.5, 145.9, 138.6, 138.0, 132.1, 123.9; EI-HRMS calculated for $C_6H_2N_2O_3BrCl$: 295.8658; observed 295.8660. R_f = 0.36 (1:3 EtOAc/hexanes).

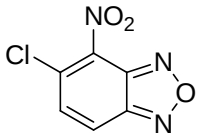

5-chloro-4-nitrobenz-[2,1,3-*d*]-oxadiazole (**3.23**).

5-chlorobenzoxadiazole (**3.18**) (100 mg, 0.65 mmol, 1 equiv) was dissolved in an ice-bath cooled mixture of H_2SO_4 (0.65 mL) and 70% HNO_3 (0.05 mL) and allowed to stir for 4 h, warming to room temperature. The reaction mixture was

quenched onto 20 mL of ice. The resulting orange precipitate was filtered and was further purified by normal phase flash column chromatography (EtOAc/hexanes) (61 mg, 48%). ^{1}H NMR (400 MHz, $CDCl_3$): δ 8.11 (d, 1H, ^{3}J = 9.4 Hz), 7.59 (d, 1H, ^{3}J = 9.4 Hz); ^{13}C NMR (100 MHz, $CDCl_3$): δ 148.7, 143.9, 135.3, 134.6, 133.4, 121.7; IR (microscope): ν = 3104, 3059, 3044, 2919, 2864, 1625, 1530, 1461, 1342cm^{-1}. EI-HRMS calculated for $C_6H_2N_3O_3Cl$: 198.9785; observed 198.9782. R_f = 0.40 (1:3 EtOAc/Hexanes).

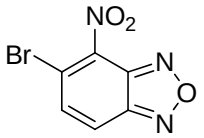

5-bromo-4-nitrobenz-[2,1,3-*d*]-oxadiazole (**3.24**).

5-bromobenzoxadiazole (**3.3**) (74 mg, 0.38 mmol, 1 equiv) was cooled in an icebath and dissolved in H_2SO_4 (0.39 mL) and HNO_3 (0.03 mL) and allowed to stir for 4 h. The reaction mixture was quenched onto ice and the resulting orange precipitate was filtered and further purified by normal phase flash column chromatography (EtOAc/hexanes) (31 mg, 33%). ^{1}H NMR (400 MHz, $CDCl_3$): δ 8.02 (d, 1H, ^{3}J = 9.4 Hz), 7.84 (d, 1H, ^{3}J = 9.4 Hz); ^{13}C NMR (100 MHz, $CDCl_3$): δ 148.9, 144.2, 137.6, 136.9, 121.8, 121.1; IR (microscope): ν = 3091, 2921, 1622, 1538, 1348 cm^{-1}. EI-HRMS calculated for $C_6H_2N_3O_3Br$: 242.9279; observed: 242.9274. R_f = 0.21 (1:3 EtOAc/hexanes).

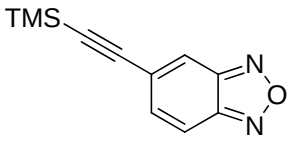

5-((Trimethylsilyl)ethynyl)benz-[2,1,3-*d*]-oxadiazole (**3.25**).

5-Bromobenzoxadiazole (**3.3**) (150 mg, 0.75 mmol, 1 equiv) was dissolved in acetonitrile (12 mL). $PdCl_2(PPh_3)_2$ (52 mg, 0.075 mmol, 0.1 equiv), DIPEA (0.50 mL, 2.8 mmol, 3.77 equiv), CuI (15 mg, 0.075 mmol, 0.1 equiv) and trimethylsilyl acetylene (0.52 mL, 3.75 mmol, 5 equiv) were subsequently added. The reaction mixture was degassed with three freeze-thaw cycles then heated at 80 °C for 24 h. The reaction mixture was then diluted with EtOAc, washed with NH_4Cl and dried over $MgSO_4$. The crude product was concentrated *in vacuo*, and purified by gradient flash column chromatography (EtOAc/hexanes) (150 mg, 92%). ^{1}H NMR (400 MHz, $CDCl_3$): δ 7.93 (s, 1H), 7.77 (d, 1H, ^3J = 10.5 Hz), 7.38 (d, 1H, ^3J = 10.5 Hz), 0.27 (s, 9H); EI-HRMS calculated for $C_{11}H_{12}N_2OSi$: 216.0718; observed: 216.0717. R_f = 0.68 (1:9 EtOAc/hexanes).

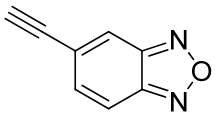

5-Ethynylbenz-[2,1,3-*d*]-oxadiazole (**3.26**).

5-((Trimethylsilyl)ethynyl)benzoxadiazole (**3.25**) (73 mg, 0.34 mmol, 1 equiv) was dissolved in methanol (7 mL). Tetrabutylammonium fluoride (0.29 mL, 1 mmol, 3 equiv) was then added, and the reaction mixture was heated at 60 °C for 20 min, until starting material was no longer visible by TLC. The reaction was quenched with distilled water, and concentrated in vacuo. The crude product was extracted with dichloromethane, dried over $MgSO_4$, concentrated in vacuo and purified by column chromatography (EtOAc/hexanes) giving a brown-yellow powder (35 mg, 72%). m.p. 66.0-66.5 ^{o}C; ^{1}H NMR (400 MHz, $CDCl_3$): δ 8.03 (s, 1H), 7.84 (d, 1H, ^3J = 10.4 Hz), 7.43 (d, 1H, ^3J = 10.4 Hz), 3.37 (s, 1H); ^{13}C NMR

(100 MHz, $CDCl_3$): δ 149.0, 148.4, 134.4, 125.8, 120.7, 116.9, 82.1, 82.0; IR (neat film): ν = 3290, 3270, 3109, 3054, 2110 cm^{-1}; EI-HRMS calculated for $C_8H_4N_2O$: 144.0324; observed: 144.0320. R_f = 0.29 (1:9 EtOAc/hexanes).

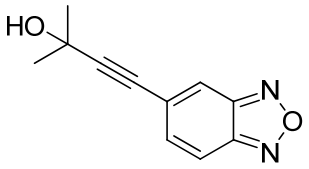

4-(benzo-[2,1,3-*d*]-oxadiazol-5-yl)-2-methylbut-3-yn-2-ol (**3.27**).

5-chlorobenzoxadiazole (**3.18**) (150 mg, 0.98 mmol, 1 equiv), 2-methyl-3-butyn-2-ol (0.12 mL, 1.72 mmol, 1.2 equiv) and $PdCl_2(PPh_3)_2$ (20 mg, 0.03 mmol, 0.03 equiv) were dissolved in TBAF (0.86 mL, 2.94 mmol, 3 equiv) and heated at 80 ^oC for 4 h.(Liang, Y., Xie, Y.-X., et al. 2005) The crude product was washed with water, extracted with ether, and the solvent removed in vacuo. Normal phase flash column chromatography was performed (EtOAc/hexanes) to isolate the pure product (91 mg, 46%). ^1H NMR (400 MHz, $CDCl_3$): δ 7.85 (t, 1H, ^4J = 0.9 Hz), 7.75 (dt, 1H, ^3J = 9.2 Hz, ^4J = 1.1 Hz), 7.32 (dt, 1H, ^3J = 9.3 Hz, ^4J = 1.3 Hz), 2.66 (broad s, 1 H), 1.64 (s, 6H); ^{13}C NMR (100 MHz, $CDCl_3$): δ 149.1, 148.3, 134.6, 126.5, 119.2, 116.6, 98.9, 80.8, 65.8, 31.5. R_f = 0.28 (1:3 EtOAc/hexanes).

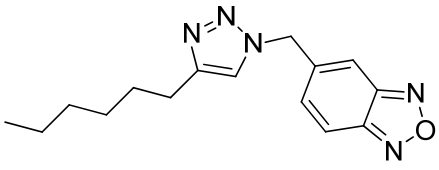

5-((4-Hexyl-1H-1,2,3-triazol-1-yl)methyl)benz-[2,1,3-*d*]-oxadiazole (**3.28**).

5-(Azidomethyl)benzoxadiazole (**3.2**) (40 mg, 0.228 mmol, 1 equiv) was dissolved in 1:1 water/methanol (5 mL) and *n*-octyne (0.17 mL, 1.14 mmol, 5 equiv) was added. Copper sulphate (7 mg, 0.046 mmol, 0.2 equiv) and ascorbic

acid (12 mg, 0.068 mmol, 0.3 equiv) were then added. A white precipitate formed and was filtered after approximately 40 m of stirring at room temperature and then purified by column chromatography (EtOAc/hexanes). Product was obtained as a white powder (41 mg, 63%). m.p. 92.0-92.7 ^{o}C; ^{1}H NMR (400 MHz, $CDCl_3$): δ 7.87 (d, 1H, ^{3}J = 10.0 Hz), 7.67 (s, 1H), 7.34 (s, 1H),7.33 (d, 1H, ^{4}J = 1.24 Hz, ^{3}J = 9.2 Hz), 5.62 (s, 2H), 2.74 (t, 2H, ^{3}J = 8.4 Hz), 1.66 (m, 3H), 1.33 (m, 6H), 0.88 (m, 3H); ^{13}C NMR (100 MHz, $CDCl_3$): δ 150.0, 149.2, 148.9, 139.3, 131.3, 121.1, 118.1, 115.1, 53.7, 31.8, 29.5, 29.1, 26.0, 14.3; IR (microscope): ν = 3109, 3055, 2965, 2956, 2854, 1556 cm^{-1}; ES-HRMS calculated for $C_{15}H_{20}N_5O$: 286.1662; observed: 286.1666. R_f = 0.61 (3:2 EtOAc/hexanes).

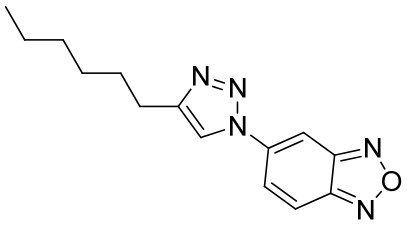

5-(4-Hexyl-1H-1,2,3-triazol-1-yl)benz-[2,1,3-*d*]-oxadiazole (**3.29**).

5-Azidobenzoxadiazole (**3.4**) (30 mg, 0.19 mmol, 1 equiv) was dissolved in 1:1 water/methanol (5 mL) and *n*-octyne (0.14 mL, 0.93 mmol, 5 equiv) was added. Copper sulphate (6 mg, 0.037 mmol, 0.2 equiv) and ascorbic acid (10 mg, 0.056 mmol, 0.3 equiv) were then added. The reaction was then allowed to stir at room temperature for 6 h. The reaction was quenched with distilled water, and the crude product was extracted with chloroform followed by water and brine washes. The organic layer was then dried over $MgSO_4$ and concentrated in vacuo. Purification was performed by column chromatography (EtOAc/hexanes). The product was obtained as white crystals (25 mg, 50%). m.p. 113.2-115.4 ^{o}C; ^{1}H NMR (400

MHz, $CDCl_3$): δ 8.19 (dd, 1H, ^4J = 3.8 Hz, ^4J = 1.84 Hz), 8.06 (m, 2H), 7.91 (s, 1H), 2.85 (t, 2H, ^3J = 8.0 Hz), 1.77 (m, 2H), 1.31-1.47 (m, 6H), 0.91 (m, 3H); ^{13}C NMR (100 MHz, $CDCl_3$): δ150.5, 149.0, 148.4, 139.1, 126.8, 119.1, 118.9, 104.5, 31.8, 29.4, 29.1, 25.9, 22.8, 14.3; IR (microscope): ν = 3147, 3114, 3095, 3059, 2956, 2929, 2857, 1637, 1540 cm^{-1}; ES-HRMS calculated for $C_{14}H_{18}N_5O$: 272.1506; observed: 272.1513. R_f = 0.51 (1:3 EtOAc/hexanes).

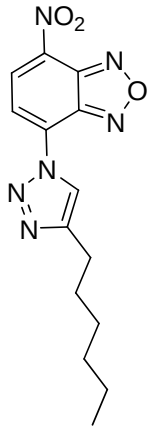

4-(4-Hexyl-1H-1,2,3-triazol-1-yl)-7-nitrobenz-[2,1,3-*d*]-oxadiazole (**3.30**).

A solution of *n*-octyne (0.143 mL, 0.97 mmol, 5 equiv), copper sulphate (6 mg, 0.039 mmol, 0.2 equiv), and ascorbic acid (10 mg, 0.06 mmol, 0.3 equiv) in 1:1 water/methanol (5 mL) was allowed to stir at room temperature for 5 m. 4-Azido-7-nitrobenzoxadiazole (**3.6**) (40 mg, 0.194 mmol, 1 equiv) was then added slowly. A green precipitate was visible after 45 m, and the reaction was allowed to stir for approximately 1.5 h. The solvent was removed in vacuo, and the crude product was purified by column chromatography (EtOAc/hexanes), giving a yellow powder. The purified product was obtained as a green-yellow powder (41 mg, 68%). m.p. 108.3-109.5 ^oC; ^{1}H NMR (400 MHz, $CDCl_3$): δ 8.75 (s, 1H), 8.72 (d, 1H, ^3J = 8.0 Hz), 8.52 (d, 1H, ^3J = 8.0 Hz), 2.89 (t, 2H, ^3J = 8.4 Hz), 1.80 (q, 2H,

^{3}J = 8 Hz), 1.40 (m, 6H), 0.93 (m, 3H); ^{13}C NMR (100 MHz, $CDCl_3$): δ 151.0, 144.1, 143.9, 135.0, 131.9, 130.8, 122.8, 117.7, 31.8, 29.3, 29.1, 25.8, 22.8, 14.3; IR (microscope): ν = 3159, 3114, 3090, 2955, 2930, 2855, 1597, 1559, 1542 , 1337 cm^{-1}; ES-HRMS calculated for $C_{14}H_{17}N_6O_3$: 317.1357; observed: 317.1350.R_f = 0.43 (3:2 EtOAc/hexanes).

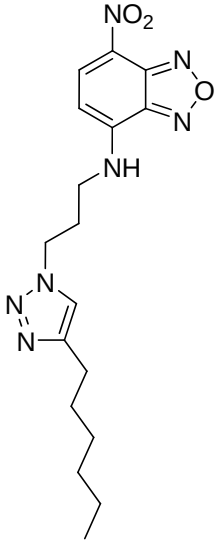

***N*-(3-(4-Hexyl-1H-1,2,3-triazol-1-yl)propyl)-7-nitrobenz-[2,1,3-*d*]-oxadiazol-4-amine** (**3.31**).

N-(3-Azidopropyl)-7-nitrobenzoxadiazol-4-amine (**3.8**) (20 mg, 0.076 mmol, 1 equiv), *n*-octyne (0.06 ml, 0.38 mmol, 5 equiv), copper sulphate (3 mg, 0.015 mmol, 0.2 equiv) and ascorbic acid (4 mg, 0.023 mmol, 0.3 equiv) were dissolved in 1:1 water/methanol (5 mL). The reaction mixture was allowed to stir at room temperature for approximately 6 h. The solvent was then removed in vacuo, and the crude product was extracted with chloroform, then washed with water and brine. The organic layer was then dried over $MgSO_4$ and concentrated in vacuo. Purification was performed by column chromatography (EtOAc/hexanes). The product was obtained in 32% yield as an orange powder. m.p. 125.5-126.6 ^{o}C; ^{1}H NMR (400 MHz, $CDCl_3$): δ 8.47 (d, 1H, ^{3}J = 10.0 Hz), 7.39 (s, 1H), 6.94 (broad

s, 1H), 6.19 (d, 1H, ^{3}J = 8.8 Hz), 4.57 (t, 2H, ^{3}J = 7.6 Hz), 3.66 (m, 2H), 2.73 (t, 2H, ^{3}J = 7.6 Hz), 2.45 (q, 2H, ^{3}J = 6.4 Hz), 2.04 (broad s, 1H), 1.67 (q, 2H, ^{3}J = 6.4 Hz), 1.30 (m, 6H), 0.90 (m, 3H); ^{13}C NMR (100 MHz, $CDCl_3$): δ 149.3, 144.5, 144.1, 144.0, 136.5, 124.5, 121.4, 99.2, 47.6, 41.3, 31.8, 29.6, 29.2, 28.9, 25.8, 22.8, 14.3; IR (microscope): ν = 3357, 3213, 3142, 3064, 2956, 2930, 2859, 1619, 1590, 1529, 1307 cm^{-1}; ES-HRMS calculated for $C_{17}H_{24}N_7O_3$: 374.1935; observed: 374.1933. R_f = 0.56 (3:2 EtOAc/hexanes).

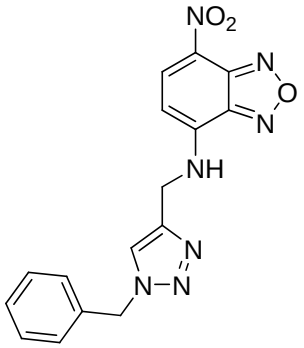

***N*-((1-Benzyl-1H-1,2,3-triazol-4-yl)methyl)-7-nitrobenz-[2,1,3-*d*]-oxadiazol-4-amine** (**3.32**).

7-Nitro-*N*-(prop-2-ynyl)benzoxadiazol-4-amine (**3.12**) (20 mg, 0.092 mmol, 1 equiv), benzyl azide (0.05 mL, 0.46 mmol, 5 equiv), copper sulphate (3 mg, 0.02 mmol, 0.2 equiv) and ascorbic acid (5 mg, 0.028 mmol, 0.3 equiv) were dissolved in 1:1 water/methanol (5 mL). The reaction mixture was allowed to stir at room temperature for approximately 6 h. The solvent was then removed *in vacuo*, and the crude product was extracted with chloroform, and washed with water and brine. The organic layer was then dried over $MgSO_4$ and concentrated in vacuo. Purification was performed by column chromatography (EtOAc/hexanes). The product was obtained in as a yellow powder (15 mg, 46%). m.p. 198.8-199.7 ^{o}C; ^{1}H NMR (400 MHz, $(CD_3)_2CO$): δ 8.54 (d, 1H, ^{3}J = 8.8 Hz), 8.08 (s, 1H), 7.35

(m, 5H), 6.63(d, 1H, ^{3}J = 8.8 Hz), 5.62 (s, 2H), 4.94 (s, 2H); ^{13}C NMR (100 MHz, DMSO-D_6): δ 144.4, 144.1, 137.6, 135.9, 128.7, 128.1, 127.9, 123.6, 121.3, 99.9, 52.8, 40.1; IR (microscope): ν = 3265, 3204, 3142, 3062 , 2961, 2899, 1620, 1588, 1527, 1296 and 1274; ES-HRMS calculated for $C_{16}H_{14}N_7O_3$: 352.1153; observed: 352.1152. R_f = 0.26 (3:2 EtOAc/hexanes).

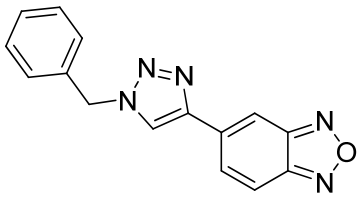

5-(1-Benzyl-1*H*-1,2,3-triazol-4-yl)benz-[2,1,3-*d*]-oxadiazole (**3.33**).

5-Ethynylbenzoxadiazole (**3.26**) (26 mg, 0.18 mmol, 1 equiv) was dissolved in 1:1 water/methanol and benzyl azide (0.095 mL, 0.90 mmol, 5 equiv) was added. Copper sulphate (6 mg, 0.036 mmol, 0.2 equiv) and ascorbic acid (10 mg, 0.025 mmol, 0.3 equiv) were then added to the solution. The reaction mixture was allowed to stir at room temperature for 1.5 h turning an opaque white colour. The solvent was removed *in vacuo* and the crude product was dissolved in chloroform, washed with water, dried over $MgSO_4$ and concentrated *in vacuo*. Purification was performed by column chromatography (EtOAc/hexanes). Product was obtained as a white powder in (30 mg, 60%). m.p. 149.5-148.7 ^{o}C; ^{1}H NMR (400 MHz, $CDCl_3$): δ 8.19 (s, 1H), 8.02 (dd, 1H, ^{4}J = 1.2 Hz, ^{3}J = 9.6 Hz), 8.01 (dd, 1H, ^{4}J = 1.2 Hz, ^{3}J = 9.6 Hz), 7.88 (s, 1H), 7.40-7.48 (m, 3H), 7.34-7.40 (m, 2H), 5.64 (s, 2H); ^{13}C NMR (100 MHz, $CDCl_3$): δ 149.6, 149.0, 146.2, 133.8, 131.2, 129.6, 129.4, 128.5, 121.4, 117.3, 111.3, 54.8; IR (microscope): ν = 3138, 3122, 3071,

3040, 2924, 2853, 1630, 1564 cm^{-1}; ES-HRMS calculated for $C_{15}H_{12}N_5O$: 278.1036; observed: 278.1032. R_f = 0.18 (1:3 EtOAc/hexanes).

3.5.4 Normalized UV-vis absorbance spectra of 3.2-3.33 in ethanol

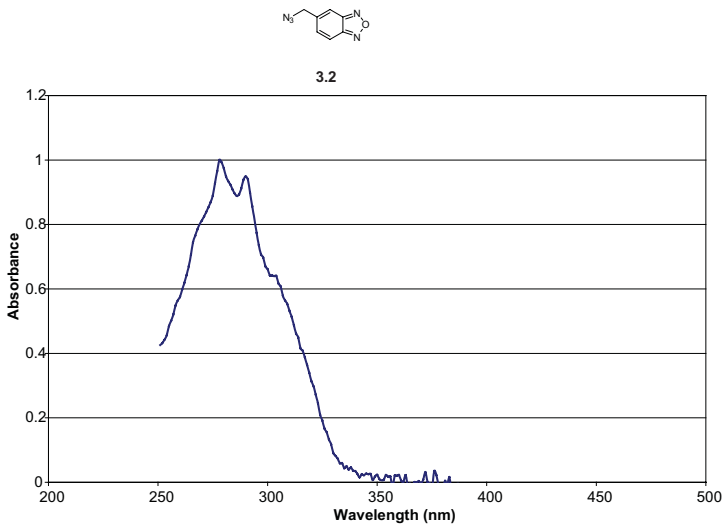

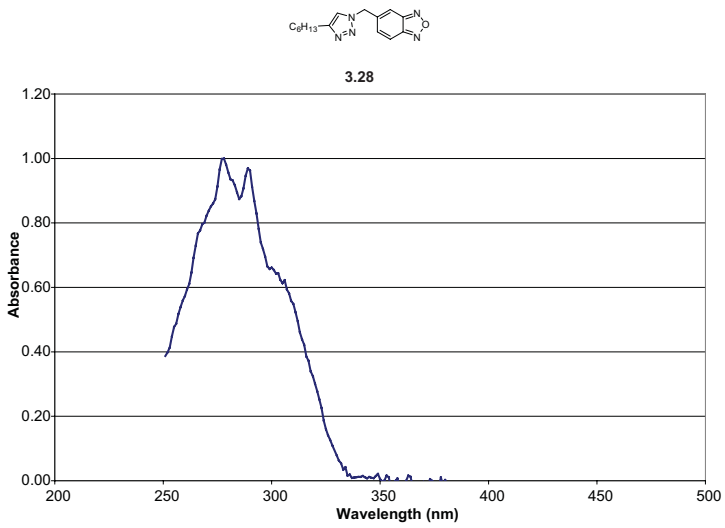

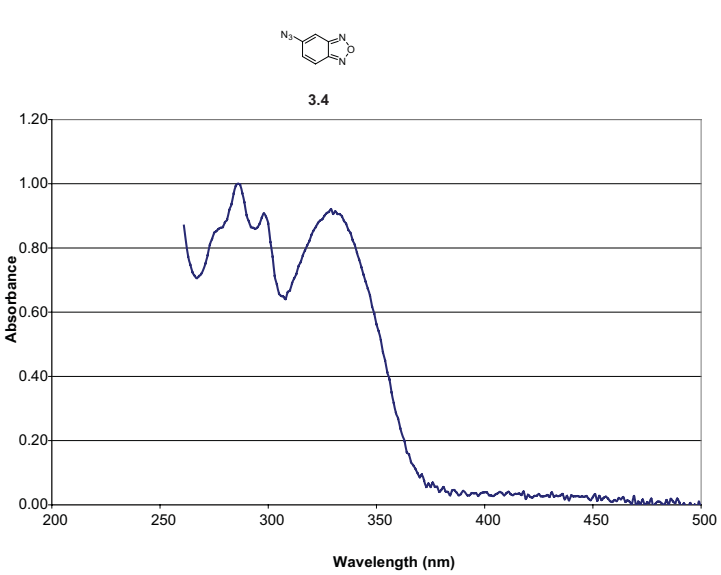
3.4
Absorbance
Wavelength (nm)
1.20
1.00
0.80
0.60
0.40
0.20
0.00
200
250
300
350
400
450
500

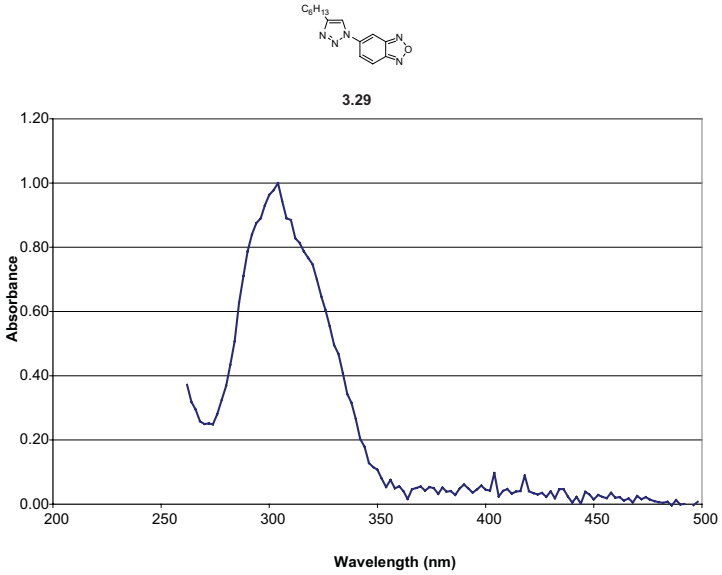
3.29
Absorbance
Wavelength (nm)
1.20
1.00
0.80
0.60
0.40
0.20
0.00
200
250
300
350
400
450
500

3.6

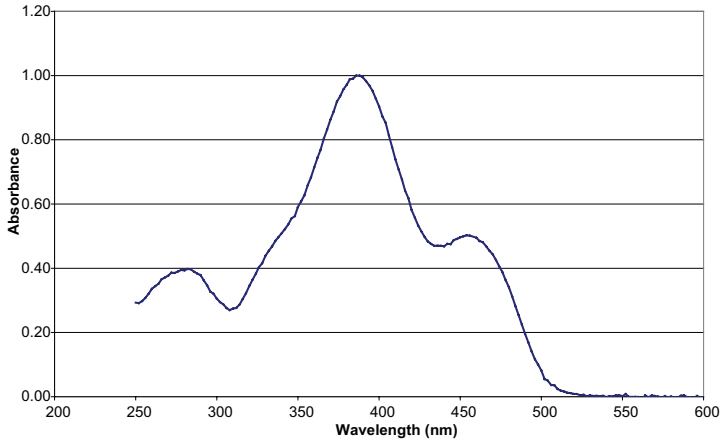
Absorbance
1.20
1.00
0.80
0.60
0.40
0.20
0.00
200
250
300
350
400
450
500
550
600
Wavelength (nm)

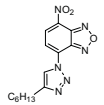

3.30

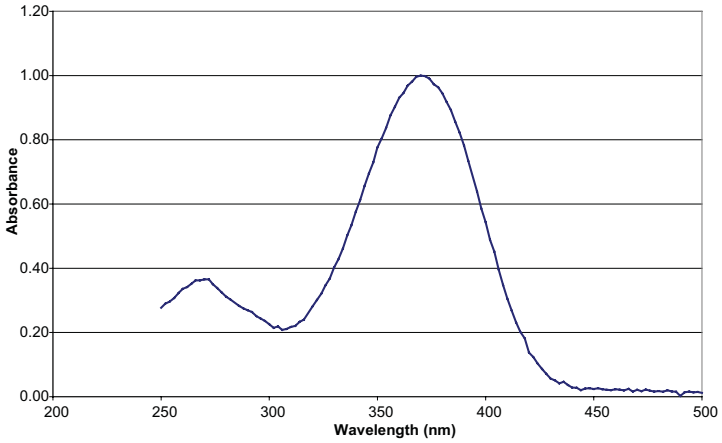
Absorbance
1.20
1.00
0.80
0.60
0.40
0.20
0.00
200
250
300
350
400
450
500
Wavelength (nm)

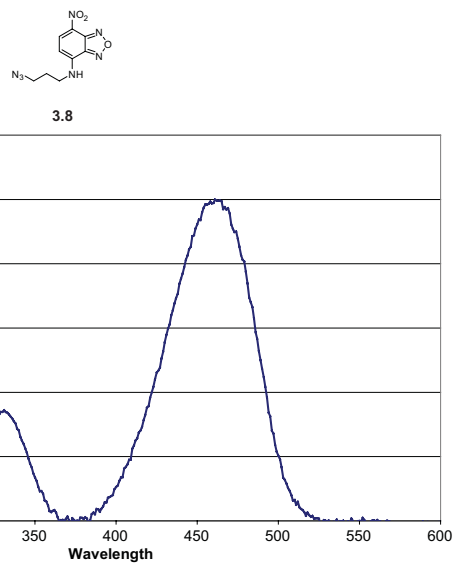
3.8
Absorbance
Wavelength
1.20
1.00
0.80
0.60
0.40
0.20
0.00
200
250
300
350
400
450
500
550
600

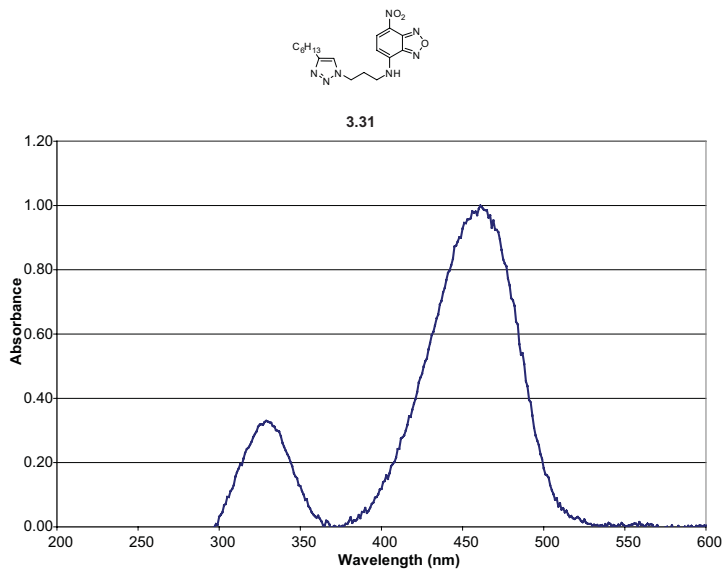
3.31
Absorbance
Wavelength (nm)
1.20
1.00
0.80
0.60
0.40
0.20
0.00
200
250
300
350
400
450
500
550
600

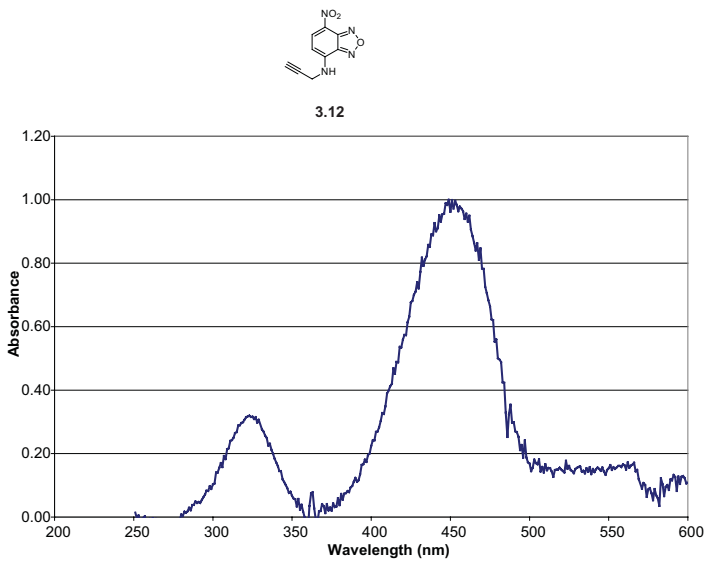
3.12
Absorbance
Wavelength (nm)
1.20
1.00
0.80
0.60
0.40
0.20
0.00
200
250
300
350
400
450
500
550
600

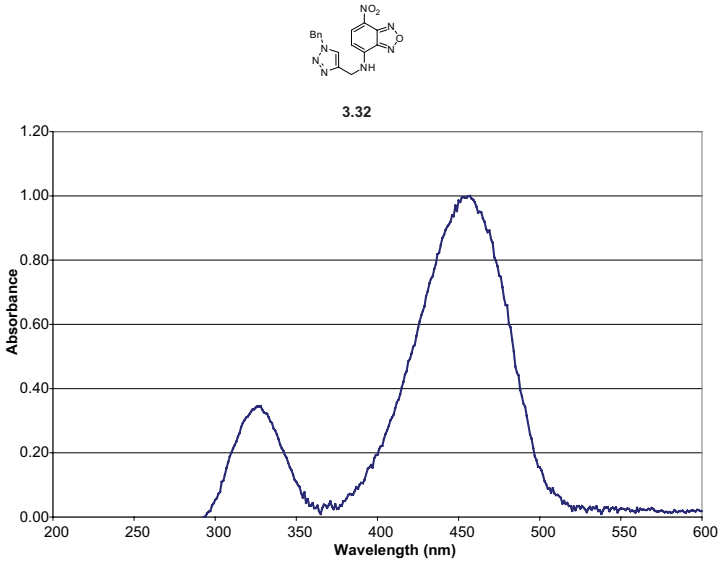
3.32
Absorbance
Wavelength (nm)
1.20
1.00
0.80
0.60
0.40
0.20
0.00
200
250
300
350
400
450
500
550
600

3.26

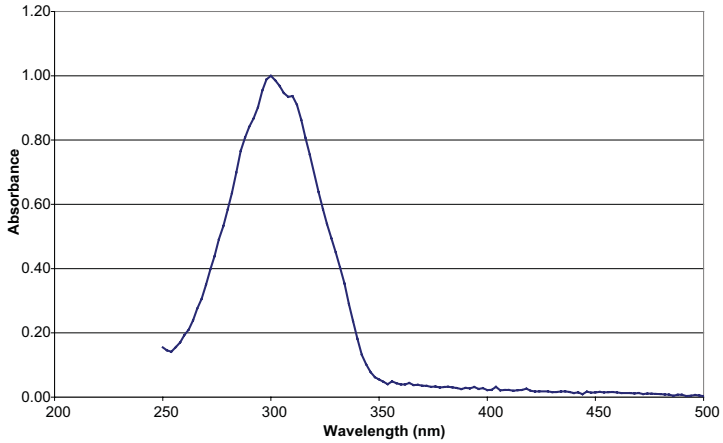
1.20
1.00
0.80
0.60
0.40
0.20
0.00
Absorbance
200
250
300
350
400
450
500
Wavelength (nm)

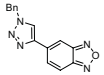

3.33

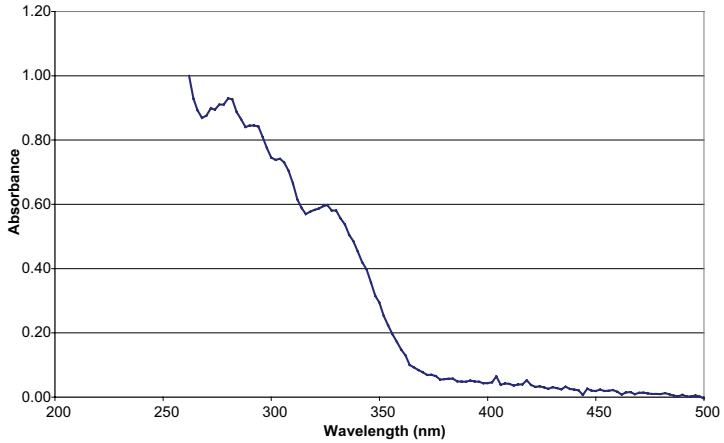
1.20
1.00
0.80
0.60
0.40
0.20
0.00
Absorbance
200
250
300
350
400
450
500
Wavelength (nm)

3.5.5 Fluorescence emission of 3.4-3.33 in ethanol

3.4

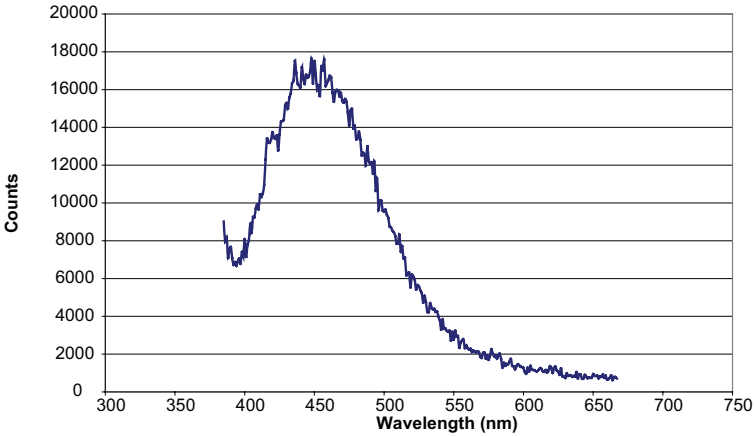

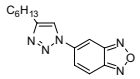

3.29

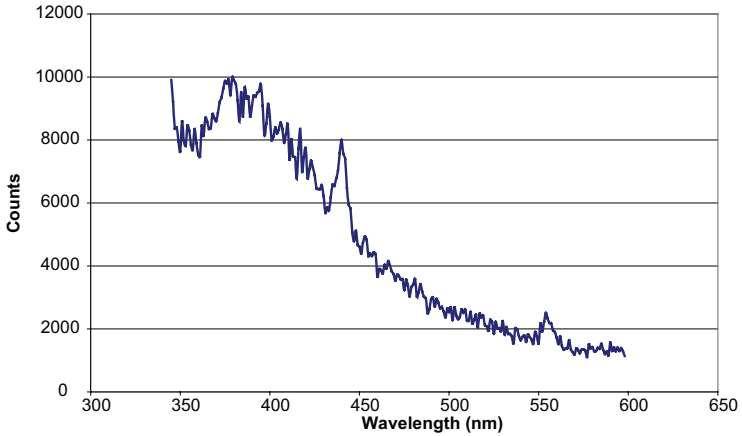

3.6

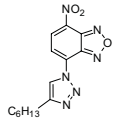

3.30

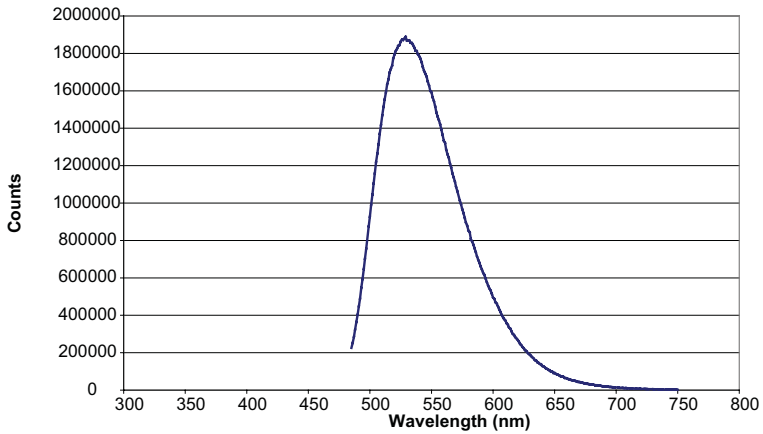
Counts
2000000
1800000
1600000
1400000
1200000
1000000
800000
600000
400000
200000
0
300 350 400 450 500 550 600 650 700 750 800
Wavelength (nm)

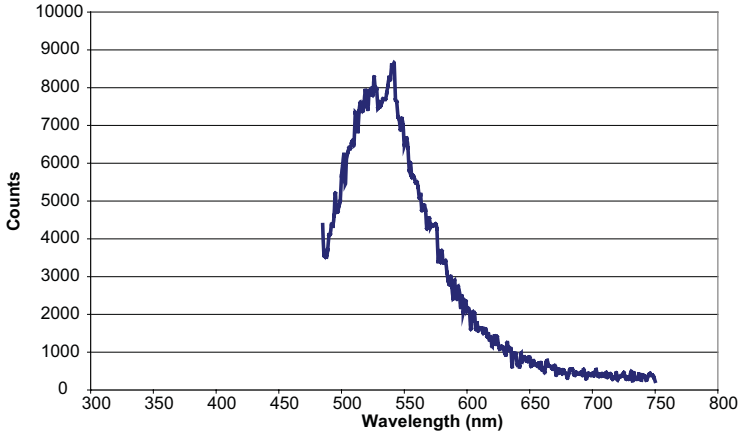
Counts
10000
9000
8000
7000
6000
5000
4000
3000
2000
1000
0
300 350 400 450 500 550 600 650 700 750 800
Wavelength (nm)

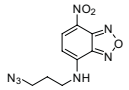

3.8

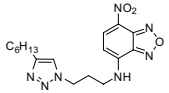

3.31

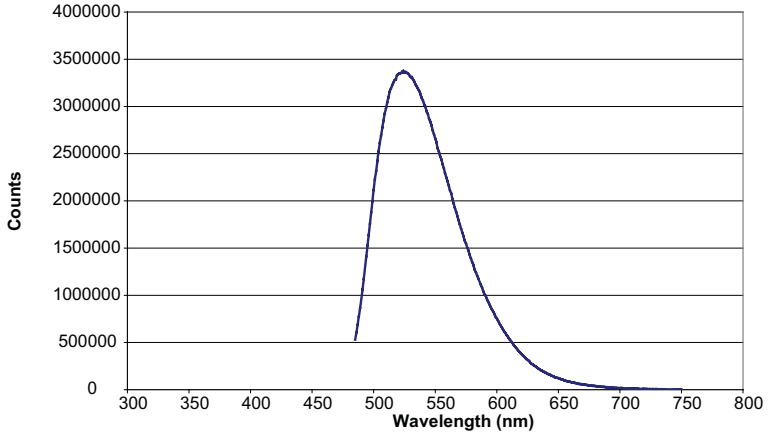
Counts
4000000
3500000
3000000
2500000
2000000
1500000
1000000
500000
0
300
350
400
450
500
550
600
650
700
750
800
Wavelength (nm)

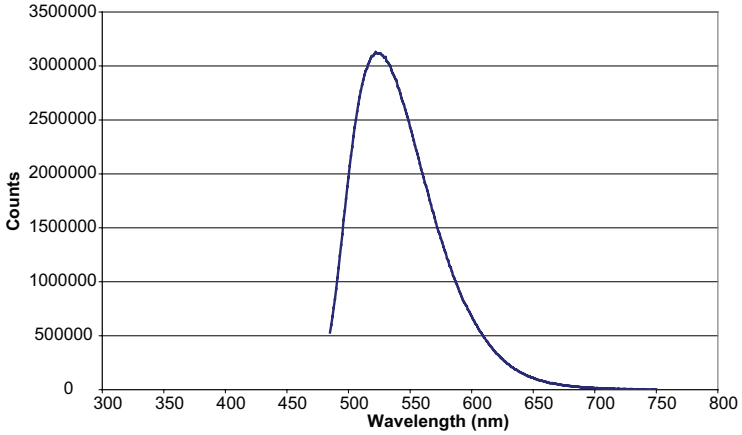
Counts
3500000
3000000
2500000
2000000
1500000
1000000
500000
0
300
350
400
450
500
550
600
650
700
750
800
Wavelength (nm)

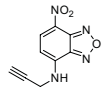

3.12

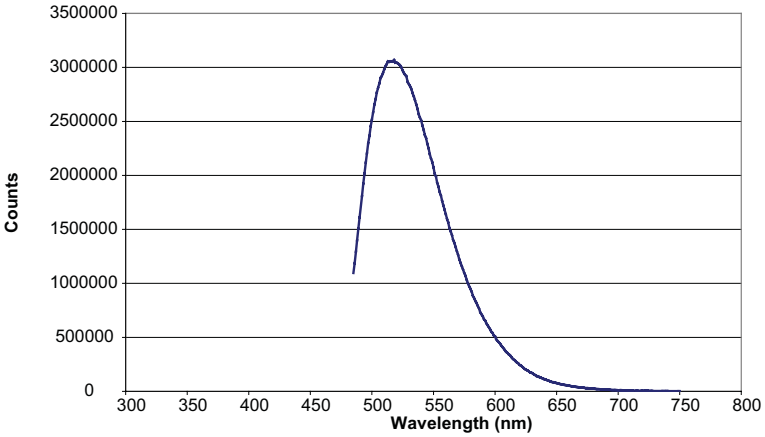
Counts
3500000
3000000
2500000
2000000
1500000
1000000
500000
0
300 350 400 450 500 550 600 650 700 750 800
Wavelength (nm)

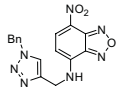

3.32

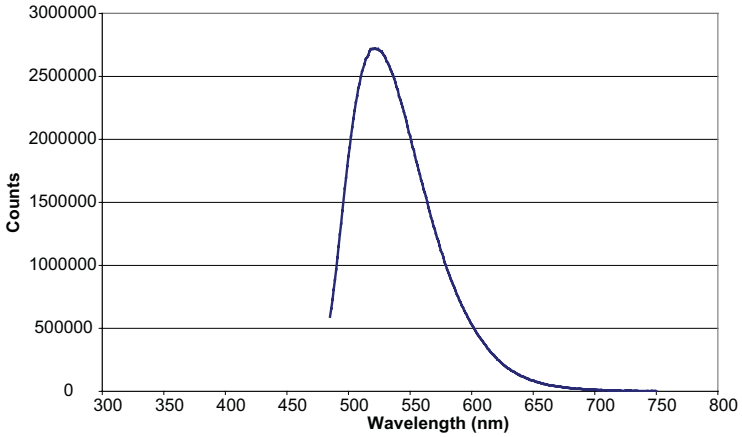
Counts
3000000
2500000
2000000
1500000
1000000
500000
0
300 350 400 450 500 550 600 650 700 750 800
Wavelength (nm)

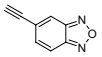

3.26

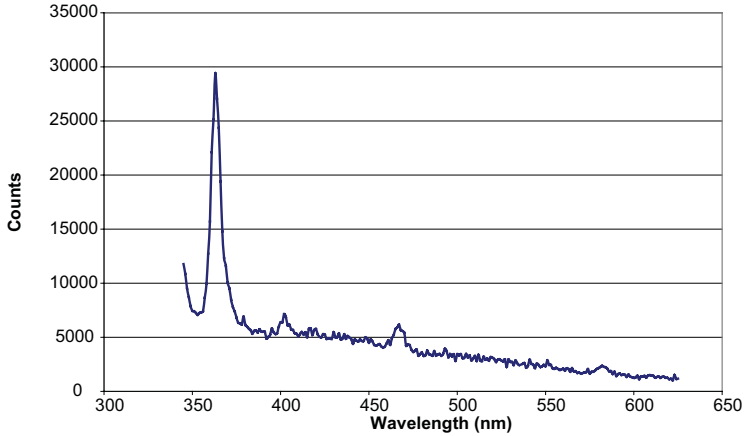
35000
30000
25000
20000
15000
10000
5000
0
Counts
300
350
400
450
500
550
600
650
Wavelength (nm)

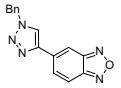
Bn

3.33

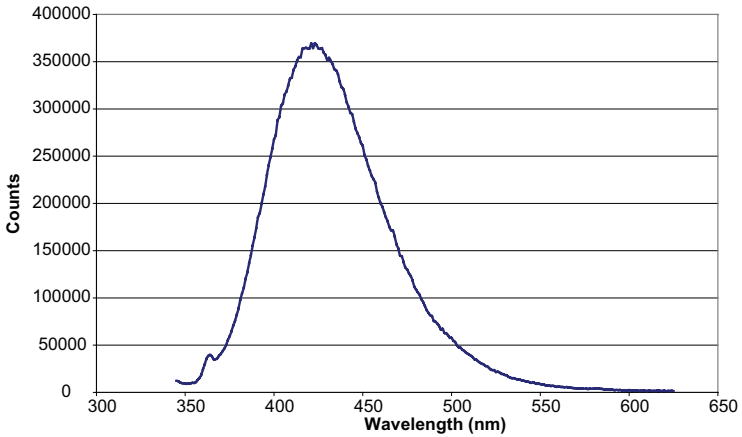
400000
350000
300000
250000
200000
150000
100000
50000
0
Counts
300
350
400
450
500
550
600
650
Wavelength (nm)

3.5.6 Normalized UV-vis absorbance of 3.2-3.33 in n*-hexane*

3.2

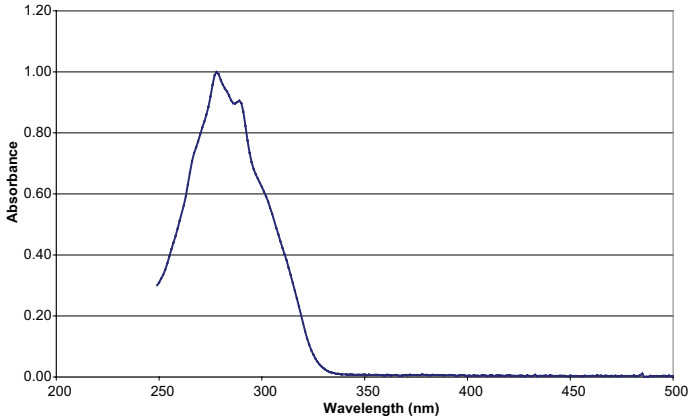

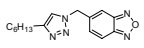

3.28

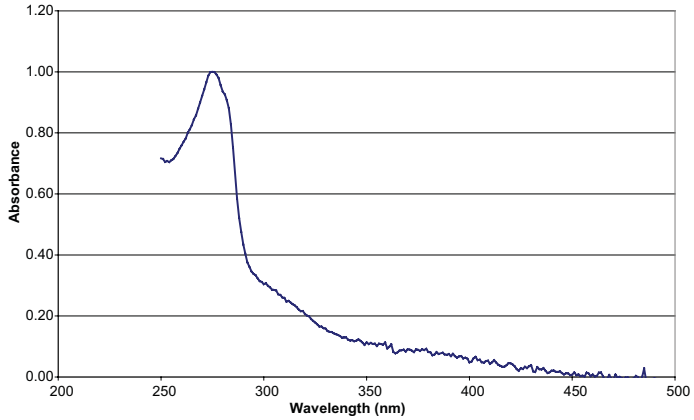

3.4

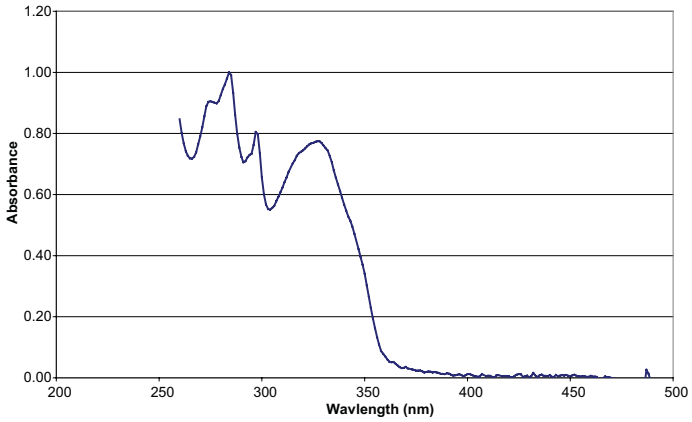
Absorbance
1.20
1.00
0.80
0.60
0.40
0.20
0.00
200
250
300
350
400
450
500
Wavlength (nm)

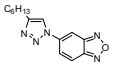

3.29

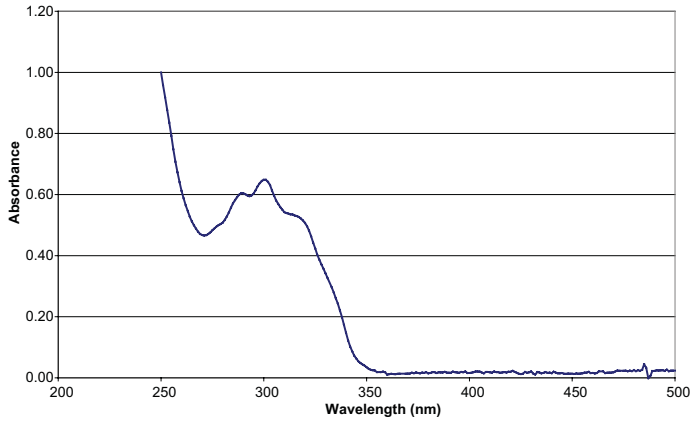
Absorbance
1.20
1.00
0.80
0.60
0.40
0.20
0.00
200
250
300
350
400
450
500
Wavelength (nm)

3.6

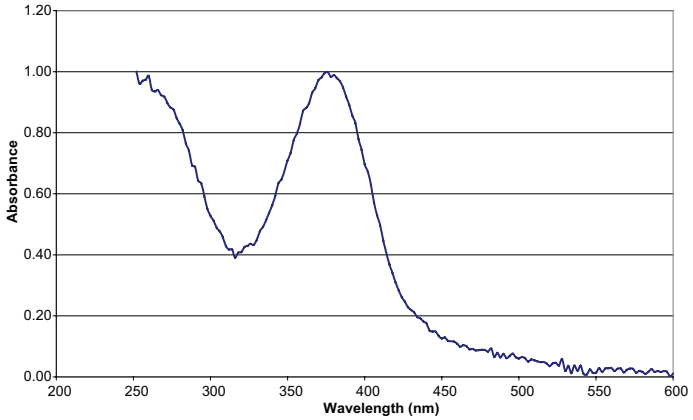
Absorbance
1.20
1.00
0.80
0.60
0.40
0.20
0.00
200
250
300
350
400
450
500
550
600
Wavelength (nm)

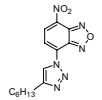

3.30

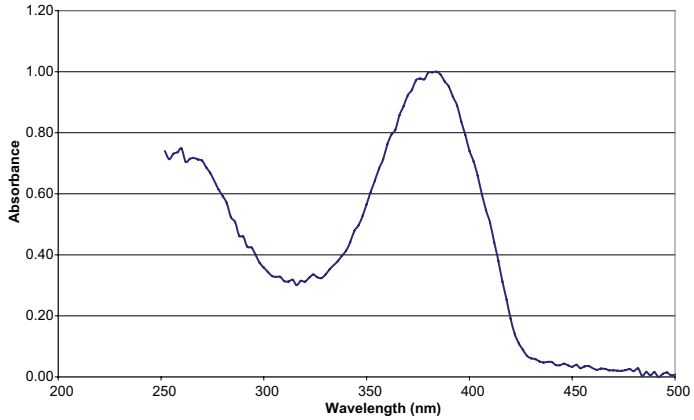
Absorbance
1.20
1.00
0.80
0.60
0.40
0.20
0.00
200
250
300
350
400
450
500
Wavelength (nm)

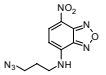

3.8

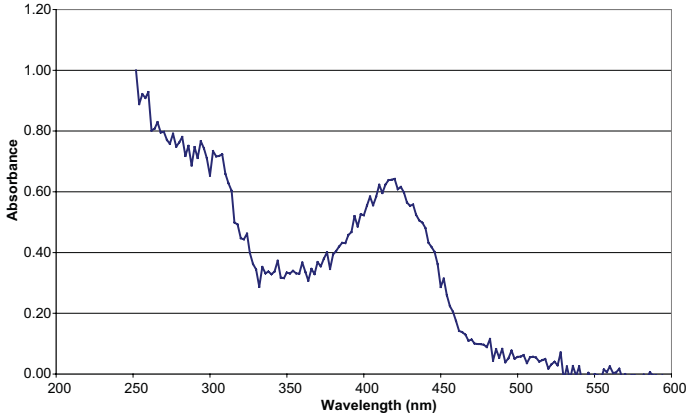
1.20
1.00
0.80
0.60
0.40
0.20
0.00
Absorbance
200
250
300
350
400
450
500
550
600
Wavelength (nm)

3.12

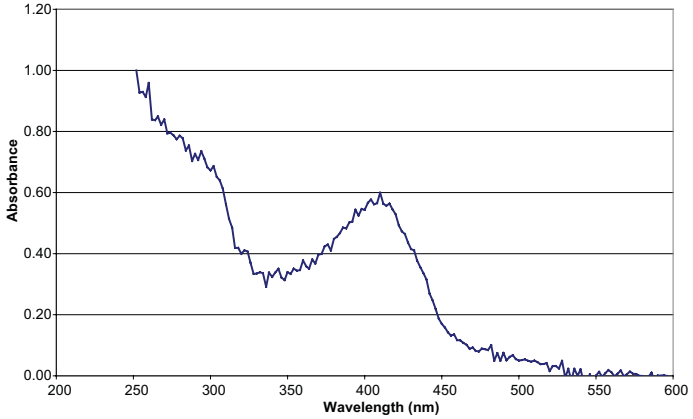
Absorbance
1.20
1.00
0.80
0.60
0.40
0.20
0.00
200
250
300
350
400
450
500
550
600
Wavelength (nm)

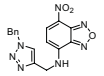

3.32

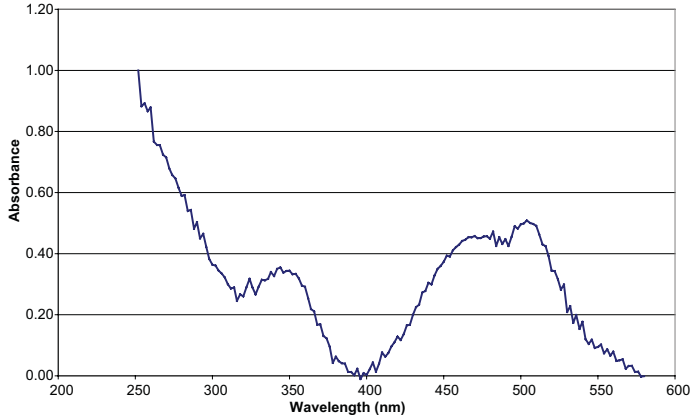
Absorbance
1.20
1.00
0.80
0.60
0.40
0.20
0.00
200
250
300
350
400
450
500
550
600
Wavelength (nm)

3.26

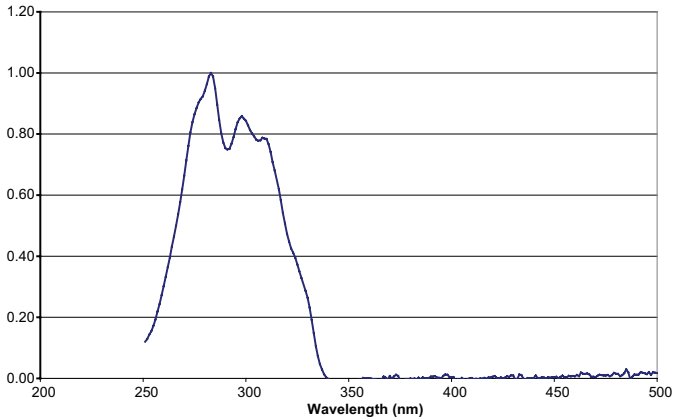
1.20
1.00
0.80
0.60
0.40
0.20
0.00
200
250
300
350
400
450
500
Wavelength (nm)

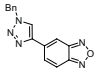

3.33

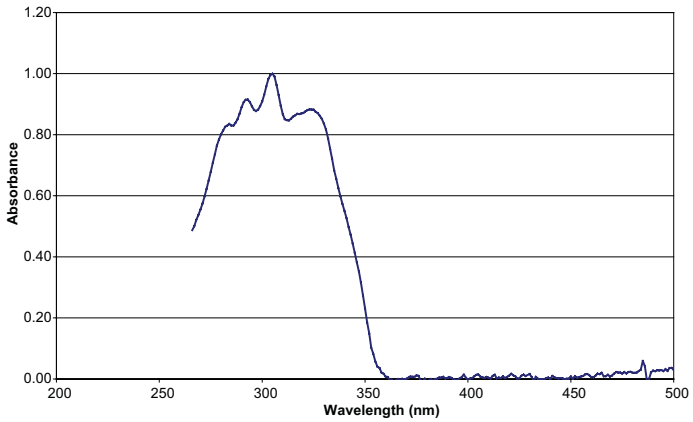
Absorbance
1.20
1.00
0.80
0.60
0.40
0.20
0.00
200
250
300
350
400
450
500
Wavelength (nm)

3.6 References

Angell, Y. and Burgess, K. (2007) Base dependence in copper-catalyzed Huisgen reactions: Efficient formation of bistriazoles. *Angewandte Chemie-International Edition*, 46, 3649-3651.

Demchenko, A.P., Mély, Y., Duportail, G. and Klymchenko, A.S. (2009) Monitoring Biophysical Properties of Lipid Membranes by Environment-Sensitive Fluorescent Probes. *Biophysical Journal*, 96, 3461-3470.

Dorogov, M.V., Filimonov, S.I., Kobylinsky, D.B., Ivanovsky, S.A., Korikov, P.V., Soloviev, M.Y., Khahina, M.Y., Shalygina, E.E., Kravchenko, D.V. and Ivachtchenko, A.V. (2004) A Convenient Synthesis of Novel 3-(Heterocyclylsulfonyl)propanoic Acids and their Amide Derivatives. *Synthesis*, 2004, 2999,3004.

Gottlieb, H.E., Kotlyar, V. and Nudelman, A. (1997) NMR Chemical Shifts of Common Laboratory Solvents as Trace Impurities. *The Journal of Organic Chemistry*, 62, 7512-7515.

Key, J.A., Cairo, C.W. and Ferguson, M.J. (2008) 7,7 '-(3,3 '-dibenzyl-3H,3 ' H-4,4 '-bi-1,2,3-triazole-5,5 '-diyl)bis(4-methyl-2H-chromen-2-one). *Acta Crystallographica Section E-Structure Reports Online*, 64, O1910-U3631.

Key, J.A., Koh, S., Timerghazin, Q.K., Brown, A. and Cairo, C.W. (2009) Photophysical characterization of triazole-substituted coumarin fluorophores. *Dyes and Pigments*, 82, 196-203.

Lakowicz, J.R. (2006) Principles of Fluorescence Spectroscopy. Springer, New York, NY.

Lavis, L.D. and Raines, R.T. (2008) Bright ideas for chemical biology. *ACS Chemical Biology*, 3, 142-155.

LeDroumaguet, C., Wang, C. and Wang, Q. (2010) Fluorogenic click reaction. *Chemical Society Reviews*, 1233 - 1239.

Lemieux, G.A., de Graffenried, C.L. and Bertozzi, C.R. (2003) A Fluorogenic Dye Activated by the Staudinger Ligation. *Journal of the American Chemical Society*, 125, 4708-4709.

Liang, Y., Xie, Y.-X. and Li, J.-H. (2005) Modified Palladium-Catalyzed Sonogashira Cross-Coupling Reactions under Copper-, Amine-, and Solvent-Free Conditions. *The Journal of Organic Chemistry*, 71, 379-381.

Lord, S.J., Lee, H.-l.D., Samuel, R., Weber, R., Liu, N., Conley, N.R., Thompson, M.A., Twieg, R.J. and Moerner, W.E. (2009) Azido Pushâˆ’Pull Fluorogens Photoactivate to Produce Bright Fluorescent Labelsâ€ *The Journal of Physical Chemistry B*.

Loura, L.M.S., Fernandes, F., Fernandes, A.C. and Ramalho, J.P.P. (2008) Effects of fluorescent probe NBD-PC on the structure, dynamics and phase transition of DPPC. A molecular dynamics and differential scanning calorimetry study. *Biochimica et Biophysica Acta (BBA) - Biomembranes*, 1778, 491-501.

Meldal, M. and Tornoe, C.W. (2008) Cu-catalyzed azide-alkyne cycloaddition. *Chemical Reviews*, 108, 2952-3015.

Sandbhor, M.S., Key, J.A., Strelkov, I.S. and Cairo, C.W. (2009) A Modular Synthesis of Alkynyl-Phosphocholine Headgroups for Labeling Sphingomyelin and Phosphatidylcholine. *The Journal of Organic Chemistry*, 74, 8669-8674.

Sawa, M., Hsu, T.L., Itoh, T., Sugiyama, M., Hanson, S.R., Vogt, P.K. and Wong, C.H. (2006) Glycoproteomic probes for fluorescent imaging of fucosylated glycans in vivo. *Proceedings of the National Academy of Sciences of the United States of America*, 103, 12371-12376.

Sivakumar, K., Xie, F., Cash, B.M., Long, S., Barnhill, H.N. and Wang, Q. (2004) A fluorogenic 1,3-dipolar cycloaddition reaction of 3-azidocoumarins and acetylenes. *Organic Letters*, 6, 4603-4606.

Smith, M.B. and March, J. (2007) March's Advanced Organic Chemistry: *Reactions, Mechanisms and Structure* John Wiley & Sons, Inc, Hoboken, NJ.

Uchiyama, S., Santa, T., Fukushima, T., Homma, H. and Imai, K. (1998) Effects of the substituent groups at the 4- and 7-positions on the fluorescence characteristics of benzofurazan compounds. *Journal of the Chemical Society-Perkin Transactions 2*, 2165-2173.

Uchiyama, S., Santa, T. and Imai, K. (1999) Semi-empirical PM3 calculation reveals the relationship between the fluorescence characteristics of 4,7-disubstituted benzofurazan compounds, the LUMO energy and the dipole moment directed from the 4- to the 7-position. *Journal of the Chemical Society-Perkin Transactions 2*, 569-576.

Uchiyama, S., Takehira, K., Kohtani, S., Santa, T., Nakagaki, R., Tobita, S. and Imai, K. (2002) Photophysical study of 5-substituted benzofurazan compounds as fluorogenic probes. *Physical Chemistry Chemical Physics*, 4, 4514-4522.

Zhou, Z. and Fahrni, C.J. (2004) A fluorogenic probe for the copper(I)-catalyzed azide-alkyne ligation reaction: modulation of the fluorescence emission via

3(n,pi)-1(pi,pi) inversion. *Journal of the American Chemical Society*, 126, 8862-8863.

Chapter 4

Detection of cellular sialic acid content using nitrobenzoxadiazole carbonyl-reactive chromophores[4]

[4] Portions of the work described in this chapter have been published in Key, J.A., Li, C. and Cairo, C.W. (Submitted) Detection of cellular sialic acid content using nitrobenzoxadiazole carbonyl-reactive chromophores. *Bioconjugate Chemistry*.

4.1 Introduction

Sensitive detection of biomolecules by derivatization with fluorescent dyes is a critical technique used in histology, cell biology, and biochemistry. (Cairo, C.W., Key, J.A., et al. 2010, Demchenko, A.P., Mely, Y., et al. 2009, Lavis, L.D. and Raines, R.T. 2008) Specific detection of conjugates relies on chemoselective ligation of functional groups found on the biomolecule and the label. As a result, strategies to introduce reactive functional groups into biomolecules have been developed. Typical strategies include the metabolic incorporation of synthetic labels and chemical modification of native biomolecules. (Sletten, E.M. and Bertozzi, C.R. 2009, Tiefenbrunn, T.K. and Dawson, P.E. 2010)

A popular strategy for labelling of glycoproteins is the use of sodium periodate to generate a reactive handle by oxidizing the glycerol side-chain of sialic acid to an aldehyde.(Van lenten, L. and Ashwell, G. 1971) While this method is more commonly used *in vitro*, it has recently been extended to the labelling of glycans in live cells. (De Bank, P.A., Kellam, B., et al. 2003, Zeng, Y., Ramya, T.N.C., et al. 2009) Live cell labelling requires mild conditions and near quantitative reactions; which has been achieved by performing the oxidation reaction at low temperature, and accelerating the conjugation reaction with an aniline catalyst. (Zeng, Y., Ramya, T.N.C., et al. 2009) This method of periodate oxidation and aniline-catalyzed ligation (PAL) can then be used to label glycoconjugates for microscopy.

Sialic acids are a class of carbohydrates which have important biological functions in embryogenesis, development, and immune response. (Bi, S. and Baum, L.G. 2009, Du, J., Meledeo, M.A., et al. 2009, Varki, N.M. and Varki, A. 2007) Methods of detecting sialylation include metabolic labelling, lectins, and chemical modification.(Chen, X. and Varki, A. 2010) Metabolic labelling affords the introduction of unique functional groups that allow for sensitive detection; however, this strategy can suffer from incomplete label incorporation.(Dube, D.H. and Bertozzi, C.R. 2003) Lectins are relatively large proteins which may suffer from relatively low affinities. Importantly, many lectins or antibodies can perturb cells by crosslinking receptors – limiting their application in live cells.(Anderson, J. and Melchers, F. 1976, Hernandez, J.D. and Baum, L.G. 2002) Selective chemical modification of sialic acids using PAL presents an attractive alternative. (Zeng, Y., Ramya, T.N.C., et al. 2009)

Previous reports of PAL have relied upon biotin-amino-oxy conjugates which were then detected by fluorescently-labelled streptavidin. This two-step method required the use of a 60 kDa tetrameric protein for labelling a single carbohydrate residue (c.a. 300 Da).(De Bank, P.A., Kellam, B., et al. 2003, Diamandis, E.P. and Christopoulos, T.K. 1991, Zeng, Y., Ramya, T.N.C., et al. 2009) Such a bulky label could mask other epitopes on the same cell or macromolecule, and may have reduced labelling capacity due to molecular crowding.

Small molecule fluorophores which contain either hydrazine or amino-oxy functional groups can be applied to bioorthogonal and PAL labelling

strategies.(Rayo, J., Amara, N., et al.) 7-nitro-benz-[2,1,3-*d*]-oxadiazoles (NBDs) are a class of small, synthetically accessible, and environmentally sensitive fluorophores which can be easily modified for use with PAL. In general NBDs possess relatively high fluorescence emission quantum yields and long excitation and emission wavelengths when compared to fluorophores of similar size, such as coumarins. (Key, J.A., Koh, S., et al. 2009) Interestingly, the attachment of a hydrazine functional group to these dyes results in fluorogenic derivatives which allow direct detection of carbonyl derivatives upon formation of the corresponding hydrazone. Reported fluorogenic and fluorescent hydrazino-NBD derivatives include: 7-hydrazino-4-nitrobenzo-2-oxa-1,3,-diazole (NBDH) (Gubitz, G., Wintersteiger, R., et al. 1984), 4-(*N*,*N*-dimethylaminosulphonyl)-7-hydrazino-benz-2,1,3-oxadiazole (DBDH) (Uzu, S., Kanda, S., et al. 1990), 4-4-aminosulphonyl-7-hydrazino-2,1,3-benzoxadiazole (ABDH) (Uzu, S., Kanda, S., et al. 1990), 4-(*N*,*N*-dimethylaminosulfonyl)-7-*N*-methylhydrazino-benz-2,1,3-oxadiazole (MDBDH) (Jachmann, N. and Karst, U. 2001), 4-[2-(*N*,*N*-dimethylamino)ethylaminosulfonyl]-7-*N*-methylhydrazino-benz-2,1,3-oxadiazole (DAABD-MHz) (Santa, T., Al-Dirbashi, O.Y., et al. 2008), and *N*-methyl-4-hydrazino-7-nitrobenzofurazan (MNBDH) (**Figure 4.1**). (Buldt, A. and Karst, U. 1999) Several of these derivatives are commercially available and have found application in biological assays (Raindlová, V., Pohl, R., et al. 2010) as well as the detection of trace carbonyls in air samples such as automobile exhaust. (Jachmann, N. and Karst, U. 2001)

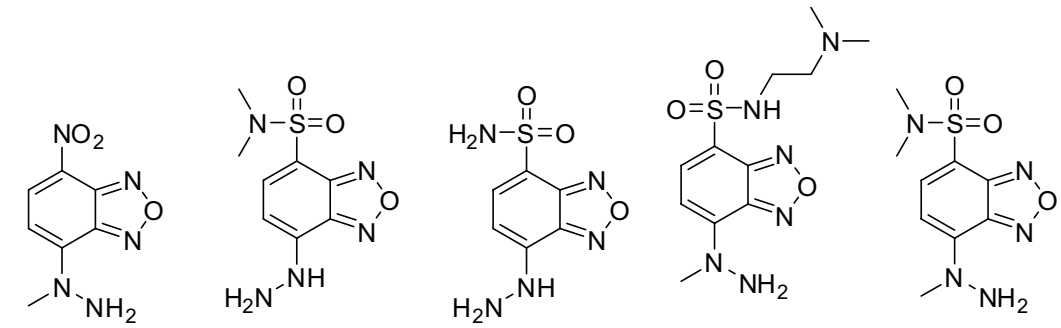

Figure 4.1. Reported fluorogenic and fluorescent hydrazino-NBD derivatives. NBDH, DBDH and ABDH are reported fluorogenic reagents, while DAABD-MHz and MDBDH are reported fluorescent.

We considered that small molecule labels compatible with PAL should be of interest for fluorescence microscopy of glycoconjugates. Herein we describe the synthesis of a novel amino-oxy fluorophore, NBDAO (**4.5**), for selective labelling of sialic acid glycoconjugates on live cells and contrast its properties to a known carbonyl reactive fluorophore, NBDH (**4.2**).(Gubitz, G., Wintersteiger, R., et al. 1984) We observe labelling of cells by fluorescence microscopy, flow cytometry, and with a fluorescence microplate reader. As well, NBDAO was used to label a glycoprotein in conjunction with PAL, followed by fluorescence detection in SDS-PAGE. We conclude that these dyes can be used as an effective one-step live-cell labelling strategy for glycoconjugates.

4.2 Fluorophore synthesis

NBDH (**4.2**) was synthesized from commercially available 7-nitro-4-chlorobenz-2,1,3-oxadiazole (NBD-Cl) (**4.1**) in chloroform by reaction with 1% hydrazine as described by Gubitz et al.(Gubitz, G., Wintersteiger, R., et al. 1984)

Alternatively, the NBDH·NH_2NH_2 salt may be prepared from 7-nitro-4-fluorobenz-2,1,3-oxadiazole using the method of Uzu and colleagues.(Uzu, S., Kanda, S., et al. 1990) A hydrazone derivative, **4.3**, was then generated in good yield by conjugation with benzaldehyde in methanol at room temperature (**Scheme 4.1**). NBDAO (**4.5**) was synthesized by an initial S_NAr of NBD-Cl (**4.1**) with ethyl *N*-hydroxyacetimidate under basic conditions, to generate the ethyl acetohydroxamate intermediate (**4.4**).(Miyazawa, E., Sakamoto, T., et al. 1997)

The acetimidate functions as a protected amino-oxy group, and reported deprotection protocols for aryl substrates involve the use of strong acids, such as perchloric acid and hydrofluoric acid.(Carpino, L.A. 1960, Miyazawa, E., Sakamoto, T., et al. 1997) We found that the amino-oxy functional group could be unveiled in moderate yield by hydrolysis with aqueous trifluoroacetic acid. Care must be taken at the deprotection step to avoid alkaline workup conditions. In our hands, basic solutions lead to decomposition of the amino-oxy compound, presumably to the corresponding phenolate.(Salahuddin, S., Renaudet, O., et al. 2004) Additionally, we found that care should be taken to remove any trace amounts of ketone or aldehyde contaminants (such as acetone) to avoid the rapid formation of the oxime. A representative oxime derivative (**4.6**) was generated by reaction with neat MEK at room temperature.

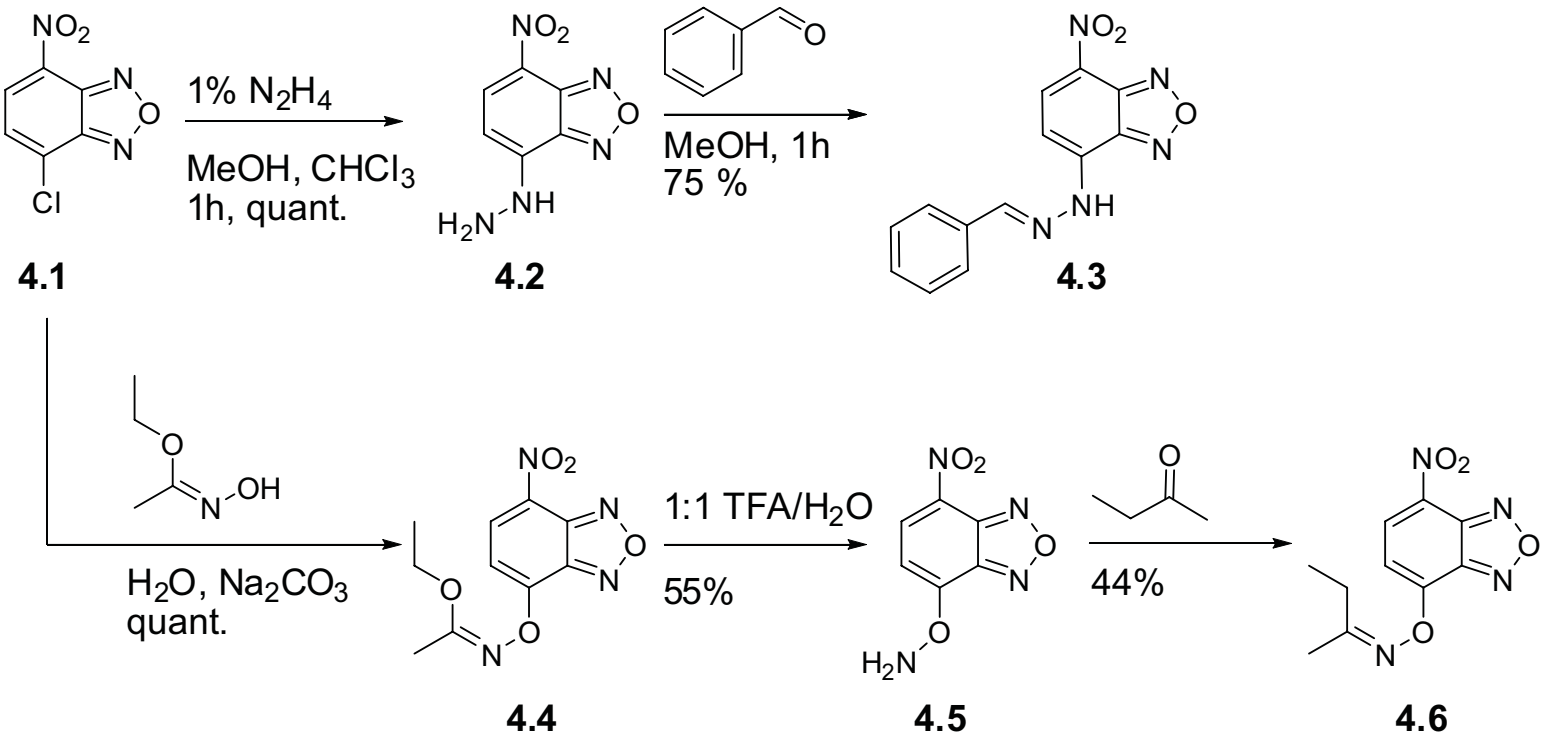

Scheme 4.1. Synthesis of NBDH (4.2) and NBDAO (4.5) carbonyl reactive chromophores and model hydrazone and oxime ligation products (4.3 and 4.6). Carbonyl reactive NBDs were generated by S_NAr and strong acid deprotection (NBDAO). Hydrazone and oxime forming reactions were performed neat.

4.3 Fluorophore characterization

The NBD dyes (**4.2** and **4.5**) and corresponding hydrazone (**4.3**) and oxime (**4.6**) conjugates were characterized to determine their absorbance spectra, fluorescence emission, molar absorption coefficients, and emission quantum yields (QY) (**Table 4.1**). Quantum yield was determined using a Rhodamine 6G standard in ethanol (see section 2.10). Similar to other NBD derivatives, the photophysical properties of these compounds were found to be environmentally sensitive.(Demchenko, A.P., Mely, Y., et al. 2009, Key, J.A. and Cairo, C.W. 2011) Consistent with previous reports, we confirmed that conversion of **4.2** to **4.3** is fluorogenic with an 8.5-fold increase in QY and a 15-fold increase in brightness in acetonitrile. Additionally, we observed that NBDH derivatization was fluorogenic in water, particularly at low pH. For example, at pH 5.4 the hydrazone (**4.3**) has a 9.2-fold increase in QY and 32-fold increase in brightness relative to the starting hydrazine (**4.2**). However, NBDH and its hydrazone derivative show less fluorescence in water relative to ethanol and acetonitrile solutions.

The derivatization of NBDAO (**4.5**) to an oxime (**4.6**) leads to an increase in the absorption coefficient of the dye; however, there is only a slight shift in the emission wavelength (**Figure 4.2**). Both NBDAO and its oxime conjugate (**4.6**) show an increased Stokes shift relative to NBDH, which may lead to improved sensitivity. Both NBDAO and the oxime derivative have reduced environmental sensitivity when compared to compounds **4.2** and **4.3**, respectively.

Compound	*Solvent*	λ *max*$_{abs\ (nm)}$	λ *max*$_{fluor}$	Φ *Quantum yield* [b]	Δ Φ *(% increase)*	ε *Absorption coefficient* ($cm^{-1}M^{-1}$)[d]	*Brightness* (ε x Φ)	Δ *Brightness (%)*
NBDH (**4.2**)	7.4	271, 374, <u>494</u>	NA	0		NA		
	5.4	271, 372, <u>496</u>	552	0.001		14800	10	
	CH_3CN	280, 405, <u>425</u>	531, 548	0.003		56700	170	
	EtOH	334, <u>470</u>	537	0.28		110500	31547	
Hydrazone (**4.3**)	7.4	360, <u>444</u>	NA	0		67900	34	
	5.4	356, 440, <u>495</u>	552	0.006	920	52100	320	3239
	CH_3CN	306, 323, <u>492</u>	555	0.026	853	98000	2501	1473
	EtOH	307, 327, <u>493</u>	555	0.038	14	25600	977	3
NBDAO (**4.5**)	4.7	291, 381, <u>470</u>	552	0.006		8000	46	
	EtOH	275, 376, <u>472</u>	540	0.054		10200	548	
	CH_3CN	279, 376, <u>466</u>	541	0.133		14000	1863	
Oxime (**4.6**)	4.7	390, <u>465</u>	566	0.003	44	16700	42	92
	EtOH	270, 378, <u>467</u>	545	0.16	298	7900	1263	230
	CH_3CN	264, 380, <u>470</u>	538	0.138	104	15600	2150	115

Table 4.1. Photophysical properties of NBDH, NBDAO and carbonyl ligation products.

a. Absorbance maxima are listed with the peak used for fluorescence excitation underlined

b. Quantum yield standards were fluorescein in 0.1 M sodium hydroxide or rhodamine 6G in ethanol

c. Φ measured with excitation at 485 nm.

d. Molar absorption coefficient ε measured at 485 nm.

e. ΔΦ calculated as ($\Phi_{\text{ligation product}}/\Phi_{\text{hydrazine or amino-oxy}}$) x 100%

f. Δ Brightness calculated as (brightness $_{\text{ligation product}}$ /brightness $_{\text{hydrazine or amino-oxy}}$) x 100%

Both dyes (**4.5** and **4.6**) exhibited a smaller range of brightness between water, ethanol, and acetonitrile as compared to the hydrazine and hydrazone derivatives (**4.2** and **4.3**). The conversion of NBDAO to the oxime appeared to be fluorogenic in certain solvent environments (ethanol), but was relatively static in others. However, we note that several of these values are close to the lower limit of detection, and therefore may not be accurate enough to make this determination. We observed that NBDAO (**4.5**) underwent degradation to the corresponding phenolate in the presence of alkaline water, which could complicate its use in assays which require high pH.(Salahuddin, S., Renaudet, O., et al. 2004) In labelling experiments, we found that this degradation product could be easily removed by performing a wash step after dye treatment.

4.4 Reaction kinetics

The mechanism of oxime or hydrazone formation by NBDAO and NBDH is expected to be accelerated in the presence of aniline, which acts as a nucleophilic catalyst in acidic media.(Cordes, E.H. and Jencks, W.P. 1963, Dirksen, A., Hackeng, T.M., et al. 2006) Differences in the fluorescent properties of these dyes and their conjugates could be used as a method to observe the rate of the reaction directly. To confirm the role of aniline in these reactions, we observed the kinetics of ligation for NBDH (**4.2**) or NBDAO (**4.5**) with MEK in the presence or absence of aniline using a time-based fluorescence assay (**Figure 4.3**).

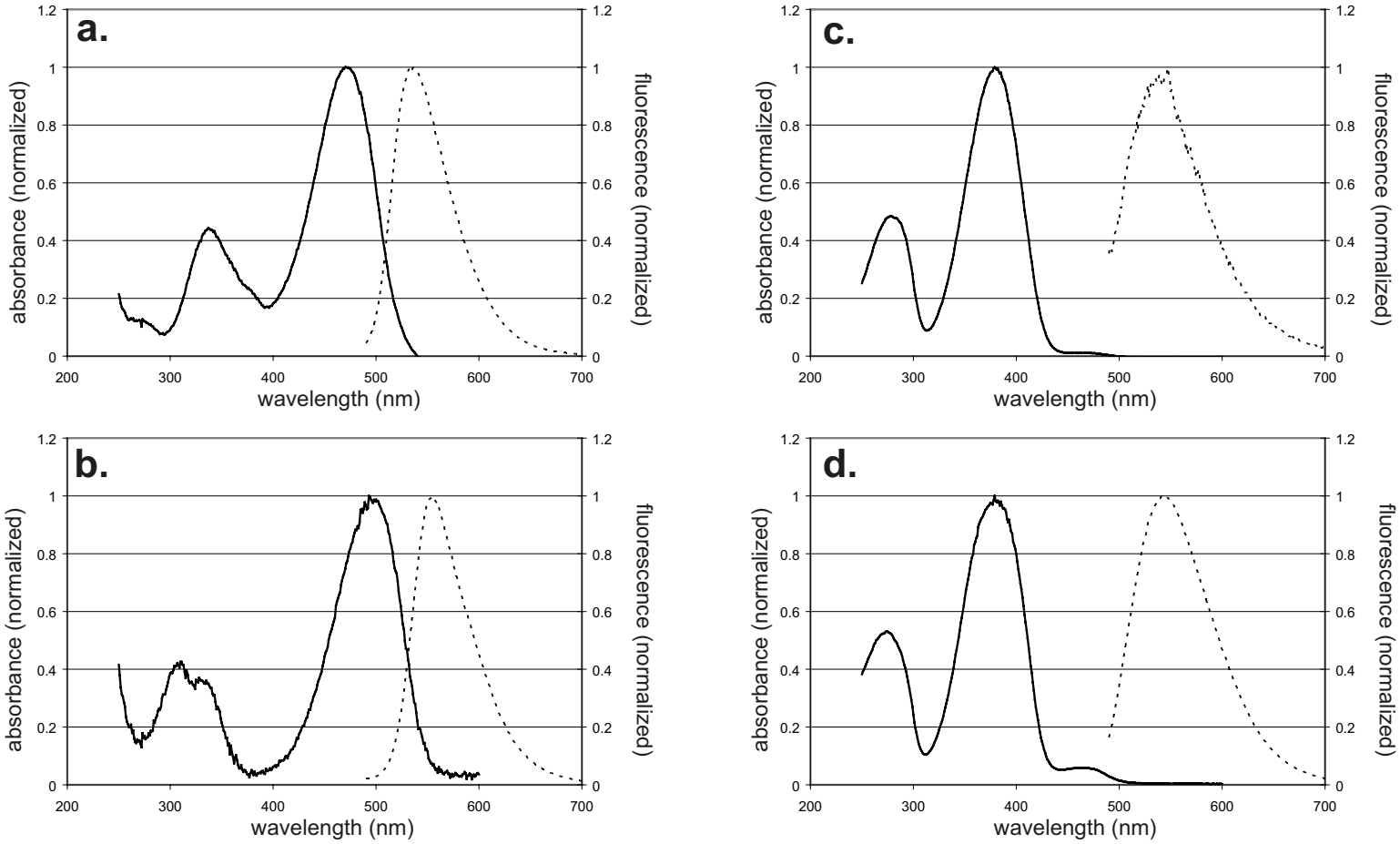

Figure 4.2. Normalized Absorbance and emission spectra in ethanol of a. NBDH (4.2), b. hydrazone (4.3), c. NBDAO (4.5), and d. oxime (4.6). Excitation was performed at 475 nm for all compounds.

As expected, we found that aniline did increase the rate of reaction for both dyes at pH 4.7. In the case of NBDH, the rate acceleration was limited to the early phase of the reaction (< 400 sec). In the case of the NBDAO dye, the rate acceleration was more substantial, with limited formation of the oxime in the absence of aniline. These findings suggest that NBDAO may be a more selective labelling agent than NBDH when used with aniline catalysis. At pH 7.4, we found that aniline did not increase the rate of reaction for either dye.

4.5 Glycoprotein labelling

To explore the utility of NBDAO for the detection of glycoconjugates, we tested the ability of the dyes to specifically label a known glycoprotein in SDS PAGE. Fetal calf serum fetuin is a commonly used, commercially available sialoprotein.(Dziegielewska, K.M., Brown, W.M., et al. 1990, Yang, Y. and Orlando, R. 1996) Detection of fetuin was performed by treatment with periodate followed by labelling with NBDAO in the presence of aniline (**Figure 4.4**). Labelling of a band (~64 kDa) corresponding to the protein was visible by fluorescence imaging. To demonstrate the specificity of this methodology for sialic acid, controls were performed using fetuin which was treated with neuraminidase (NEU). As expected, the dye only labelled the glycoprotein when sialic acid was present, and only after periodate treatment – confirming that the labelling chemistry is specific for sialylated proteins. We observed only minor residual staining in control samples; and factors that may contribute to background staining could include non-specific binding and naturally occurring

protein oxidation.(Matsushita, Y., Takahashi, M., et al. 1986, Ahn, B., Rhee, S.G., et al. 1987)

IgG glycosylation analysis is difficult due to the high level of heterogeneity in the many possible glycoforms, typically requiring elegant ms/ms strategies.(Huhn, C., Selman, M.H.J., et al. 2009) However, understanding the glycosylation patterns of different IgG clones remains an important target in the expanding field of therapeutic antibodies. Murine polyclonal IgG (pIgG) is expected to contain glycoforms with one or more sialylated glycans; commonly found in the bi-antennary glycan at the conserved N-link site of the heavy chain. Recent studies by Yasukawa et al, have identified sialic acid-containing glycans in the light chain of IgG, including disialic acid and Neu5Gc modifications.(Yasukawa, Z., Sato, C., et al. 2005, Yasukawa, Z., Sato, C., et al. 2006)

To confirm the presence of sialic acid glycoforms, pIgG was treated with periodate and then labelled with NBDH (Figure **4.5a**) or NBDAO in the presence of aniline (**Figure 4.5b**). Labelling of bands corresponding to the heavy chains (~50 kDa) and light chains (~25 kDa) of the protein were visible by fluorescence imaging. As a control, protein without periodate oxidation was included to determine background staining. For both dyes, we observed increased signal over control samples; however, NBDH gave greater signal intensity. Factors contributing to background staining again are likely due to non-specific binding and naturally occurring protein oxidation.

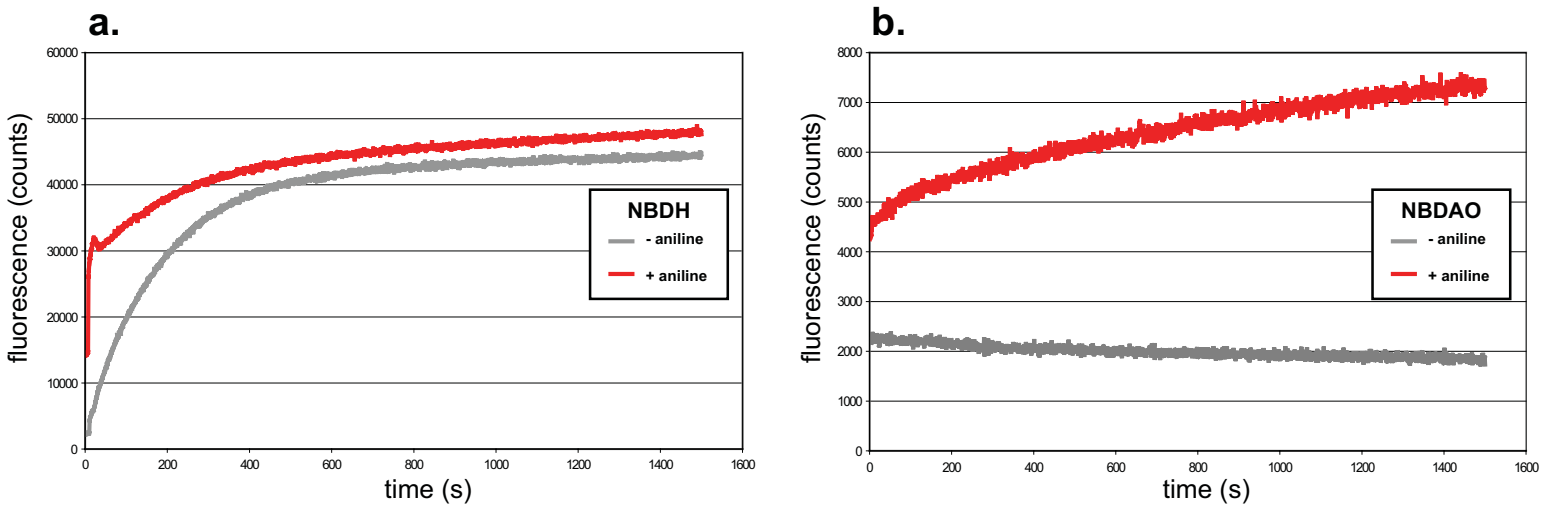

Figure 4.3. Reaction kinetics of a. NBDH (4.2) and b. NBDAO (4.5) with MEK at pH 4.7. The rates of both reactions are enhanced by the presence of aniline in the reaction mixture. The excitation wavelength was 485 nm, and emission was monitored at 540 nm for 1500 sec.

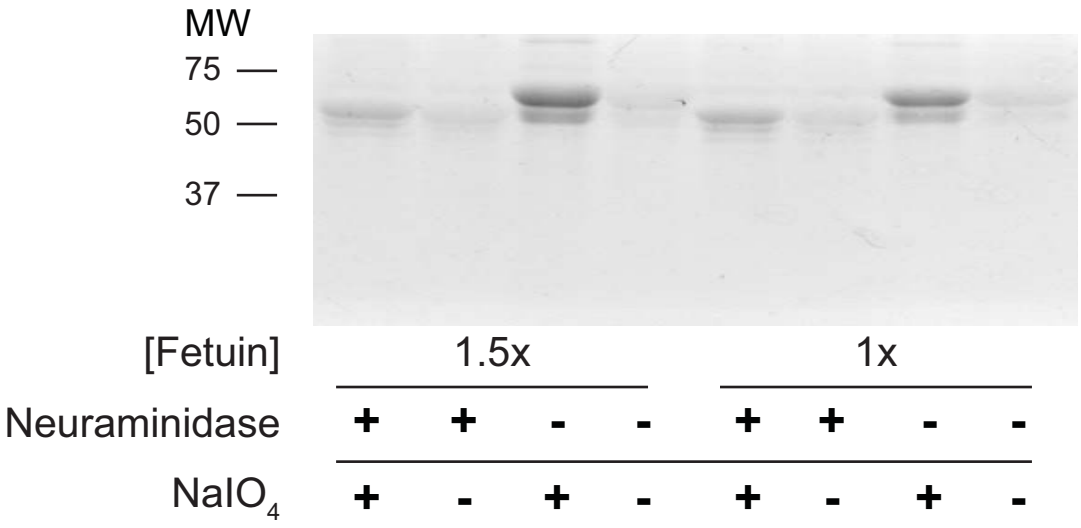

Figure 4.4. Fluorescent detection of glycoproteins in SDS PAGE. Labelling of fetal calf serum fetuin by PAL with NBDAO. Control lanes used protein which was treated with neuraminidase (NEU), and protein not treated with periodate. Molecular weights are given in kDa.

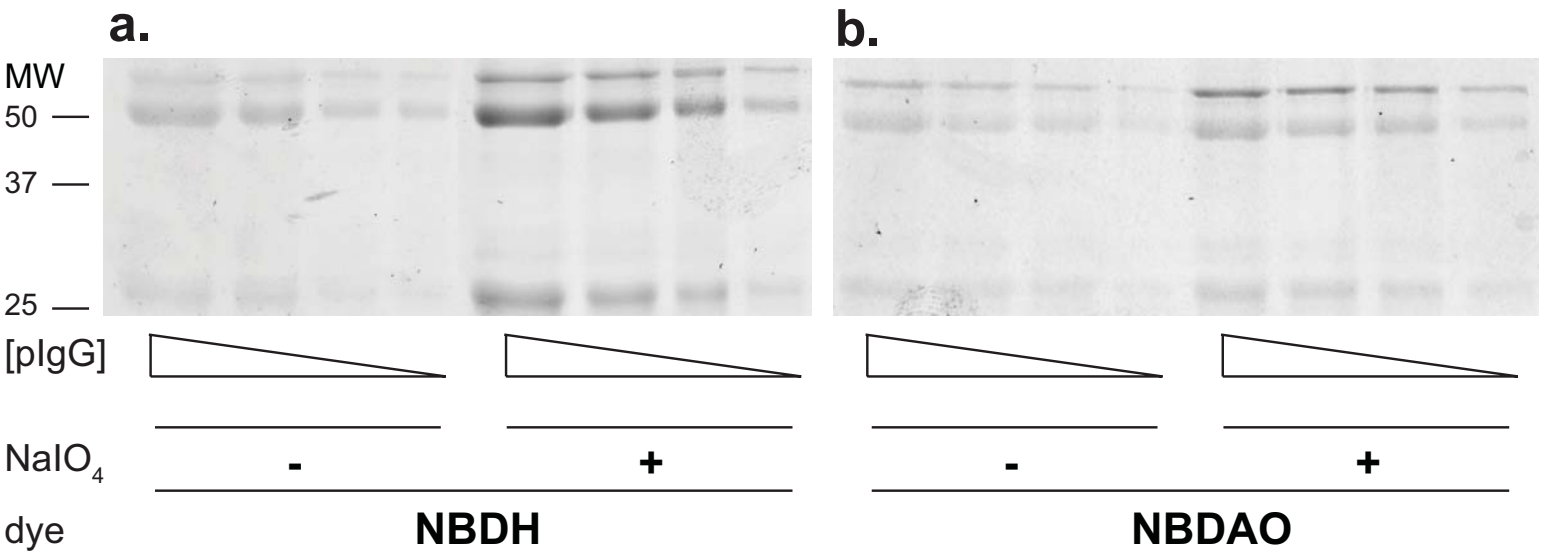

Figure 4.5. Labelling of murine polyclonal IgG (pIgG) by PAL with NBDH (a) and NBDAO (b). Control lanes used protein which was not treated with periodate. Molecular weights are given in kDa.

4.6 Live cell labelling

We tested the ability of NBDH (**4.2**) and NBDAO (**4.5**) to detect glycans on live cells using PAL. HeLa cells were cultured in a microplate and exposed to periodate, washed, and then treated with one of the carbonyl-reactive dyes. Control wells lacked the periodate oxidation step, but were otherwise identical. After labelling, the fluorescence of treated cells was compared to that of the control wells. We found that the mean fluorescence after PAL with both dyes resulted in specific labelling when performed at acidic pH. The hydrazine dye gave an increase of 3.3-fold at pH 4.7, while NBDAO gave a larger increase of 4.3-fold. Both dyes were similar to control when the labelling was performed at pH 7.4 (**Figure 4.6**).

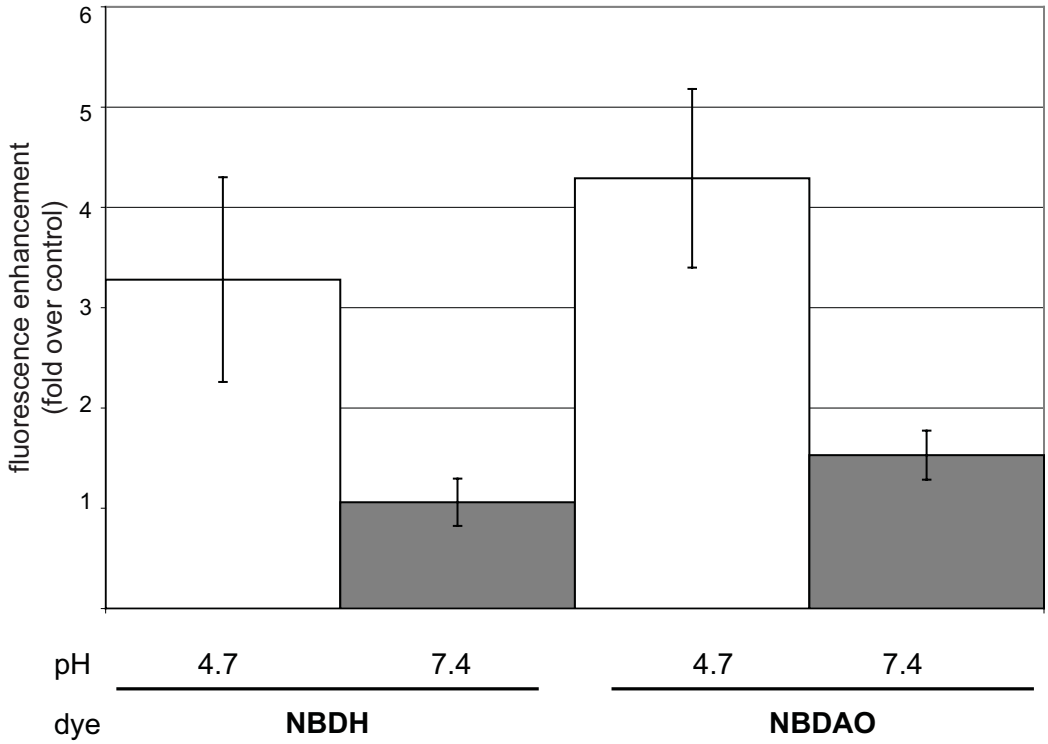

Figure 4.6. Fluorescence enhancement, expressed as fold enhancement over negative control, of 96 well plates after PAL treatment with NBDH (4.2) or NBDAO (4.5) at pH 4.7 or 7.4. Each point represents at least 8 wells, error is shown as the standard deviation. Excitation 485 nm, emission 538 nm.

4.6.1 Fluorescence microscopy of cell glycans

In order to explore the utility of these dyes for imaging applications, we tested their ability to label glycoconjugates in fixed and live cells. HeLa cells were treated with periodate, followed by a solution of dye containing aniline. Both the oxidation and labelling steps were performed at low temperature based on the protocol of Zeng et al.(Zeng, Y., Ramya, T.N.C., et al. 2009) Cells were then imaged using fluorescence microscopy and differential interference contrast (DIC) (**Figure 4.7**). To determine the background staining, we included controls that were treated with no periodate and no dye (--), no periodate and dye (-+), and periodate and dye (++). We employed conditions for staining of live and fixed cells for all treatments. We evaluated labelling conditions at pH 4.7, 5.4, 6.1 and 7.4. In our hands, pH 4.7 gave the best results for both dyes.

Fluorescence images of NBDH-treated cells showed membrane-staining of cells which was dependent on the use of both periodate and dye. Additional controls performed with compound **4.6** typically showed only background staining. The staining intensity was relatively weak for NBDH treatment when compared to NBDAO. Although all conditions were identical, experiments which employed NBDAO staining showed reduced background, and improved fluorescence signal intensity. Based on these results, we conclude that NBDAO is more suited to fluorescence imaging, and presents a significant improvement over NBDH. We also note that PAL labelling protocols which exploit small-molecule

fluorophores require fewer steps, and may have advantages over biotin-streptavidin reagents typically employed. (Zeng, Y., Ramya, T.N.C., et al. 2009)

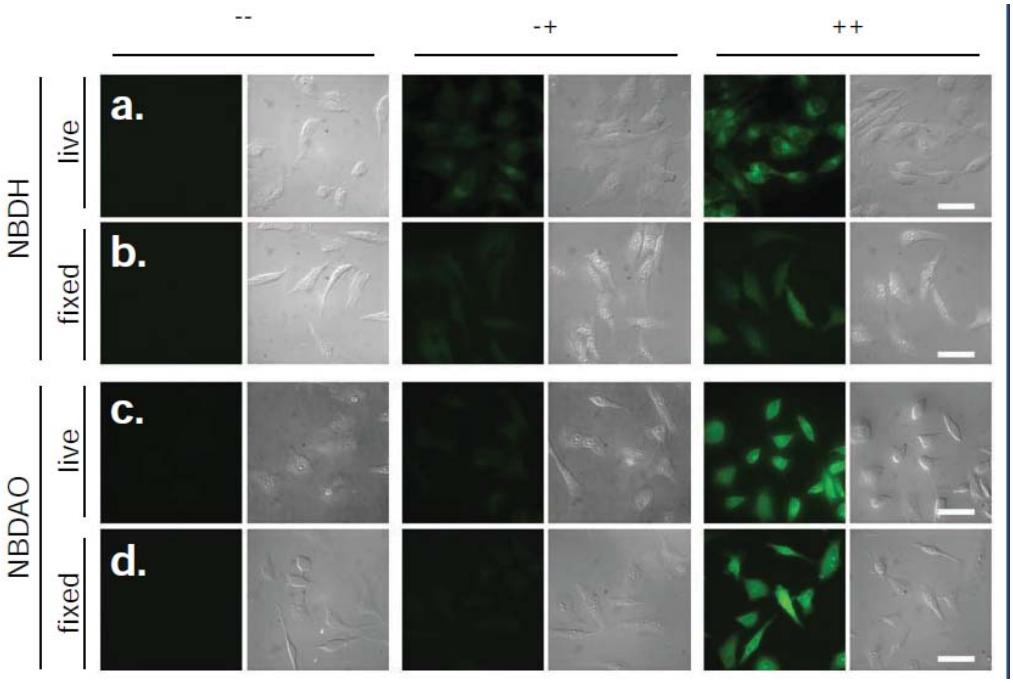

Figure 4.7. Fluorescence and brightfield images of HeLa cells labelled with NBDH and NBDAO. For each dye, cells were observed after one of the following treatments: no periodate, no dye (--), no periodate and dye (-+), and periodate and dye (++). Fluorescence images (488 ex/515 em) are shown on the left, and DIC images of the same field are shown on the right. Scale bars represent 50 μm. NBDH labelling is shown for live (**a.**) and fixed cells (**b.**) NBDAO labelling is shown for live (**c.**) and fixed cells (**d.**)

4.6.2 Flow cytometry measurement of cellular glycan

To determine the applicability of small molecule dyes for quantitation of cellular sialic acid content, we examined labelling of Jurkat cells by flow cytometry. Cells were treated with periodate, followed by a solution of NBDAO

dye containing aniline. As with the experiments described above, the oxidation and labelling step was performed at low temperature. To determine the background staining, we included samples that were treated with no periodate and no dye (--), periodate and no dye (+-), no periodate and dye (-+), and both periodate and dye (++). Non-specific background staining (-+) was observed to increase the mean fluorescence intensity (MFI) of cells by approximately 4.5 fold (**Figure 4.8**). However, PAL treatment and fluorophore (++) resulted in a 30-fold increase in MFI (**Figure 4.8a**). We compared these results to those obtained with commercially available fluorophores of similar excitation/emission profiles: NBDH and Bodipy FL hydrazide (**Table 4.2**).

The NBDAO and NBDH-treated cells showed minor non-specific background staining (-+) which increased the mean fluorescence intensity (MFI) of cells by approximately 4.5- and 2.5-fold over untreated controls, respectively. In contrast, the Bodipy FL hydrazide dye gave a larger increase in background staining (> 500-fold). This result likely indicates that the Bodipy fluorophore is more hydrophobic, leading to integration of the dye into the cell membrane.

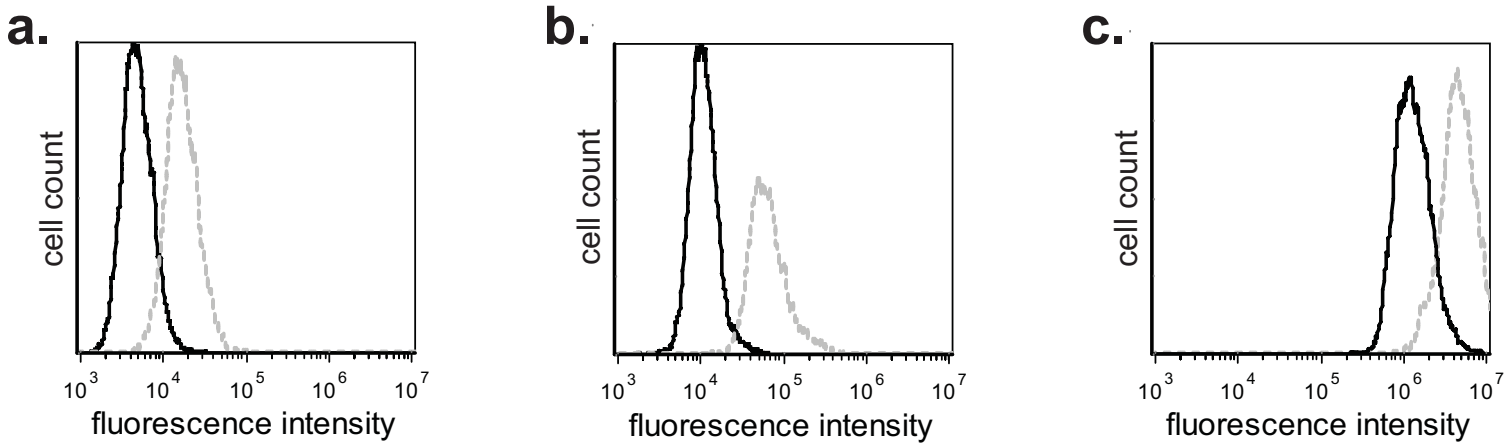

Figure 4.8. Representative flow cytometry histograms of the relative fluorescence of Jurkat cells. Cells were treated with a solution containing only the fluorophore (-+, solid black line), or the fluorophore after PAL-treatment of the cells (++, dashed grey line). Dyes shown are a. NBDH, b. NBDAO, and c. Bodipy FL hydrazide. Experiments were performed in triplicate, 488 nm excitation; 533 nm detection.

To determine the fidelity of sialic acid detection for each dye, we compared cells which were dye treated (-+) to those which were PAL and fluorophore treated (++). In the case of the NBDAO dye, cells showed an almost 7-fold increase in fluorescence after staining. This was the largest increase we observed, as both commercial dyes (NBDH and Bodipy FL hydrazide) gave only 2-3 fold increases over background. Based on these data we concluded that NBDAO gave the best combination of low background and high signal to noise for sialic acid detection. Jurkat cells that were treated with bacterial neuraminidase for one hour, followed by PAL and NBDAO, showed reduced MFI (78 ± 8%) compared to untreated cells, suggesting that this method may be useful to monitor enzymatic changes to sialoproteins *in vivo*.

Fluorophore	*Periodate Oxidation*	*Mean Fluorescence Intensity (MFI)*	*Fold MFI increase oxidized over non-oxidized*
None	-	$2456 \pm 6.8 \times 10^2$	N/A
	+	$2559 \pm 2.3 \times 10^2$	
NBDAO	-	$11519 \pm 1.0 \times 10^3$	6.7 ± 0.2
	+	$77576 \pm 1.1 \times 10^4$	
NBDH	-	$6159 \pm 5.6 \times 10^2$	2.9 ± 0.1
	+	$17908 \pm 6.0 \times 10^2$	
Bodipy FL Hydrazide	-	$1650433 \pm 4.8 \times 10^5$	2.5 ± 0.4
	+	$4144324 \pm 9.4 \times 10^5$	

Table 4.2. Comparison of flow cytometry Mean Fluorescence Intensity (MFI) values observed with NBDAO, NBDH, and Bodipy FL with or without PAL conditions. Experiments were performed in triplicate, 488 nm excitation; 533 nm detection.

4.7 Conclusion

We report the synthesis and application of two carbonyl reactive fluorophores, NBDAO and NBDH, for the selective labelling of sialic acid using PAL. We demonstrate that these dyes can be used to follow the kinetics of hydrazone or oxime formation when combined with an aldehyde substrate. Importantly, when used in conjunction with aniline catalysis these dyes are ideal for labelling of glycoproteins, detection of the sialic acid content of whole cells, and as small-molecule fluorophore stains of glycans on live cells.(Kohler, J.J. 2009) We demonstrate that these dyes can be used as a simple procedure for sialic acid labelling when combined with the recent development of periodate oxidation as a method for modifying sialic acids in vivo.(Kohler, J.J. 2009, Zeng, Y., Ramya, T.N.C., et al. 2009) As well, we have shown a procedure for quantitative detection of sialic acid content by flow cytometry. The NBDAO dye showed significant staining of sialic acid over background (6.7-fold); which was superior to the commercially available fluorophores NBDH (2.9-fold) and Bodipy FL hydrazide (2.5-fold). We expect this methodology will prove useful for a variety of applications in glycobiology, particularly in the study of changes to sialic acid content and subcellular location in live cells. These dyes may also prove useful in other popular carbonyl ligation strategies.(Brustad, E.M., Lemke, E.A., et al. 2008, Chen, I., Howarth, M., et al. 2005, Rannes, J.B., Ioannou, A., et al. , Whitman, C.M., Yang, F., et al.) We postulate that these compounds will supplement current fluorogenic bioorthogonal strategies, and will enable multi-colour bioorthogonal reaction labelling experiments: for example labelling one

biomolecule of interest by PAL and a carbonyl reactive fluorophore while labelling another by Sharpless-Meldal reaction. However, further development of long-wavelength bioorthogonal fluorophores, such as Cy dyes, are required.

4.8 Experimental

4.8.1 General experimental methods

Reagents were purchased from commercial sources such as Sigma-Aldrich (Oakville, Ont) and used without additional purification. Proton (^{1}H) and Carbon (^{13}C) NMR spectra were obtained on Varian 300, 400, 500 or 700 MHz instruments at room temperature as noted. Deuterated solvents were obtained from Cambridge Isotope Laboratories (Andover, MA). Mass spectrometry was performed using an MS50G positive electron impact instrument from Kratos Analytical (Manchester, UK) and a Mariner Biospectrometry positive ion electrospray instrument from Applied Biosystems (Foster City, CA).

4.8.2 Spectroscopy

Absorbance spectra for all compounds were collected at room temperature with a Hewlett-Packard (Palo Alto, CA) model 8453 diode array UV-visible spectrophotometer or Varian (Walnut Creek, CA) Cary 50 spectrophotometer. Fluorescence spectra for all compounds were collected at room temperature with a Photon Technology International (Birmingham, NJ) model MP1 steady-state fluorimeter. Absorbance and fluorescence measurements were taken using NSG Precision Cells (Farmingdale, NY) ES quartz cuvettes (190 – 2000 nm).

4.8.3 Synthesis of dyes and model conjugates

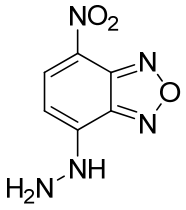

4-Hydrazinyl-7-nitrobenz-[2,1,3-*d*]-oxadiazole (4.2, NBDH).

4-Chloro-7-nitrobenz-[2,1,3-*d*]-oxadiazole (**4.1**) (100 mg, 0.5 mmol, 1 equiv) was dissolved in chloroform (50 mL). A 1% hydrazine solution (0.77 mL hydrazine in 50 mL methanol) was then added to the solution and allowed to stir at room temperature for 1 h. A yellow-brown precipitate was formed and isolated without further purification (104 mg, quant.) ^{1}H NMR (400 MHz, D_2O): δ 7.04 (d, 1H, ^{3}J = 10.5 Hz), 6.37 (d, 1H, ^{3}J = 10.5 Hz); ^{13}C NMR (100 MHz, D_2O): δ 147.6, 145.4, 131.4, 121.9, 120.8, 115.1; IR (microscope): ν = 3378, 3278, 3191, 3051, 2984, 2692, 1618, 1542, 1500, 1465, 1213, 1019, 982, 873, 794 cm^{-1}. ES-HRMS calculated for $C_5H_5N_5O_3Na$: 218.0285, observed: 218.0284.

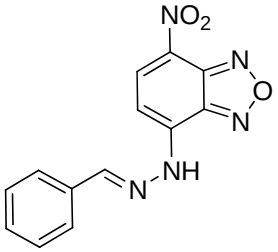

4-(2-Benzylidenehydrazinyl)-7-nitrobenz-[2,1,3-*d*]-oxadiazole (4.3).

4-Hydrazinyl-7-nitrobenz-[2,1,3-*d*]-oxadiazole (**4.2**) (25 mg, 0.13 mmol, 1 equiv) was dissolved in methanol (10 mL). Benzaldehyde (0.13 mL, 1.3 mmol, 10 equiv) was added, turning the reaction mixture a red colour. The product gradually formed as a dark red-black precipitate and was isolated by vacuum filtration.

Additional product was isolated from the supernatant after flash column chromatography (EtOAc/hexanes). The precipitate and column fractions were combined (27 mg, 74%). ^{1}H NMR (400 MHz, $(CD_3)_2CO$): 8.62 (d, 1H, ^{3}J = 8.8 Hz), 8.59 (s, 1H), 7.92-7.79 (m, 2H), 7.56-7.39 (m, 3H), 7.31 (d, 1H, ^{3}J = 8.8 Hz); ^{13}C NMR (100 MHz, $(CD_3)_2CO$): δ 149.9, 145.2, 144.1, 141.0, 137.0, 134.9, 131.6, 129.8, 128.4, 126.0, 102.7; IR (microscope): ν = 3486, 3307, 3219, 3144, 3060, 2955, 1603, 1581, 1515, 1446, 1406, 1295, 1117, 997 cm^{-1}. ES-HRMS calculated for $C_{13}H_{10}N_5O_3$: 284.0778, observed: 284.0778. R_f = 0.23 (1:3 EtOAc/hexanes).

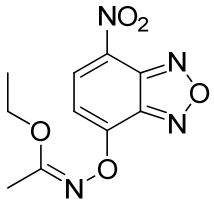

Ethyl *N*-7-nitrobenz-[2,1,3-*d*]-oxadiazol-4-yloxyacetimidate (4.4).

Ethyl *N*-hydroxyacetimidate (35 mg, 0.34 mmol, 3 equiv) was dissolved in H_2O (2 mL). Sodium carbonate (100 mg, 0.94 mmol, 7.5 equiv) was added and the reaction mixture was allowed to stir for 10 min. 4-Chloro-7-nitrobenz-[2,1,3-*d*]-oxadiazole (**4.1**) (25 mg, 0.125 mmol, 1 equiv) was then added and allowed to stir at room temperature for approximately 15 min. The resulting brown-yellow precipitate was isolated by vacuum filtration without further purification (35 mg, quant.). ^{1}H NMR (300 MHz, $CDCl_3$): δ 8.54 (d, 1H, ^{3}J = 8.4 Hz), 7.25 (d, 1H, ^{3}J = 8.4 Hz), 4.27 (q, 2H, ^{3}J = 6.9 Hz), 2.32 (s, 3H), 1.42 (t, 3H, ^{3}J = 6.9 Hz); ^{13}C NMR (100 MHz, $CDCl_3$): δ 170.2, 154.3, 144.2, 143.9, 134.6, 129.7, 106.2, 64.4, 15.3, 14.5; IR (microscope): ν = 3133, 3090, 2999, 2988, 1933, 1713, 1645,

1623, 1537, 1451, 1379, 1164, 997, 854 cm^{-1}. ES-HRMS calculated for $C_{10}H_{10}N_4O_5Na$: 289.0543, observed: 289.0541. R_f = 0.69 (1:3 EtOAc/hexanes).

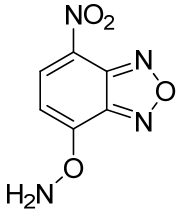

***O*-(7-Nitrobenz-[2,1,3-*d*]-oxadiazol-4-yl)hydroxylamine (4.5, NBDAO)**.

Ethyl *N*-7-nitrobenz-[2,1,3-*d*]-oxadiazol-4-yloxyacetimidate (**4.4**) (250 mg, 0.94 mmol, 1 equiv) was dissolved in 1:1 TFA/water (25 mL) and allowed to stir at room temperature for 2 h. The TFA was removed in vacuo, and the resulting aqueous solution was concentrated by lyophilization. The product was isolated by flash column chromatography with a dichloromethane mobile phase (94 mg, 55%). ^{1}H NMR (700 MHz, $CDCl_3$): δ 8.56 (d, 1H, ^3J = 8.4 Hz), 7.40 (d, 1H, ^3J = 8.4 Hz), 6.51 (s, 2H). ^{13}C NMR (175 MHz, $CDCl_3$): δ 156.0, 143.9, 143.5, 134.0, 130.1, 105.7; IR (microscope): ν = 3325, 3255, 3167, 3104, 2918, 2851, 1641, 1588, 1537, 1328, 1083, 997, 729 cm^{-1}. ES-HRMS calculated for $C_6H_4N_4O_4Na$: 219.0125, observed: 219.0127. R_f = 0.25 (1:3 EtOAc/hexanes).

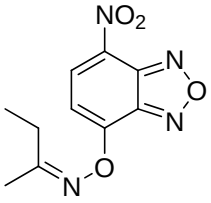

Butan-2-one *O*-7-nitrobenz-[2,1,3-*d*]-oxadiazol-4-yl oxime (4.6).

O-(7-Nitrobenz-[2,1,3-*d*]-oxadiazol-4-yl)hydroxylamine (**4.5**) (27 mg, 0.14 mmol, 1 equiv) was dissolved in methylethylketone (MEK) (0.08 mL, 0.83 mmol, 6 equiv). The reaction was allowed to run at room temperature for 2 h. Excess

MEK was removed in vacuo and the remaining residue was purified as an inseparable mixture of E/Z isomers (1.36:1) using flash column chromatography (EtOAc/hexanes) (15 mg, 44%). ^{1}H NMR (400 MHz, $CDCl_3$): δ 8.56 (d, 1H, ^{3}J = 9.3 Hz), 7.35 (d, 1H, ^{3}J = 9.6 Hz), 2.73 (q, 0.90H, ^{3}J = 7.8 Hz), 2.48 (q, 1.29H, ^{3}J = 7.5 Hz), 2.25 (s, 1.88H), 2.14 (s, 1.38H), 1.26 (m, 5.23H); ^{13}C NMR (125 MHz, $CDCl_3$): δ 169.7, 168.8, 153.98, 153.92, 144.0, 143.8, 134.4, 129.8, 106.6, 29.8, 24.0, 19.3, 15.5, 10.4; IR (microscope): ν = 3113, 3092, 2987, 2987, 2919, 2849, 1633, 1533, 1453, 1369, 1327, 887, 854, 733 cm^{-1}. ES-HRMS calculated for $C_{10}H_{11}N_4O_4$: 251.0775, observed: 251.0778. R_f = 0.67 (1:1 EtOAc/hexanes).

4.8.4 Reaction kinetics

Dye solutions of NBDH (6.88 x 10^{-5} M) or NBDAO (2.50 x 10^{-5} M) were prepared in 1 mL aliquots with or without aniline (4.38 x 10^{-4} M) in buffer (0.1 M sodium acetate, pH 4.7; or 0.1 M HEPES, pH 7.4). An aliquot of MEK (10 μL, 1.11 x 10^{-4} M) was added and the fluorescence emission of the reaction was monitored for 1,500 sec (ex. 480 nm; em. 540 nm).

4.8.5 Glycoprotein labelling

Fetal calf serum fetuin (1 mg/mL, 0.5 mL aliquots) was treated with 1 mL aliquots of neuraminidase from *Clostriduim perfringens* (*C. Welchii*) (0.1 mg/mL) in sodium acetate buffer (0.1 M, pH 5.4) for 0.5 h at 37 °C. Sodium acetate buffer was removed by ultrafiltration (Millipore, Billerica, MA) for 15 min at 1600 g, followed by a water wash (1 mL). Oxidation was performed by treatment with sodium periodate (300 μL, 0.1 M) for 30 min at 4 °C. Excess periodate was

removed by ultrafiltration for 15 min at 1600 g, followed by a water wash (1 mL). Aliquots of the protein (20 μL or 10 μL) were then treated with a labelling solution (20 μL) consisting of NBDAO (1.25×10^{-5} M) and aniline (4.38×10^{-4} M) in sodium acetate buffer (0.1 M, pH 4.7) for 0.5 – 1 h at 4 °C. Labelled proteins were resolved by SDS PAGE (stacking 4%, resolving 12%). The resulting gels were imaged using a FujiFilm Fluorescent Image Analyzer FLA-5000 (Fujifilm medical systems USA Inc., Stamford, CT) with 473 nm excitation and a low band pass filter. Coomassie staining was used to detect molecular weight standards.

4.8.6 Microplate assay

HeLa cells were grown in Dulbecco's modified Eagle medium (DMEM) with 10% fetal bovine serum (FBS) at 37 °C under 5% CO_2 to approximately 80% confluency. Cells were trypsinized, and then added to 96 well plates (~2,000 cells/well) (tissue culture treated; Corning, Corning, NY). The plate was then incubated for 96 h at 37 °C in a humidified incubator. The growth media was removed and the plates were washed with Dulbecco's phosphate buffered saline (DPBS). Wells were then treated with sodium periodate (80 μL, 1 mM) or DPBS buffer control (80 μL) for 30 min at 4 °C. The solution was removed by inversion, and the plates were washed with DPBS (2 × 100 μL). Control and sample wells were treated with dye for 1 h at 4 °C (NBDH, 6.88×10^{-5} M; or NBDAO, 2.5×10^{-5} M). Dye solutions were prepared in 1 mL aliquots with or without aniline (4.38×10^{-4} M) in DPBS (pH 7.4) or 0.1 M sodium acetate buffer (pH 4.7) as

indicated. Fluorescence measurements were taken on a Molecular Devices M2e plate reader (Sunnyvale, CA).

4.8.7 Fluorescence microscopy

HeLa cells were added to a 6-well plate (~10,000 cells/well) containing treated coverglass (1% BSA in TBS), and grown to 60% confluence. The growth media was removed and the wells were washed with DPBS. Sample wells received sodium periodate in DPBS (1 mL, 1 mM) treatment; control wells received DPBS (2 mL); samples were then incubated for 30 min at 4 °C. Cells can optionally be fixed at this point by washing with sodium acetate buffer (0.1 M, pH 4.7; 2 × 2 mL), incubation for 10 min in a 1:1 solution of sodium acetate buffer and methanol, and incubation for 5 min in methanol. Fixing solution is then removed, and the samples are washed with sodium acetate buffer (2 × 2 mL). The double negative control was treated with buffer solution, while control and experimental wells were then treated with dye for 0.5 to 1 h at 4 °C (NBDH, 6.88 x 10^{-5} M; or NBDAO, 2.50 x 10^{-5} M). Dye solutions were prepared in 1 mL aliquots with aniline (4.38 x 10^{-4} M) in sodium acetate buffer (0.1 M, pH 4.7). Each treatment was observed in triplicate. Cells were washed with buffer after staining, and then visualized using a Nikon Eclipse Ti inverted fluorescence microscope with 60x objective (NA 1.49). Images were acquired with a Photometrics QuantEM 512SC camera.

4.8.8 Flow cytometry

Jurkat cells were grown in RPMI 1640 media (Invitrogen, Carlsbad, CA) with 10% fetal bovine serum (FBS) at 37 °C under 5% CO_2 to approximately 1 x 10^6 cells/mL. The growth media was removed and the cells were washed with DPBS. Control cell aliquots were incubated in DPBS for 1 h at 37 °C. Sialidase-treated cell aliquots were incubated at 37 °C in the presence of bacterial neuraminidase (0.4 mg/mL). Cells were pelleted by centrifugation (2000 g x 4 m) and washed with DPBS. Oxidation-treated aliquots received sodium periodate in DPBS (1 mL, 1 mM) oxidation treatment; non-oxidation treatment aliquots received DPBS (1 mL); samples were then incubated for 30-45 m at 4 °C. Cells were again pelleted by centrifugation (2000 g x 4 min) and washed three times with DPBS. Unlabelled control aliquots were treated with buffer solution, while a set of unoxidized and oxidized experimental aliquots were then treated with dye (100 μL) for 1-1.5 h at 4 °C (NBDAO, 2.50 x 10^{-5} M, Bodipy FL hydrazide 6.53 x 10^{-5} M (Invitrogen, Carlsbad, CA), NBDH 1.02 x 10^{-4} M). Dye solutions were prepared in 1 mL aliquots with aniline (4.38 x 10^{-4} M) in sodium acetate buffer (0.1 M, pH 4.7). Cells were pelleted by centrifugation (2000 g x 4 min) and washed three times with DPBS before flow cytometry. Flow cytometry was performed on an Accuri C6 cytometer (Ann Arbor, MI) operating at 488 nm excitation; 533 nm detection. Each treatment was observed in triplicate.

4.8.9 Absorption/emission spectra (excitation 475 nm) for NBDH (4.2)

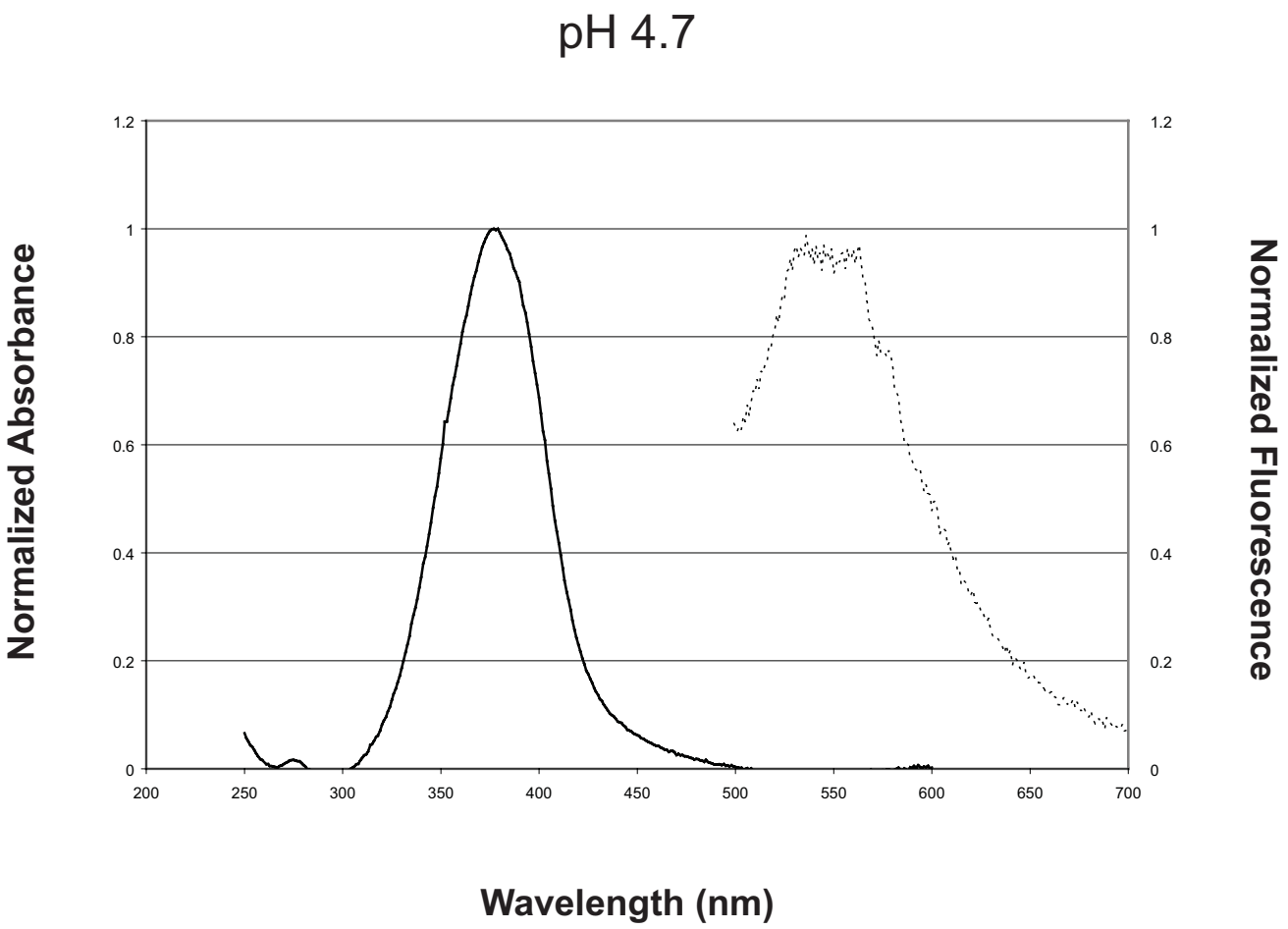

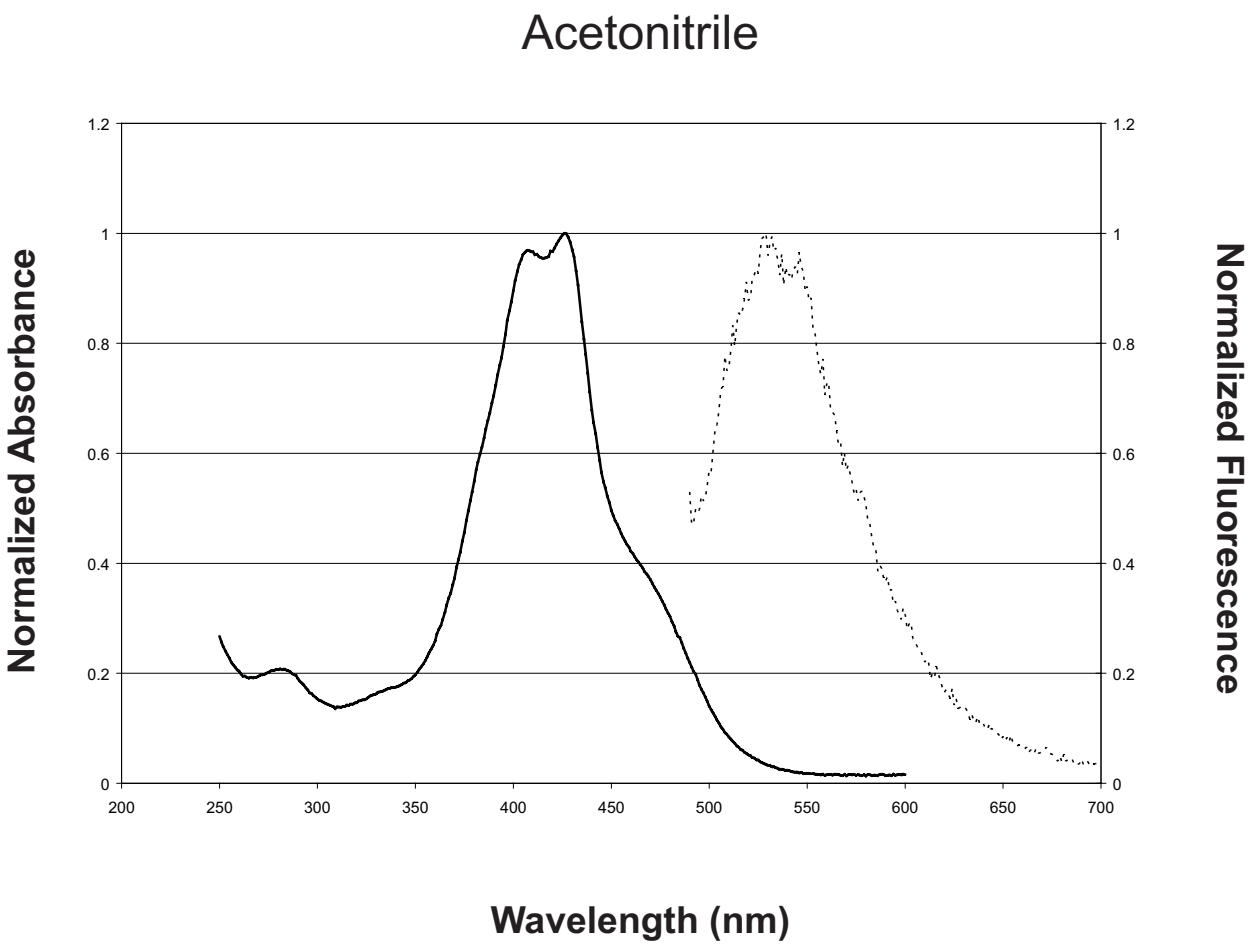
Acetonitrile
Normalized Absorbance
Normalized Fluorescence
Wavelength (nm)
1.2
1
0.8
0.6
0.4
0.2
0
200
250
300
350
400
450
500
550
600
650
700

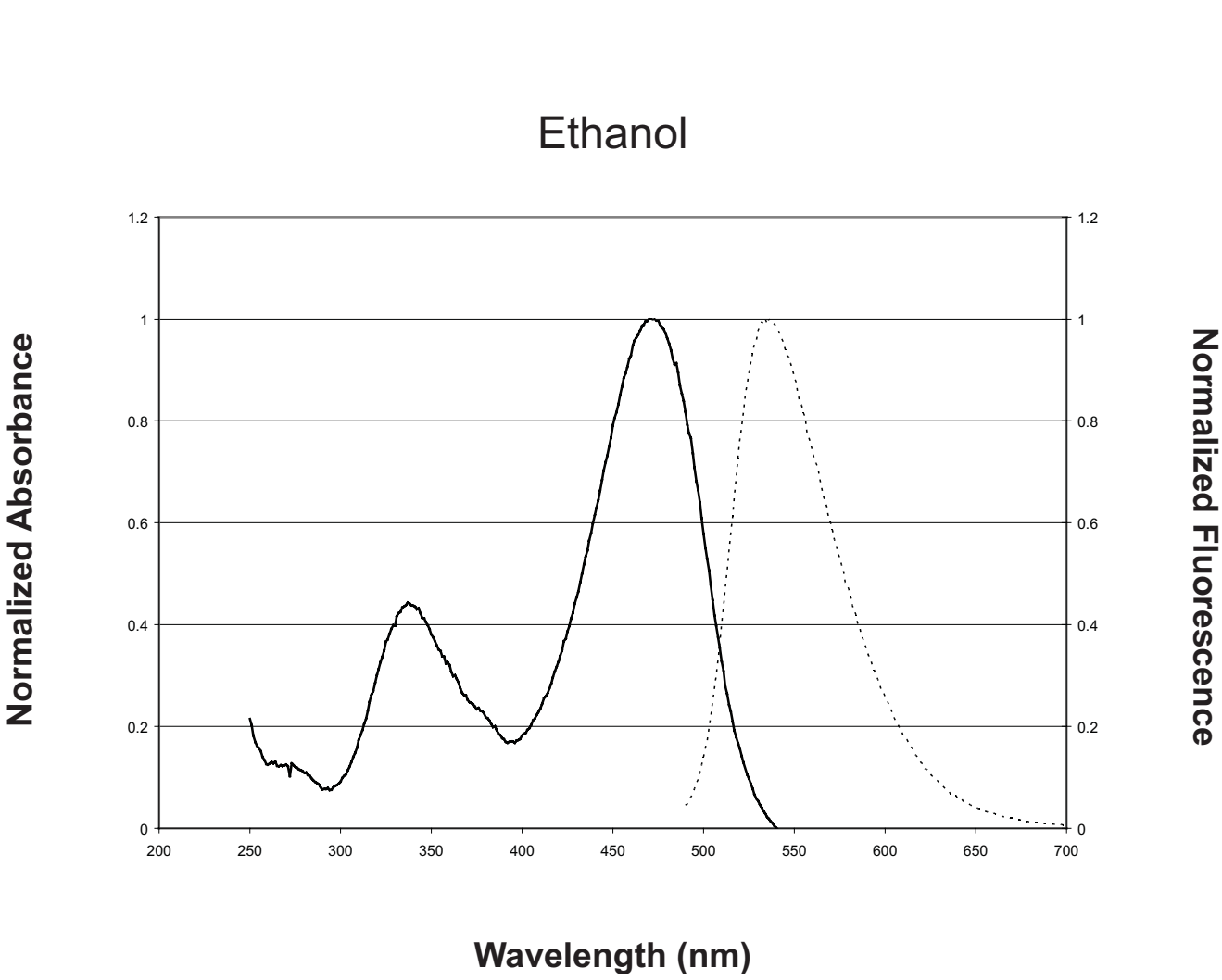
Ethanol
Normalized Absorbance
Normalized Fluorescence
Wavelength (nm)
1.2
1
0.8
0.6
0.4
0.2
0
200
250
300
350
400
450
500
550
600
650
700

4.8.10 Absorption/emission spectra (excitation 475 nm) for hydrazone (4.3)

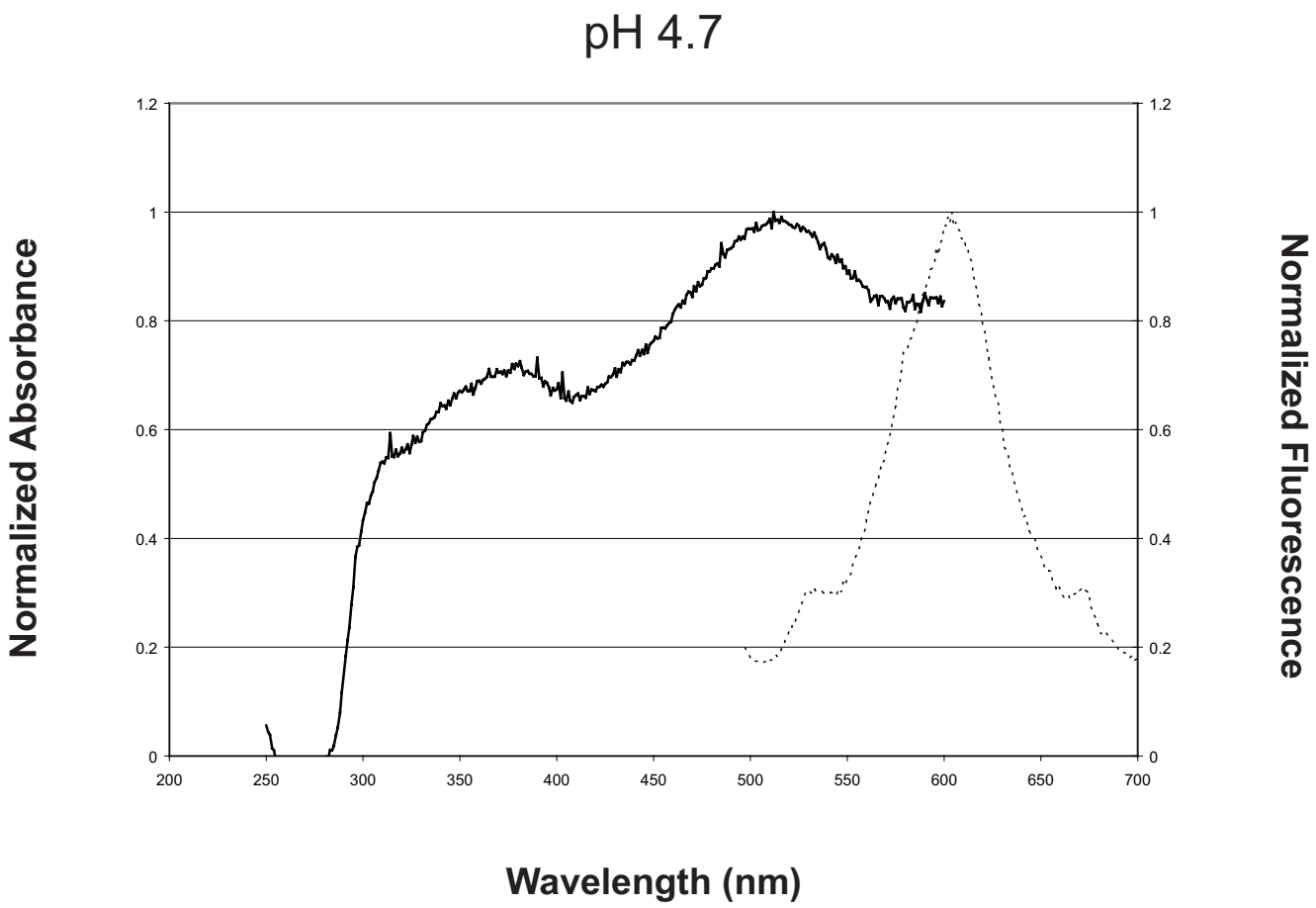

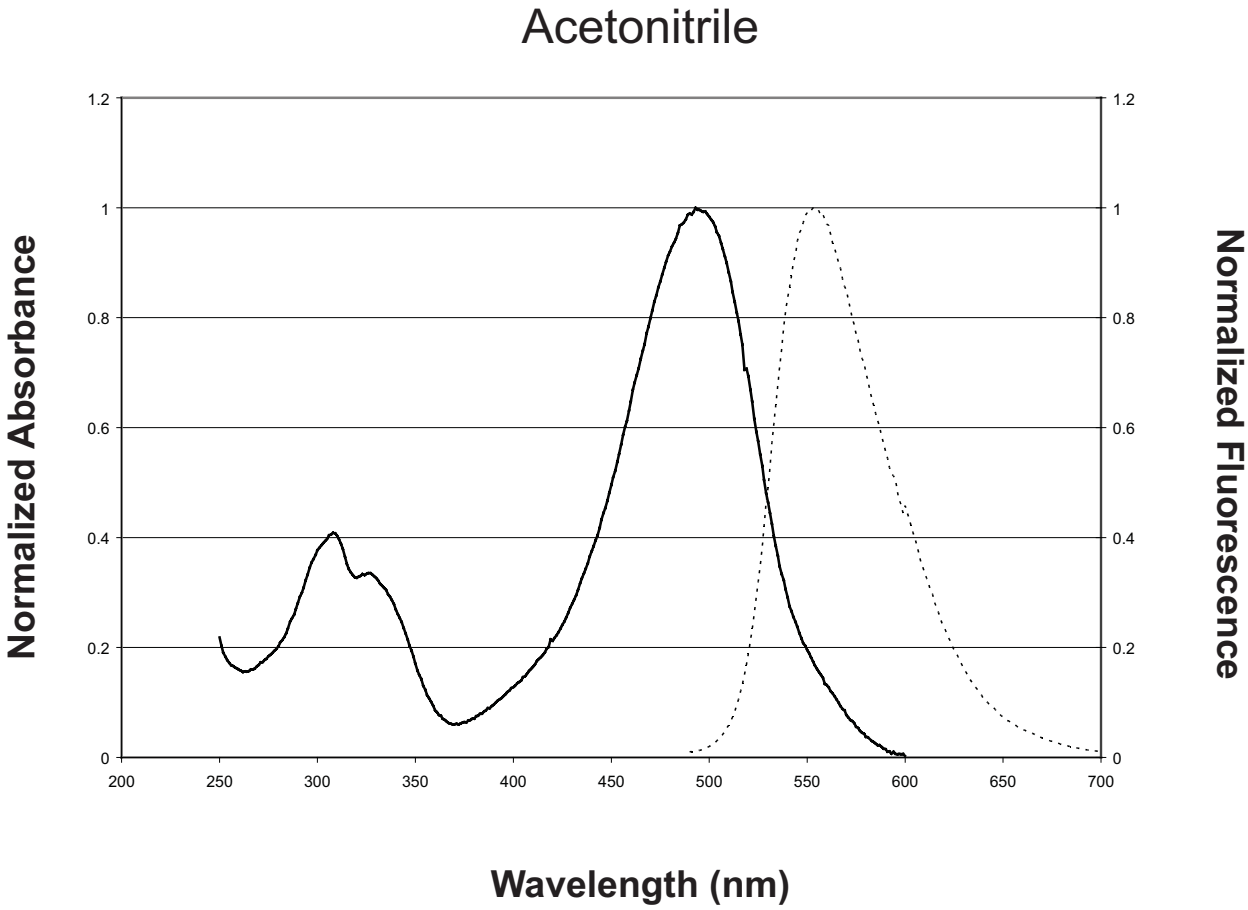
Acetonitrile
Normalized Absorbance
Normalized Fluorescence
Wavelength (nm)
1.2
1
0.8
0.6
0.4
0.2
0
200
250
300
350
400
450
500
550
600
650
700

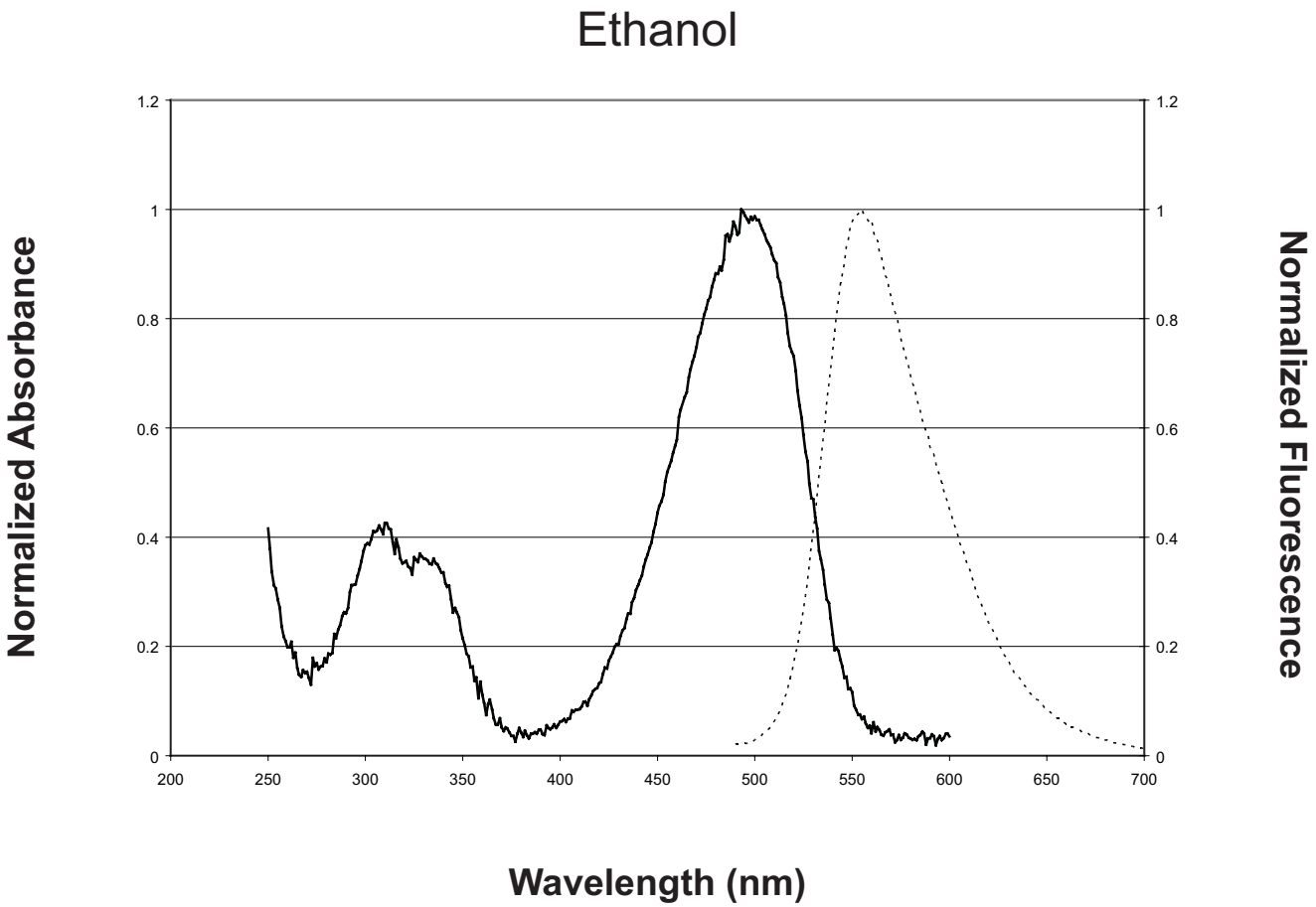
Ethanol
Normalized Absorbance
Normalized Fluorescence
Wavelength (nm)
1.2
1
0.8
0.6
0.4
0.2
0
200
250
300
350
400
450
500
550
600
650
700

4.8.11 Absorption/emission spectra (excitation 475 nm) for NBDAO (4.5)

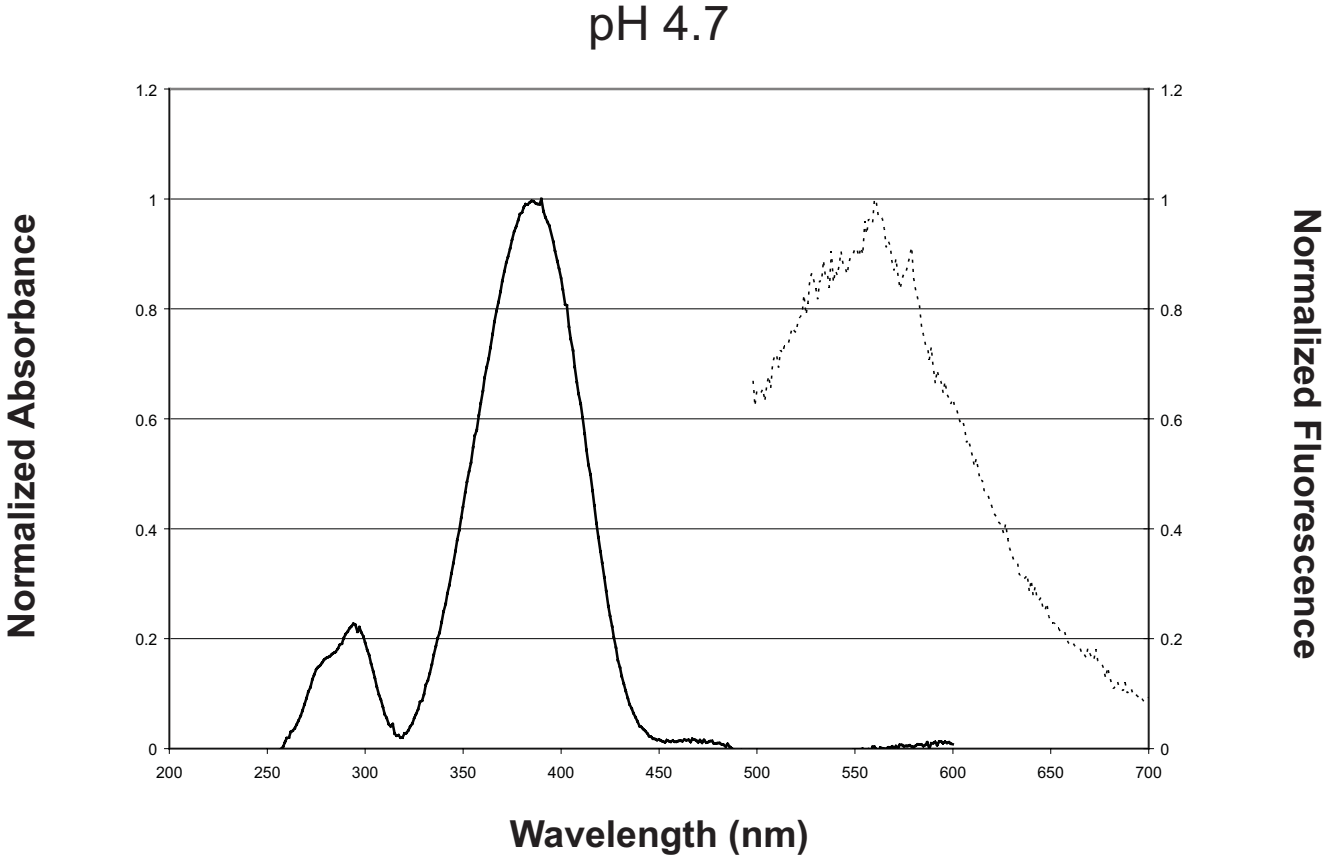

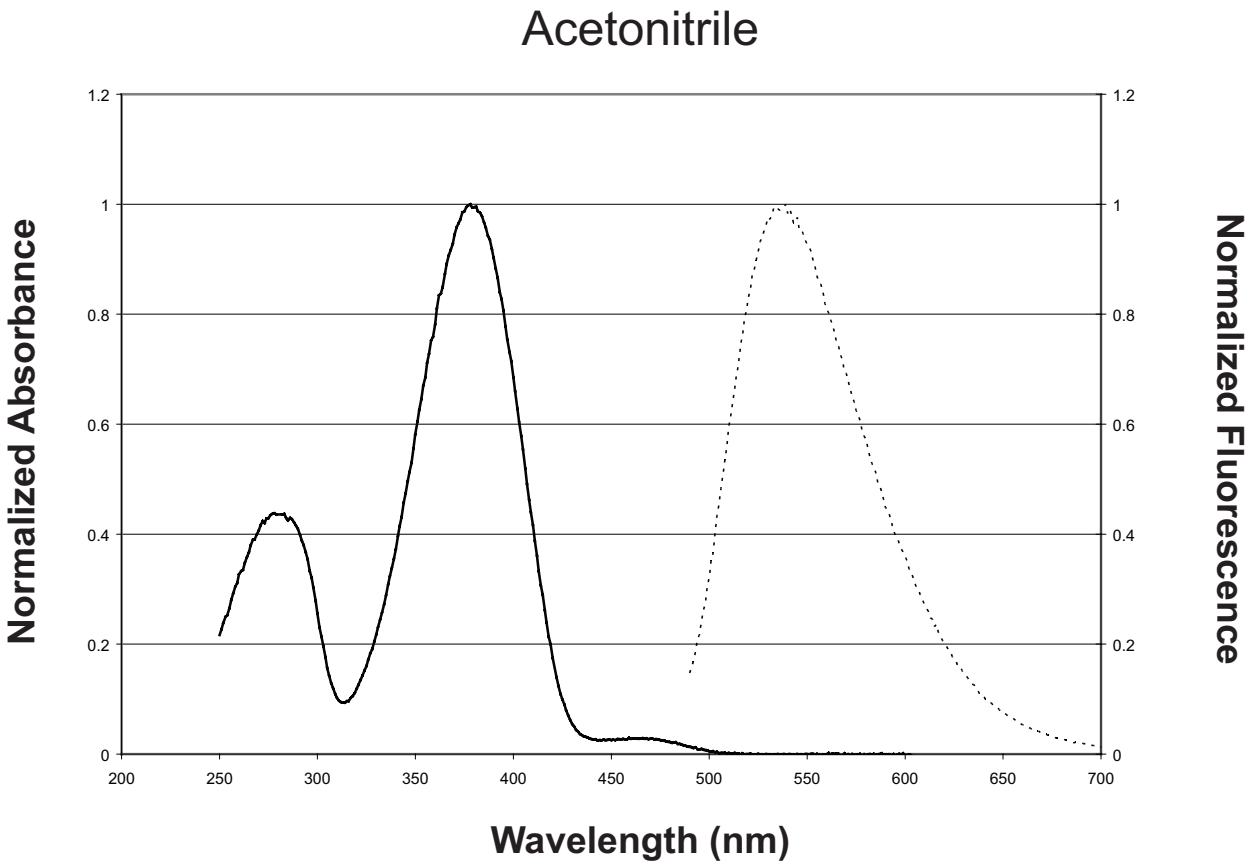
Acetonitrile
Normalized Absorbance
Normalized Fluorescence
Wavelength (nm)
1.2
1
0.8
0.6
0.4
0.2
0
200
250
300
350
400
450
500
550
600
650
700

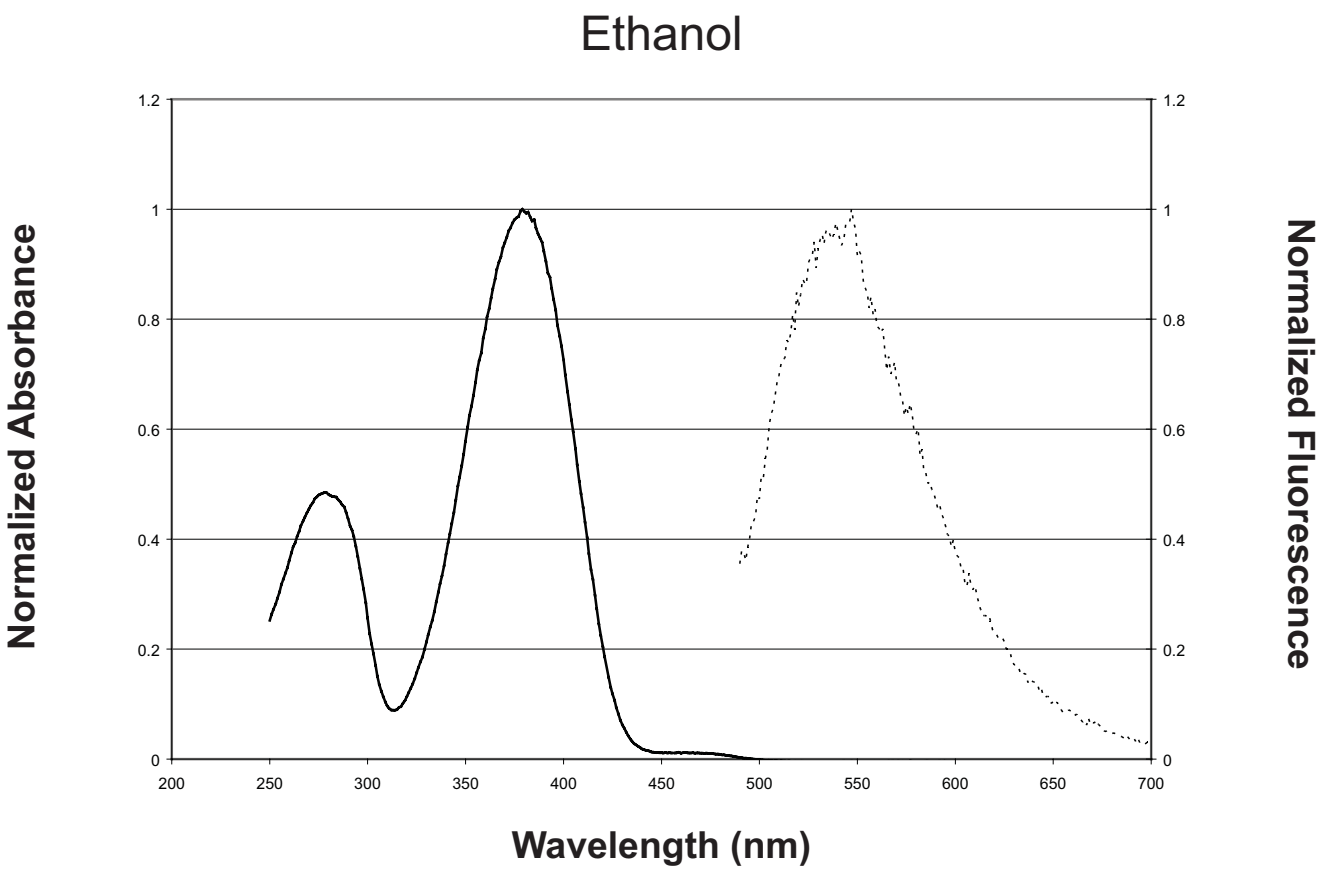
Ethanol
Normalized Absorbance
Normalized Fluorescence
Wavelength (nm)
1.2
1
0.8
0.6
0.4
0.2
0
200
250
300
350
400
450
500
550
600
650
700

4.8.12 Absorption/emission spectra (excitation 475 nm) for oxime (4.6)

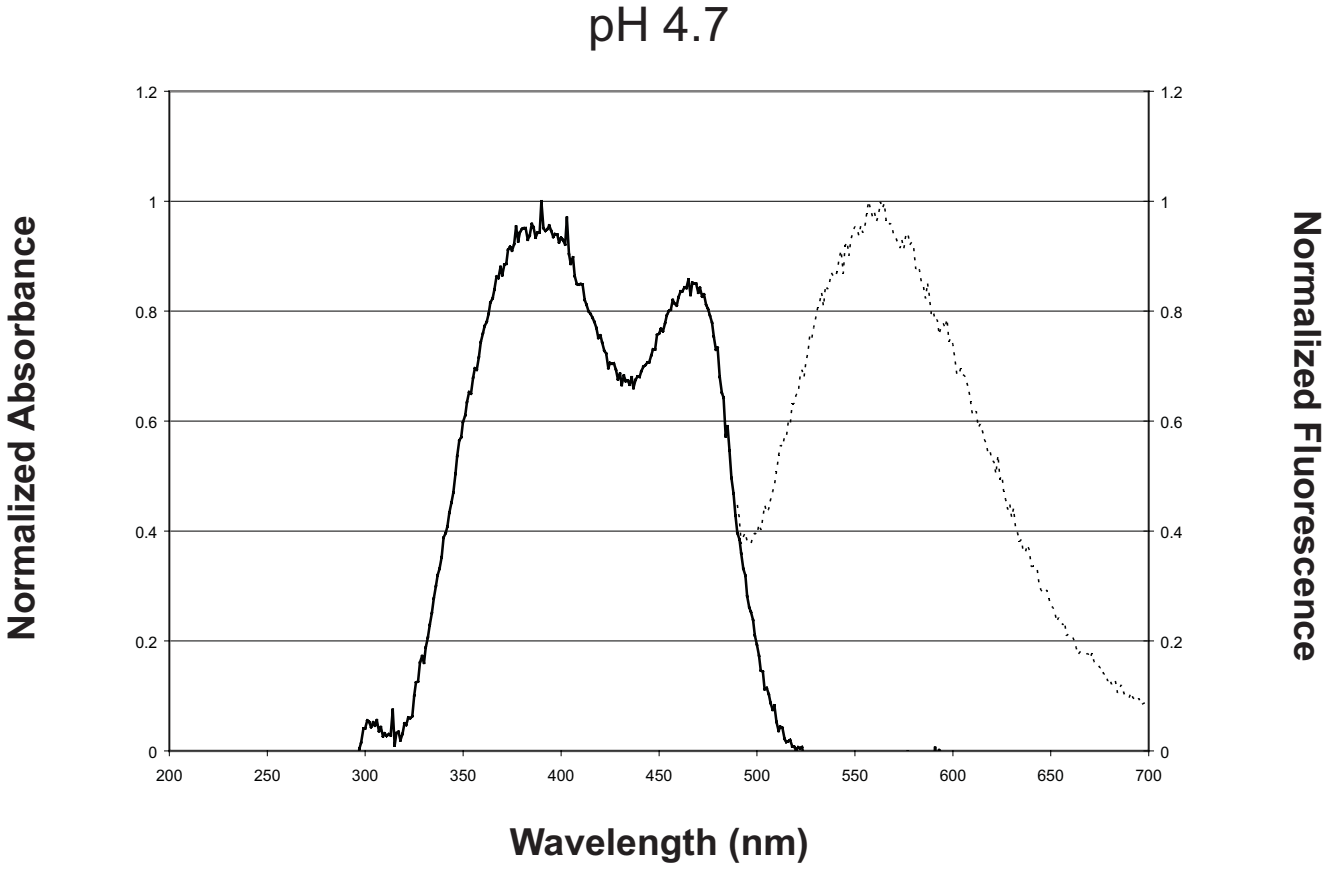

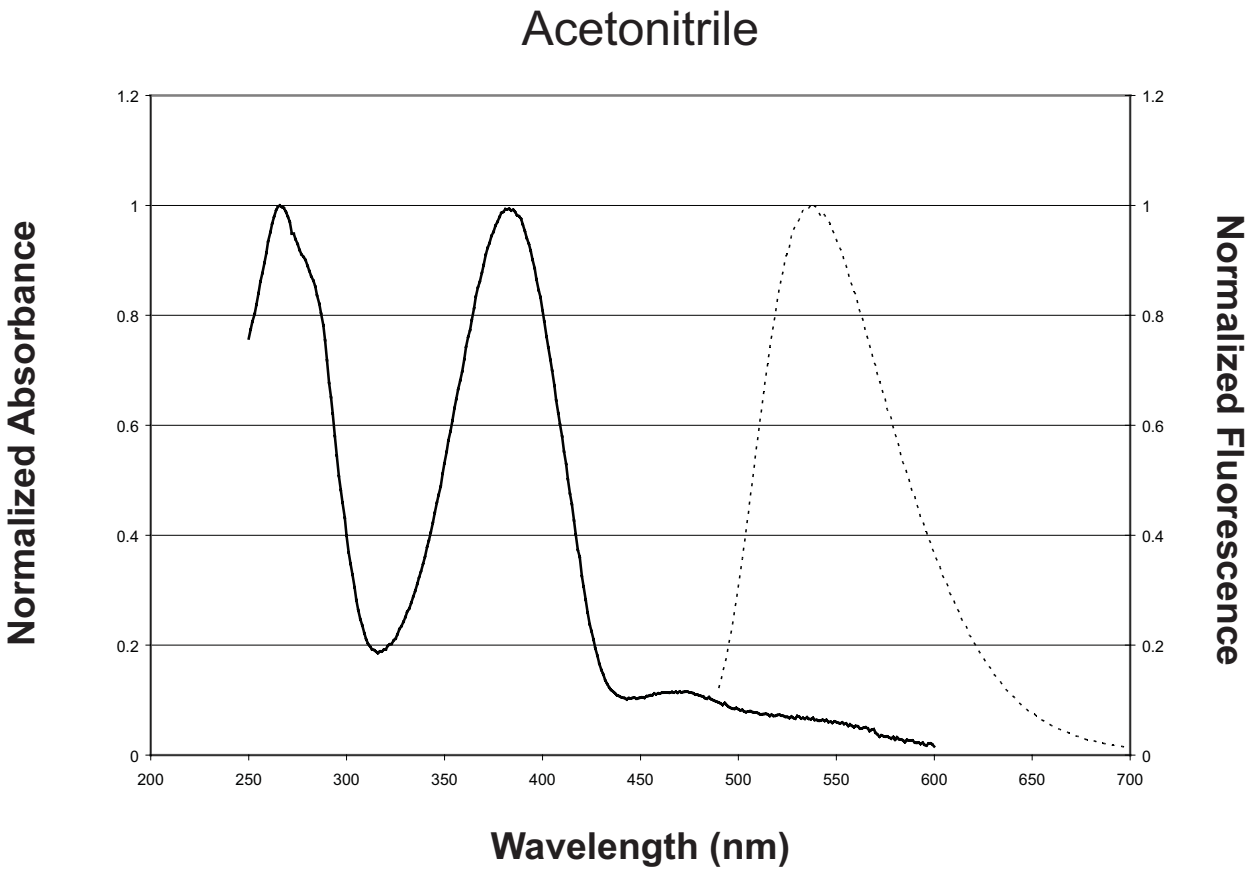
Acetonitrile
Normalized Absorbance
Normalized Fluorescence
Wavelength (nm)
1.2
1
0.8
0.6
0.4
0.2
0
200
250
300
350
400
450
500
550
600
650
700

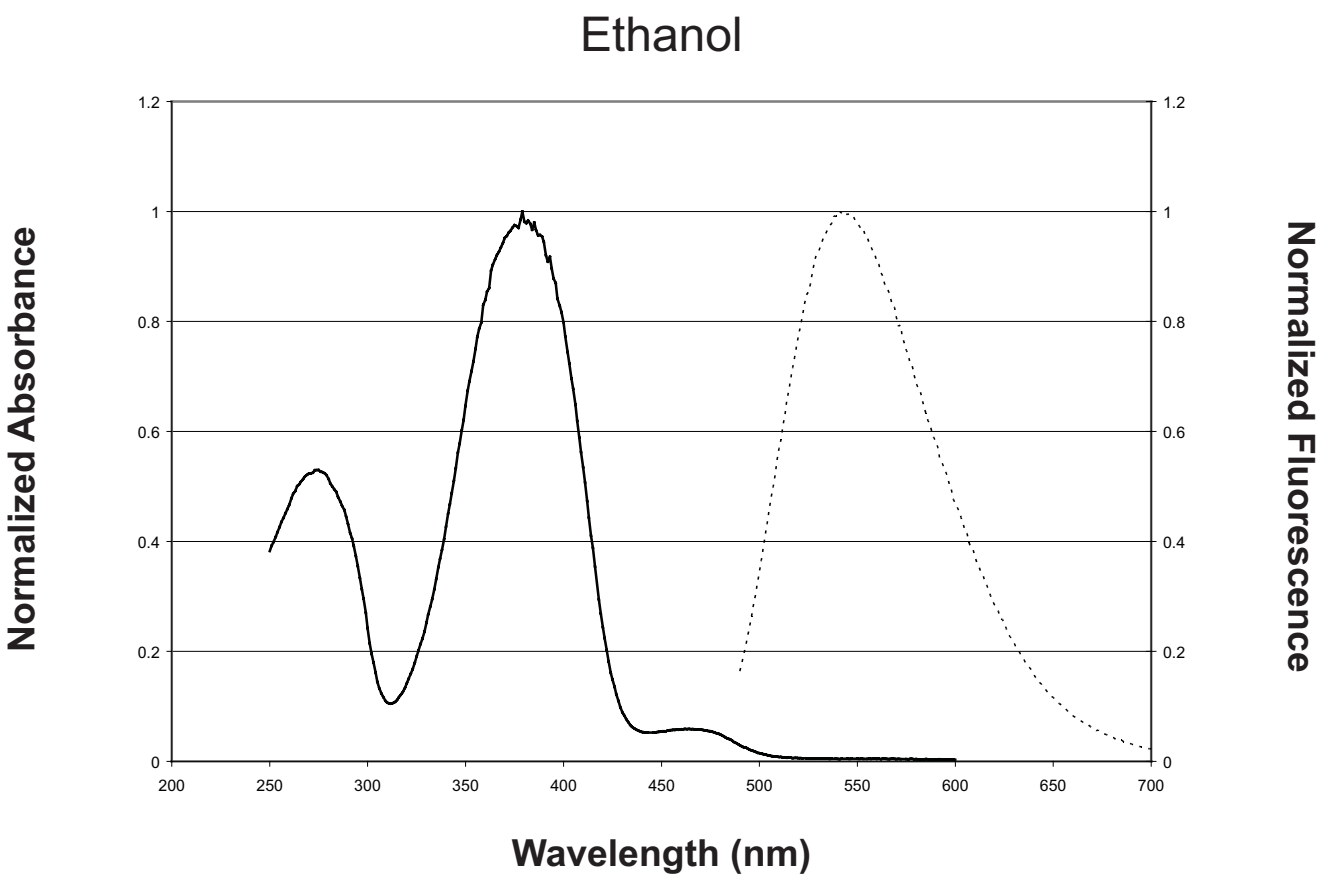
Ethanol
Normalized Absorbance
Normalized Fluorescence
Wavelength (nm)
1.2
1
0.8
0.6
0.4
0.2
0
200
250
300
350
400
450
500
550
600
650
700

4.8.13 Representative flow cytometry histograms

The relative fluorescence of Jurkat cells treated with PAL conditions (+-, blue/left), fluorophore solution only (-+, black/middle), and both PAL and fluorophore solution (++, red/right). Dyes shown are **a.** NBDH, **b.** NBDAO, and **c.** Bodipy FL hydrazide. Experiments were performed in triplicate, 488 nm excitation; 533 nm detection.

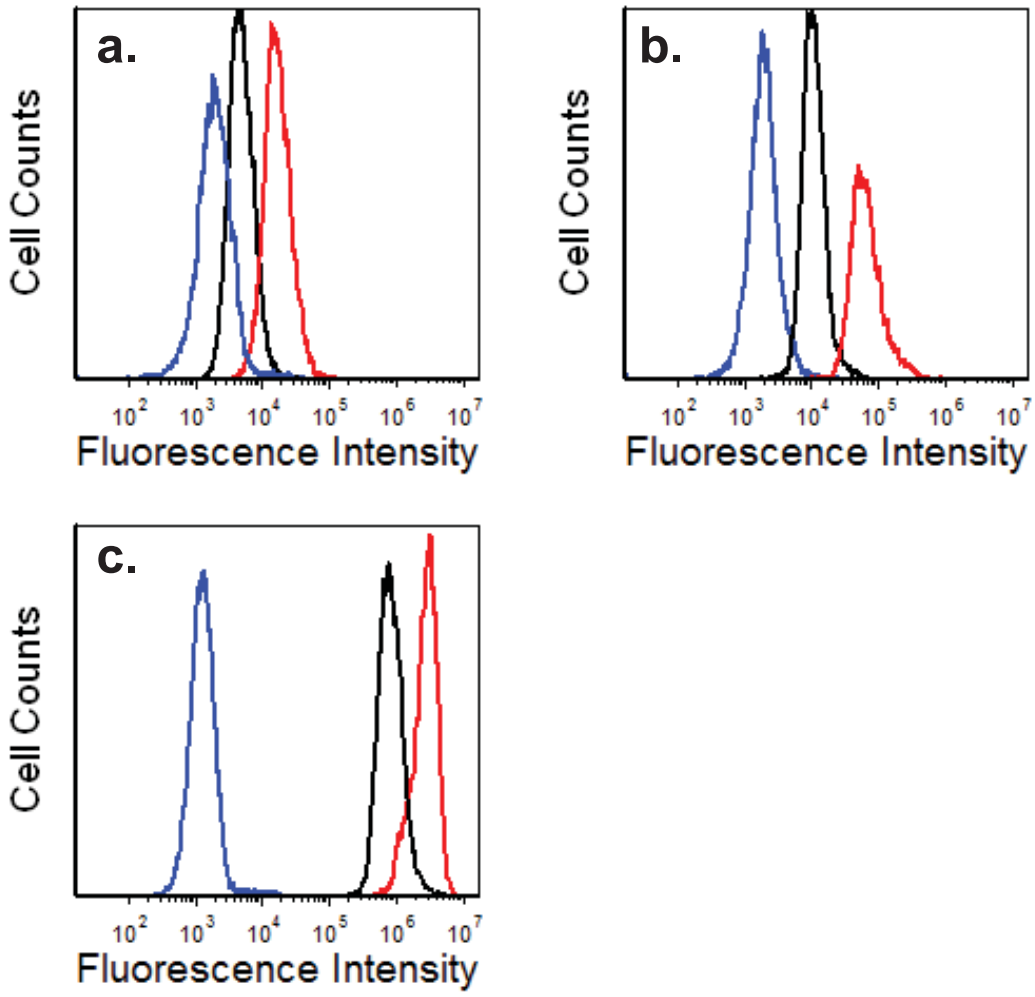

4.9 References

Ahn, B., Rhee, S.G. and Stadtman, E.R. (1987) Use of fluorescein hydrazide and fluorescein thiosemicarbazide reagents for the fluorometric determination of protein carbonyl groups and for the detection of oxidized protein on polyacrylamide gels. *Analytical Biochemistry*, 161, 245-257.

Anderson, J. and Melchers, F. (1976) Lymphocyte stimulation by concanavalin A. In Bittiger, H. and Schnebli, H.P. (eds), Concanavalin A as a Tool. John Wiley & Sons, New York, pp. 505-522.

Bi, S. and Baum, L.G. (2009) Sialic acids in T cell development and function. *Biochimica et Biophysica Acta*, 1790, 1599-1610.

Brustad, E.M., Lemke, E.A., Schultz, P.G. and Deniz, A.A. (2008) A General and Efficient Method for the Site-Specific Dual-Labeling of Proteins for Single Molecule Fluorescence Resonance Energy Transfer. *Journal of the American Chemical Society*, 130, 17664-17665.

Buldt, A. and Karst, U. (1999) *N*-methyl-4-hydrazino-7-nitrobenzofurazan as a new reagent for air monitoring of aldehydes and ketones. *Analytical Chemistry*, 71, 1893-1898.

Cairo, C.W., Key, J.A. and Sadek, C.M. (2010) Fluorescent small-molecule probes of biochemistry at the plasma membrane. *Current Opinion in Chemical Biology*, 14, 57-63.

Carpino, L.A. (1960) O-acylhydroxylamines .2. o-mesitylenesulfonyl-hydroxylamine, o-para-toluenesulfonyl-hydroxylamine and o-mesitylhydroxylamine. *Journal of the American Chemical Society*, 82, 3133-3135.

Chen, I., Howarth, M., Lin, W. and Ting, A.Y. (2005) Site-specific labeling of cell surface proteins with biophysical probes using biotin ligase. *Nat Meth*, 2, 99-104.

Chen, X. and Varki, A. (2010) Advances in the Biology and Chemistry of Sialic Acids. *ACS Chemical Biology*, 5, 163-176.

Cordes, E.H. and Jencks, W.P. (1963) The Mechanism of Hydrolysis of Schiff Bases Derived from Aliphatic Amines. *Journal of the American Chemical Society*, 85, 2843-2848.

De Bank, P.A., Kellam, B., Kendall, D.A. and Shakesheff, K.M. (2003) Surface engineering of living myoblasts via selective periodate oxidation. *Biotechnology and Bioengineering*, 81, 800-808.

Demchenko, A.P., Mely, Y., Duportail, G. and Klymchenko, A.S. (2009) Monitoring Biophysical Properties of Lipid Membranes by Environment-Sensitive Fluorescent Probes. *Biophysical Journal*, 96, 3461-3470.

Diamandis, E.P. and Christopoulos, T.K. (1991) The biotin-(strept)avidin system: principles and applications in biotechnology. *Clinical Chemistry*, 37, 625-636.

Dirksen, A., Hackeng, T.M. and Dawson, P.E. (2006) Nucleophilic Catalysis of Oxime Ligation. *Angewandte Chemie International Edition*, 45, 7581-7584.

Du, J., Meledeo, M.A., Wang, Z.Y., Khanna, H.S., Paruchuri, V.D.P. and Yarema, K.J. (2009) Metabolic glycoengineering: Sialic acid and beyond. *Glycobiology*, 19, 1382-1401.

Dube, D.H. and Bertozzi, C.R. (2003) Metabolic oligosaccharide engineering as a tool for glycobiology. *Current Opinion in Chemical Biology*, 7, 616-625.

Dziegielewska, K.M., Brown, W.M., Casey, S.J., Christie, D.L., Foreman, R.C., Hill, R.M. and Saunders, N.R. (1990) The complete cDNA and amino acid sequence of bovine fetuin - its homology with alpha 2HS glycoprotein and relation to other members of the cystatin superfamily. *Journal of Biological Chemistry*, 265, 4354-4357.

Gubitz, G., Wintersteiger, R. and Frei, R.W. (1984) Fluorogenic labeling of carbonyl compounds with 7-hydrazino-4-nitrobenzo-2-oxa-1,3,-diazole (NBD-H). *Journal of Liquid Chromatography*, 7, 839-854.

Hernandez, J.D. and Baum, L.G. (2002) Ah, sweet mystery of death! Galectins and control of cell fate. *Glycobiology*, 12, 127R-136R.

Huhn, C., Selman, M.H.J., Ruhaak, L.R., Deelder, A.M. and Wuhrer, M. (2009) IgG glycosylation analysis. *Proteomics*, 9, 882-913.

Jachmann, N. and Karst, U. (2001) Synthesis and application of 4-(N,N-dimethylaminosulfonyl)-7-N-methylhydrazino-2,1,3-benzoxadiazole (MDBDH) as a new derivatizing agent for aldehydes. *Fresenius' Journal of Analytical Chemistry*, 369, 47-53.

Key, J.A. and Cairo, C.W. (2011) Identification of fluorogenic and quenched benzoxadiazole reactive chromophores. *Dyes and Pigments*, 88, 95-102.

Key, J.A., Koh, S., Timerghazin, Q.K., Brown, A. and Cairo, C.W. (2009) Photophysical characterization of triazole-substituted coumarin fluorophores. *Dyes and Pigments*, 82, 196-203.

Kohler, J.J. (2009) Aniline: a catalyst for sialic acid detection. *ChemBioChem*, 10, 2147-2150.

Lavis, L.D. and Raines, R.T. (2008) Bright ideas for chemical biology. *ACS Chemical Biology*, 3, 142-155.

Matsushita, Y., Takahashi, M. and Moriguchi, I. (1986) Binding of fluorescent 7-amino-4-nitrobenzoxadiazole derivatives to bovine serum albumin. *Chemical & Pharmaceutical Bulletin*, 34, 333-339.

Miyazawa, E., Sakamoto, T. and Kikugawa, Y. (1997) Preparation of ring-substituted phenoxylamine derivatives. *Organic Preparations and Procedures International*, 29, 594-600.

Raindlová, V., Pohl, R., Scaronanda, M. and Hocek, M. (2010) Direct Polymerase Synthesis of Reactive Aldehyde-Functionalized DNA and Its Conjugation and Staining with Hydrazines. *Angewandte Chemie International Edition*, 49, 1064-1066.

Rannes, J.B., Ioannou, A., Willies, S.C., Grogan, G., Behrens, C., Flitsch, S.L. and Turner, N.J. Glycoprotein Labeling Using Engineered Variants of Galactose Oxidase Obtained by Directed Evolution. *Journal of the American Chemical Society*, ASAP.

Rayo, J., Amara, N., Krief, P. and Meijler, M.M. (2011) Live Cell Labeling of Native Intracellular Bacterial Receptors Using Aniline-Catalyzed Oxime Ligation. *Journal of the American Chemical Society*, 133, 7469–7475.

Salahuddin, S., Renaudet, O. and Reymond, J.L. (2004) Aldehyde detection by chromogenic/fluorogenic oxime bond fragmentation. *Organic & Biomolecular Chemistry*, 2, 1471-1475.

Santa, T., Al-Dirbashi, O.Y., Ichibangase, T., Rashed, M.S., Fukushima, T. and Imai, K. (2008) Synthesis of 4-[2-(*N*,*N*-dimethylamino)ethylaminosulfonyl]-7-N-methylhydrazino-2,1,3-benz oxadiazole (DAABD-MHz) as a derivatization reagent for aldehydes in liquid chromatography/electrospray ionization-tandem mass spectrometry. *Biomedical Chromatography*, 22, 115-118.

Sletten, E.M. and Bertozzi, C.R. (2009) Bioorthogonal Chemistry: Fishing for Selectivity in a Sea of Functionality. *Angewandte Chemie, International Edition in English*, 48, 6974-6998.

Tiefenbrunn, T.K. and Dawson, P.E. (2010) Chemoselective Ligation Techniques: Modern Applications of Time-Honored Chemistry. *Biopolymers*, 94, 95-106.

Uzu, S., Kanda, S., Imai, K., Nakashima, K. and Akiyama, S. (1990) Fluorogenic Reagents - 4-Aminosulphonyl-7-Hydrazino-2,1,3-Benzoxadiazole, 4-(*N*,*N*-Dimethylaminosulphonyl)-7-Hydrazino-2,1,3-Benzoxadiazole and 4-Hydrazino-7-Nitro-2,1,3-Benzoxadiazole Hydrazine for Aldehydes and Ketones. *Analyst*, 115, 1477-1482.

Van lenten, L. and Ashwell, G. (1971) Studies on chemical and enzymatic modification of glycoproteins - general method for tritiation of sialic acid-containing glycoproteins. *Journal of Biological Chemistry*, 246, 1889-1894.

Varki, N.M. and Varki, A. (2007) Diversity in cell surface sialic acid presentations: implications for biology and disease. *Laboratory Investigation*, 87, 851-857.

Whitman, C.M., Yang, F. and Kohler, J.J. Modified GM3 gangliosides produced by metabolic oligosaccharide engineering. *Bioorganic & Medicinal Chemistry Letters*, In Press, Accepted Manuscript.

Yang, Y. and Orlando, R. (1996) Identifying the glycosylation sites and site-specific carbohydrate heterogeneity of glycoproteins by matrix-assisted laser desorption/ionization mass spectrometry. *Rapid Communications in Mass Spectrometry*, 10, 932-936.

Yasukawa, Z., Sato, C. and Kitajima, K. (2005) Inflammation-dependent changes in alpha 2,3-, alpha 2,6-, and alpha 2,8-sialic acid glycotopes on serum glycoproteins in mice. *Glycobiology*, 15, 827-837.

Yasukawa, Z., Sato, C., Sano, K., Ogawa, H. and Kitajima, K. (2006) Identification of disialic acid-containing glycoproteins in mouse serum: a novel modification of immunoglobulin light chains, vitronectin, and plasminogen. *Glycobiology*, 16, 651-665.

Zeng, Y., Ramya, T.N.C., Dirksen, A., Dawson, P.E. and Paulson, J.C. (2009) High-efficiency labeling of sialylated glycoproteins on living cells. *Nature Methods*, 6, 207-209.

Chapter 5

Synthesis, photophysical characterization, and application of bifunctional bioorthogonal cyanine-5 derivatives for labelling of phospholipids[5]

[5] Portions of the work described in this chapter have been published in Sandbhor, M.S., Key, J.A., Strelkov, I.S. and Cairo, C.W. (2009) A Modular Synthesis of Alkynyl-Phosphocholine Headgroups for Labeling Sphingomyelin and Phosphatidylcholine. *The Journal of Organic Chemistry*, 74, 8669-8674.

5.1 Introduction

Phospholipids are an important part of the cell membrane, with roles in structure, metabolism and signalling.(Dowhan, W. 1997) However, it is difficult to directly interrogate phospholipids using genetic methods as mutations to enzymes in the biosynthetic pathway may directly alter lipid structure or be detrimental to the cell. These kinds of mutations can result in loss of cell integrity or may affect multiple cell functions simultaneously, obscuring the results obtained.(Dowhan, W. 1997) Therefore, bioorthogonal chemical probes provide an attractive strategy to examine phospholipids and their interactions with biomolecules.

Our group has previously developed synthetic strategies to generate alkyne-modified phosphatidylcholine and sphingomyelin (**3.35**) (53% yield over five steps) which allowed successful elaboration of the lipid with an azido-substituted benzoxadiazole probe (**3.2**) to generate the triazole product (**3.36**) (see Chapter 3, Scheme 3.6).(Sandbhor, M.S., Key, J.A., et al. 2009) Although synthetically challenging, this method allowed for the incorporation of a chemically defined phospholipid analogue into cells (**Figure 5.1**). Additionally, our modification of the headgroup with an alkyne or triazole moiety did not prevent cleavage of the phosphodiester by sphingomyelinase, as observed by TLC assay. This strategy is unique in that it allows for post-synthetic bioorthogonal modification of the lipid through the solvent-exposed headgroup.

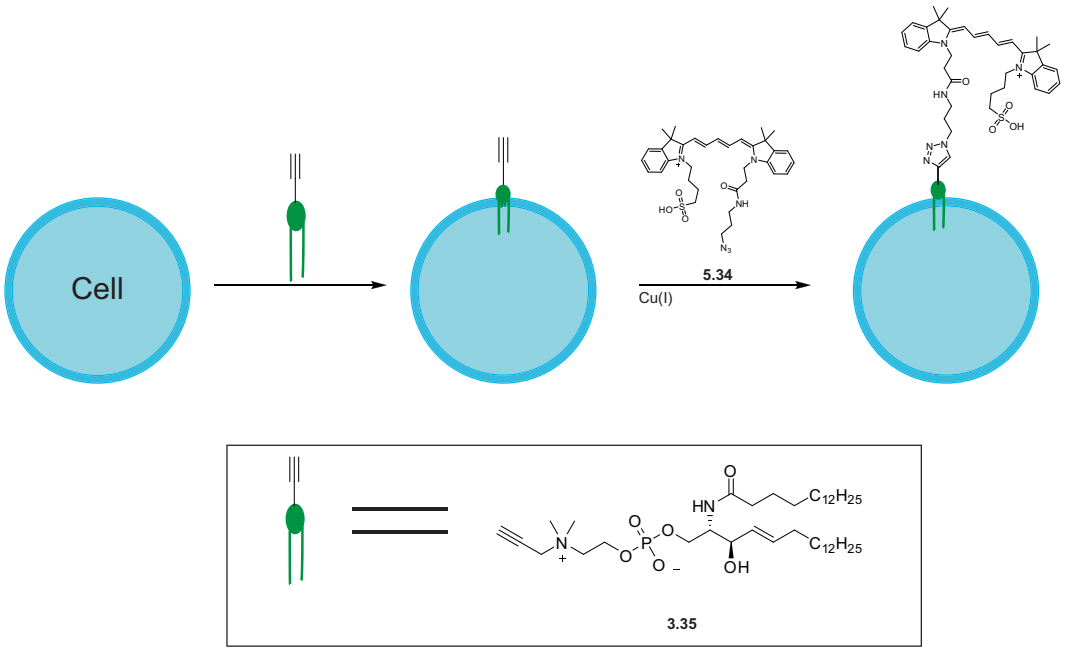

Figure 5.1. Cellular incorporation of alkyne-modified phosphatidylcholine (3.35) and subsequent labelling with an azido-cyanine dye (5.34). Synthetic lipids may passively insert into the cell membrane, allowing for labelling and examination of distribution, mobility and activity of a substrate.

A complementary approach was recently reported by Jao and colleagues which takes advantage of the primary mammalian choline pathway to metabolically label choline-containing phospholipids. Exogenous choline is absorbed and phosphorylated upon entry into mammalian cells by choline kinase. Subsequently, phosphocholine undergoes a rate limiting conversion to cytidine diphosphate choline (CDP-choline), catalyzed by the enzyme CTP:phosphocholine cytidylyltransferase. Phosphatidylcholine, the main choline reservoir in mammals, is then synthesized from CDP-choline. This reaction is catalyzed by the enzyme CDP-choline:1,2-diacylglycerol cholinephosphotransferase. Phosphatidylcholine may be used as a primary lipid in

the cell membrane, elaborated into other lipids (such as sphingomyelin) or degraded by phospholipases.(Kent, C. 1995, Li, Z. and Vance, D.E. 2008)

Jao and colleagues utilized the choline pathway to incorporate an alkyne choline analog into phosphatidylcholine, sphingomyelin and ether phospholipids.(Jao, C.Y., Roth, M., et al. 2009) Cells were incubated with propargyl choline (**5.3**) overnight followed by Cu(I)-catalyzed cycloaddition with an azido-fluorophore to label all classes of choline phospholipids (**Figure 5.2**) and subsequently examined phospholipid distribution and synthesis by fluorescence microscopy. While this method has the advantage of facile synthesis using precedented or commercially available reagents, it is not specific for interrogation of any single class of phospholipid.

We postulate that combining these two methodologies and expanding the repertoire of bioorthogonal reactivity which may be used in Jao's technique would enable superior interrogation of phospholipid functions *in vivo*. In their report, Jao and colleagues use only a propargyl-choline derivative, however, they do not examine the feasibility of an azido-choline for metabolic labelling. Azides are very popular metabolic labels, particularly in glycoform remodelling strategies, due to their small size and narrow reaction profiles.(Du, J., Meledeo, M.A., et al. 2009, Saxon, E., Luchansky, S.J., et al. 2002) Aldehydes and ketones are also popular metabolic labels, as they are normally absent from the cell surface and can selectively react with nucleophiles enhanced by the alpha effect.(Fina, N.J. and Edwards, J.O. 1973, Hang, H.C. and Bertozzi, C.R. 2001, Rannes, J.B., Ioannou, A., et al.) The use of this strategy has increased with the development of

aqueous aniline catalysis, improving reaction rates by 30-400%, via formation of an aniline Schiff base intermediate.(Dirksen, A., Dirksen, S., et al. 2006, Kohler, J.J. 2009) As well, aldehydes may also be generated and examined *in situ* using periodate oxidation and aniline-catalyzed ligation (PAL) strategies for glycoconjugates (see Chapter 4).(Zeng, Y., Ramya, T.N., et al. 2009) To date, no other bioorthogonal chemistries have been developed for choline labelling.

We propose azido and carbonyl-containing cholines may expand the palette of metabolic labels for Jao's methodology. Furthermore, additional bioorthogonal reactivities should enable multi-colour and pulse-chase experiments which are currently impractical for these biomolecules. To test this hypothesis, we employed the blue and green emitting fluorophores detailed in chapters 3-4 in conjunction with a new series of cyanine-5 fluorophores, substituted with bioorthogonal handles, which emit in the red region of the spectrum.

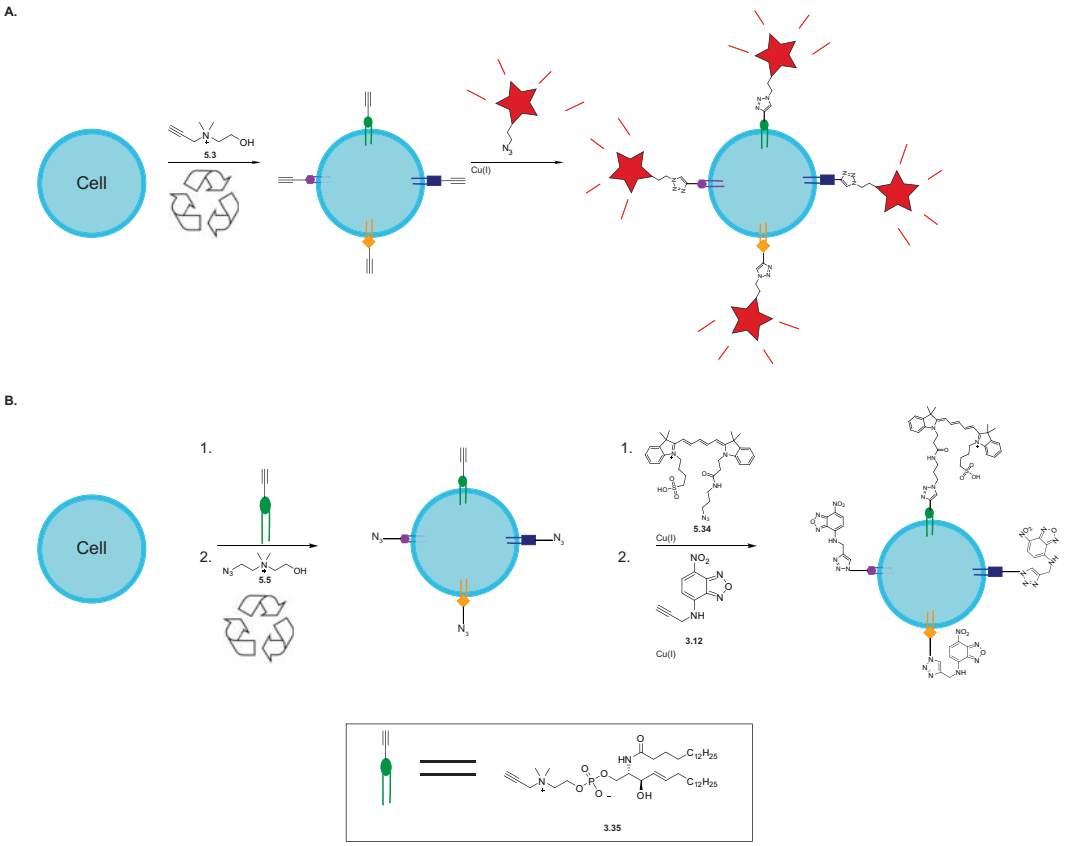

Figure 5.2. Metabolic labelling of choline-containing phospholipids including phosphatidylcholine, sphingomyelin and ether phospholipids. A) Choline-containing phospholipids including phosphatidylcholine, sphingomyelin and ether phospholipids can be metabolically labelled with choline derivatives and subsequently examined using fluorophore probes. **B)** A combined strategy utilizing a synthetic lipid derivative and metabolic labelling strategies to enable multi-colour fluorescence microscopy experiments for examination of lipid distribution and function.

The first component of our strategy rests on the development of new choline derivatives for label incorporation. We synthesized alkynyl, azido and carbonyl choline derivatives (**5.3, 5.5** and **5.8**) and examined their metabolic incorporation into Jurkat T cell phospholipids by fluorophore labelling using flow cytometry and fluorescence microscopy. With potential metabolic precursors in hand, we also set out to develop additional bright fluorophores with complementary reactive handles for labelling analysis. We purchased or synthesized a series of amine linkers with alkynyl, azido, and amino-oxy functional groups. The amine linkers were incorporated via amide bond formation from a common carboxylic acid precursor (**5.32**) to generate a series of Cy 5 fluorophores (**Scheme 5.1**).

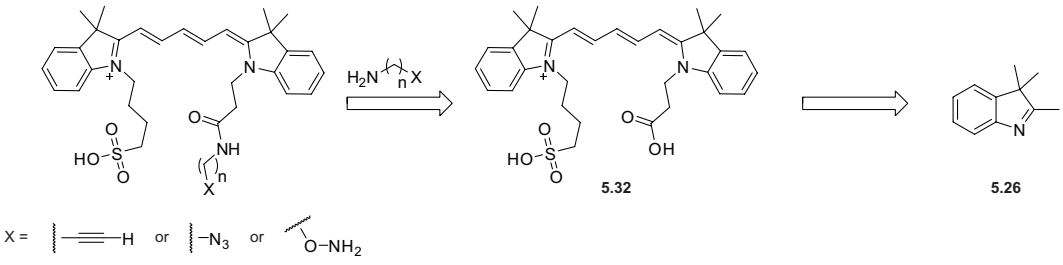

Scheme 5.1. Retrosynthesis of a series of Cy 5 fluorophores with alkynyl, azido, and amino-oxy reactive handles. The reactive handles may be installed by amide bond formation with a series of amine linkers.

5.2 Synthesis of choline derivatives

Choline analogs having a methyl group replaced with an alkyl chain of up to five carbons in length may be efficiently incorporated into phospholipids.(Bridges, R.G. and Ricketts, J. 1970, Jao, C.Y., Roth, M., et al. 2009) An alkynyl choline derivative (**5.3**) suitable for click-chemistry metabolic

labelling was previously tested by Jao and colleagues, and may be synthesized by nucleophilic displacement of bromoethanol (**5.1**) and *N,N*-dimethylprop-2-yn-1-amine (**5.2**) in excellent yield (**Scheme 5.2**). Similarly, an azido choline derivative (**5.5**) may be generated by nucleophilic displacement of 2-azido-*N,N*-dimethylethanamine (**5.4**) with bromoethanol (**5.1**).[6]

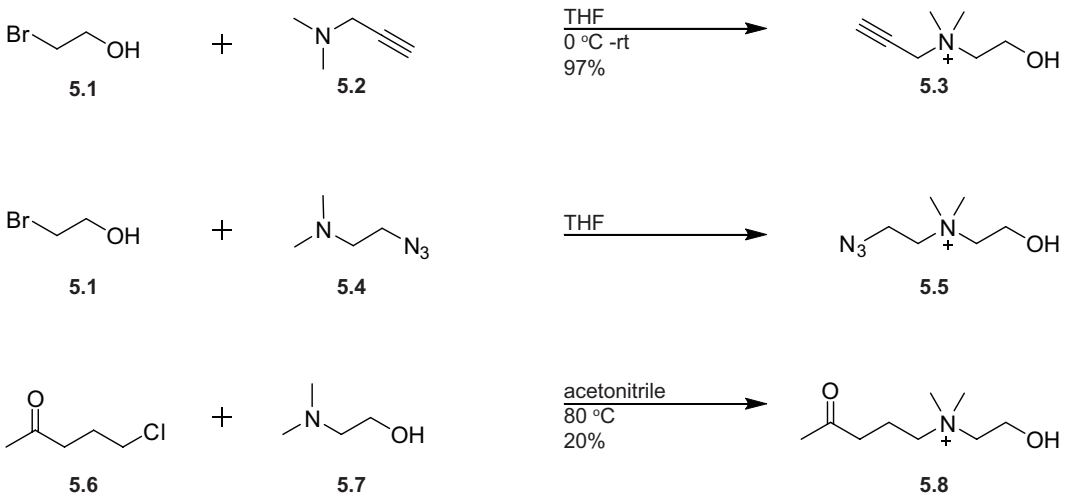

Scheme 5.2. Synthesis of alkynyl (5.3), azido (5.5) and carbonyl (5.8) choline analogs. Choline analogues were generated by nucleophilic substitution of alkyl halides.

We set out to design a choline derivative containing a carbonyl for use in hydrazone/oxime forming bioorthogonal strategies. Synthesis of a suitable carbonyl-containing choline derivative proved more challenging, as the position of the carbonyl group was critical to the stability of the product. We first attempted nucleophilic displacement of 1-bromobutan-2-one (**5.9**) with *N,N*-dimethylaminoethanol (**5.7**) in polar aprotic solvents (**Scheme 5.3**). A promising white precipitate formed readily in excellent yield; however, characterization

[6] Compound **5.5** was previously synthesized and characterized by Dr. Mahendra Sandbhor; Sandbhor and Cairo, unpublished.

indicated this compound to be a remarkably stable 6-membered cyclic hemiketal, **5.10**. Similarly, the nucleophilic displacement of *N*,*N*-dimethylaminoacetone (**5.11**) with bromoethanol (**5.1**) also generated a stable hemiketal, **5.12**.

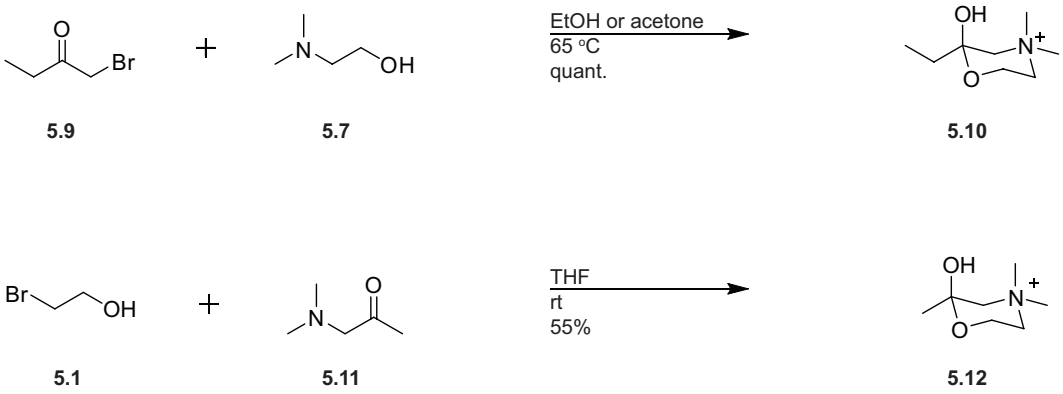

Scheme 5.3. Formation of undesired hemiketal products 5.10 and 5.12. Isolated products of nucleophilic attack at bromide and subsequent ring closure to hemiketals **5.10** and **5.12**.

To circumvent the formation of the cyclic hemiketal we envisioned using protecting group strategies at both the carbonyl and hydroxyl functionalities. The hydroxyl group of *N,N*-dimethylaminoethanol (**5.7**) was protected with triethylsilane (TES) in the presence of catalytic sodium metal in hexanes to afford **5.13** in good yield (**Scheme 5.4**). Acetal protection of 1-bromobutan-2-one (**5.9**) with ethylene glycol (**5.14**) under Dean-Stark generated **5.15** in excellent yield. Attempts to perform nucleophilic substitution with protected compounds (**5.13** and **5.15**) were complicated by formation of side products, likely due to loss of the protecting groups under typical reaction conditions. This was readily observed with the TES protected compound (**5.13**), which upon reaction with bromoethanol (**5.1**) in THF at 65 ^{o}C resulted in formation of the diol **5.16**.

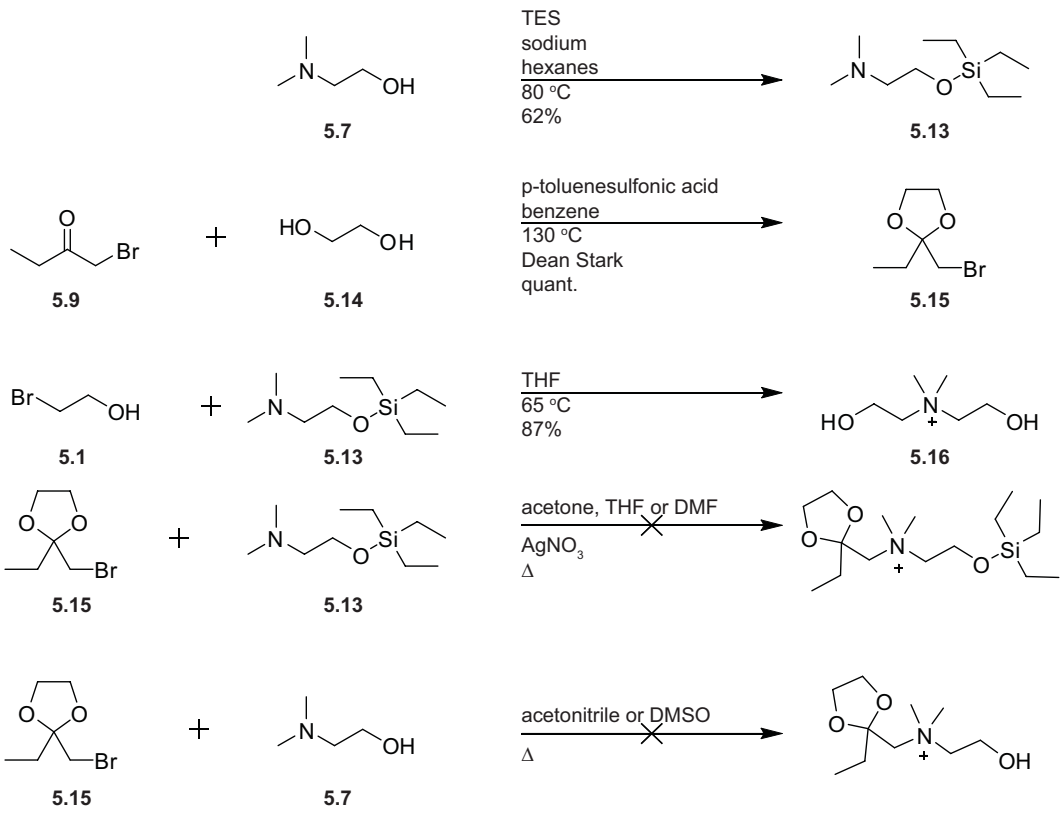

Scheme 5.4. Synthesis of protected starting materials 5.16 and 5.18 and attempts to generate a carbonyl choline. The protected starting materials **5.13** and **5.15** decomposed under reaction conditions.

An alternate stategy was attempted to generate a suitable carbonyl choline compound (**5.17**) via hydration of propargyl choline (**5.3**). We attempted several known reaction conditions for this transformation (**Table 5.1**), including the use of formic acid (Menashe, N., Reshef, D., et al. 1991), mercury sulphate/sulphuric acid (Rose, N.C. 1966), and a TMSOTf-promoted reaction (Park, J.Y., Ullapu, P.R., et al. 2008). These conditions were unsuccessful, yielding starting materials, decomposition products, or trace amounts of carbonyl product (as detected by IR).

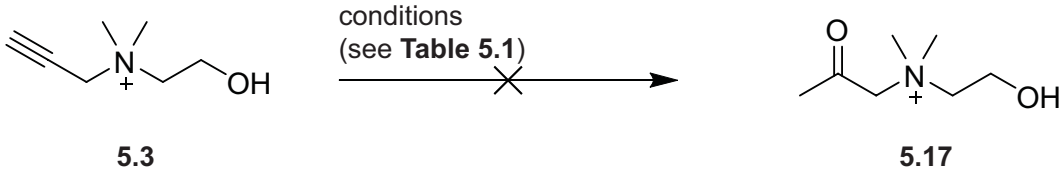

5.3 **5.17**

Scheme 5.5. Attempted synthesis of carbonyl choline 5.17.

Reaction Conditions	*Results*
Formic acid, 100 - 150 ^{o}C	No reaction
Water, 160 ^{o}C, 5 days	<5% product
$HgSO_4$, H_2SO_4, 70 - 105 ^{o}C	No reaction
TMSOTf, formaldehyde, ethyl ether -78 ^{o}C to rt	Decomp.

Table 5.1. Reaction conditions tested for the synthesis of compound 5.17.

Hydration of the alkyne **5.3** was attempted using popular conditions such as formic acid and mercury catalysis, however was unsuccessful. (Menashe, N., Reshef, D., et al. 1991, Park, J.Y., Ullapu, P.R., et al. 2008, Rose, N.C. 1966)

Although hydration of alkynes is a well precedented reaction for many types of substrates, there are no prior examples which include quaternary amines. We tested several conditions (**Table 5.1**) and were unable to generate significant amounts of the desired carbonyl-choline derivative. This may not be unexpected based on the AD_E2 mechanism of acid catalyzed alkyne hydration. This reaction is believed to go through a rate limiting proton transfer step affording a vinyl cation.(Allen, A.D., Chiang, Y., et al. 1982) Formation of the vinyl cation during the rate limiting step is likely very unfavourable due to the adjacent quaternary amine.

We next turned our attention to generating a carbonyl choline via an S_N2 substitution of alkyl chloride **5.6**. A suitable carbonyl choline (**5.8**) was

synthesized in modest yield by the nucleophilic displacement of 5-chloropentan-2-one (**5.6**) and *N,N*-dimethylaminoethanol (**5.7**) in acetonitrile with heating. Significant loss of product occurred due to multiple ion exchange purification steps required to isolate the product. Unreacted dimethylaminoethanol (**5.7**) eluted closely with the product in both reverse phase and ion exchange chromatography. No evidence of a cyclic hemiketal product was observed in this reaction, which may be rationalized by the increased penalty from strain of a larger 8-membered cycle.(Prelog, V. 1963)

5.3 Amine-linkers for bioorthogonal strategies

With alkynyl, azido and carbonyl choline derivatives in hand, we next turned our attention to designing complementary bioorthogonal amine linkers (**5.18**, **5.20** and **5.25**). These linkers will be covalently attached to the cyanine-dyes, via amide bond formation for visualization of dye ligation to the derivativized phospholipids. Bioorthogonal amine linkers were either purchased, (**5.18**) or synthesized following routes described in the literature (**Scheme 5.6**).(Carrasco, M.R., Alvarado, C.I., et al. 2010, Lewis, W.G., Magallon, F.G., et al. 2004) The 3-azidopropylamine linker (**5.20**) was synthesized in one step in moderate yield, following the route of Lewis and colleagues, by nucleophilic displacement of 3-bromopropylamine hydrobromide (**5.19**) with sodium azide under aqueous conditions.(Lewis, W.G., Magallon, F.G., et al. 2004) Extreme caution should be used when performing this reaction and concentrating the azide product, as 3-azidopropylamine (**5.20**) is suspected to be unstable.

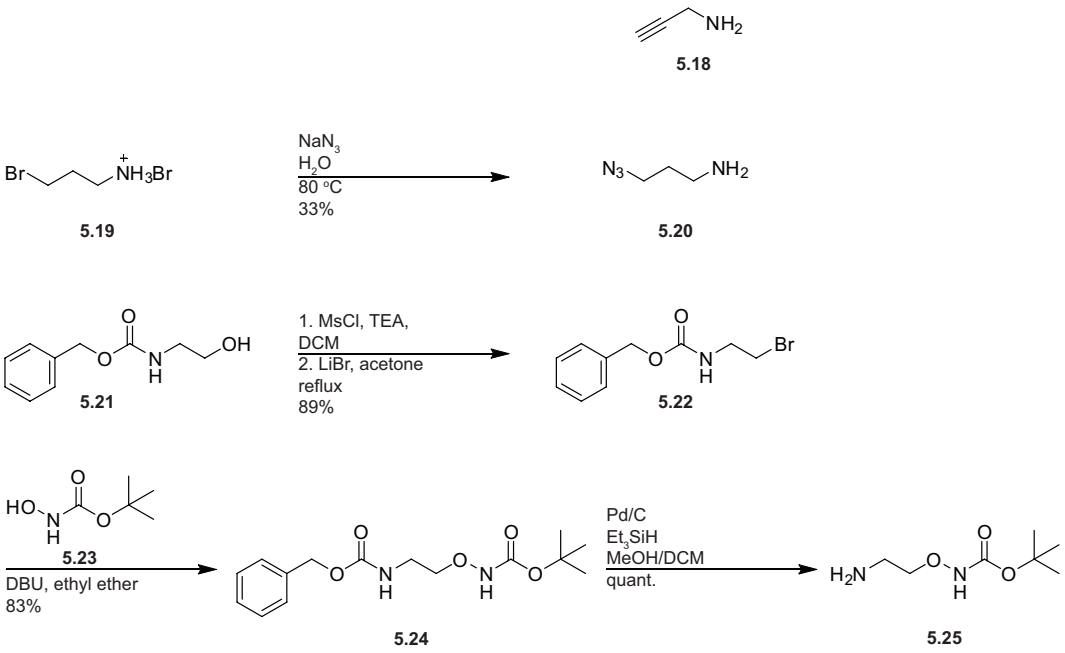

Scheme 5.6. Synthesis of amine linkers. The 3-azidopropylamine linker (**5.20**) was synthesized in one step by nucleophilic displacement.(Lewis, W.G., Magallon, F.G., et al. 2004) Boc-protected amino-oxy linker (**5.25**) was synthesized in 74% total yield over three steps.(Carrasco, M.R., Alvarado, C.I., et al. 2010)

Consequently, the azide product should be stored in toluene at low temperatures (-20 ^{o}C). The amino-oxy linker (**5.25**) was synthesized following the route described by Carrasco and colleagues in 74% total yield over three steps.(Carrasco, M.R., Alvarado, C.I., et al. 2010) The starting material, *N*-Z-ethanolamine (**5.21**), was reacted with methanesulfonyl chloride to facilitate nucleophilic substitution with lithium bromide affording the bromide (**5.22**) in excellent yield. The protected amino-oxy moiety was installed by a subsequent nucleophilic displacement with *N*-Boc-*N*-methylhydroxylamine (**5.23**) giving compound **5.24** in good yield. Deprotection of the CBZ group was performed

using hydrogenation over Pd/C to generate the free amine end on the Boc-protected amino-oxy linker (**5.25**) in quantitative yield.

5.4 Cyanine-5 fluorophore synthesis

Cyanine dyes have become popular labels for use in microarrays and high resolution microscopy due to their extremely high absorption coefficients and long-wavelength absorption and emission profiles.(Lavis, L.D. and Raines, R.T. 2008) These compounds are cationic and feature two nitrogen heterocycles linked by a polymethine bridge (**Figure 5.3**). The length of this bridge contributes to the numerical notation in the abbreviation, for example a cyanine dye with a five carbon linker would be described as Cy 5. As the length of the polymethine bridge is increased by one unit, the dye will exhibit a bathochromic shift in absorption and emission maxima of approximately 100 nm; however, the fluorescence quantum yield will decrease due to greater molecular flexibility. Cy dye functional group diversity is usually introduced by varying nitrogen substituents, changing the heterocycles, or altering the polymethine chain. However, very few functional groups are stable to the reaction conditions employed in the condensation step of their synthesis.(Mojzych, M. and Henary, M. 2008) As well, due to the cationic and polar nature of many cyanine dyes, purification is often very challenging. Therefore, synthesis of chemically well defined bifunctional cyanine dyes remains an active area of research with several recent examples appearing in the literature.(Bouteiller, C., Clave, G., et al. 2007, Pavlik, C., Biswal, N.C., et al. 2011, Shao, F., Weissleder, R., et al. 2008, Shao, F., Yuan, H., et al. 2011)

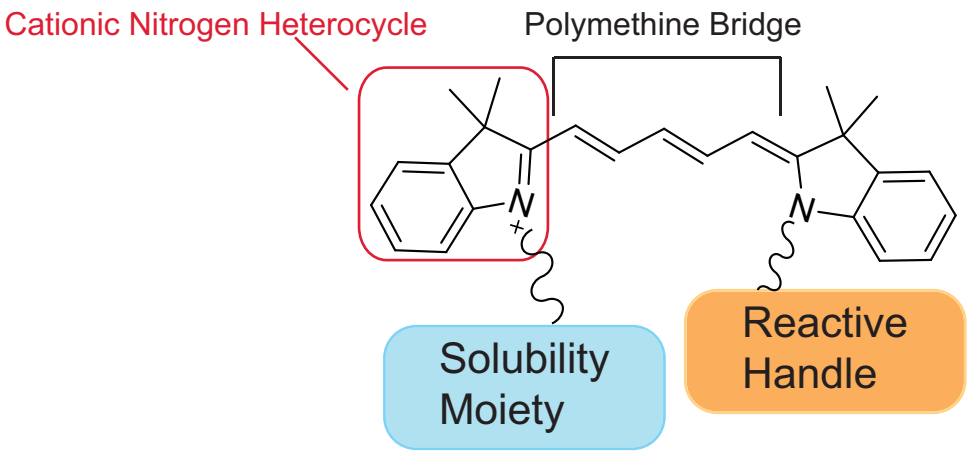

Figure 5.3. General structure of cyanine-5 dyes. Structural features such as the nitrogen heterocycle and polymethine bridge are indicated. Solubility moieties and reactive handles are typically sulphonates or carboxylic acids.

We sought to synthesize a series of customizable bioorthogonal Cy 5 derivatives by introducing a sulphonate group on one indole hemisphere to improve water solubility and a carboxylic acid on the other to act as a reactive handle for a bioorthogonal amine linker (**Figure 5.3**). The starting material 2,3,3-trimethyl-3H-indole (**5.26**) was quaternized to the sulphonate bearing indolium (**5.28**) by heating with 1,4-butanesultone (**5.27**) for 3 h at 120 ^{o}C following the procedure established by Kiyose and colleagues (**Scheme 5.7**).(Kiyose, K., Aizawa, S., et al. 2009) Similarly, heating **5.26** at 105 ^{o}C, neat with 3-iodopropionic acid (**5.29**) generated the quaternized acid-bearing indolium (**5.30**). Trimethyl-1-(4-sulfobutyl)-3H-indolium (**5.28**) and malonaldehyde dianilide hydrochloride (**5.31**) were condensed in acetic anhydride at room temperature to

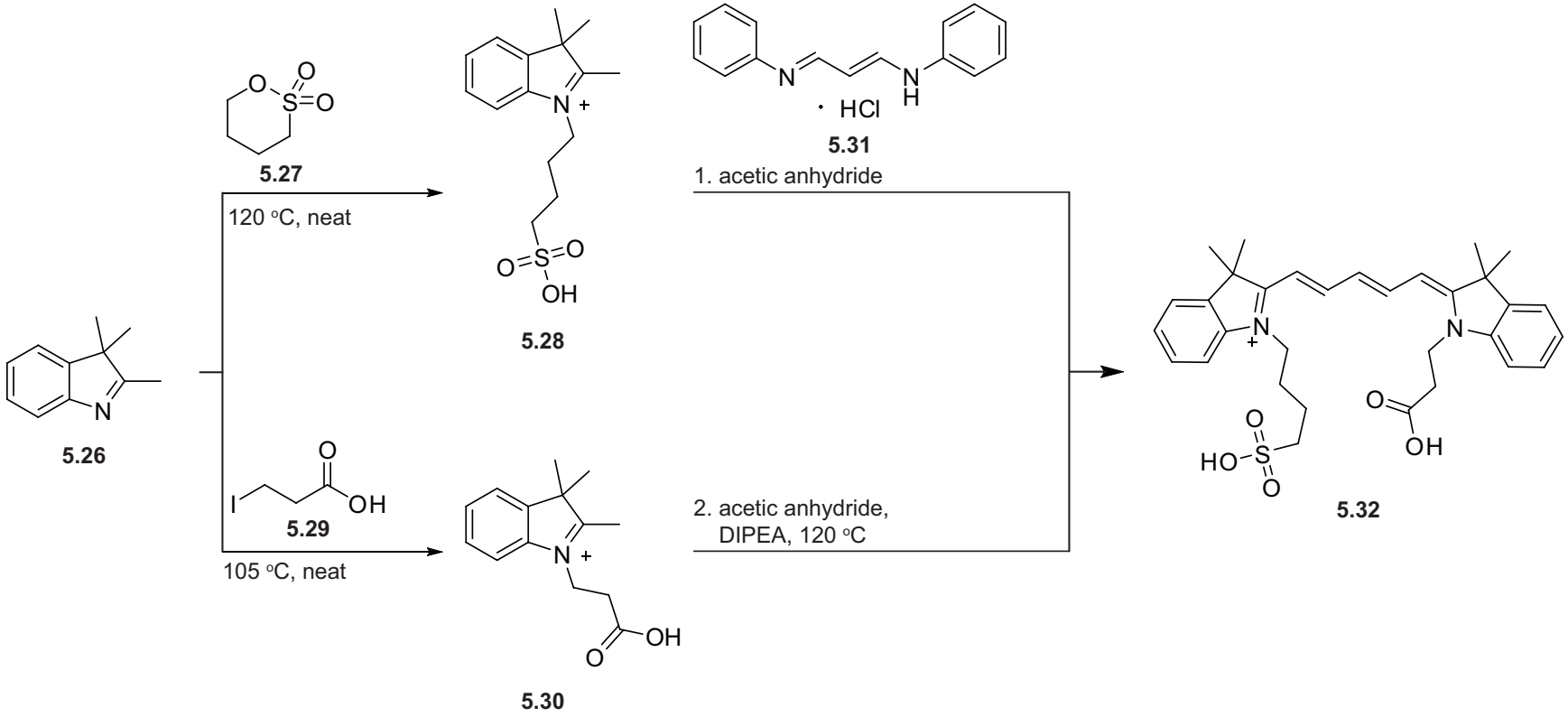

Scheme 5.7. Synthesis of bifunctional cyanine-5 dye 5.32. Substituted cationic indoliums **5.28** and **5.30** were synthesized neat and carried forward without purification to the condensation step with malonaldehyde dianilide hydrochloride (**5.31**).

provide a 3,3-dimethyl-2-((1E,3E)-4-(phenylamino)buta-1,3-dienyl)-1-(4-sulfobutyl)-3H-indolium intermediate. To avoid formation of a monofunctional disulphonate Cy 5, it is critical that the indolium (**5.28**) and malonaldehyde (**5.31**) are reacted at equimolar concentrations and that the resulting intermediate is enriched using a short normal phase silica plug. This intermediate can then be condensed with 1-(2-carboxyethyl)-2,3,3-trimethyl-3H-indolium (**5.30**) in acetic anhydride in the presence of DIPEA with heating at 120 ^{o}C for 3 h. The use of dianilide linker condensations to generate cyanine dyes is well precedented and can be performed in large scales. However, the most challenging aspect of cyanine dye synthesis is purification. Purification must be performed using reverse phase HPLC to obtain the desired bifunctional Cy 5 (**5.32**). A number of possible side products are formed in this reaction, reducing the yield substantially. Several side products elute closely to the desired cyanine **5.32**, complicating isolation and identification. Compound **5.32** can be obtained in 10-30 milligram quantities after multiple purification steps (5-10 runs), using a semi-preparative C18 RP-HPLC column.

We next modified the dyes for use in bioorthogonal reactions with choline derivatives by attachment of the amine linkers. The bifunctional Cy 5 (**5.32**) was subjected to coupling with amine bearing bioorthogonal linkers (**5.18**, **5.20**, **5.25**) to afford the amide derivatives (**5.33**-**5.35**) (**Scheme 5.8**). We found that the choice of coupling agent was critical during this step. Coupling with *N,N′*-dicyclohexylcarbodiimide (DCC) resulted in poor yields and impurities, which may be attributed to lower reactivity of the activated ester. The lowered reactivity

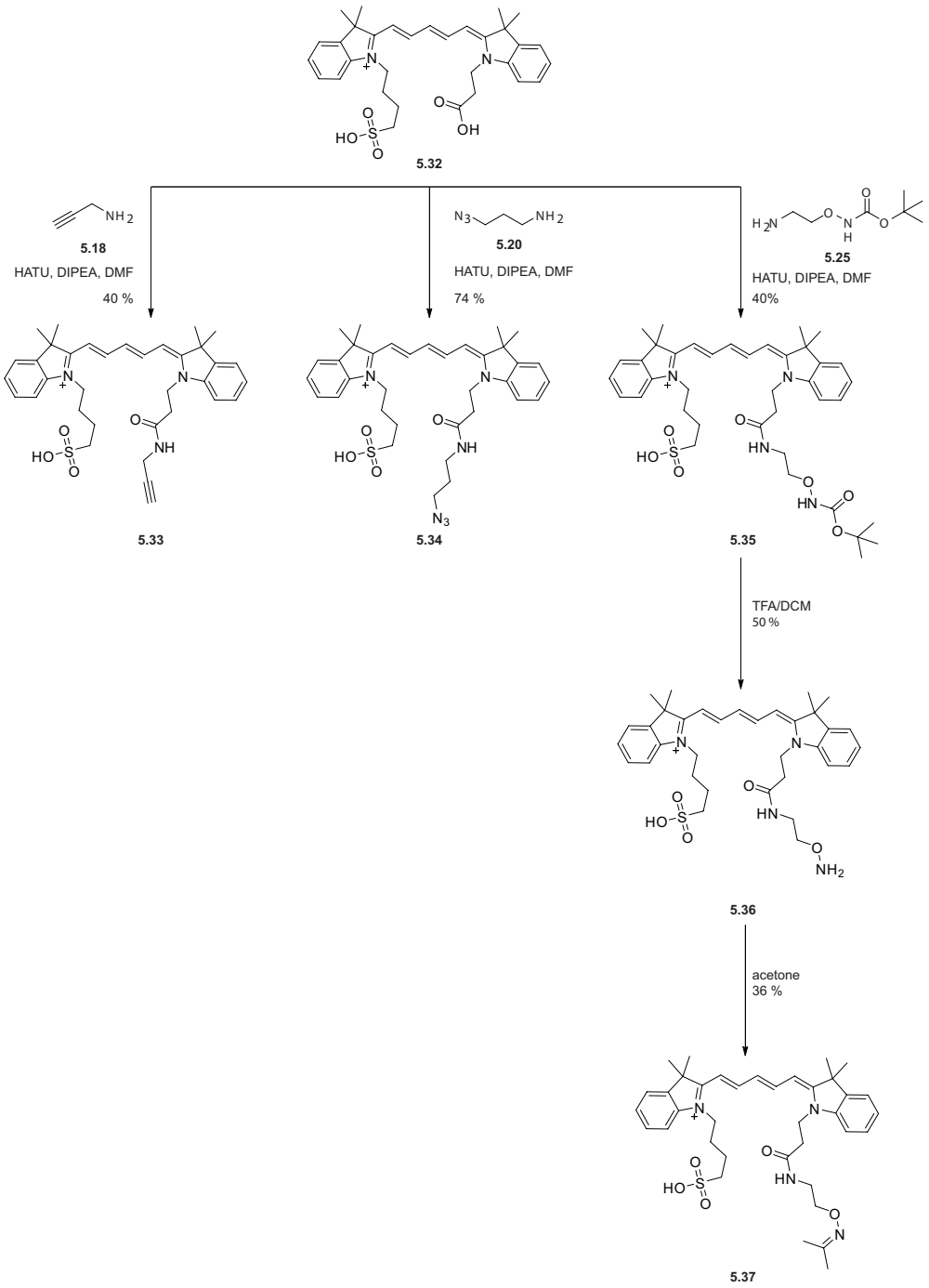

Scheme 5.8 Synthesis of bioorthogonal cyanine-5 derivatives (5.33, 5.34, and 5.46). Bifunctional Cy 5 (**5.32**) was subjected to coupling with amine-bearing bioorthogonal linkers (**5.18**, **5.20**, and **5.25**). Coupling with HATU consistently gave moderate to good yields (40-74%).

in activated ester formation using propionic acid bearing cyanine dyes has been noted by Majumdar and colleagues; however, they chose to address this problem by switching to longer hexanoic acid moieties.(Mujumdar, R.B., Ernst, L.A., et al. 1993) We explored alternative coupling reagents and found that *O*-(7-azabenzotriazol-1-yl)-*N*,*N*,*N*',*N*'-tetramethyluronium hexafluorophosphate (HATU) gave moderate to good yields (40-74%). The Boc-protected amino-oxy Cy 5 (**5.35**) was deprotected using TFA/DCM affording the amino-oxy Cy 5 (**5.36**) in moderate yield. The amino-oxy Cy 5 (**5.36**) was found to be very reactive, and readily underwent oxime formation with acetone, affording **5.37** in moderate yield.

5.5 Fluorophore characterization

Cyanine compounds (**5.32**, **5.33**, **5.34**, and **5.36**) were characterized to determine their UV-vis absorbance, fluorescence emission, molar absorption coefficients, and emission quantum yields (**Table 5.2**). We performed spectral characterization in methanol, using cresyl violet as the quantum yield standard (see section 2.10). The compounds examined range in absorption maxima between 642-644 nm and emission maxima between 662-663 nm. The cyanine compounds displayed high absorption coefficients between 6.5 x 10^4 and 19.1 x 10^4 cm^{-1} M^{-1}, and good quantum yields between 0.15 and 0.21, indicative of bright fluorophores. We speculate that the lower absorption coefficient of azide **5.34** is the result of intramolecular quenching of the azide on the linker.

Compound	λ max_{abs} (nm)	λ max_{fluor} (nm)[a]	ε Absorption Coefficient (cm^{-1} M^{-1})[b]	Φ Quantum Yield[a,c]	Brightness (ε x Φ)
5.32	643	663	19.1 x 10^4	0.21	4.0 x 10^4
5.33	642	662	16.0 x 10^4	0.21	3.4 x 10^4
5.34	643	662	6.5 x 10^4	0.15	1.0 x 10^4
5.36	644	662	12.9 x 10^4	0.15	1.9 x 10^4

Table 5.2. Spectral properties of Cy 5 compounds in methanol.

a. Excitation was at 590 nm.

b. Absorption coefficients were measured at 640 nm.

c. Cresyl violet was used as a quantum yield standard (Φ = 0.54) in methanol.

5.6 Flow cytometry and fluorescence microscopy of metabolically labelled Jurkat cells

To evaluate the effectiveness of metabolic incorporation of choline derivatives, live Jurkat T cells were incubated with choline analogs (**5.3, 5.5,** and **5.8**) overnight (320-520 μM) and treated with the corresponding bioorthogonal Cy 5 fluorophores (**5.34, 5.33** and **5.36**, respectively) following the protocol of Jao and colleagues. Labelling with alkynyl (**5.33**) and azido cyanine (**5.34**) dyes (2.5 μM) was performed in the presence of $CuSO_4$ (1 mM) and ascorbic acid (75 mmol) in PBS buffer for approximately 20 min. Labelling with amino-oxy cyanine dye **5.36** (2.4 μM) or NBDH **4.2** (19.2 μM) was performed using dye solutions with aniline (4.38 x 10^{-4} M) in sodium acetate buffer (0.1 M, pH 4.7) for 1 h. To determine the background staining, we included samples that were treated with no choline and no dye (--), choline and no dye (+-), no choline and dye (-+), and both choline and dye (++) and examined the fluorescence intensity of cells by flow cytometry (**Figure 5.4**).

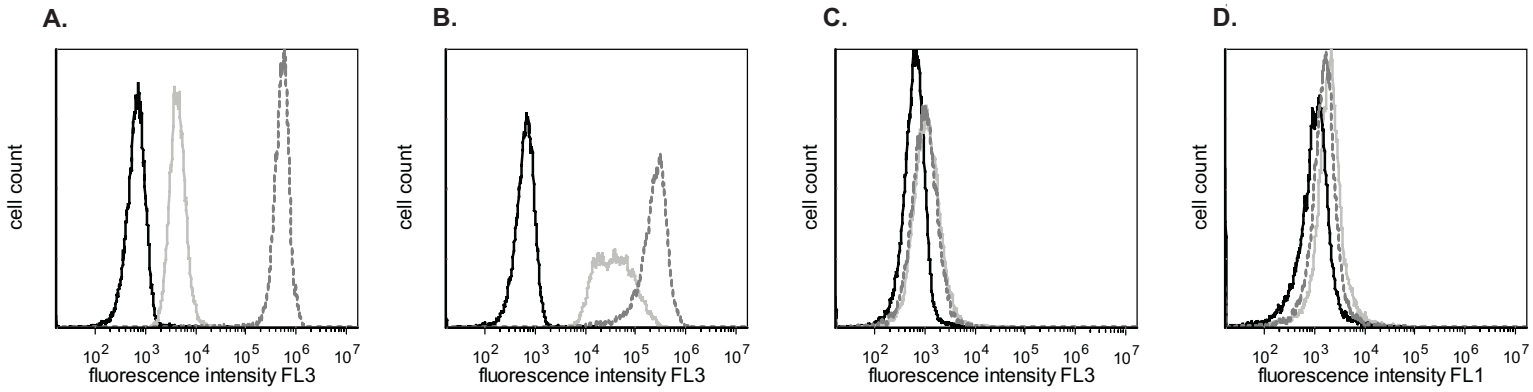

Figure 5.4. Flow cytometry histograms of Jurkat cells treated with choline derivatives. Conditions shown include cells treated with choline and no fluorophore solution (+-, Black), no choline and fluorophore solution (-+, Grey), or both choline and fluorophore solution (++, Dashed). **A)** Cells were grown in the presence of propargyl choline **5.3** and azido Cy 5 **5.34**, followed by incubation with $CuSO_4$ (1 mM) and ascorbic acid (75 mmol) in PBS buffer for 20 min. **B)** Cells were grown in the presence of azido choline **5.5** and alkynyl Cy 5 **5.33** following incubation with $CuSO_4$ (1 mM) and ascorbic acid (75 mmol) in PBS buffer for 20 min. **C)** Cells were grown in the presence of carbonyl choline **5.8** and amino-oxy Cy 5 **5.36** following incubation with aniline (4.38×10^{-4} M) in sodium acetate buffer (0.1 M, pH 4.7) for 1 h. **D)** Cells were grown in the presence of carbonyl choline **5.8** and NBDH **4.2** following incubation with aniline (4.38×10^{-4} M) in sodium acetate buffer (0.1 M, pH 4.7) for 1 h. Experiments were performed in triplicate with a minimum 10,000 events, filter sets as indicated (FL1: 488 nm ex/530 nm em; FL 3: 488 nm ex/670 nm em). Representative histograms are shown.

Although cells treated with fluorophore **5.34** alone (-+) show a minor increase in background signal (6.8-fold MFI over control cells (--)), cells treated with propargyl choline (**5.3**) and azide Cy 5 (**5.34**) (++) show an almost 1000-fold increase in MFI. Azido choline **5.5** also appears to be incorporated as cells treated with alkynyl Cy 5 **5.33** were successfully labelled. Based on flow cytometry data, compound **5.5** has a higher proportion of events with low front and side scatter, which we speculate may be from increased debris or dead cells. We observed higher background (-+) signal (approximately 75-fold MFI over control (--)) using alkynyl Cy 5 **5.33**. The increased background may be attributed to the more hydrophobic nature of the alkyne group of **5.33**. Cells that received both choline **5.5** and alkyne **5.33** (++) had an increase in MFI of approximately 500-fold over control (--). The carbonyl choline, **5.8**, did not show evidence of metabolic incorporation based on flow cytometry. No significant increase in MFI was observed upon treatment with both choline **5.8** and amino-oxy Cy 5 **5.36** or NBDH **4.2** fluorophores. These results suggest that **5.8** is not significantly incorporated, or else is degraded or processed by the cells. Further experiments will be required to determine the cause of this observation; however, other groups have reported that larger alkyl substituents reduce choline analog incorporation.(Bridges, R.G. and Ricketts, J. 1970)

To visualize the labelling by **5.3**, **5.5** and **5.8** we performed fluorescence and DIC microscopy on aliquots of cells from the flow cytometry assay (**Figure 5.5**). The results obtained were consistent with the flow cytometry assay for all three choline-dye pairs. Membrane staining was observed for cells treated with propargyl choline (**5.3**)-azide Cy 5 (**5.34**) (++) (**Figure 5.6**). While no fluorescence was observed for cells that only received the fluorophore **5.34** (-+). The

azide choline (**5.5**)-alkyne Cy 5 (**5.33**) (++) also exhibited strong fluorescence localized at the cell membranes; however, cells that only received the fluorophore **5.33** (-+) showed minor background fluorescence. Cells exposed to the carbonyl choline (**5.8**)-Cy 5 amino-oxy (**5.36**) (++) and cells that received only fluorophore (-+) showed background staining only. Thus, microscopy and flow cytometry assays both confirm that the alkyne and azide choline derivatives (**5.3** and **5.5**) are incorporated into cells, and can be detected with the corresponding Cy 5 labels (**5.34** and **5.33**).

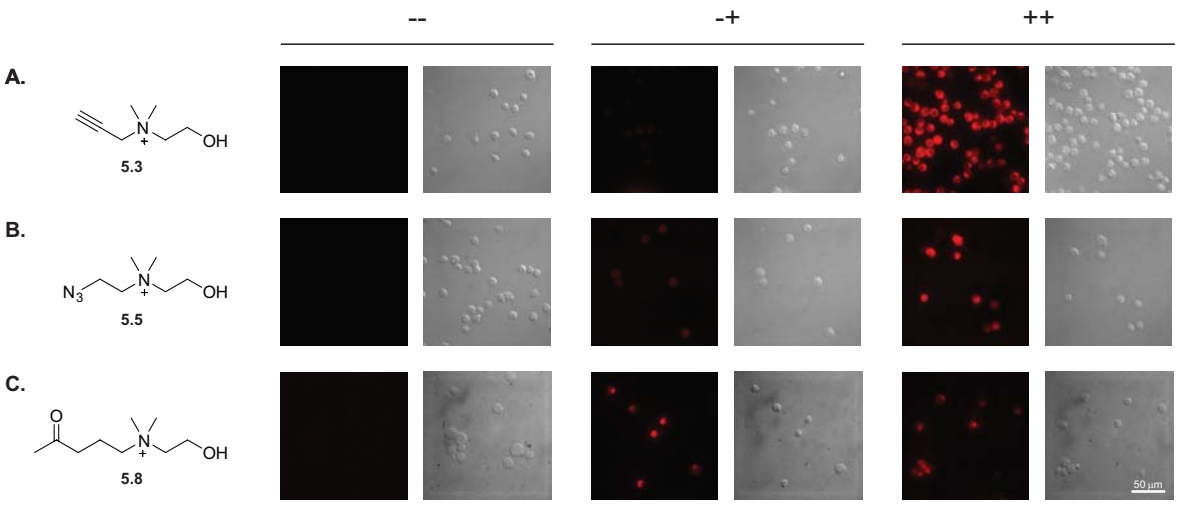

Figure 5.5. Fluorescence microscopy imaging of live Jurkat T cells with metabolically labelled choline and complementary cyanine dye (5.34, 5.33 and 5.36). For each dye, cells were observed after one of the following treatments: no choline, no dye (--), no choline and dye (-+), and choline and dye (++). **A and B)** Alkyne and azide cholines were incubated with complementary fluorophore labels in the presence of $CuSO_4$ (1 mM) and ascorbic acid (75 mmol) in PBS buffer for approximately 20 min. **C)** Carbonyl Choline was incubated with amino-oxy cyanine dye 5.36 in the presence of aniline (4.38×10^{-4} M) in sodium acetate buffer (0.1 M, pH 4.7) for 1 h. Fluorescence images (625-650 ex/670 em) are shown on the left, and DIC images of the same field are shown on the right. Scale bar represents 50 μm.

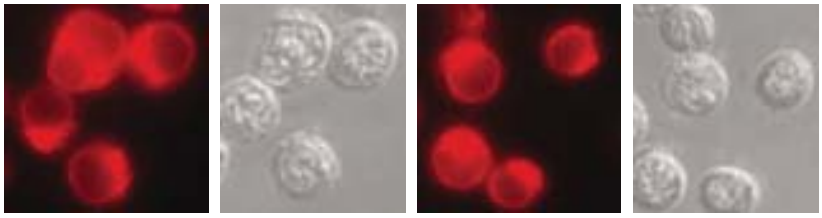

Figure 5.6. Expanded fluorescence microscopy image of live Jurkat T cells with propargyl choline 5.3 and azido cyanine dye 5.34. Jurkat cells were incubated with propargyl choline (320-520 μM) overnight, and labelled with azido fluorophore **5.34** (2.5 μM) in the presence of $CuSO_4$ (1 mM) and ascorbic acid (75 mmol) in PBS buffer for approximately 20 min. Fluorescence images (625-650 ex/670 em) are shown on the left, and DIC images of the same fields are shown on the right. Each image represents an approximately 30 μm x 30 μm field of view.

5.7 Conclusion

We sought to evaluate the use of choline based metabolic labels for interrogation of phospholipid functions *in vivo*, and to develop new dyes and labelling strategies for this system. We synthesized propargyl, azido, and carbonyl containing cholines (**5.3**, **5.5**, and **5.8**) by nucleophilic substitution of alkyl halides. A series of Cy 5 derivatives (**5.33**, **5.34**, and **5.36**) containing functional groups compatible with bioorthogonal labelling was synthesized from acid **5.32**. The carboxylic acid served as a reactive handle for derivatization with bioorthogonal amine linkers (**5.18**, **5.20** and **5.25**) via amide bond formation. A sulphonate group was incorporated on the opposite hemisphere of the cyanine dye to improve water solubility. The photophysical properties of the cyanine dyes were characterized in methanol, and displayed long wavelength absorption maxima ranging between 642-644 nm and emission maxima between 662-663 nm. The emission quantum yields of the fluorophores ranged between 0.15 and 0.21, while absorption coefficients were high, between 6.5-19.1 x 10^4 cm^{-1} M^{-1}.

Jurkat cells were incubated with choline metabolic handles (**5.3**, **5.5**, and **5.8**) overnight following the protocol of Jao and colleagues, and treated with the corresponding bioorthogonal Cy 5 fluorophores (**5.34**, **5.33** and **5.36**). Flow cytometry and fluorescence microscopy was used to evaluate the level of incorporation after fluorescent labelling. We observed that the propargyl and azido cholines (**5.3** and **5.5**) were readily incorporated into cells and showed strong fluorescence labelling by both flow cytometry and fluorescence microscopy. Additionally, alkynyl Cy 5 (**5.33**) displayed increased levels of

background, possibly due to its higher hydrophobicity resulting in membrane incorporation. Examination and comparison of partition coefficients for these compounds may support the speculated higher hydrophobicity of **5.33**. The carbonyl-containing choline, **5.8**, did not show evidence of incorporation into cells as a metabolic label. We did not observe significant labelling by flow cytometry or microscopy experiments.

Further investigation into this methodology may clarify and augment the results observed in this study. To determine if choline **5.8** is being degraded or processed by cells, high-resolution mass spectrometry could be used on cell lysates. The presence and ratio of signals corresponding to the unique masses of the starting material, or phosphocholine analog and CDP-choline analog intermediates may provide evidence towards elucidating the fate of this compound. To identify which lipids are being labelled and quantify the efficiency of label incorporation for the propargyl choline **5.3**, Jao and colleagues performed electrospray tandem mass spectrometry experiments.(Jao, C.Y., Roth, M., et al. 2009) Similar tandem mass spectrometry experiments may also be performed for the azide and carbonyl choline analogs **5.5** and **5.8**. As well, lipid extracts from labelled cells may be subjected to TLC experiments to identify chemical incorporation. Identity and relative quantities may be determined by comparing the retention factors (R*f*s) and intensities of labelled lipid extracts to known standards. These experiments are currently under investigation in our laboratory. We also observed a higher amount of low scatter events in the flow cytometry experiments using azide choline (**5.5**), often a sign of increased debris or dead

cells. A toxicity assay, such as trypan blue exclusion, should be performed for cells exposed to all three choline analogs to determine toxicity.

The choline-based metabolic labelling strategy, when coupled with the partner cyanine dyes developed here, demonstrates promise for use in phospholipid quantification and characterization. In particular, this methodology can complement the use of synthetic alkyne-modified phosphatidylcholine (**3.35**). This strategy should facilitate examination of cell surface phosphocholine biomolecules using single molecule fluorescence microscopy and multicolour experiments.

5.8 Experimental

5.8.1 General

Reagents were purchased reagent grade from commercial sources such as Sigma-Aldrich (Oakville, Ont) and used without additional purification. ^{1}H and ^{13}C NMR were performed on Varian 300, 400, or 500 MHz instruments at room temperature as noted. Deuterated solvents were obtained from Cambridge Isotope Laboratories (Andover, MA). NMR spectra were referenced to CD_3OD, $(CD_3)_2SO$, and $CDCl_3$ solvent peaks (3.31, 2.50, and 7.26 ppm for ^{1}H; 49.0, 39.5, and 77.2 ppm for ^{13}C, respectively) as internal chemical shift standards. For NMR spectra examined in D_2O, $(CD_3)_2CO$ was used as external standard (^{1}H: 2.23 ppm; ^{13}C: 31.07 ppm). Some spectra contain small amounts of contaminating solvents.(Gottlieb, H.E., Kotlyar, V., et al. 1997) Mass spectrometry was performed using an MS-50G positive electron impact instrument from Kratos

Analytical (Manchester, UK) and a Mariner Biospectrometry positive ion electrospray instrument from Applied Biosystems (Foster City, CA).

5.8.2 Spectroscopy

Absorbance spectra for all compounds were collected at room temperature with a Hewlett-Packard (Palo Alto, CA) model 8453 diode array UV-visible spectro-photometer or Varian (Walnut Creek, CA) Cary 50 spectrophotometer. Absorbance measurements were taken using Eppendorf (Hamburg, Germany) UVette cuvettes (220 – 1600 nm) or NSG Precision Cells (Farmingdale, NY) ES quartz cuvettes (190 – 2000 nm). Fluorescence spectra for all compounds were collected at room temperature with a Photon Technology International (Birmingham, NJ) model MP1 steady-state fluorimeter. Fluorescence measurements were taken using NSG Precision Cells (Farmingdale, NY) ES quartz cuvettes (190 – 2000 nm).

5.8.3 Synthesis

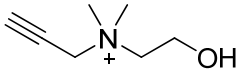

***N*-(2-hydroxyethyl)-*N*,*N*-dimethylprop-2-yn-1-aminium** (**5.3**).

N,*N*-dimethylprop-2-yn-1-amine (**52**) (0.96 mL, 9 mmol, 1 equiv) and bromoethanol (**5.1**) (0.63 mL, 9 mmol, 1 equiv) were dissolved in THF and allowed to stir at room temperature for 12 h. The THF was then removed in vacuo, and the resulting oily liquid was then purified by C18 reverse phase chromatography (water) (1.117 g, 97%). ^{1}H NMR (500 MHz, D_2O): δ 4.43 (s,

2H), 4.16 (broad s, 2H), 3.72 (m, 2H), 3.36 (partially obscured d, 1H), 3.34 (s, 6H); APT ^{13}C NMR (125 MHz, D_2O): δ 82.7, 72.1, 66.0, 56.5, 56.4, 52.3, 43.1; IR (microscope): $\tilde{\nu}$ = 3293, 3017, 2931, 2125, 1474, 1088 cm^{-1}; ES-HRMS calculated for $C_7H_{14}NO$: 128.107; observed: 128.107. R_f = 0.07 (9:1 DCM/methanol).

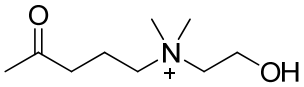

***N*-(2-hydroxyethyl)-*N*,*N*-dimethyl-4-oxopentan-1-aminium** (**5.8**).

5-chloropentan-2-one (**5.6**) (0.3 mL, 2.6 mmol, 2.6 equiv) was dissolved in acetonitrile (5 mL) and one crystal of iodine was added. This was allowed to stir for 0.5 h at room temperature. *N*,*N*-dimethylaminoethanol (**5.7**) (0.1 mL, 1 mmol, 1 equiv) was then added, and the reaction mixture was heated at 80 ^{o}C for 48 h. The solvent was then removed in vacuo, and dissolved in deionized water. This solution was then washed with ethyl acetate (3 x 30 mL). The water layer was lyophilized and subjected to cation exchange chromatography on AG 50W-X8 resin using a water/HCl eluent system. The product was obtained as a yellow oil (34 mg, 20%). ^{1}H NMR (300 MHz, D_2O): δ 4.02 (m, 2H), 3.48 (t, 2H, ^3J = 4.8 Hz), 3.31 (m, 2H), 3.12 (s, 6H), 2.67 (t, 2H, ^3J = 6.9 Hz), 2.18 (s, 3H), 1.97 (m, 2H); ^{13}C NMR (125 MHz, $CDCl_3$): δ 214.2, 65.9, 65.1, 56.3, 52.3, 39.9, 30.2, 17.3; IR (microscope): $\tilde{\nu}$ = 3349, 2971, 1709 cm^{-1}; ES-HRMS calculated for $C_9H_{20}NO_2$: 174.1489; observed: 174.1487. R_f = 0.18 (5:1 DCM/methanol).

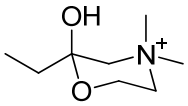

(±) 2-ethyl-2-hydroxy-4,4-dimethylmorpholin-4-ium (**5.10**).

1-bromobutan-2-one (**5.9**) (0.02 mL, 0.66 mmol, 1 equiv) and *N*,*N*-dimethylaminoethanol (**5.10**) (0.02 mL, 0.66 mmol, 1 equiv) were dissolved in acetone or THF (3 mL) and heated for 12 h at 60 ^{o}C. A white precipitate formed, and was filtered (39 mg, quant). ^{1}H NMR (500 MHz, D_2O): δ 4.53 (dd, 1H, ^{2}J = 13.5 Hz, ^{3}J = 3.5 Hz), 4.02 (broad d, 1H, ^{2}J = 13.5 Hz), 3.60 (m, 3H), 3.50 (s, 3H), 3.44 (d, 1H, ^{2}J = 13.5 Hz), 3.30 (s, 3H), 1.81 (q, 2H, ^{3}J = 7.5 Hz), 1.019 (t, 3H, ^{3}J = 7.5 Hz); APT ^{13}C NMR (125 MHz, D_2O): δ 96.5, 65.0, 61.1, 59.0, 55.7, 51.6, 34.1, 7.1; IR (microscope): $\tilde{\nu}$ = 3226, 2970, 1086 cm^{-1}; ES-HRMS calculated for $C_8H_{18}NO_2$: 160.1332; observed: 160.1331.

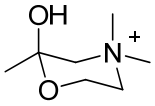

(±) 2-hydroxy-2,4,4-trimethylmorpholin-4-ium (**5.12**).

N,*N*-dimethylaminoacetone (**5.11**) (0.05 mL, 0.4 mmol, 1 equiv) and bromoethanol (**5.1**) (0.03 mL, 0.4 mmol, 1 equiv) were dissolved in THF, cooled in an ice bath and allowed to stir at room temperature for 36 h. A brownish precipitate formed and was filtered off to give the product (32 mg, 55%). ^{1}H NMR (500 MHz, D_2O): δ 4.53 (dd, 1H, ^{2}J = 11.5 Hz, ^{3}J = 3.3 Hz), 4.02 (broad d, 1H, ^{2}J = 14.5 Hz), 3.60 (m, 3H), 3.50 (s, 3H), 3.44 (d, 1H, ^{2}J = 13.0 Hz), 3.29 (s, 3H), 1.56 (s, 3H); ^{13}C NMR (125 MHz, D_2O): δ 94.6, 66.0, 60.9, 58.9, 55.7, 51.5, 27.6; IR (microscope): $\tilde{\nu}$ = 3242, 3013, 2934, 1728, 1271 cm^{-1}; ES-HRMS calculated for $C_7H_{16}NO_2$: 146.1176; observed: 146.1175.

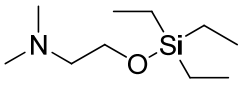

***N*,*N*-dimethyl-2-(triethylsilyloxy)ethanamine** (**5.13**).

N,*N*-dimethylaminoethanol (**5.7**) (0.5 mL, 5 mmol, 1 equiv), and triethylsilane (0.8 mL, 5 mmol, 1 equiv) were dissolved in hexanes (5 mL) and a catalytic amount of sodium metal was added. The reaction mixture was heated at 80 ^{o}C for 16 h. The solvent was removed in vacuo and purified by normal phase column chromatography (DCM/methanol) as a colourless oil (0.54 g, 62%). ^{1}H NMR (300 MHz, CD_3OD): δ 3.75 (t, 2H, ^{3}J = 6.0 Hz), 2.49 (t, 2H, ^{3}J = 6.0 Hz), 2.27 (s, 6H), 0.98 (t, 9H, ^{3}J = 8.1 Hz), 0.63 (q, 6H, ^{3}J = 8.1 Hz); ^{13}C NMR (100 MHz, CD_3OD): δ 61.2, 60.6, 44.9, 5.9, 4.0; (microscope): $\tilde{\nu}$ = 2954, 2912, 2818, 2769, 1458, 1108 cm^{-1}; EI-HRMS calculated for $C_{10}H_{25}NOSi$: 203.1705; observed: 203.1706. R_f = 0.29 (9:1 DCM/methanol).

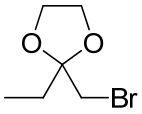

2-(bromomethyl)-2-ethyl-1,3-dioxolane (**5.15**).

1-bromobutan-2-one (**5.9**) (0.1 mL, 1 mmol, 1 equiv), ethylene glycol (**5.14**) (0.06 mL, 1.1 mmol, 1.1 equiv), and *p*-Toluenesulfonic acid (5 mg, 0.02 mmol, 0.02 equiv) were dissolved in benzene (25 mL) and heated for 6 h at 130 ^{o}C using a Dean Stark apparatus. The reaction mixture was then washed with 10% NaOH (20 mL), water (20 mL) and back extracted into EtOAc (30 mL), then dried over magnesium sulphate. The solvent was removed in vacuo to afford a yellow oil (230 mg, quant). ^{1}H NMR (400 MHz, $CDCl_3$): δ 4.02 (m, 4H), 3.38 (s, 2H), 1.85 (q, 2H, ^{3}J = 7.6 Hz), 0.92 (t, 3H, ^{3}J = 7.6 Hz); ^{13}C NMR (100 MHz, $CDCl_3$): δ

109.0, 65.4, 34.9, 28.5, 7.2; IR (microscope): $\tilde{\nu}$ = 2975, 2885, 1223, 1083, 1055 cm^{-1}; MALDI-TOF MS: calculated for $C_6H_{12}BrO_2$: 195.0015; observed: 195.0016. R_f = 0.26 (3:2 EtOAc /hexanes).

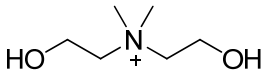

2-hydroxy-*N*-(2-hydroxyethyl)-*N*,*N*-dimethylethanaminium (**5.16**).

N,*N*-dimethyl-2-(triethylsilyloxy)ethanamine (**5.13**) (137 mg, 0.674 mmol, 1 equiv) was dissolved in THF (2 mL) and cooled on an ice bath. Bromoethanol (**5.1**) (0.05 mL, 0.674 mmol, 1 equiv) was then added and the reaction mixture was then heated at 65 ^oC for 24 h. A white precipitate was visible and filtered off (79 mg, 87%). ^1H NMR (500 MHz, CD_3OD): δ 4.00 (m, 4H), 3.57 (m, 4H), 3.24 (s, 6 H); APT ^{13}C NMR (125 MHz, CD_3OD): δ 68.0, 56.9, 53.1; IR (microscope): $\tilde{\nu}$ = 3329, 3016, 2959, 1473, 1076 cm^{-1}; ES-HRMS calculated for $C_6H_{16}NO_2$: 134.1176; observed: 134.1176.

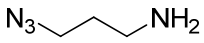

3-azidopropan-1-amine (**5.20**).

3-azidopropan-1-amine was prepared following a modification of the method reported by Lewis et al.(Lewis, W.G., Magallon, F.G., et al. 2004) Bromopropylamine (**5.19**) (1 g, 4.57 mmol, 1 equiv) and sodium azide (0.89 g, 13.7 mmol, 3 equiv) were dissolved in water (15 mL) and heated at 80 ^oC for 12 h. The reaction mixture was made alkaline using 5% NaOH (25 mL), followed by toluene extractions (3 x 20 mL). Caution – this material may be unstable and should be treated with care. The product was stored in as a stabilizer, yield was

determined by ^{1}H NMR (150 mg, 33%). ^{1}H NMR (300 MHz, $CDCl_3$): δ 3.41 (t, 2H, ^{3}J = 6.9 Hz), 2.84 (t, 2H, ^{3}J = 6.9 Hz), 1.77 (q, 2H, ^{3}J = 6.9 Hz).

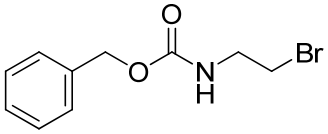

Benzyl 2-bromoethylcarbamate (**5.22**).

Benzyl 2-bromoethylcarbamate was prepared following the procedure reported by Carrasco et al.(Carrasco, M.R., Alvarado, C.I., et al.) *N*-Z-ethanolamine (**5.21**)(1.95 g, 10 mmol, 1 equiv) and methanesulfonyl chloride (0.93 mL, 12 mmol, 1.2 equiv) were dissolved in dichloromethane (30 mL), and triethylamine (1.8 mL, 13 mmol, 1.3 equiv) was added dropwise and allowed to stir for 45 min at room temperature. Lithium bromide (8.7 g, 100 mmol, 10 equiv) and acetone (30 mL) were then added, and the reaction was allowed to stir at room temperature for approximately 12 h. The solvent was removed in vacuo, and redissolved in ether (30 mL). The ether layer was washed with water (40 mL), 0.1 M sodium bisulfite (20 mL), brine (20 mL) and dried with magnesium sulphate. Solvent was then removed in vacuo resulting in a yellow oil, which may solidify (2.296 g, 89%). ^{1}H NMR (400 MHz, $CDCl_3$): δ 7.39 (m, 5H), 5.14 (s, 2H), 3.63 (m, 2H), 3.49 (m, 2H); ^{13}C NMR (100 MHz, $CDCl_3$): δ 156.4, 136.5, 128.8, 128.5, 128.4, 67.3, 43.0, 32.7; IR (microscope): $\tilde{\nu}$ = 3310, 3062, 2972, 2949, 1682, 1543, 1453, 1273 cm^{-1}; EI-HRMS calculated for $C_{10}H_{12}NO_2Br$: 257.0051; observed: 257.0055. R_f = 0.30 (1:6 EtOAc/hexanes).

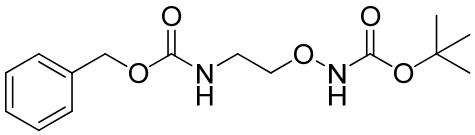

Benzyl 2- (tert-butoxycarbonylaminooxy)ethylcarbamate (**5.24**).

Benzyl 2-bromoethylcarbamate (**5.22**) (1g, 3.89 mmol, 1 equiv), *N*-Boc-*N*-methylhydroxylamine (**5.23**) (0.73 g, 5.5 mmol, 1.4 equiv), and DBU (0.87 mL, 5.8 mmol, 1.5 equiv) were dissolved in ether and allowed to stir overnight at room temperature. The reaction mixture was then taken up into ethyl acetate (30 mL) and washed with water (30 mL), 0.1 M sodium bisulfite (30 mL), and brine (30 mL). Magnesium sulphate was used to dry the organic layer, followed by evaporation *in vacuo* resulting in a volatile yellow oil (1 g, 83%). ^{1}H NMR (400 MHz, $CDCl_3$): δ 7.39 (m, 5H), 5.13 (s, 2H), 3.88 (t, 2H, ^{3}J = 4.7 Hz), 3.45 (m, 2H), 1.49 (s, 9H); ^{13}C NMR (100 MHz, $CDCl_3$): δ 157.7, 157.1, 136.9, 128.7, 128.3, 128.4, 82.4, 66.9, 39.4, 28.4; IR (microscope): $\tilde{\nu}$ = 3596, 3066, 2979, 2935, 1705, 1522, 1456, 1252, 1162, 1111 cm^{-1}; EI-HRMS calculated for (M+H - Boc C_4H_9 fragment) $C_{11}H_{14}N_2O_5$: 254.0903; observed: 254.09104. R_f = 0.65 (1:1 EtOAc/hexanes).

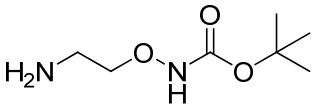

tert-butyl 2-aminoethoxycarbamate (**5.25**).

Benzyl 2-(tert-butoxycarbonylamino-oxy)ethylcarbamate (**5.24**) (0.93 g, 3 mmol, 1 equiv), was dissolved in chloroform (0.3 mL) and methanol (9 mL), and 10% Pd/C (0.74 g) was added. Triethylsilane (4.8 mL, 30 mmol, 10 equiv) was then added dropwise over 1 h. The reaction mixture was filtered over celite and dried

in vacuo, giving an off-white solid (0.59 g, quant.) ^{1}H NMR (400 MHz, $CDCl_3$): δ 9.03 (broad s, 1H), 8.20 (broad s, 2H), 4.21 (broad s, 2H), 3.39 (broad s, 2H), 1.46 (s, 9H); ^{13}C NMR (100 MHz, $CDCl_3$): δ 158.1, 82.5, 72.1, 38.3, 28.6, 28.5; IR (microscope): ν̃ = 3411, 2980, 2937, 1713, 1609, 1479, 1455, 1166, 1111 cm^{-1}; ES-HRMS calculated for $C_7H_{17}N_2O_3$: 177.1234; observed: 177.1236.

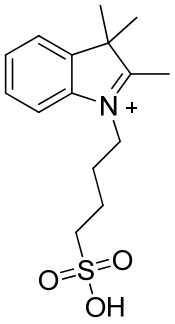

2,3,3-trimethyl-1-(4-sulfobutyl)-3H-indolium (**5.28**).

2,3,3-trimethyl-1-(4-sulfobutyl)-3H-indolium was prepared following a modification of the method reported by Kiyose et al.(Kiyose, K., Aizawa, S., et al. 2009) 1,4-butanesultone (**5.27**) (0.37 mL, 3.65 mmol, 1.05 equiv) and 2,3,3-trimethyl-3H-indole (**5.26**) (0.56 mL, 3.5 mmol, 1 equiv) were heated neat for 3 h at 120 ^{o}C. The reaction mixture was allowed to cool to room temperature and washed with ether and the resulting purple-red sticky solid was then used without further purification. ^{1}H NMR (400 MHz, CD_3OD): δ 7.93 (m, 1H), 7.76 (m, 1H), 7.64 (m, 2H), 4.55 (t, 2H, , ^{3}J = 8.0 Hz) 3.30 (s, 3H), 2.89 (t, 2H, ^{3}J = 6.8 Hz), 2.14 (q, 2H, ^{3}J = 8.4 Hz) 1.94 (q, 2H, ^{3}J = 7.6 Hz), 1.60 (s, 6 H); ^{13}C APT NMR (100 MHz, CD_3OD): δ 196.9, 142.2, 141.4, 130.0, 129.4, 123.4, 115.5, 54.8, 51.3, 50.6, 50.4, 29.3, 27.5, 26.2, 25.2, 22.6, 22.1; IR (microscope): ν̃ = 3445, 3051, 2969, 2930, 1647, 1483, 1186, 1038 cm^{-1}; ES-MS calculated for $C_{14}H_{18}NO_2Na$: 318.1; observed: 318.1.

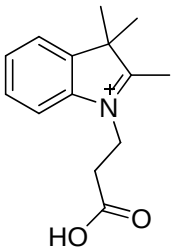

1-(2-Carboxyethyl)-2,3,3-trimethyl-3H-indolium (**5.30**).

1-(2-Carboxyethyl)-2,3,3-trimethyl-3H-indolium was prepared following a modification of the method used by Kiyose et al.(Kiyose, K., Aizawa, S., et al. 2009) 2,3,3-trimethyl-3H-indole (**5.26**) (1.6 mL, 10 mmol, 1 equiv) and 3-iodopropionic acid (**5.29**) (2.8 g, 14 mmol, 1.4 equiv) were combined and heated at 105 ^{o}C, neat. The reaction was allowed to proceed for 2.5 h then quenched with deionized water. A DCM wash (2 x 20 mL) was performed, and the aqueous layer was lyophilized. An orange, oily product (2.91 g) was obtained and used without further purification. ^{1}H NMR (400 MHz, Ac-D_6): δ 8.11 (m, 1H), 7.88 (m, 1H), 7.66 (m, 2H), 4.93 (t, 2H, , ^{3}J = 6.4 Hz) 3.29 (s, 3H), 3.12 (m, 2H) 1.69 (s, 6 H); APT ^{13}C NMR (125 MHz, Ac-D_6): δ 198.5, 142.4, 141.5, 129.9, 129.4, 123.8, 116.1, 55.1, 49.0, 44.9, 31.5, 22.2, 15.4, 15.2; IR (microscope): ṽ = 3422, 3034, 2974, 1731, 1626, 1460, 1176 cm^{-1}; ES-HRMS calculated for $C_{14}H_{18}NO_2$: 232.1332; observed: 232.1329.

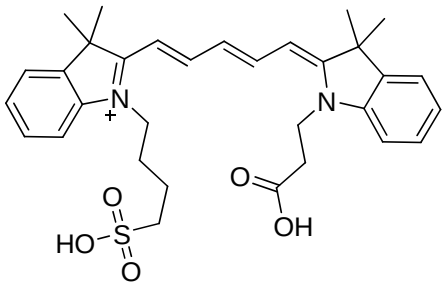

2-((1E,3E,5Z)-5-(1-(2-Carboxyethyl)-3,3-dimethylindolin-2-ylidene)penta-1,3-dienyl)-3,3-dimethyl-1-(4-sulfobutyl)-3H-indolium (**5.33**).

Trimethyl-1-(4-sulfobutyl)-3H-indolium (**5.28**), carried forward from above, and malonaldehyde dianilide hydrochloride (**5.31**) (0.9 g, 3.5 mmol, 1 equiv) were dissolved in acetic anhydride (15 mL) and allowed to stir at room temperature for approximately 1 h. The solvent was then removed in vacuo and the reaction mixture was then run through a short silica plug column (10:1 DCM/methanol) to enrich for the 3,3-dimethyl-2-((1E,3E)-4-(phenylamino)buta-1,3-dienyl)-1-(4-sulfobutyl)-3H-indolium intermediate (0.46 g crude, R_f = 0.16 (9:1 DCM/methanol). The mixture(0.46g, 0.98 mmol, 1 equiv) was then dissolved in acetic anhydride (5 mL) with 1-(2-carboxyethyl)-2,3,3-trimethyl-3H-indolium (**5.33**) (0.23 g, 0.98 mmol, 1 equiv) and DIPEA (0.17 mL, 0.98 mmol, 1 equiv) with heating at 120 ^{o}C for 3 h. The solvent was then removed in vacuo and the resulting blue, oily, solid was washed with ether (3 x 40 mL). Purification was performed using C18 RP-HPLC using a 1% TFA in water/acetonitrile gradient (acetonitrile 5% to 80%). Yield as determined by the integration of an analytical scale RP-HPLC trace at 254 nm was 23%. ^{1}H NMR (500 MHz, CD_3OD): δ 8.23 (q, 2H, ^{3}J = 13.0 Hz), 7.49 (d, 1H, ^{3}J = 8.5 Hz), 7.35-7.47 (m, 4H), 7.28 (t, 2H, ^{3}J = 8.5 Hz), 7.22 (t, 1H, ^{3}J = 6.0 Hz), 6.65 (t, 1H, ^{3}J = 12.0 Hz), 6.41 (d, 1H, ^{3}J = 14.0 Hz), 6.28 (d, 1H, ^{3}J = 13.5 Hz), 4.36 (t, 2H, ^{3}J = 7.5 Hz), 4.17 (t, 2H, ^{3}J = 6.5

Hz), 2.88 (t, 2H, ^{3}J = 7.0 Hz), 2.80 (t, 2H, ^{3}J = 7.0 Hz), 1.97 (m, 4H), 1.71 (d, 12H, ^{3}J = 6.5 Hz). APT ^{13}C NMR (125 MHz, CD_3OD): δ 175.7, 173.9, 156.2, 155.1, 143.4, 142.9, 142.4, 129.9, 129.6, 127.2, 126.6, 125.9, 123.4, 123.3, 112.5, 111.7, 105.4, 104.0, 51.7, 50.8, 50.3, 49.9, 45.0, 40.8, 32.6, 28.0, 27.9, 27.3, 23.5; IR (microscope): ṽ = 3359, 2998, 2715, 1682, 1492, 1457, 1205, 1338 cm^{-1}; ES-HRMS calculated for $C_{32}H_{38}N_2O_5SNa$: 585.2394.; observed: 585.2385.

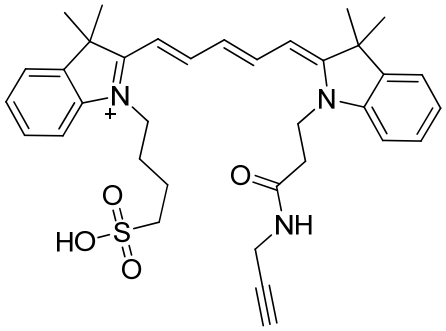

2-((1E,3E,5Z)-5-(3,3-dimethyl-1-(3-oxo-3-(prop-2-ynylamino)propyl)indolin-2-ylidene)penta-1,3-dienyl)-3,3-dimethyl-1-(4-sulfobutyl)-3H-indolium (**5.33**).

2-((1E,3E,5Z)-5-(1-(2-carboxyethyl)-3,3-dimethylindolin-2-ylidene)penta-1,3-dienyl)-3,3-dimethyl-1-(4-sulfobutyl)-3H-indolium (**5.32**) (10 mg, 0.019 mmol, 1 equiv), and propargylamine (**5.18**) (0.01 mL, 0.149 mmol, 8 equiv) were dissolved in DMF (1.5 mL). DIPEA (0.02 mL, 0.095 mmol, 5 equiv) was then added and the solution was allowed to stir for approximately 10 min. HATU (15 mg, 0.038 mmol, 2 equiv) was then added and the reaction was allowed to stir for 24 h at room temperature. The reaction mixture was then diluted with water and lyophilized. The resulting blue solid was washed with ether (2 x 20 mL) and purified by flash column chromatography (DCM/methanol) followed by C18 RP-HPLC using a 1% TFA in water/acetonitrile gradient (acetonitrile 5% to 80%) (4.6 mg, 40%). ^{1}H NMR (500 MHz, CD_3OD): δ 8.23 (q, 2H, ^{3}J = 13.5 Hz), 7.49

(d, 1H, ^{3}J = 7.4 Hz), 7.44 (d, 1H, ^{3}J = 7.7 Hz), 7.41 (d, 1H, ^{3}J = 7.2 Hz), 7.37 (m, 2H), 7.27 (t, 2H, ^{3}J = 7.2 Hz), 7.21 (t, 1H, ^{3}J = 7.5 Hz), 6.65 (t, 1H, ^{3}J = 12.4 Hz), 6.41 (d, 1H, ^{3}J = 13.9 Hz), 6.26 (d, 1H, ^{3}J = 13.5 Hz), 4.36 (t, 2H, ^{3}J = 6.9 Hz), 4.17 (t, 2H, ^{3}J = 6.9 Hz), 3.87 (d, 2H, ^{4}J = 2.6 Hz), 2.89 (t, 2H, ^{3}J = 7.15 Hz), 2.69 (t, 2H, ^{3}J = 6.8 Hz), 2.53 (t, 1H, ^{4}J = 2.6 Hz), 1.97 (m, 4H), 1.71 (d, 12H, ^{3}J = 5.14 Hz). ^{13}C NMR (125 MHz, CD_3OD): δ 175.6, 173.9, 171.8, 156.2, 155.2, 143.4, 143.3, 142.8, 142.4, 129.9, 129.6, 127.2, 126.6, 125.9, 123.4, 123.3, 112.5, 111.8, 105.3, 104.1, 80.2, 72.5, 51.7, 50.8, 50.3, 49.9, 49.6, 45.0, 41.4, 34.3, 29.6, 28.1, 27.9, 27.3, 23.5; IR (microscope): ṽ = 3290, 3058, 2971, 2930, 2870, 2118, 1669, 1576, 1492, 1455, 1387, 1140, 1046, 1018 cm^{-1}; ES-HRMS calculated for $C_{35}H_{42}N_3O_4S$: 600.2891; observed: 600.2890. R_f = 0.65 (5:1 DCM/methanol).

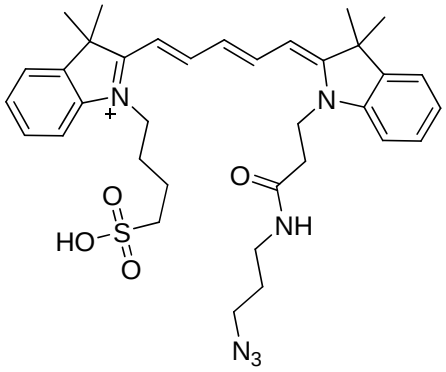

2-((1E,3E,5Z)-5-(1-(3-(3-azidopropylamino)-3-oxopropyl)-3,3-dimethylindolin-2-ylidene)penta-1,3-dienyl)-3,3-dimethyl-1-(4-sulfobutyl)-3H-indolium (**5.34**).

2-((1E,3E,5Z)-5-(1-(2-carboxyethyl)-3,3-dimethylindolin-2-ylidene)penta-1,3-dienyl)-3,3-dimethyl-1-(4-sulfobutyl)-3H-indolium (**5.32**) (12 mg, 0.021 mmol, 1 equiv), and 3-azidopropan-1-amine (**5.20**) (1.7 mg, 0.17 mmol, 8 equiv) were dissolved in DMF (1.5 mL). DIPEA (0.02 mL, 0.105 mmol, 5 equiv) was then added and the solution was allowed to stir for approximately 10 min. HATU (16

mg, 0.042 mmol, 2 equiv) was then added and the reaction was allowed to stir for 24 h at room temperature. The reaction mixture was then diluted with water and lyophilized. The resulting blue solid was washed with ether (2 x 20 mL) and purified by flash column chromatography (DCM/methanol) followed by C18 RP-HPLC using a 1% TFA in water/acetonitrile gradient (acetonitrile 5% to 80%). The final product was found to be a blue solid (10 mg, 74%). ^{1}H NMR (500 MHz, CD_3OD): δ 8.24 (q, 2H, ^{3}J = 13.2 Hz), 7.49 (d, 1H, ^{3}J = 7.4 Hz), 7.45 (d, 1H, ^{3}J = 7.4 Hz), 7.41 (d, 1H, ^{3}J = 7.2 Hz), 7.37 (q, 2H, ^{3}J = 8.0 Hz), 7.28 (t, 2H, ^{3}J = 7.2 Hz), 7.22 (t, 1H, ^{3}J = 7.4 Hz), 6.65 (t, 1H, ^{3}J = 12.4 Hz), 6.42 (d, 1H, ^{3}J = 13.8 Hz), 6.26 (d, 1H, ^{3}J = 13.5 Hz), 4.36 (t, 2H, ^{3}J = 6.6 Hz), 4.18 (t, 2H, ^{3}J = 7.6 Hz), 3.87 (d, 2H, ^{4}J = 2.6 Hz), 3.16 (m, 4H), 2.89 (t, 2H, ^{3}J = 7.2 Hz), 2.66 (t, 2H, ^{3}J = 6.7 Hz), 1.97 (m, 4H), 1.72 (s, 12H), 1.60 (q, 2H, ^{3}J = 6.8 Hz). ^{13}C NMR (125 MHz, CD_3OD): δ 175.7, 173.2, 172.4, 156.2, 155.1, 143.44, 143.41, 142.9, 142.3, 129.9, 129.6, 127.2, 126.7, 125.9, 123.4, 123.3, 112.6, 111.9, 105.4, 104.0, 73.5, 62.3, 51.7, 50.9, 50.3, 49.9, 45.0, 41.5, 37.9, 34.8, 29.6, 28.1, 27.9, 27.3, 23.5; IR (microscope): $\tilde{\nu}$ = 3258, 3058, 2920, 2849, 2097, 1648, 1478, 1374, 1129, 1037 cm^{-1}; ES-HRMS calculated for $C_{35}H_{45}N_6O_4S$: 645.3218; observed: 645.3213. R_f = 0.81 (5:1 DCM/methanol).

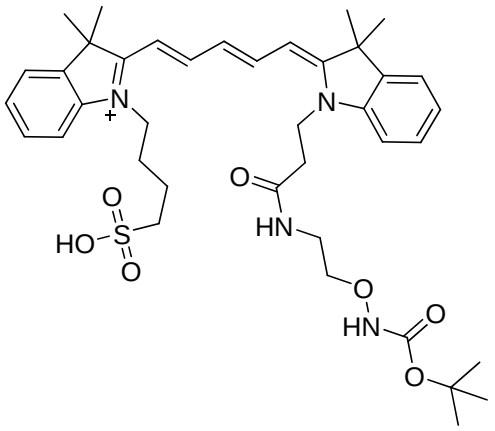

2-((1E,3E,5Z)-5-(1-(2,2-dimethyl-4,10-dioxo-3,6-dioxa-5,9-diazadodecan-12-yl)-3,3-dimethylindolin-2-ylidene)penta-1,3-dienyl)-3,3-dimethyl-1-(4-sulfobutyl)-3H-indolium (**5.35**).

2-((1E,3E,5Z)-5-(1-(2-carboxyethyl)-3,3-dimethylindolin-2-ylidene)penta-1,3-dienyl)-3,3-dimethyl-1-(4-sulfobutyl)-3H-indolium (**5.32**) (12 mg, 0.021 mmol, 1 equiv), and tert-butyl 2-aminoethoxycarbamate (**5.25**) (30 mg, 0.17 mmol, 8 equiv) were dissolved in DMF (1.5 mL). DIPEA (0.02 mL, 0.105 mmol, 5 equiv) was then added and the solution was allowed to stir for approximately 10 min. HATU (16 mg, 0.042 mmol, 2 equiv) was then added and the reaction was allowed to stir for 24 h at room temperature. The reaction mixture was then diluted with water and lyophilized. The resulting blue solid was washed with ether (2 x 20 mL) and purified by flash column chromatography (DCM/methanol) followed by C18 RP-HPLC using a 1% TFA in water/acetonitrile gradient (acetonitrile 5% to 80%). The final product was found to be a blue solid (6 mg, 40%). ^{1}H NMR (500 MHz, CD_3OD): δ 8.23 (q, 2H, ^{3}J = 12.6 Hz), 7.49 (d, 1H, ^{3}J = 7.3 Hz), 7.45 (d, 1H, ^{3}J = 7.4 Hz), 7.41 (d, 1H, ^{3}J = 7.2 Hz), 7.37 (m, 2H), 7.28 (m, 2H), 7.22 (t, 1H, ^{3}J = 7.3 Hz), 4.38 (t, 2H, ^{3}J = 6.7 Hz), 4.17 (t, 2H, ^{3}J = 6.8 Hz), 3.70 (t, 2H, ^{3}J = 5.2 Hz), 3.32 (t, 2H, ^{3}J = 5.2 Hz), 2.88 (t, 2H, ^{3}J = 7.2 Hz),

2.69 (t, 2H, ^{3}J = 6.7 Hz), 1.97 (m, 4H), 1.72 (d, 12H, ^{3}J = 4.5 Hz), 1.43 (s, 9H). APT ^{13}C NMR (125 MHz, CD_3OD): δ 175.6, 174.0, 172.4, 159.4, 156,1, 155.2, 143.4, 142.8, 142.4, 129.9, 129.6, 127.1, 126.6, 125.9, 123.4, 123.3, 112.5, 111.9, 105.3, 104.1, 82.4, 75.6, 51.7, 50.8, 50.3, 49.9, 45.0, 41.6, 39.0, 34.8, 28.6, 28.1, 27.9, 27.3, 23.5; IR (microscope): $\tilde{\nu}$ = 3256, 3059, 2975, 2931, 1632, 1494, 1458, 1386, 1337, 1139, 1113 cm^{-1}; ES-HRMS calculated for $C_{39}H_{53}N_4O_7S$: 721.3629; observed: 721.3629. R_f = 0.55 (5:1 DCM/methanol).

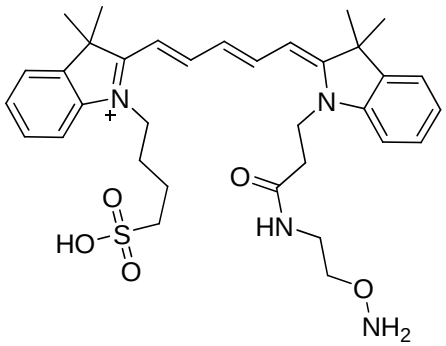

2-((1E,3E,5Z)-5-(1-(3-amino-3-oxopropyl)-3,3-dimethylindolin-2-ylidene)penta-1,3-dienyl)-3,3-dimethyl-1-(4-sulfobutyl)-3H-indolium (**5.36**).

2-((1E,3E,5Z)-5-(1-(2,2-dimethyl-4,10-dioxo-3,6-dioxa-5,9-diazadodecan-12-yl)-3,3-dimethylindolin-2-ylidene)penta-1,3-dienyl)-3,3-dimethyl-1-(4-sulfobutyl)-3H-indolium (**5.35**) (7 mg, 0.001 mmol, 1 equiv) was dissolved in 1:1 TFA/DCM (2 mL) and allowed to react at room temperature for 15 min. The solvent was then removed *in vacuo* and the crude product was washed with ethyl ether (3 x 5 mL). The resulting blue solid was characterized without further purification (3 mg, 50%). ^{1}H NMR (500 MHz, CD_3OD): δ 8.22 (m, 2H), 7.50 (d, 1H, ^{3}J = 7.2 Hz), 7.46 (d, 1H, ^{3}J = 7.0 Hz), 7.41 (m, 4H), 7.28 (m, 2H), 7.22 (t, 1H, ^{3}J = 7.4 Hz), 6.65 (t, 1H, ^{3}J = 12.4 Hz), 6.46 (d, 1H, ^{3}J = 13.9 Hz), 6.25 (d, 1H, ^{3}J = 13.4 Hz), 4.35 (t, 2H, ^{3}J = 6.9 Hz), 4.18 (t, 2H, ^{3}J = 7.2 Hz), 4.04 (t, 2H, ^{3}J = 5.1 Hz), 3.44

(t, 2H, ^3J = 5.2 Hz), 2.92 (t, 2H, ^3J = 7.0 Hz), 2.70 (t, 2H, ^3J = 7.0 Hz), 1.98 (m, 4H), 1.71 (d, 12H, ^3J = 5.5 Hz). APT ^{13}C NMR (125 MHz, CD_3OD): δ 175.9, 173.6, 173.3, 156.1, 154.7, 143.4, 143.3, 142.9, 142.4, 129.9, 129.6, 127.4, 126.7, 125.9, 123.5, 112.5, 111.5, 105.8, 104.0, 75.0, 51.5, 50.9, 50.3, 49.9, 44.5, 41.3, 38.4, 34.3, 28.1, 27.9, 27.1, 23.4; IR (microscope): ṽ = 3293, 2938, 2871, 1684, 1494, 1457, 1379, 1137, 1045 cm^{-1}; ES-HRMS calculated for $C_{34}H_{45}N_4O_5S$: 621.3105; observed: 621.3105. R_f = 0.13 (5:1 DCM/methanol).

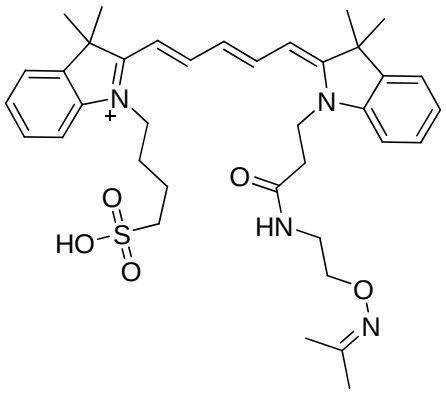

2-((1E,3E,5Z)-5-(3,3-dimethyl-1-(3-oxo-3-(2-(propan-2-ylideneamino-oxy)ethylamino)propyl)indolin-2-ylidene)penta-1,3-dienyl)-3,3-dimethyl-1-(4-sulfobutyl)-3H-indolium (**5.37**).

2-((1E,3E,5Z)-5-(1-(2,2-dimethyl-4,10-dioxo-3,6-dioxa-5,9-diazadodecan-12-yl)-3,3-dimethylindolin-2-ylidene)penta-1,3-dienyl)-3,3-dimethyl-1-(4-sulfobutyl)-3H-indolium (**5.35**) (5 mg, 0.009 mmol) was deprotected *in situ* with 1:1 TFA/DCM (2 mL) and exposed to excess acetone for one hour at room temperature. The resulting oxime product was purified by normal phase flash column chromatography (DCM/methanol) and the resulting product was a blue solid (2.1 mg, 36%). ^{1}H NMR (500 MHz, CD_3OD): δ 8.23 (q, 2H, ^3J = 15.5 Hz), 7.49 (d, 1H, ^3J = 7.5 Hz), 7.45 (d, 1H, ^3J = 7.5 Hz), 7.41 (d, 1H, ^3J = 7.3 Hz), 7.37 (m, 2H), 7.28 (m, 2H), 7.22 (t, 1H, ^3J = 7.4 Hz), 6.64 (t, 1H, ^3J = 12.3 Hz), 6.41

(d, 1H, ^3J = 13.8 Hz), 6.27 (d, 1H, ^3J = 13.6 Hz), 4.35 (t, 2H, ^3J = 6.8 Hz), 4.17 (t, 2H, ^3J = 7.0 Hz), 3.89 (t, 2H, ^3J = 5.6 Hz), 3.34 (t, 2H, ^3J = 5.6 Hz), 2.89 (t, 2H, ^3J = 7.2 Hz), 2.80 (t, 2H, ^3J = 6.7 Hz), 1.97 (m, 4H), 1.81 (s, 3H), 1.78 (s, 3H), 1.71 (d, 12H, ^3J = 6.8 Hz). APT ^{13}C NMR (125 MHz, CD_3OD): δ 175.6, 173.9, 172.4, 157.1, 156.2, 155.2, 143.4, 142.8, 142.4, 129.9, 129.6, 127.1, 126.6, 125.9, 123.4, 123.3, 112.5, 111.9, 105.3, 104.1, 72.3, 51.7, 50.8, 50.4, 49.9, 49.6, 45.0, 41.5, 40.2, 34.6, 30.8, 28.1, 27.9, 27.3, 23.5, 21.7, 15.6; IR (microscope): $\tilde{\nu}$ = 3288, 3060, 2926, 2856, 2396, 1687, 1481, 1452, 1133, 1105, 1037, 1016 cm^{-1}; ES-HRMS calculated for $C_{37}H_{49}N_4O_5S$: 661.3418; observed: 661.3411. R_f = 0.79 (5:1 DCM/methanol).

5.8.4 Flow cytometry and fluorescence microscopy

Jurkat cells were grown in RPMI 1640 media (Invitrogen, Carlsbad, CA) with 10% fetal bovine serum (FBS) at 37 °C under 5% CO_2 to approximately 1 x 10^6 cells/mL. Cells were incubated with (+) or without (-) choline derivatives (**5.3**, **5.5**, or **5.8**) at 382-520 μM concentrations in RPMI media at 37 ^oC overnight. The growth media was removed and the cells were washed with DPBS. Cells were pelleted by centrifugation (2000 g x 4 m) and washed with DPBS. Control aliquots (-- and +-) were treated with buffer solution, while background (-+) and experimental (++) aliqouts were then treated with dye solutions. For Cy dyes **5.33** and **5.34**, CuAAC conditions were used. The dyes were dissolved in methanol (10 μM). 50 μL aliquots of this solution were diluted to a final volume of 400 uL using a stock solution of $CuSO_4$ (1 mM) and ascorbic acid (75 mmol) in PBS buffer. Cell samples in PBS (100 μL) were incubated with 60 μL of the

fluorophore solutions for approximately 20 min. For oxime and hydrazone labelling: Dye solutions were prepared with aniline (4.38×10^{-4} M) in sodium acetate buffer (0.1 M, pH 4.7) with cyanine **5.36** (2.4 μM) or NBDH **4.2** (19.2 μM). Cell samples in 150 μL PBS were incubated with 200 μL dye solution for 1 h at 4 ^{o}C. After incubation, cell samples were washed three times with DPBS before flow cytometry. Flow cytometry was performed on an Accuri C6 cytometer (Ann Arbor, MI) operating at (FL1: 488 nm excitation/530 nm detection; FL3: 488 nm excitation/670 nm detection), collecting 10,000 events per sample.

Jurkat cells treated identically as above were transferred to a microscope slide and visualized using a Nikon Eclipse Ti inverted fluorescence microscope with 60x objective (NA 1.49). Images were acquired with a Photometrics QuantEM 512SC camera, excitation 625-650 nm/670 nm detection.

5.8.5 UV-vis absorbance spectra of 5.32 to 5.36 in methanol

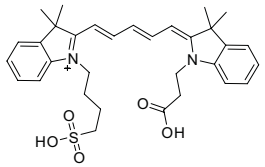

5.32

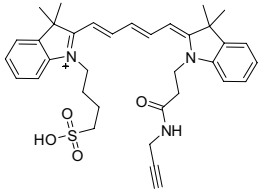

5.33

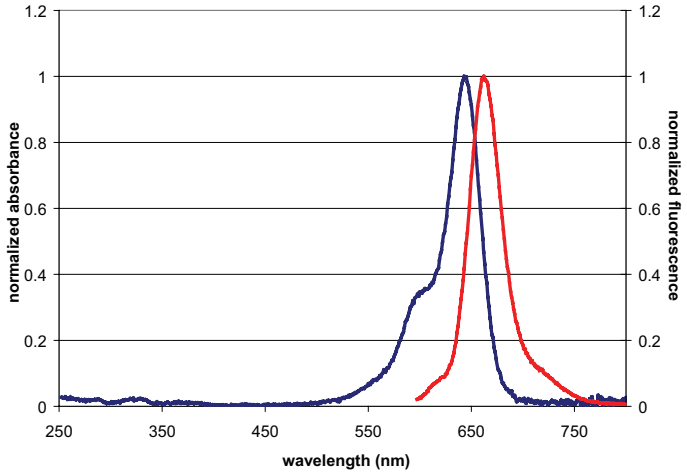

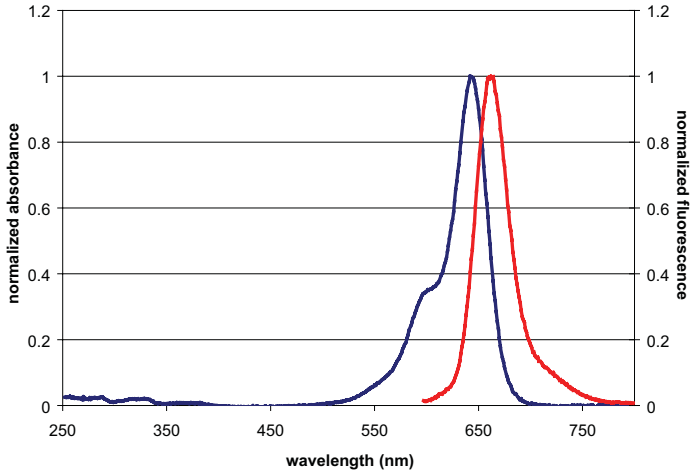

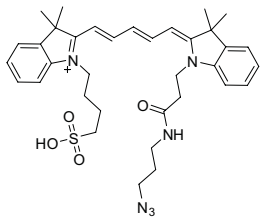

5.34

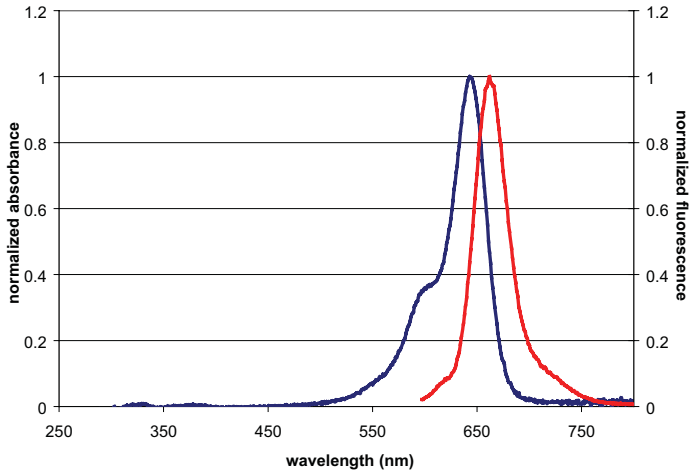
normalized absorbance
normalized fluorescence
wavelength (nm)
0
0.2
0.4
0.6
0.8
1
1.2
250
350
450
550
650
750

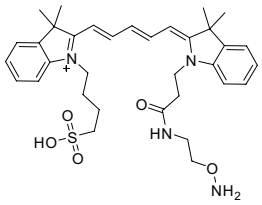

5.36

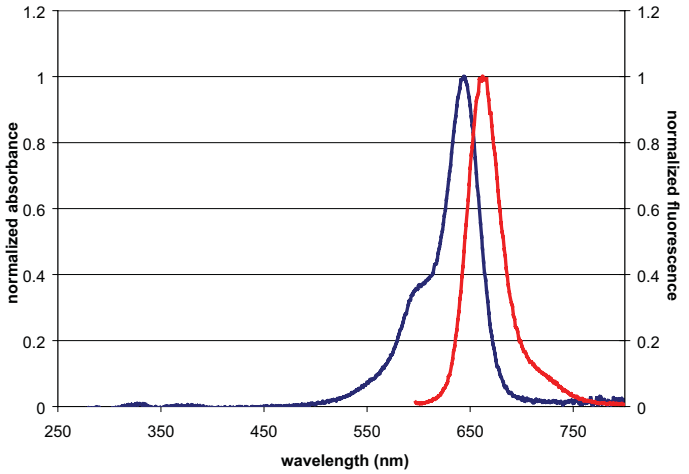
normalized absorbance
normalized fluorescence
wavelength (nm)
0
0.2
0.4
0.6
0.8
1
1.2
250
350
450
550
650
750

5.9 References

Allen, A.D., Chiang, Y., Kresge, A.J. and Tidwell, T.T. (1982) Substituent effects on the acid hydration of acetylenes. *The Journal of Organic Chemistry*, 47, 775-779.

Bouteiller, C., Clave, G., Bernardin, A., Chipon, B., Massonneau, M., Renard, P.-Y. and Romieu, A. (2007) Novel Water-Soluble Near-Infrared Cyanine Dyes: Synthesis, Spectral Properties, and Use in the Preparation of Internally Quenched Fluorescent Probes. *Bioconjugate Chemistry*, 18, 1303-1317.

Bridges, R.G. and Ricketts, J. (1970) The incorporation of analogues of choline into the phospholipids of the larva of the housefly, Musca domestica. *Journal of Insect Physiology*, 16, 579-593.

Carrasco, M.R., Alvarado, C.I., Dashner, S.T., Wong, A.J. and Wong, M.A. (2010) Synthesis of Aminooxy and *N*-Alkylaminooxy Amines for Use in Bioconjugation. *The Journal of Organic Chemistry*, 75, 5757-5759.

Dirksen, A., Dirksen, S., Hackeng, T.M. and Dawson, P.E. (2006) Nucleophilic Catalysis of Hydrazone Formation and Transimination: Implications for Dynamic Covalent Chemistry. *Journal of the American Chemical Society*, 128, 15602-15603.

Dowhan, W. (1997) Molecular basis for membrane phospholipid diversity: Why are there so many lipids? *Annual Review of Biochemistry*, 66, 199-232.

Du, J., Meledeo, M.A., Wang, Z.Y., Khanna, H.S., Paruchuri, V.D.P. and Yarema, K.J. (2009) Metabolic glycoengineering: Sialic acid and beyond. *Glycobiology*, 19, 1382-1401.

Fina, N.J. and Edwards, J.O. (1973) The alpha effect. A review. *International Journal of Chemical Kinetics*, 5, 1-26.

Gottlieb, H.E., Kotlyar, V. and Nudelman, A. (1997) NMR Chemical Shifts of Common Laboratory Solvents as Trace Impurities. *The Journal of Organic Chemistry*, 62, 7512-7515.

Hang, H.C. and Bertozzi, C.R. (2001) Ketone Isosteres of 2-N-Acetamidosugars as Substrates for Metabolic Cell Surface Engineering. *Journal of the American Chemical Society*, 123, 1242-1243.

Jao, C.Y., Roth, M., Welti, R. and Salic, A. (2009) Metabolic labeling and direct imaging of choline phospholipids in vivo. *Proceedings of the National Academy of Sciences of the United States of America*, 106, 15332-15337.

Kent, C. (1995) Eukaryotic Phospholipid Biosynthesis. *Annual Review of Biochemistry*, 64, 315-343.

Kiyose, K., Aizawa, S., Sasaki, E., Kojima, H., Hanaoka, K., Terai, T., Urano, Y. and Nagano, T. (2009) Molecular Design Strategies for Near-Infrared Ratiometric Fluorescent Probes Based on the Unique Spectral Properties of Aminocyanines. *Chemistry – A European Journal*, 15, 9191-9200.

Kohler, J.J. (2009) Aniline: A Catalyst for Sialic Acid Detection. *ChemBioChem*, 10, 2147-2150.

Lavis, L.D. and Raines, R.T. (2008) Bright ideas for chemical biology. *ACS Chemical Biology*, 3, 142-155.

Lewis, W.G., Magallon, F.G., Fokin, V.V. and Finn, M.G. (2004) Discovery and Characterization of Catalysts for Azide-Alkyne Cycloaddition by Fluorescence Quenching. *Journal of the American Chemical Society*, 126, 9152-9153.

Li, Z. and Vance, D.E. (2008) Thematic Review Series: Glycerolipids. Phosphatidylcholine and choline homeostasis. *Journal of Lipid Research*, 49, 1187-1194.

Menashe, N., Reshef, D. and Shvo, Y. (1991) The reaction of alkynes and formic acid. *The Journal of Organic Chemistry*, 56, 2912-2914.

Mojzych, M. and Henary, M. (2008) Synthesis of Cyanine Dyes. Heterocyclic Polymethine Dyes, pp. 1-9.

Mujumdar, R.B., Ernst, L.A., Mujumdar, S.R., Lewis, C.J. and Waggoner, A.S. (1993) Cyanine dye labeling reagents: Sulfoindocyanine succinimidyl esters. *Bioconjugate Chemistry*, 4, 105-111.

Park, J.Y., Ullapu, P.R., Choo, H., Lee, J.K., Min, S.-J., Pae, A.N., Kim, Y., Baek, D.-J. and Cho, Y.S. (2008) TMSOTf-Promoted Addition of Alkynes to Aldehydes: A Novel Synthesis of Chroman-4-ones. *European Journal of Organic Chemistry*, 2008, 5461-5469.

Pavlik, C., Biswal, N.C., Gaenzler, F.C., Morton, M.D., Kuhn, L.T., Claffey, K.P., Zhu, Q. and Smith, M.B. (2011) Synthesis and fluorescent characteristics of imidazole-indocyanine green conjugates. *Dyes and Pigments*, 89, 9-15.

Prelog, V. (1963) Conformation and reactivity of medium-sized ring compounds. *Pure and Applied Chemistry*, 6, 545-560.

Rannes, J.B., Ioannou, A., Willies, S.C., Grogan, G., Behrens, C., Flitsch, S.L. and Turner, N.J. Glycoprotein Labeling Using Engineered Variants of Galactose

Oxidase Obtained by Directed Evolution. *Journal of the American Chemical Society*, ASAP.

Rose, N.C. (1966) Hydration of an alkyne: Undergraduate organic chemistry experiment. *Journal of Chemical Education*, 43, 324-null.

Sandbhor, M.S., Key, J.A., Strelkov, I.S. and Cairo, C.W. (2009) A Modular Synthesis of Alkynyl-Phosphocholine Headgroups for Labeling Sphingomyelin and Phosphatidylcholine. *The Journal of Organic Chemistry*, 74, 8669-8674.

Saxon, E., Luchansky, S.J., Hang, H.C., Yu, C., Lee, S.C. and Bertozzi, C.R. (2002) Investigating cellular metabolism of synthetic azidosugars with the Staudinger ligation. *Journal of the American Chemical Society*, 124, 14893-14902.

Shao, F., Weissleder, R. and Hilderbrand, S.A. (2008) Monofunctional Carbocyanine Dyes for Bio- and Bioorthogonal Conjugation. *Bioconjugate Chemistry*, 19, 2487-2491.

Shao, F., Yuan, H., Josephson, L., Weissleder, R. and Hilderbrand, S.A. (2011) Facile synthesis of monofunctional pentamethine carbocyanine fluorophores. *Dyes and Pigments*, 90, 119-122.

Zeng, Y., Ramya, T.N., Dirksen, A., Dawson, P.E. and Paulson, J.C. (2009) High-efficiency labeling of sialylated glycoproteins on living cells. *Nature Methods*, 6, 207-209.

Chapter 6

Conclusions and future directions

6.1 Summary and conclusions

Herein we have examined a series of fluorophores suitable for bioorthogonal labelling strategies. We ascended from shorter wavelength alkynyl coumarins (see Chapter 2), to alkynyl, azido, hydrazine and amino-oxy benzoxadiazoles (see Chapters 3 and 4), and finally a series of alkynyl, azido and amino-oxy long wavelength cyanine dyes (see Chapter 5). Substitution patterns on some of these fluorophore backbones resulted in dramatic changes to their photophysical properties following conjugation. In the coumarin system we observed increases in QY between 1.2- to 9-fold and bathochromic shifts of up to 23 nm upon triazole formation. While examining benzoxadiazoles, we found triazole formation could lead to fluorogenic, quenching and static properties of fluorophores. In particular, the 5-ethynyl-benzoxadiazole, **3.26**, showed a 48-fold increase in QY upon conversion to a triazole. However, the NBD-azide, **3.6**, suffered a 470-fold decrease in QY upon triazole formation. Hydrazine and amino-oxy derivatives of NBD showed fluorogenic properties upon hydrazone and oxime formation, but were highly environmentally sensitive. These striking changes in fluorescence properties upon ligation could be exploited to ameliorate assay detection limits, or quantitate biomolecules *in vitro* and *in vivo*.

The strength of fluorogenic bioorthogonal labels is demonstrated by the use of NBDAO in PAL sialic acid detection assays ranging from SDS PAGE fluorescence imaging, microplate assay, fluorescence microscopy, and flow cytometry. This probe showed optimal signal to noise (6.7-fold over background) compared to commercially available compounds NBDH (2.9-fold) and Bodipy FL

hydrazide (2.5-fold) in live cell applications. As well, we have examined the applicability of novel choline derivatives as metabolic labelling substrates with long wavelength cyanine-5 bioorthogonal fluorophores. The propargyl and azido cholines (**5.3** and **5.5**) showed strong fluorescence labelling in experimental samples by both flow cytometry and fluorescence microscopy, confirming their viability as metabolic labels. However, the carbonyl containing choline, **5.8**, did not show evidence of metabolic incorporation, with no significant fluorescence labelling observed. The fluorophores developed here have proven useful in biolabelling applications, there remains room for improvement in future generations of bioorthogonal labels. Predicting fluorophore photophysical properties remains challenging *a priori*, the following sections will address potential future directions for the field of fluorogenic and fluorescent bioorthogonal labelling.

6.2 Improving upon the properties of the fluorophores examined

Although fluorophores with remarkable photophysical properties were examined in the previous chapters, there still remain many modifications that could be tested in the future. Quantum yield, brightness and photobleaching properties may be improved with additional modifications to the fluorophore. In the coumarin system, we generated the starting material 4-difluororesorcinol (**2.12**) in 4 steps in an overall yield of 68%. However, we did not find the opportunity to develop a series of fluorinated coumarins to examine their photophysical properties. Fluorinated coumarins typically possess increased emission quantum yields, reduced pKa's, and improved photostability compared

to the parent compound.(Sun, W.-C., Gee, K.R., et al. 1998) Therefore 7-alkynyl, azido, and amino-oxy fluorinated coumarins may have improved photophysical properties over those examined in Chapter 2 (**Scheme 6.1**). The alkyne (**6.2**), similar to our previous coumarins, may be generated by Sonogashira cross-coupling of hydroxycoumarin **6.1**. The amino-oxy (**6.3**) may be generated by amination, or by nucleophilic displacement of the same hydroxycoumarin starting material. (Salahuddin, S., Renaudet, O., et al. 2004)

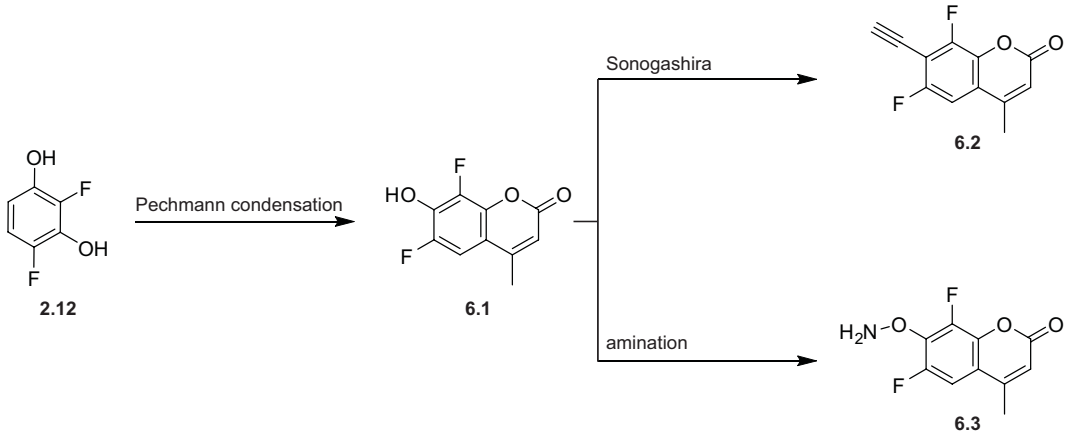

Scheme 6.1. Synthesis of fluorinated coumarin bioorthogonal labelling probes. Probes suitable for bioorthogonal labelling may be generated from the starting alcohol **6.1**, using Sonogashira cross-coupling or amination.(Salahuddin, S., Renaudet, O., et al. 2004, Sun, W.-C., Gee, K.R., et al. 1998)

Additionally, coumarin fluorescence is known to be sensitive to substitution at the 7- and 3- positions. Our 3-substituted 7-alkynyl coumarin derivative, **2.7.2**, had the largest bathochromic shift upon triazole formation. The synthesis and examination of additional 3-substituted 7-alkynyl coumarins may generate additional profluorophores with desirable properties. Interesting candidates would likely include compounds with additional π bonding (**6.4**),

electron withdrawing groups (**6.5**) and electron donating groups (**6.6**). In addition to altering the photophysical properties, introduction of an electron withdrawing group to the alkyne may lower its LUMO and increase the rate of reaction by improving the azide-HOMO/alkyne-LUMO interaction.

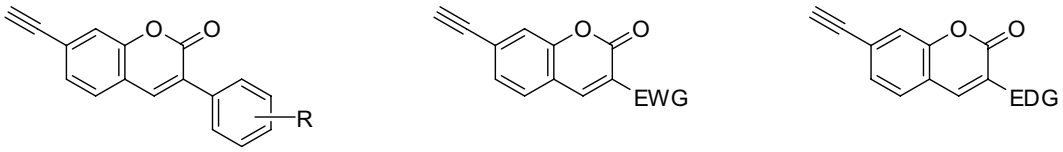

6.4 6.5 6.6

Figure 6.1. Candidate 3-substituted 7-alkynyl coumarins. Substitution of various groups at the 3- position may show interesting photophysical properties upon triazole formation. These compounds should be synthetically accessible from commercially available Pechmann and Knoevenagel condensation substrates.(P. Bandgar, B., S. Uppalla, L., et al. 1999, Valizadeh, H. and Vaghefi, S. 2009, Wiener, C., Schroeder, C.H., et al. 1957)

For the benzoxadiazole system, novel alkynes and azides containing the sulphonate group may have improved water solubility and longer wavelength absorption and emission. Although the sulphonate compounds examined in Chapter 3 proved synthetically challenging, alternatively substituted sulphonates such as those based on the ammonium 7-fluoro-2,1,3-benzoxadiazole-4-sulphonate (SBD-F) (**6.7**) core may exhibit similar S_NAr reactivity to NBD-Cl **3.5** (**Scheme 6.2**).(Imai, K., Toyo'oka, T., et al. 1983) Examination of oxadiazoles with additional fused rings or heteroatom fused oxadiazoles may also yield interesting longer wavelength probes.(Sheremetev, A. 1999)

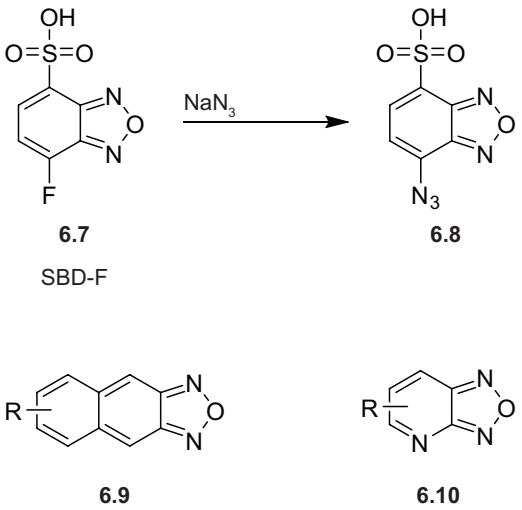

Scheme 6.2. Proposed synthesis of SBD-azide 6.8 and proposed napthoxadiazole (6.9) and pyridyloxadiazole (6.10) target compounds. These compounds may have interesting photophysical properties due to their altered electronics from benzoxadiazoles examined in chapter 3.(Sheremetev, A. 1999)

The bifunctional cyanine dyes examined in chapter 5 show excellent photophysical properties with high absorption coefficients, good quantum yields and very desirable absorption/emission profiles. The main hurdle to further adaptation and use of these fluorophores is their difficult synthesis, purification and cost. Bifunctional cyanine dyes are particularly low yielding because of the generation of undesired homodimers, which tend to elute similarly during chromatography. To address this problem, several strategies have been implemented for the synthesis of monofunctional cyanine dyes, having reactive handles incorporated into the polymethine linker chain.(Bouteiller, C., Clave, G., et al. 2007, Shao, F., Weissleder, R., et al. 2008, Shao, F., Yuan, H., et al. 2011, Ying, L.-Q. and Branchaud, B.P. 2011)

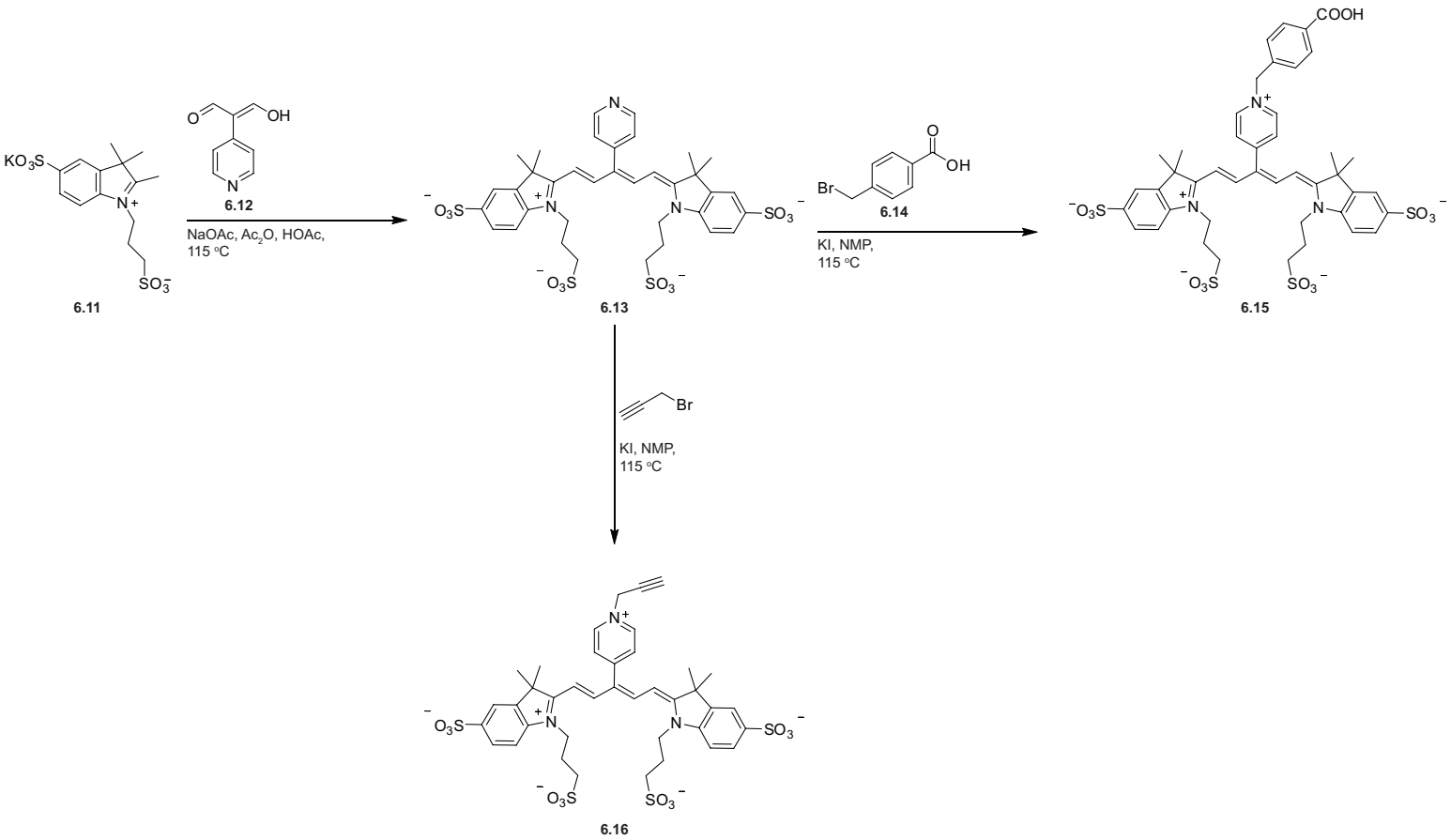

Scheme 6.3. Synthesis of monofunctional cyanine dyes. Carboxylic acid **6.15** was generated in > 60% yield, and was further substituted to a succinimidyl ester in 53% total yield.(Ying, L.-Q. and Branchaud, B.P. 2011)

These monofunctional strategies show improved yield, and purification can often be performed using low pressure reverse phase chromatography. Ying and Branchaud were able to synthesize a monofunctional Cy 5 derivative with a carboxylic handle (**6.15**) in >60% total yield (**Scheme 6.3**). They use the aldehyde **6.12** to form the polymethine chain linking two equivalents of indolium **6.11**. The polymethine linker imine may be quaternized by alkyl bromides such as 4-(bromomethyl)benzoic acid (**6.14**) to generate iminium species such as **6.15**. An interesting future direction may be to generate one of these compounds with a bioorthogonal reactive handle, such as alkyne **6.16**, directly conjugated to the polymethine linker. This compound will likely show a large bathochromic shift upon triazole formation, as one unit extensions of the polymethine chain typically elicit ~100 nm shifts.(Mojzych, M. and Henary, M. 2008)

6.3 Examination of additional fluorophore backbones

In the previous chapters, we have examined only a few carefully chosen fluorophore backbones. There are numerous other systems available, each with strengths and weaknesses.(Lavis, L.D. and Raines, R.T. 2008) Ideal candidates for future generations of fluorogenic and fluorescent bioorthogonal labels should be synthetically accessible, have high quantum yields, high absorption coefficients and good photostability. Some systems that may have potential as fluorogenic labels include dyes based on propidium (**6.17**), hydroxypyrene sulphonate (**6.18**) and hemicyanine/merocyanine dye systems (**6.19**) (**Figure 6.2**). These small fluorophores can be obtained from relatively inexpensive starting materials and are amenable to introduction of conjugated bioorthogonal handles. They have

emission in the green or longer wavelengths and can have good water solubility. Few fluorophores in the red and near infra-red (NIR) region have been developed for fluorogenic labelling strategies. Their challenging synthesis and larger size have limited their exploration. Further efforts should be applied to fluorophores in these wavelengths, as they avoid autofluorescence and are therefore most amenable to *in vivo* applications.(Weissleder, R. 2001)

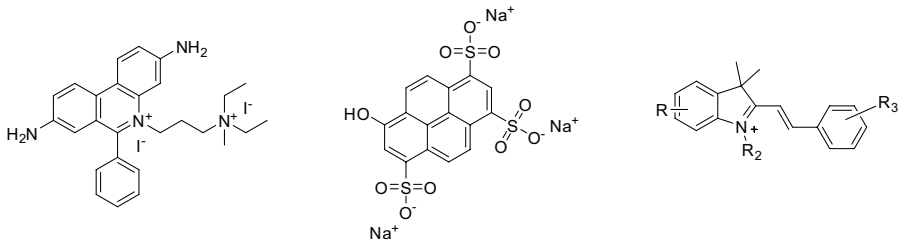

	6.17	6.18	6.19
Excitation (nm):	488	460	570
Emission (nm):	562-588	510	605

Figure 6.2. Additional fluorophore backbones which show promise for fluorogenic and fluorescent bioorthogonal ligation strategies. Emission and excitation values obtained from Sigma Aldrich and Zhan et al.(Zhan, W.H., Barnhill, H.N., et al. 2005)

6.4 Examination of additional bioorthogonal labelling strategies

We have examined two well known bioorthogonal labelling strategies: the Sharpless-Meldal reaction and oxime/hydrazone ligation. However, there are several other bioorthogonal reactions currently used, including the Staudinger ligation, and alkene based tetrazole and tetrazine reactions (see Chapter 1). Applying the fluorophores examined here to these systems may prove useful for biolabelling experiments. In particular, the tetrazine moiety which acts as a

quencher for green and red fluorophores will likely generate fluorogenic labels with the NBD (green) and cyanine (red) dyes explored here (**Scheme 6.4**). These compounds could be generated in one step from existing compounds NBD-Cl **3.5** and Cy dye **5.32** by S_NAr and amide coupling, respectively, with the tetrazine amine **6.20** reported by Deveraj et al.(Devaraj, N.K., Hilderbrand, S., et al. 2010)

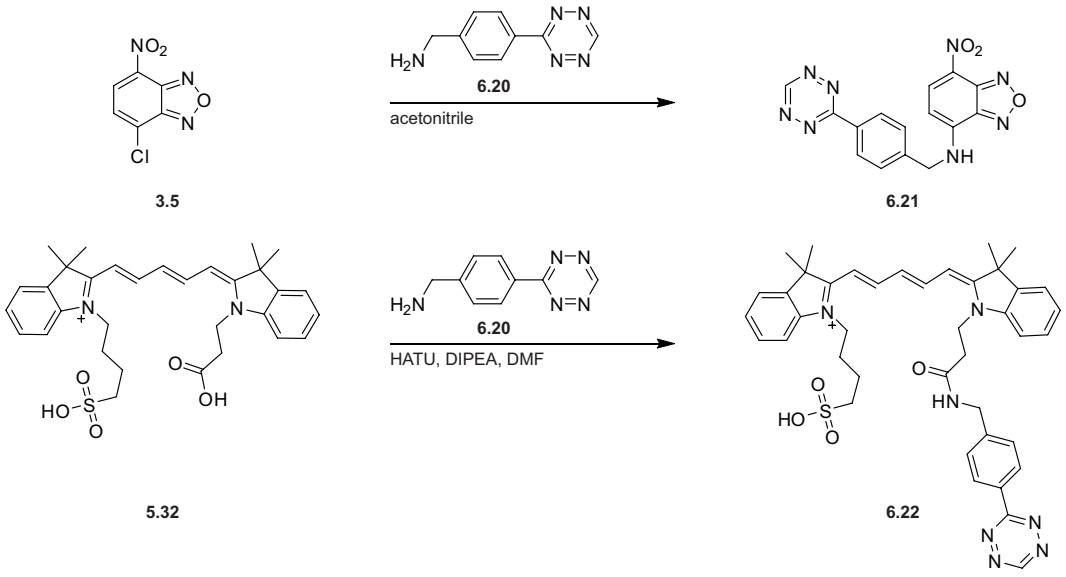

Scheme 6.4. Proposed synthesis of tetrazine substituted NBD and Cy 5 dyes. NBD-Cl **3.5** and Cy dye **5.32** could be derivatized with the tetrazine amine **6.20** by S_NAr and amide coupling, respectively. (Devaraj, N.K., Hilderbrand, S., et al. 2010)

As additional bioorthogonal strategies emerge, there will be opportunities to apply rational fluorophore design to generate novel, and more sensitive biological probes. Higher quantum yields, absorption coefficients and selectivity are some properties needed to generate improved probe sensitivity. Likewise, as new questions arise in the examination of biological phenomena there will be a need for innovative new probes.

6.5 References

Bouteiller, C., Clave, G., Bernardin, A., Chipon, B., Massonneau, M., Renard, P.-Y. and Romieu, A. (2007) Novel Water-Soluble Near-Infrared Cyanine Dyes: Synthesis, Spectral Properties, and Use in the Preparation of Internally Quenched Fluorescent Probes. *Bioconjugate Chemistry*, 18, 1303-1317.

Devaraj, N.K., Hilderbrand, S., Upadhyay, R., Mazitschek, R. and Weissleder, R. (2010) Bioorthogonal Turn-On Probes for Imaging Small Molecules inside Living Cells. *Angewandte Chemie International Edition*, 49, 2869-2872.

Imai, K., Toyo'oka, T. and Watanabe, Y. (1983) A novel fluorogenic reagent for thiols: Ammonium 7-fluorobenzo-2-oxa-1,3-diazole-4-sulfonate. *Analytical Biochemistry*, 128, 471-473.

Lavis, L.D. and Raines, R.T. (2008) Bright ideas for chemical biology. *ACS Chemical Biology*, 3, 142-155.

Mojzych, M. and Henary, M. (2008) Synthesis of Cyanine Dyes. Heterocyclic Polymethine Dyes, pp. 1-9.

P. Bandgar, B., S. Uppalla, L. and S. Kurule, D. (1999) Solvent-free one-pot rapid synthesis of 3-carboxycoumarins using focused microwaves. *Green Chemistry*, 1, 243-245.

Salahuddin, S., Renaudet, O. and Reymond, J.L. (2004) Aldehyde detection by chromogenic/fluorogenic oxime bond fragmentation. *Organic & Biomolecular Chemistry*, 2, 1471-1475.

Shao, F., Weissleder, R. and Hilderbrand, S.A. (2008) Monofunctional Carbocyanine Dyes for Bio- and Bioorthogonal Conjugation. *Bioconjugate Chemistry*, 19, 2487-2491.

Shao, F., Yuan, H., Josephson, L., Weissleder, R. and Hilderbrand, S.A. (2011) Facile synthesis of monofunctional pentamethine carbocyanine fluorophores. *Dyes and Pigments*, 90, 119-122.

Sheremetev, A. (1999) The chemistry of furazans fused to six- and seven-membered heterocycles with one heteroatom. *Russian Chemical Reviews*, 68, 137-148.

Sun, W.-C., Gee, K.R. and Haugland, R.P. (1998) Synthesis of novel fluorinated coumarins: Excellent UV-light excitable fluorescent dyes. *Bioorganic & Medicinal Chemistry Letters*, 8, 3107-3110.

Valizadeh, H. and Vaghefi, S. (2009) One-Pot Wittig and Knoevenagel Reactions in Ionic Liquid as Convenient Methods for the Synthesis of Coumarin Derivatives. *Synthetic Communications*, 39, 1666-1678.

Weissleder, R. (2001) A clearer vision for in vivo imaging. *Nature Biotechnology*, 19, 316-317.

Wiener, C., Schroeder, C.H. and Link, K.P. (1957) The synthesis of various 3-substituted-4-alkylcoumarins. *Journal of the American Chemical Society*, 79, 5301-5303.

Ying, L.-Q. and Branchaud, B.P. (2011) Facile Synthesis of Symmetric, Monofunctional Cyanine Dyes for Imaging Applications. *Bioconjugate Chemistry*, 22, 865-869.

Zhan, W.H., Barnhill, H.N., Sivakumar, K., Tian, T. and Wang, Q. (2005) Synthesis of hemicyanine dyes for 'click' bioconjugation. *Tetrahedron Letters*, 46, 1691-1695.

Appendix

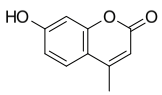

2.4.1
^{1}H NMR (300 MHz, DMSO-D_6)

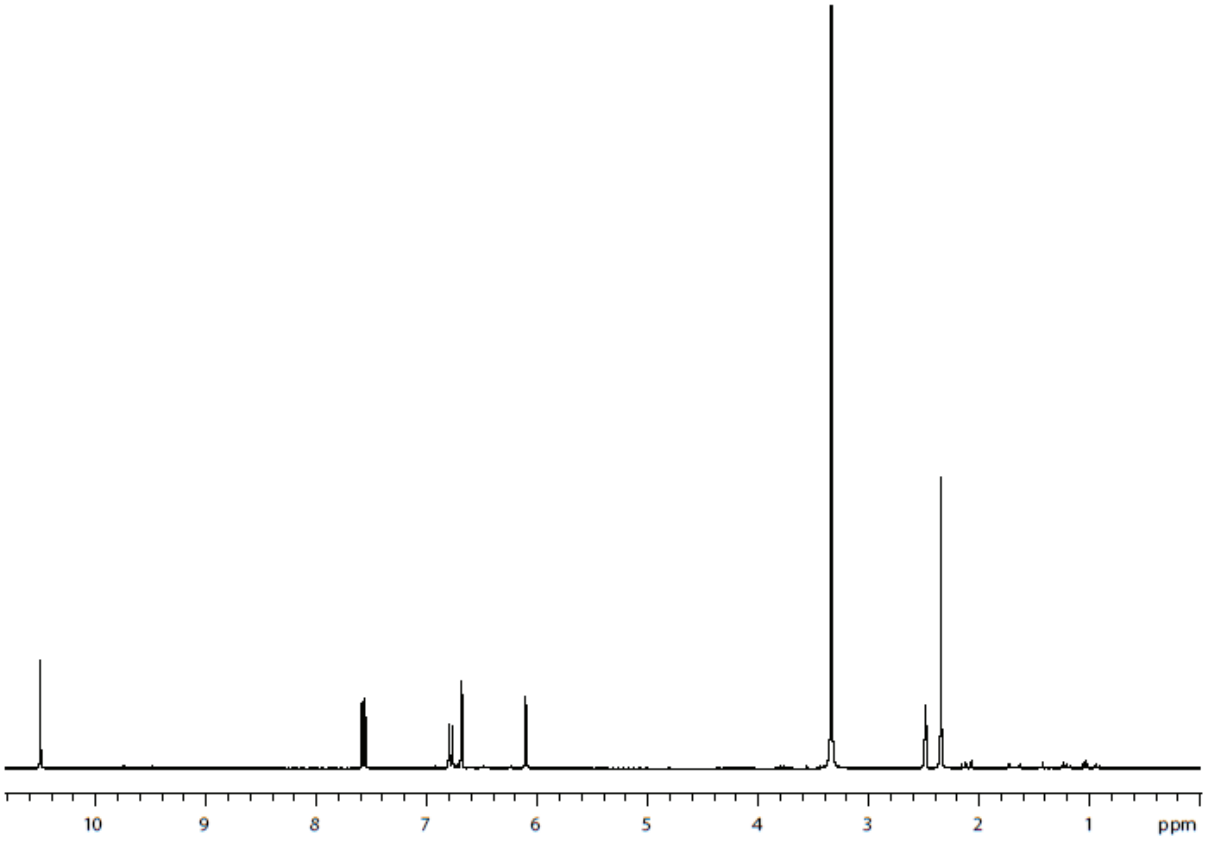

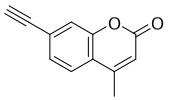

2.4.2
^{1}H NMR (400 MHz, DMSO-D_6)

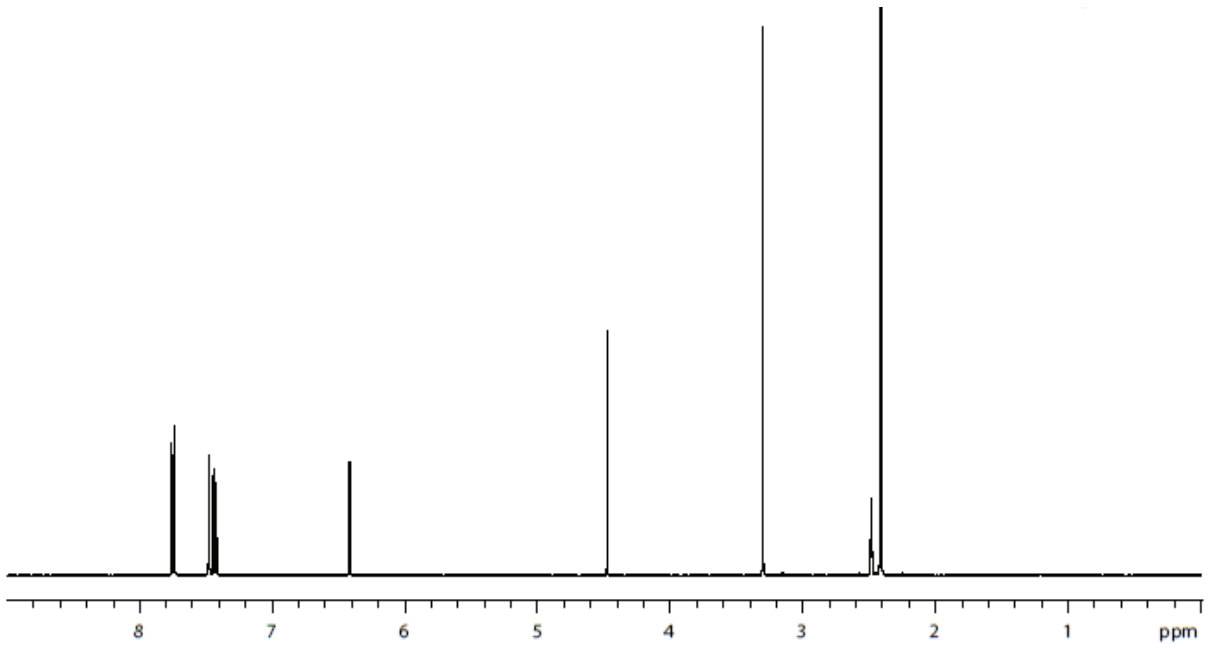

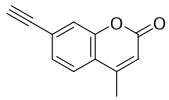

2.4.2
^{13}C NMR (100 MHz, DMSO-D_6)

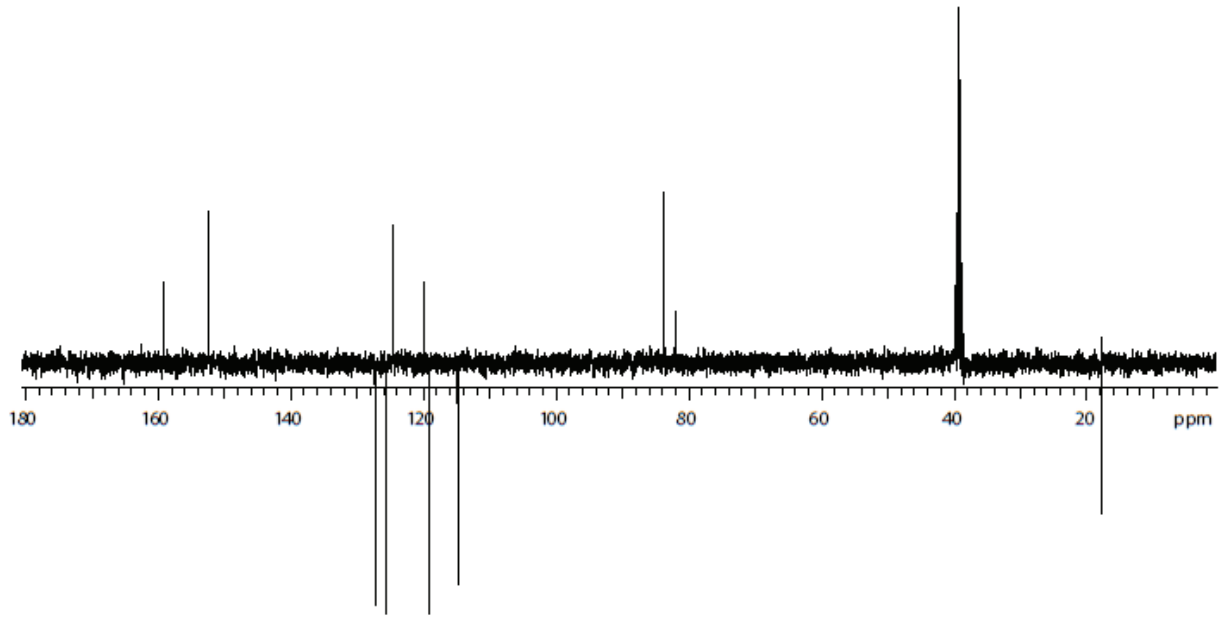

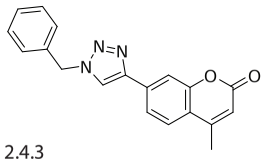

2.4.3
^{1}H NMR (500 MHz, $CDCl_3$)

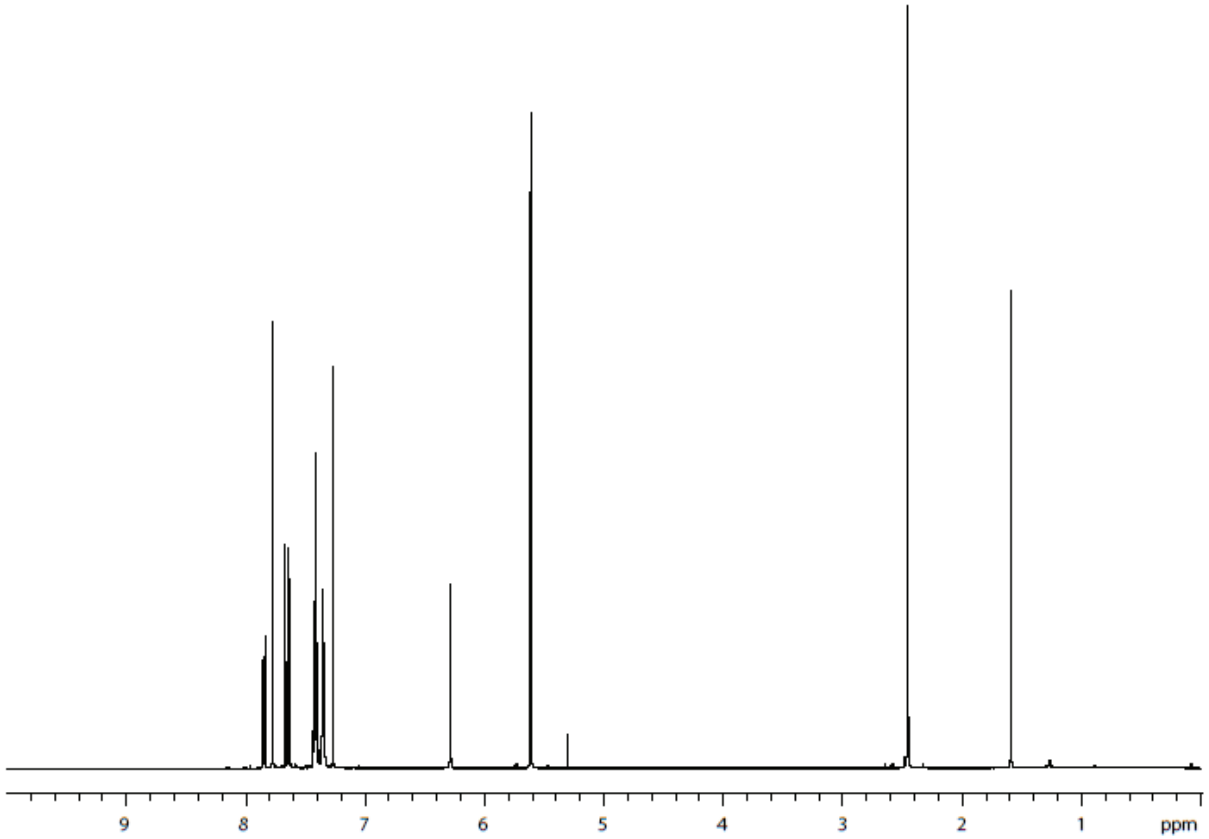

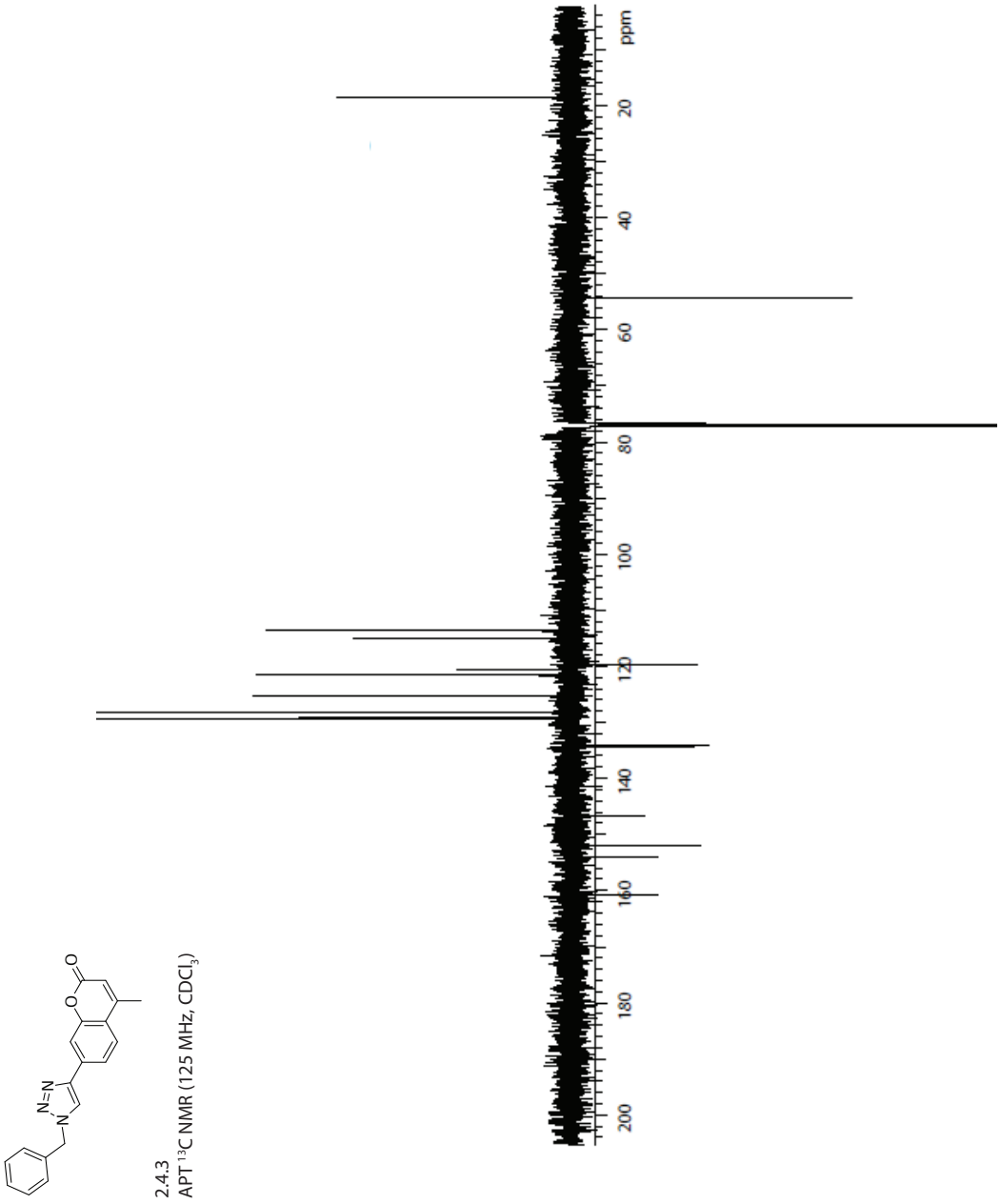

2.4.3
APT ^{13}C NMR (125 MHz, $CDCl_3$)

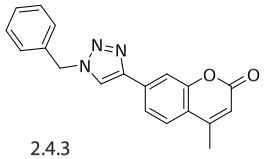

2.4.3
^{1}H COSY NMR (500 MHz, $CDCl_3$)

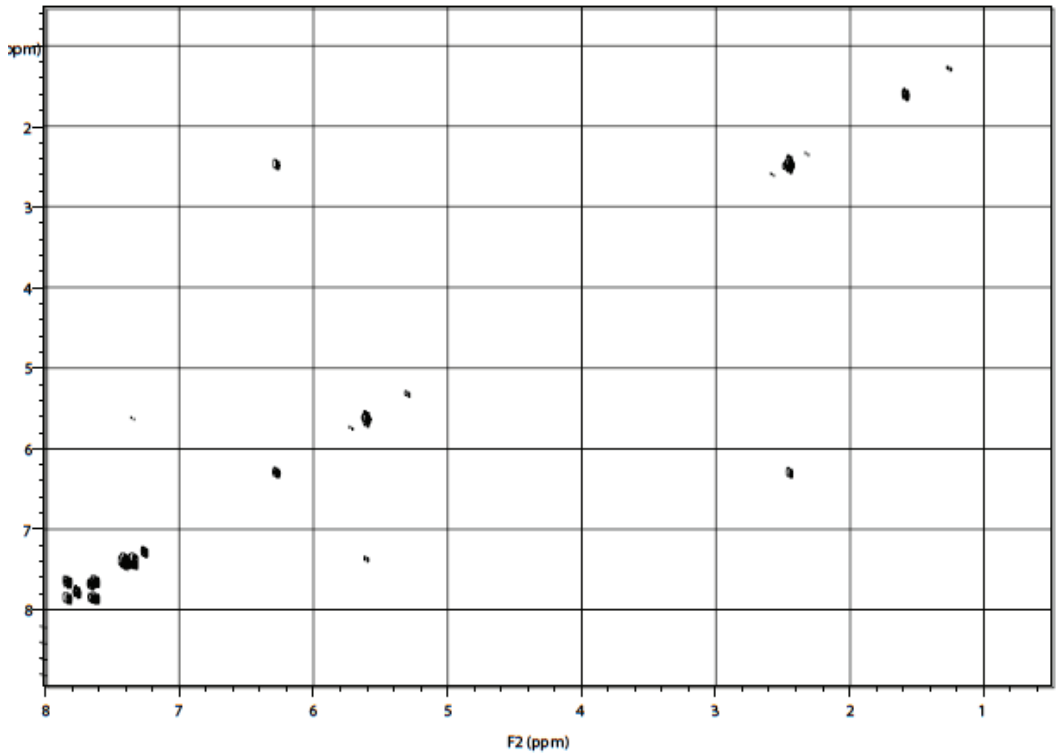

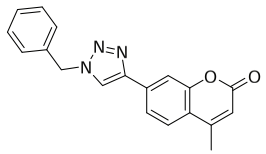

2.4.3
HMQC NMR (500 MHz, $CDCl_3$)

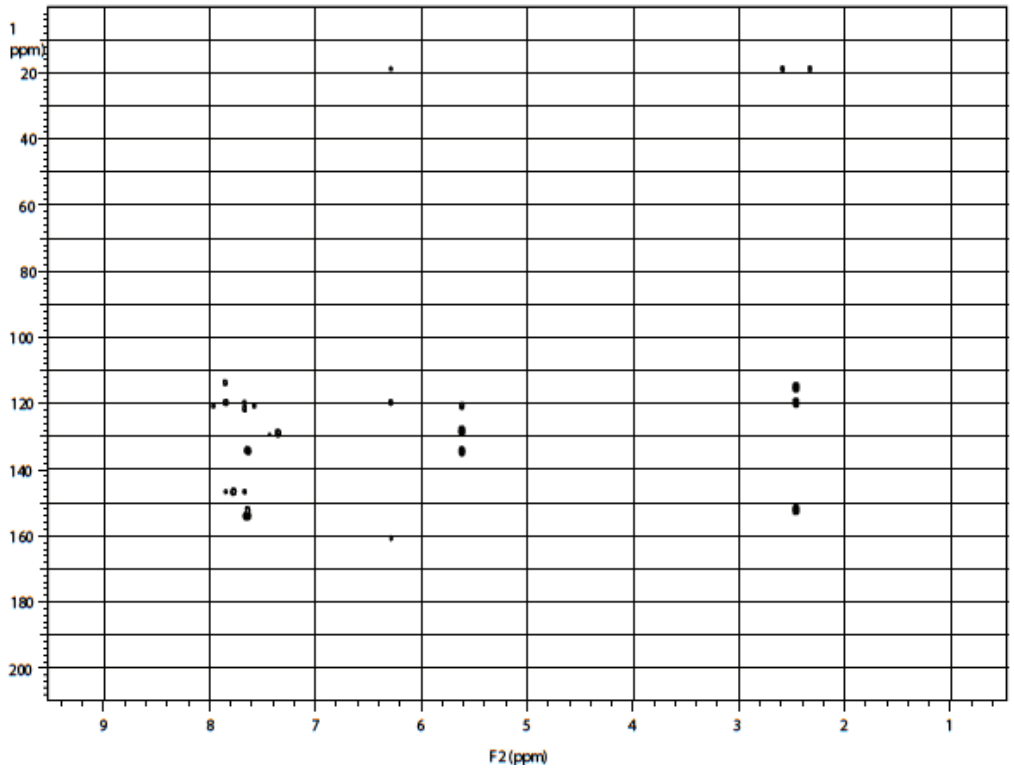

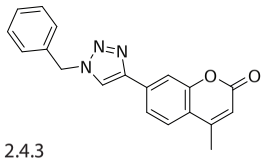

2.4.3
HSQC NMR (500 MHz, $CDCl_3$)

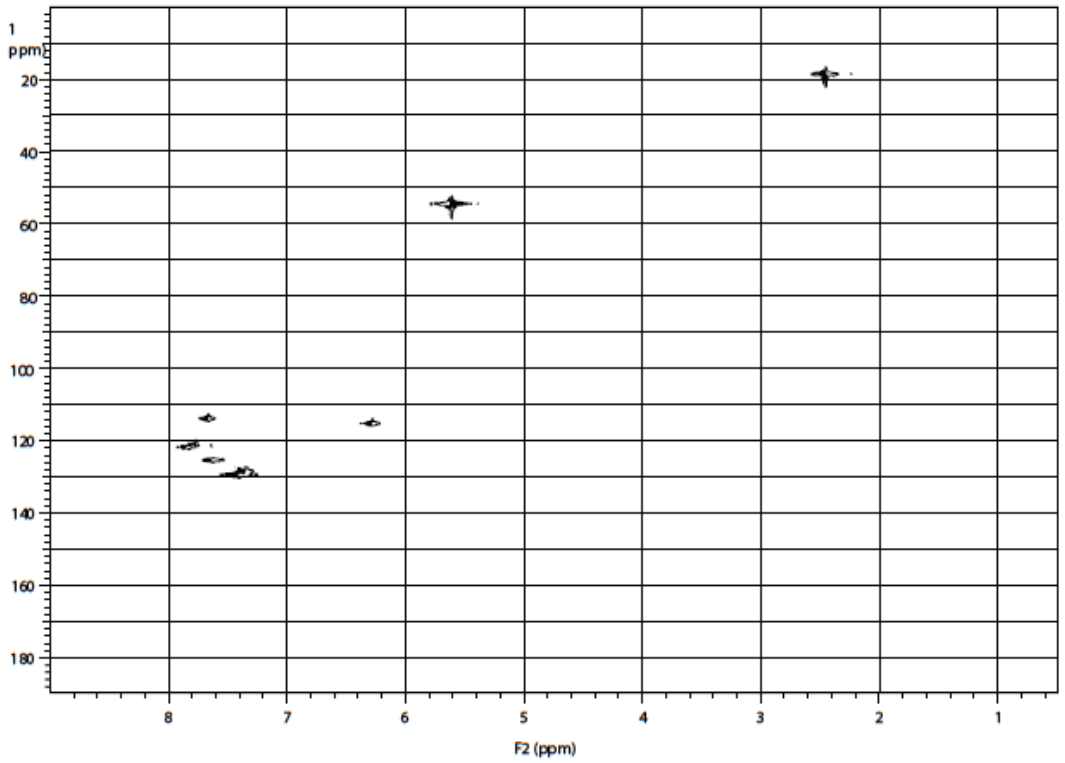

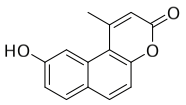

2.5.1

^{1}H NMR (400 MHz, DMSO-D_6)

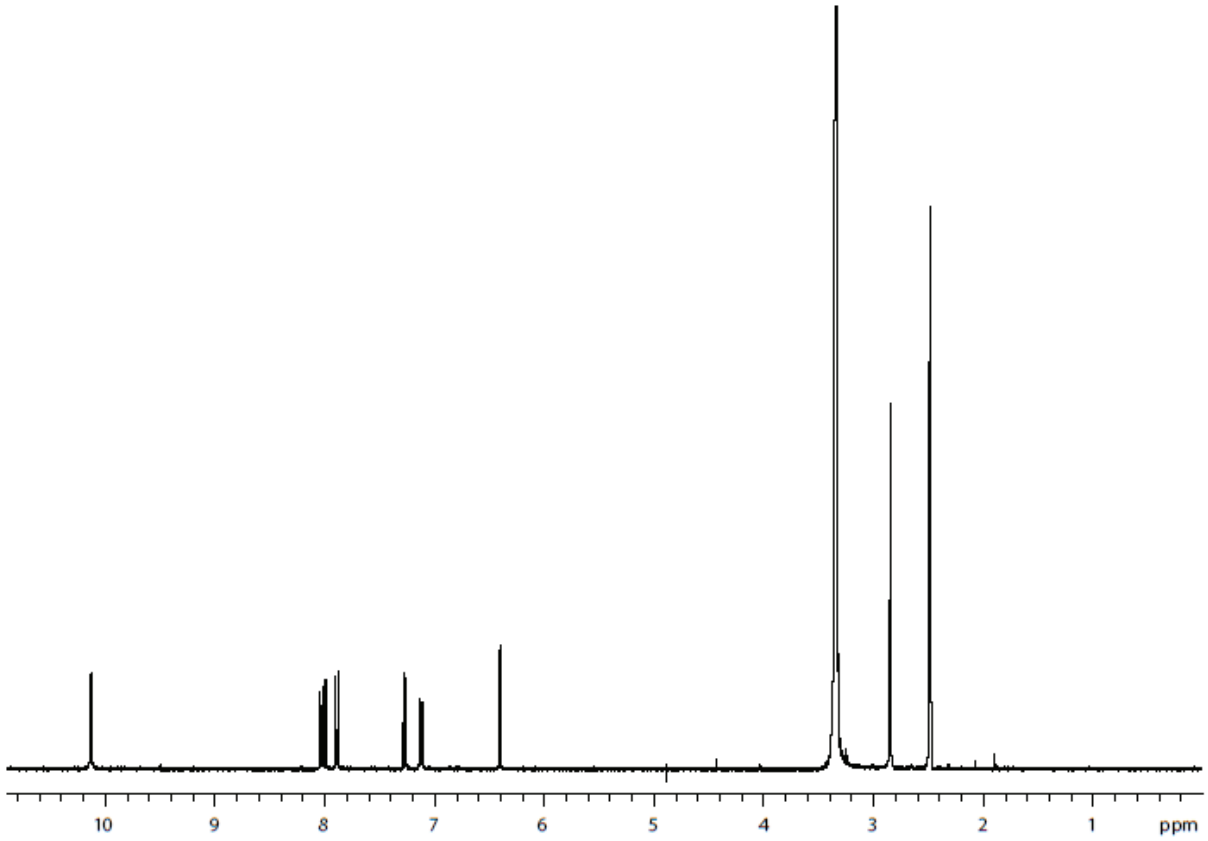

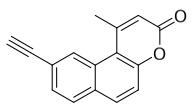

2.5.2
^{1}H NMR (600 MHz, $CDCl_3$)

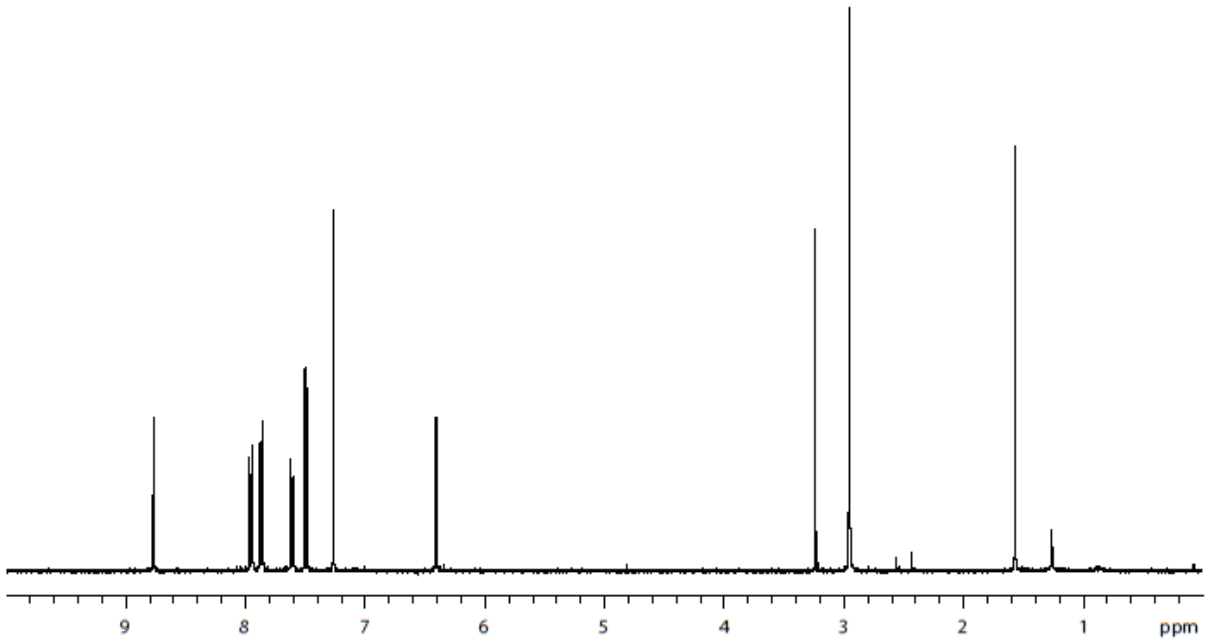

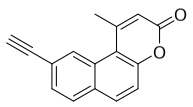

2.5.2
APT ^{13}C NMR (100 MHz, $CDCl_3$)

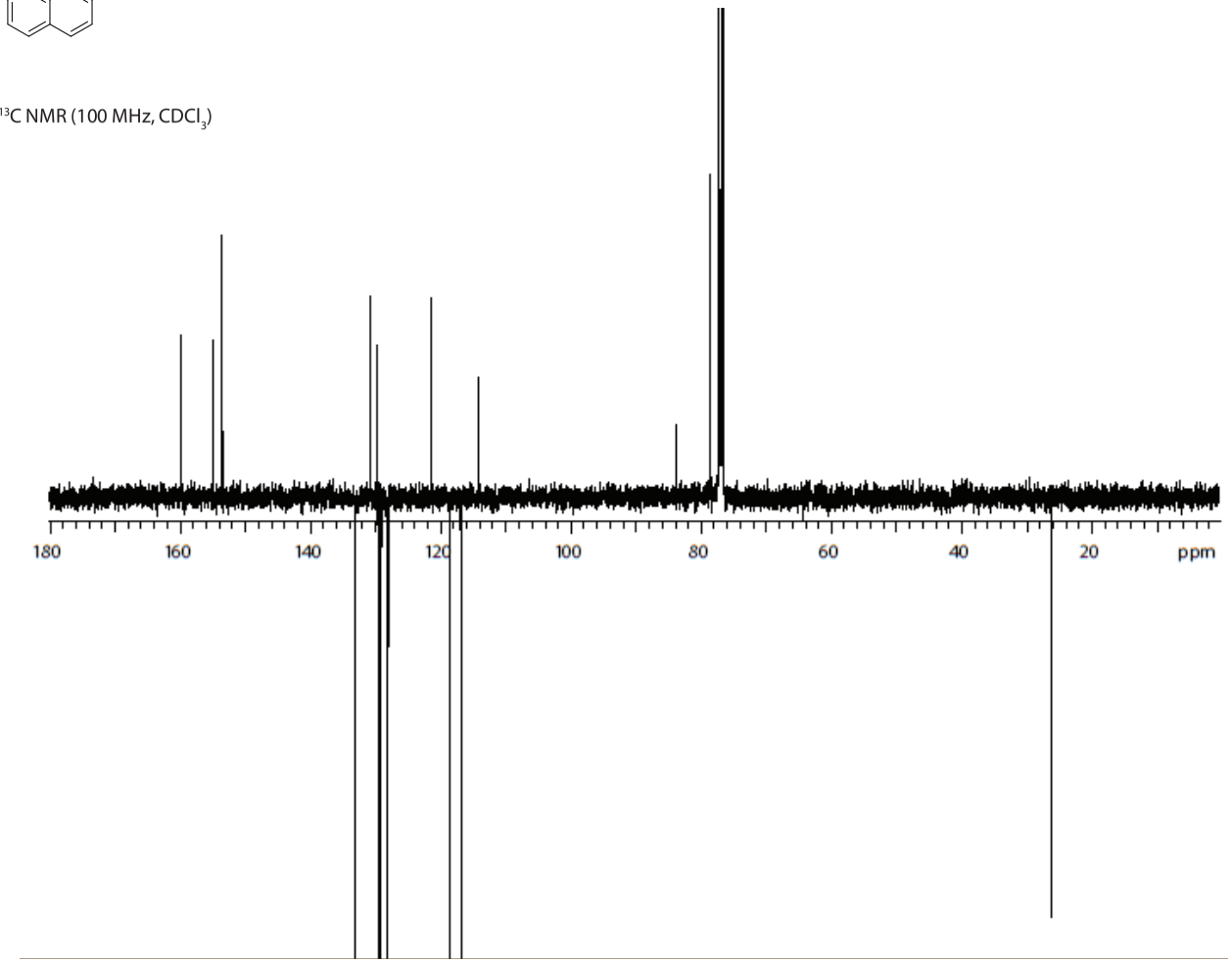

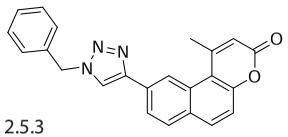

2.5.3
^{1}H NMR (500 MHz, $CDCl_3$)

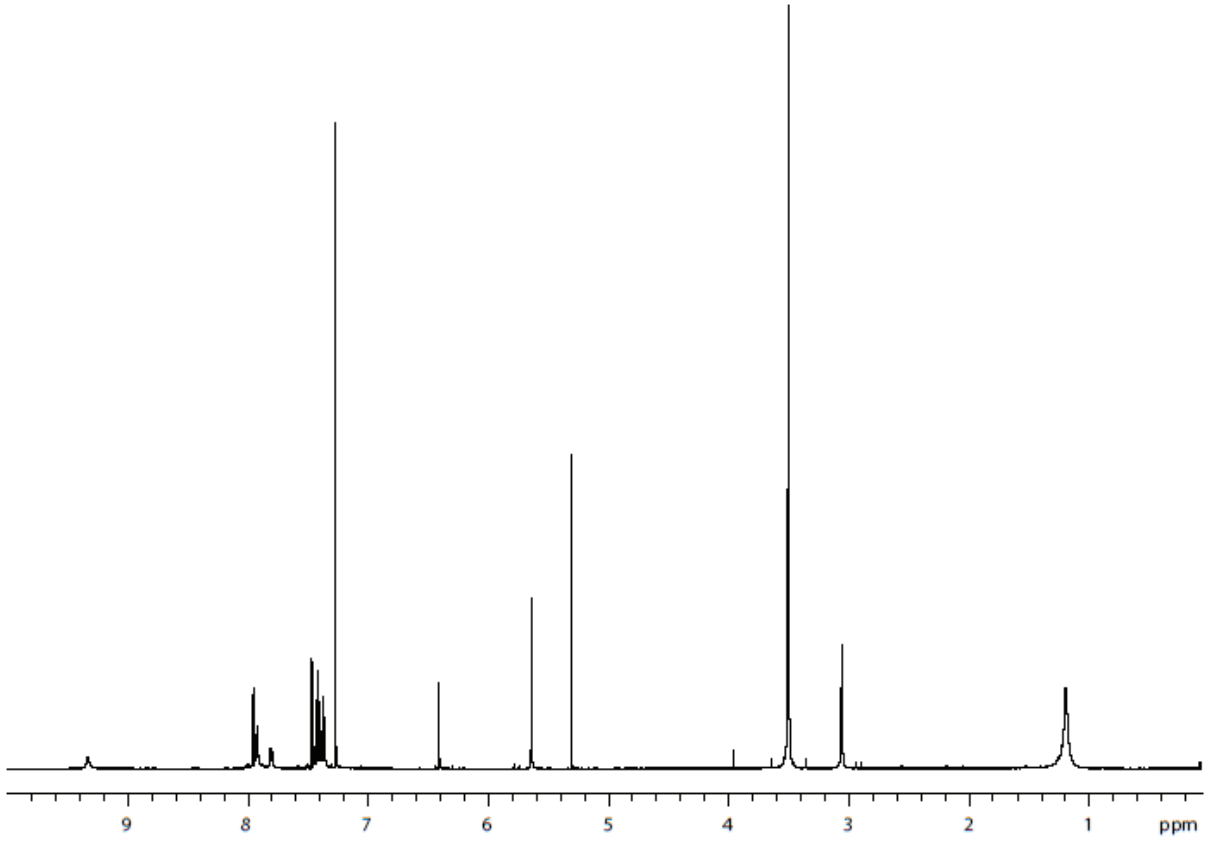

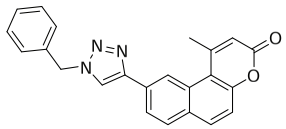

2.5.3
COSY NMR (500 MHz, $CDCl_3$)

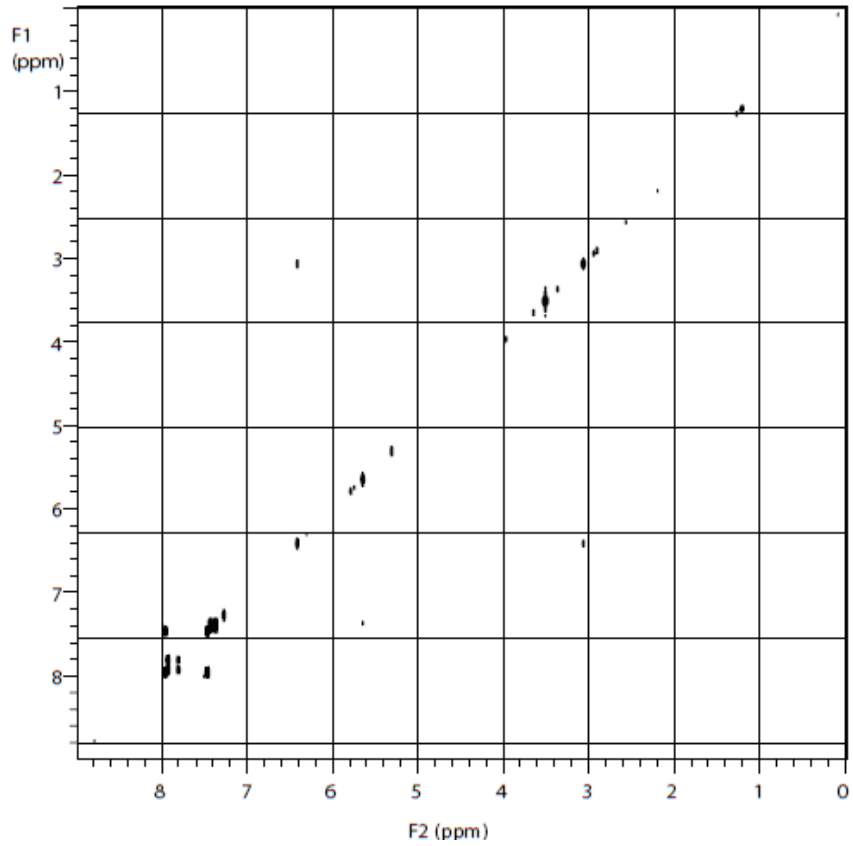

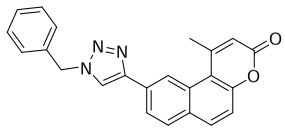

2.5.3
HMQC NMR (500 MHz, $CDCl_3$)

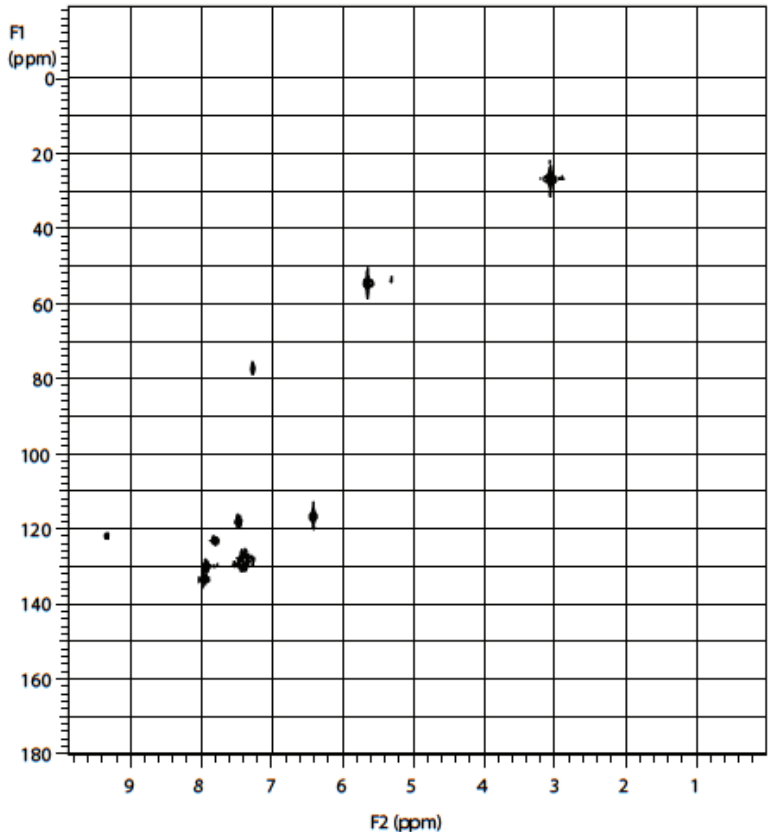

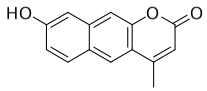

2.6.1

^{1}H NMR (300 MHz, DMSO-D_6)

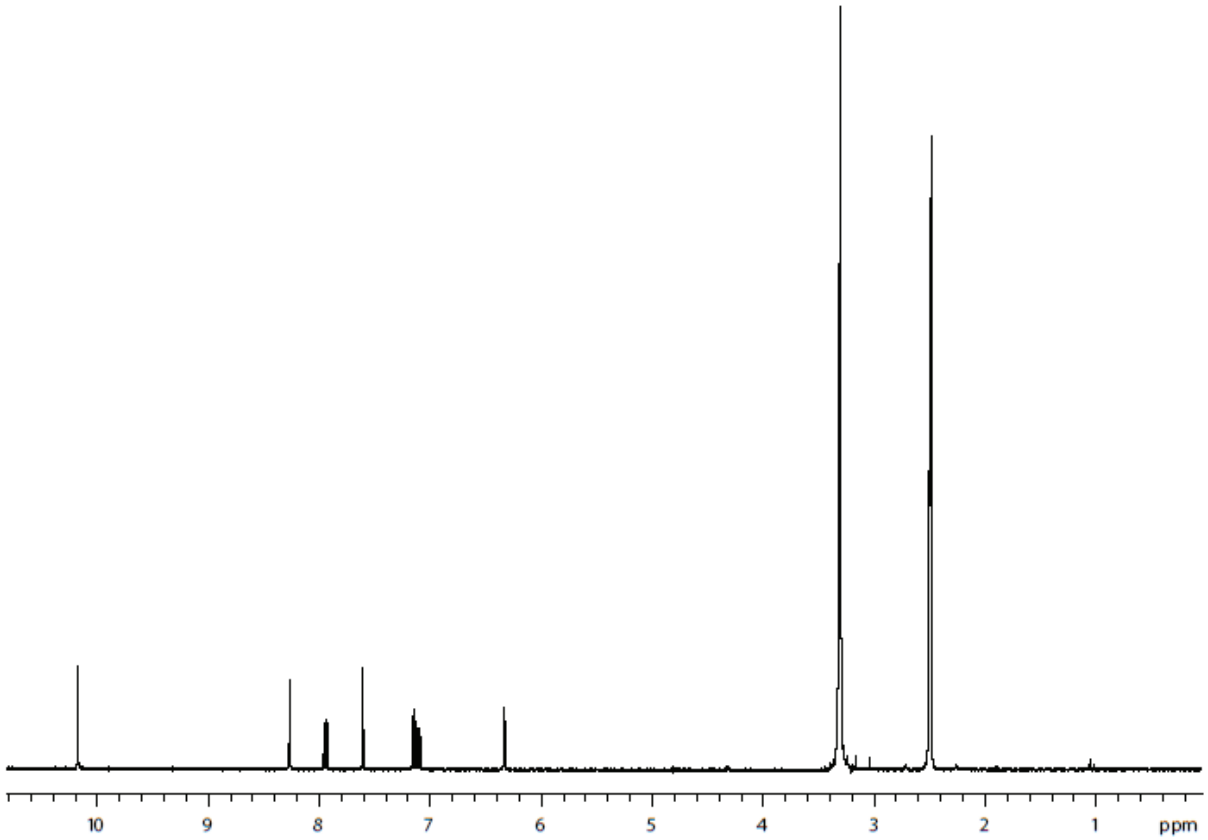

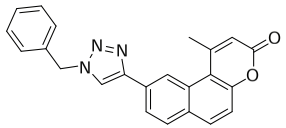

2.5.3
APT ^{13}C NMR (125 MHz, $CDCl_3$)

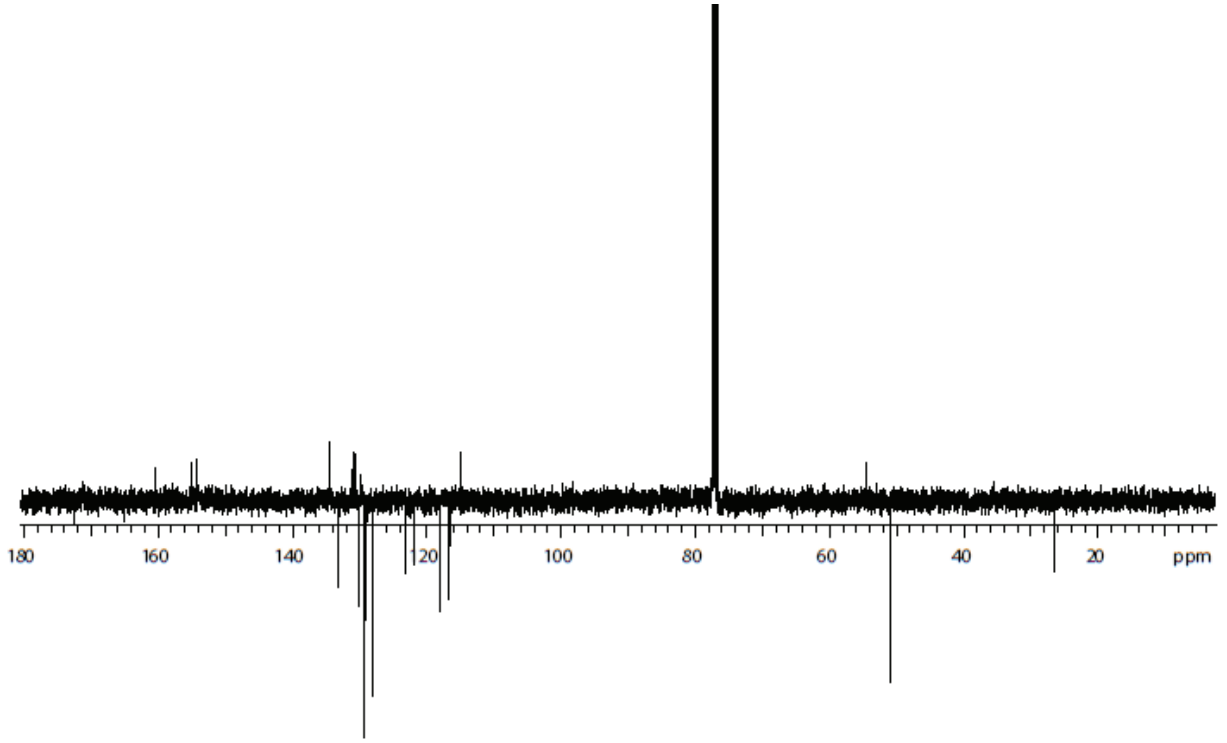

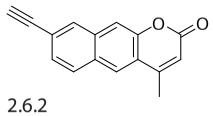

2.6.2
^{1}H NMR (600 MHz, $CDCl_3$)

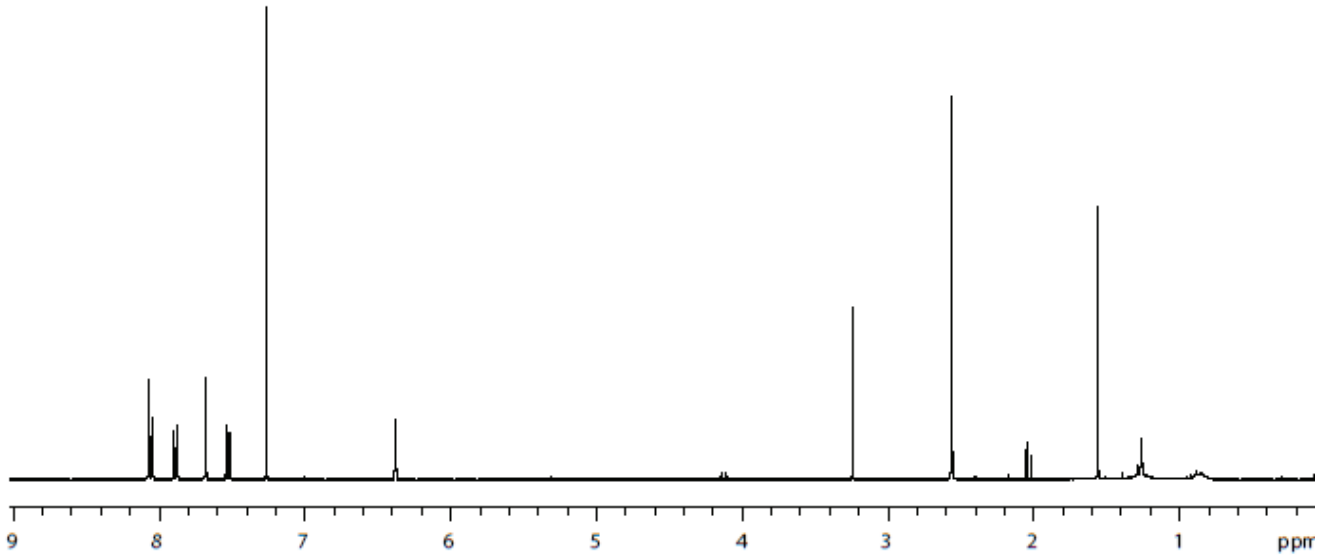

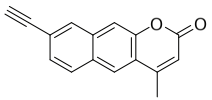

2.6.2
APT ^{13}C NMR (100 MHz, $CDCl_3$)

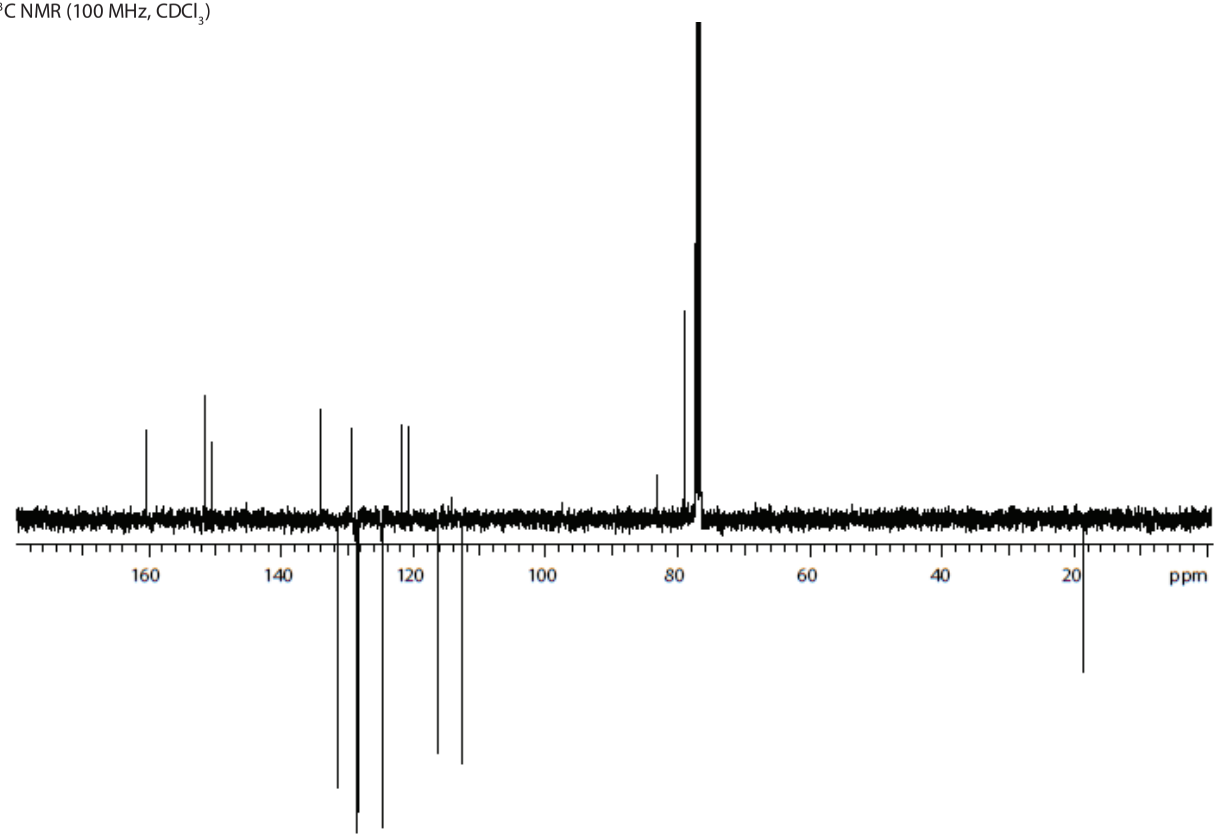

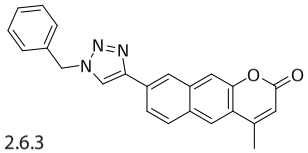

2.6.3

^{1}H NMR (500 MHz, $CDCl_3$)

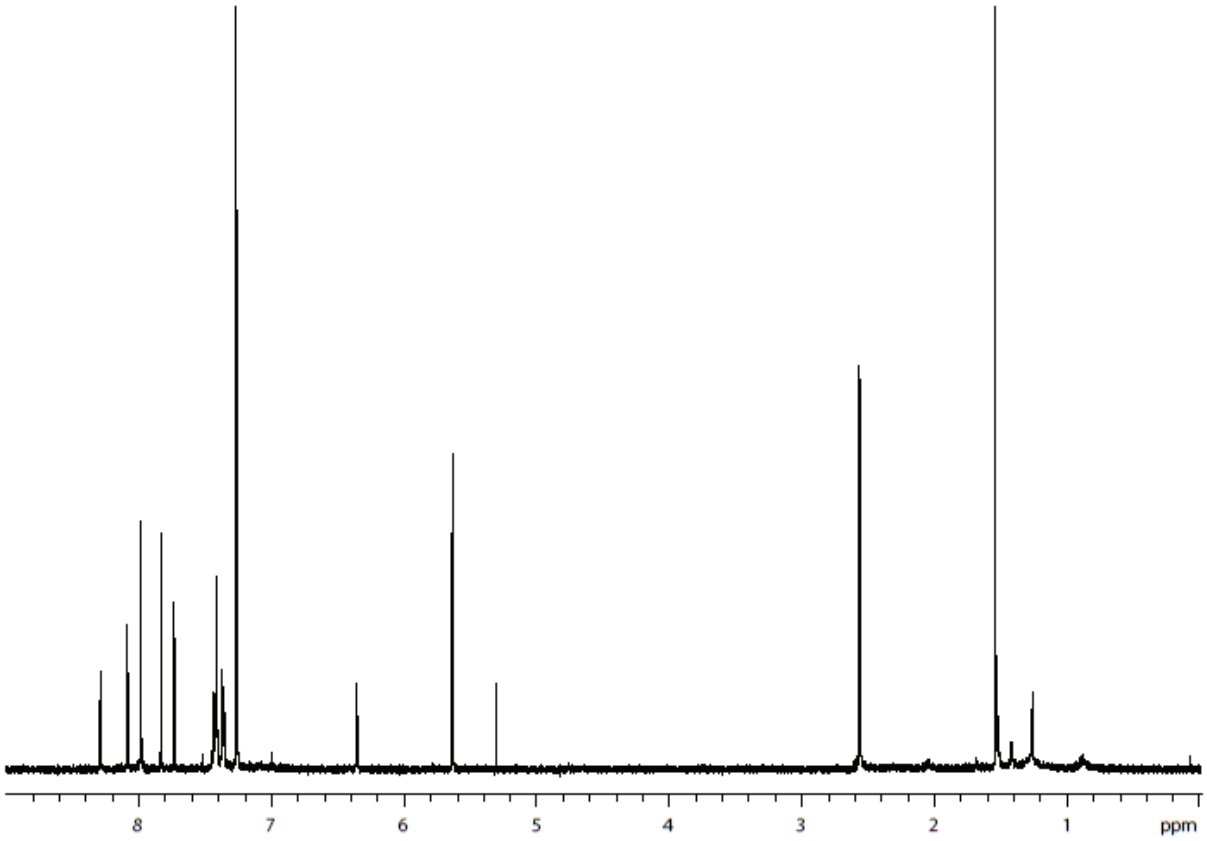

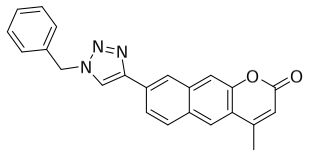

2.6.3
APT ^{13}C NMR (125 MHz, $CDCl_3$)

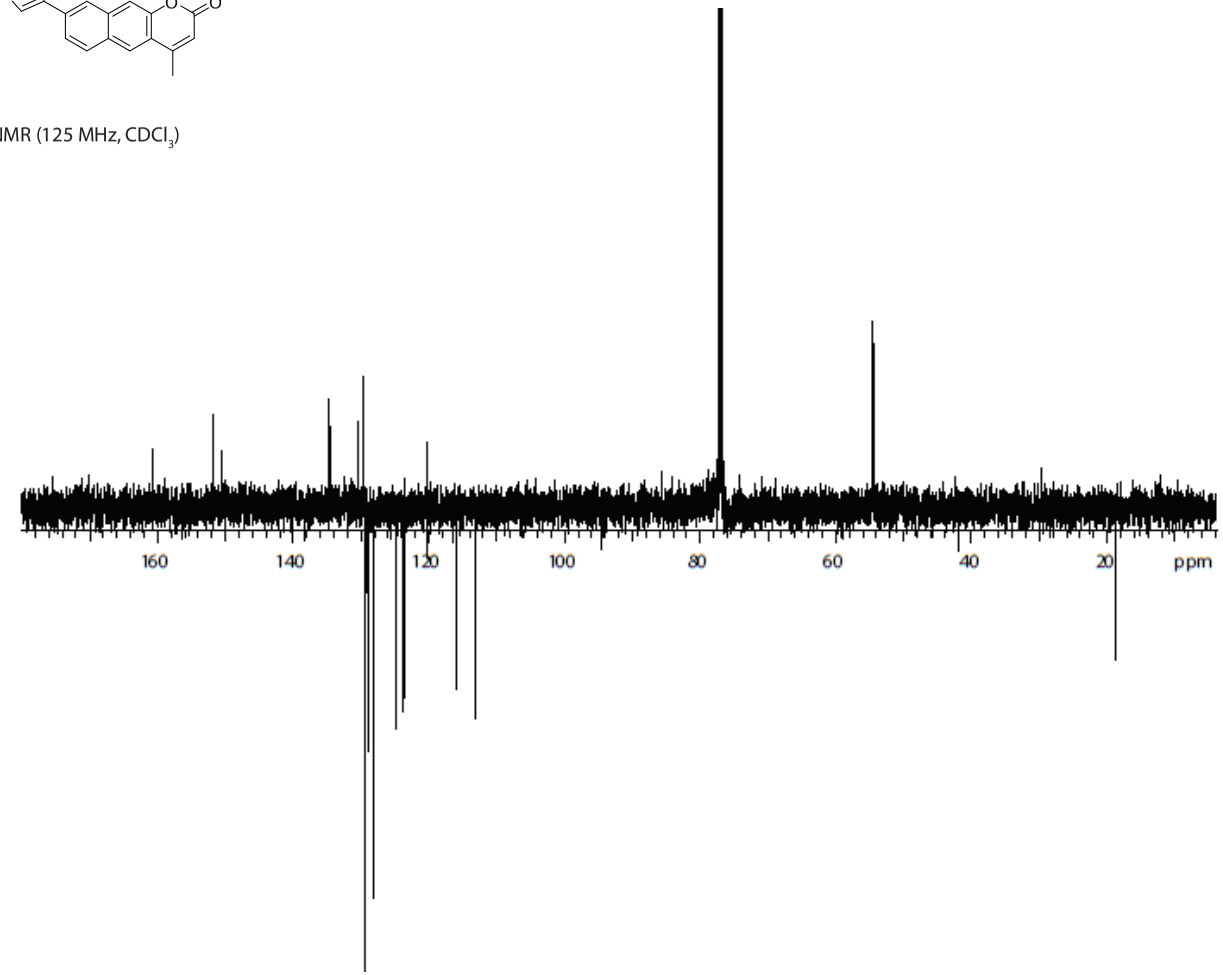

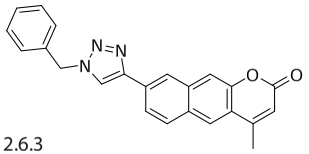

2.6.3

^{1}H COSY NMR (500 MHz, $CDCl_3$)

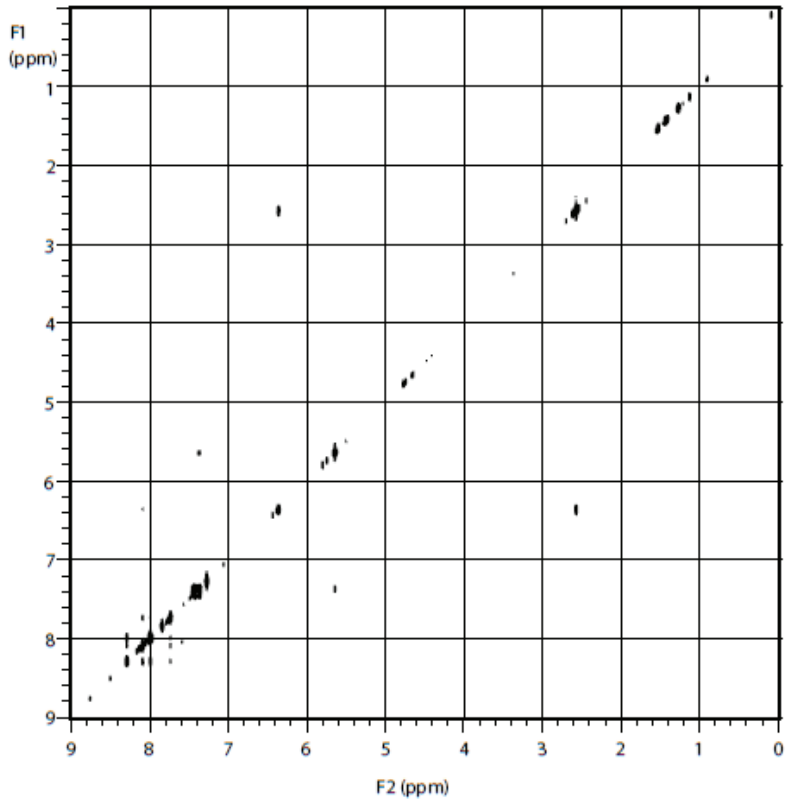

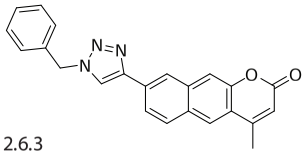

2.6.3
HMBC NMR (500 MHz, $CDCl_3$)

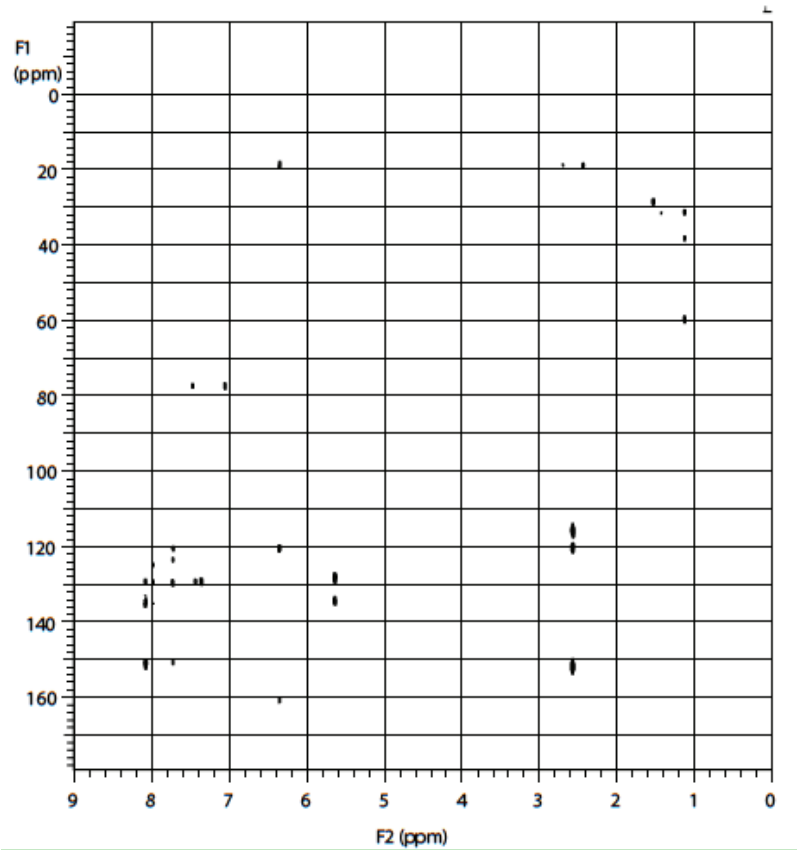

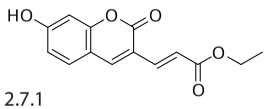

2.7.1

^{1}H NMR (300 MHz, CD_3OD)

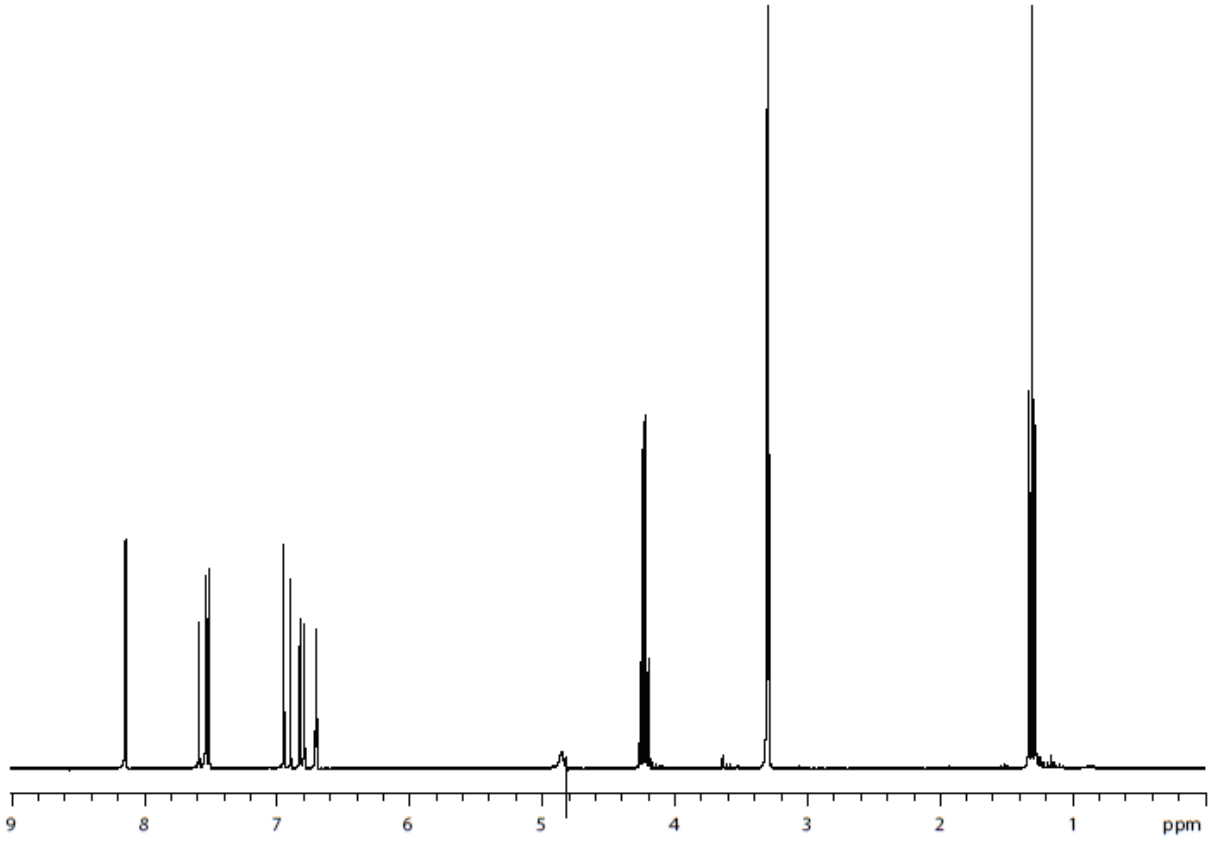

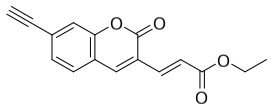

2.7.2
^{1}H NMR (400 MHz, $CDCl_3$)

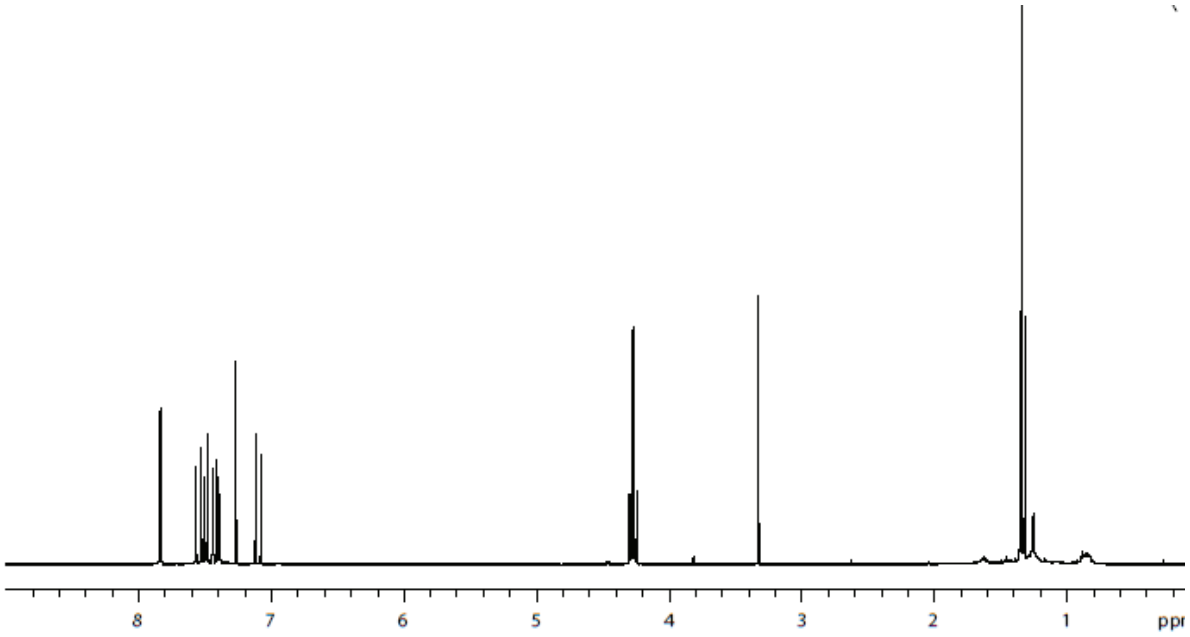

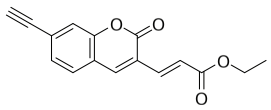

2.7.2
APT ^{13}C NMR (100 MHz, $CDCl_3$)

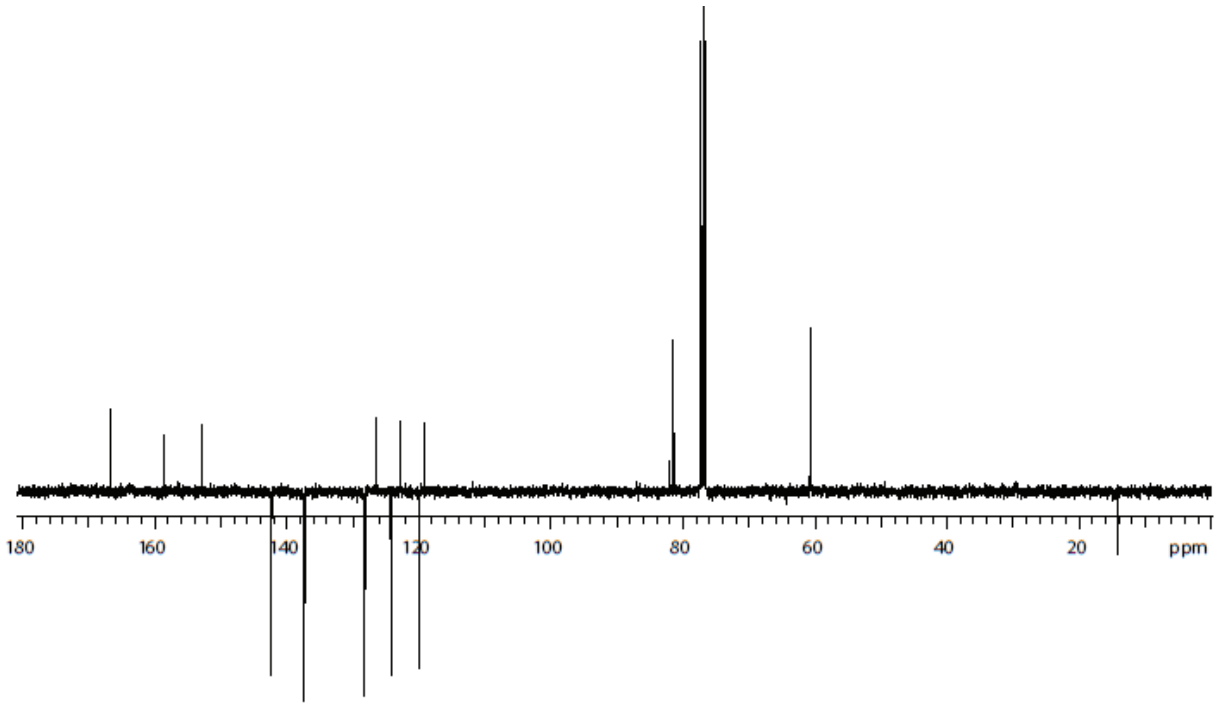

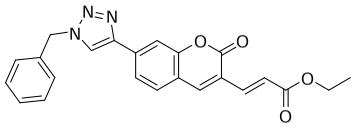

2.7.3

^{1}H NMR (500 MHz, $CDCl_3$)

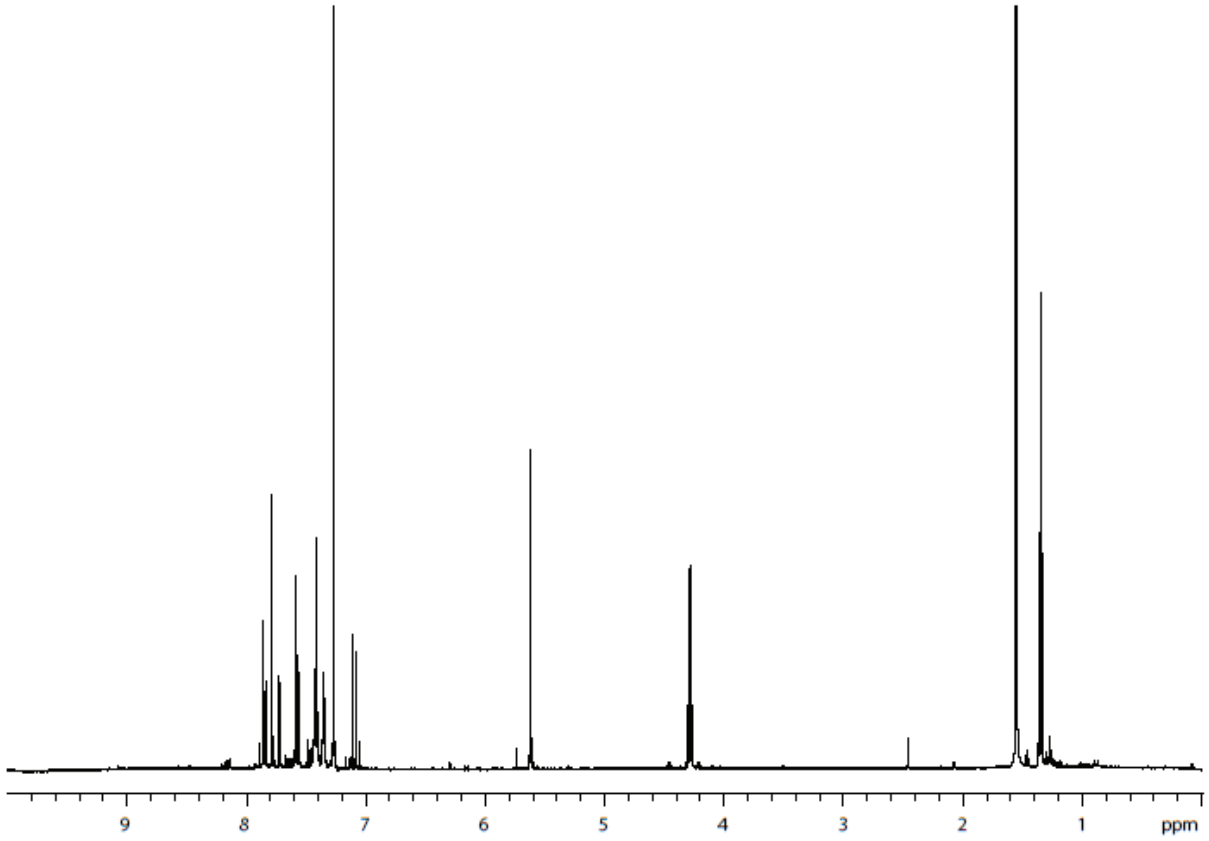

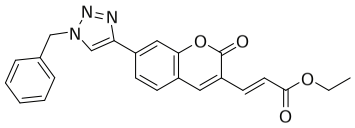

2.7.3

^{13}C NMR (125 MHz, $CDCl_3$)

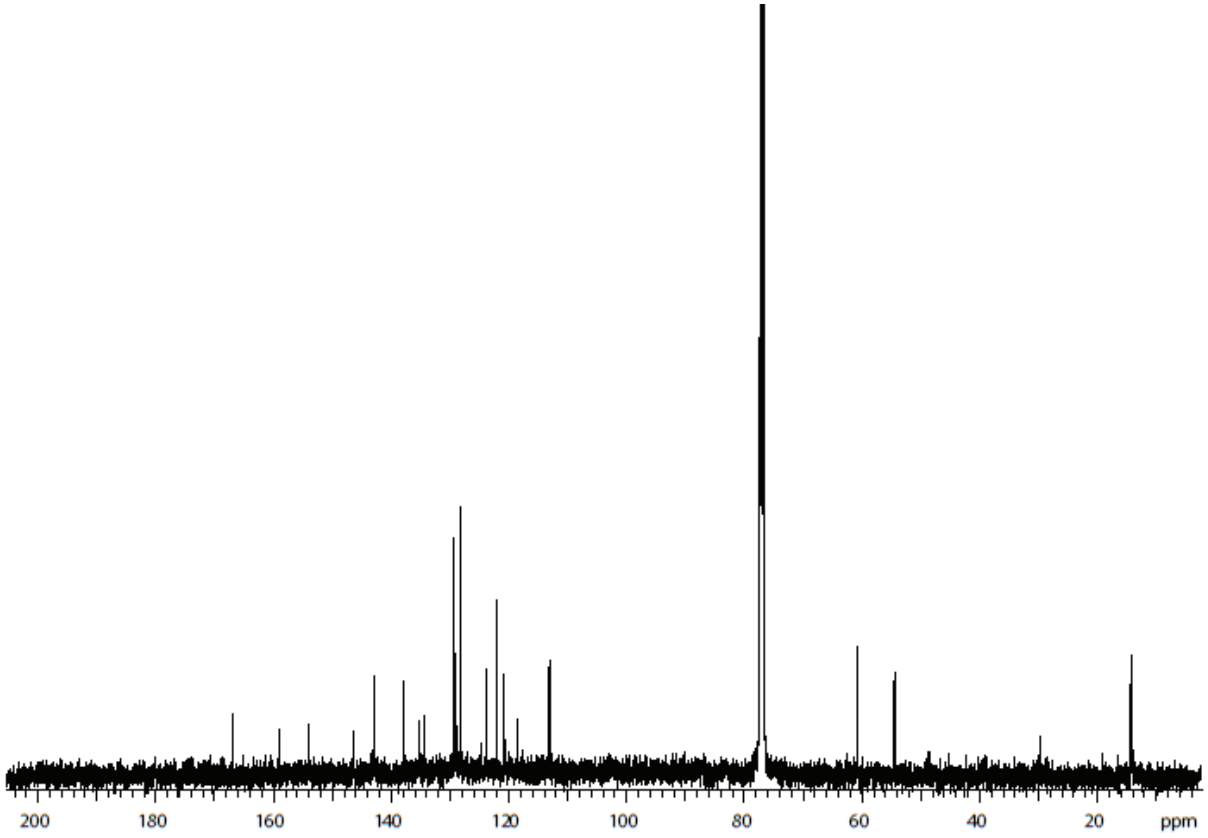

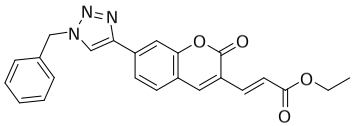

2.7.3
HSQC NMR (500 MHz, $CDCl_3$)

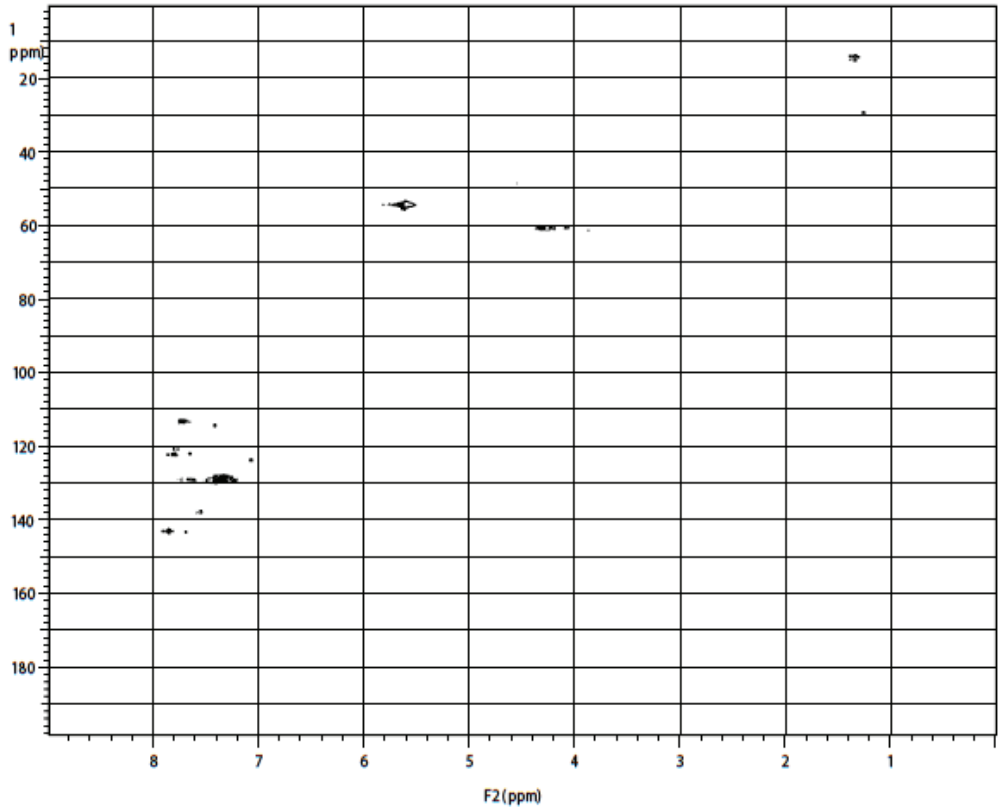

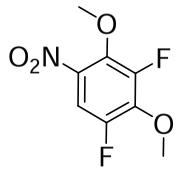

2.9
^{1}H NMR (400 MHz, MeOD)

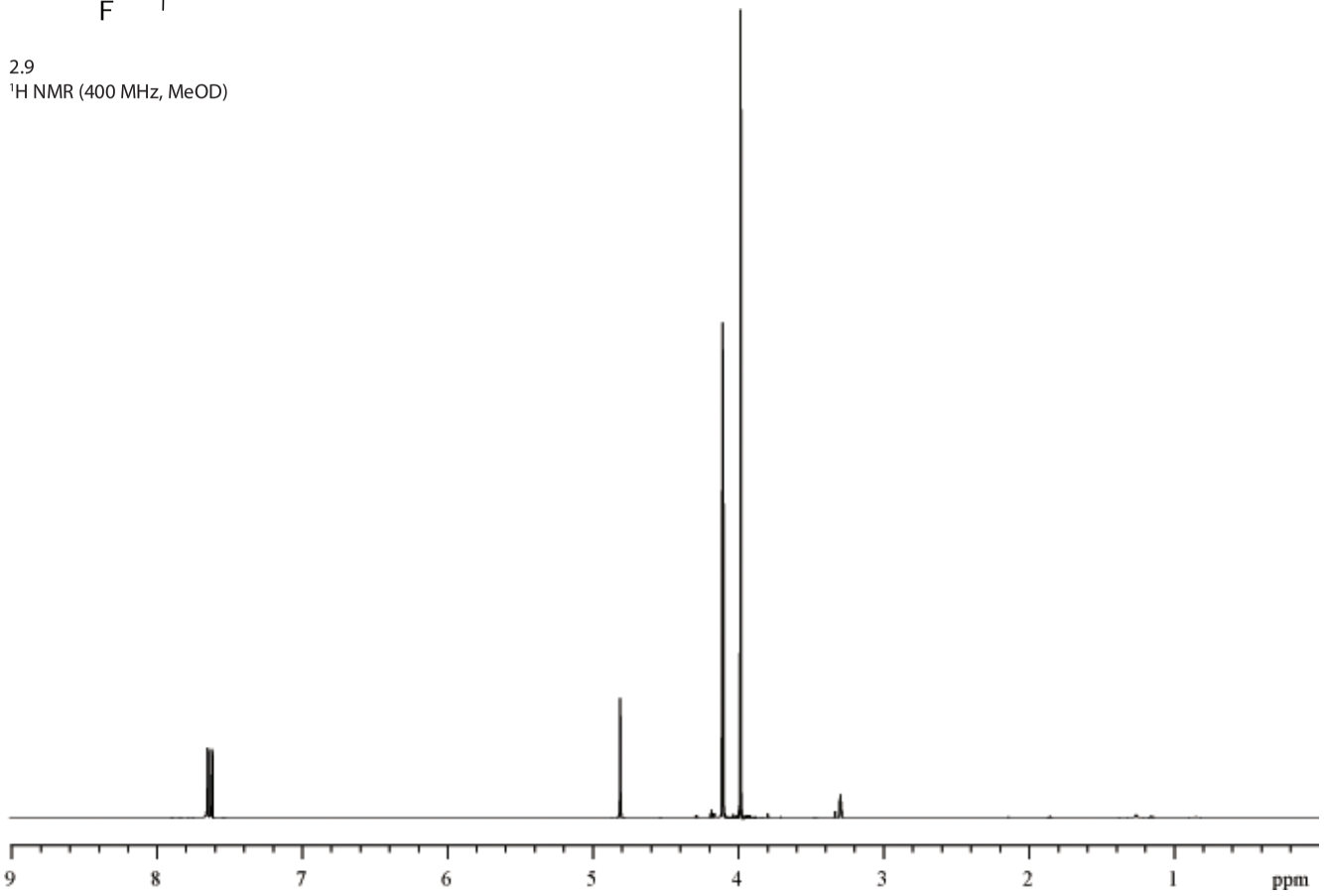

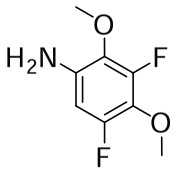

2.10
^{1}H NMR (300 MHz, $CDCl_3$)

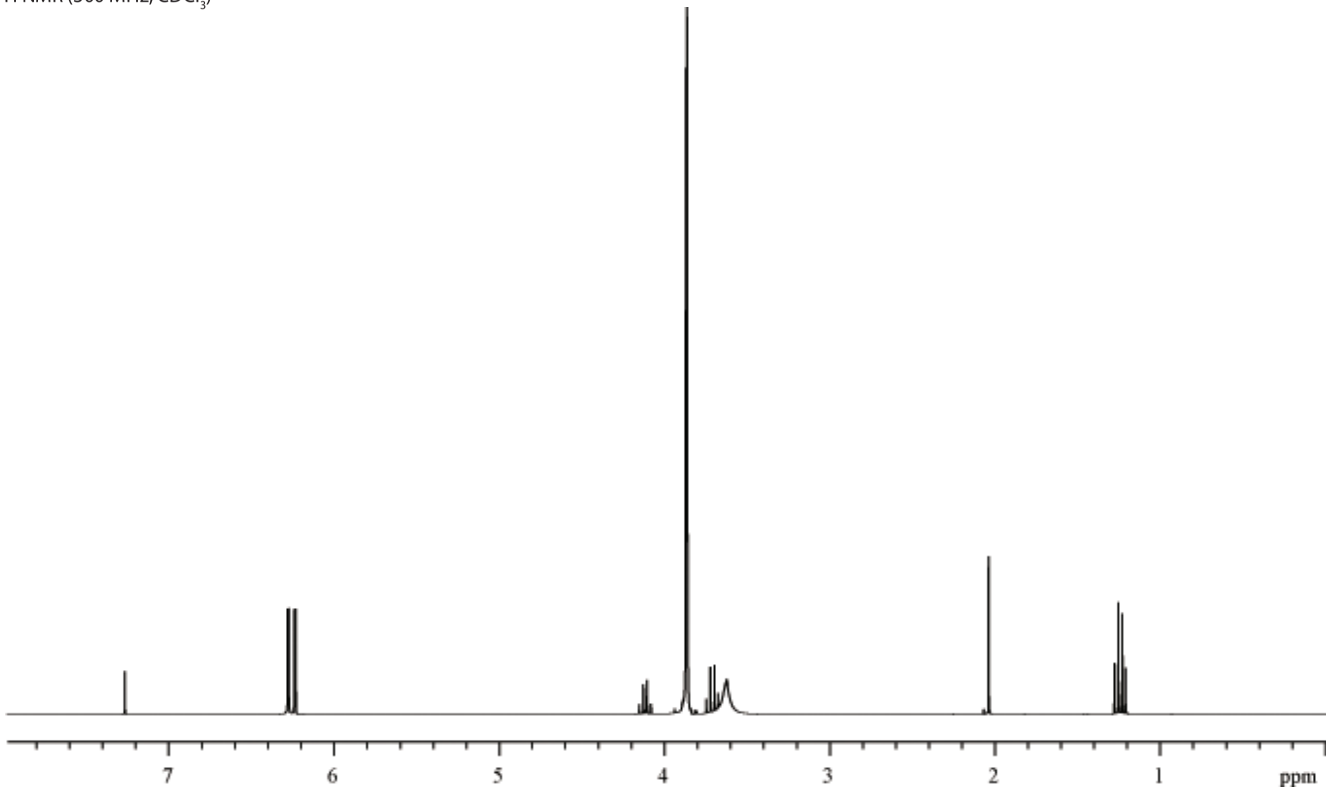

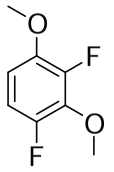

2.11
^{1}H NMR (400 MHz, $CDCl_3$)

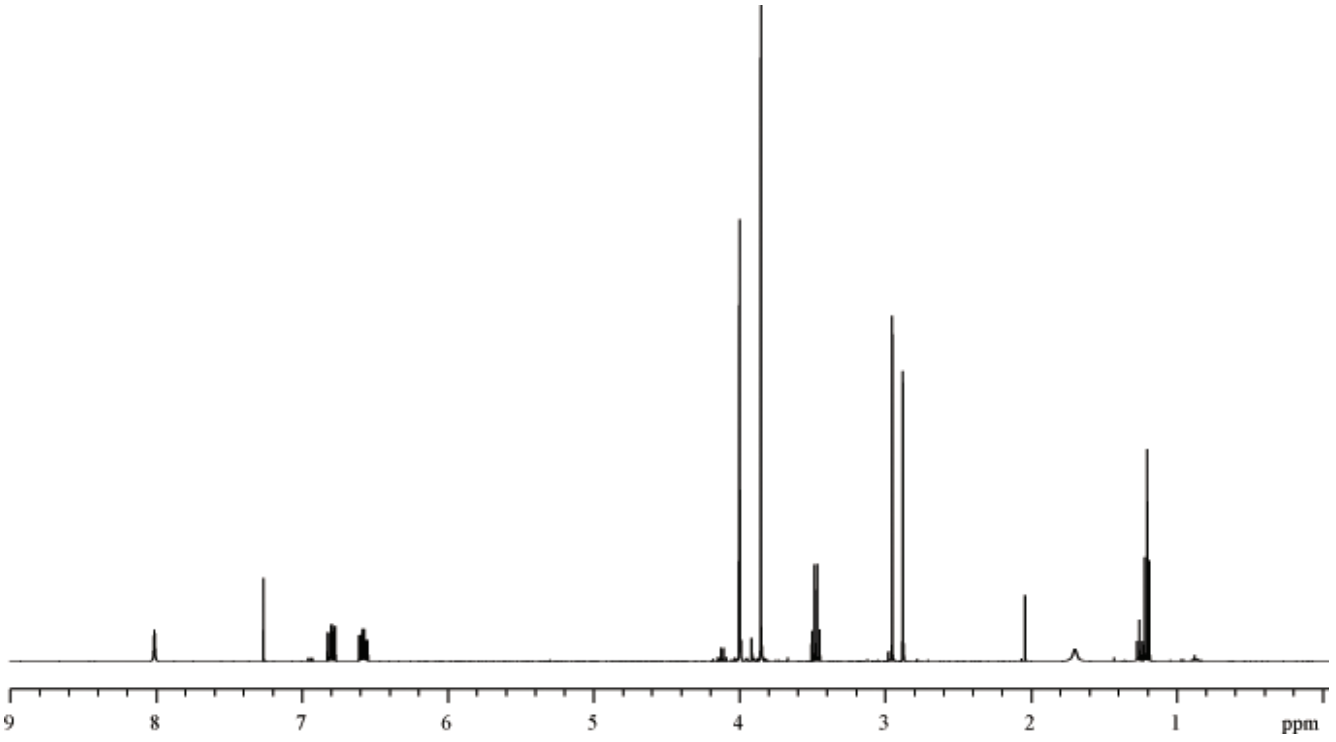

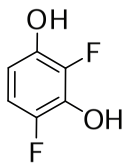

2.12
^{1}H NMR (300 MHz, $CDCl_3$

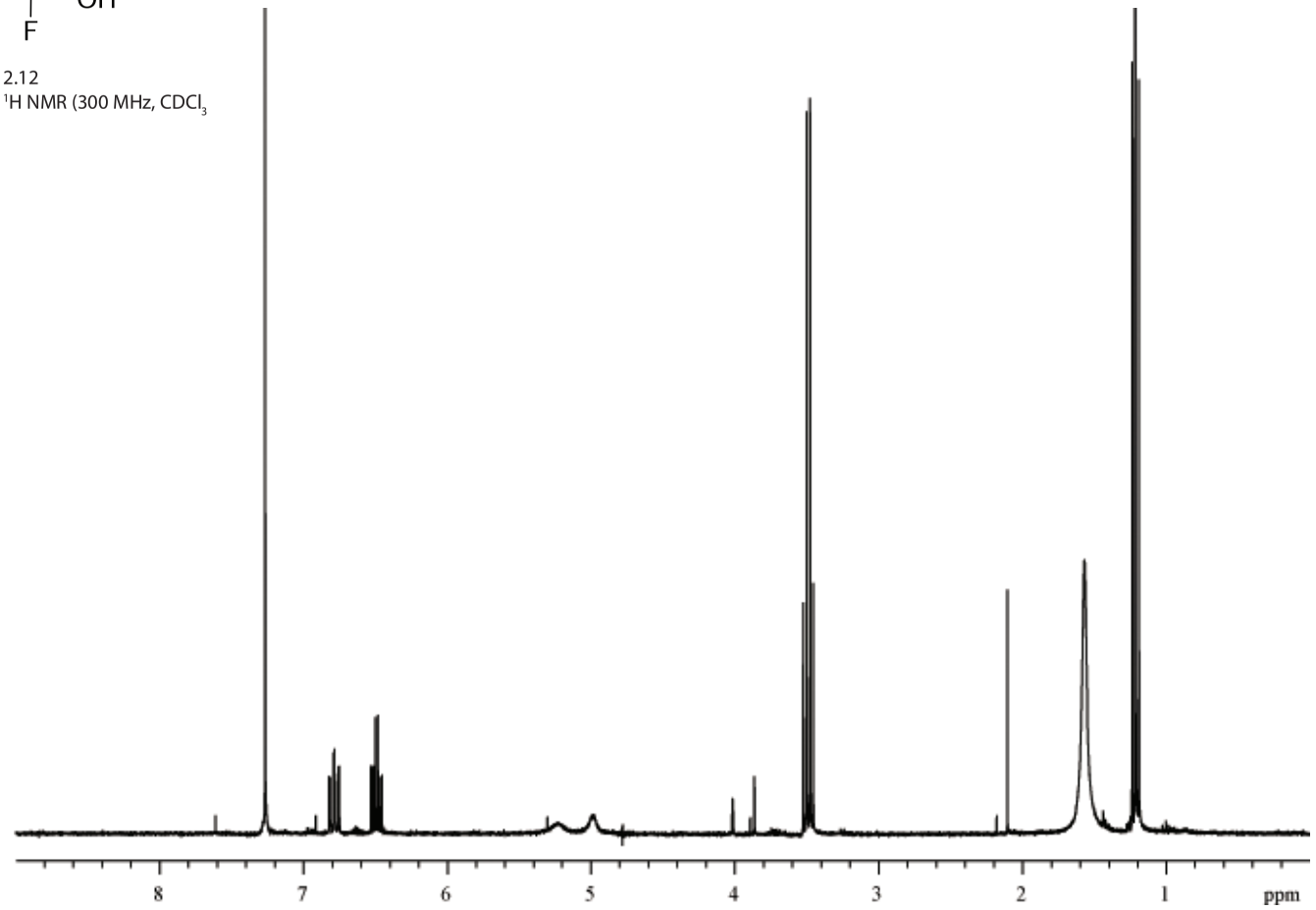

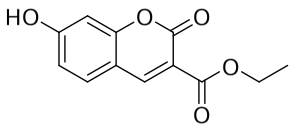

2.14

^{1}H NMR (400 MHz, DMSO-D_6)

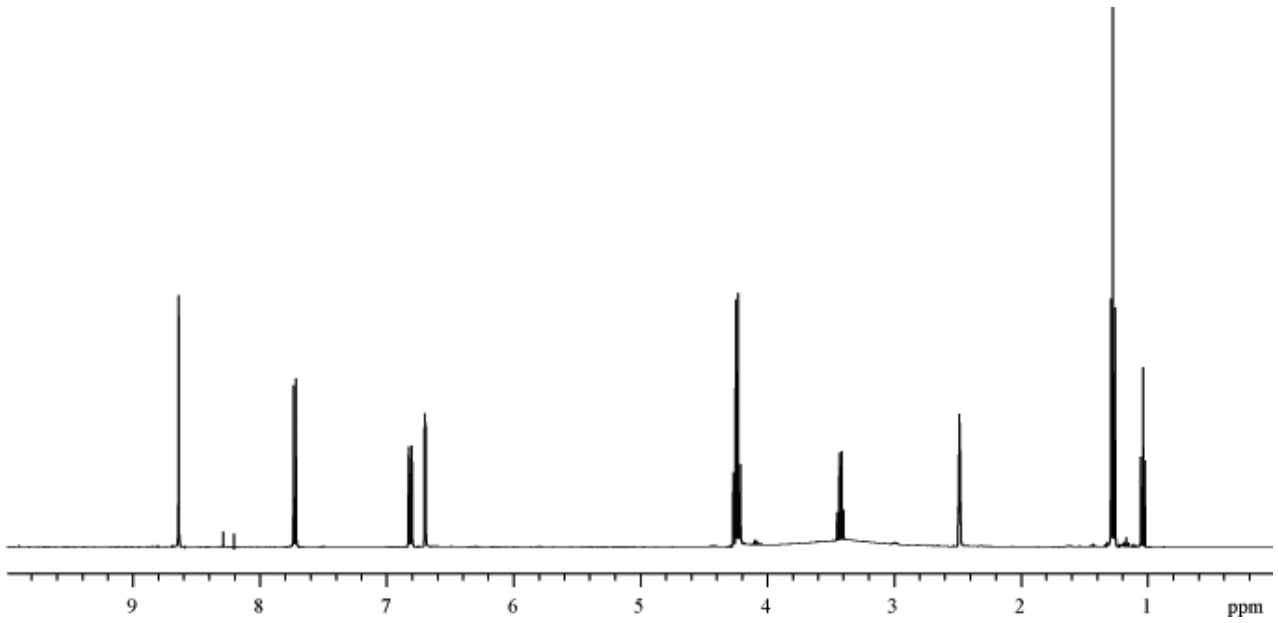

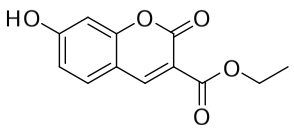

2.14
APT ^{13}C NMR (100 MHz, DMSO-D_6)

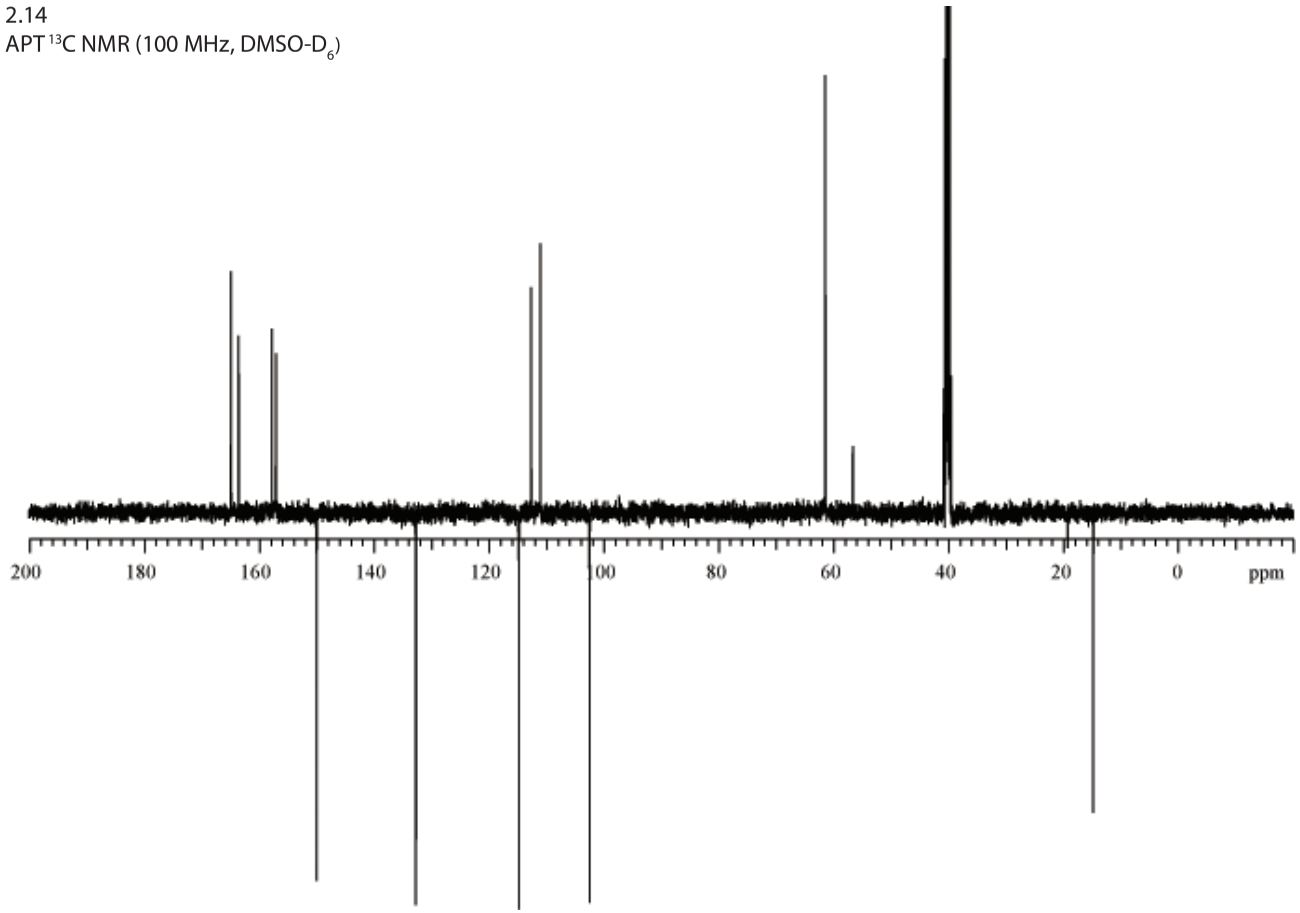

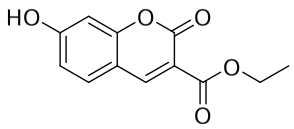

2.14

^{1}H COSY NMR (400 MHz, DMSO-D_6)

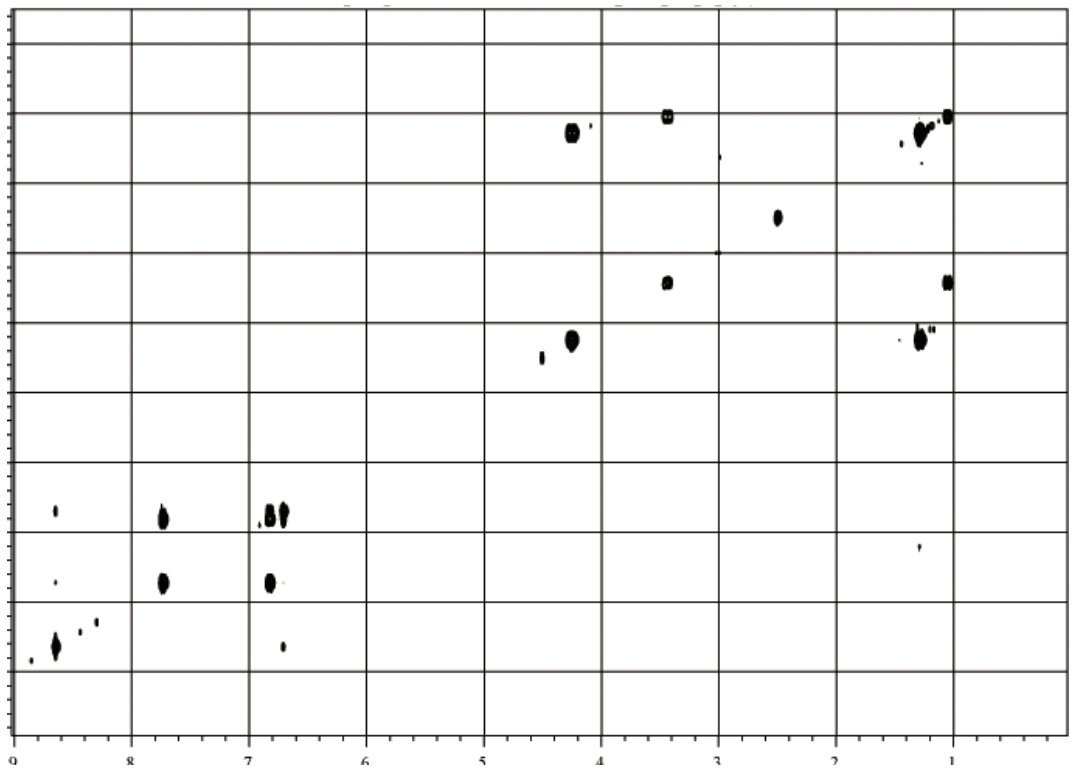

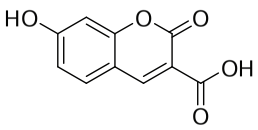

2.15

^{1}H NMR (400 MHz, DMSO -D_6)

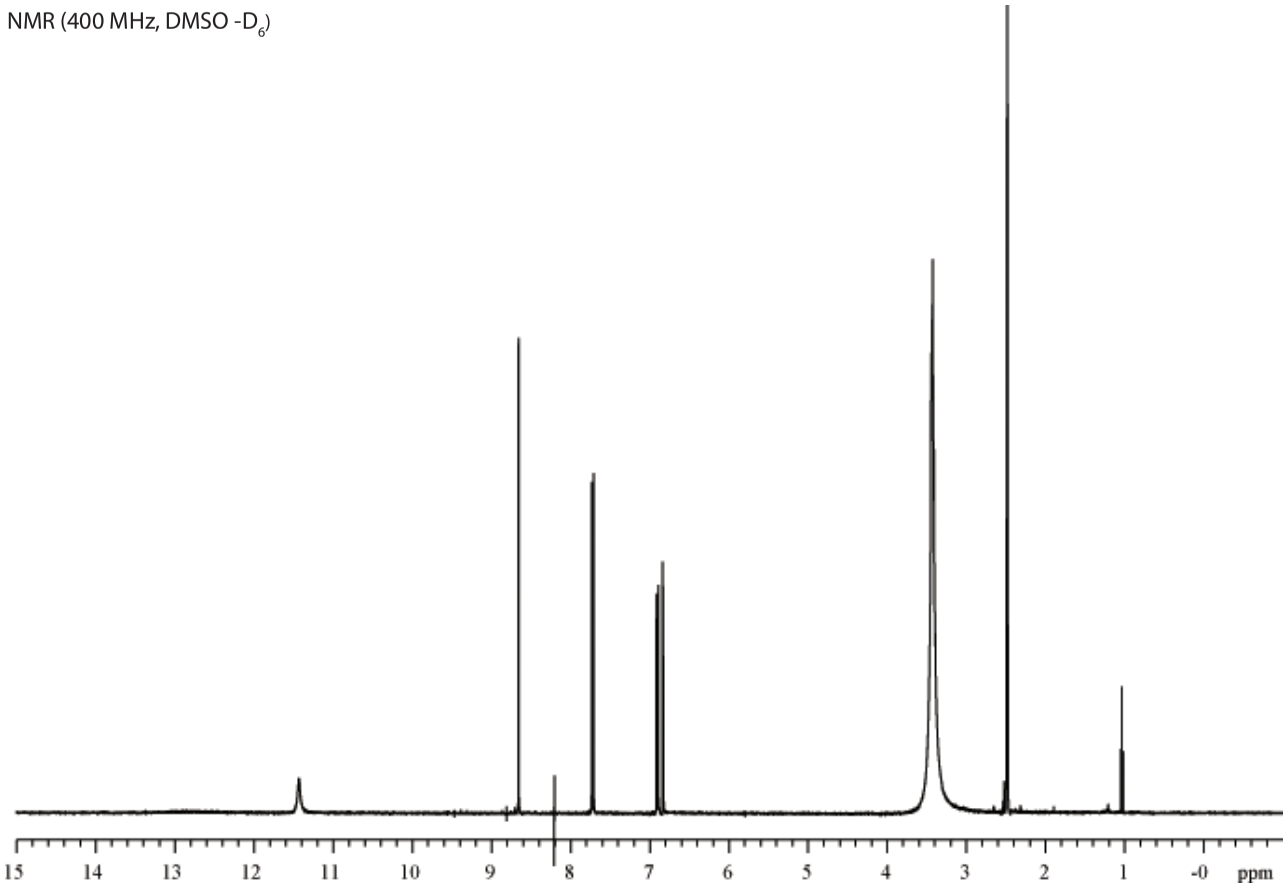

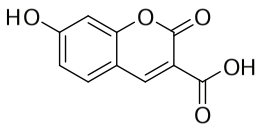

2.15

^{13}C NMR (100 MHz, DMSO -D_6)

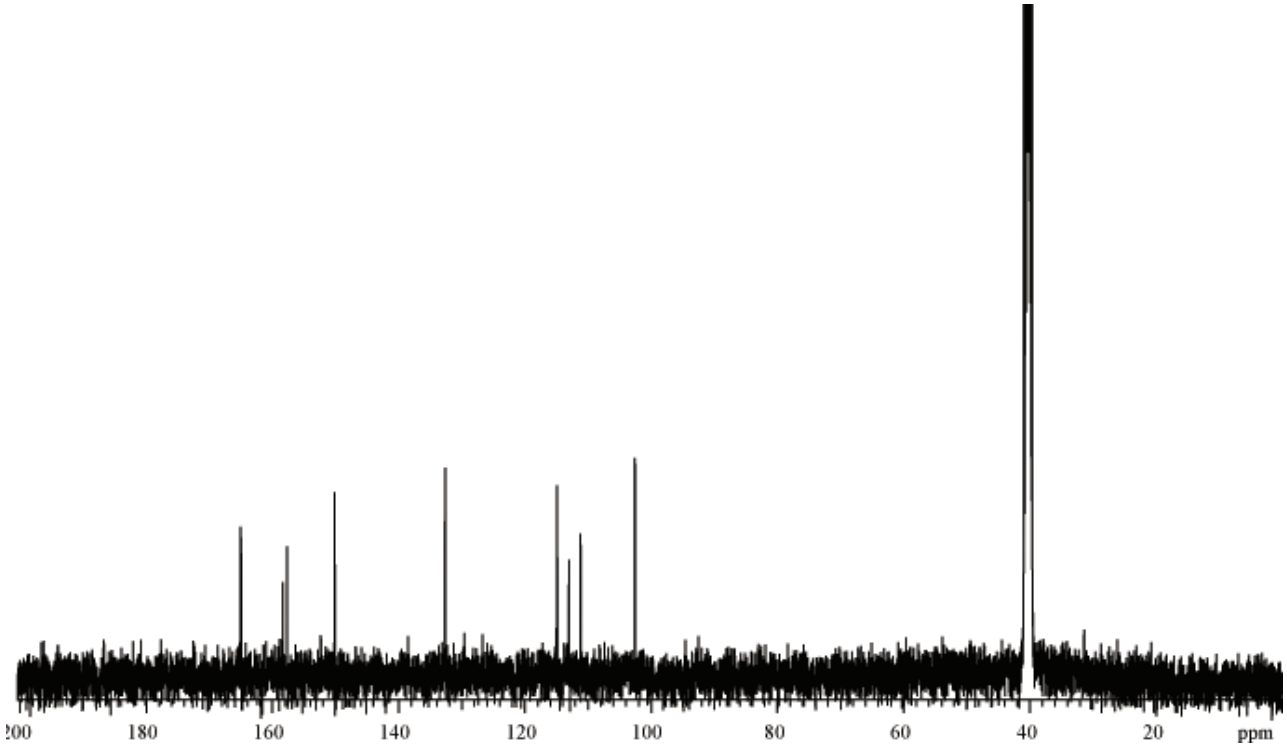

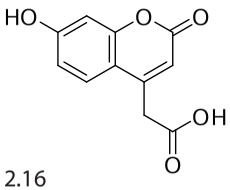

2.16

^{1}H NMR (500 MHz, CD_3OD)

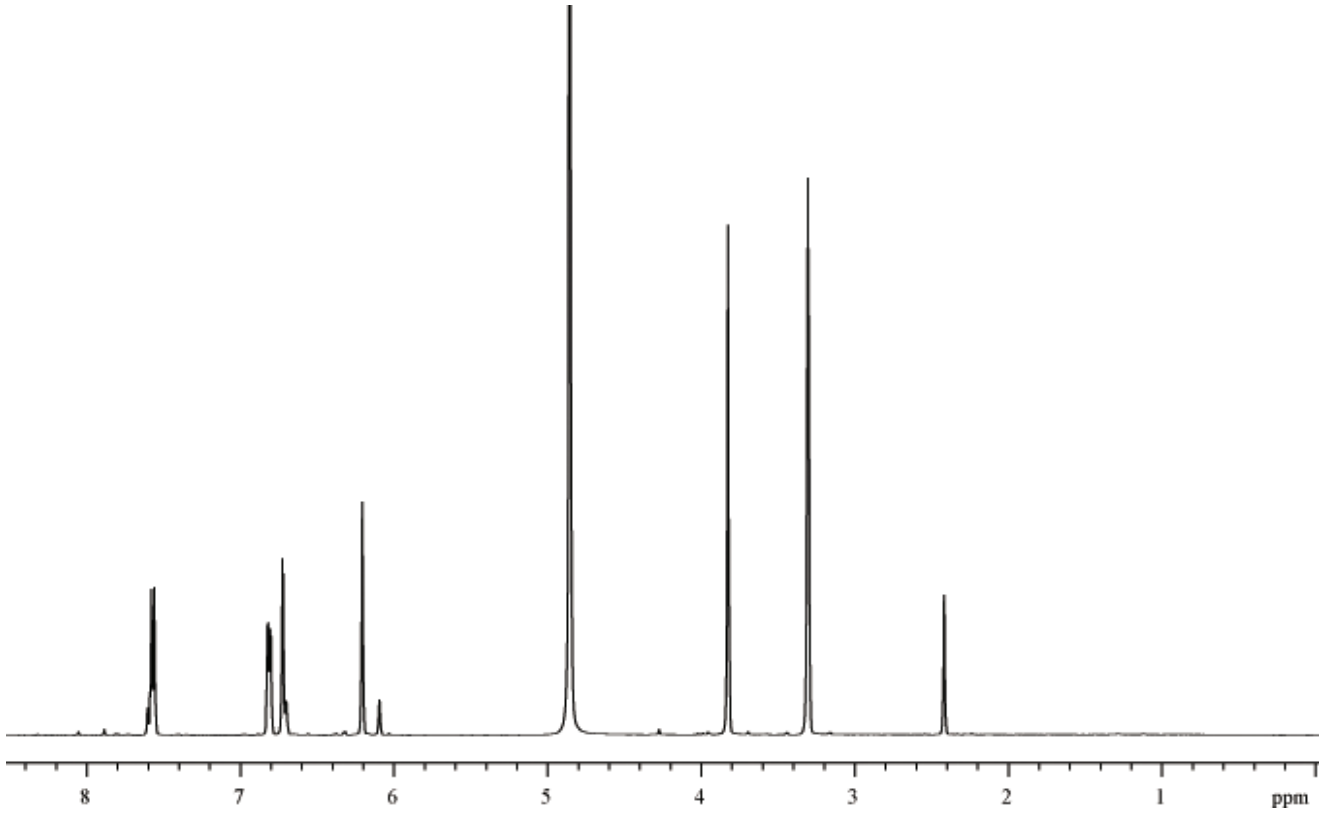

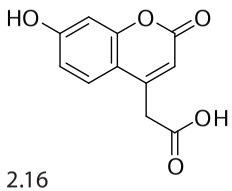

2.16

^{1}H Cosy NMR (500 MHz, CD_3OD)

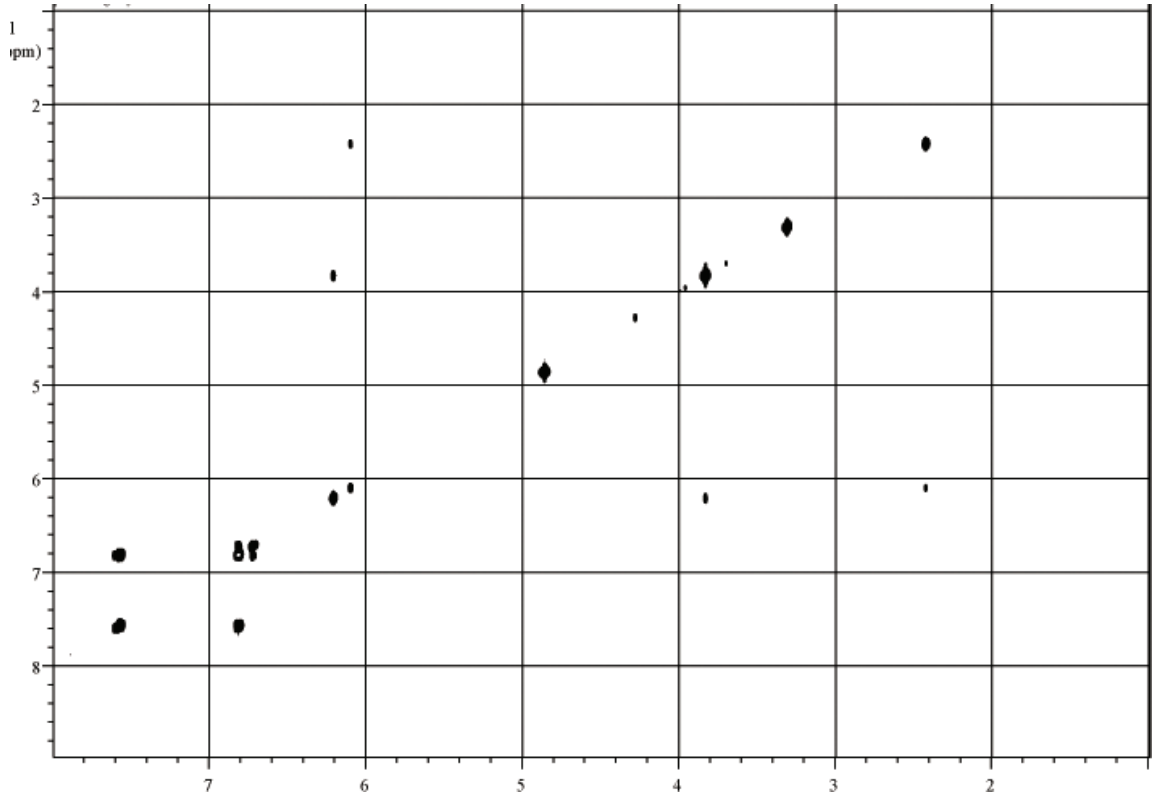

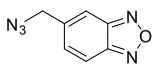

3.2
^{1}H NMR (400 MHz, $CDCl_3$)

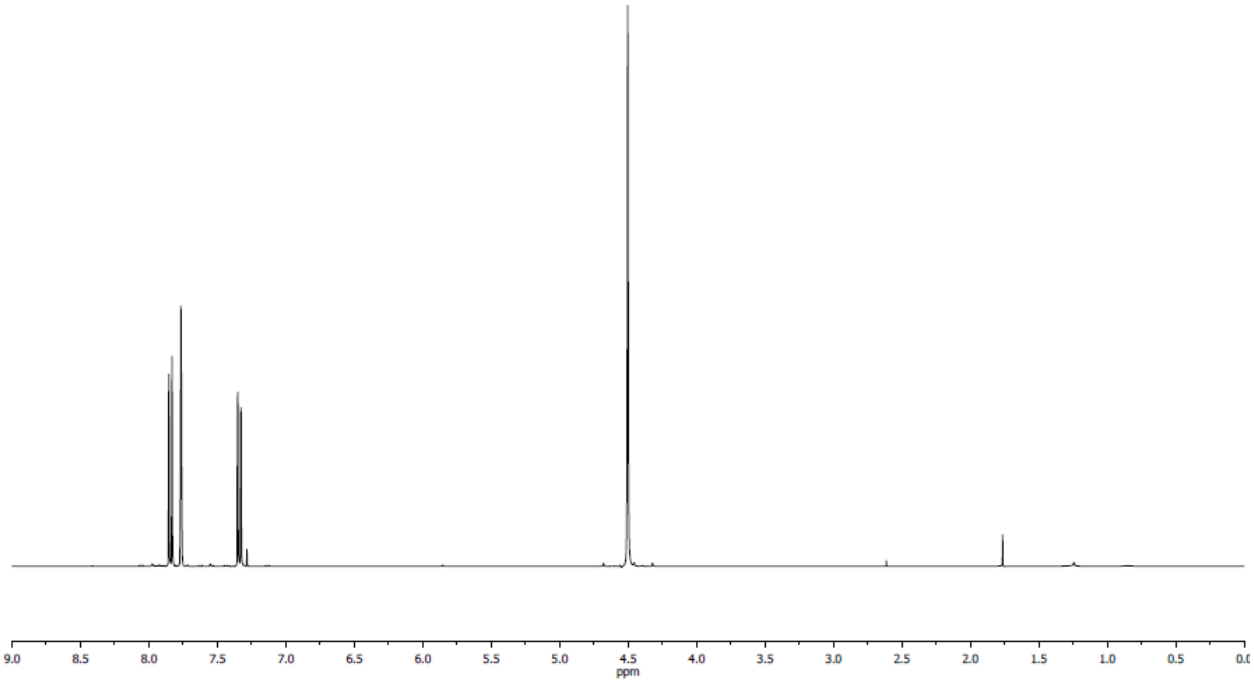

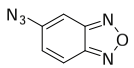

3.4
^{1}H NMR (400 MHz, $CDCl_3$)

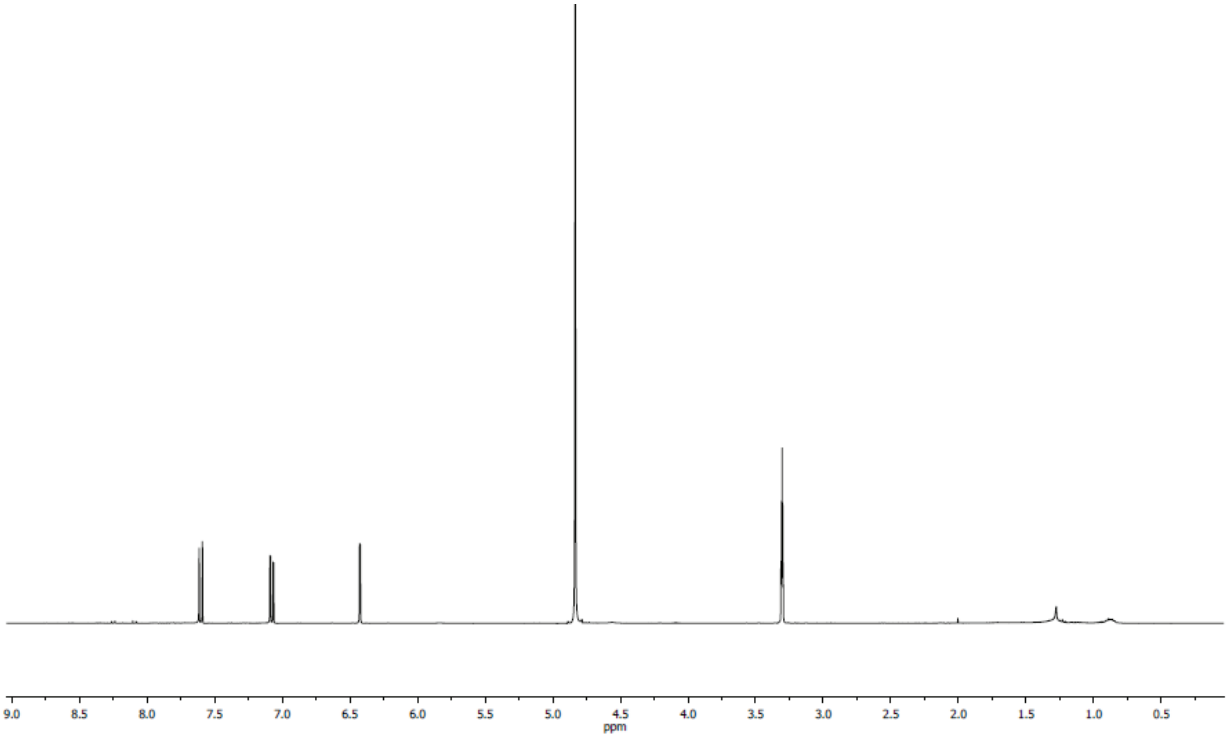

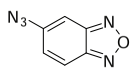

3.4
APT ^{13}C NMR (100 MHz, $CDCl_3$)

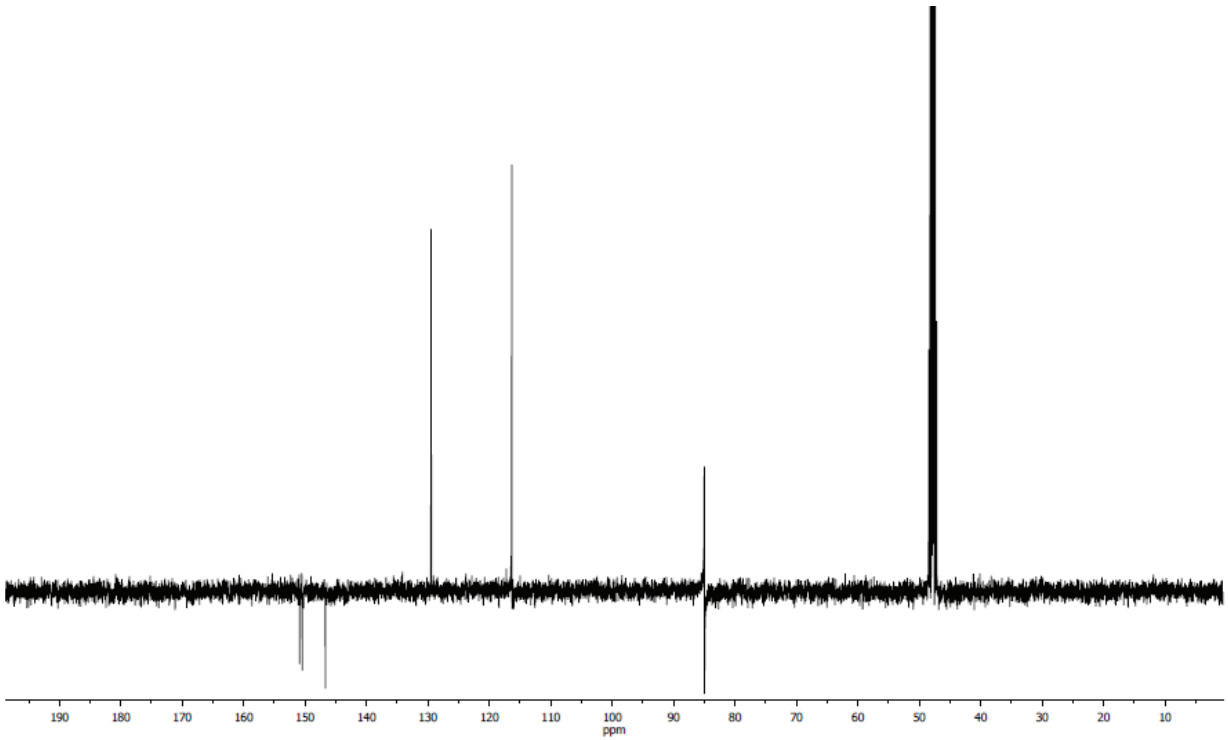

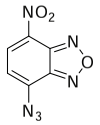

3.6

^{1}H NMR (400 MHz, $CDCl_3$)

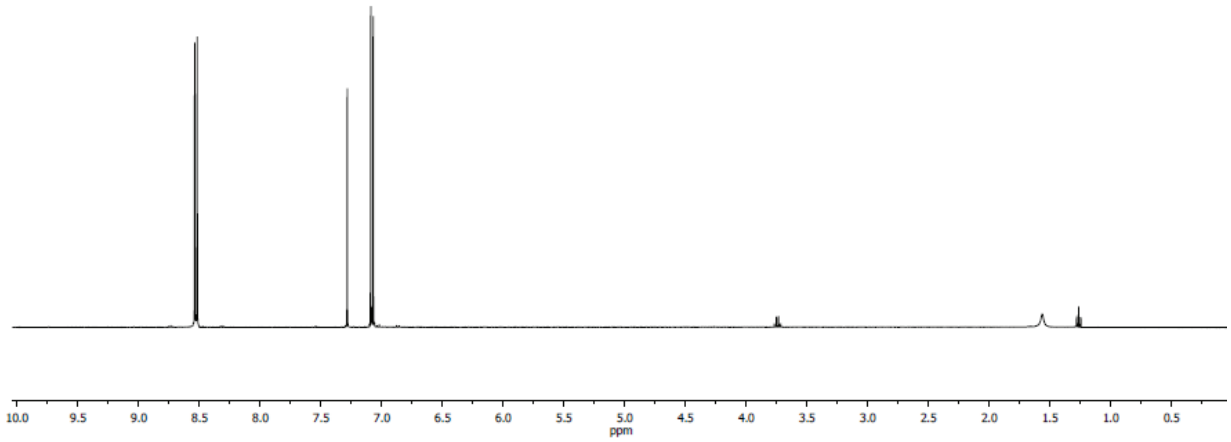

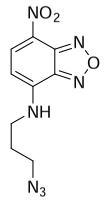

3.8

^{1}H NMR (400 MHz, $CDCl_3$)

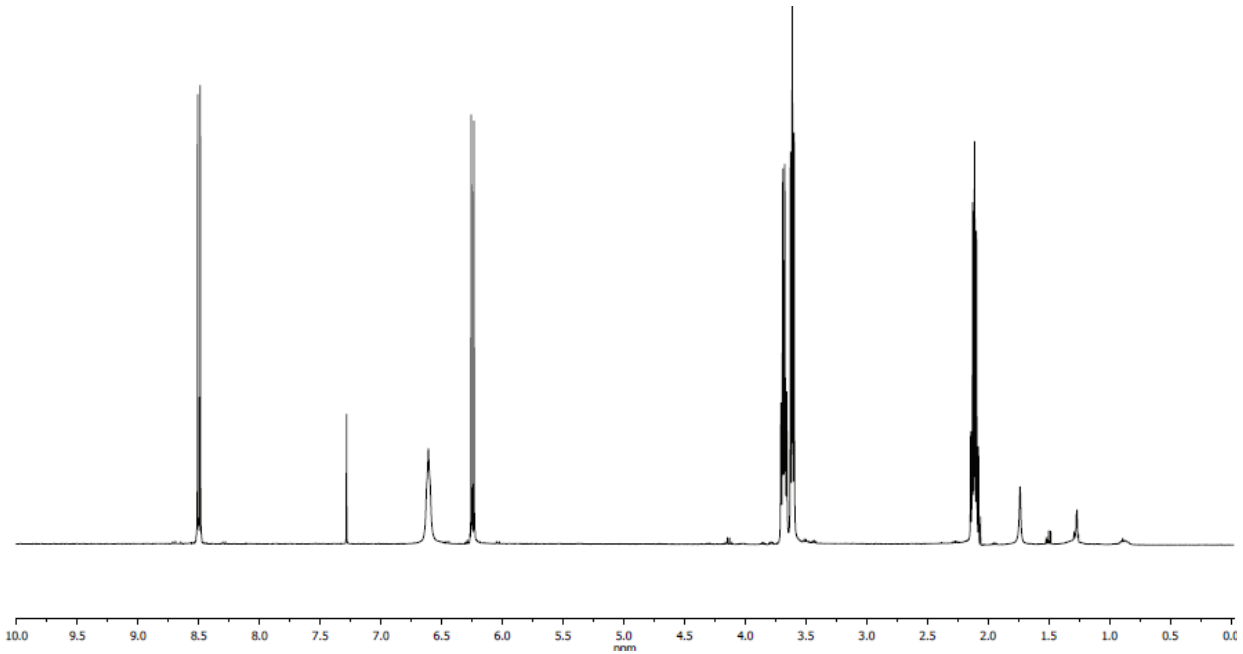

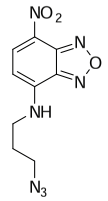

3.8

^{13}C NMR (100 MHz, $CDCl_3$)

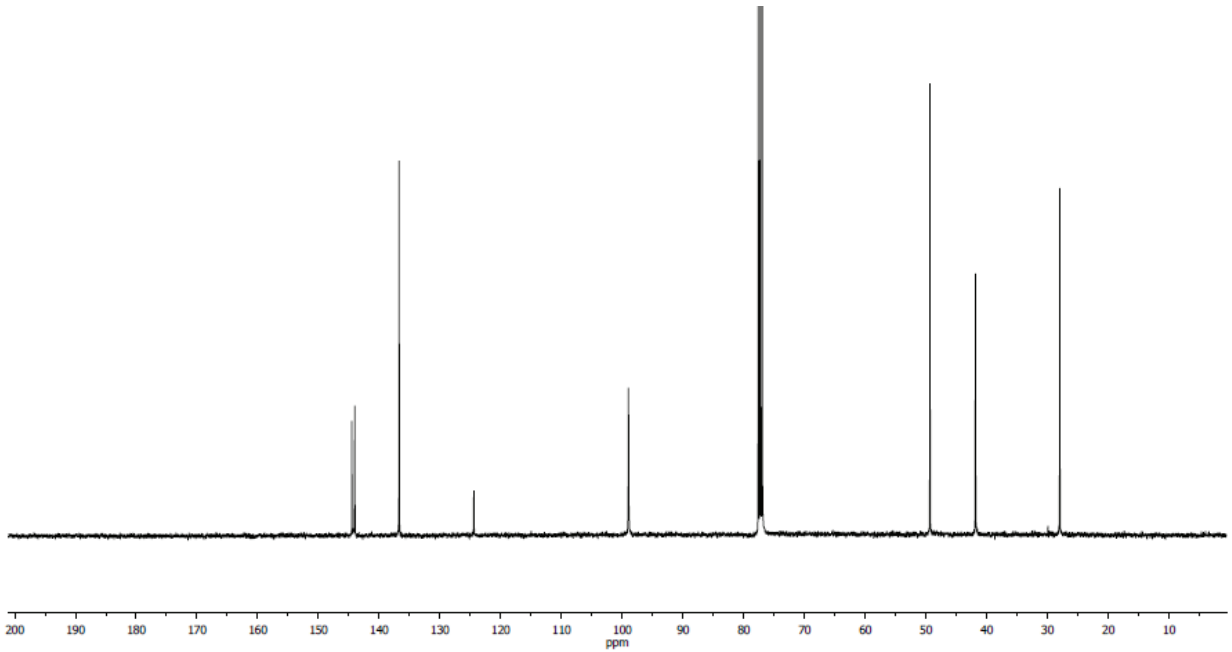

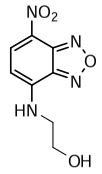

3.9

^{1}H NMR (400 MHz, CD_3OD)

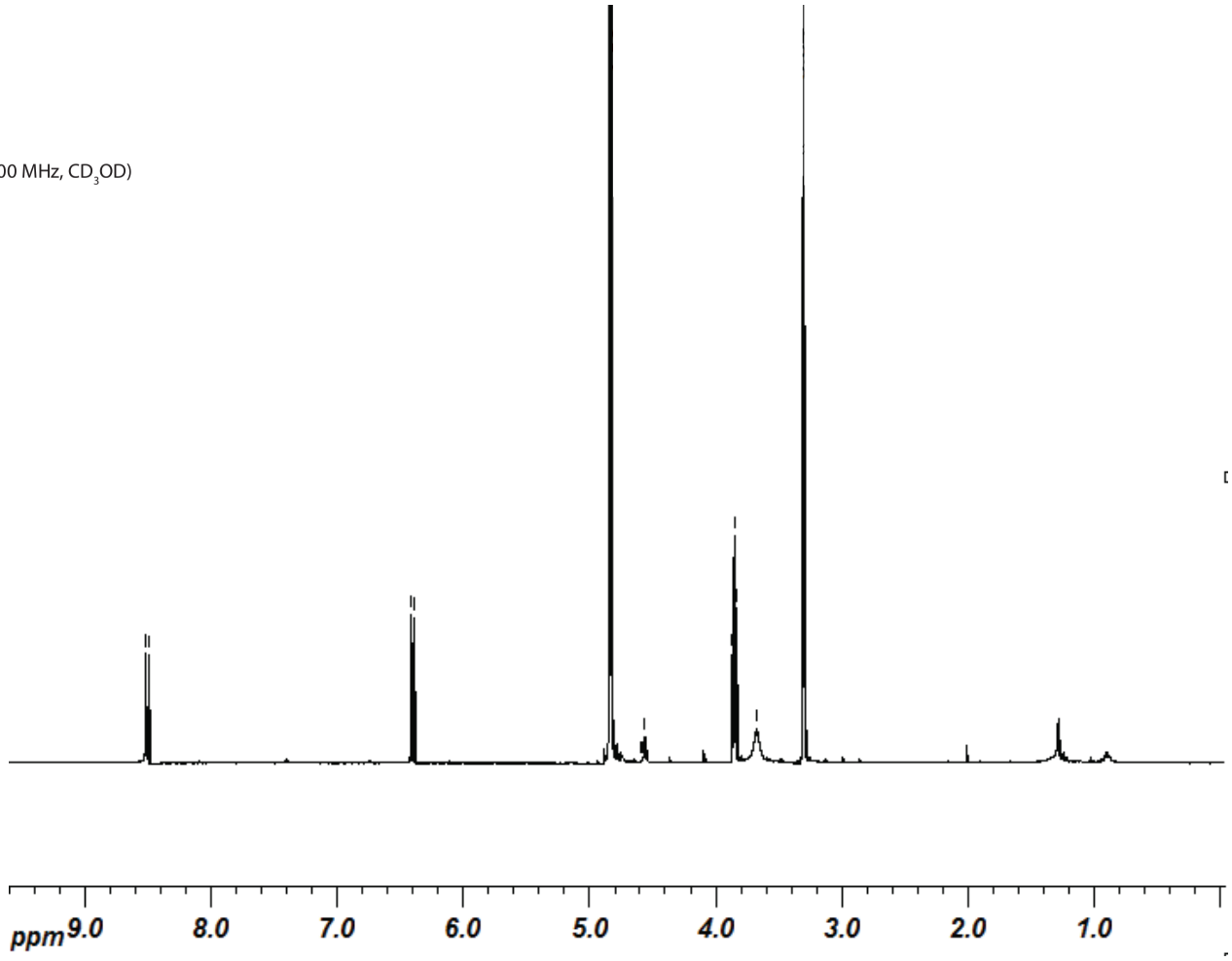

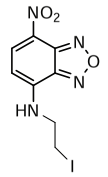

3.10

^{1}H NMR (400 MHz, $CDCl_3$)

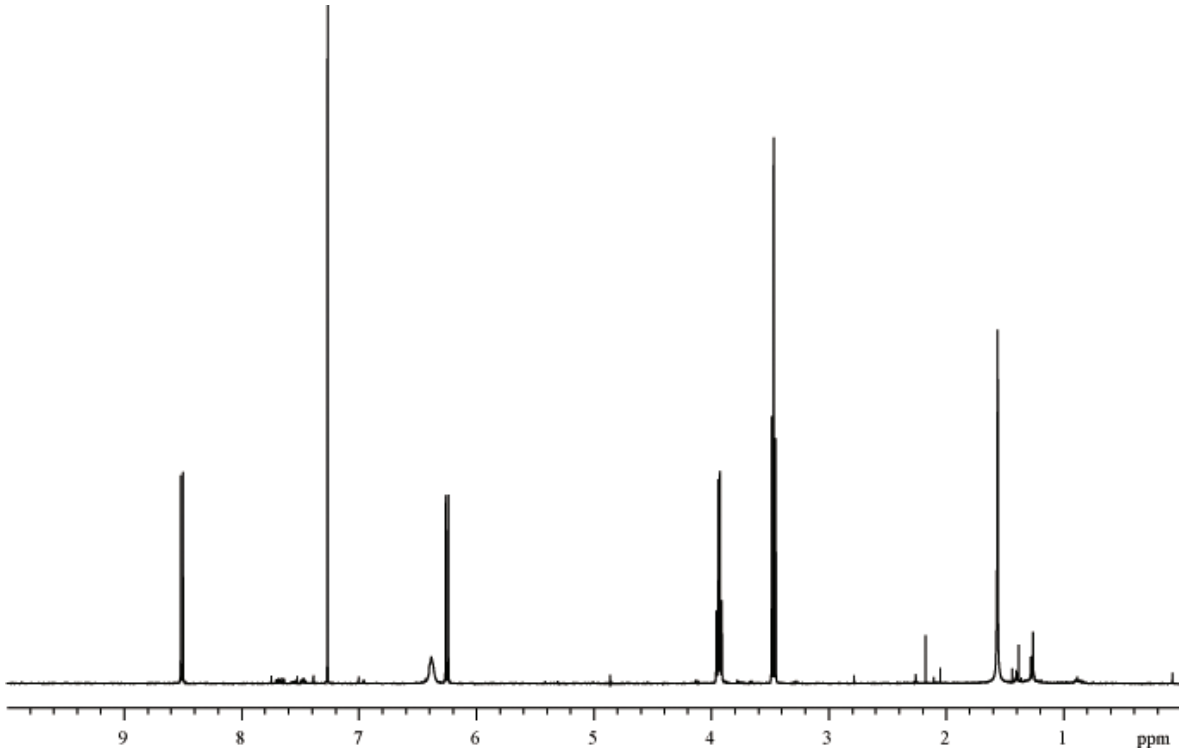

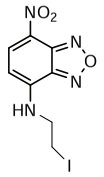

3.10

^{13}C NMR (100 MHz, $CDCl_3$)

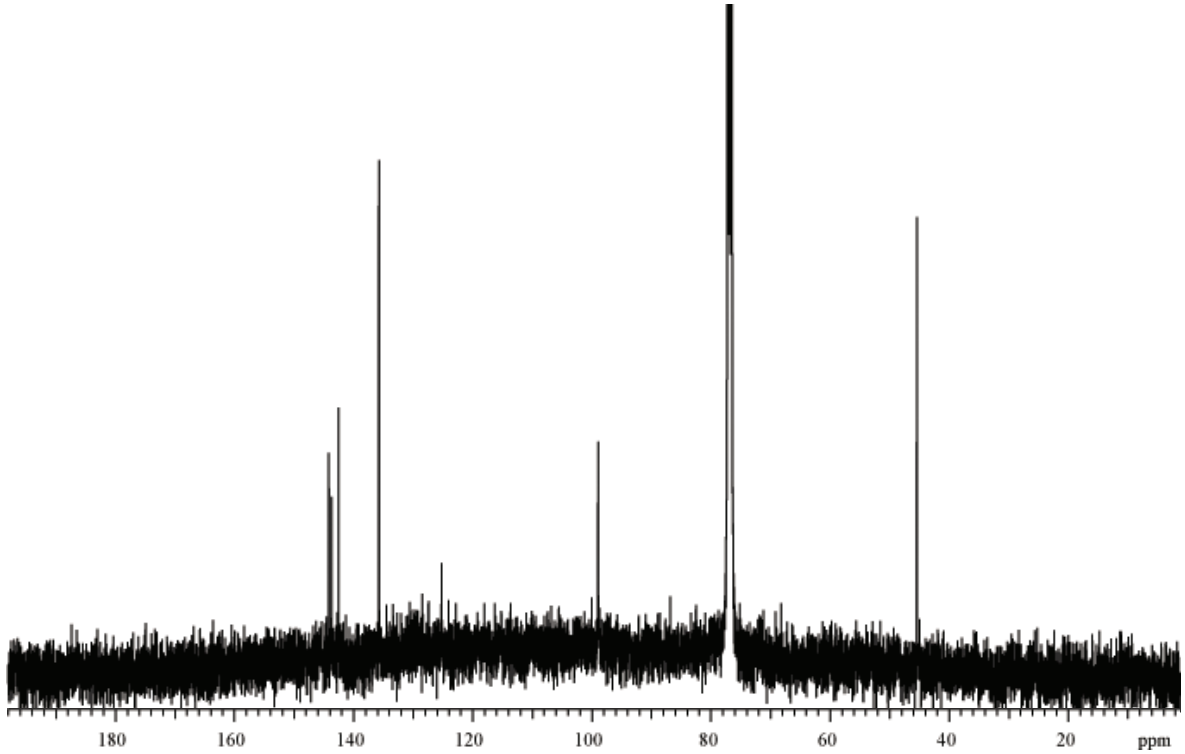

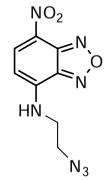

3.11

^{1}H NMR (400 MHz, $CDCl_3$)

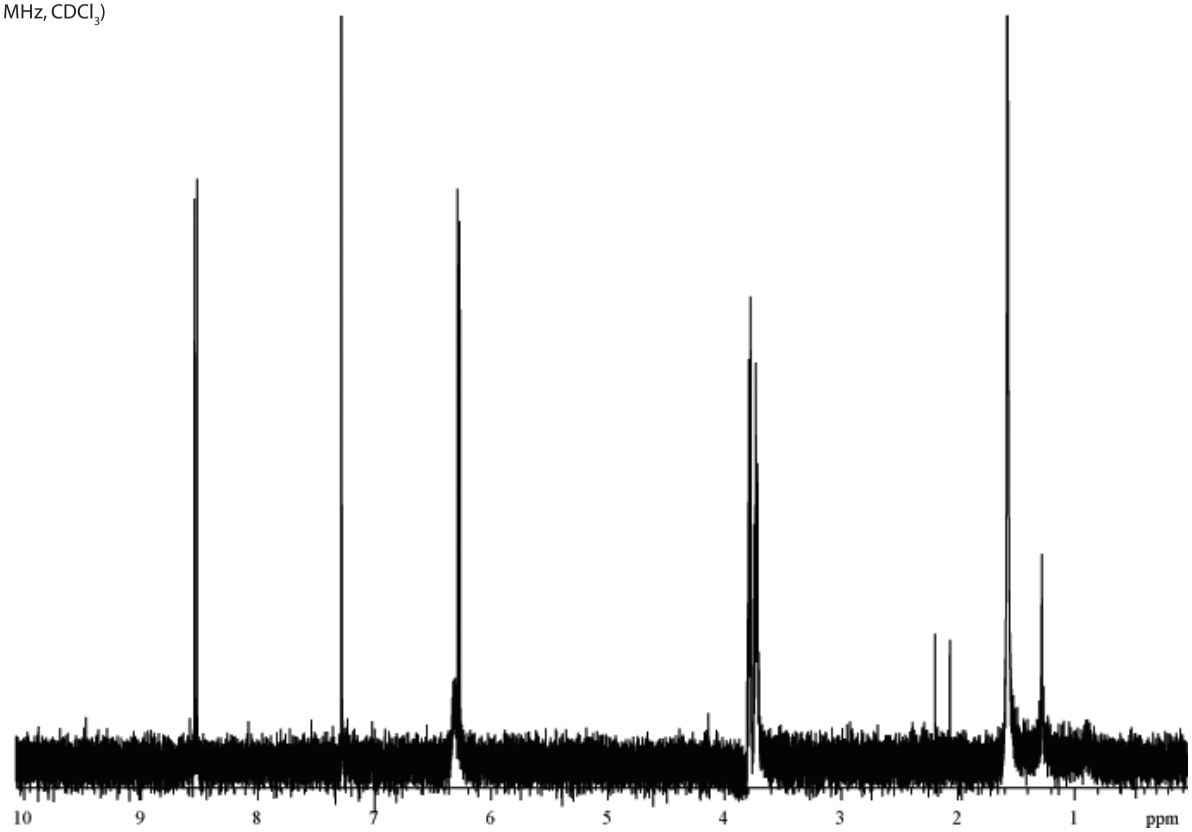

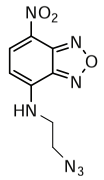

3.11

^{1}H COSY NMR (400 MHz, $CDCl_3$)

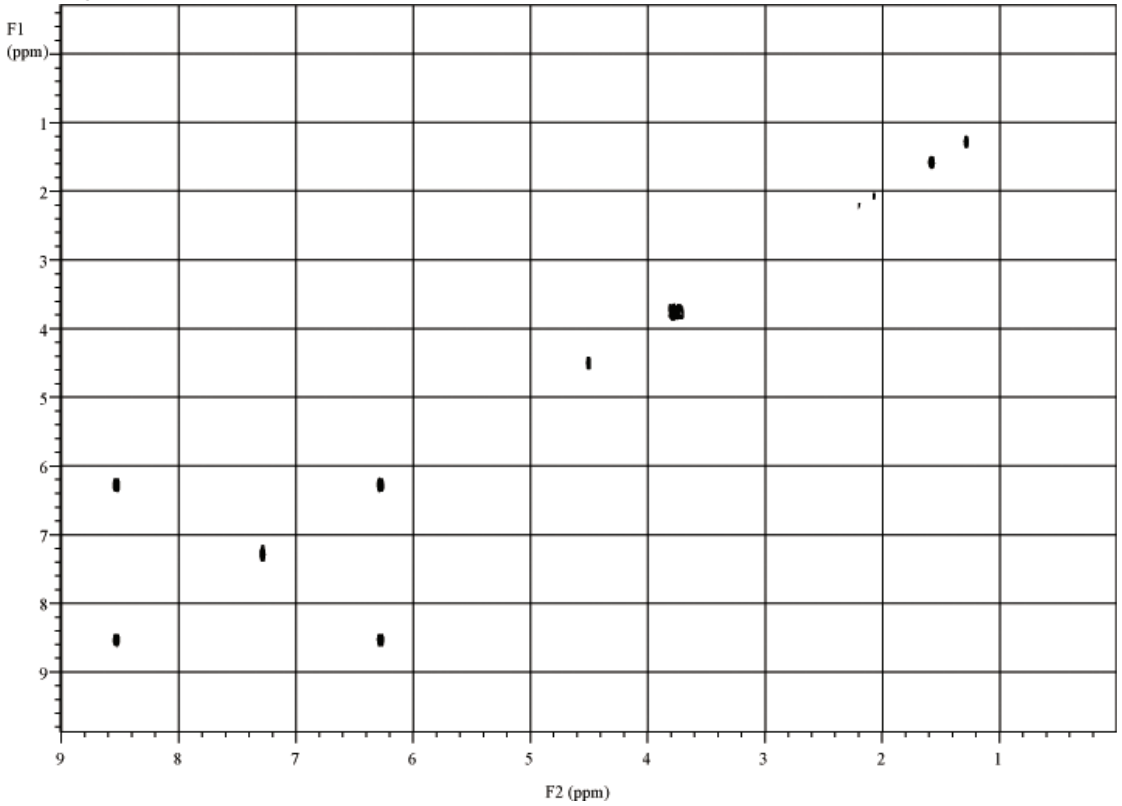

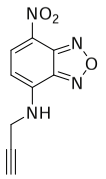

3.12
^{1}H NMR (400 MHz, $CDCl_3$)

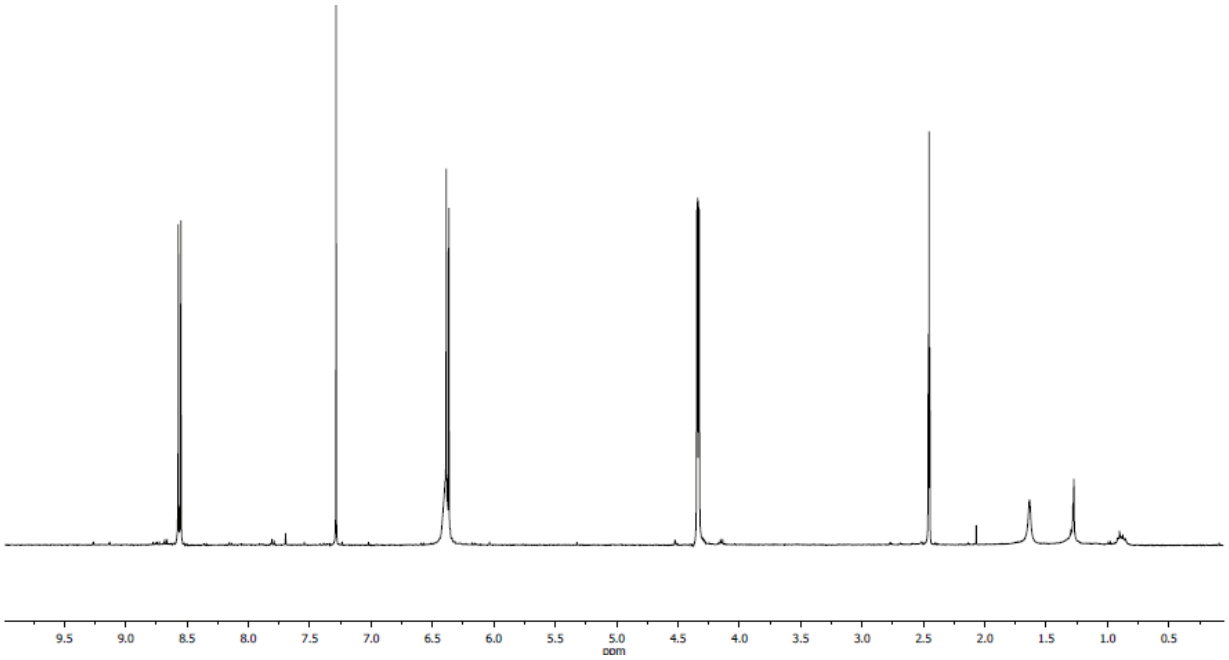

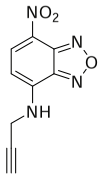

3.12

^{13}C NMR (100 MHz, $CDCl_3$)

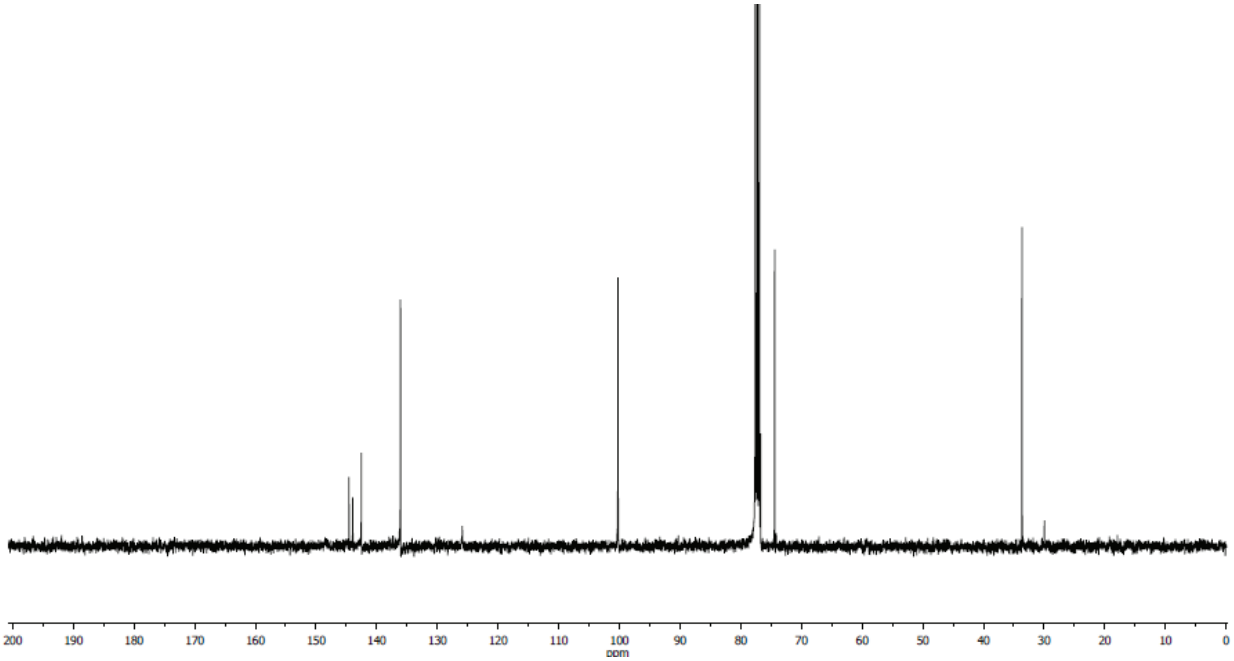

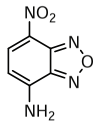

3.13
^{1}H NMR (400 MHz, CD_3OD)

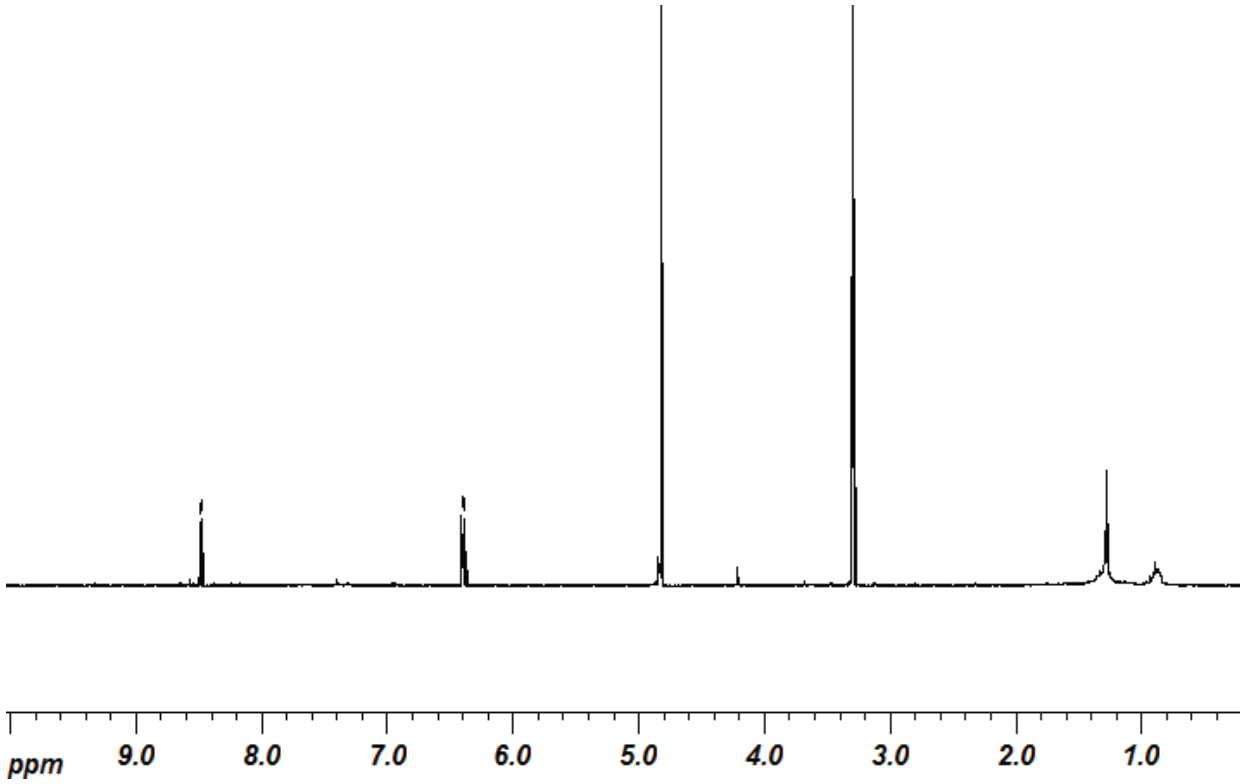

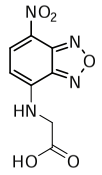

3.14

^{1}H NMR (300 MHz, D_2O)

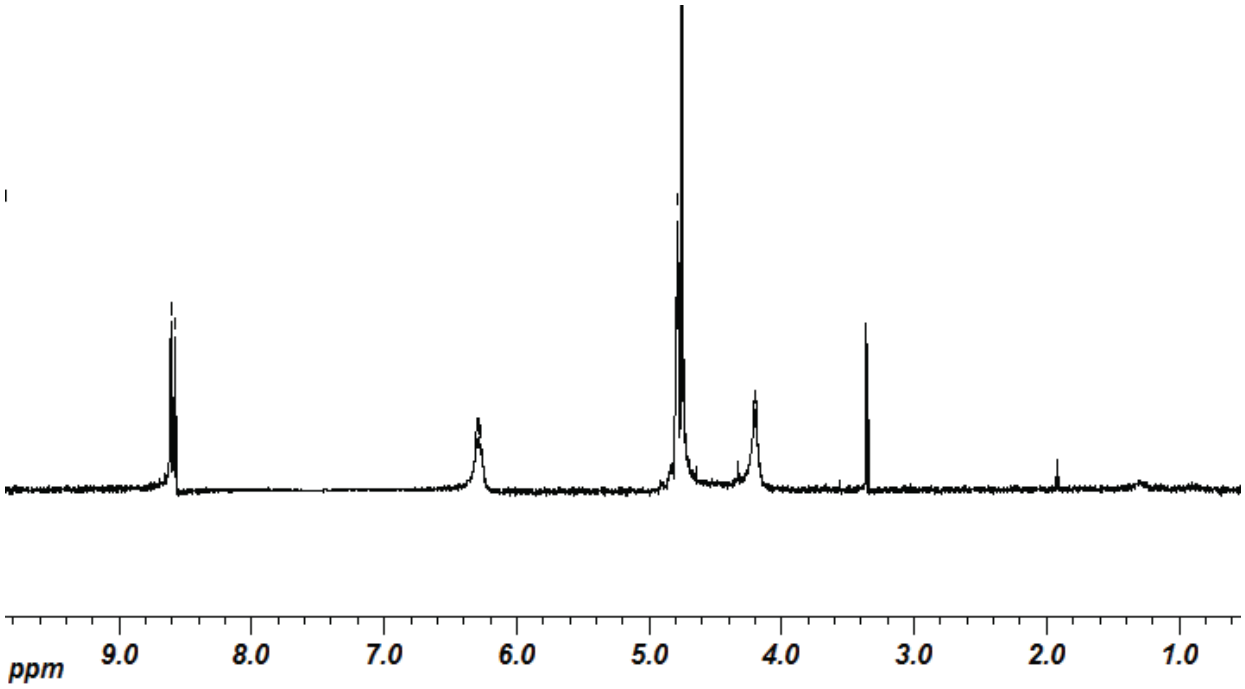

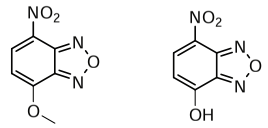

minor

major

3.15 and 3.16
^{1}H NMR (400 MHz, CD_3OD)

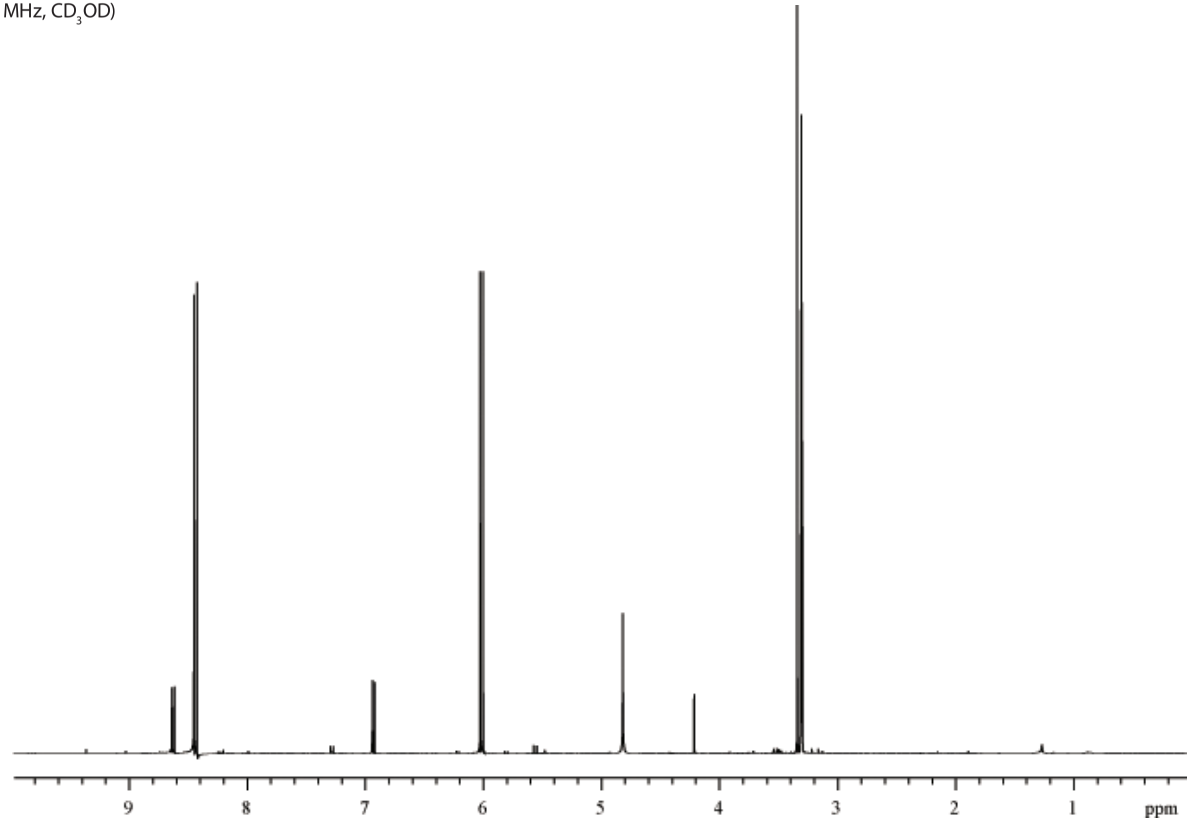

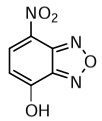

3.16
^{1}H NMR (400 MHz, CD_3OD)

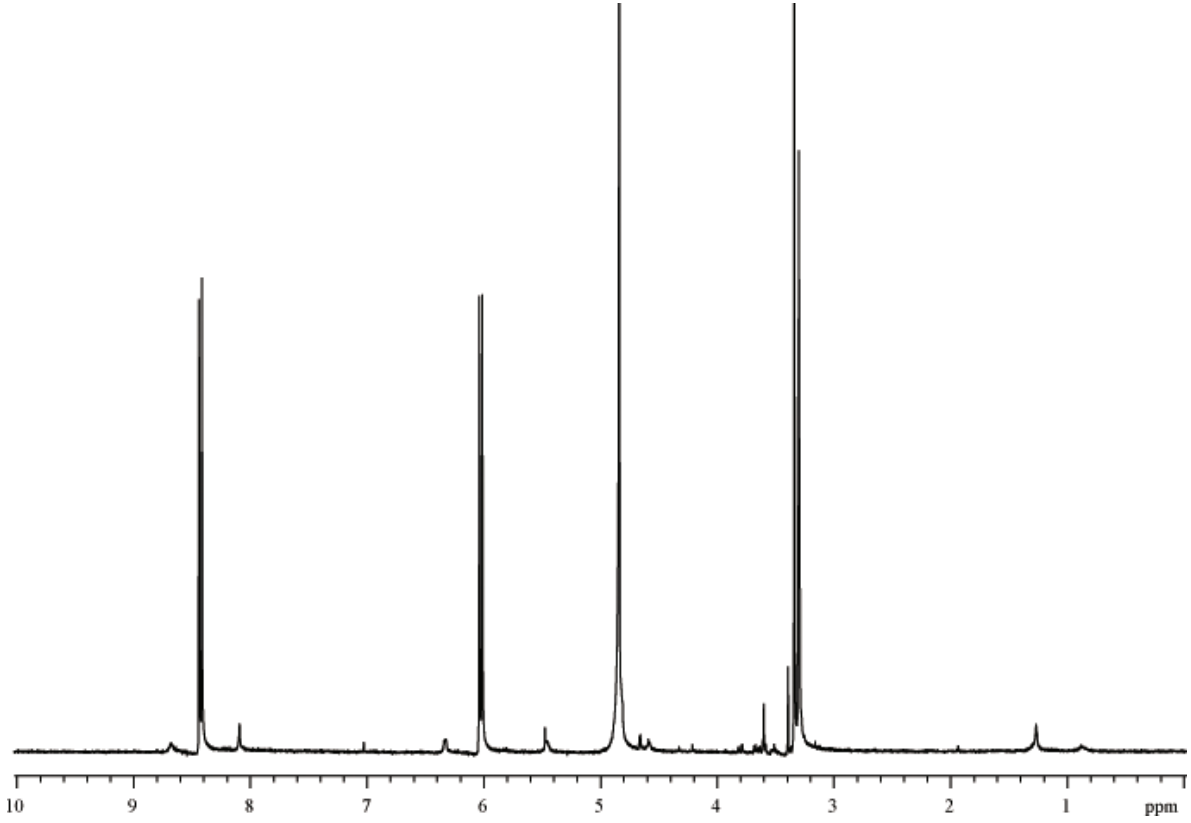

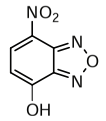

3.16

^{13}C NMR (100 MHz, CD_3OD)

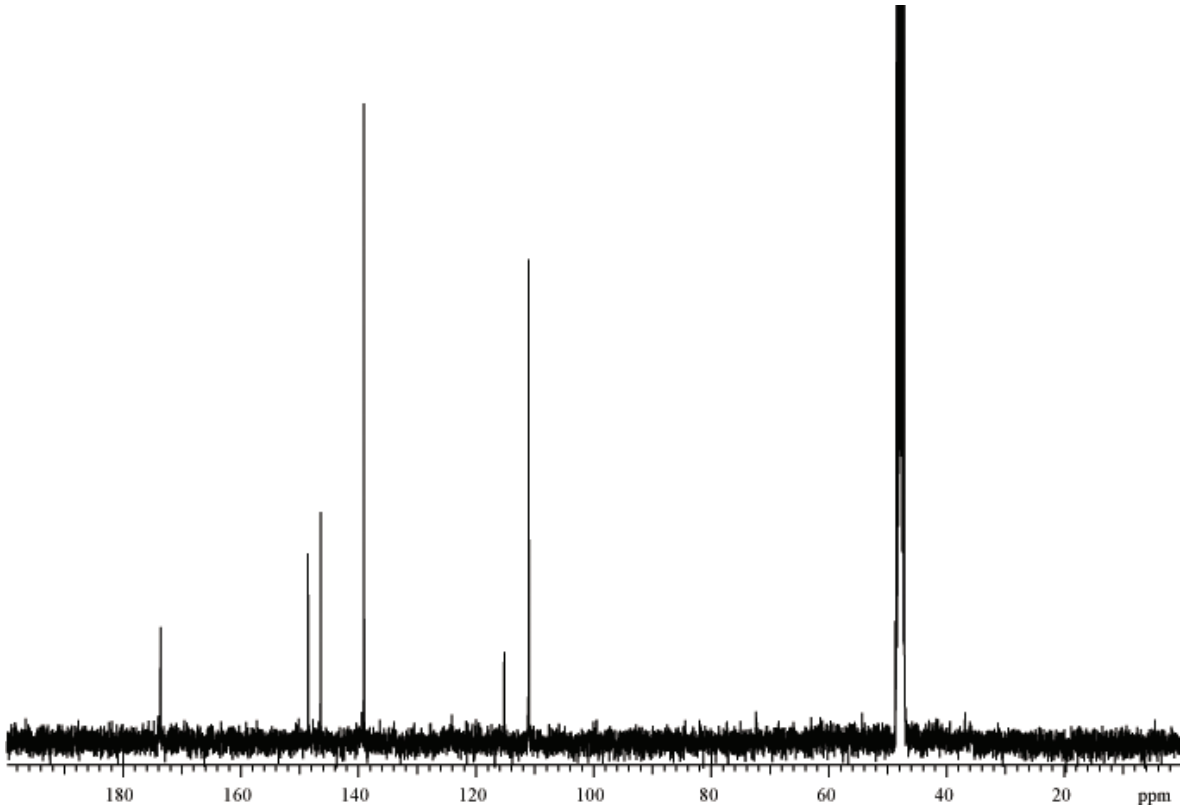

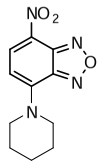

3.17
^{1}H NMR (400 MHz, $CDCl_3$)

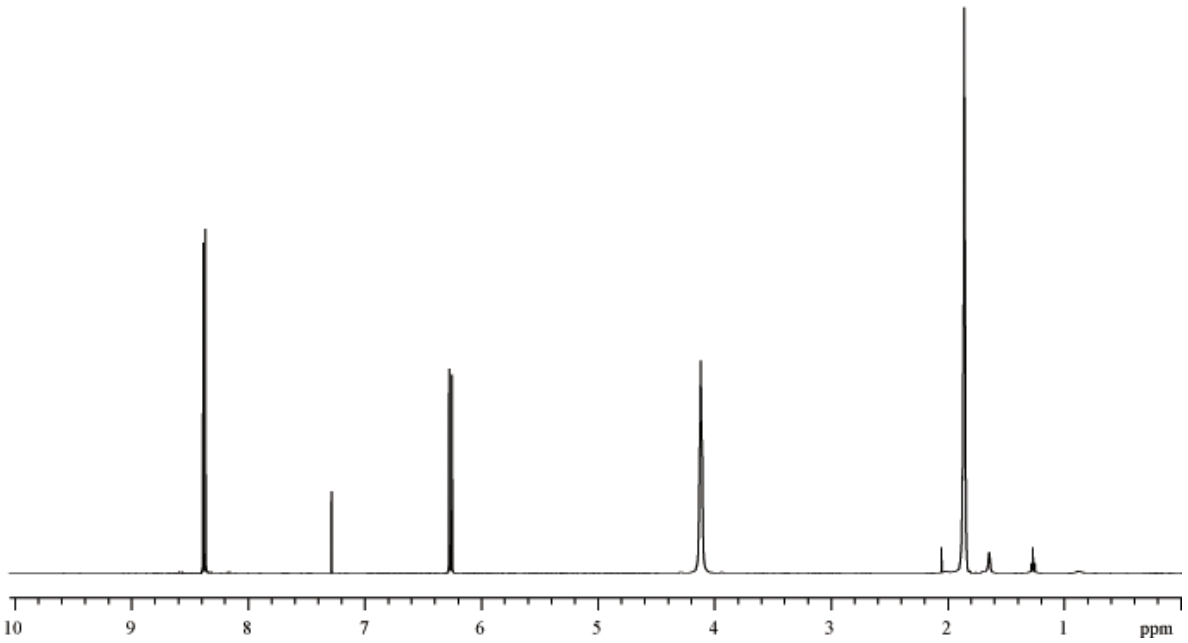

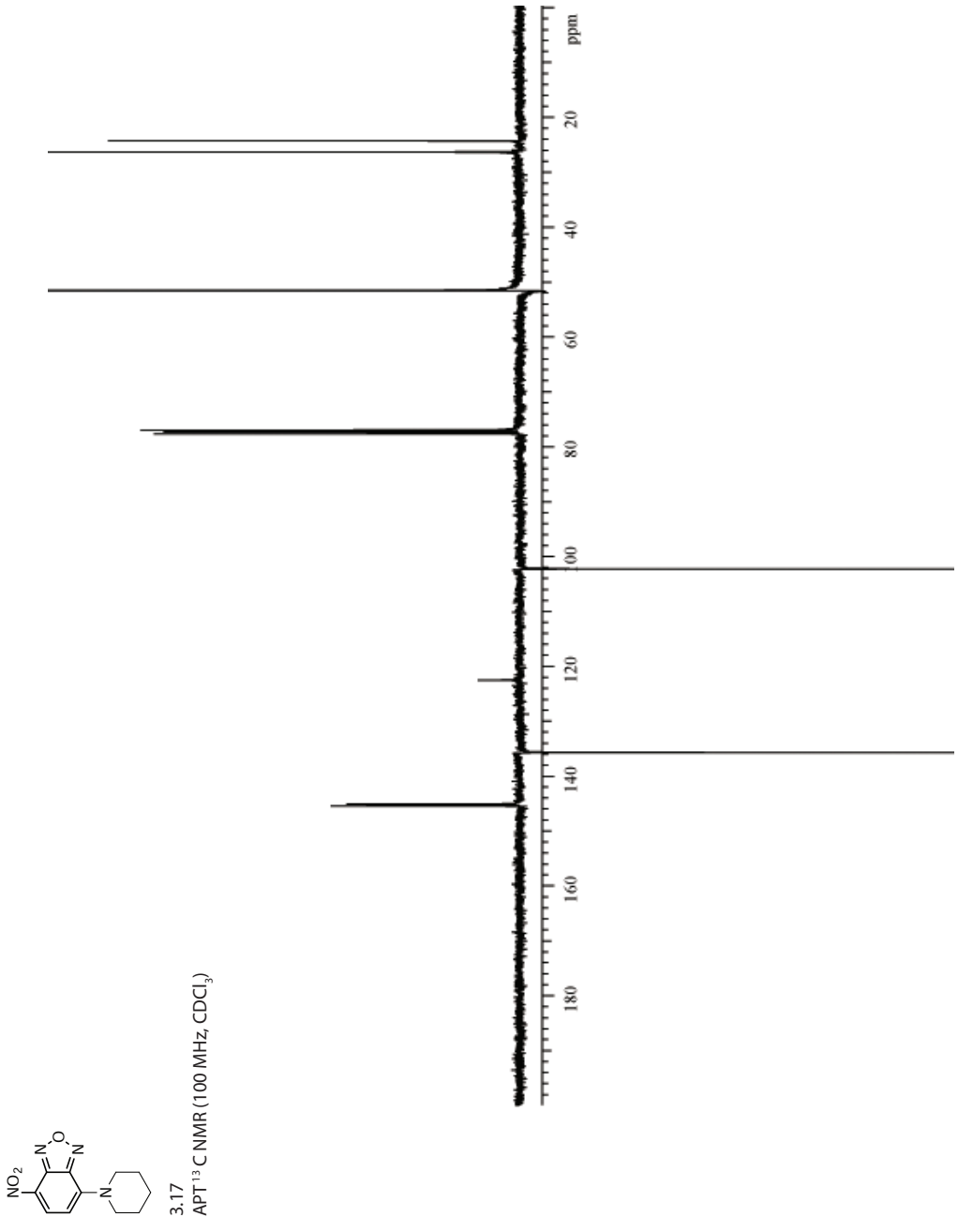
NO2
N
O
N
N
3.17
APT 13 C NMR (100 MHz, CDCl3)
ppm
20
40
60
80
100
120
140
160
180

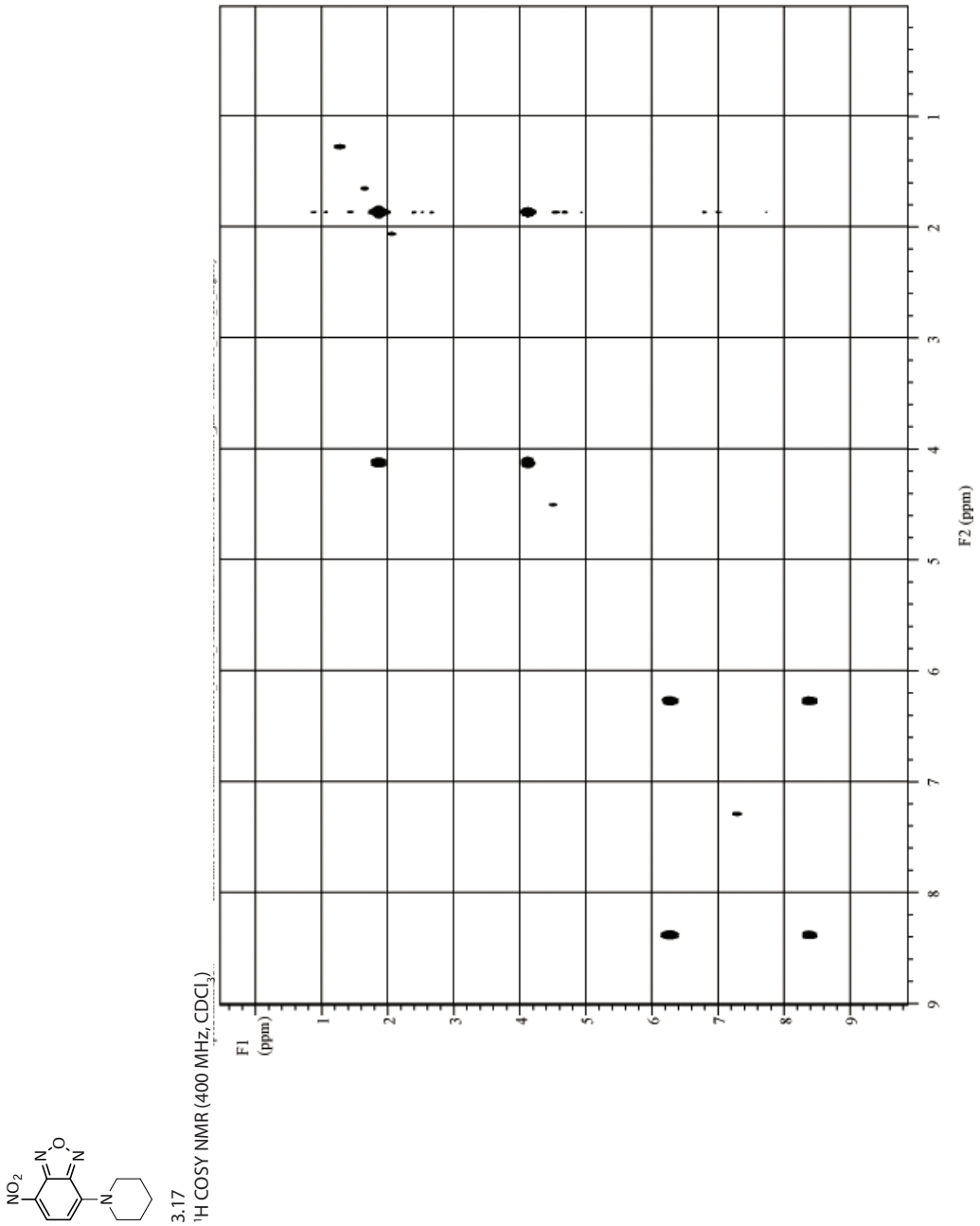
NO2
N
O
N
N
3.17
1H COSY NMR (400 MHz, CDCl3)
F1 (ppm)
F2 (ppm)

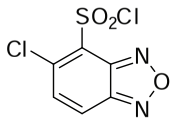

3.19

^{1}H NMR (400 MHz, $CDCl_3$)

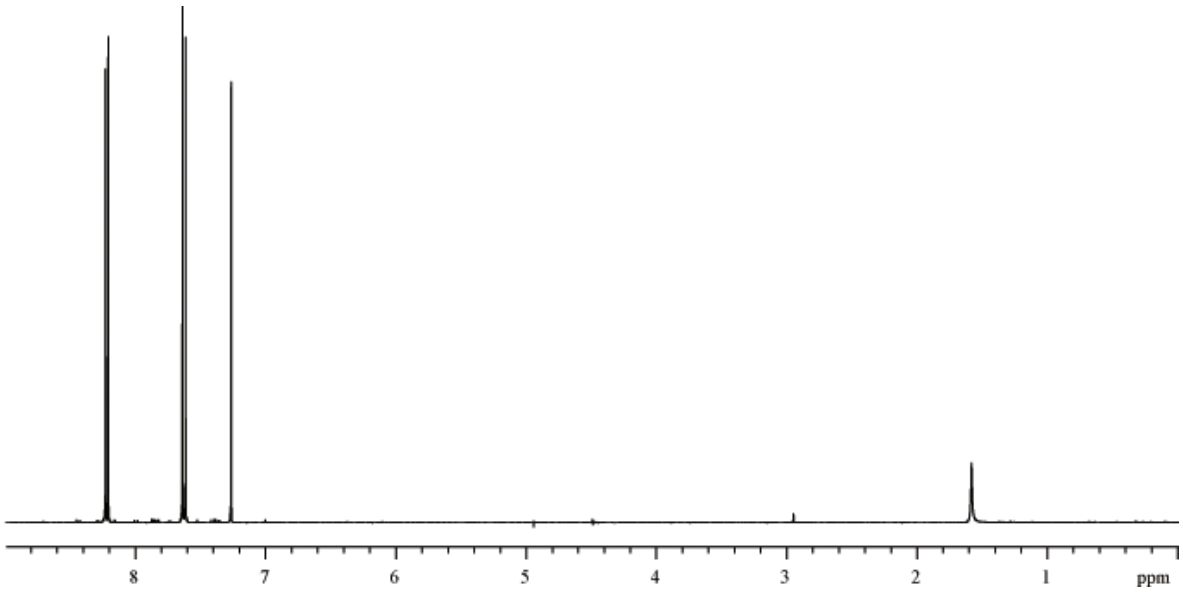

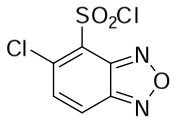

3.19
^{13}C NMR (100 MHz, $CDCl_3$)

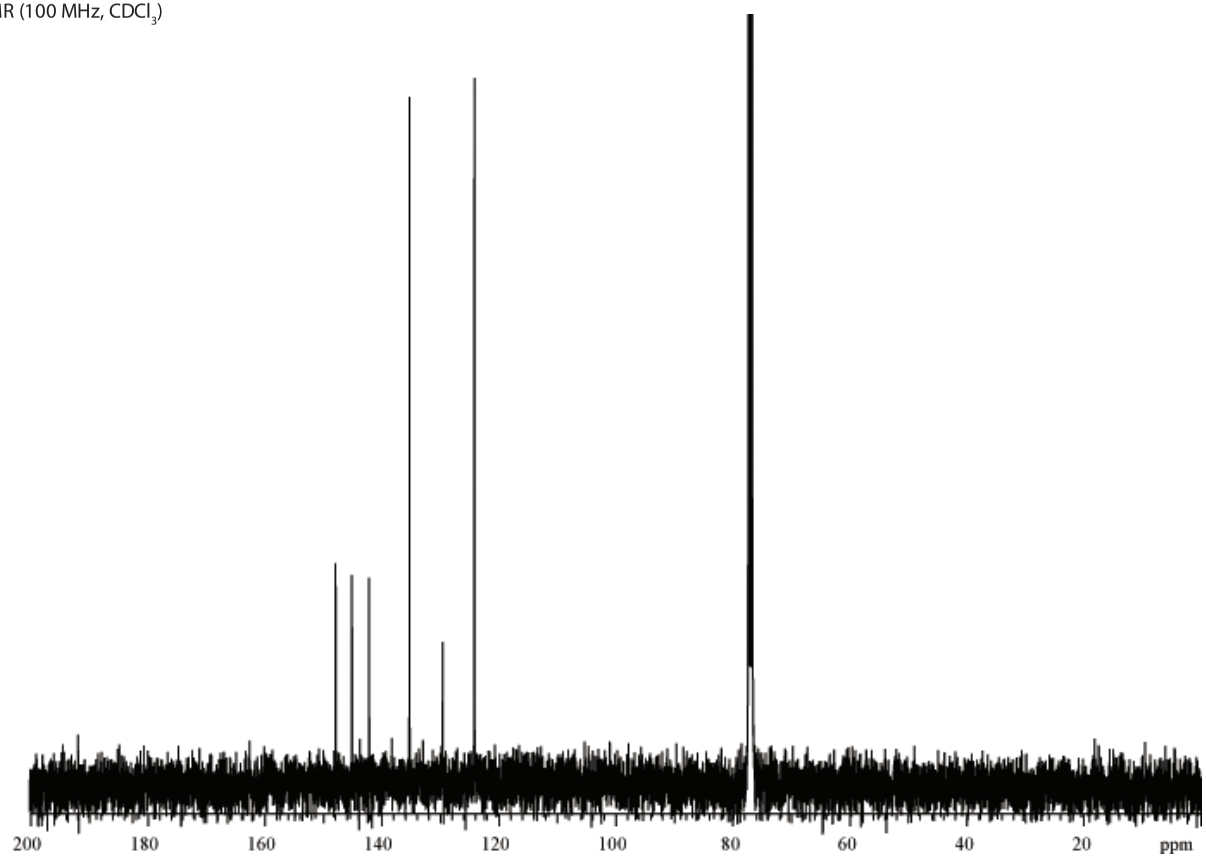

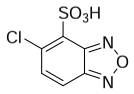

3.20
^{1}H NMR (400 MHz, CD_3OD)

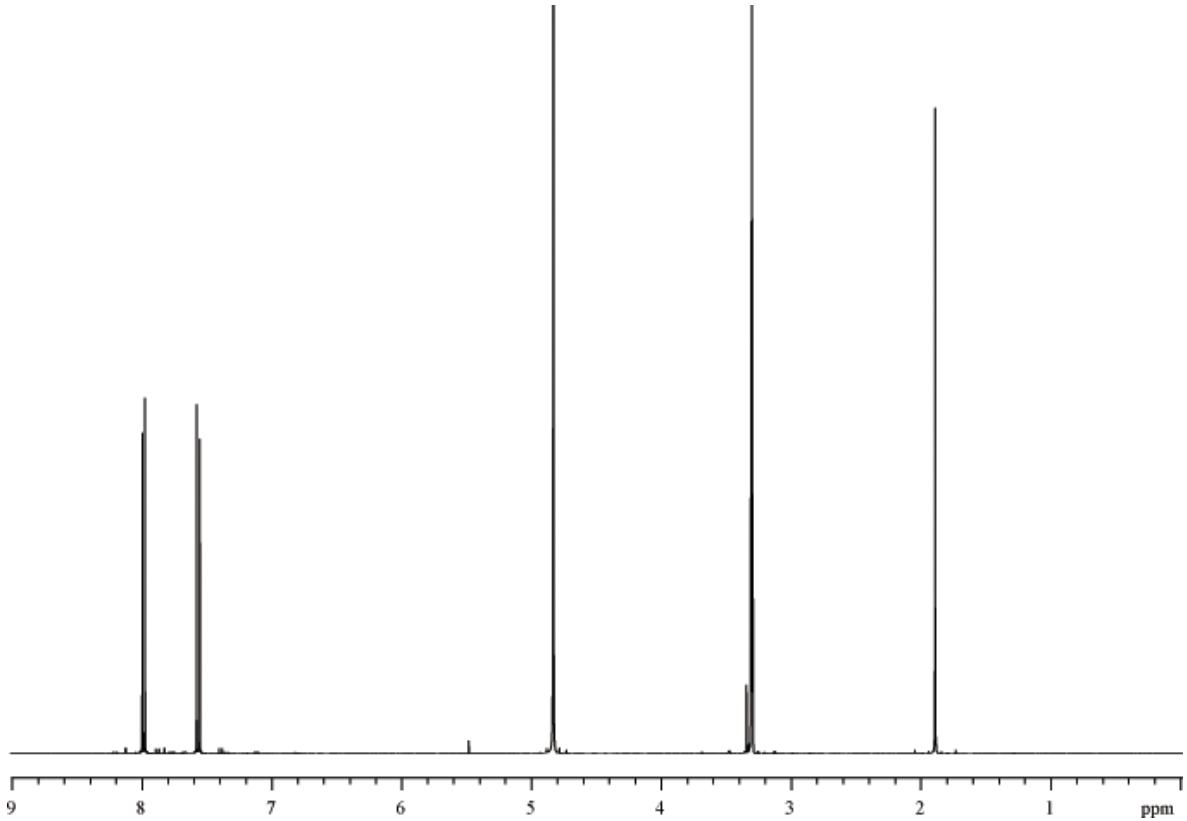

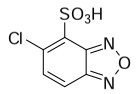

3.20
^{13}C NMR (100 MHz, CD_3OD)

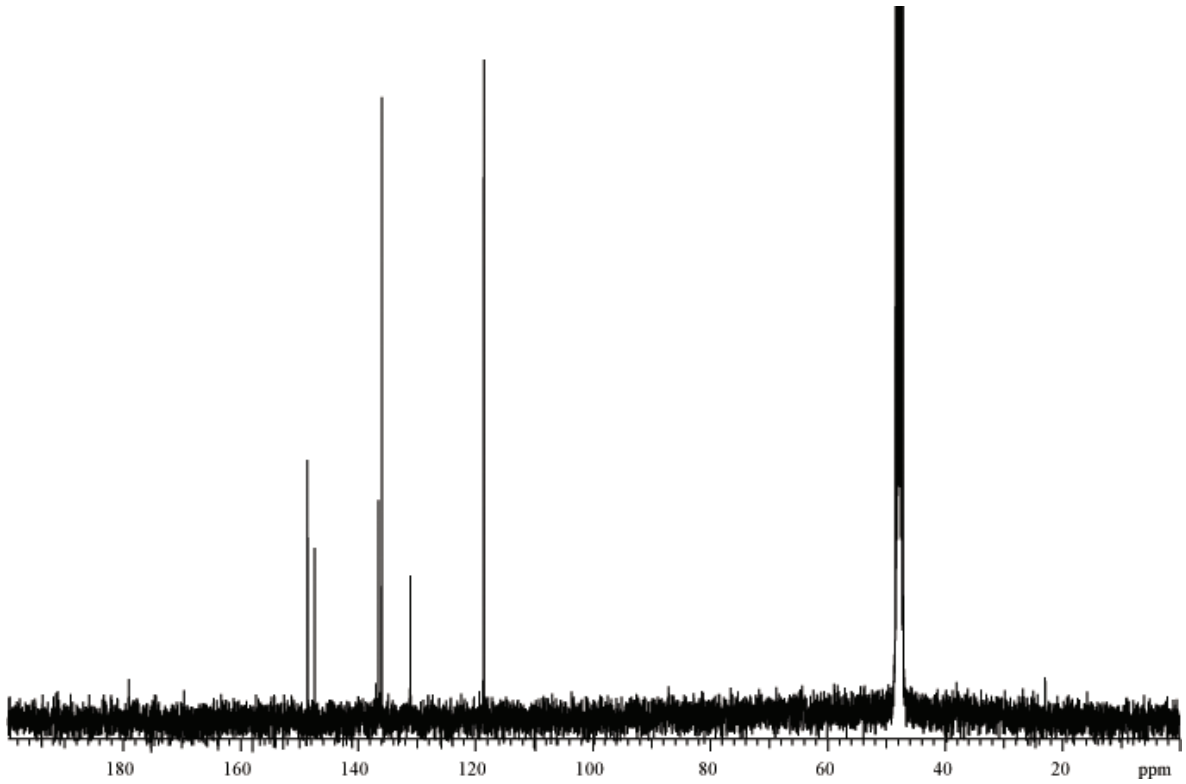

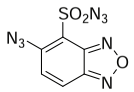

3.21
^{1}H NMR (400 MHz, $CDCl_3$)

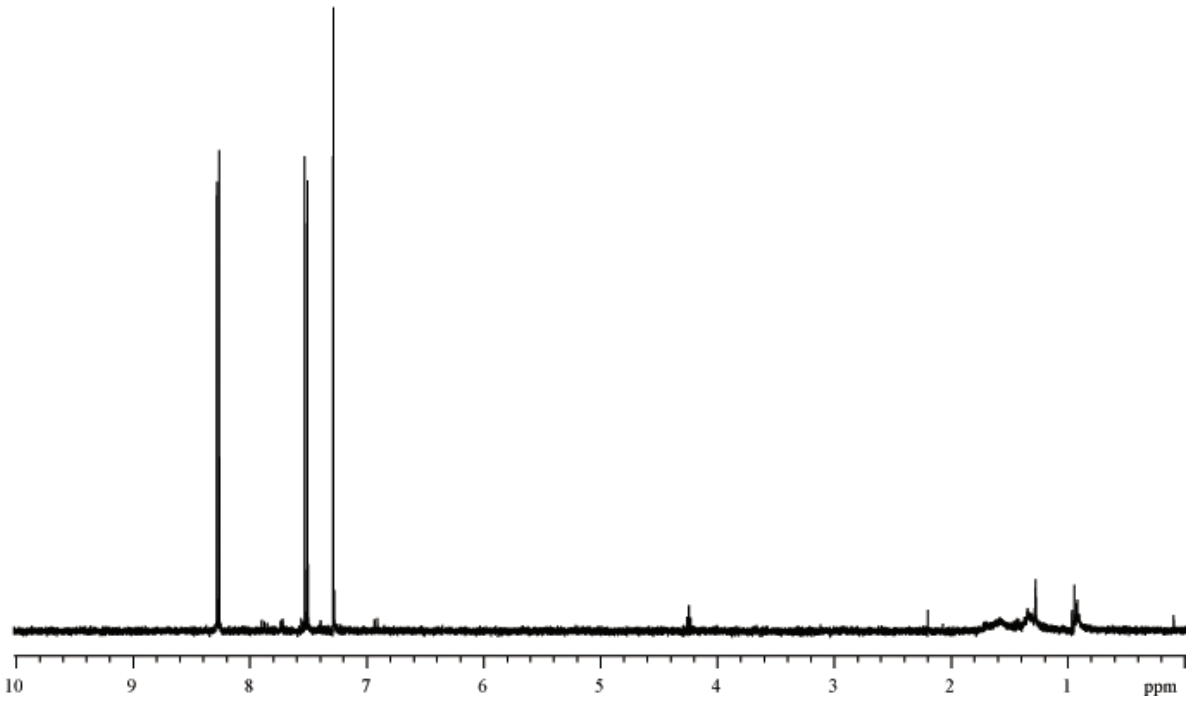

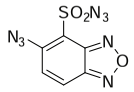

3.21

^{13}C NMR (100 MHz, $CDCl_3$)

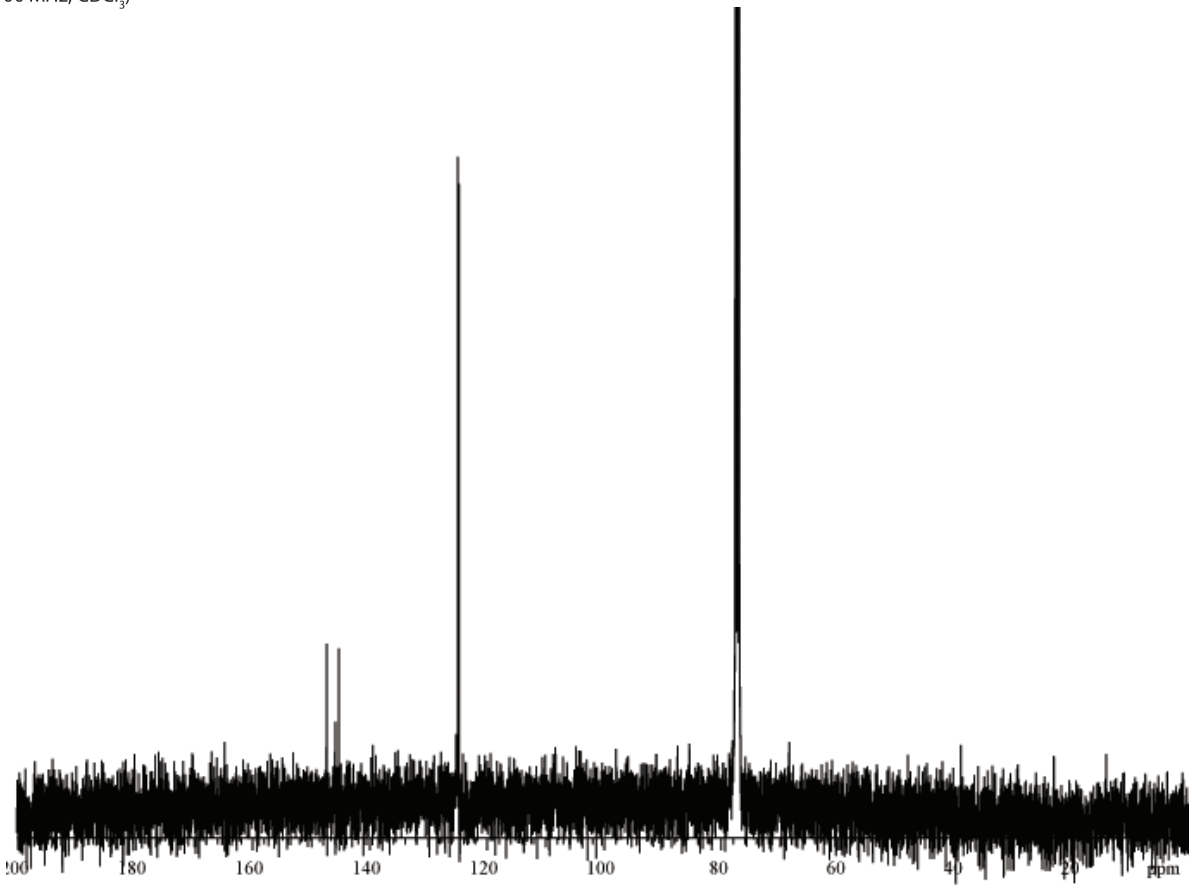

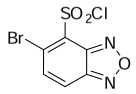

3.22
^{1}H NMR (400 MHz, $CDCl_3$)

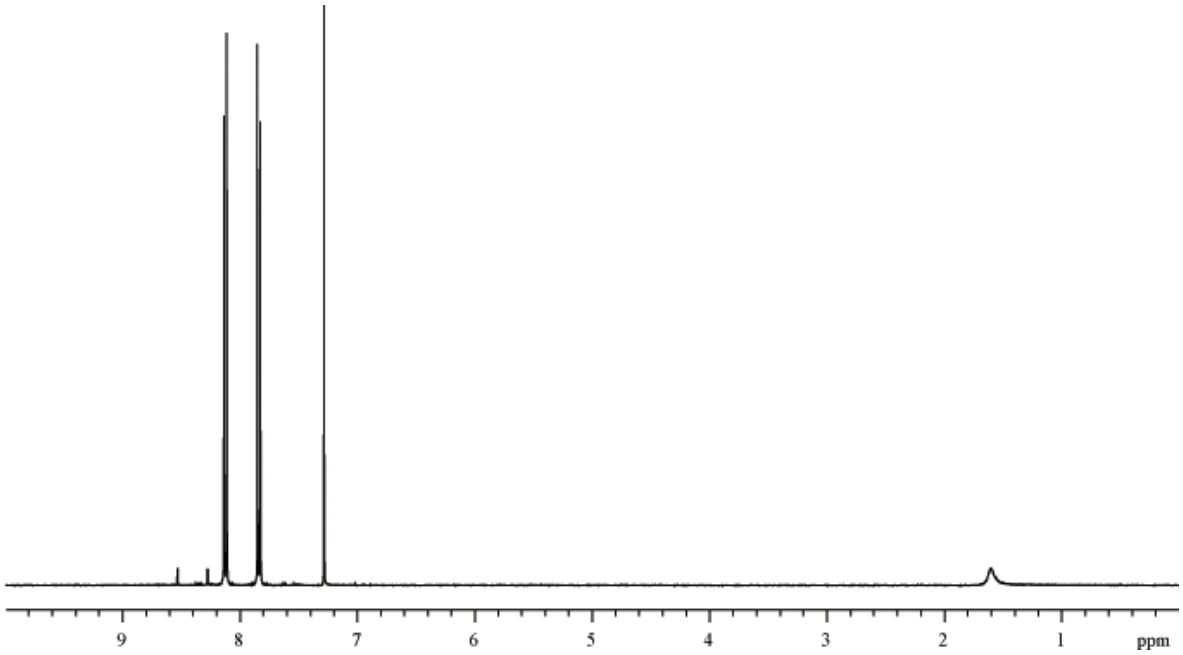

3.22
^{13}C NMR (100 MHz, $CDCl_3$)

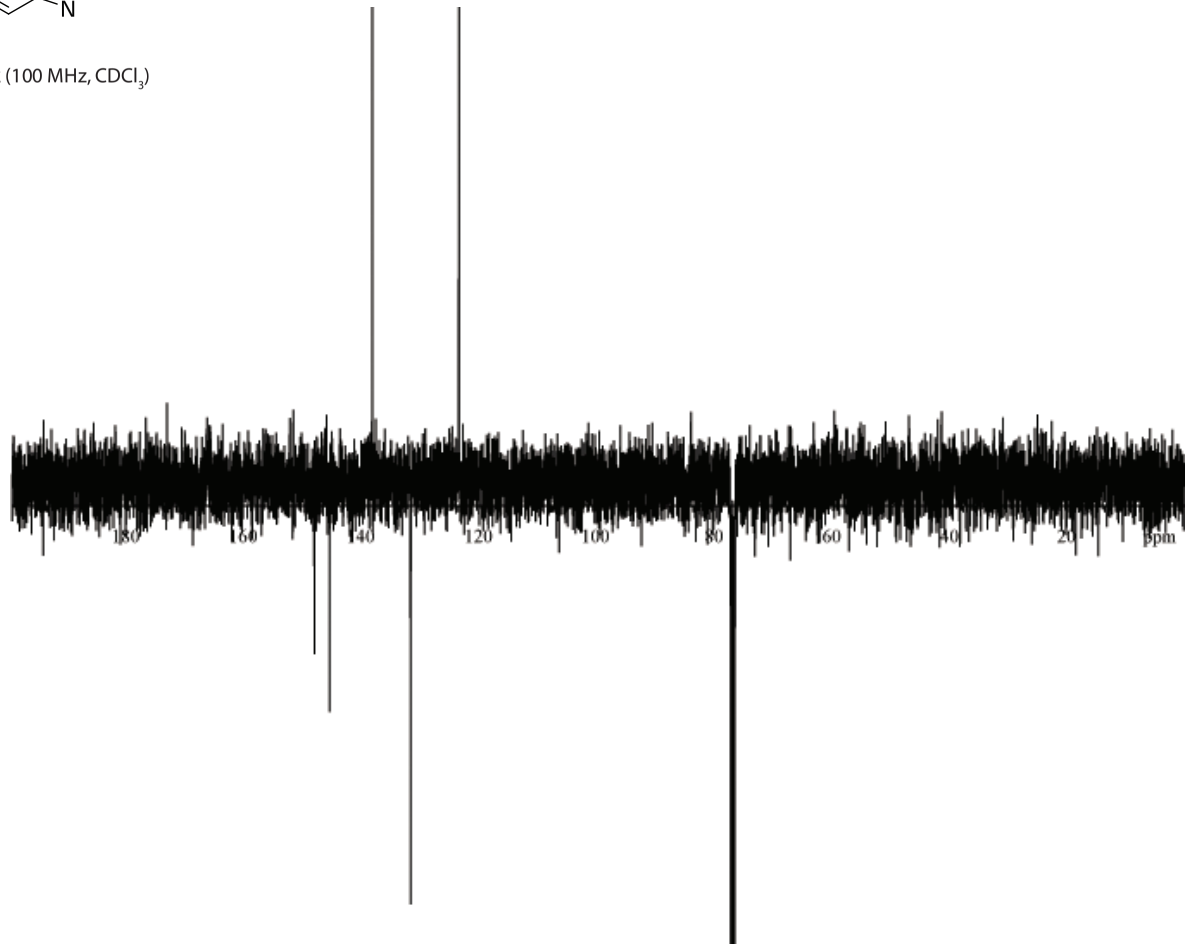

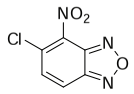

3.23
^{1}H NMR (400 MHz, $CDCl_3$)

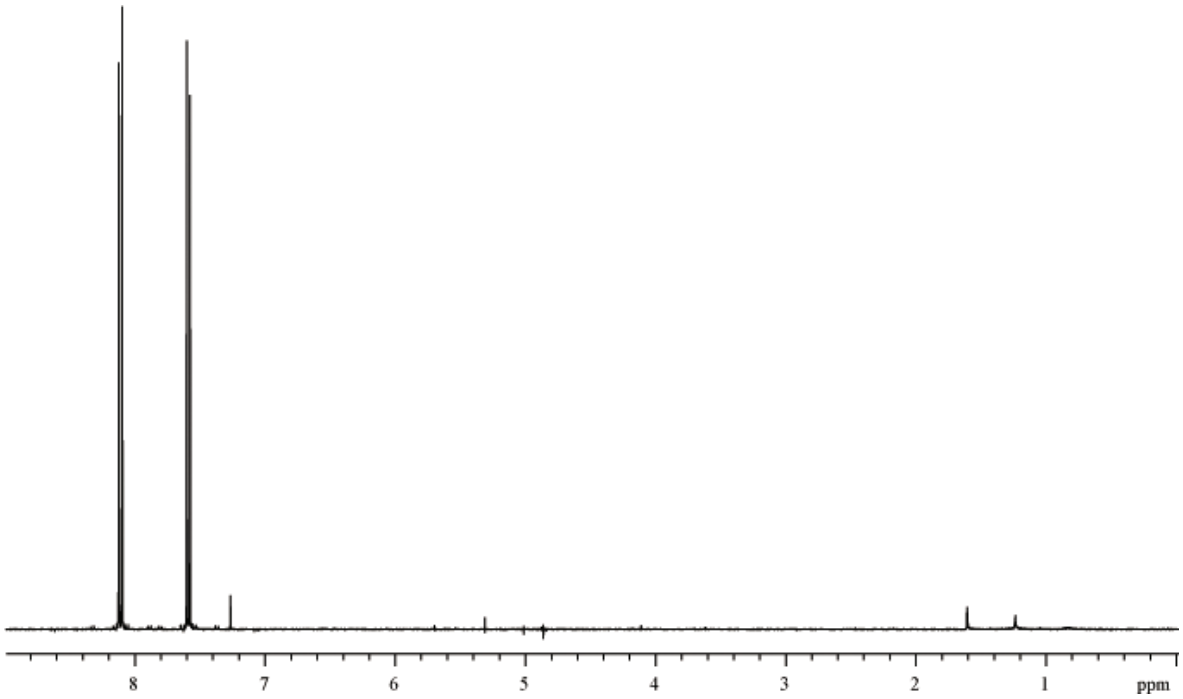

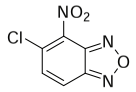

3.23

^{13}C NMR (100 MHz, $CDCl_3$)

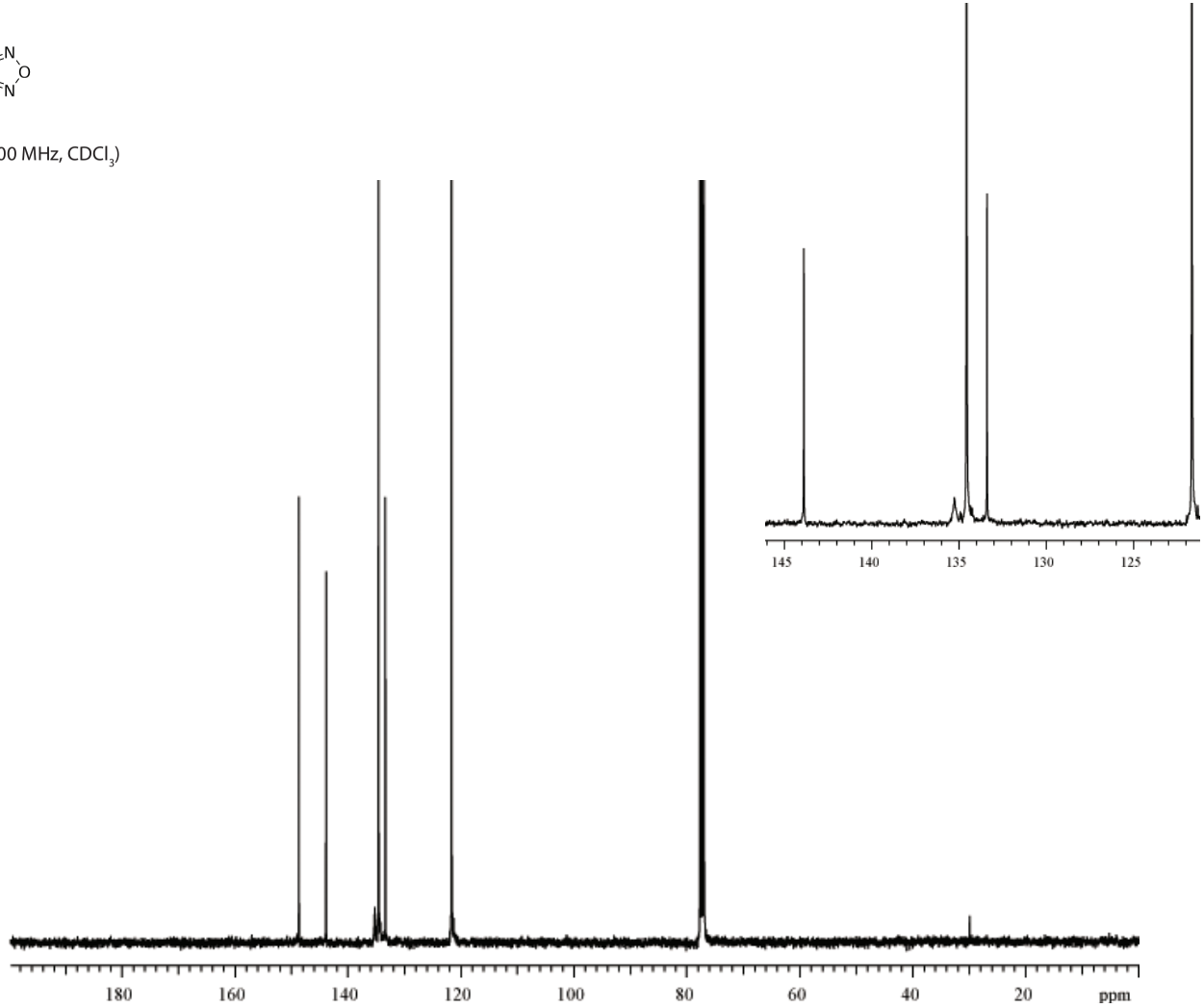

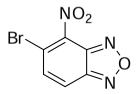

3.24
^{1}H NMR (400 MHz, $CDCl_3$)

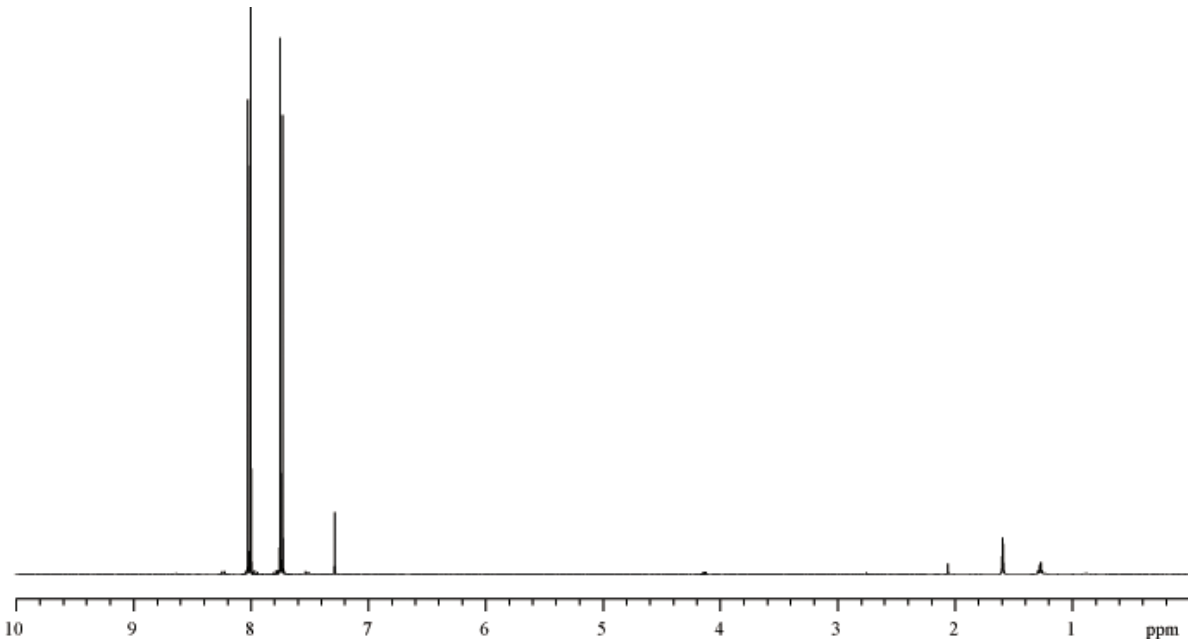

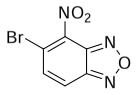

3.24

^{13}C NMR (100 MHz, $CDCl_3$)

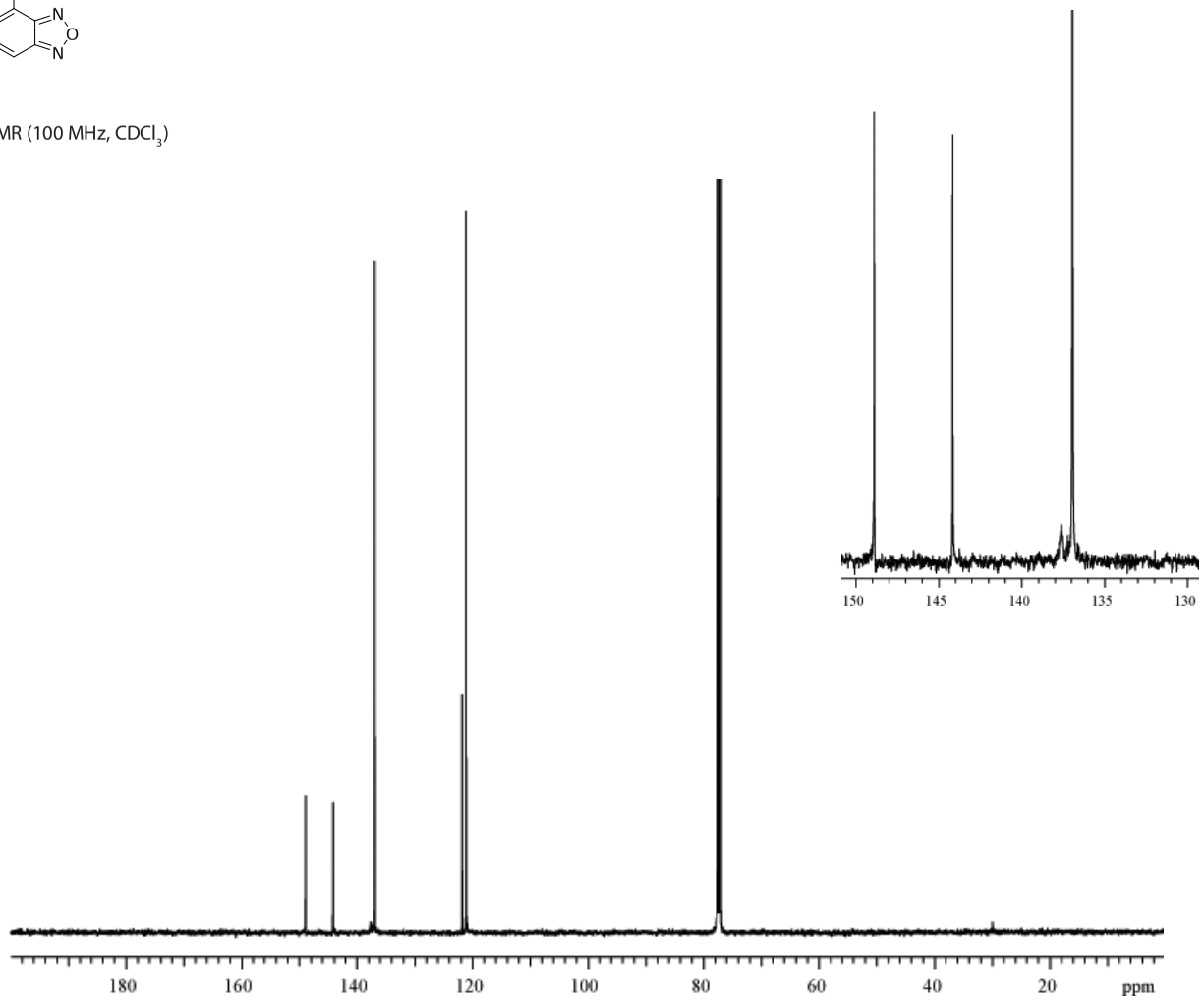

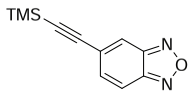

3.25

^{1}H NMR (400 MHz, $CDCl_3$)

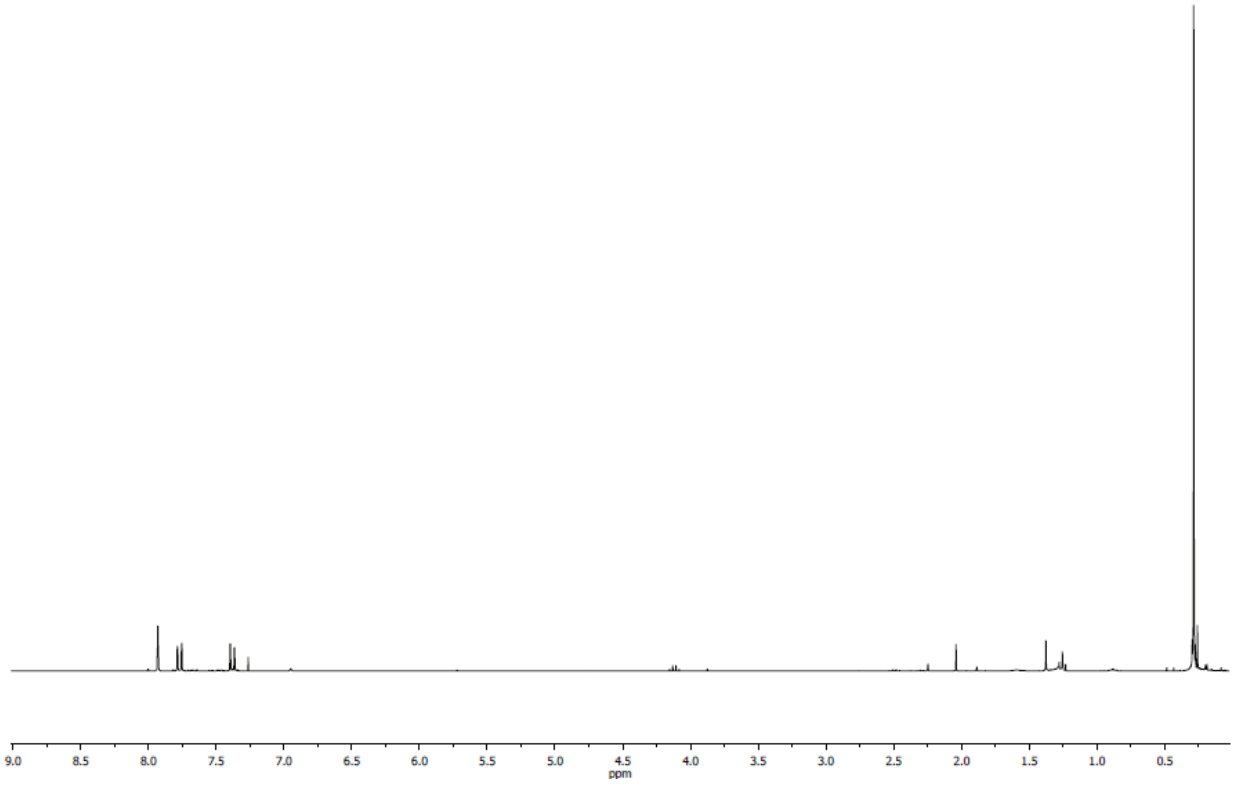

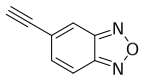

3.26
^{13}C NMR (100 MHz, $CDCl_3$)

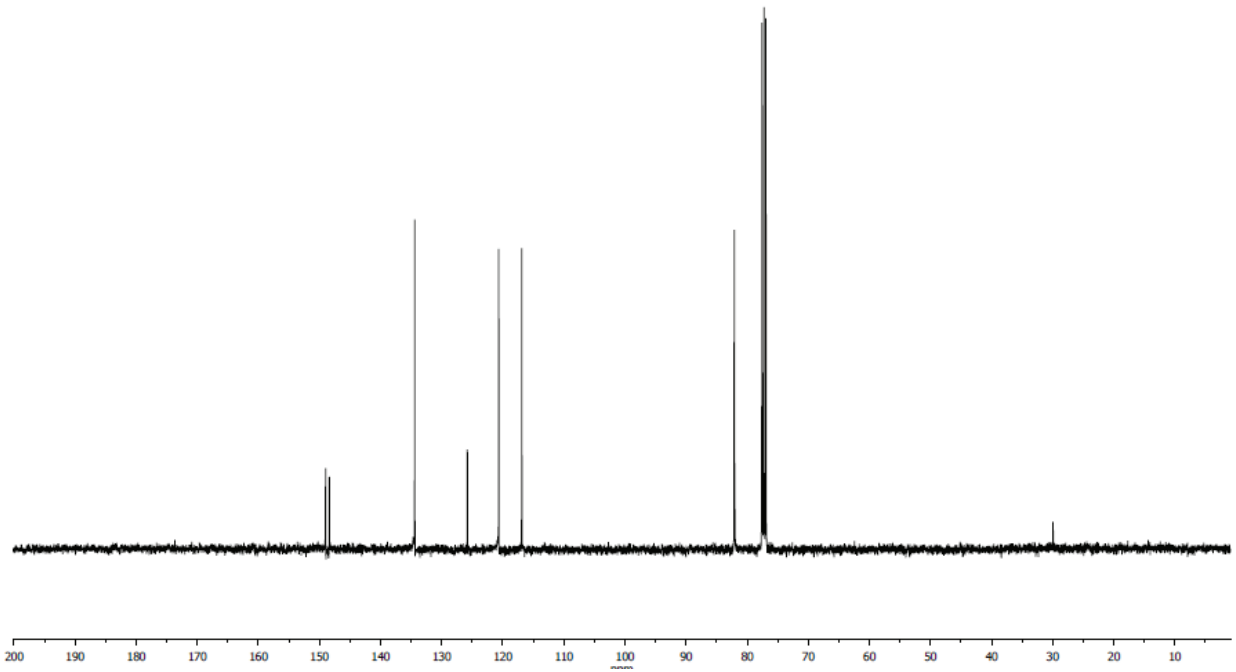

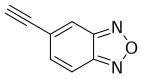

3.26
^{1}H NMR (400 MHz, $CDCl_3$)

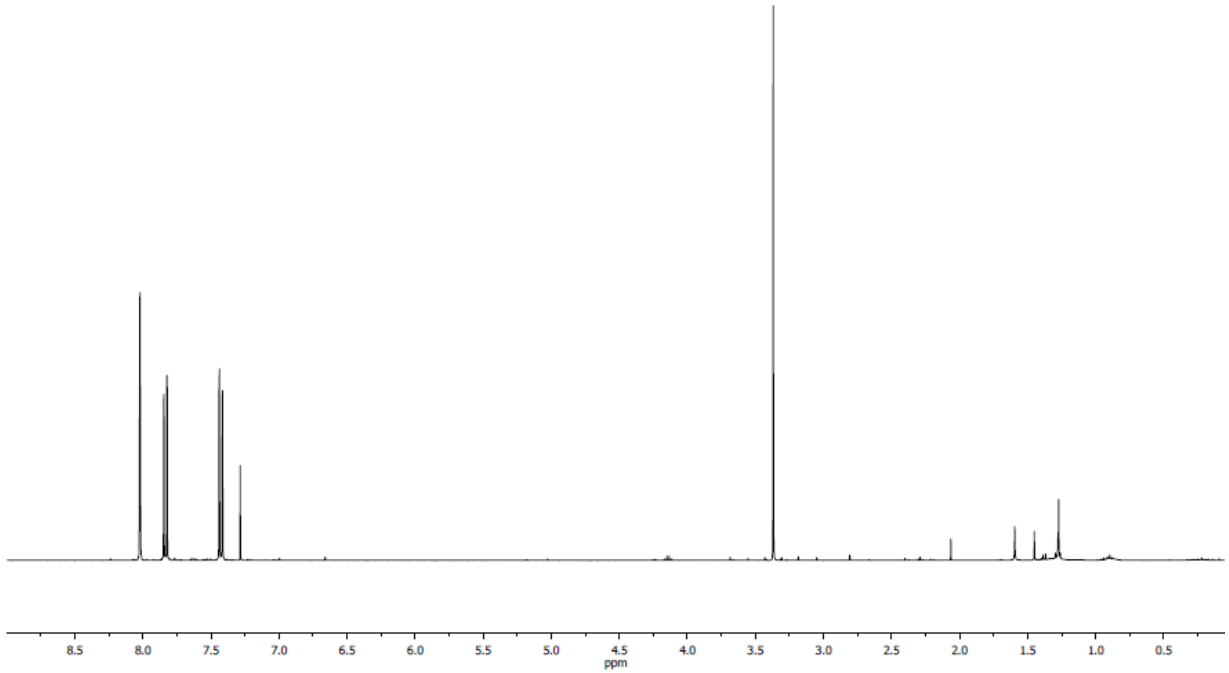

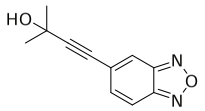

3.27

^{1}H NMR (400 MHz, $CDCl_3$)

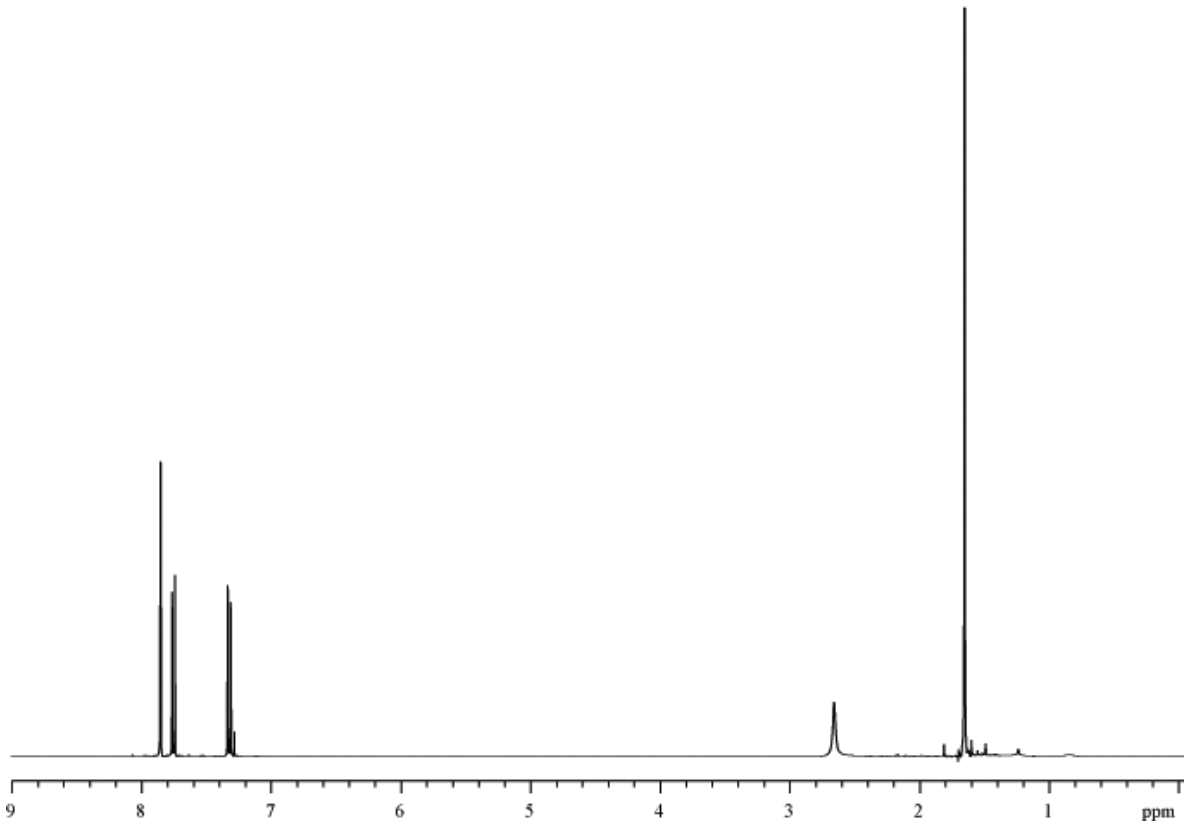

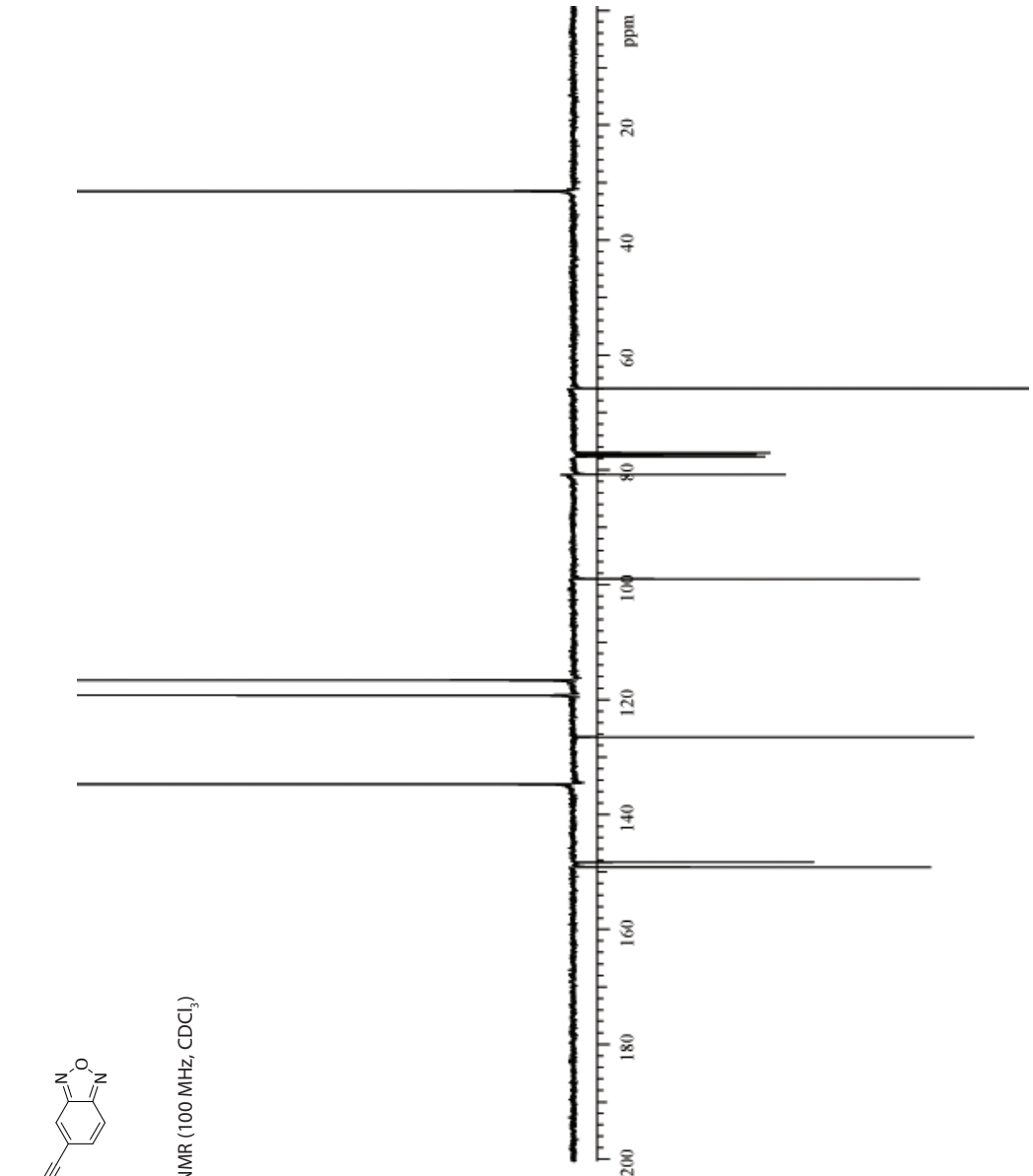
HO
N
O
N
3.27
APT ^{13}C NMR (100 MHz, $CDCl_3$)
ppm
200
180
160
140
120
100
80
60
40
20

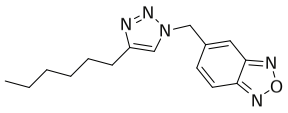

3.28
^{1}H NMR (400 MHz, $CDCl_3$)

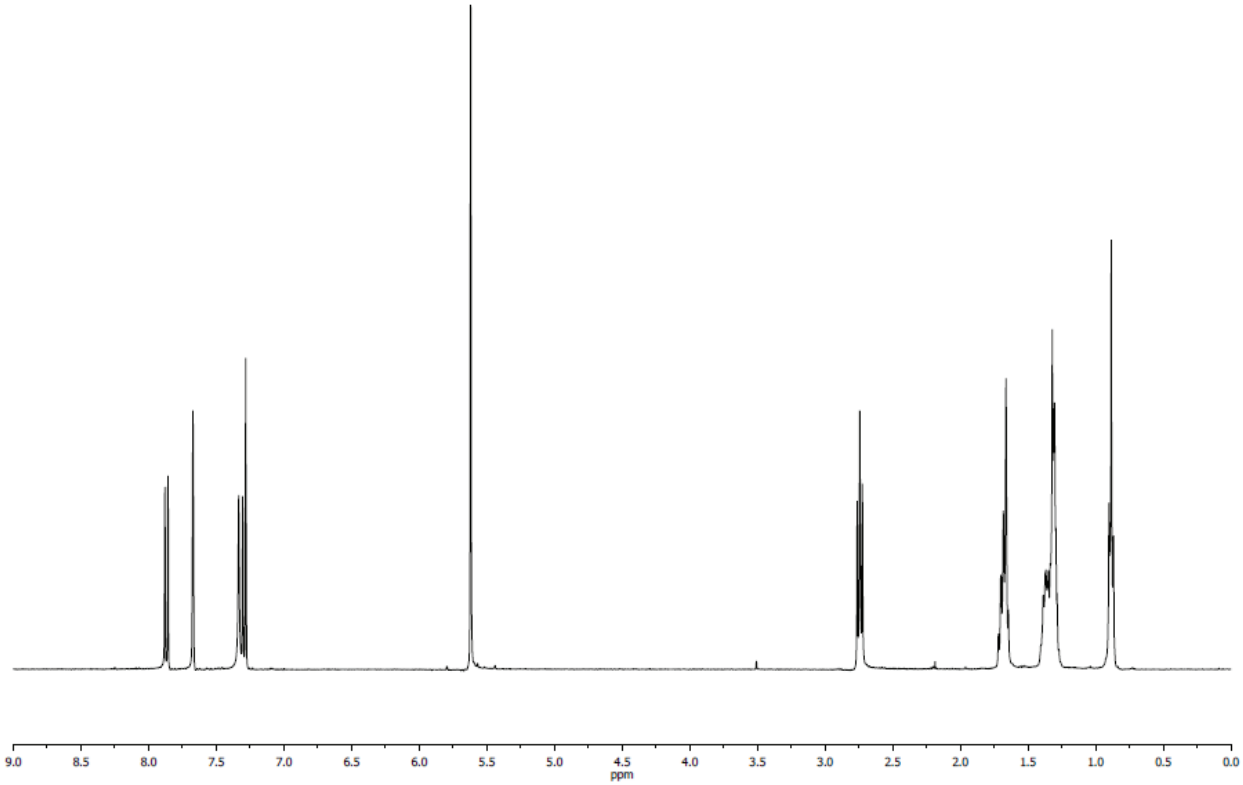

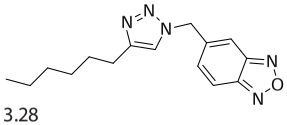

3.28

^{13}C NMR (100 MHz, $CDCl_3$)

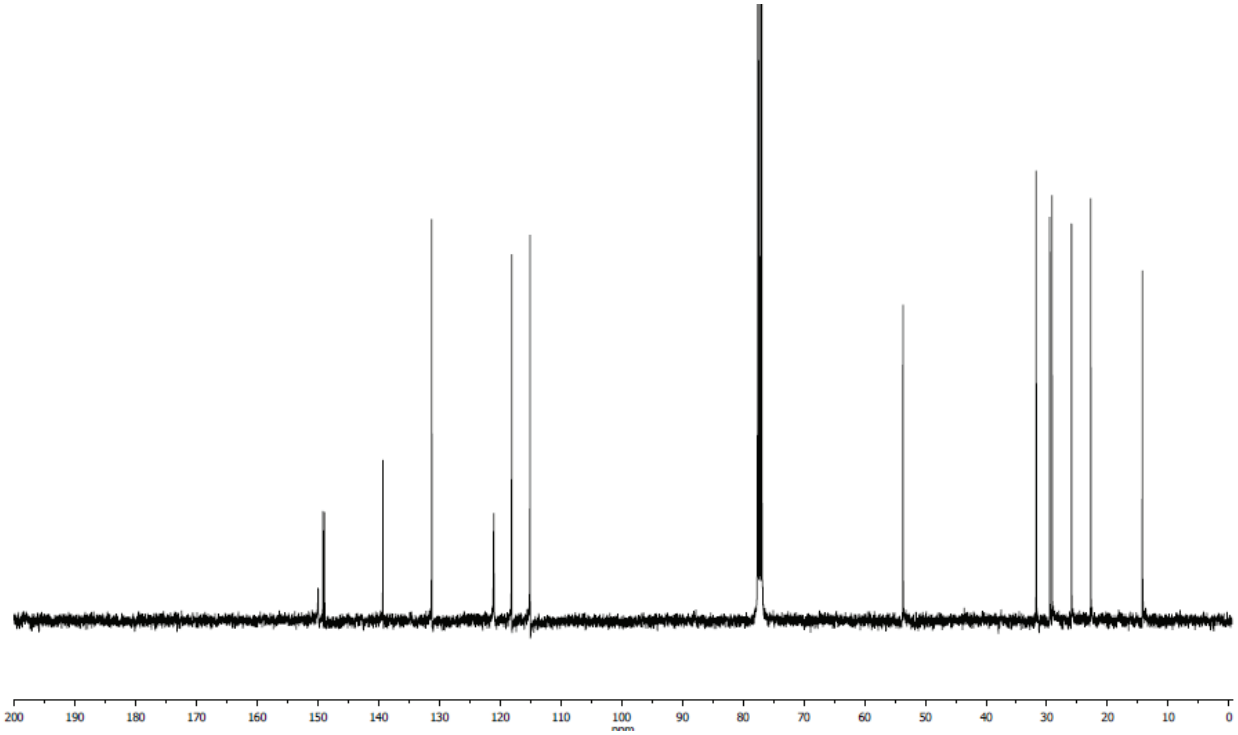

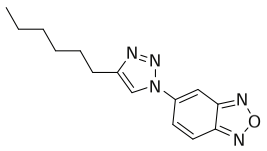

3.29
^{1}H NMR (400 MHz, $CDCl_3$)

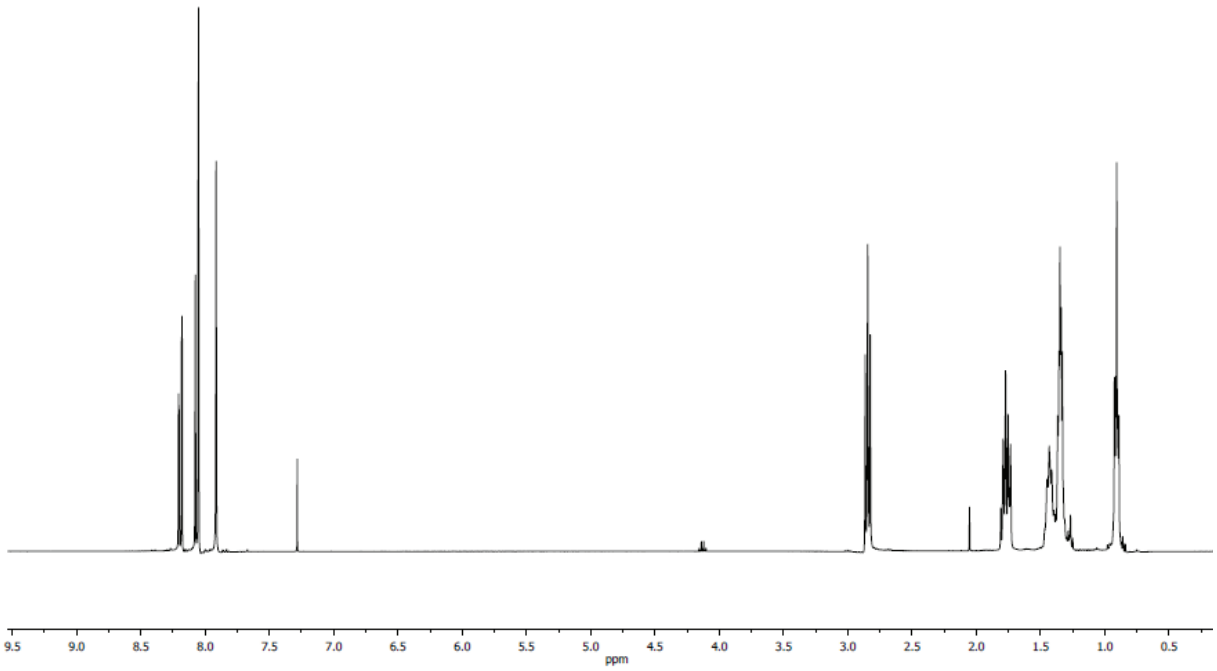

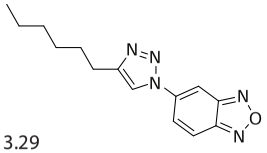

3.29

^{13}C NMR (100 MHz, $CDCl_3$)

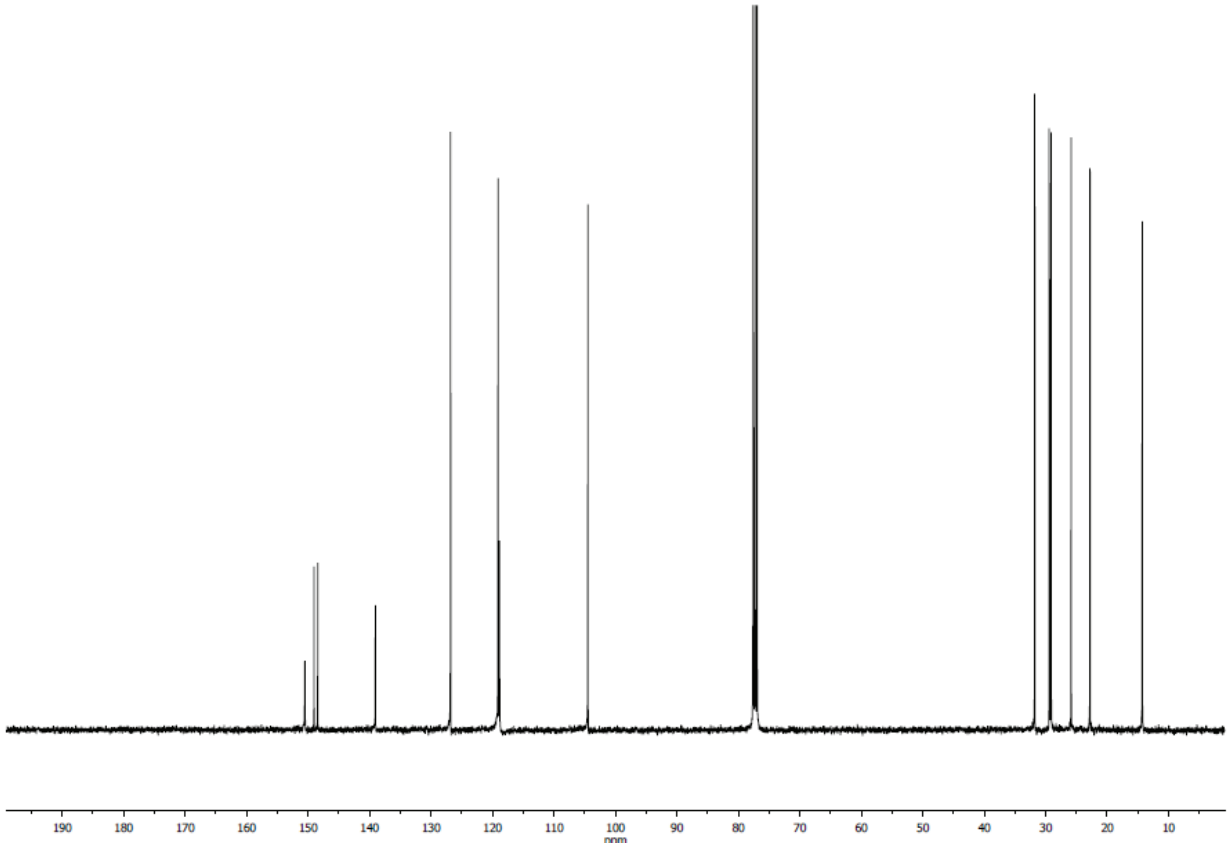

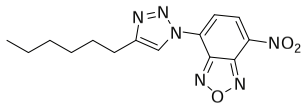

3.30

^{1}H NMR (400 MHz, $CDCl_3$)

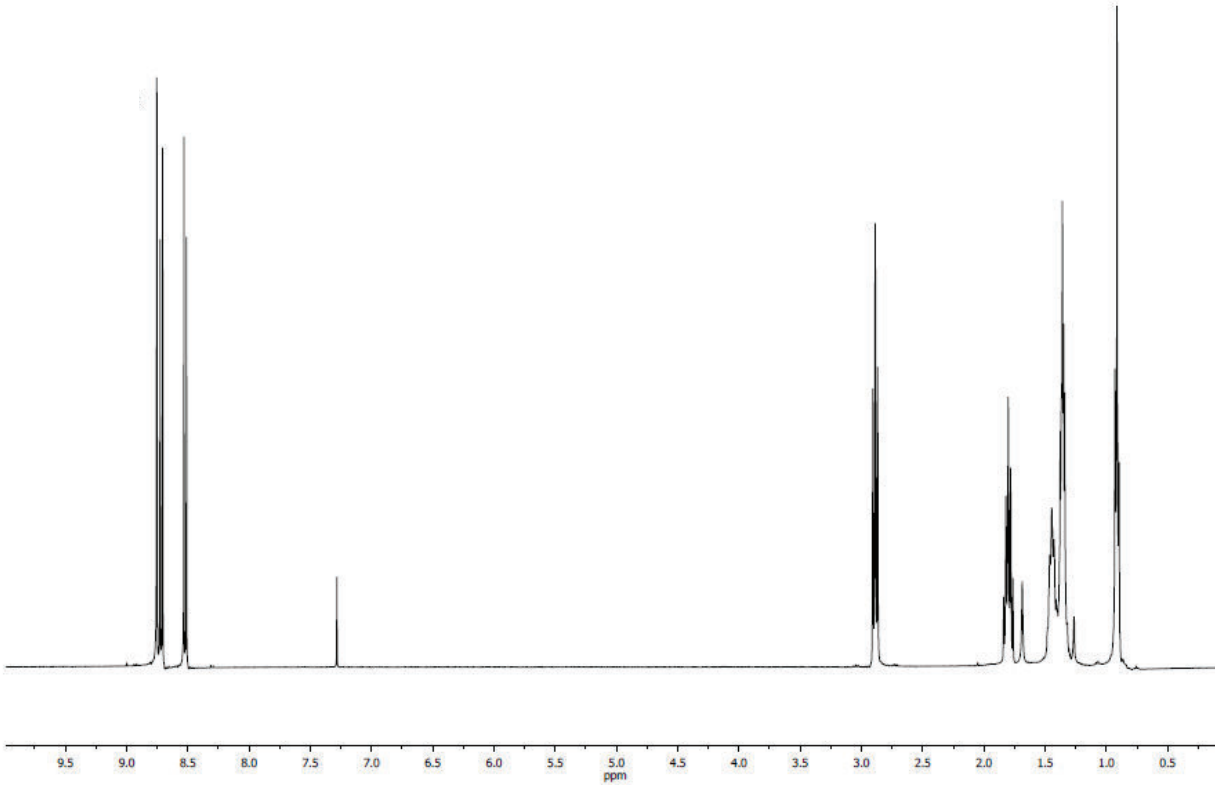

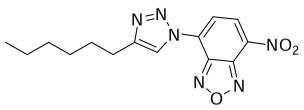

3.30

^{13}C NMR (100 MHz, $CDCl_3$)

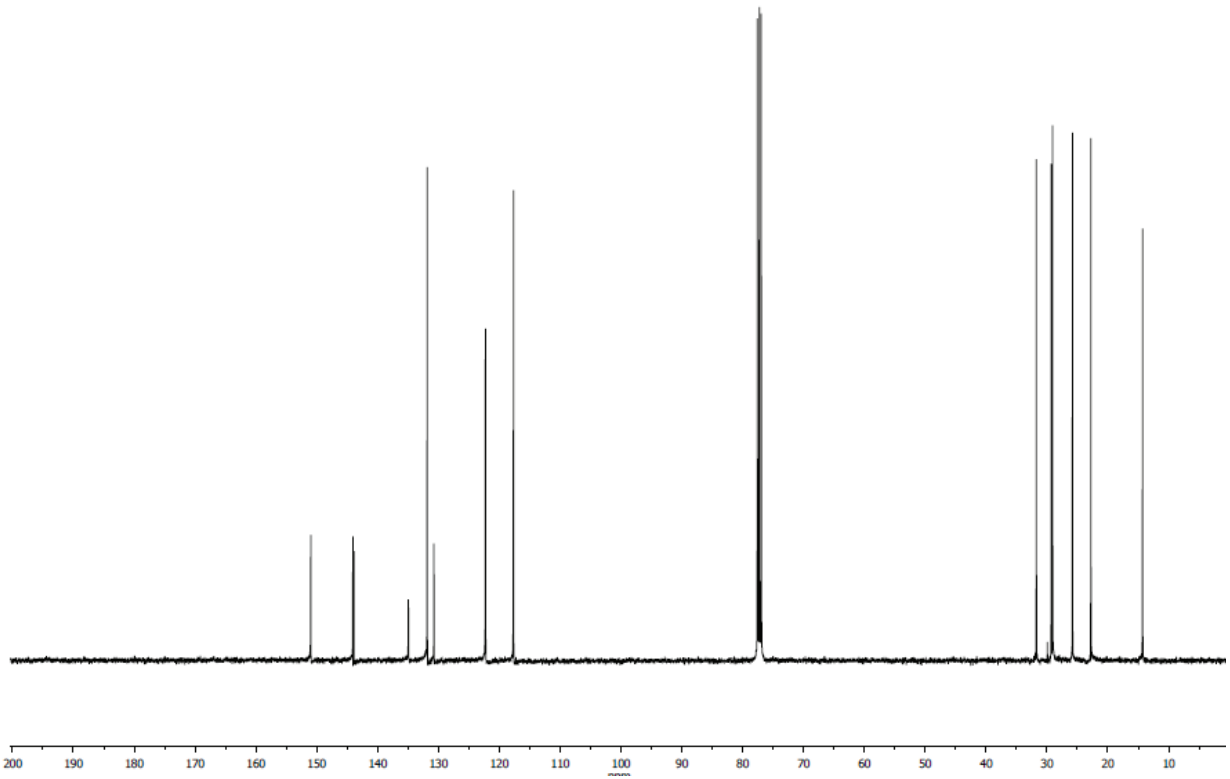

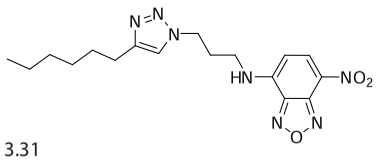

3.31

^{1}H NMR (400 MHz, $CDCl_3$)

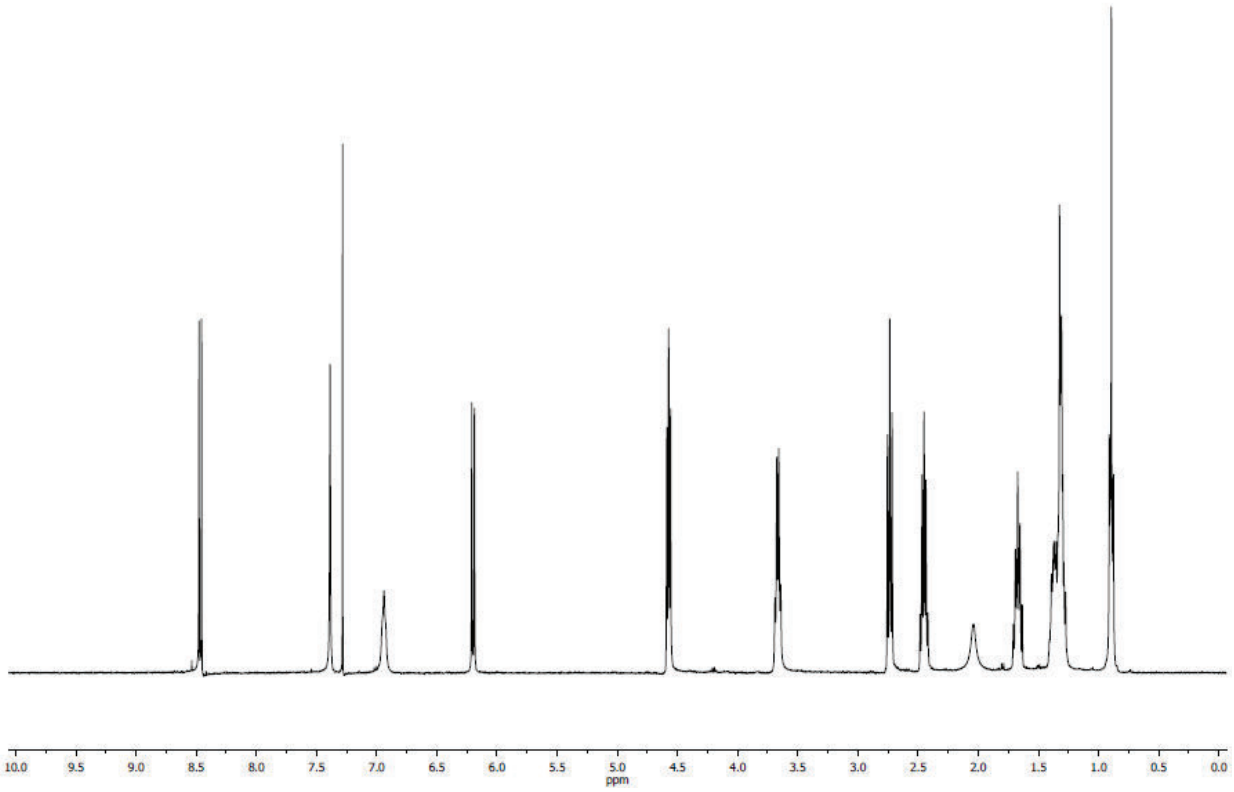

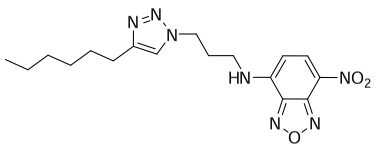

3.31

^{13}C NMR (100 MHz, $CDCl_3$)

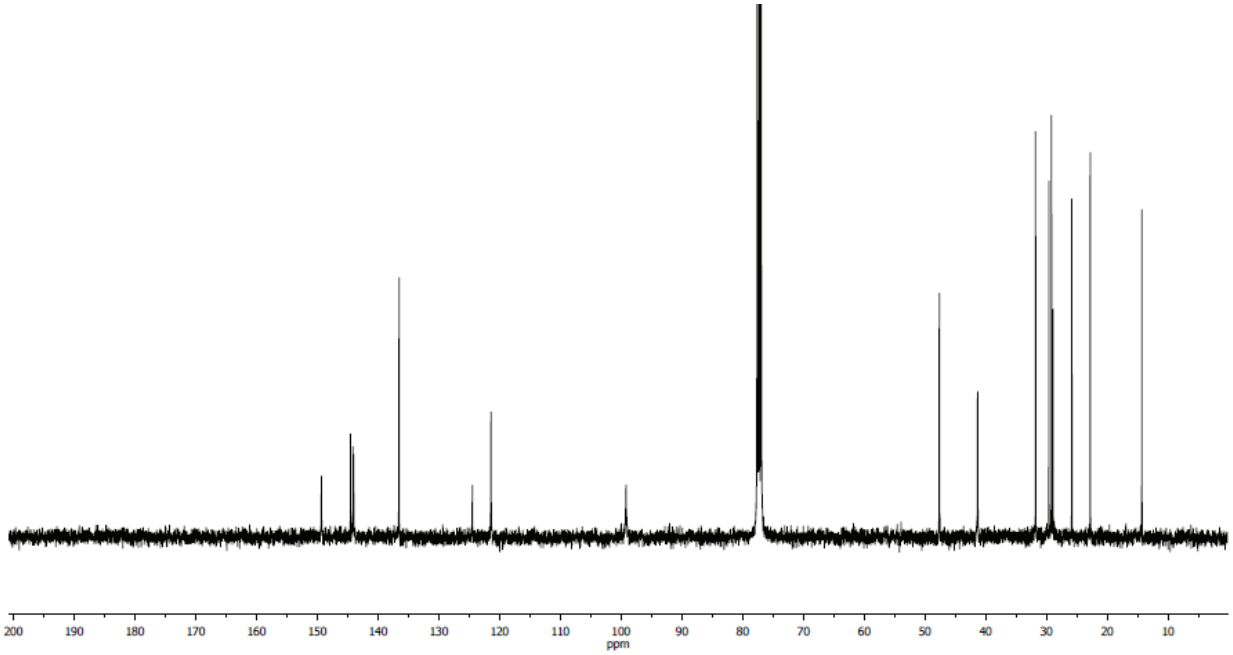

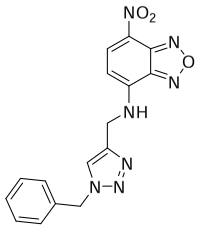

3.32

^{1}H NMR (400 MHz, $(CD_3)_2CO$)

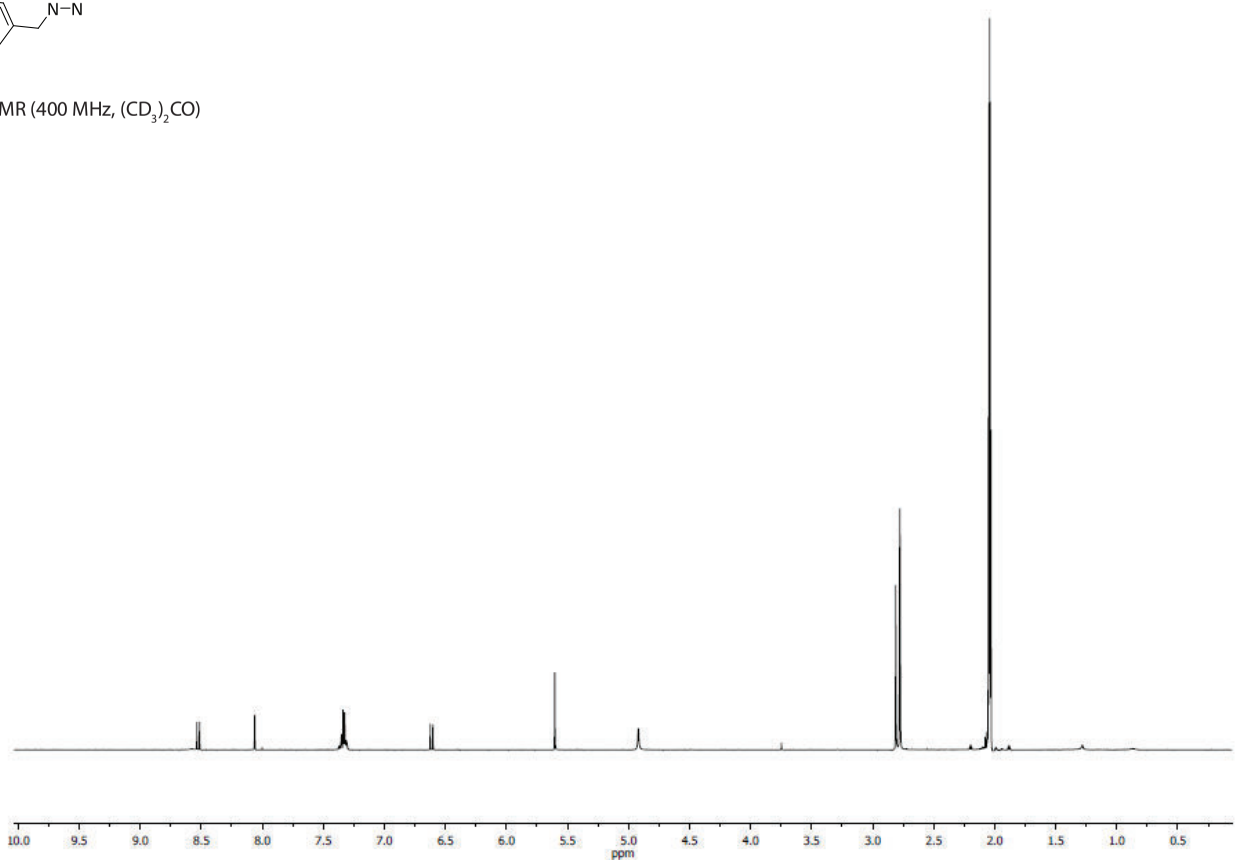

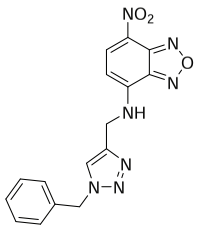

3.32

^{13}C NMR (100 MHz, DMSO-D_6)

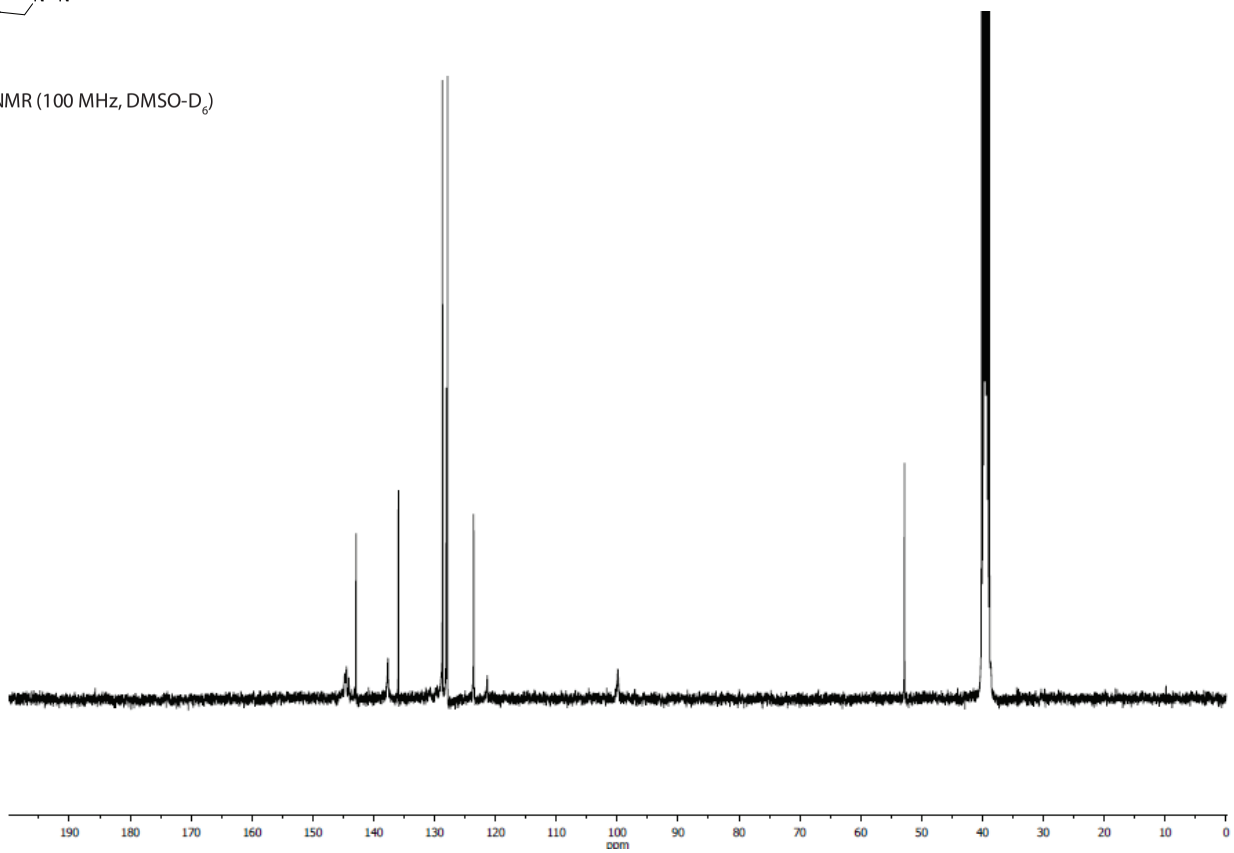

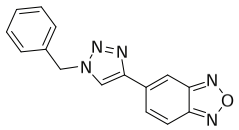

3.33
^{1}H NMR (400 MHz, $CDCl_3$)

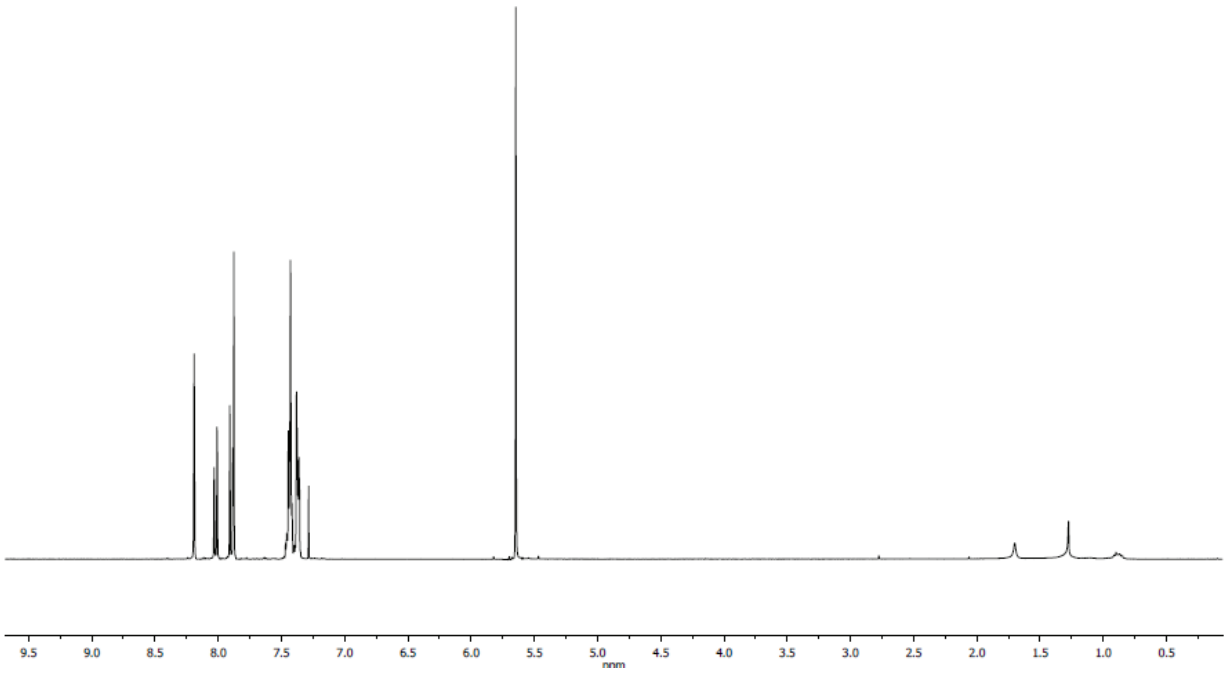

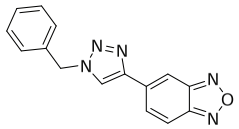

3.33

^{13}C NMR (100 MHz,$CDCl_3$)

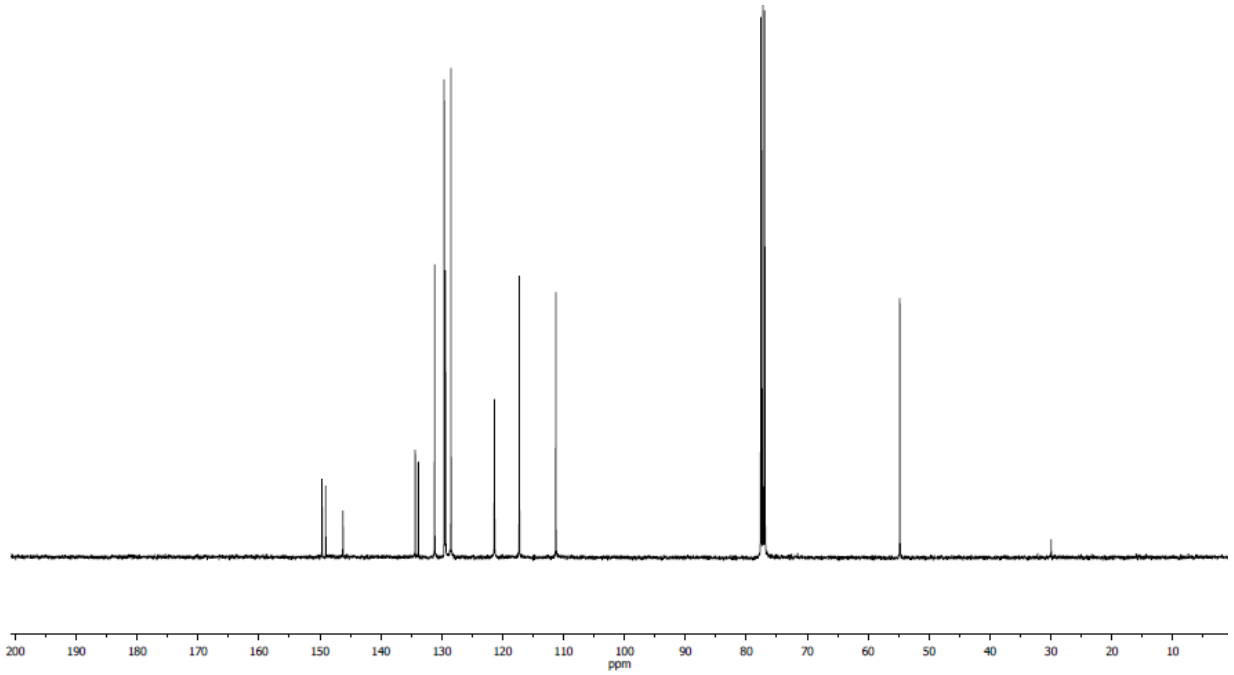

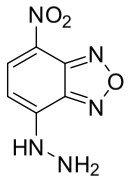

4.2

^{1}H NMR (400 MHz, D_2O)

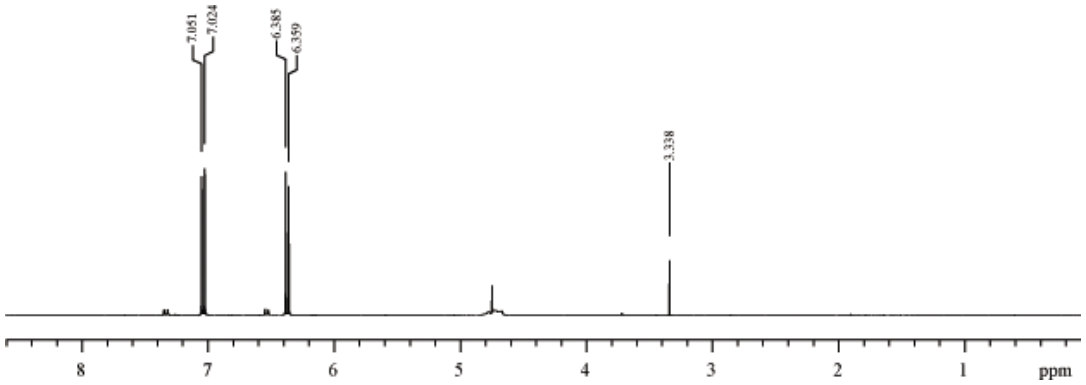

^{13}C NMR (100 MHz, D_2O)

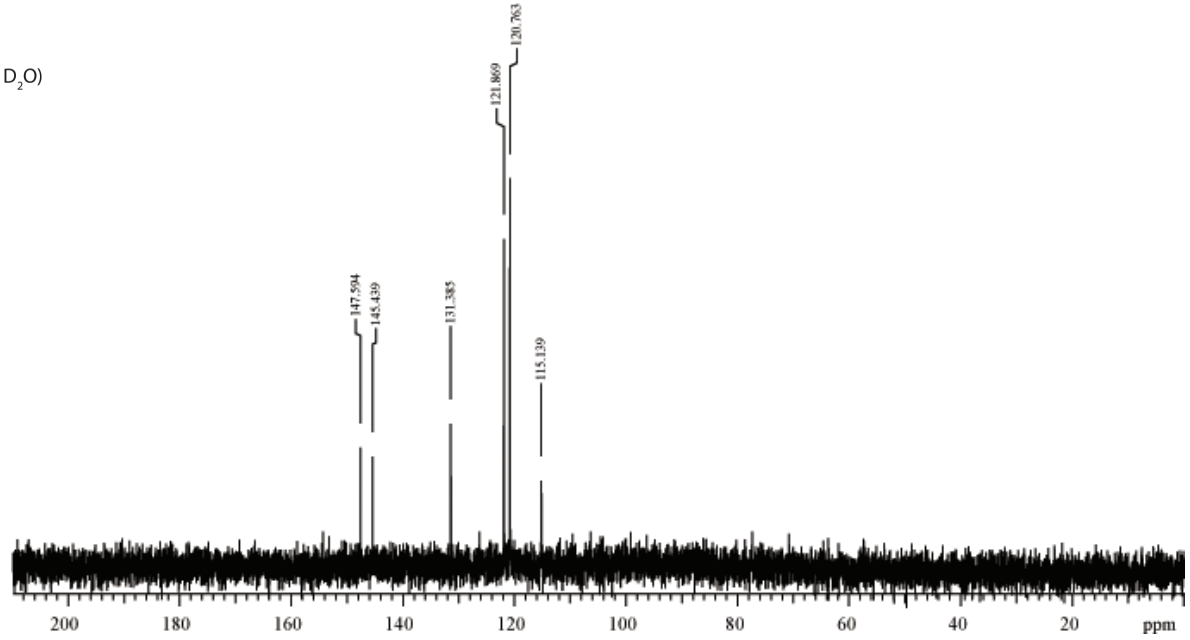

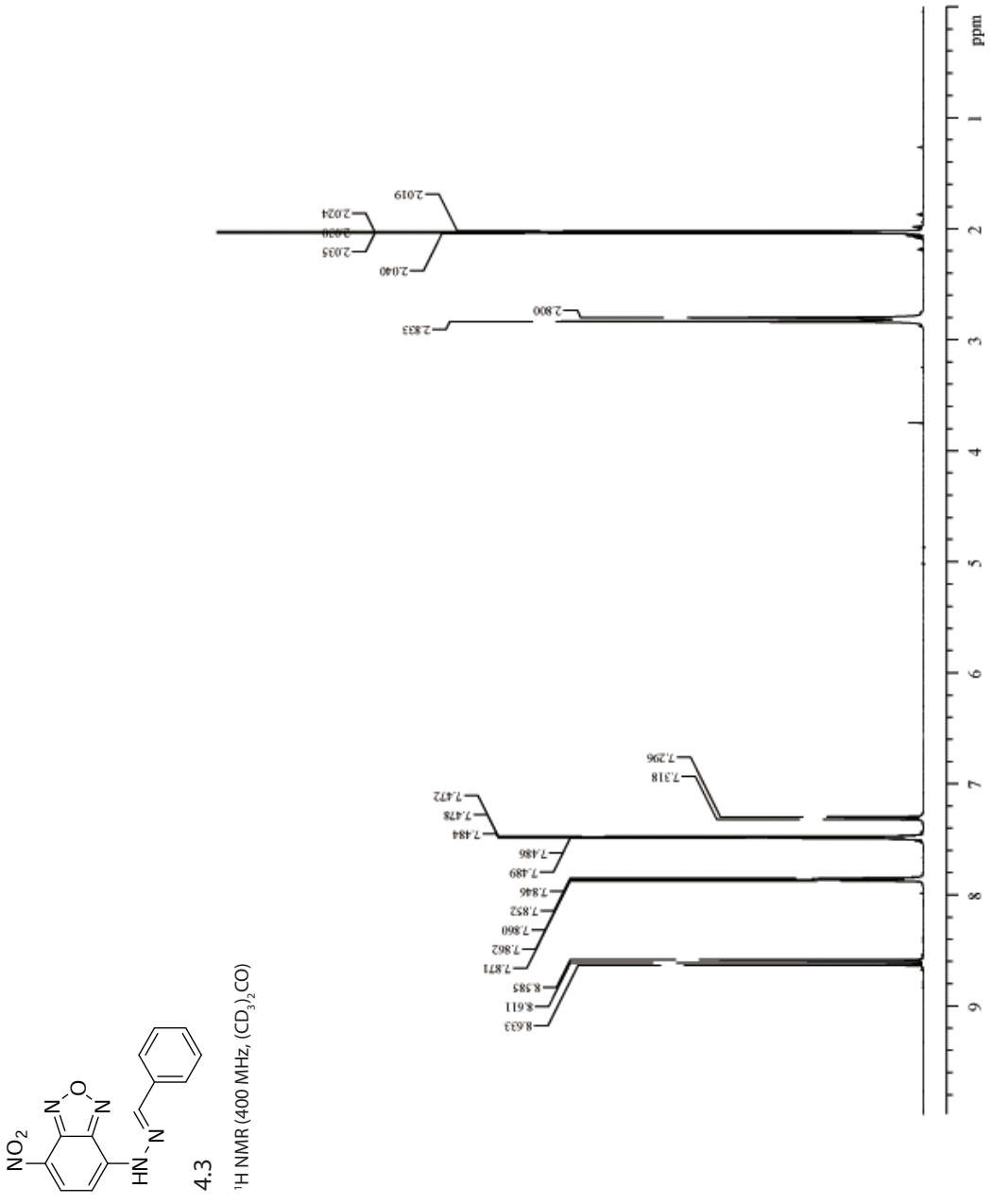
NO2
HN
N
O
N
4.3
1H NMR (400 MHz, (CD3)2CO)
8.633
8.611
8.585
7.871
7.862
7.860
7.852
7.846
7.489
7.486
7.484
7.478
7.472
7.318
7.296
2.833
2.800
2.040
2.035
2.030
2.024
2.019
ppm

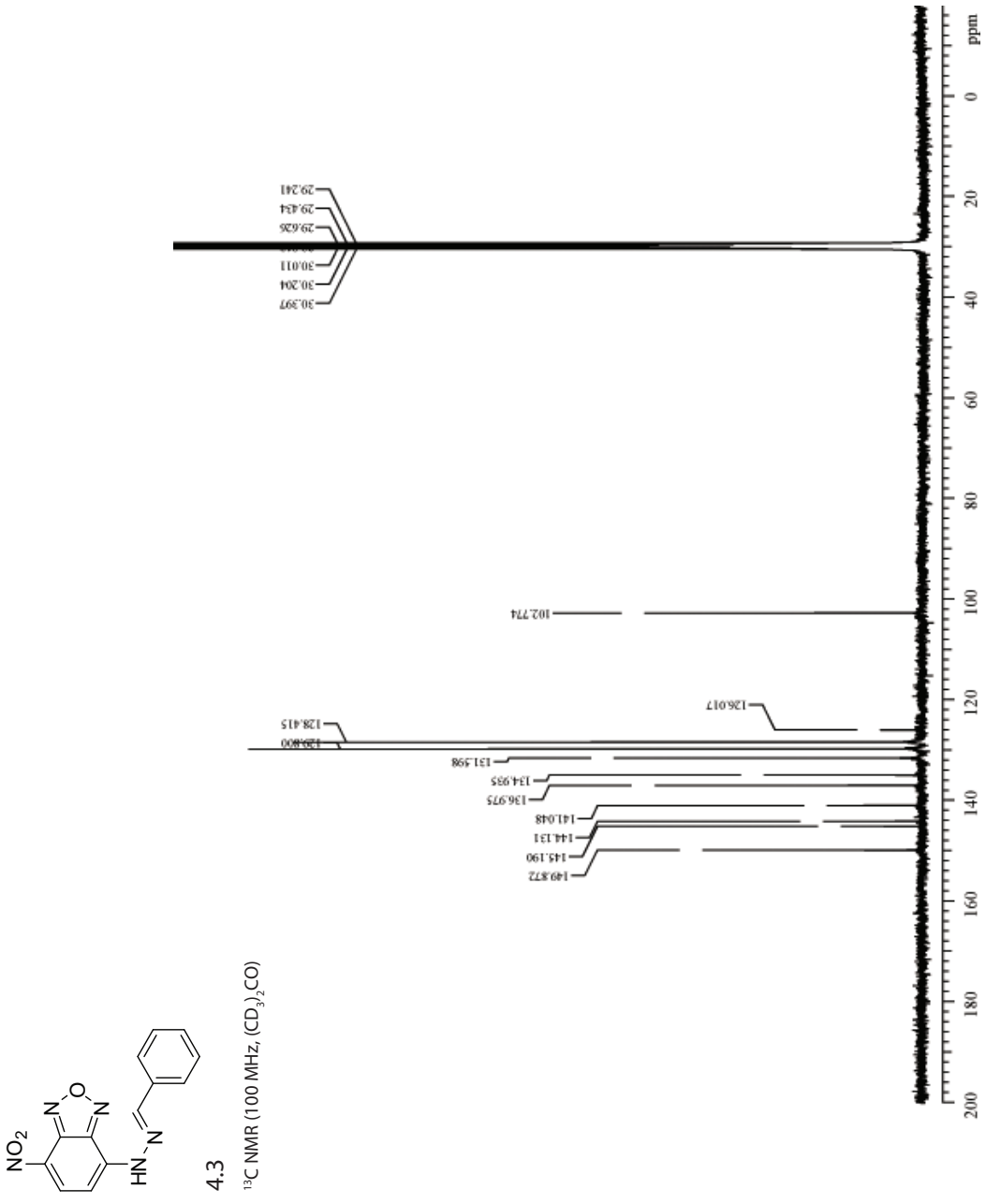
4.3
^{13}C NMR (100 MHz, $(CD_3)_2CO$)
NO_2
HN
N
O
N
N
ppm
0
20
40
60
80
100
120
140
160
180
200
29.241
29.434
29.636
30.011
30.204
30.397
102.774
126.017
128.415
128.800
131.598
134.935
136.975
141.048
144.131
145.190
149.872

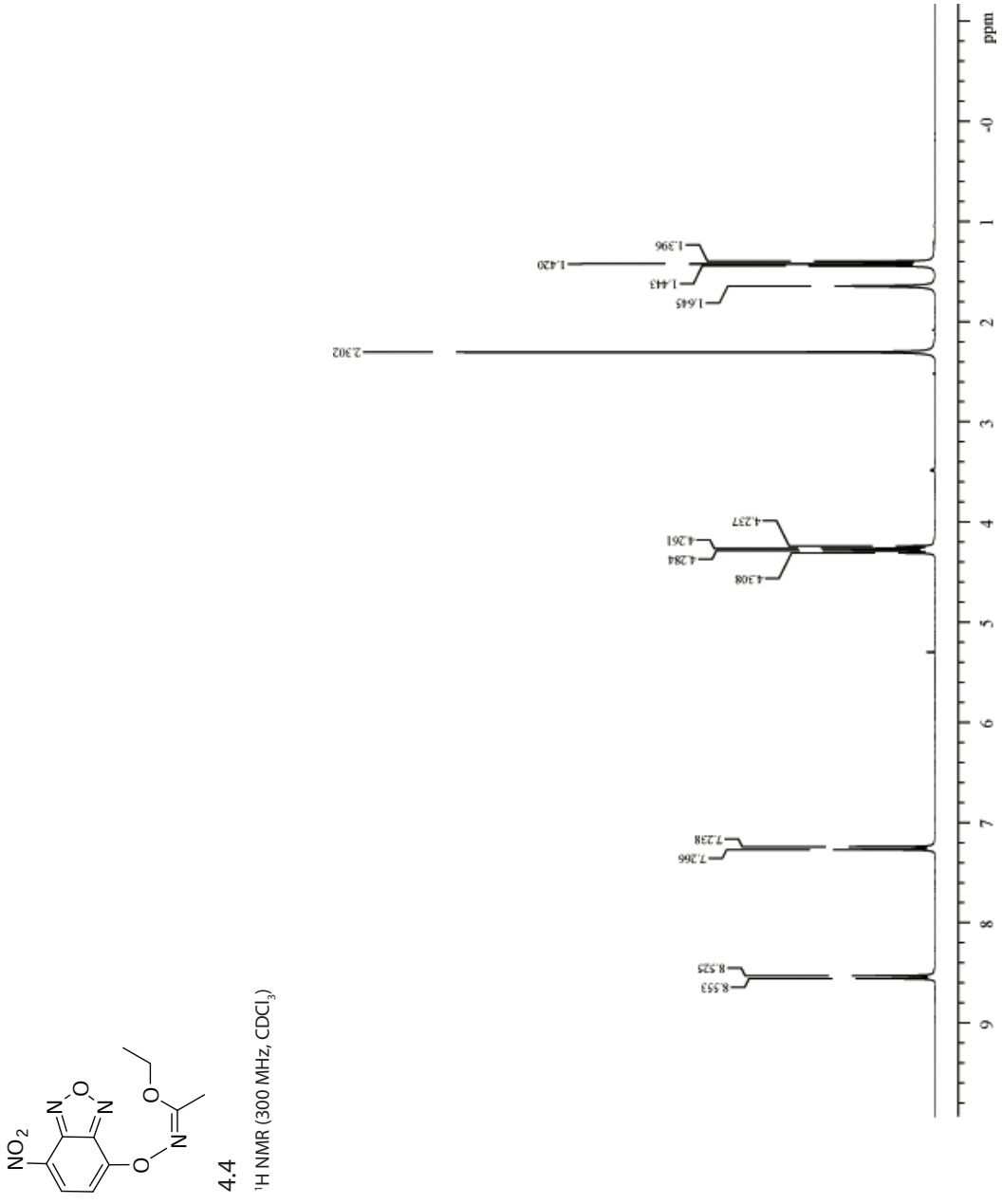

4.4

^{1}H NMR (300 MHz, $CDCl_3$)

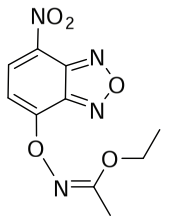

4.4

^{13}C NMR (100 MHz, $CDCl_3$)

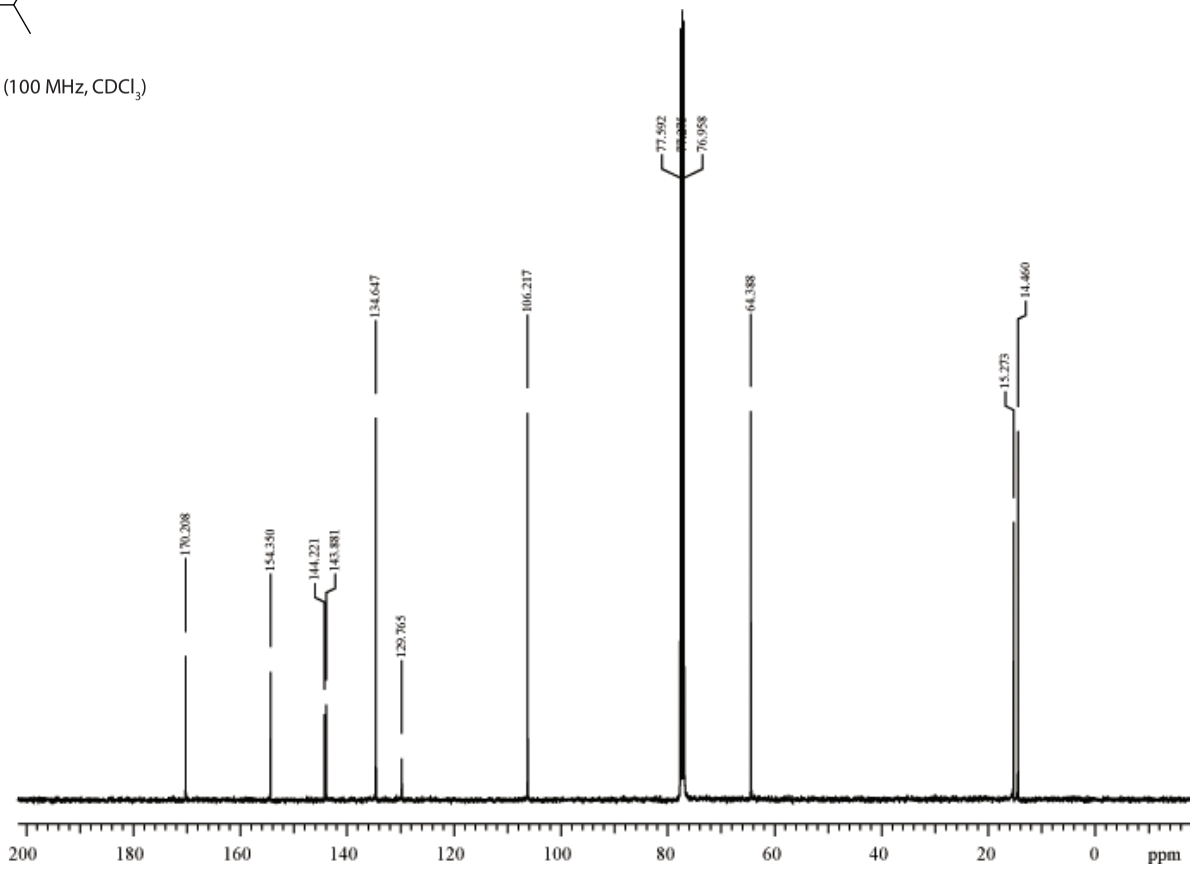

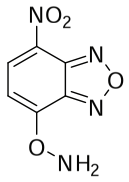

4.5

^{1}H NMR (700 MHz, $CDCl_3$)

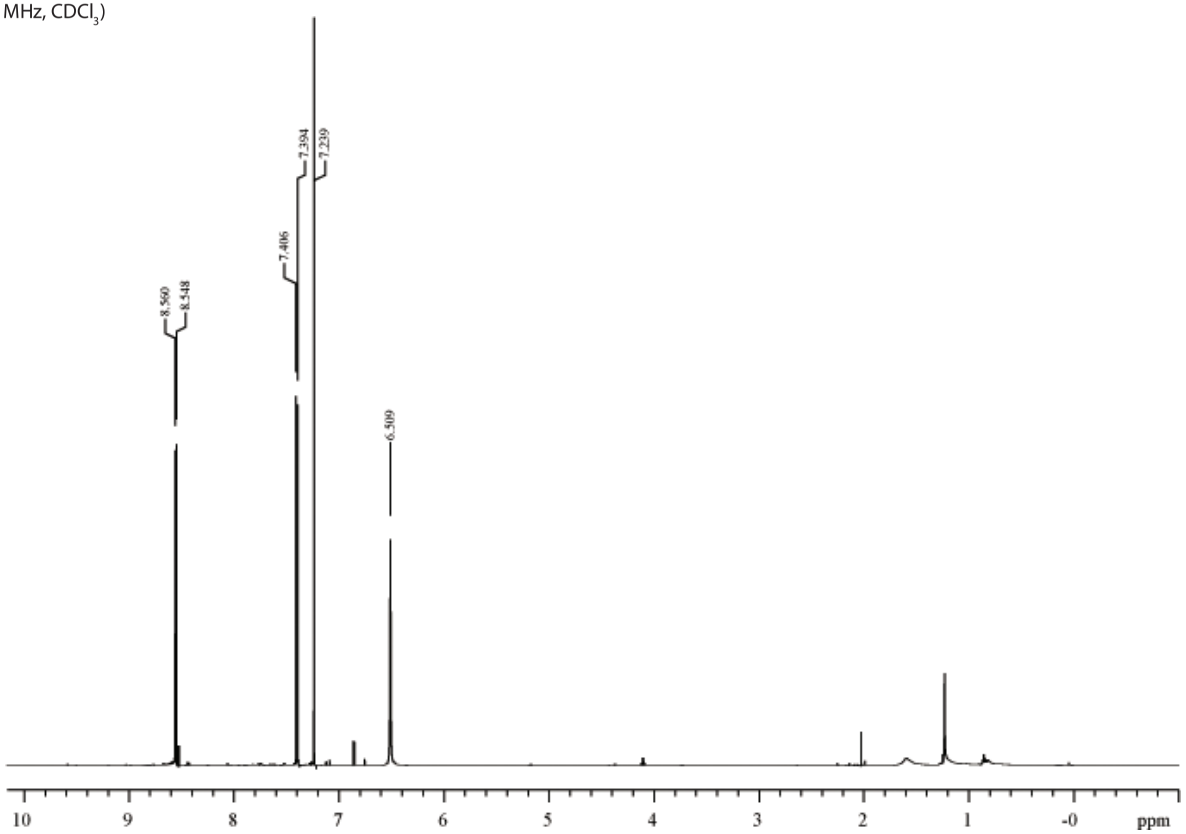

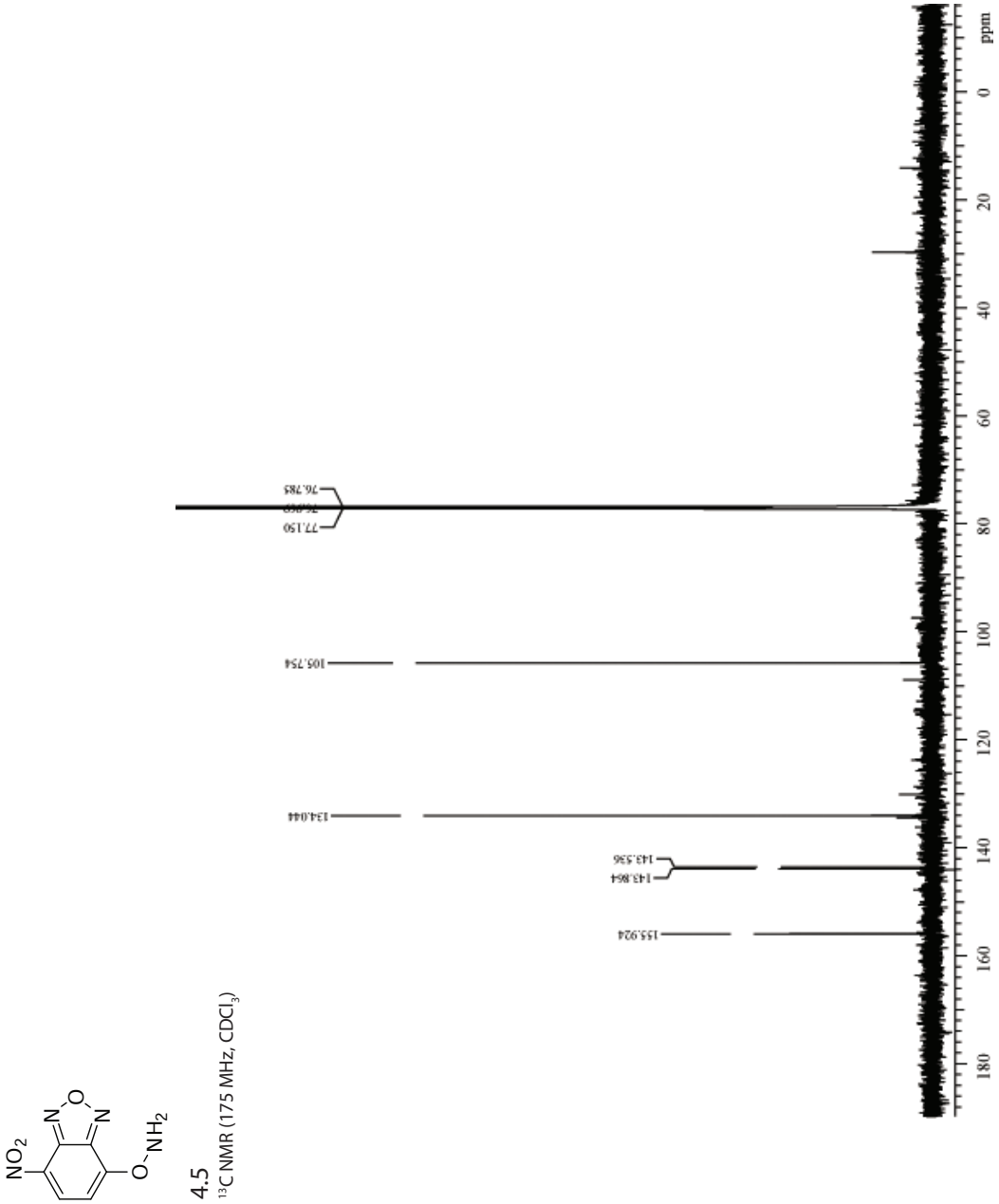
NO2
O
N
N
O
NH2
4.5
13C NMR (175 MHz, CDCl3)
155.924
143.864
143.536
134.044
105.754
77.150
76.785
ppm
0
20
40
60
80
100
120
140
160
180

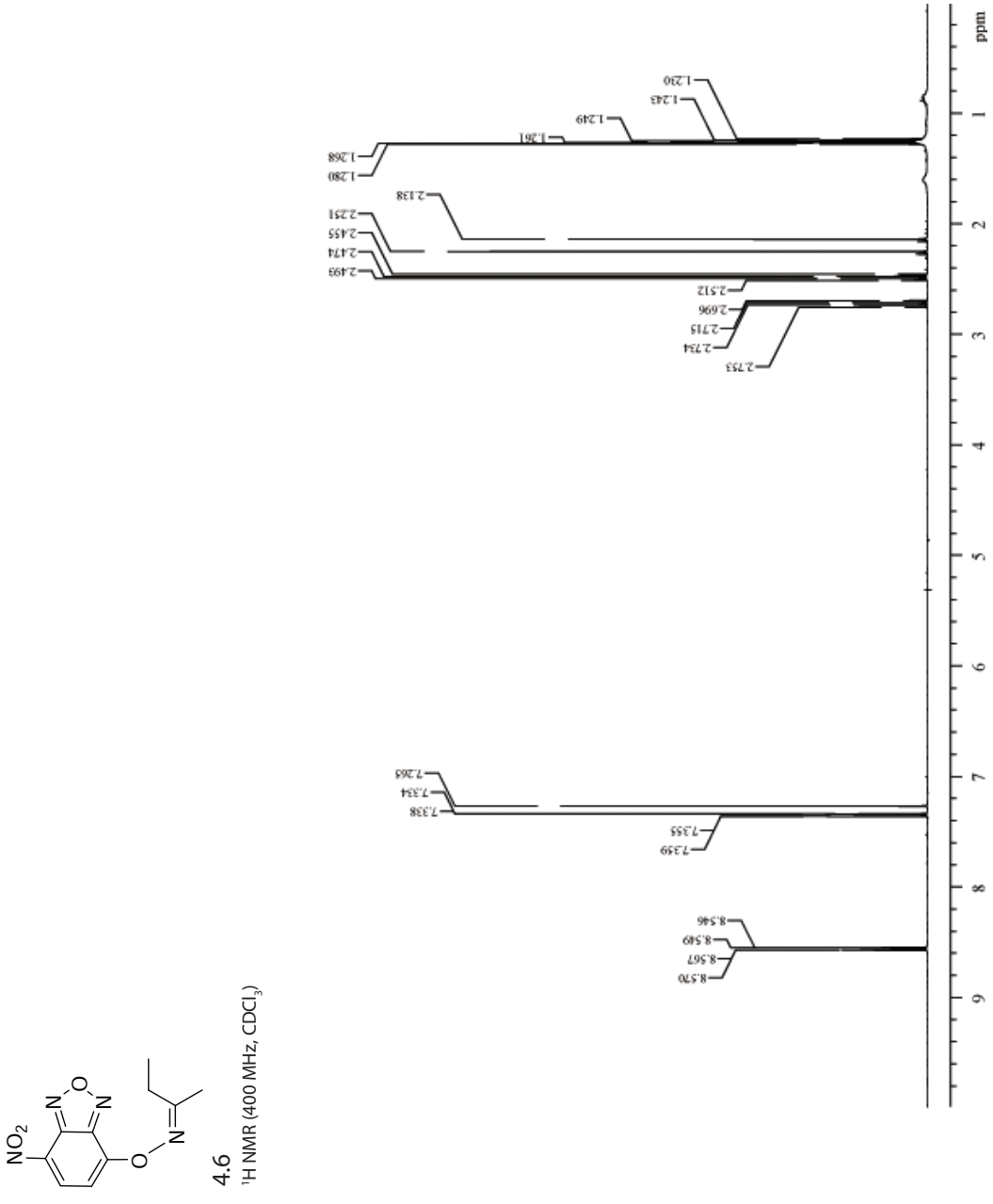
4.6
^{1}H NMR (400 MHz, $CDCl_3$)
NO_2
8.570
8.567
8.549
8.546
7.359
7.355
7.338
7.334
7.265
2.753
2.734
2.715
2.696
2.512
2.493
2.474
2.455
2.251
2.138
1.280
1.268
1.261
1.249
1.243
1.240
ppm

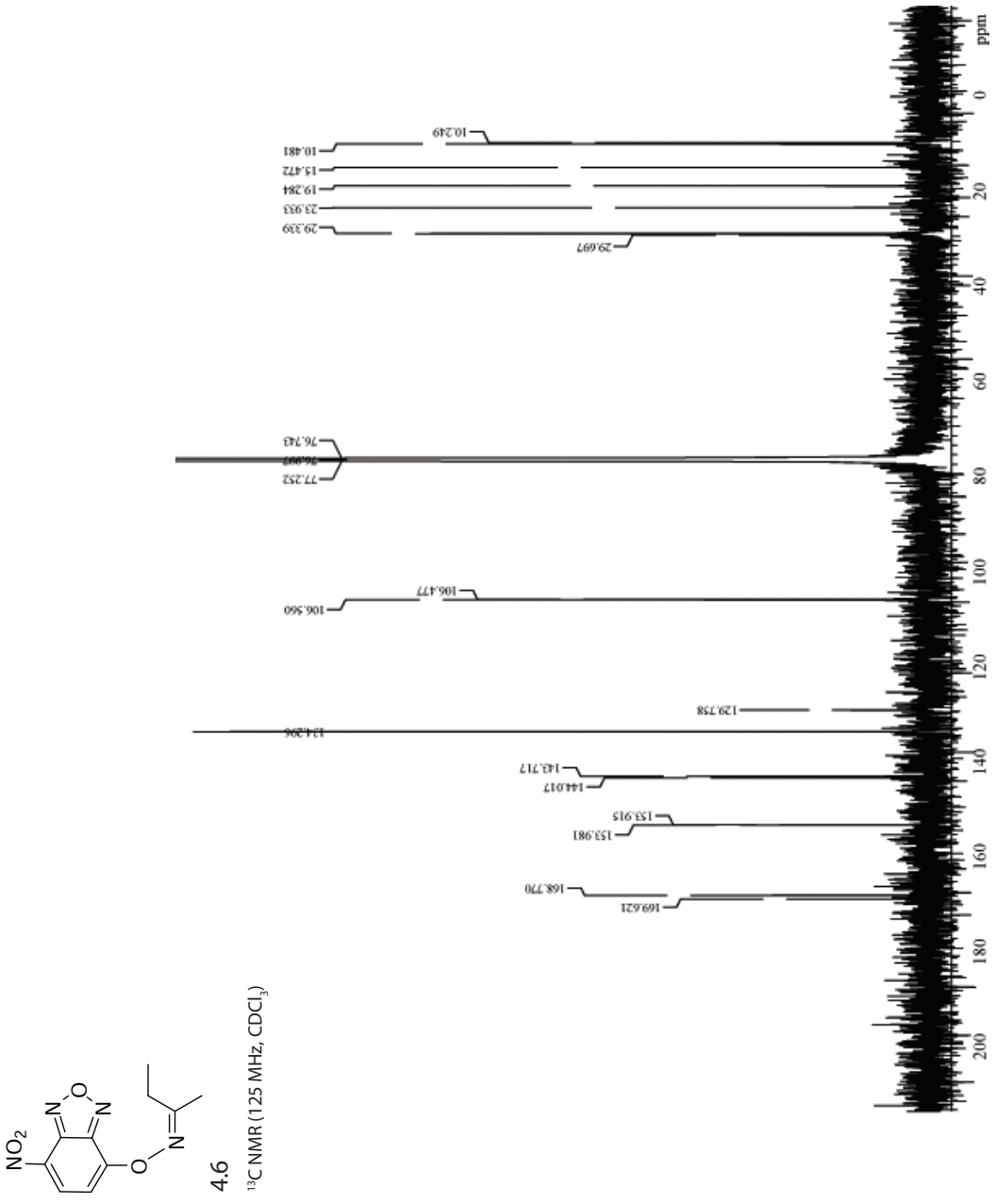
10.249
10.481
15.472
19.284
23.933
29.339
29.697
76.743
77.252
106.477
106.560
129.758
131.296
143.717
144.017
153.915
153.981
168.770
169.621
ppm
0
20
40
60
80
100
120
140
160
180
200
NO2
O
N
N
O
N
4.6
13C NMR (125 MHz, CDCl3)

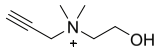

5.3
^{1}H NMR (500 MHz, D_2O)

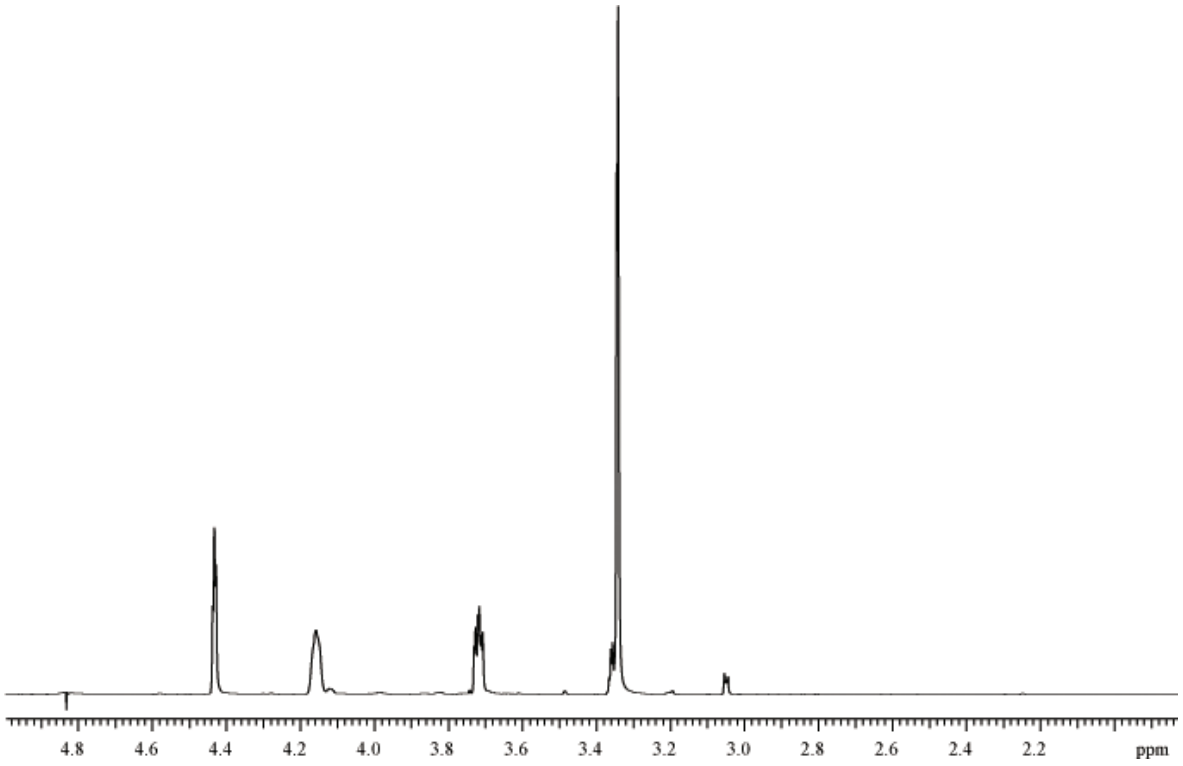

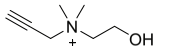

5.3
APT ^{13}C NMR (125 MHz, D_2O)

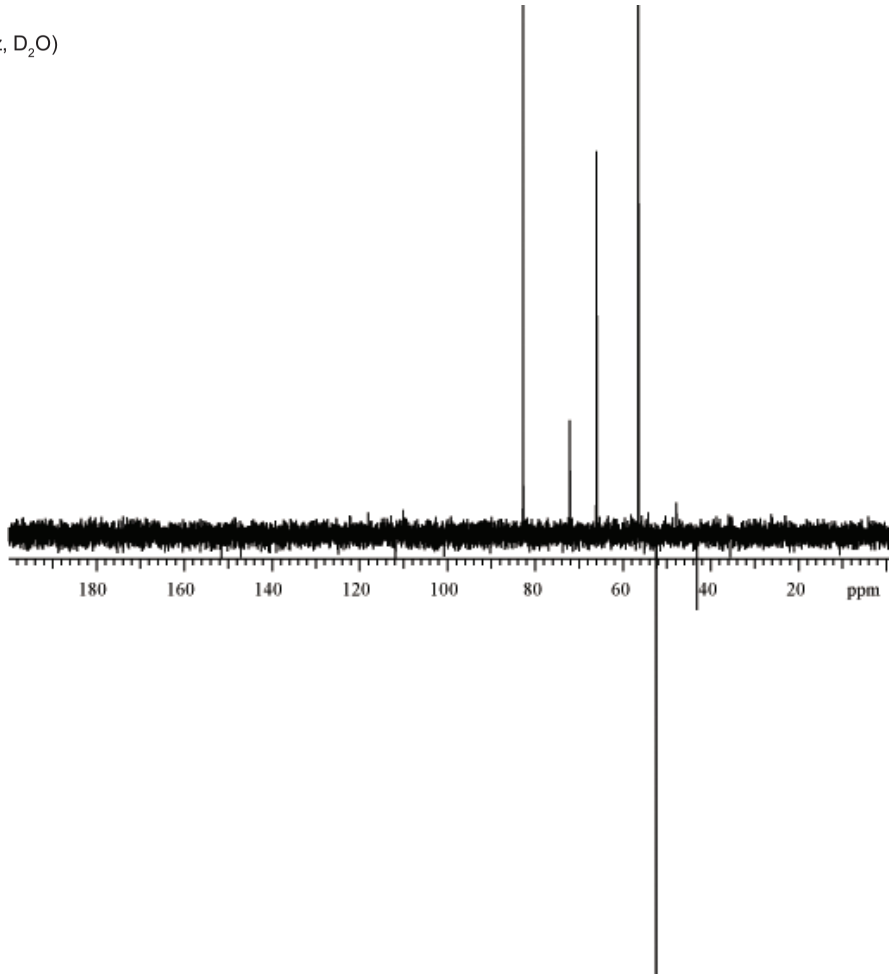

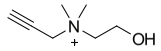

5.3

^{1}H COSY NMR (500 MHz, D_2O)

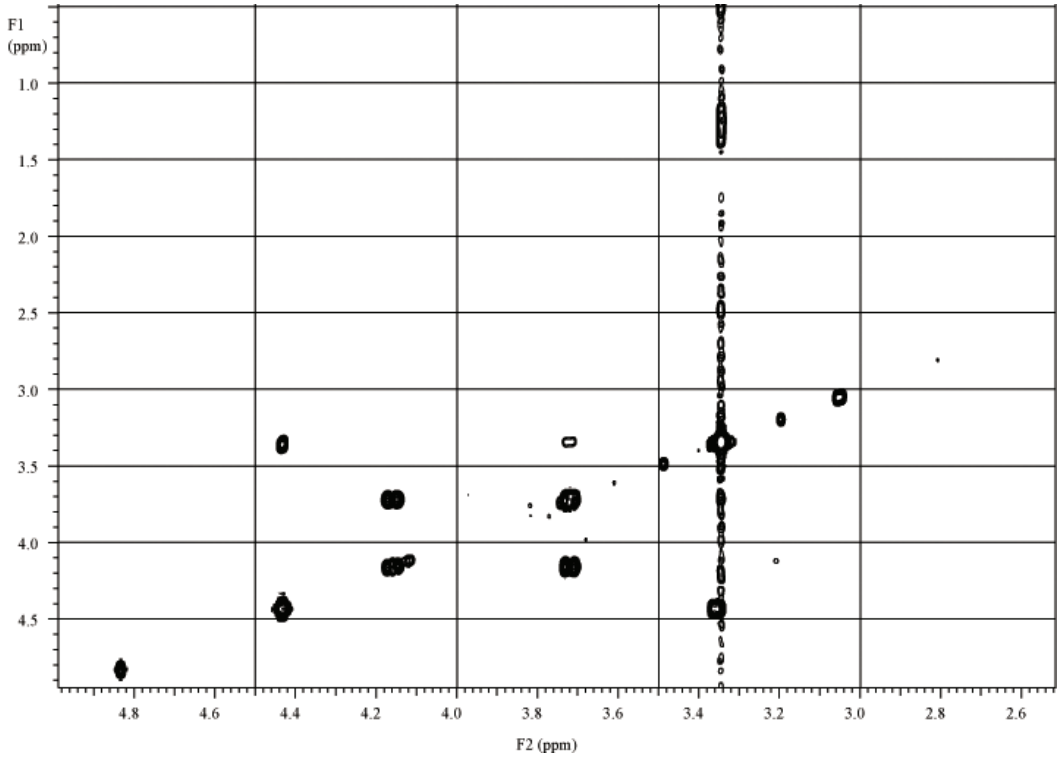

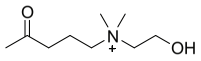

5.8
^{1}H NMR (300 MHz, D_2O)

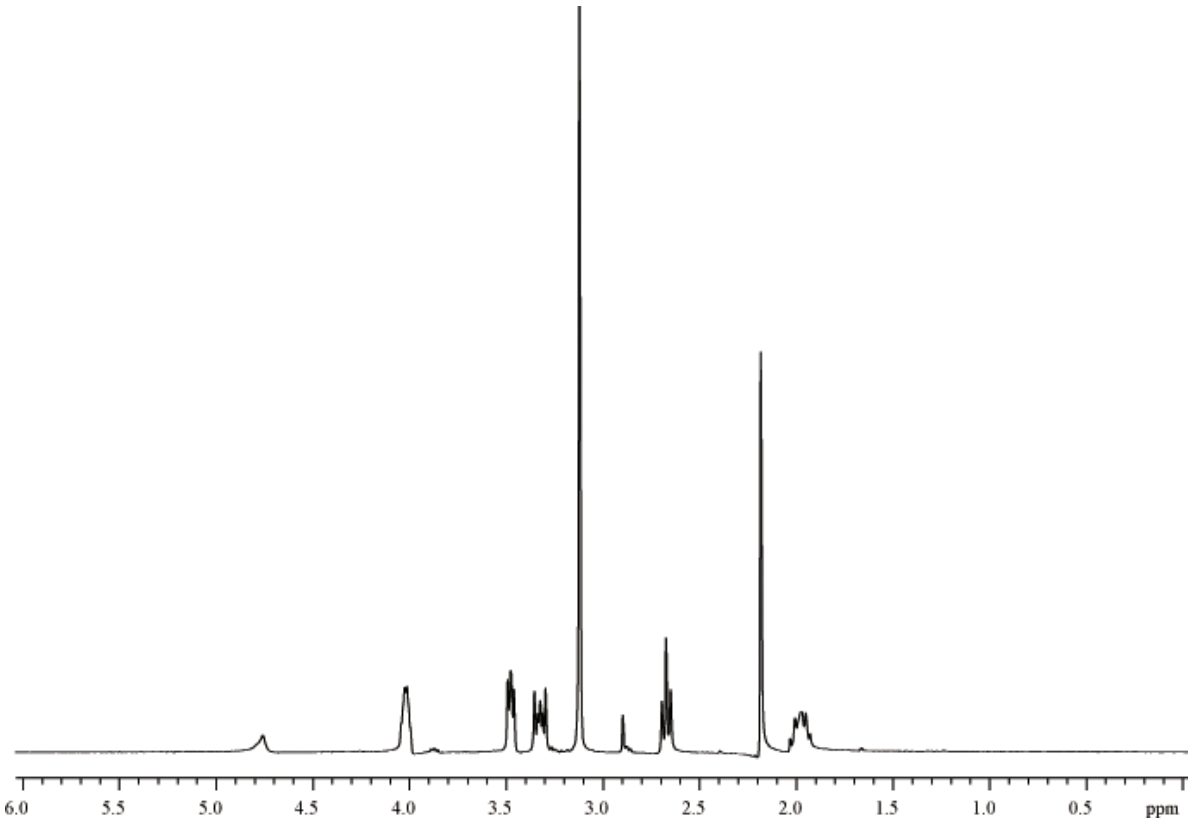

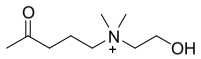

5.8

^{13}C NMR (125 MHz, D_2O)

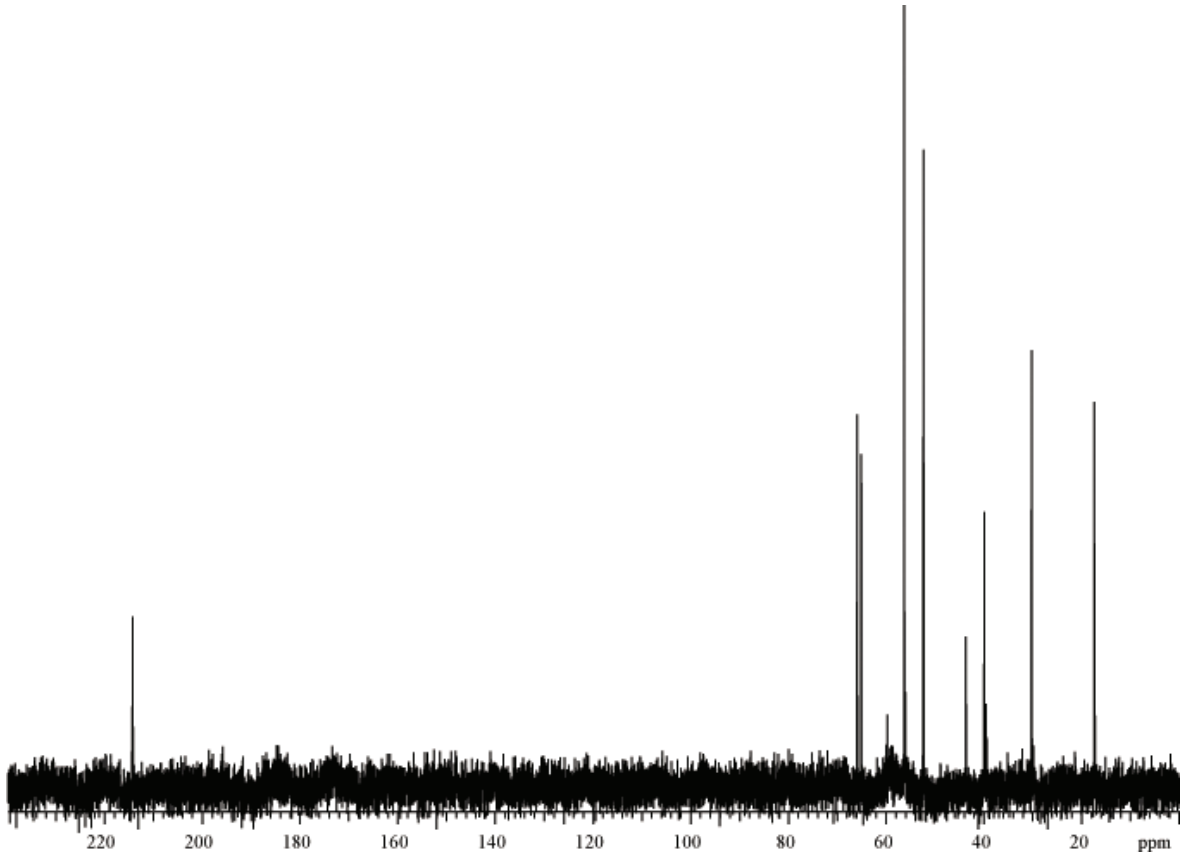

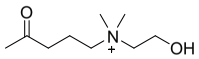

5.8

^{1}H COSY NMR (300 MHz, D_2O)

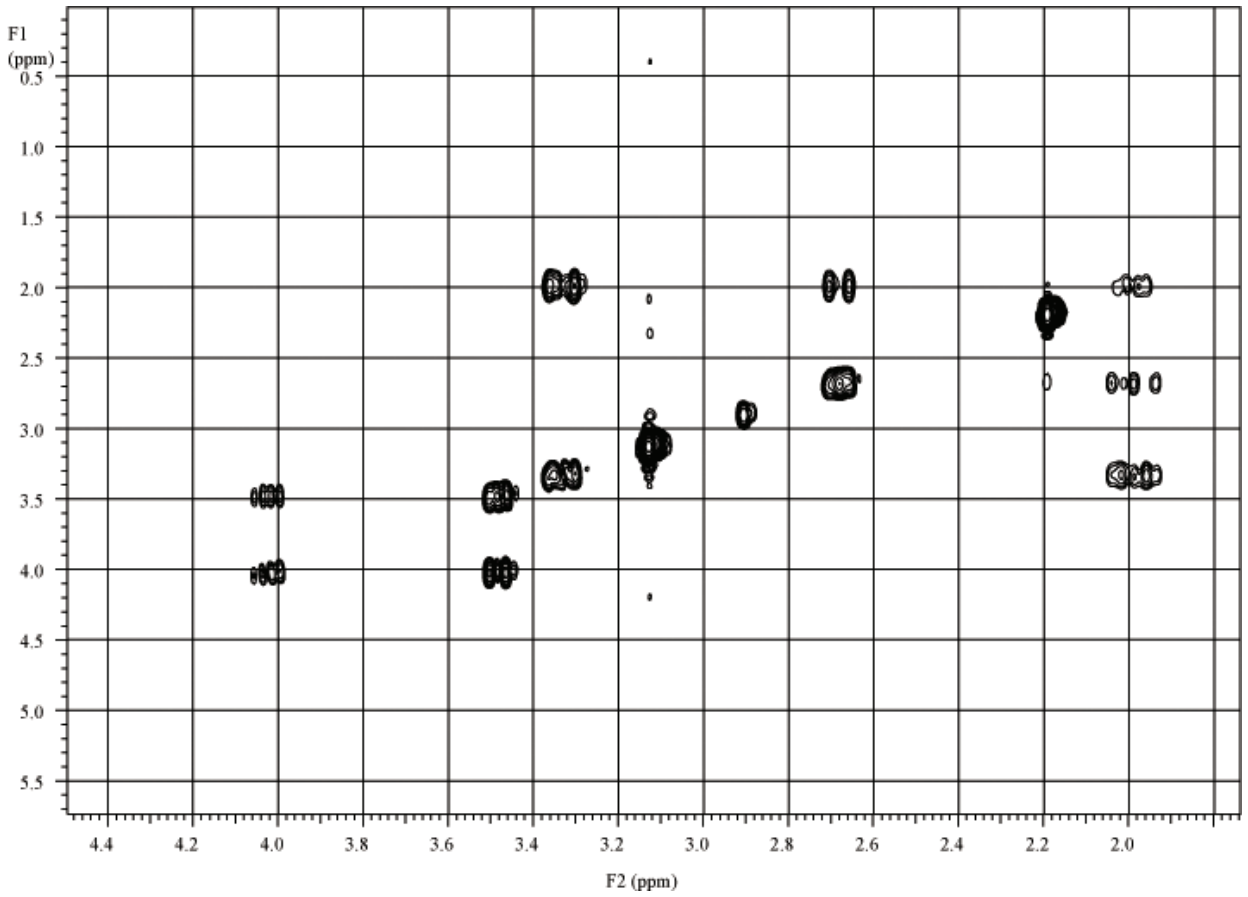

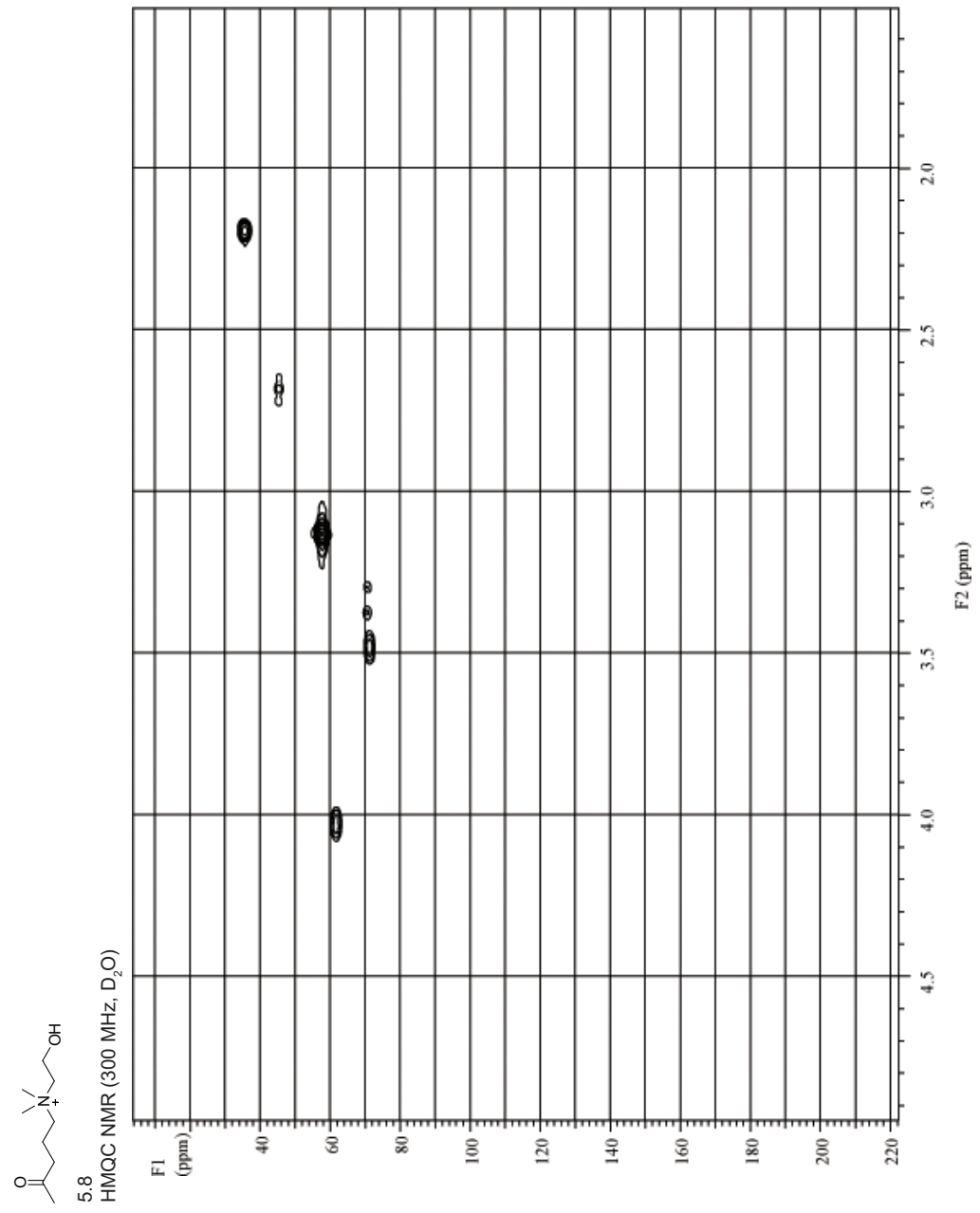
O
N+
OH
5.8
HMQC NMR (300 MHz, D2O)
F1 (ppm)
40
60
80
100
120
140
160
180
200
220
4.5
4.0
3.5
3.0
2.5
2.0
F2 (ppm)

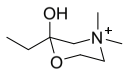

5.10
^{1}H NMR (500 MHz, D_2O)

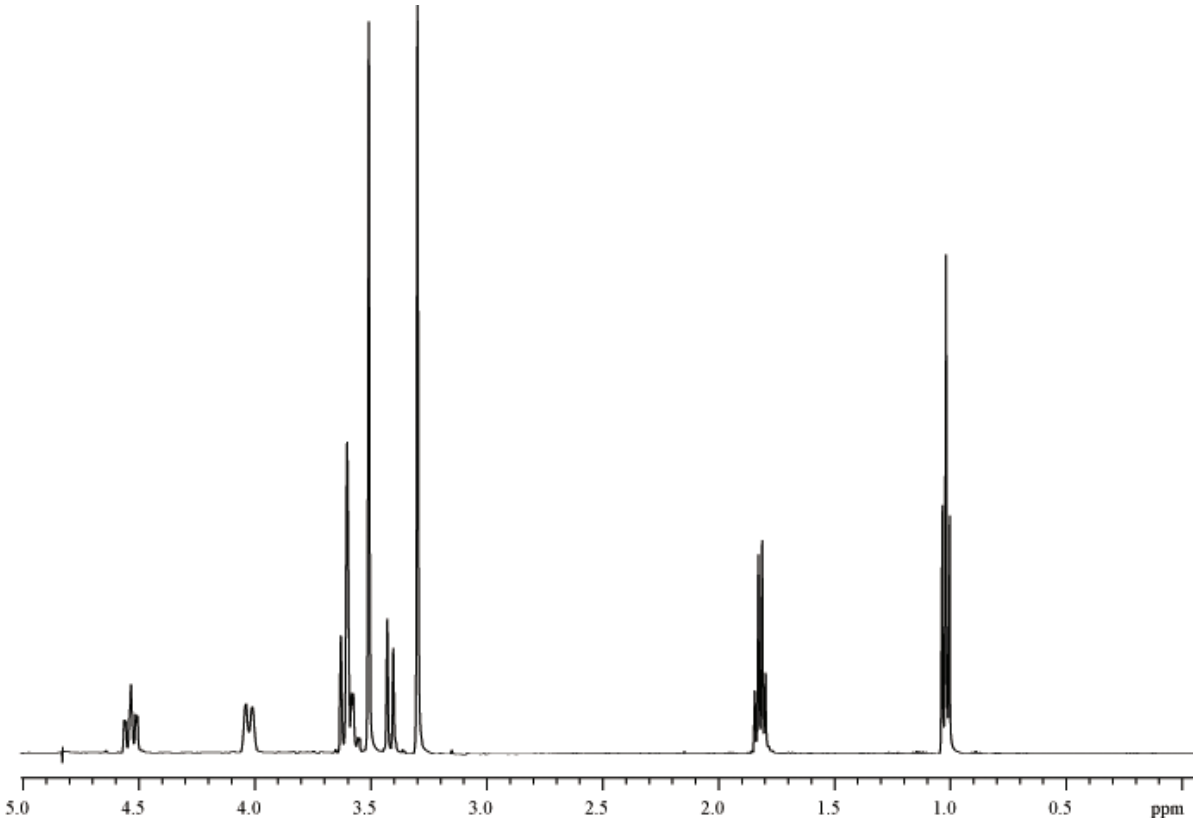

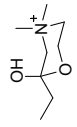

5.10
APT ^{13}C NMR (125 MHz, D_2O)

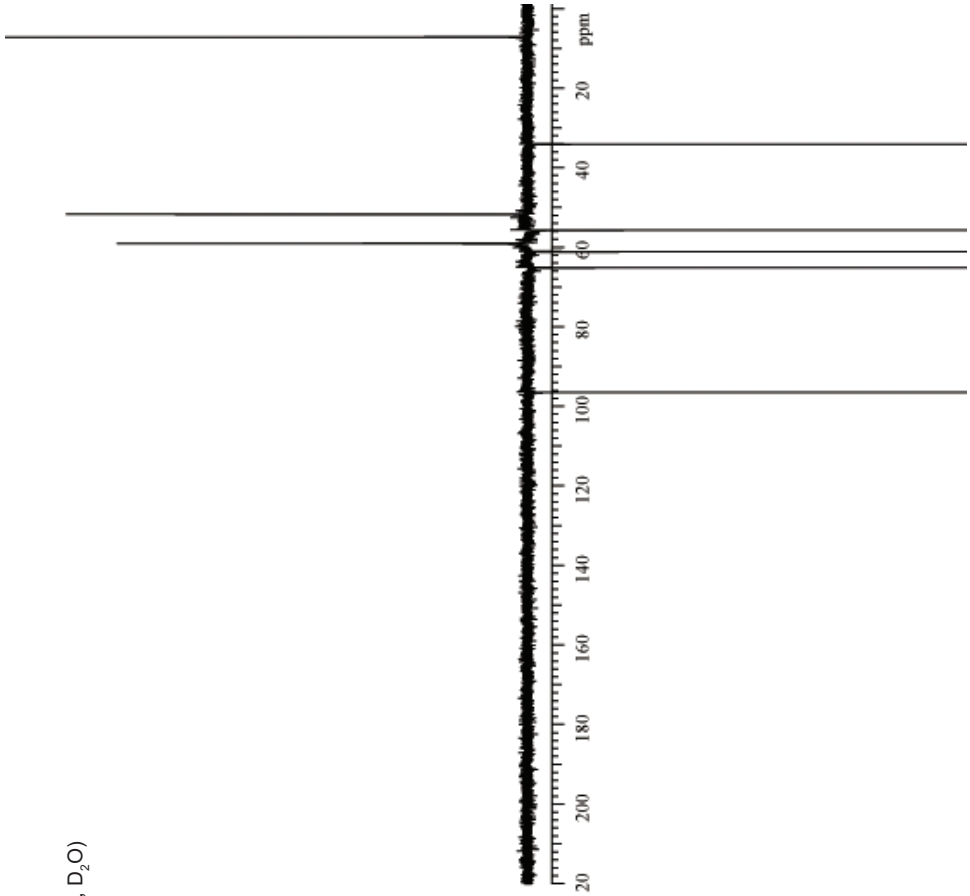

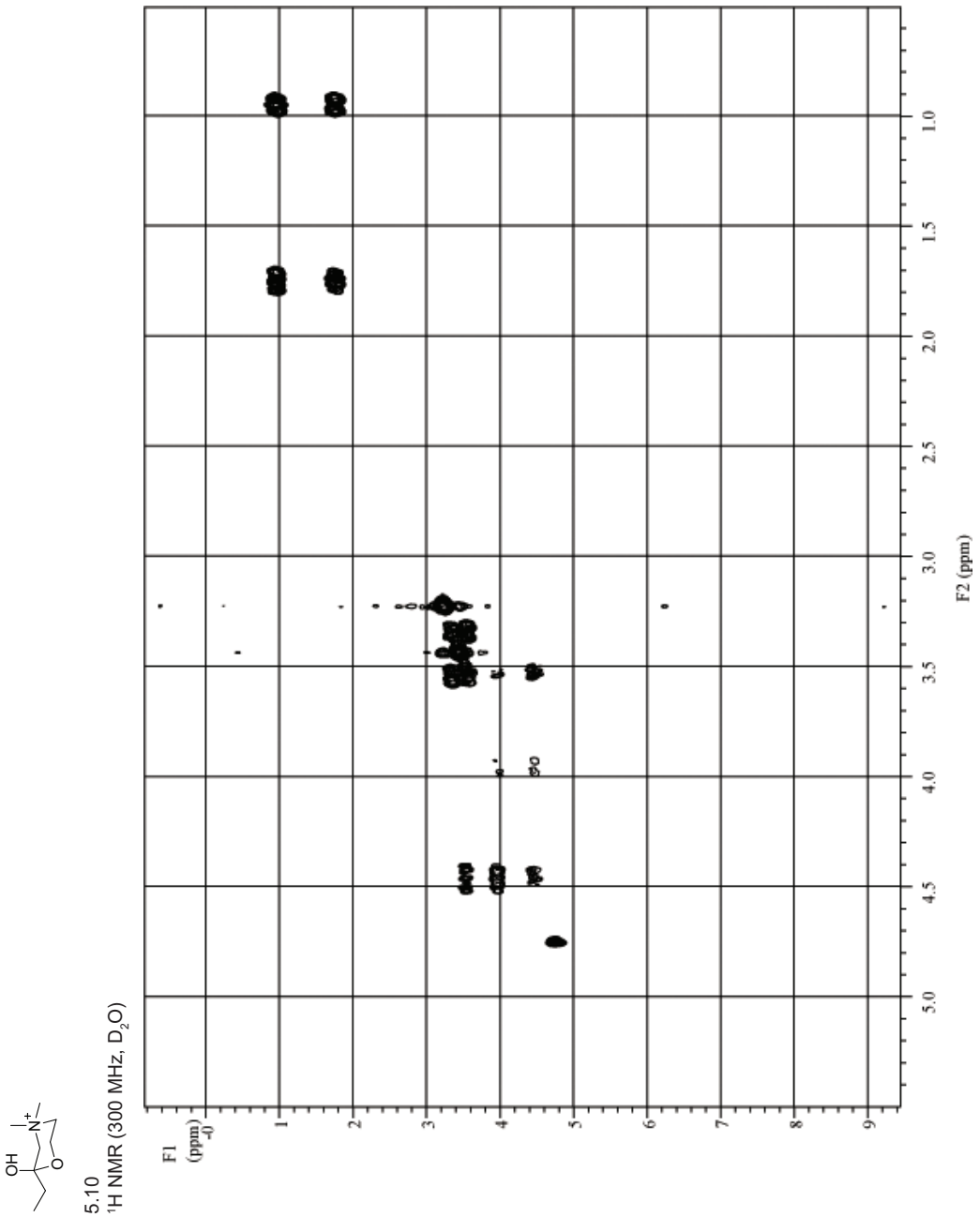

5.10
^{1}H NMR (300 MHz, D_2O)

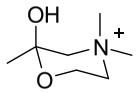

5.12
^{1}H NMR (500 MHz, D_2O)

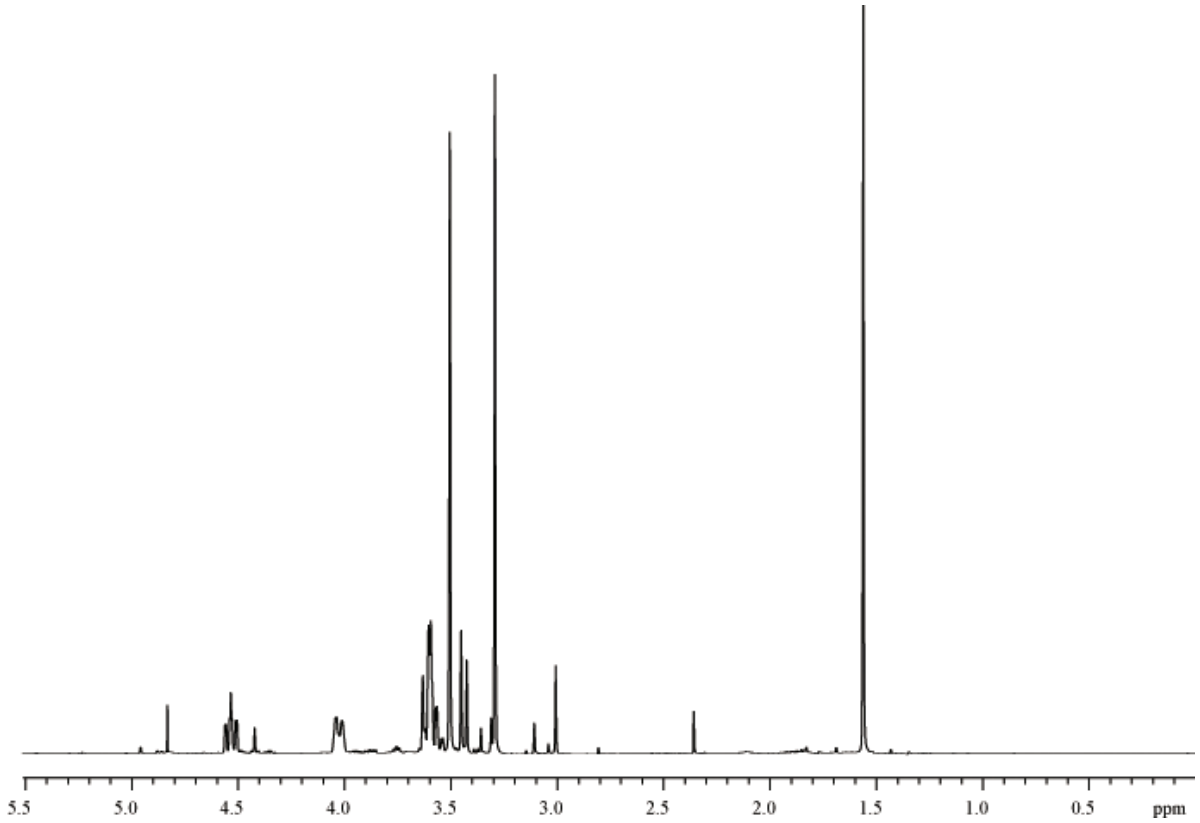

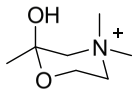

5.12
^{13}C NMR (125 MHz, D_2O)

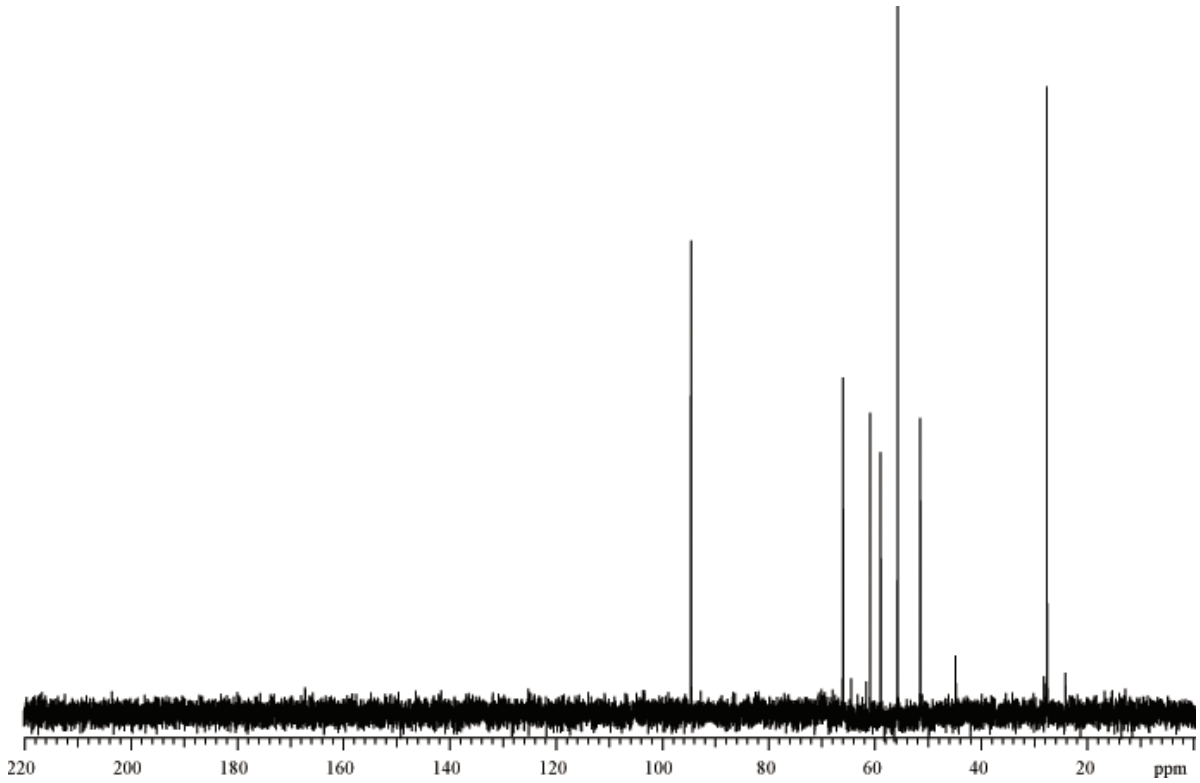

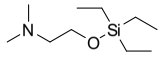

5.13
^{1}H NMR (300 MHz, CD_3OD)

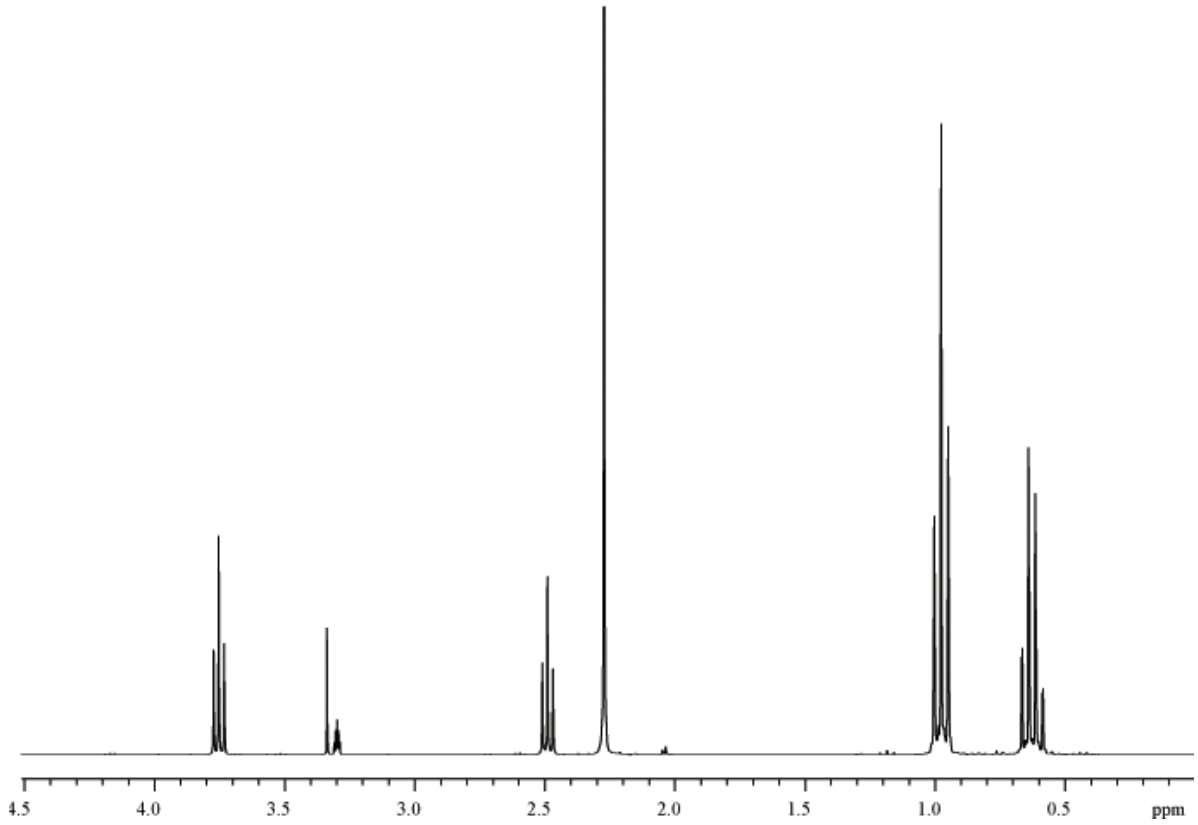

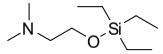

5.13
^{13}C NMR (100 MHz, CD_3OD)

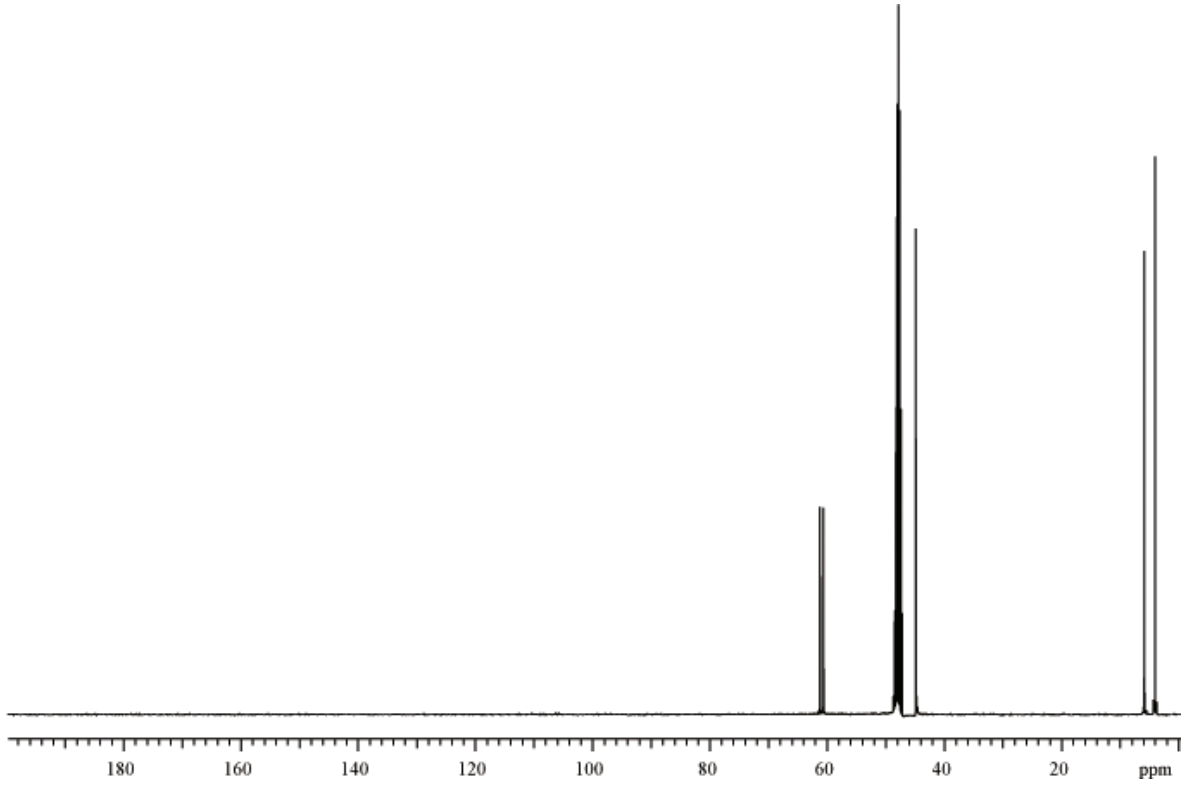

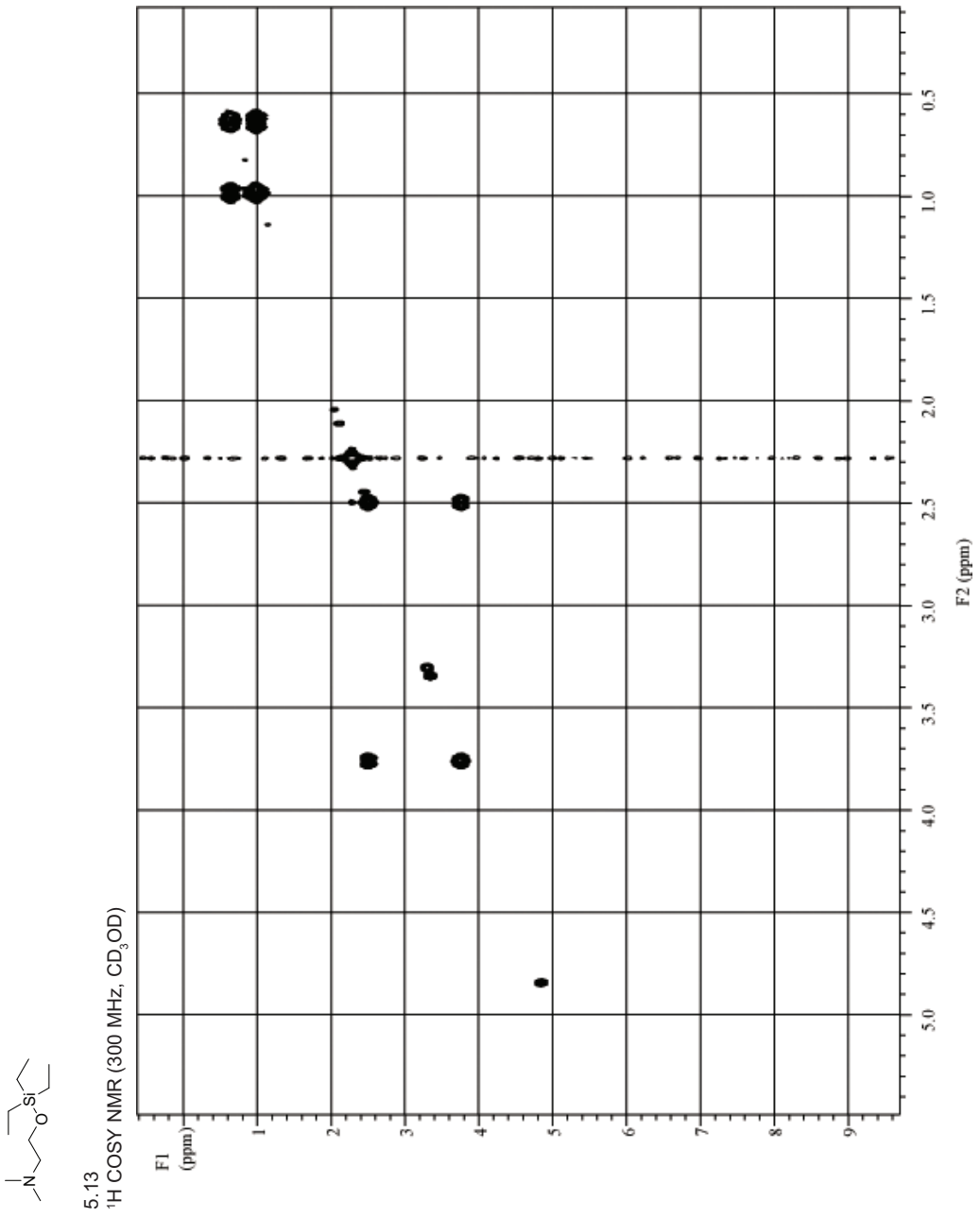
5.13
^{1}H COSY NMR (300 MHz, CD_3OD)
F1 (ppm)
F2 (ppm)
1
2
3
4
5
6
7
8
9
5.0
4.5
4.0
3.5
3.0
2.5
2.0
1.5
1.0
0.5
N
O
Si

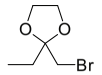

5.15

^{1}H NMR (400 MHz, $CDCl_3$)

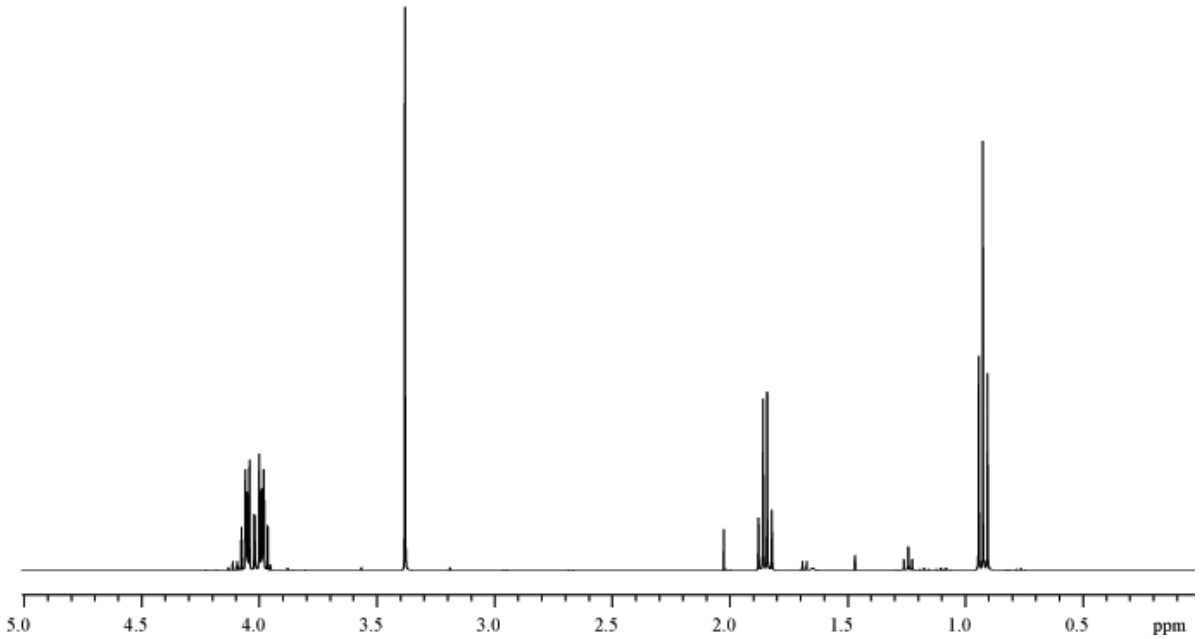

5.15
APT ^{13}C NMR (100 MHz, $CDCl_3$)

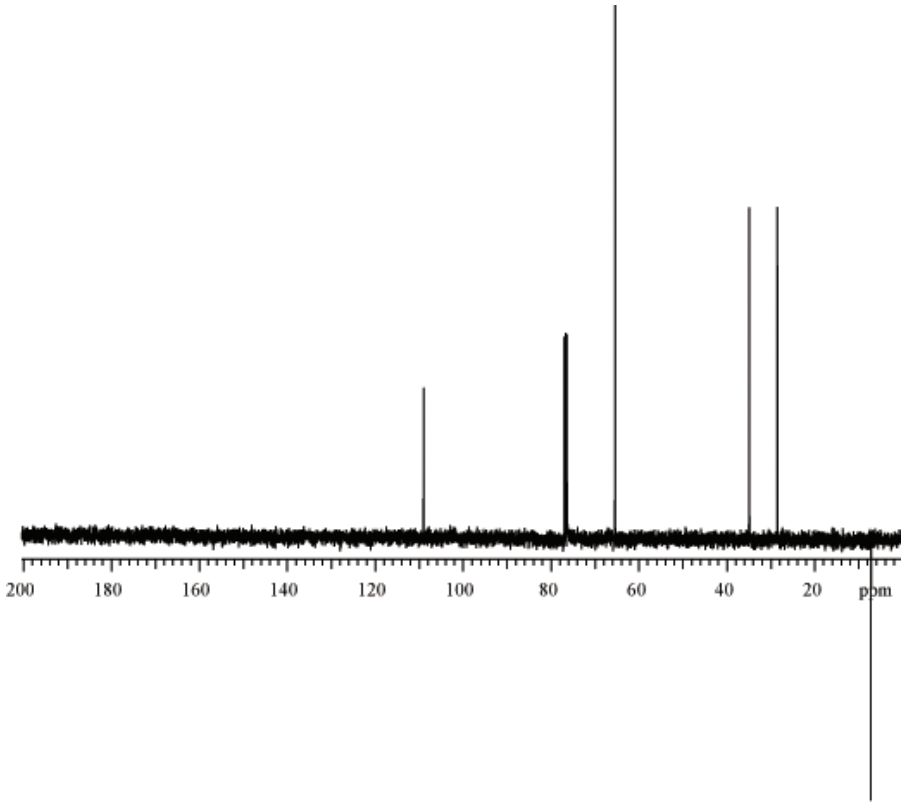

5.15
^{1}H COSY NMR (400 MHz, CD_3OD)

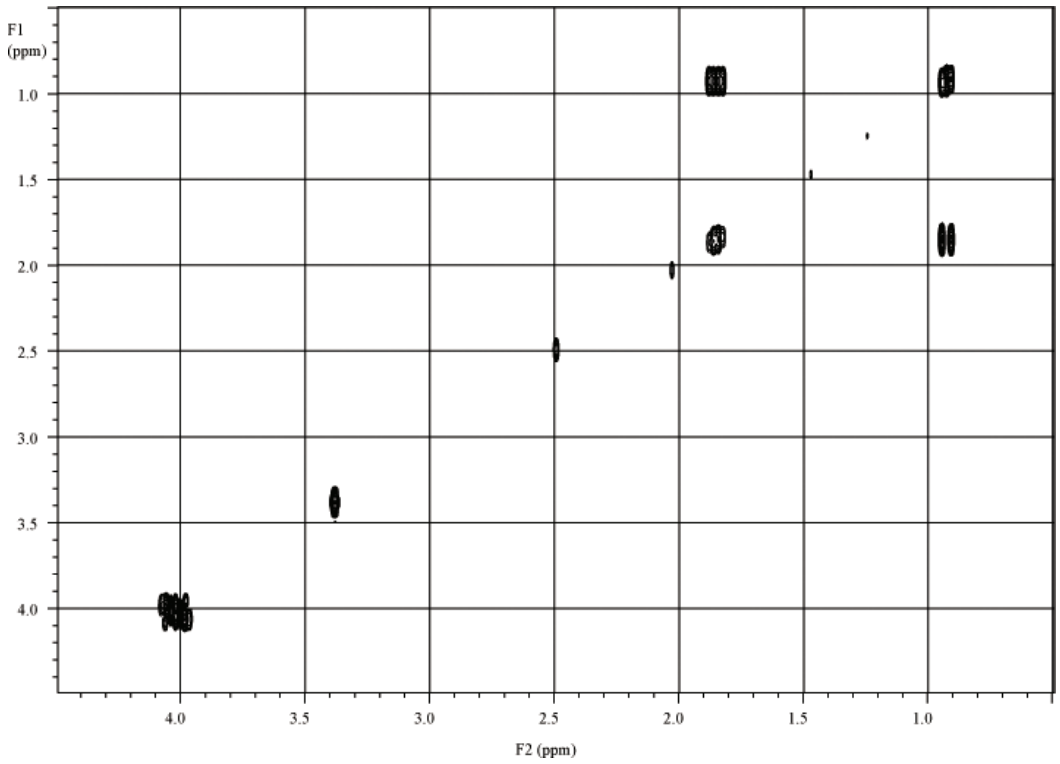

5.15
HSQC NMR (400 MHz, CD_3OD)

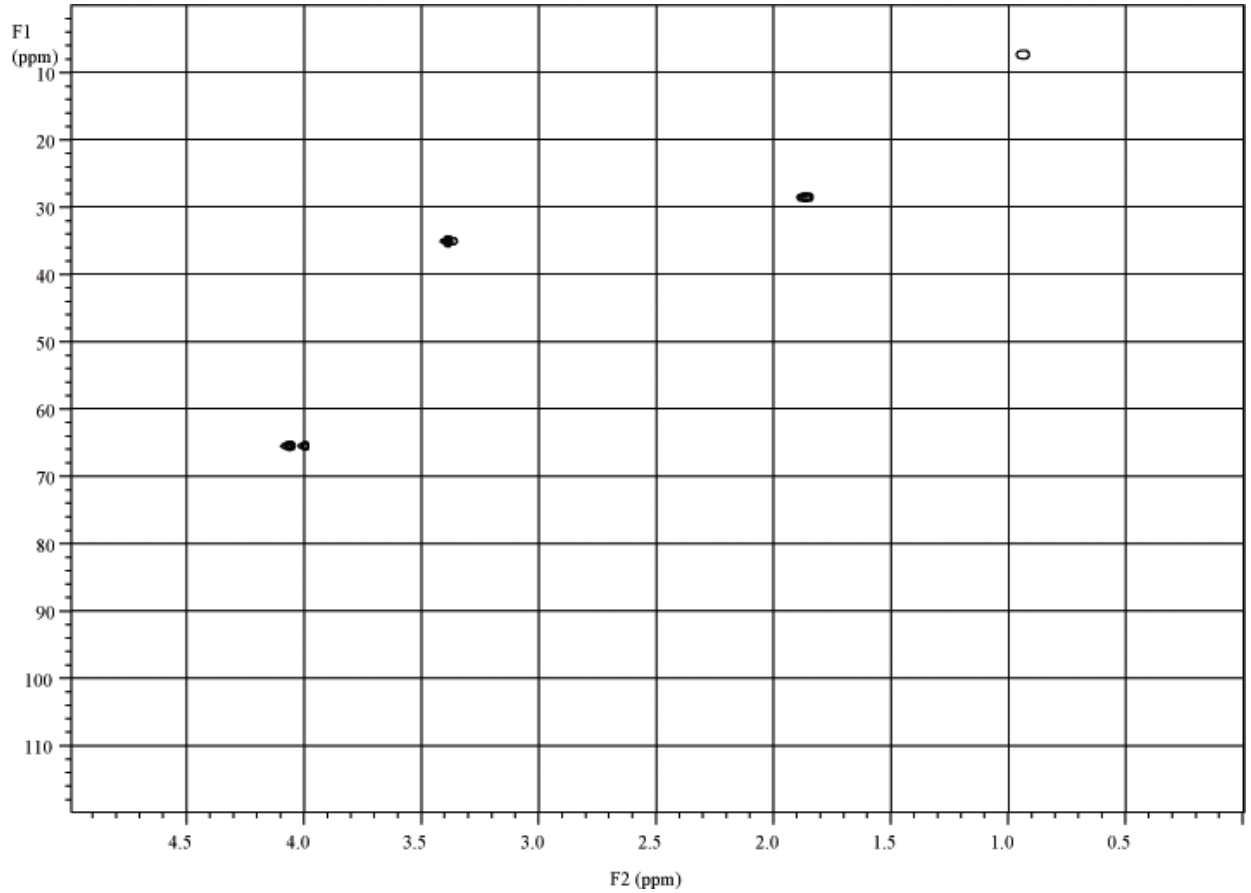

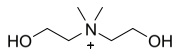

5.16
^{1}H NMR (500 MHz, CD_3OD)

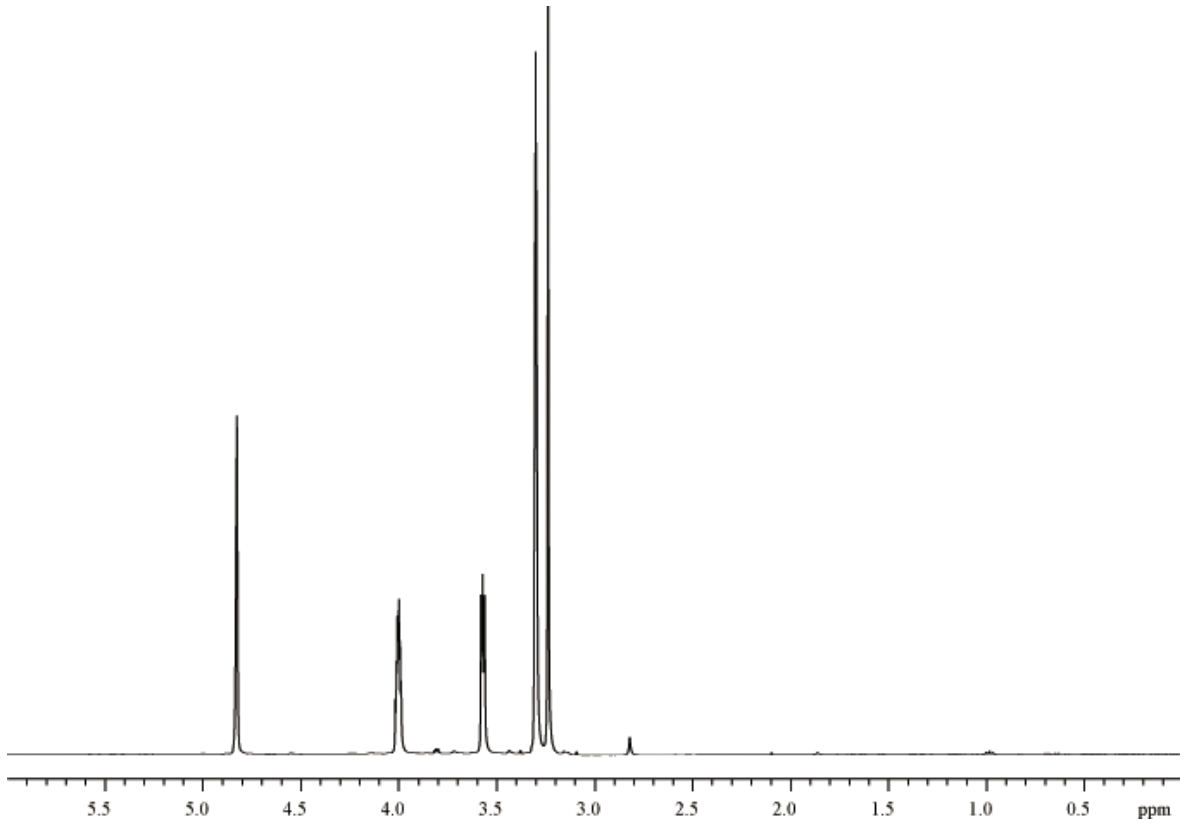

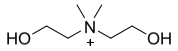

5.16
^{13}C NMR (125 MHz, CD_3OD)

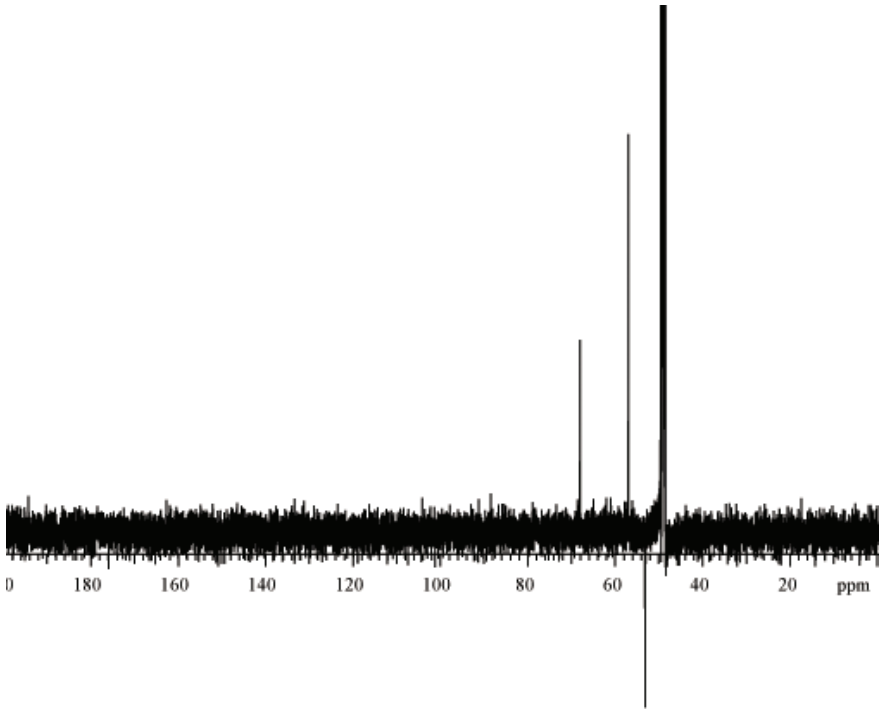

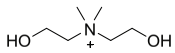

5.16

^{1}H COSY NMR (300 MHz, CD_3OD)

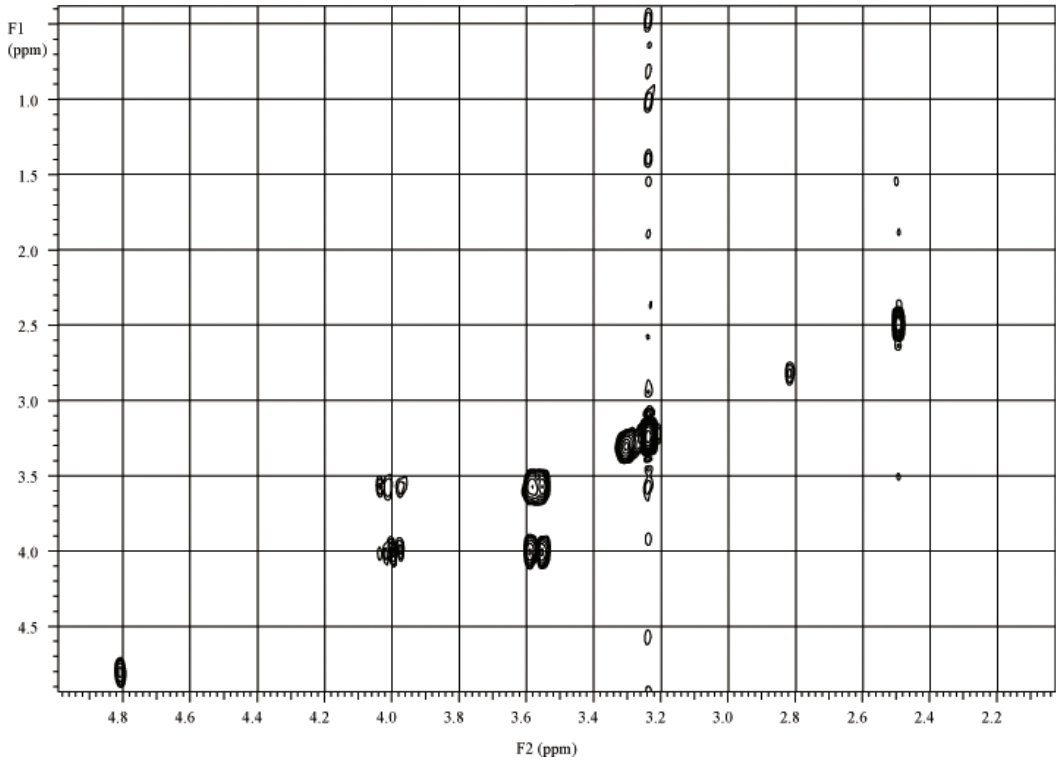

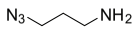

5.20
^{1}H NMR (300 MHz, $CDCl_3$)

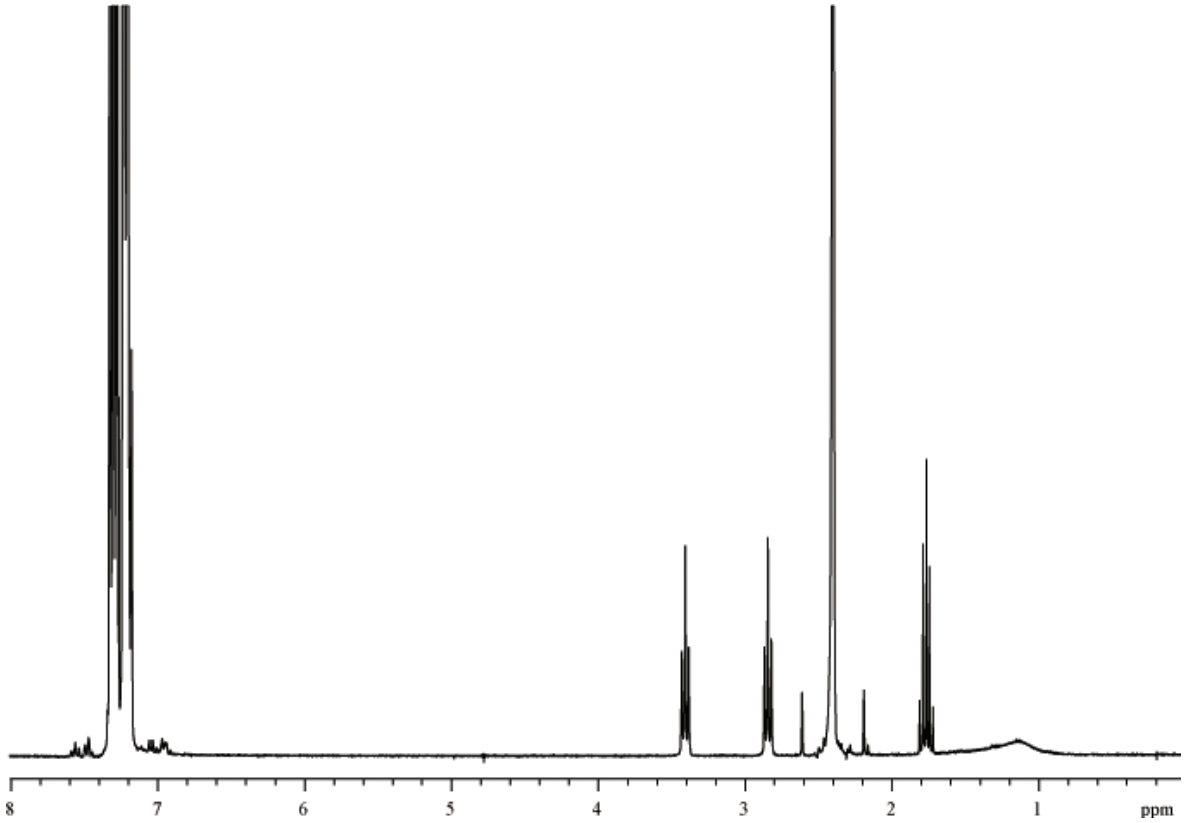

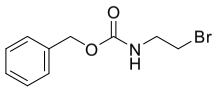

5.22
^{1}H NMR (400 MHz, $CDCl_3$)

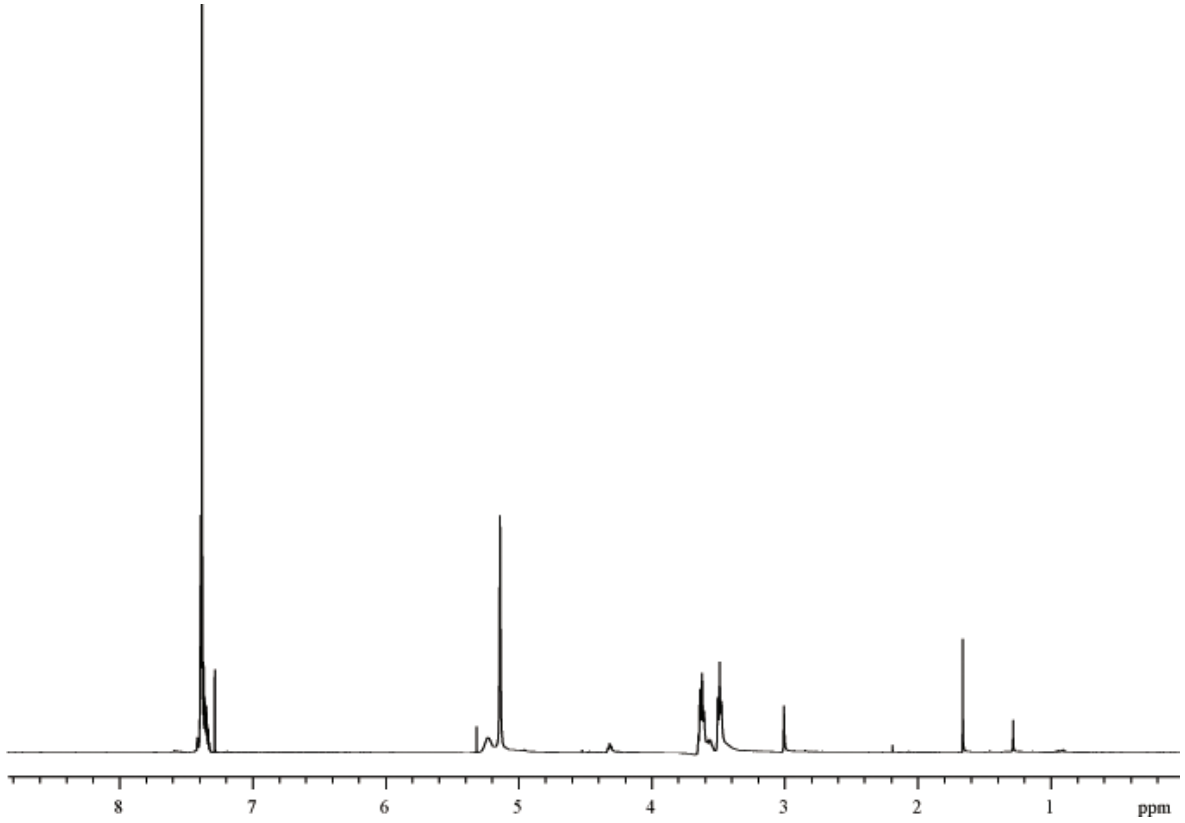

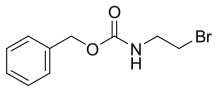

5.22

^{13}C NMR (100 MHz, $CDCl_3$)

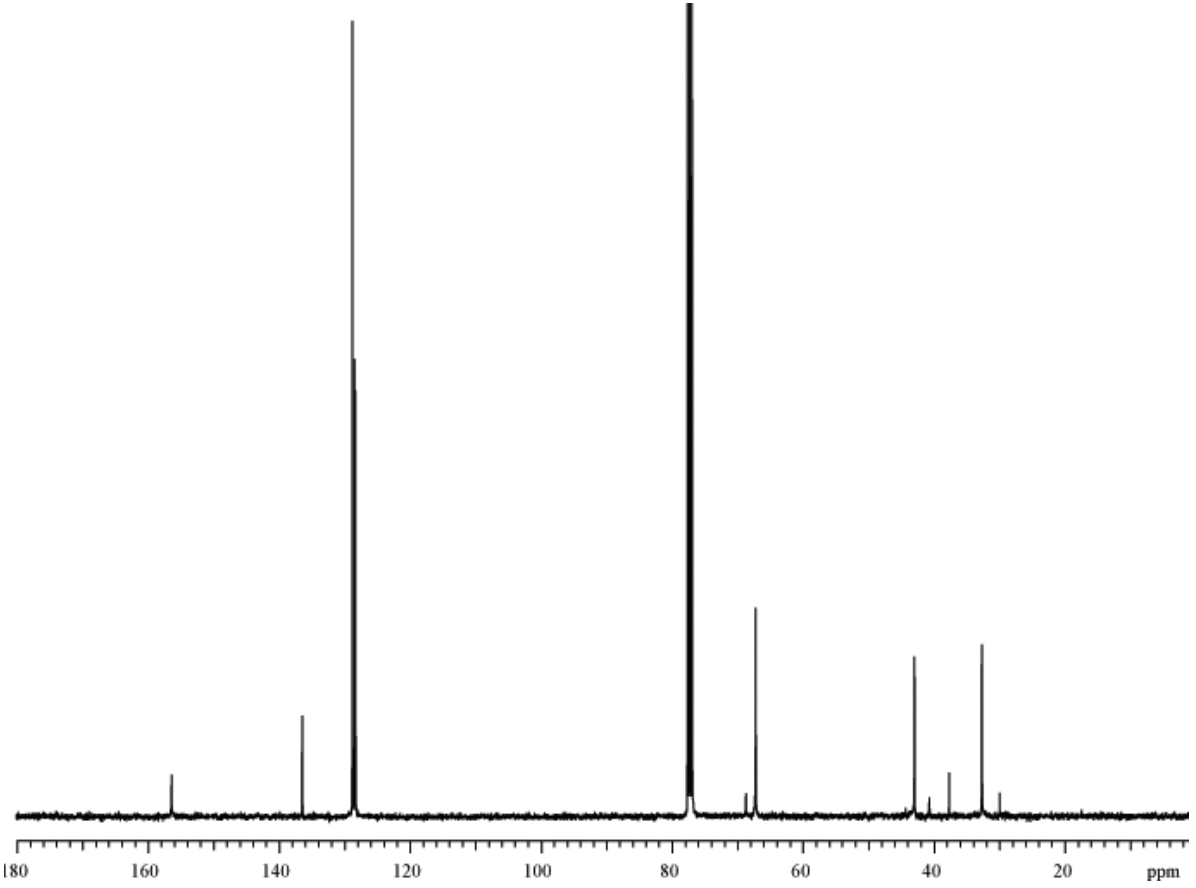

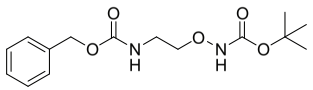

5.24
^{1}H NMR (400 MHz, $CDCl_3$)

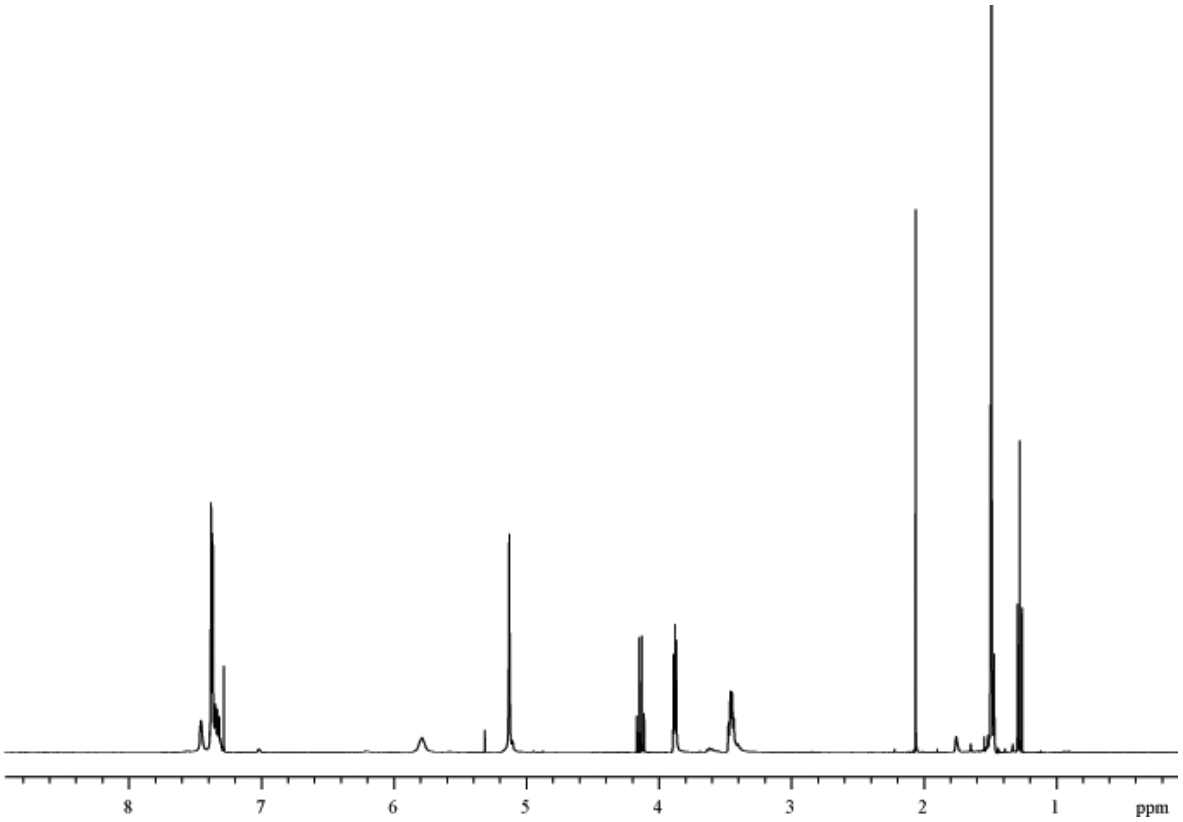

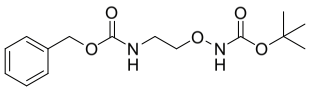

5.24

^{13}C NMR (100 MHz, $CDCl_3$)

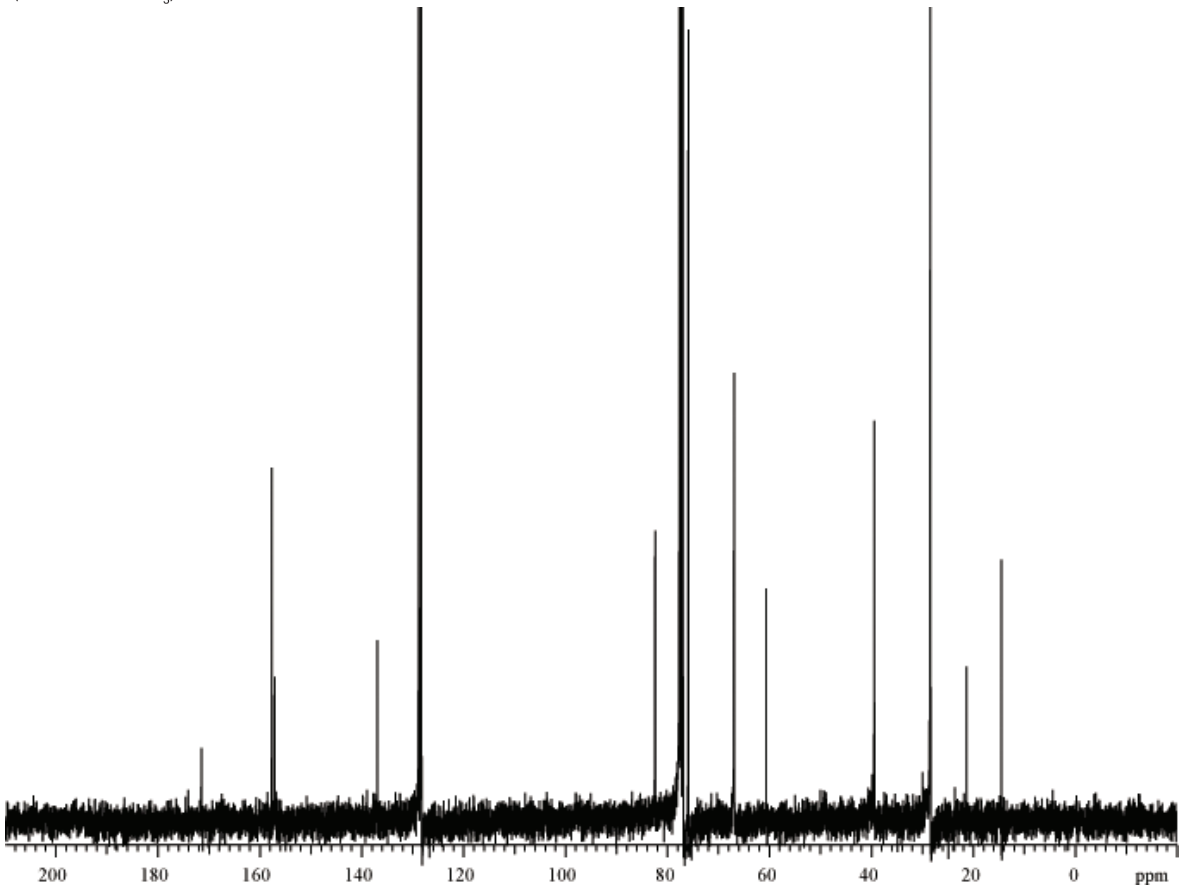

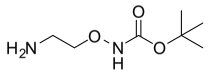

5.25
^{1}H NMR (400 MHz, $CDCl_3$)

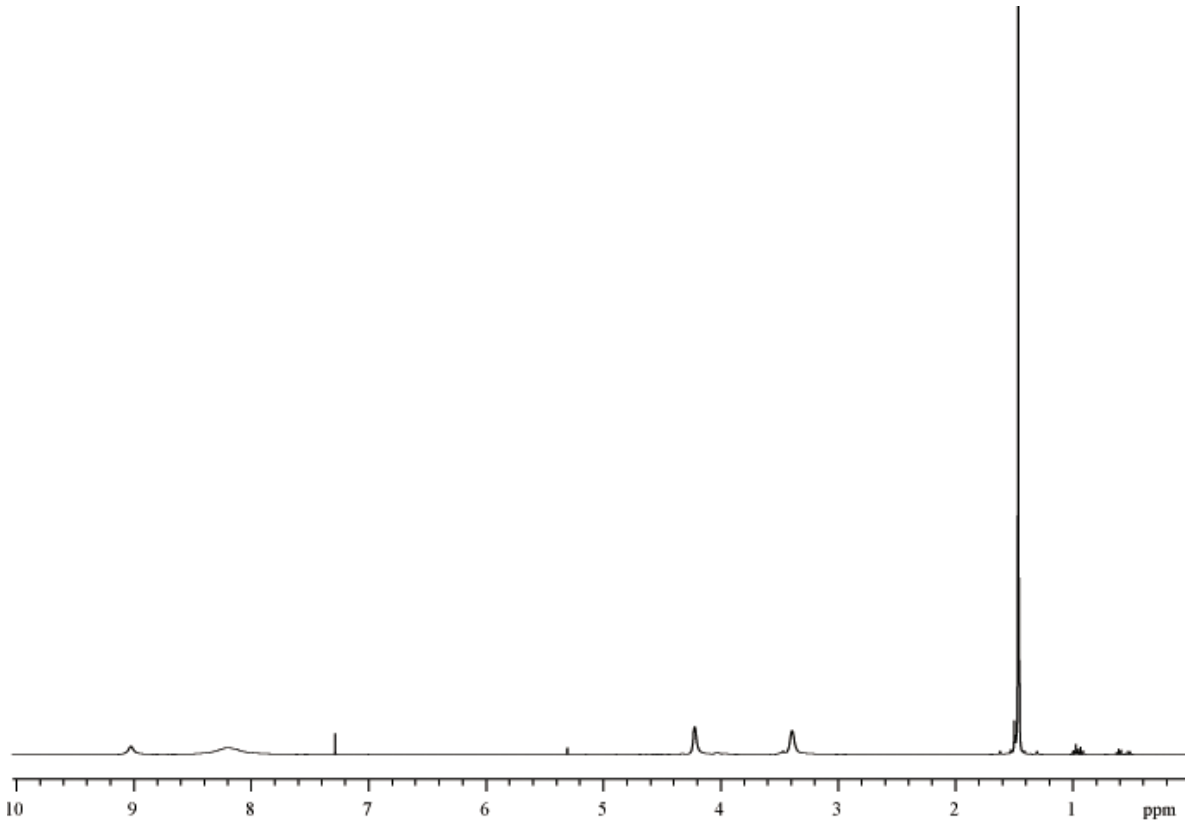

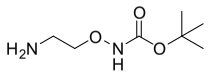

5.25
^{13}C NMR (100 MHz, $CDCl_3$)

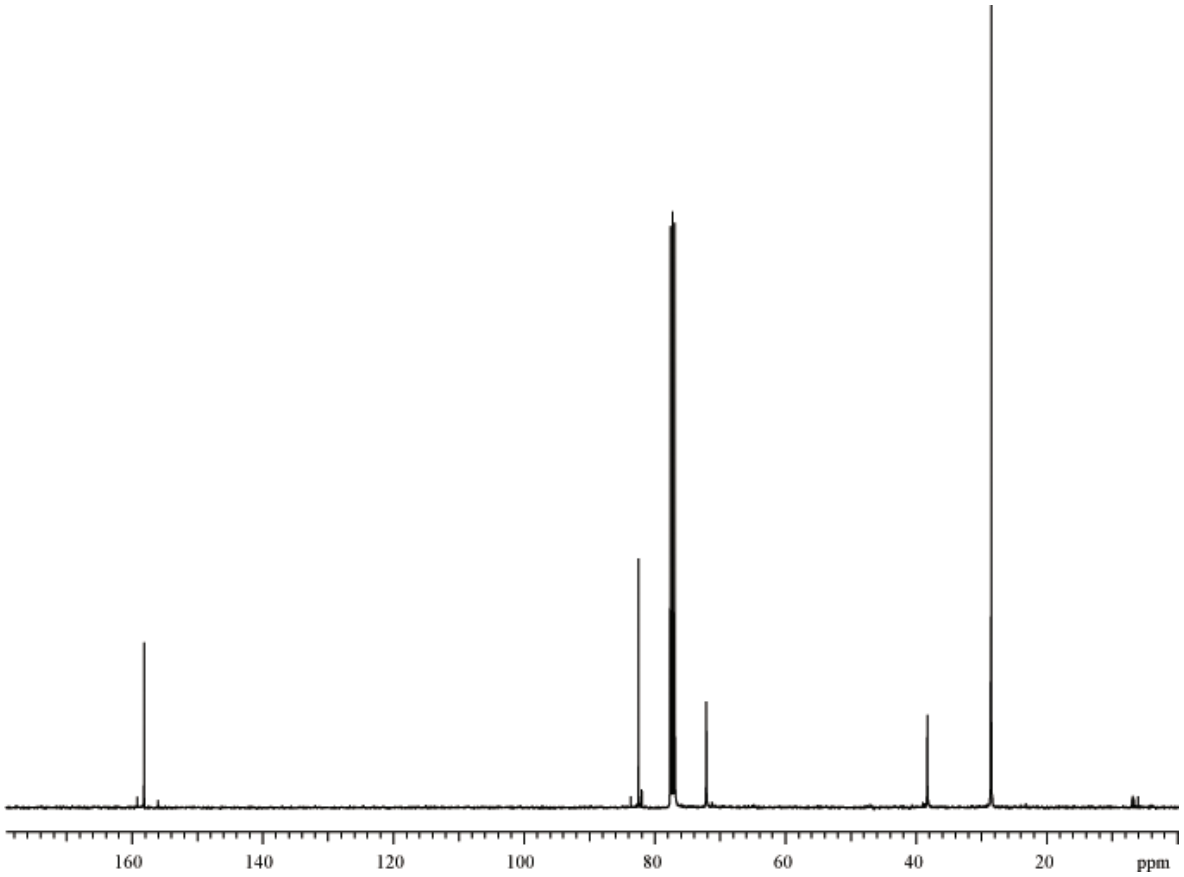

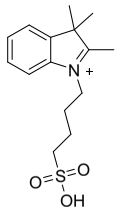

5.28
^{1}H NMR (400 MHz, CD_3OD)

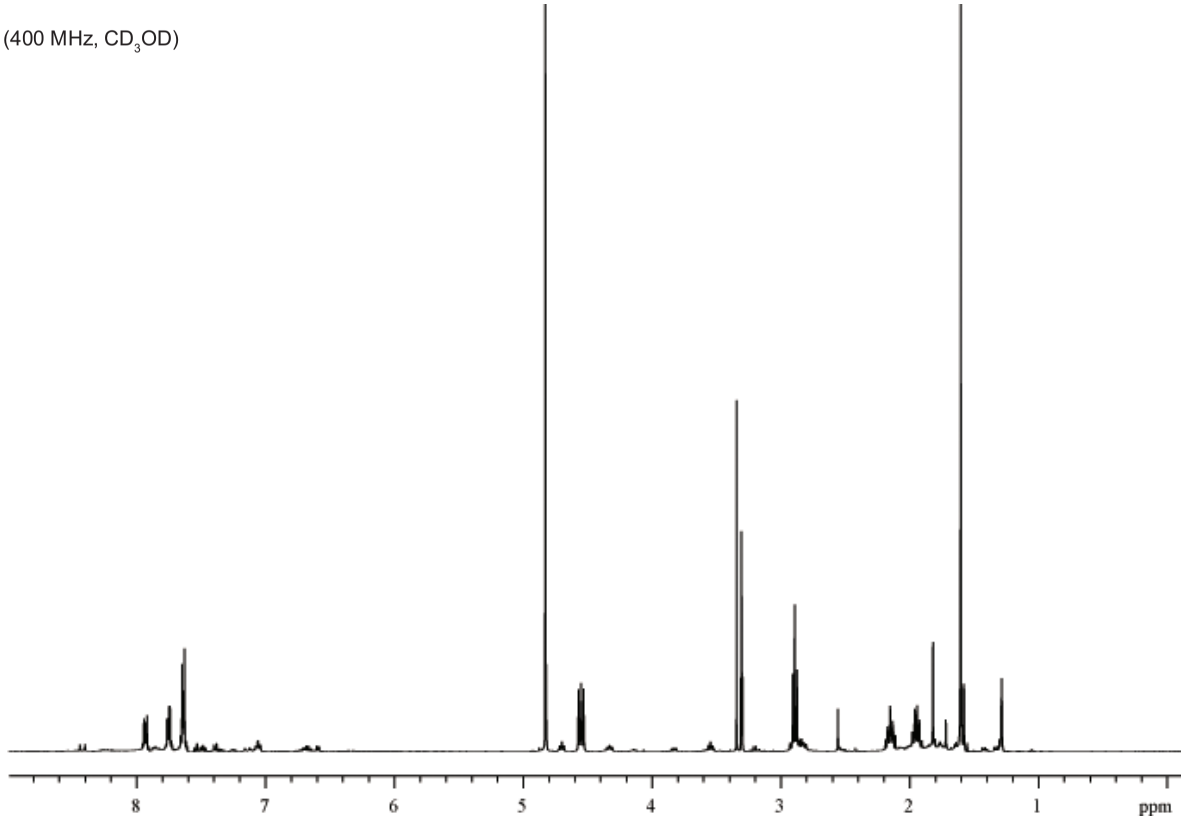

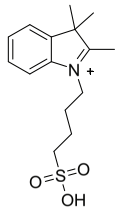

5.28
^{13}C NMR (100 MHz, CD_3OD)

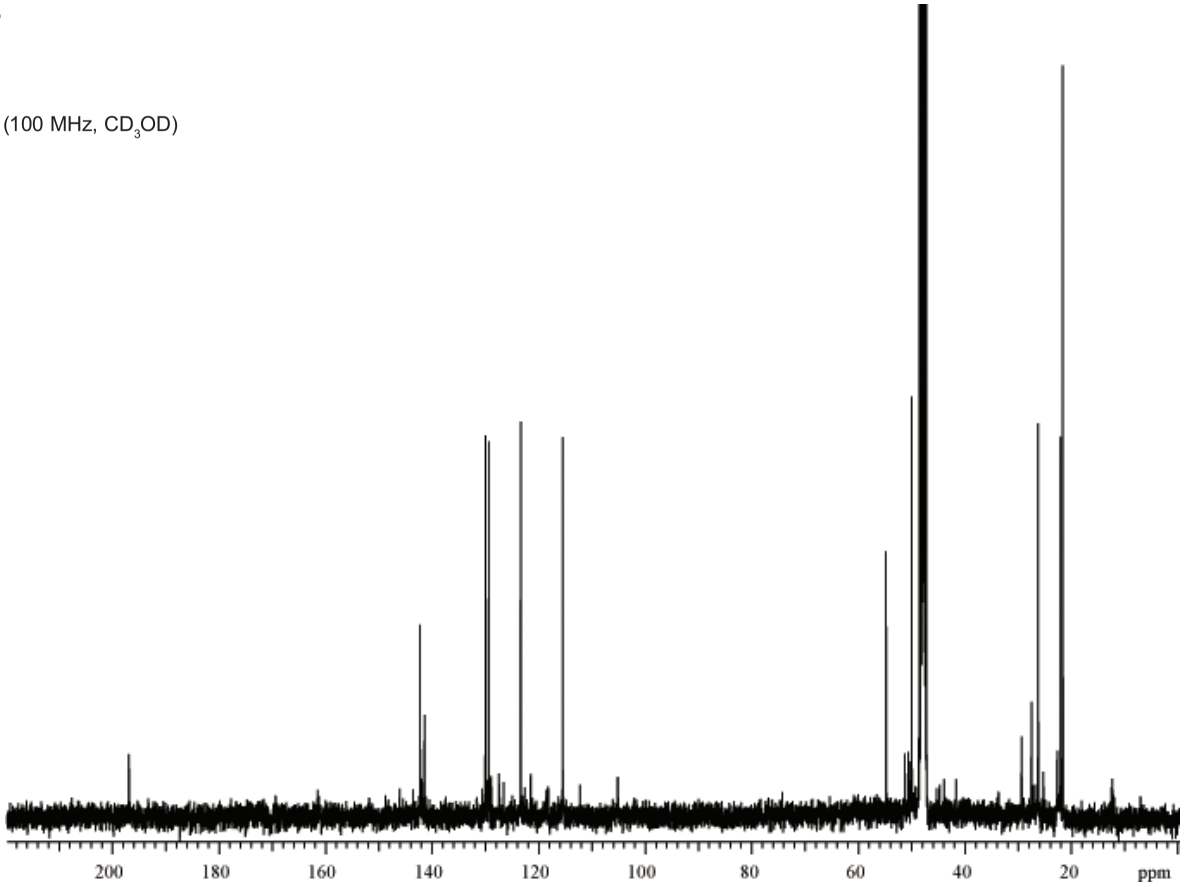

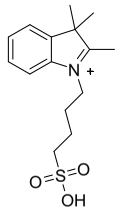

5.28

^{1}H COSY NMR (400 MHz, CD_3OD)

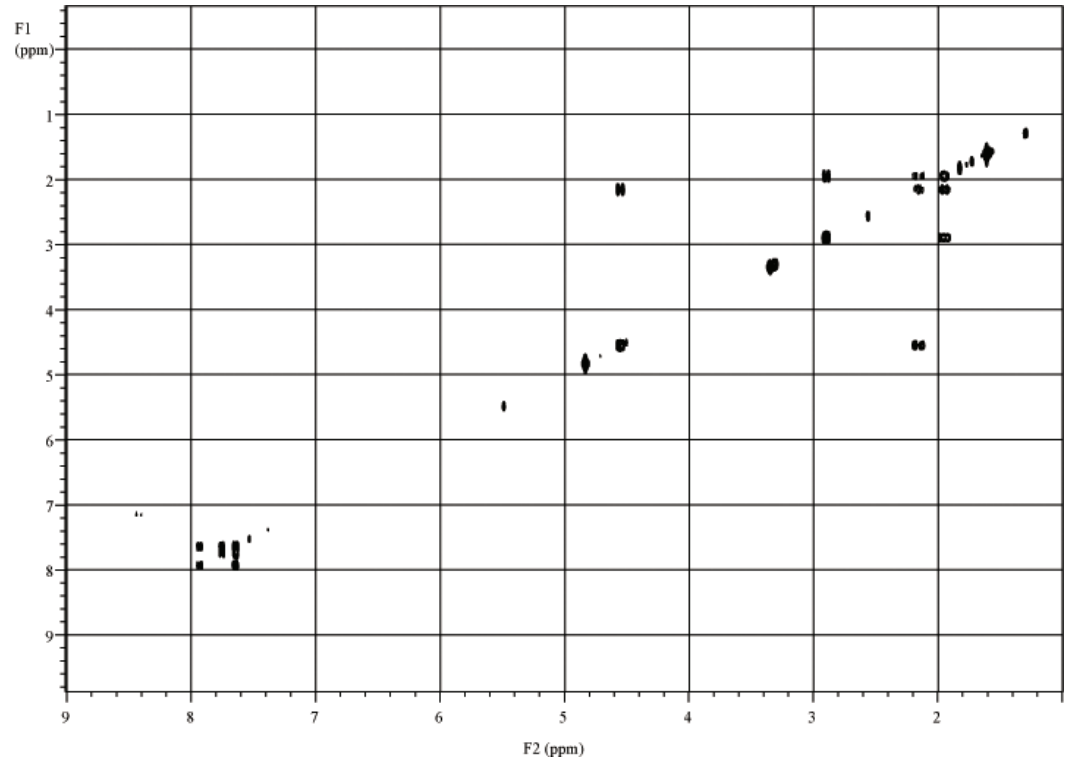

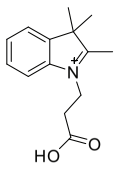

5.30
^{1}H NMR (400 MHz, Ac-D_6)

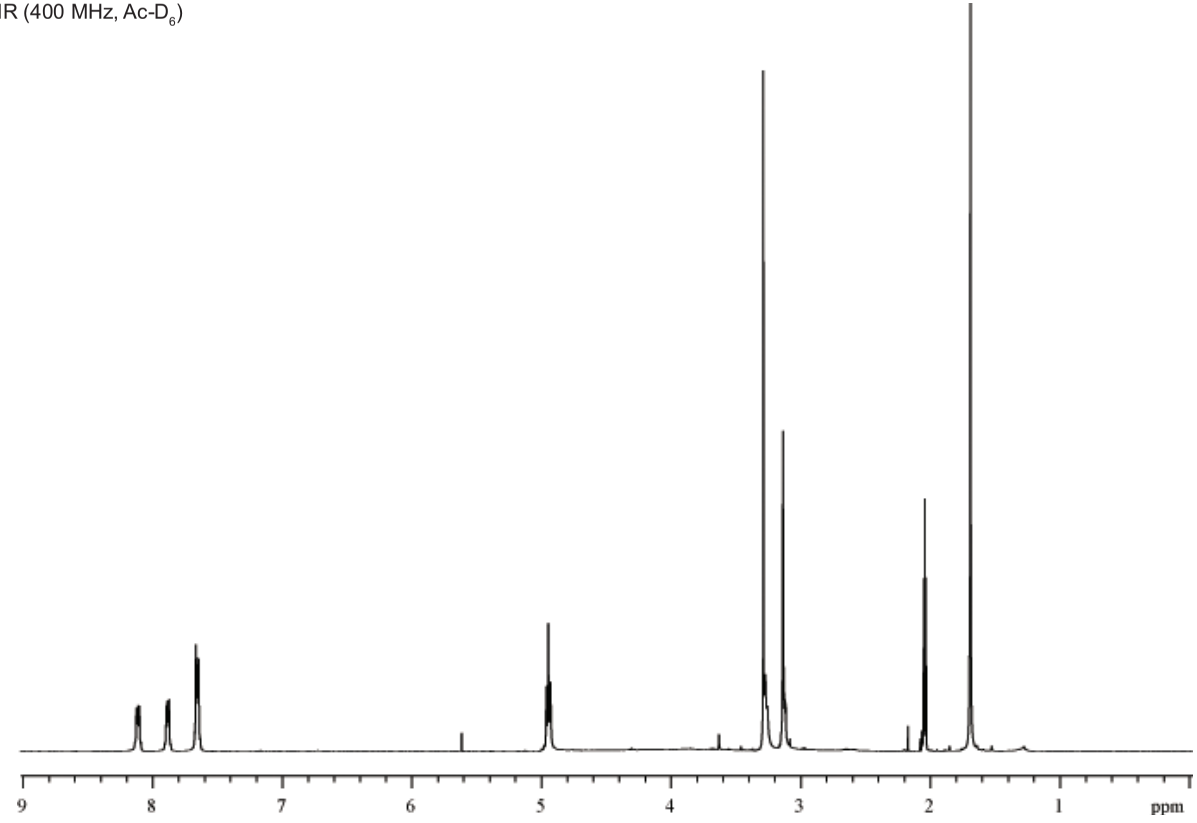

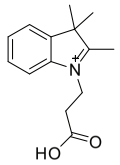

5.30

^{13}C NMR (100 MHz, Ac-D_6)

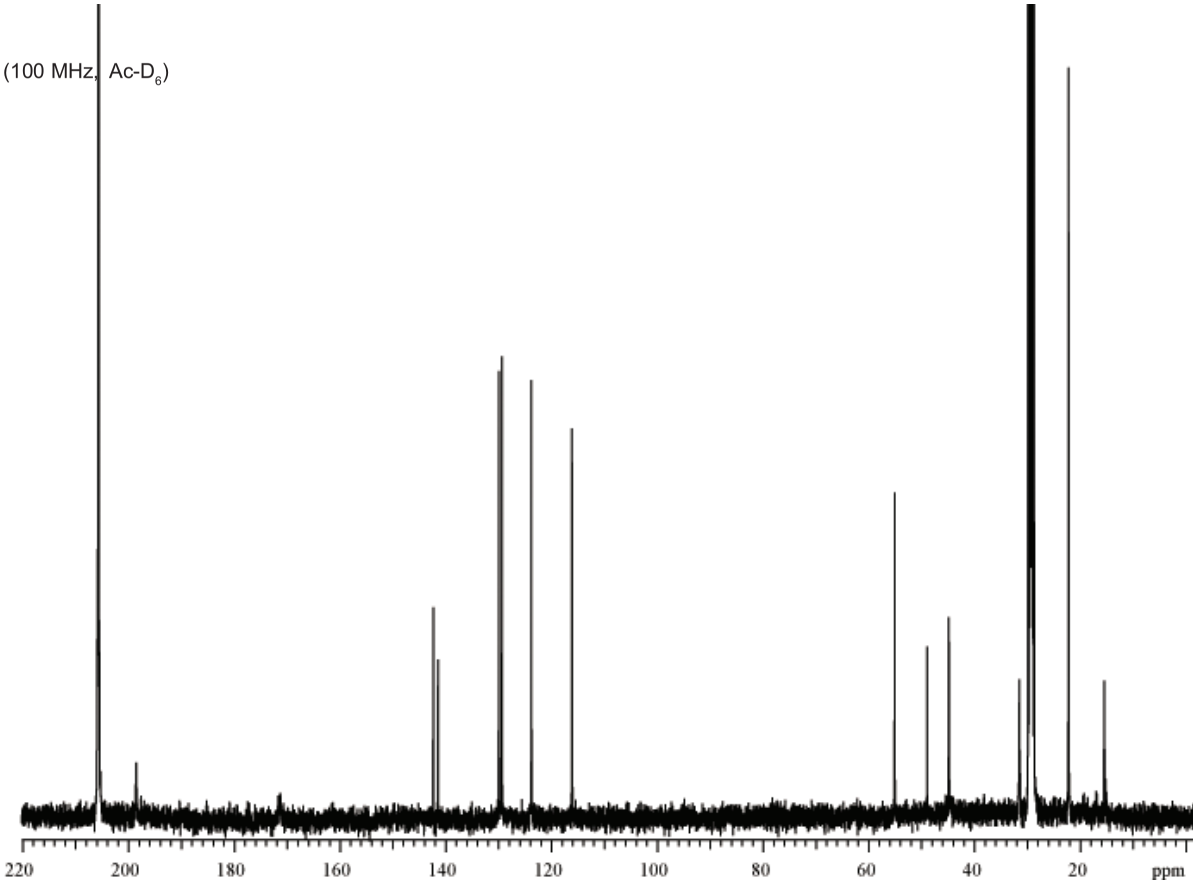

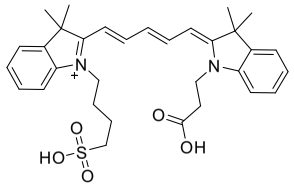

5.32
^{1}H NMR (500 MHz, CD_3OD)

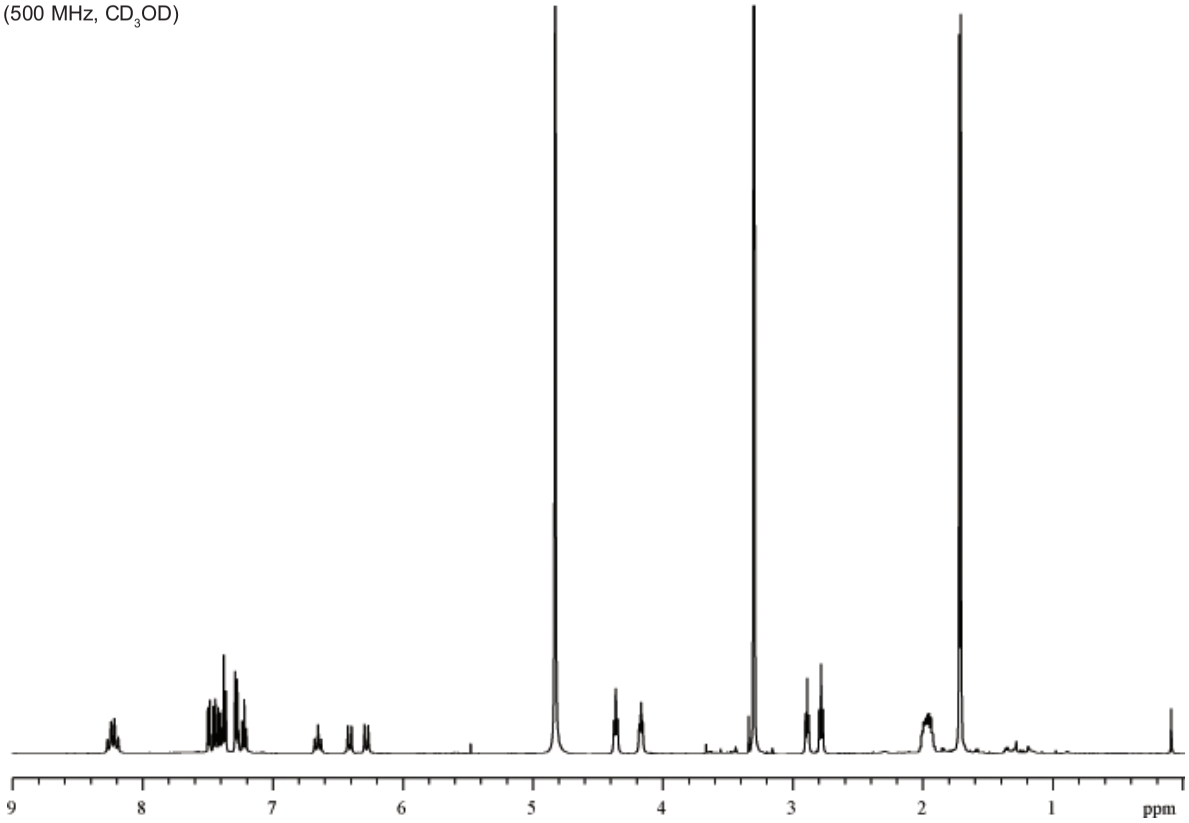

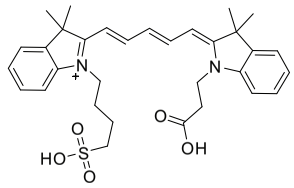

5.32
^{13}C NMR (125 MHz, CD_3OD)

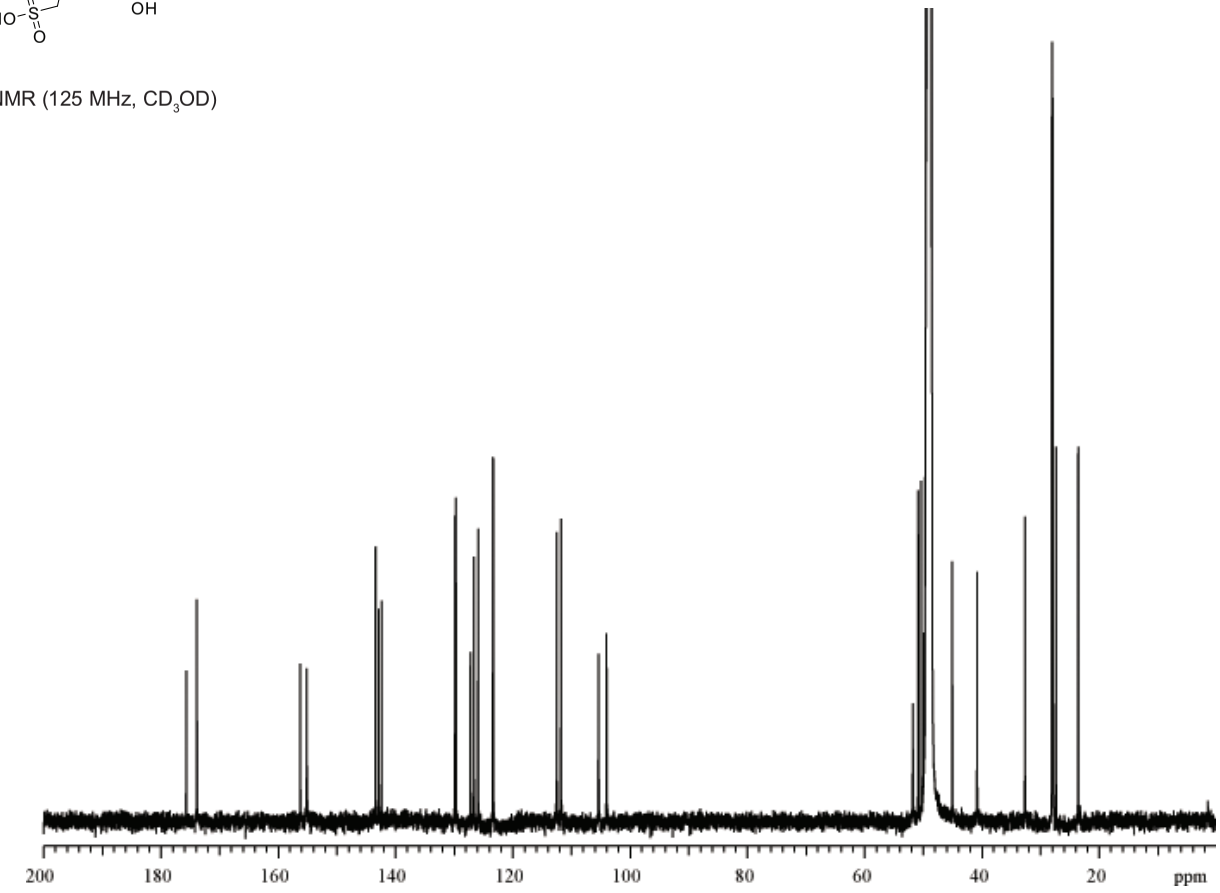

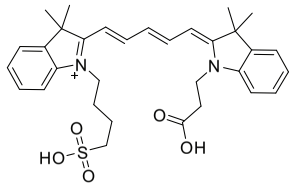

5.32

^{1}H COSY NMR (500 MHz, CD_3OD)

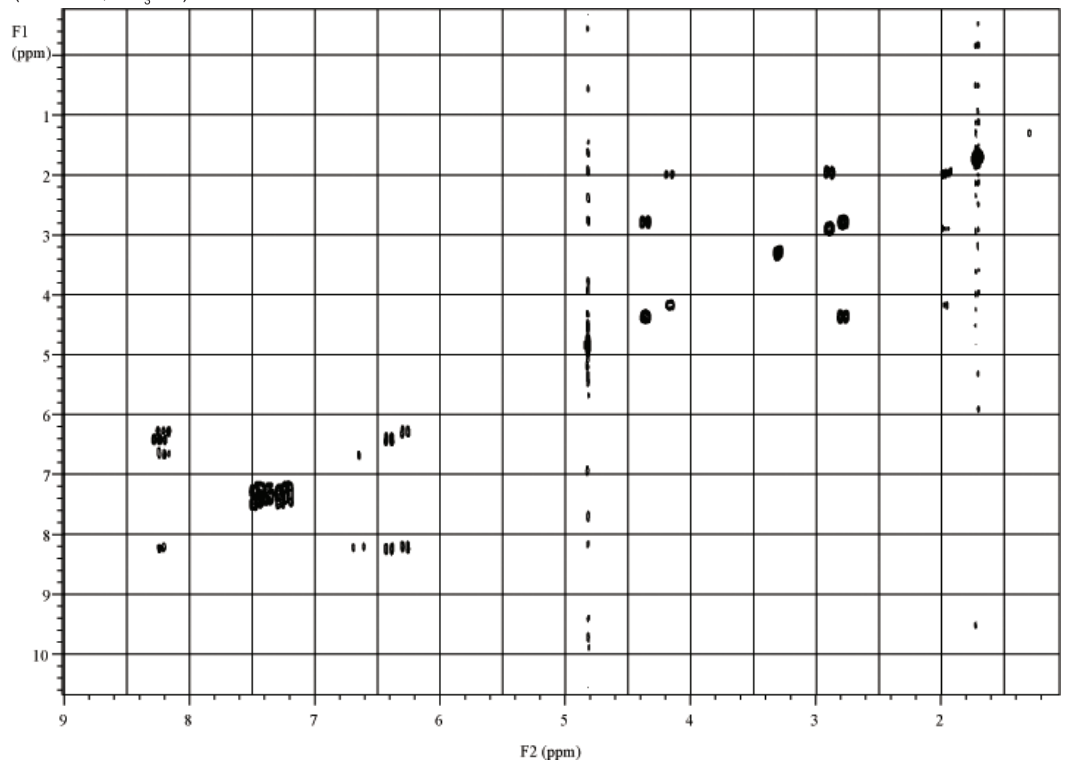

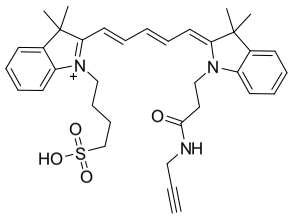

5.33
^{1}H NMR (500 MHz, CD_3OD)

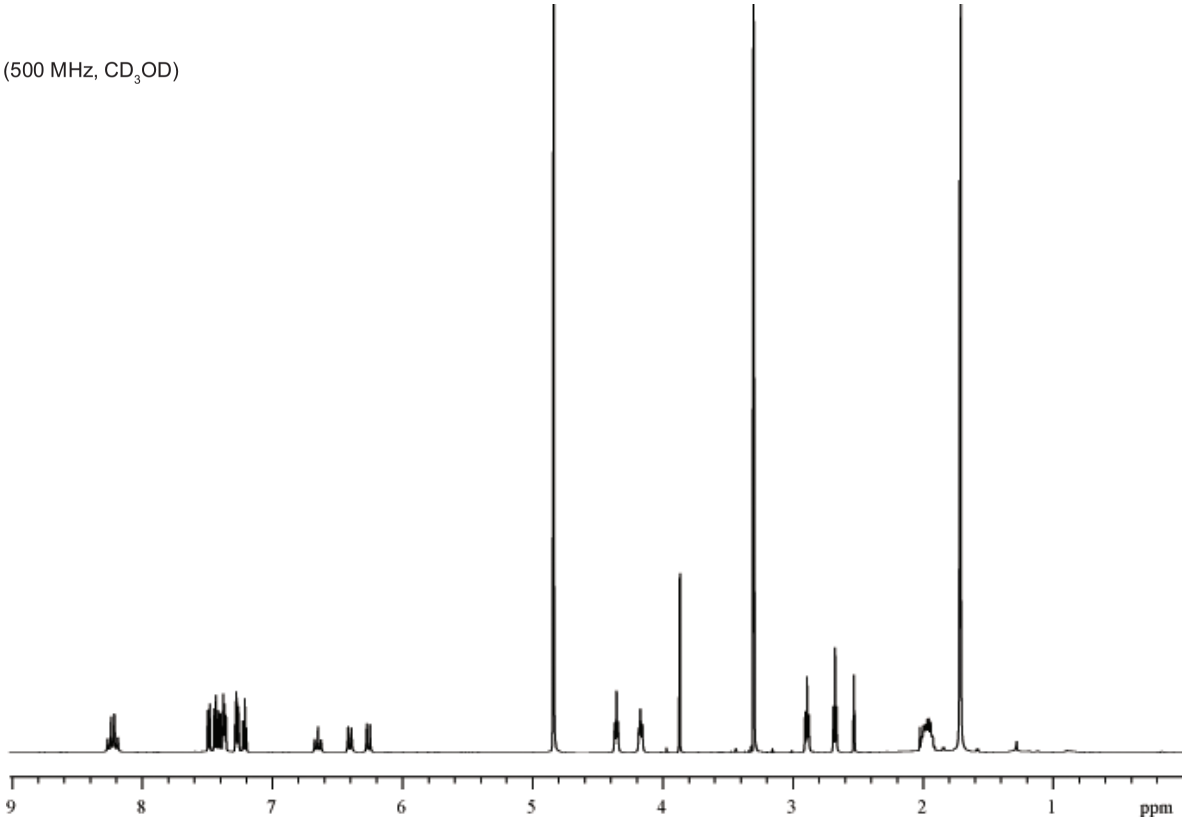

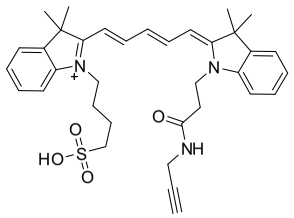

5.33
^{13}C NMR (125 MHz, CD_3OD)

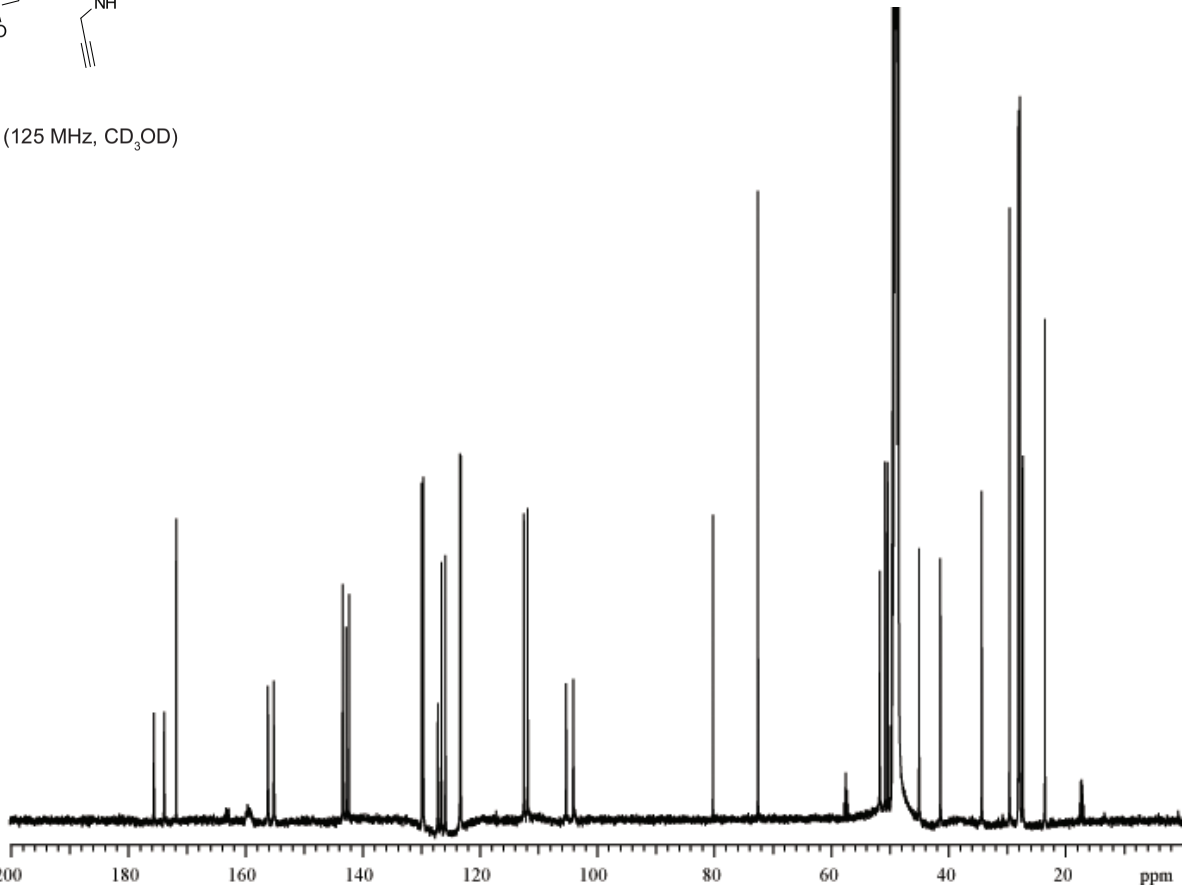

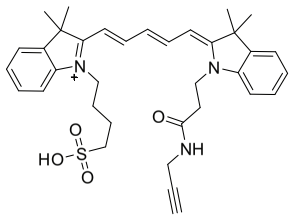

5.33
COSY NMR (500 MHz, CD_3OD)

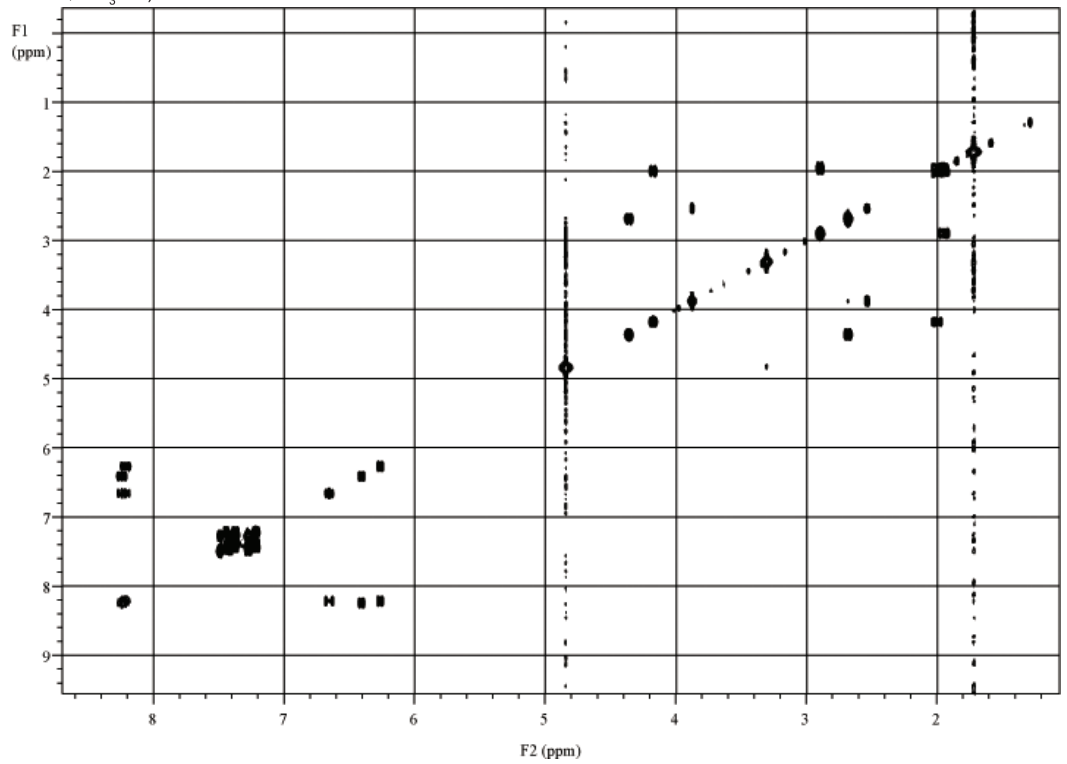

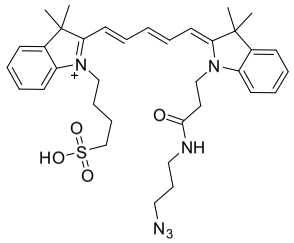

5.34
^{1}H NMR (500 MHz, CD_3OD)

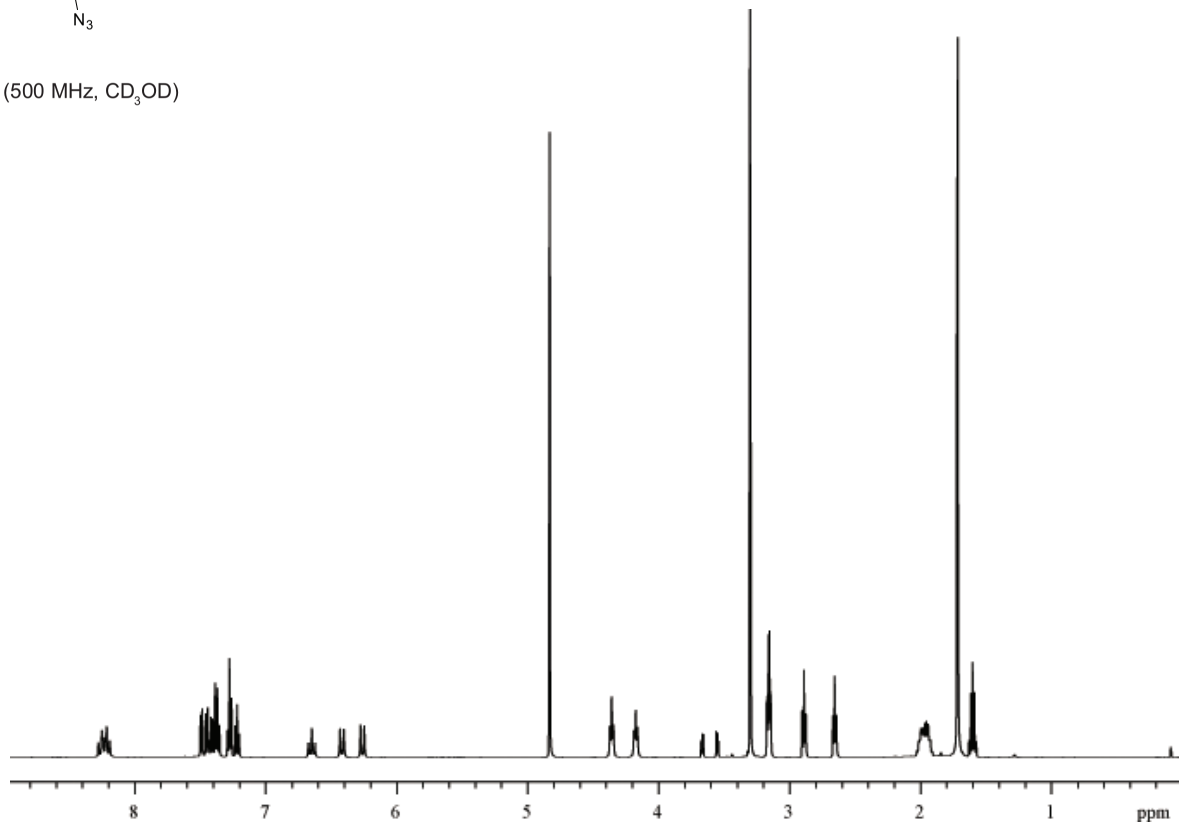

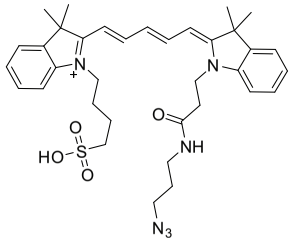

5.34
^{13}C NMR (125 MHz, CD_3OD)

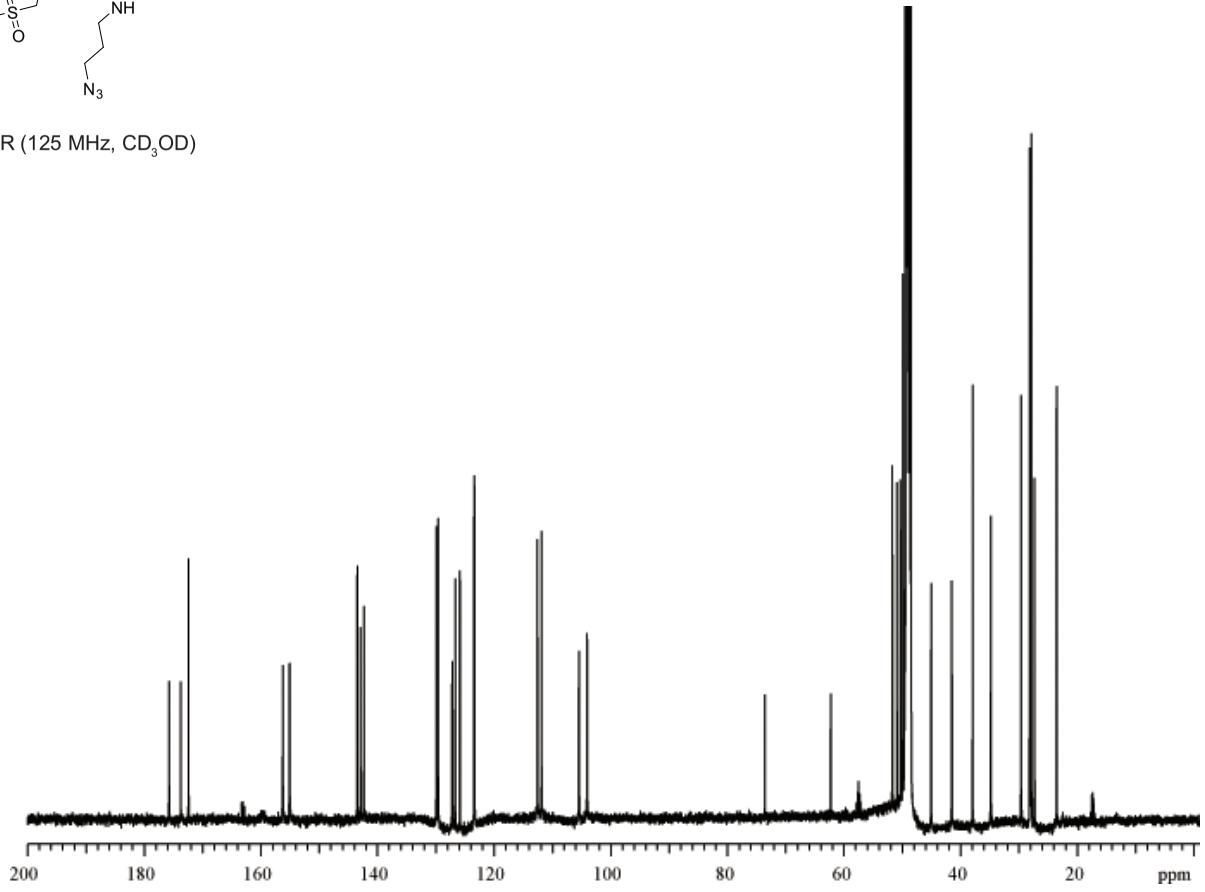

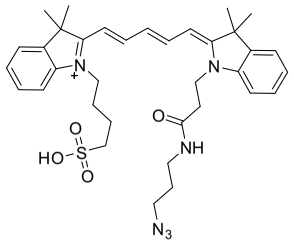

5.34

COSY NMR (300 MHz, CD_3OD)

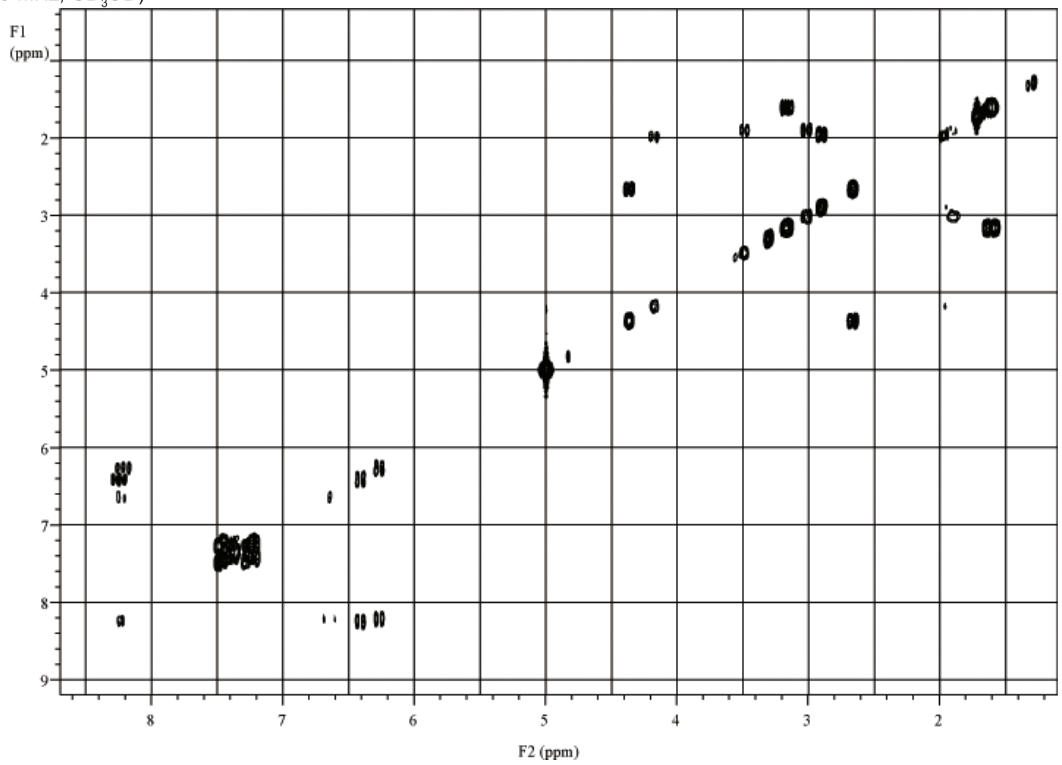

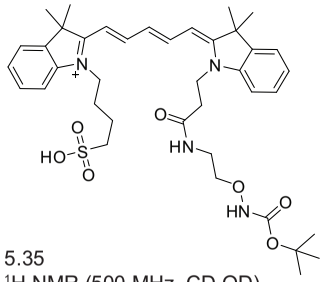

5.35
^{1}H NMR (500 MHz, CD_3OD)

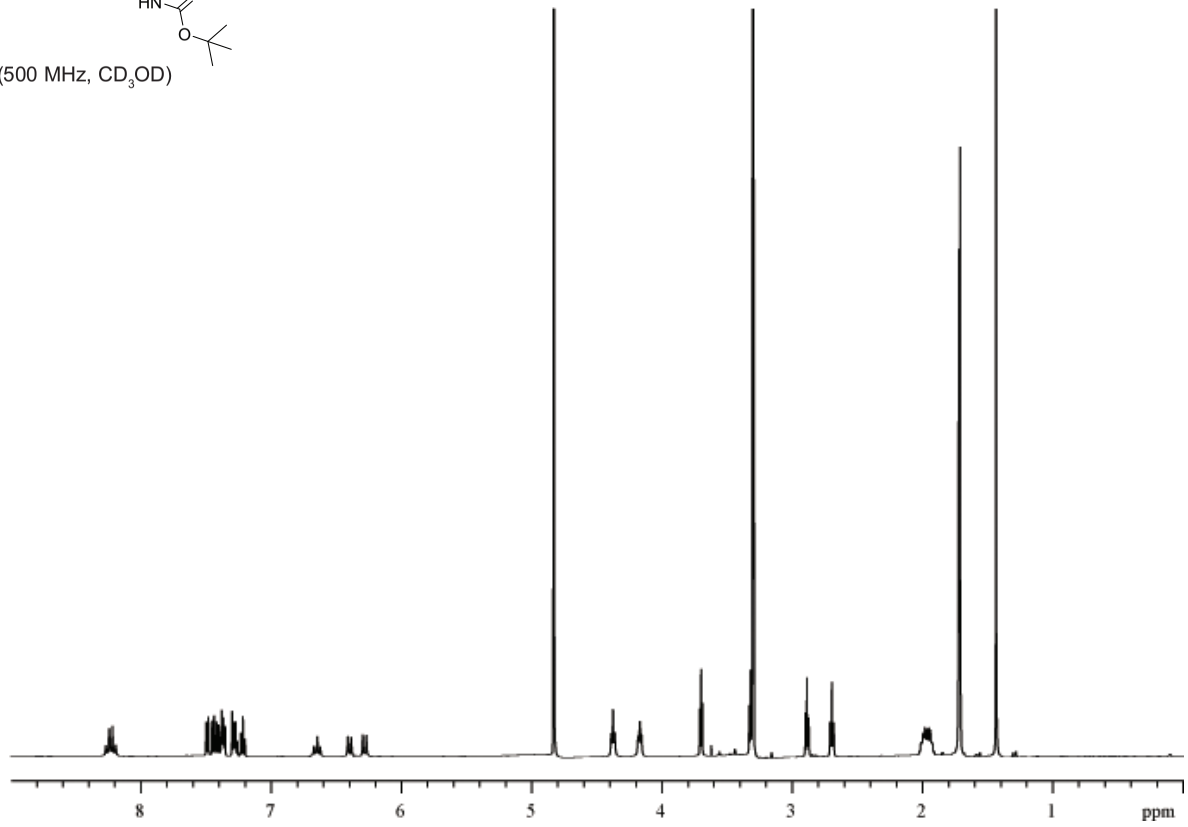

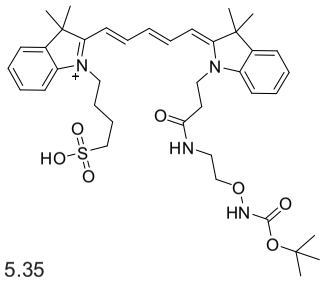

5.35
^{13}C NMR (125 MHz, CD_3OD)

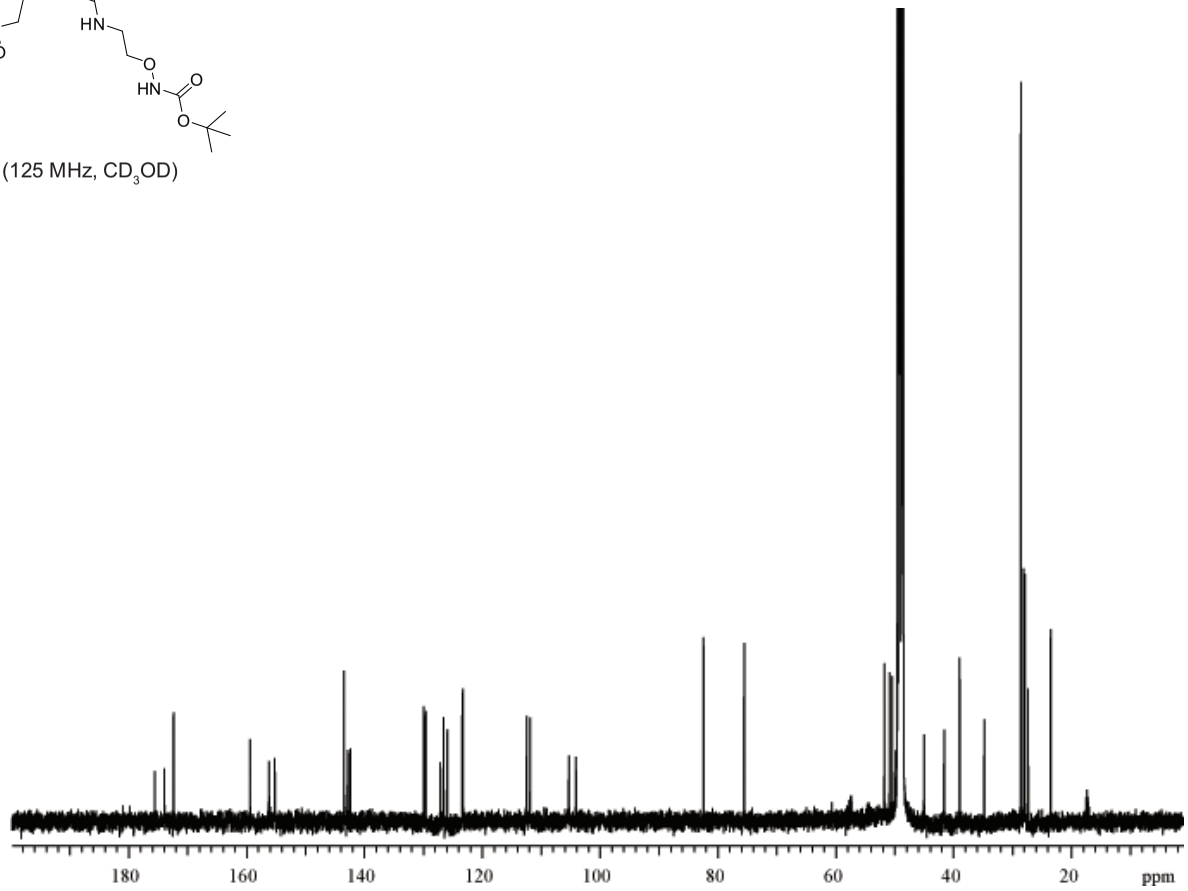

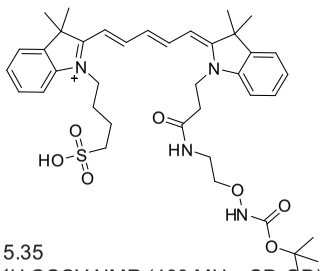

5.35

^{1}H COSY NMR (400 MHz, CD_3OD)

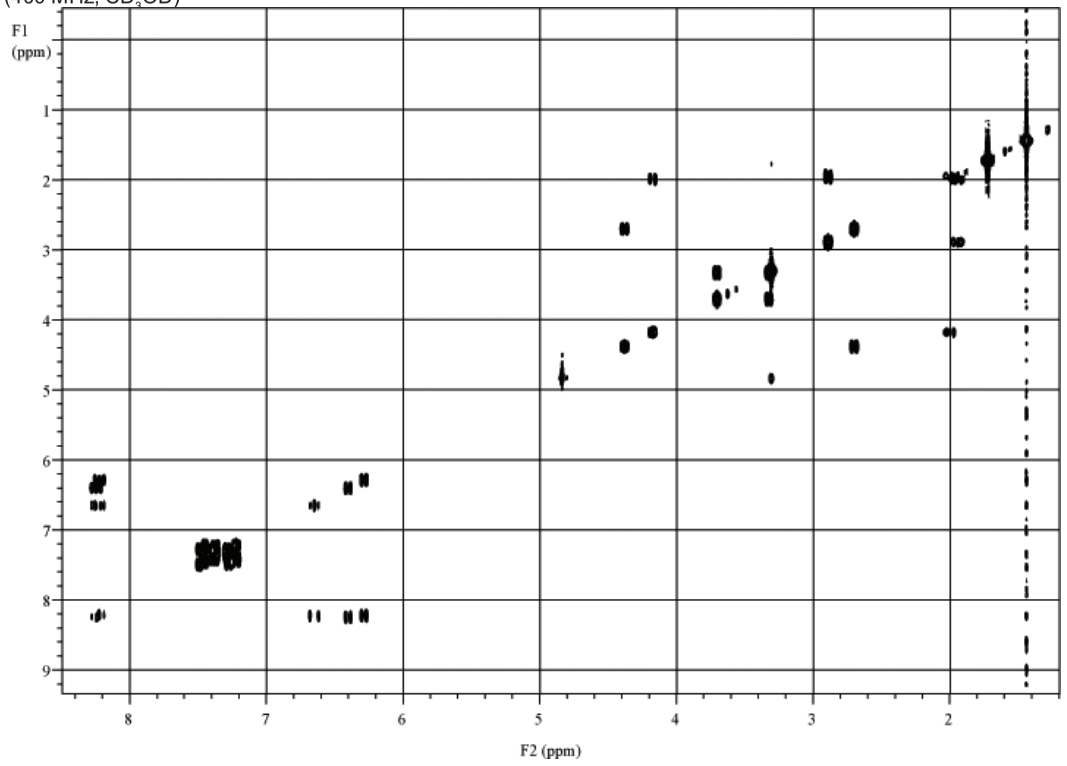

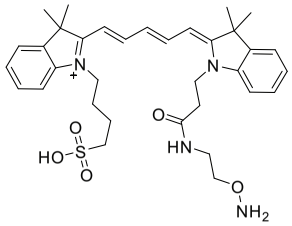

5.36
^{1}H NMR (500 MHz, CD_3OD)

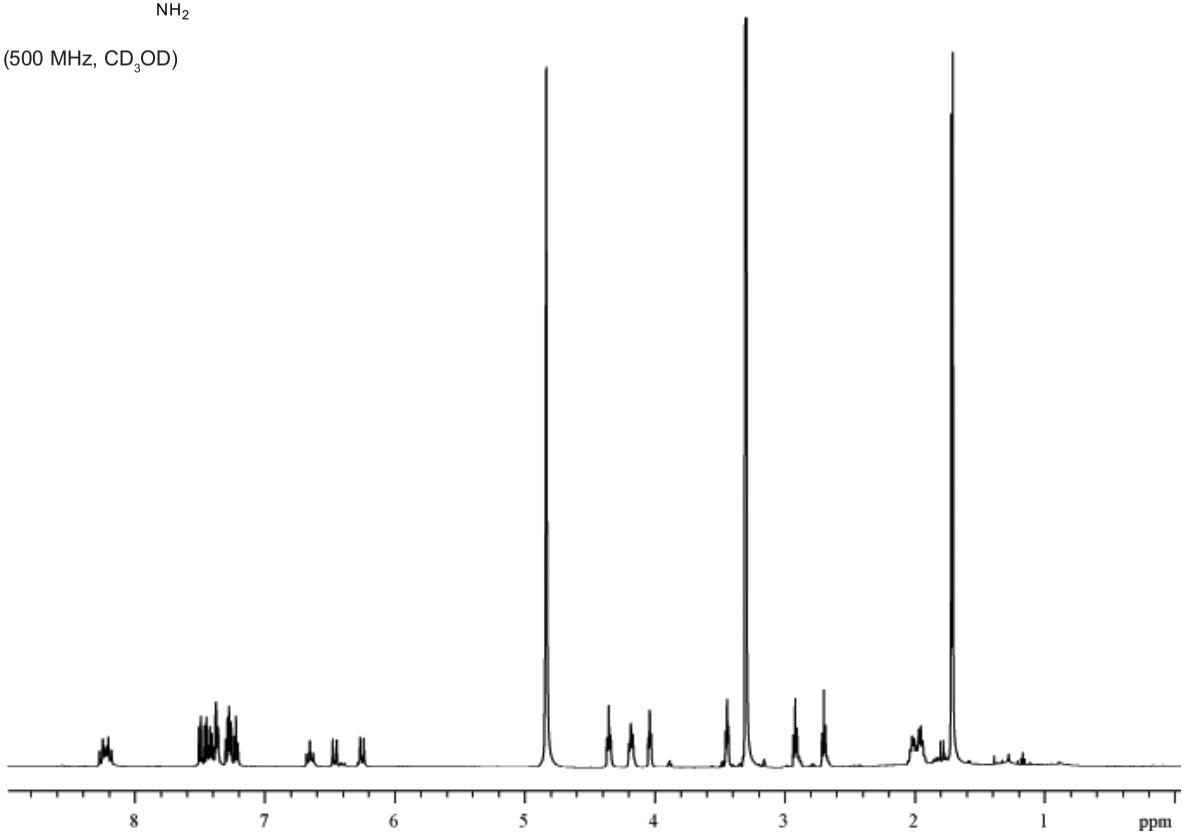

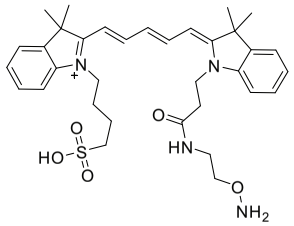

5.36
^{13}C NMR (125 MHz, CD_3OD)

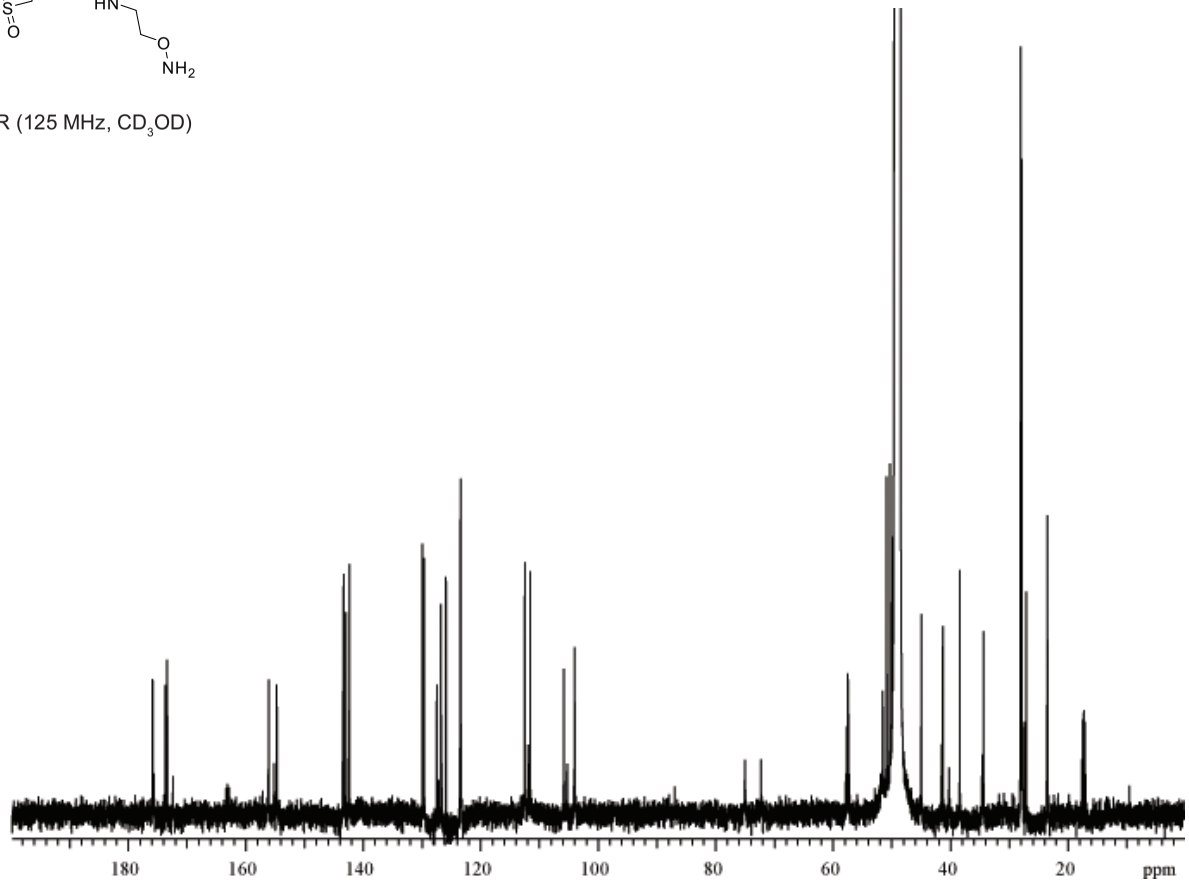

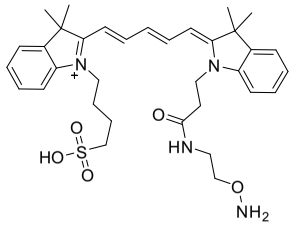

5.36

COSY NMR (500 MHz, CD_3OD)

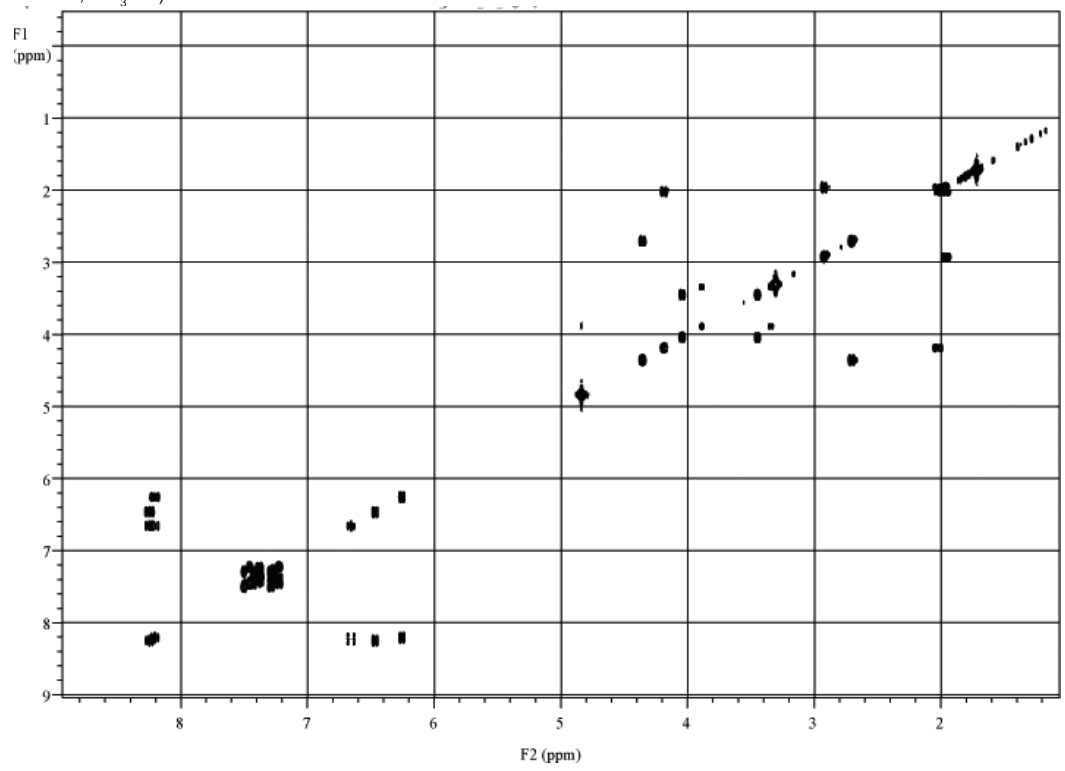

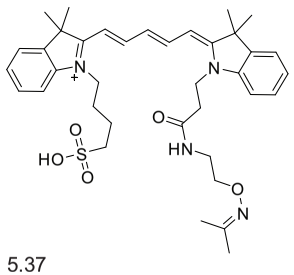

5.37
^{1}H NMR (500 MHz, CD_3OD)

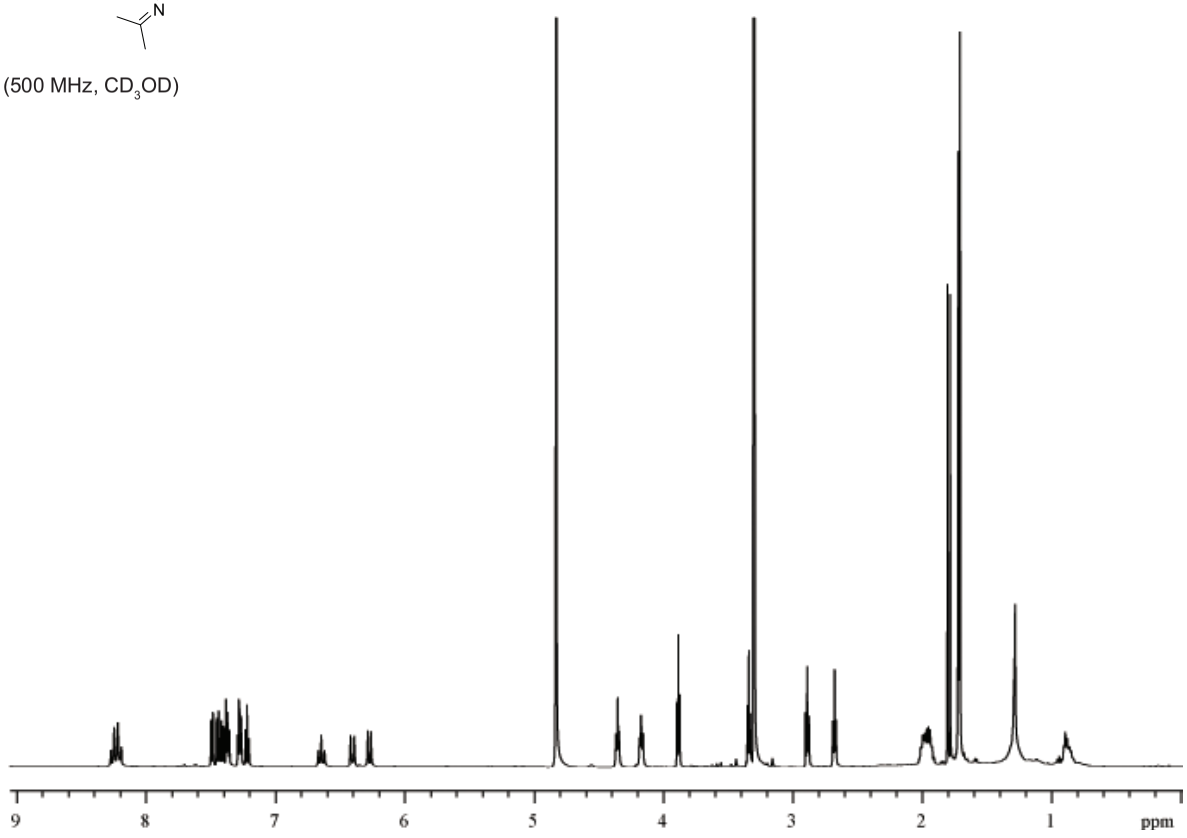

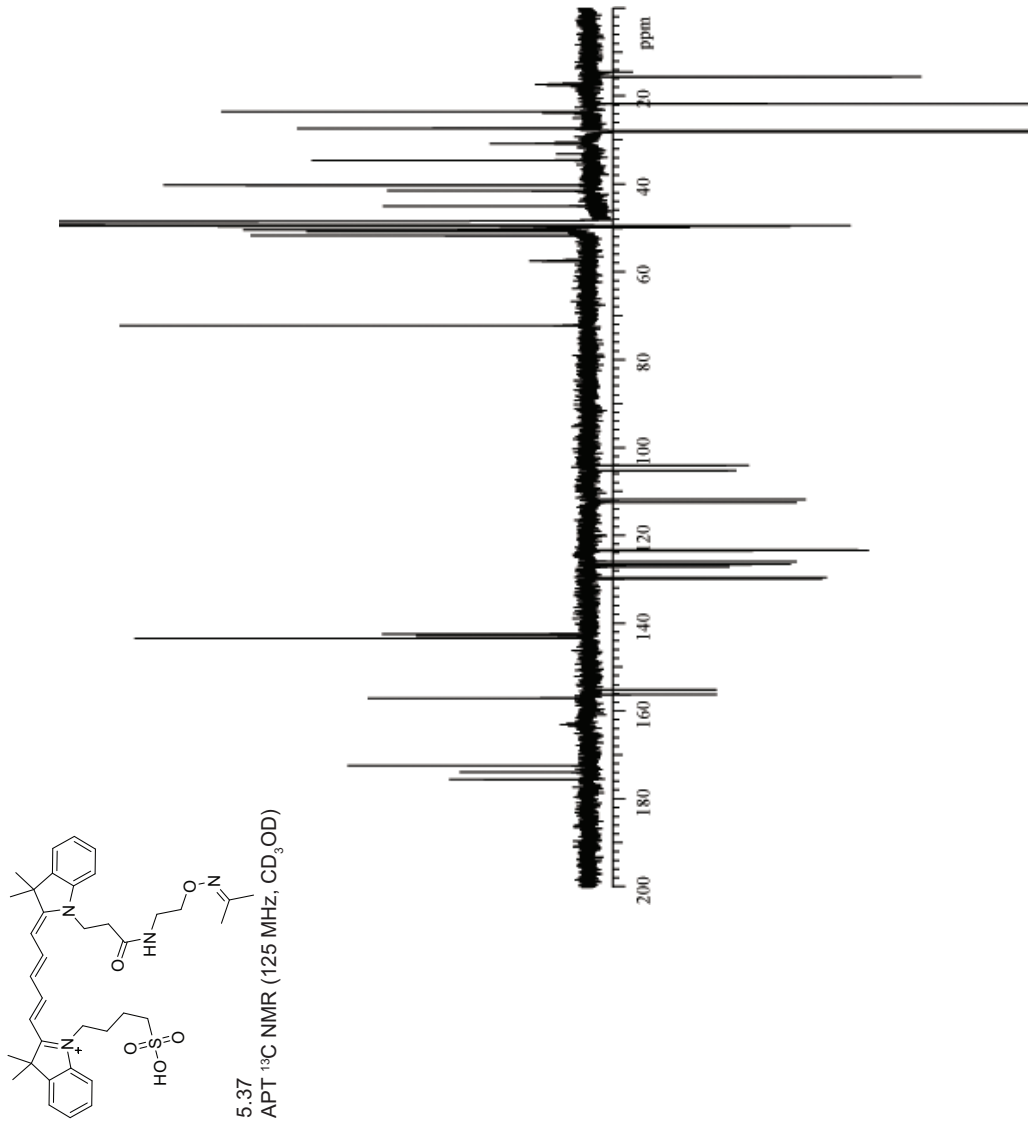
ppm
200
180
160
140
120
100
80
60
40
20
5.37
APT ^{13}C NMR (125 MHz, CD_3OD)

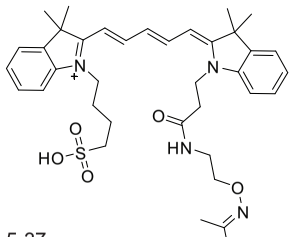

5.37

COSY NMR (500 MHz, CD_3OD)